Title
Development of a New High-Performance Steel Plate Shear Wall System with an Innovative Gusset Plate Moment Connection

Author
QIAN, XIN

Publication Date
2017

Peer reviewed|Thesis/dissertation

Development of a High-Performance Steel Plate Shear Wall System with an Innovative Gusset Plate Moment Connection

by

Xin Qian

A dissertation submitted in partial satisfaction of the

requirements for the degree of

Doctor of Philosophy

in

Engineering – Civil and Environmental Engineering

in the

Graduate Division

of the

University of California, Berkeley

Committee in charge:

Professor Abolhassan Astaneh-Asl, Chair

Professor Khalid M. Mosalam

Professor Lisa A. Pruitt

Fall 2017

COPYRIGHT

Development of a High-Performance Steel Plate Shear Wall System
with an Innovative Gusset Plate Moment Connection

Abstract

Development of a New High-Performance Steel Plate Shear Wall System
with an Innovative Gusset Plate Moment Connection

by

Xin Qian

Doctor of Philosophy in Engineering – Civil and Environmental Engineering
University of California, Berkeley

Professor Abolhassan Astaneh-Asl, Chair

This dissertation focused on developing a new High-Performance Steel Plate Shear Wall system (HPSPSW) with an innovative Gusset Plate Moment Connection (GPMC). This research and development work has resulted in the innovative concepts, the modeling methods and interim design procedures of the new connection and the system.

Among the design issues for the current fully connected steel plate shear wall (SPSW) system, three of them are fundamental: (1) the tension field anchor force of the infill plate makes the columns very large, heavy, and expensive; (2) the complete joint penetration (CJP) field-welded moment connections used in the current system are not cost effective and require field-welding and on-site ultrasonic testing; and (3) the thin infill wall is susceptible to buckling under wind loads and small frequent earthquakes. The proposed new HPSPSW system incorporates two major modifications that are targeted at solving these root problems: (1) detaching the infill wall from the boundary columns but providing side stiffeners on the two vertical free edges; and (2) replacing the CJP welded moment connection by the innovative GPMC.

The GPMC utilizes the ductility of gusset plate as the main ductile energy dissipation element, enabling the beams and columns to remain essentially elastic. The entire connection configuration is proposed to minimize the field CJP welds, doubler plates, and continuity plates, resulting in potential savings in terms of fabrication costs. The GPMC offers several configurations and finds applications in a variety of lateral force-resisting systems. Extensive nonlinear finite element (FE) analyses were conducted to examine the appropriate range of gusset plate materials, strengths, thicknesses, free gusset lengths, gusset flange thicknesses, and bolt strengths, with the aim of achieving both the desired ductile behavior and a reduction in fabrication costs. With the gusset plate acting as the fuse, the “strong-column–weak-beam” criteria for special moment frames can be suspended, resulting in greater design flexibility and cost savings. In addition, a simplified rotational hinge model was calibrated for the GPMC for use in global analysis models. An interim step-by-step design procedure was proposed, following the format of pre-qualified moment connection design procedures and was developed based on desirable objective performance criteria and limit state hierarchy.

Through nonlinear FE parametric studies, the new HPSPSW system is shown to solve issues related to the tension field action anchor force with comparable or better performance compared to the current fully connected SPSW system; it is cost-effective, flexible and versatile. The infill wall thickness and the column sections are no longer strongly dependent on each other, allowing thicker walls to be used for drift or service performance goals, and lighter and more forms and orientations of the columns to be employed. In addition, the reduction of the two vertical welds increases the reparability as well as the ease of retrofit and modular construction of the system. After a study of various shapes, the T-shaped side stiffeners were found to be the most efficient and practical for use in the HPSPSW system. Design equations for establishing the strength and stiffness of the infill wall were derived based on the collapse mechanism of plate girders, followed by design recommendations for the infill wall and its side stiffeners. An equivalent brace (EB) model was developed and verified for the new HPSPSW system both as an analysis and a design tool.

Finally, the system performance was evaluated using realistic site and prototype buildings, including a series of 3-, 9- and 20-story prototype buildings that conform to the SAC building specifications. The model used the simplified rotational hinge model for the GPMC and the EB model for infill wall with side-stiffeners. Two seismic design procedures were proposed for the new HPSPSW system: a prescriptive code-based procedure and a performance-based procedure. The performance-based procedure adopts the code-based procedure to initiate the preliminary design and uses design iterations to achieve multiple enhanced performance objectives at different seismic hazard levels. It was found that the preliminary code-based designs generally satisfy the deformation controlled performance objectives (i.e., story drift, residual drift, and connection rotation) at the median level. All designs met service-level performance goals even without explicit consideration in the design process. Some code-based designs experienced a soft-story mechanism at the maximum considered level hazard. Column yielding other than the base of the first story was also observed in some of the code-based designs, indicating a need for improvement. The performance-based designs met all deformation-controlled objectives on the 84-percentile level, and satisfied the column axial-moment interaction objective on the median level with no column yielding other than the base of the first-story columns. A comparison between the current AISC SPSW system and the new HPSPSW system showed that the new HPSPSW system effectively reduced the column over-stress and structural weight, eased the design iterations, and improved the material-utilization ratio and economy of the system efficiently while exhibiting enhanced seismic performance.

In addition to the main findings, various design, detailing, and fabrication considerations were also discussed. Recommendations for future experimental and analytical research are suggested. A test program is proposed aiming to verify, validate, and refine the proposed concepts, analytical model, and design procedures.

DEDICATION

To my family and friends,

who inspire and support all the time.

Table of Contents

List of Figures

List of Tables

Definition of Symbols

b_s	Width of rectangular side stiffeners
b_{cf}	Column flange width
c	Distance between the two plastic hinges forming in the side stiffeners
d_b	Depth of the beam
d_{eff}	Effective length of infill plate to act together with the side stiffener
f_{yp}	Minimum specified yield stress of the infill panel
f_{yf}	Minimum specified yield stress of the boundary frame
f_{ys}	Minimum specified yield stress of the side stiffener
f_{yEB}	Yield stress of the equivalent brace
f^*_{yEB}	Yield stress of the equivalent brace specifically for the proposed HPSPSW system assuming bilinear behavior with strain-hardening
$f^{*'}_{yEB}$	Modified yield stress of the equivalent brace specifically for the proposed HPSPSW system assuming elastic-perfectly plastic behavior
h	Story height, or the center to center distance between beams (horizontal boundary elements)
h_{bf}	Height of the infill panel, or the clear distance between the beams
h_p	Nominal height of the infill plate (not necessarily equal to h_{bf})
k	Correction coefficient considering non-uniform shear stress distribution on the cross-section. For rectangular cross-section, $k = 1.2$
k_s	Plate shear buckling coefficient
n	Stiffness amplification factor in a rotational spring model (Chapter III)
n_b	Number of bolts per column or vertical row in the gusset flange
n_{bc}	Number of bolts at the compression side in a gusset plate moment connection
t_g	Thickness of the gusset plate
t_{gf}	Thickness of the gusset flange plate
t_s	Thickness of rectangular side stiffeners
t_p	Infill panel thickness
t_{bw}	Thickness of beam web
t_{cw}	Thickness of column web
t_{bf}	Thickness of beam flange
t_{cf}	Thickness of column flange
A_c	Gross section area of the boundary column
A_b	Gross section area of the boundary beam
A_{bolt}	Nominal gross area of bolt
A_{EB}	Area of the equivalent brace
A^*_{EB}	Area of the equivalent brace specifically for the proposed HPSPSW system
C_{prg}	Strain hardening factor of the gusset plate material equal to $(F_{yg}+F_{ug})/2F_{yg}$
E	Young's modulus
F_{yc}	Minimum specified yield strength of the column
F_{yb}	Minimum specified yield strength of the beam
F_{ub}	Minimum specified ultimate strength of the beam

F_{yg}	Minimum specified yield strength of the gusset plate
F_{ug}	Minimum specified ultimate strength of the gusset plate
F_{nt}	Nominal tensile strength of the bolt
F_{nv}	Nominal shear strength of the bolt
F_{EXX}	Filler metal classification strength of the weld
H_{g1}	Gusset height
H_{g2}	Shorter gusset height
I_s	Out-of-plane stiffness of the side stiffeners about an axis parallel to the infill plate plane
K_s	Modified stiffness of the spring in a rotational spring model
K_{mem}	Actual stiffness of the member
K_{bc}	Modified stiffness of the elastic beam-column element in a rotational spring model
L	Center to center distance between columns (vertical boundary elements)
L_h	Distance between the plastic hinges in the gusset plate
L_{eff}	Effective tension field width
L_p	Nominal width of the infill plate (not necessarily equal to L_{cf})
L_{cf}	Width of the infill panel, or the clear distance between the columns
L_{fg}	Free gusset length
L_{wh}	Horizontal weld length in a gusset plate moment connection
M_{yb}	Minimum specified yield moment of the beam
M_{pb}	Minimum specified plastic moment capacity of the beam
M_{peb}	Expected plastic moment capacity of the beam
M_{peg}	Expected plastic moment capacity of the gusset plate
M_{prg}	Probable (expected and strain-hardened) plastic moment capacity of the gusset plate
M_{pf}	Plastic moment capacity of the side stiffener
N	Number of bolts per horizontal row in the gusset flange
R_{yg}	Expected yield strength factor of the gusset plate
R_{tg}	Expected ultimate strength factor of the gusset plate
R_{yb}	Expected yield strength factor of the beam
R_{tb}	Expected ultimate strength factor of the beam
S_{bx}	Elastic modulus of the beam about the strong axis
V_c	Shear force in the column outside the joint
V_{cu}	Shear force in the column inside the joint
V_{cn}	Nominal shear capacity of the panel zone
V_{gu}	Shear demand in the gusset plate in the middle of the plastic hinge
V_{gn}	Nominal shear capacity of the gusset plate
$V_{gravity}$	Beam shear force resulting from the gravity load combination
V_{sp}	Shear strength of the infill plate
Z_{nb}	Plastic section modulus of the net section of the beam
Z_b	Gross plastic section modulus of the beam
Z_{gx}	Plastic section modulus of the gusset plate about the strong axis

α	Angle of inclination of the tension field
$\alpha_{s,mem}$	Actual strain hardening coefficient of the member
$\alpha_{s,s}$	Strain hardening coefficient of the spring in a rotational spring model
β	Rigidity factor for the side stiffener
γ	Capacity ratio for the tension and compression braces in an equivalent brace model

σ_{yt}	Tensile yield stress for the equivalent brace
ε_{yt}	Tensile yield strain for the equivalent brace
σ_{yc}	Compression yield stress for the equivalent brace
ε_{yc}	Compression yield strain for the equivalent brace
η	Coefficient in front of $1/2 f_{yp} L_p t_p$ for establishing the ultimate shear strength of the infill plate plus side stiffeners
η_{EB}	Area reduction factor in the proposed equivalent brace model
ϕ	Effective strength factor (also written as φ)
τ_{cr}	Critical shear buckling stress of the infill plate
τ_{yw}	Shear yield stress of the infill plate
θ	Angle of the diagonal = $\tan^{-1}(L/h)$
ν	Poisson's ratio
Δ_{lim}	Architectural limit for the gusset height

Acknowledgements

I would like to give my special thanks to my research adviser and dissertation committee chair, Professor Abolhassan Astaneh-Asl for his endless support – not only for this research but also for my entire Ph.D. studies. Without his guidance and creative mind, this dissertation would not have been possible. I would also like to thank Professors Lisa Pruit and Khalid Mosalam for their review as well as the insightful and constructive comments on my work.

In addition, I would like to express my sincere appreciation for the Project Professional Advisory Panel of this research and development project, including: Mr. Brett Manning, S.E., Vice President Northwest Sales/Engineering – Pacific Division, Schuff Steel and President of Structural Steel Educational Council, (www.steeltips.org), publisher of the Steel TIPS Reports, who had given valuable suggestions on detailing and fabrication of the proposed new Gusset Plate Moment Connection and High-Performance Steel Plate Shear Wall, Mr. James O. Malley, S.E., Group Director and Senior Principal, Degenkolb Engineers, San Francisco and former Chair of the AISC Task 9-Seismic Design, as well as Mr. Rafael Sabelli, S. E., Principal, and Director of Seismic Design at Walter P. Moore, San Francisco, and current Vice-Chair of the AISC Task Committee 9-Seismic Design for their suport and input.

I would also like to acknowledge the tremendous technical support provided by Dr. Metin Ozen, President, Casey Heydar, and the analysts Kaan Divringi and Chris Cowan at Ozen Engineering Inc. (https://www.ozeninc.com/) on the use of ANSYS nonlinear structural analysis software featured in this project.

I am more than grateful for the financial support by the Professor T.Y. Lin Fellowship in Structural Engineering at the University of California, Berkeley, which partially supported my Ph.D. studies and made this research project possible.

I would like to express my gratitude to my colleague Dr. Maryam Tabbakhha, Dr. Selim Gunay, Dr. Thanh Do and Dr. Shanshan Wang and many others with whom I had numerous illuminating discussions.

Last but not least, my heartfelt appreciation to my family and friends for their love and support along the way.

Chapter I

Introduction

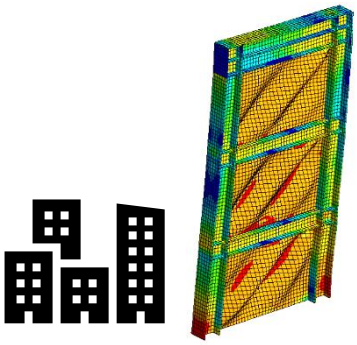

1.1 Background

During the last few decades, the Steel Plate Shear Wall (SPSW) system has become one of the main steel lateral force-resisting systems; other systems include the moment frame, concentrically braced frame, and eccentrically braced frame. The SPSW system has seen applications in a variety of building types and in different countries like Japan, North America, and China. As shown in Figure 1.1, the main components of a steel plate shear wall include the steel infill plate and the surrounding boundary beams and boundary columns. Horizontal or vertical stiffeners are also needed for stiffened steel shear wall.

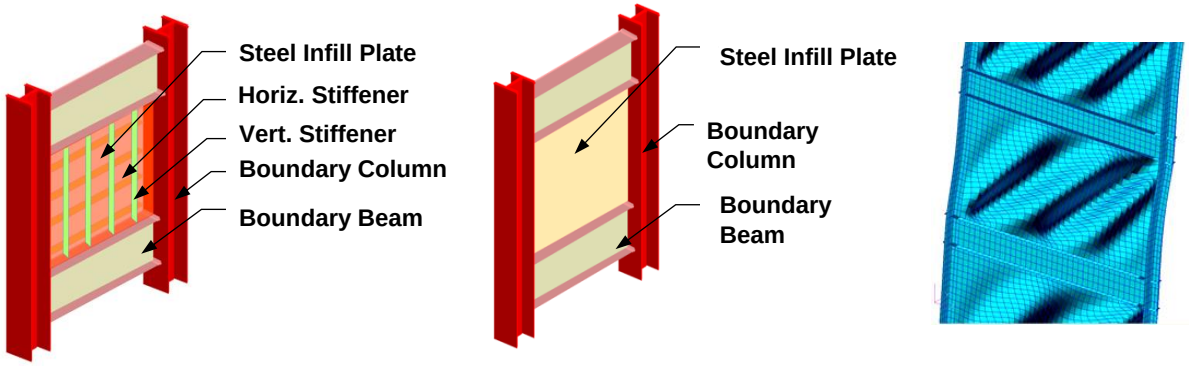

(a) *Stiffened* Steel Shear Wall

(b) *Unstiffened* Steel Shear Wall

(c) Diagonal buckling and development of tension field action

Figure 1.1 Typical stiffened and unstiffened steel shear walls

When first developed, infill plate buckling was prevented until plate shear yielding capacity had developed; this behavior was achieved by using heavily stiffened or relatively thick infill plates [Figure 1.1(a)]. Later, the thin unstiffened steel plate shear wall system became popular after the post-buckling capacity from the diagonal tension field of the infill plates was recognized [Figure 1.1(b) and (c)]. The superior shear resistance and stiffness, stable hysteresis behavior, high-energy dissipation capability and high ductility as well as the inherent redundancy have made the SPSW system a promising alternative to conventional lateral load-resisting systems in high-risk seismic and wind regions.

Stiffeners are favored because they assure the ductility and high-energy dissipation capacity of the steel shear walls without a need for thick steel plates. However, at the same time, use of stiffeners have been criticized because of the labor-intensive installation process and increased construction costs. Stiffened steel shear walls remain popular in countries like Japan and China (Figure 1.2).

Figure 1.2 Examples of stiffened steel shear walls used in Japan (Photo courtesy of Nippon Steel and Takenaka Corporation)

In contrast, unstiffened steel plate shear walls are much more popular in North America, where the economy and good-performance of thin infill unstiffened plates are very much appreciated. The unstiffened steel plate shear wall (SPSW) is composed of steel infill plates surrounded by boundary beams and columns, referred to as Horizontal Boundary Element (HBE) and Vertical Boundary Element (VBE), respectively. The steel plate shear wall is analogous conceptually to a vertically oriented plate girder, with the infill plate similar to the web, VBEs (i.e., columns) as the flanges and HBEs (i.e., beams) being analogous to transverse stiffeners in a plate girder (Figure 1.3). In addition, both SPSWs and plate girders optimize system performance by taking advantages of the post-buckling tension field action of the thin infill panels. In the remainder of this dissertation, SPSW will refer to the unstiffened steel plate shear walls if not otherwise specified.

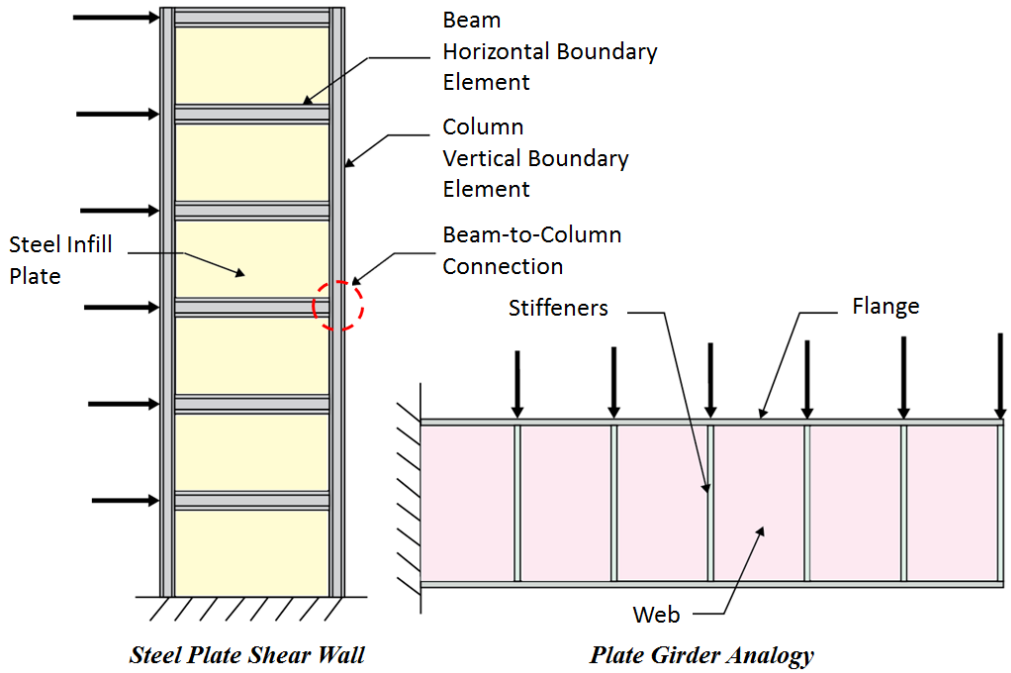

Figure 1.3 Schematic of the structural components of an SPSW system and the plate girder analogy

The history of analytical models for SPSWs dates back to 1960s when Basler and his colleague (Basler and Thuerlimann 1961; Basler et al. 1960) proposed the design of plate girders, which served as the basis for many analytical models developed later for the SPSW system. Early investigations of the post-buckling strength of steel plate shear walls were conducted at the University of Alberta, where the benchmark strip model to compute the post-buckling strength of SPSWs was proposed and verified by experimental and analytical studies (Thorburn et al. 1983; Timler and Kulak 1983; Tromposch and Kulak 1987). These studies inspired much research on the unstiffened steel plate shear wall systems, which verified the concept of the strip model and unfolded more aspects of the behavior and design of the SPSW system (Berman and Bruneau 2005; Caccese et al. 1993; Driver et al. 1998; Elgaaly 1998; Lubell 1997; Qu et al. 2008; Rezai et al. 2000; Sabouri-Ghomi and Roberts 1992). More of these benchmark studies are to be discussed in Chapter II. Further, the strip model formed the basis of the current design method in the North American design codes AISC341-05, CAN/CSA S16-01 and FEMA 450 (AISC 2005; CSA 2001; FEMA450 2003). AISC Design Guide 20 (AISC 2007) included detailed design examples for both low- and high-seismic applications.

1.2 Advantages

The unstiffened SPSW system included in the North American seismic design codes and specifications offer a number advantages over other commonly used lateral force-resisting systems in terms of performance, cost, and ease of construction.

Based on existing research, the steel shear wall system, regardless of the construction details, in general possesses high initial stiffness and strength, which are beneficial for resisting wind and moderate lateral loads, and allow fewer numbers of bays and shorter bays to be used. These characteristics are similar to all "braced-frame" type of lateral load-resisting systems, such as concrete shear walls and steel braced frames, in constrast to the more flexible "moment-frame" type systems that generally have lower initial stiffness. The system's superior ductility, stable hysteretic behavior, and relatively large energy-dissipation capacity validated by past research, also provide the basis for its satisfactory performance under severe seismic events.

Compared with reinforced concrete (RC) shear walls, the most significant advantage of steel shear wall comes from the small thickness of the steel infill plate and the associated reduced structural weight. It is well established a lighter structure will attract fewer inertia forces, and, therefore, less demand will be imposed on the structure itself and on its foundation. The much-reduced wall thickness also provides more usable floor space, especially for high-rise buildings where the lower floor RC shear walls can be very thick. In addition, all-steel construction, including steel shear wall systems, are efficient options for cold regions where the construction of concrete structures can be greatly affected by low temperatures (longer hardening periods, freeze and thaw issues, etc.) Steel plate shear walls are much easier and faster to install and erect compared to RC shear walls. In particular, if shop-welded and field-bolted construction is opted, the construction speed and quality control can be improved even further. In addition to new construction, steel shear walls are also a viable option in retrofit of deficient structures; not only would they be effective in improving the structural stiffness and strength, construction of steel shear walls would not increase the room humidity level or cause severe disruption of services, which could occur during concrete placement. These benefits are especially advantageous for hospitals, which are sensitive to operation disruption, and libraries, where relocation of books due to increased humidity during concrete placement would be required. Furthermore, due to the small required plan area, preservation of historical finishes also becomes possible when using steel shear walls for the retrofit.

Steel plate shear walls can be viewed as an alternative to braced frames: they can provide comparable strength and stiffness, they require similar or even less floor footprint area, and they sidestep the issue of obstructing views if placed on the building perimeter. Compared to the one-dimensional brace elements that rely on the formation of one or three hinges in the braces, steel infill plates are two-dimensional elements that can yield and deform over the entire panel, and have significantly higher inherent continuity and redundancy. Therefore, steel shear walls can provide higher ductility and energy-dissipation capacity for the same weight, and are much less sensitive to localized fractures. In other words, they are less fracture-critical compared to braced frames. Considerable time and cost savings can also be achieved by using steel plate shear walls since less construction and inspection efforts are needed to detail the connections of the system (gusset plates in the braced frame often require significant detailing efforts). Instead, simple continuous welded (fillet welds) or bolted connections are sufficient to attach the infill wall to the boundary frames. The steel plate shear wall system also becomes an appropriate and a very

efficient system to replace the brace frame when the required gusset plate in the braced frame becomes unrealistically large (Figure 1.4).

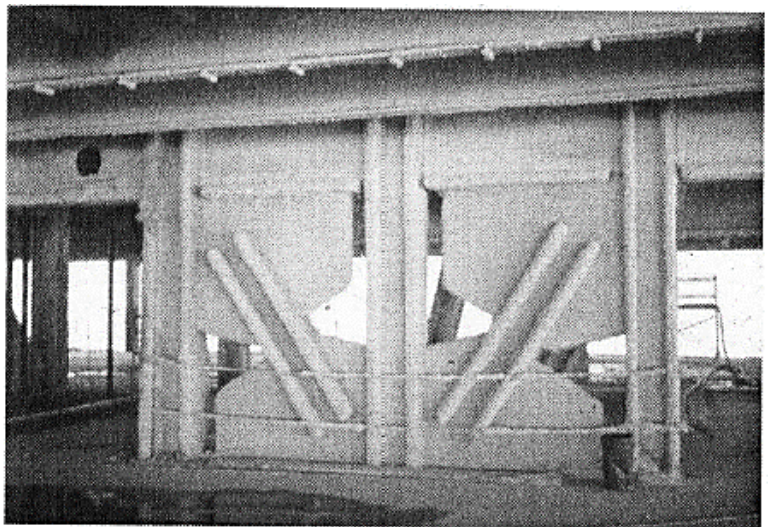

Figure 1.4 Examples of excessive brace connections in high rise buildings (Photo courtesy of M. Gilmor)

1.3 Constructed Steel Plate Shear Wall System

Buildings that use steel shear walls as the main lateral load-resisting system began to be constructed in the late 1960s (Commerce 1984; Troy and Richard 1979). Their use vary in terms of building heights and functions – ranging from low-rise single-family residential to high-rise offices and commercial buildings, and from new constructions to the retrofit of existing framed buildings.

Since the 1960s, stiffened steel shear walls have been used in Japan for new construction, and since the 1970s, they also found application in the U.S. in both seismic retrofit projects and new buildings. Later in the 1980s and 1990s, unstiffened steel shear walls became popular in the U.S. and Canada, and recently in China. Examples include a number of important high-rise buildings (Figure 1.5 – 1.9), and two buildings that withstood major earthquakes like the 1995 Kobe and 1994 Northridge earthquake (e.g., Figure 1.8 and 1.11). Several other SPSW applications in mid- and low-rise buildings and retrofit projects are shown in Figure 1.10 – 1.14. Appendix A, in the descending order of building height, summarizes the constructed buildings that use steel shear wall system as the primary lateral load-resisting system in one or more directions. Brief descriptions and researcher/designers' comments are also included for each building. The list is considered extensive but not exhaustive. Many of the constructed SPSW buildings were selected over the other lateral force-resisting systems due to the system's lighter weight, ease of construction, larger usable space, and less cost.

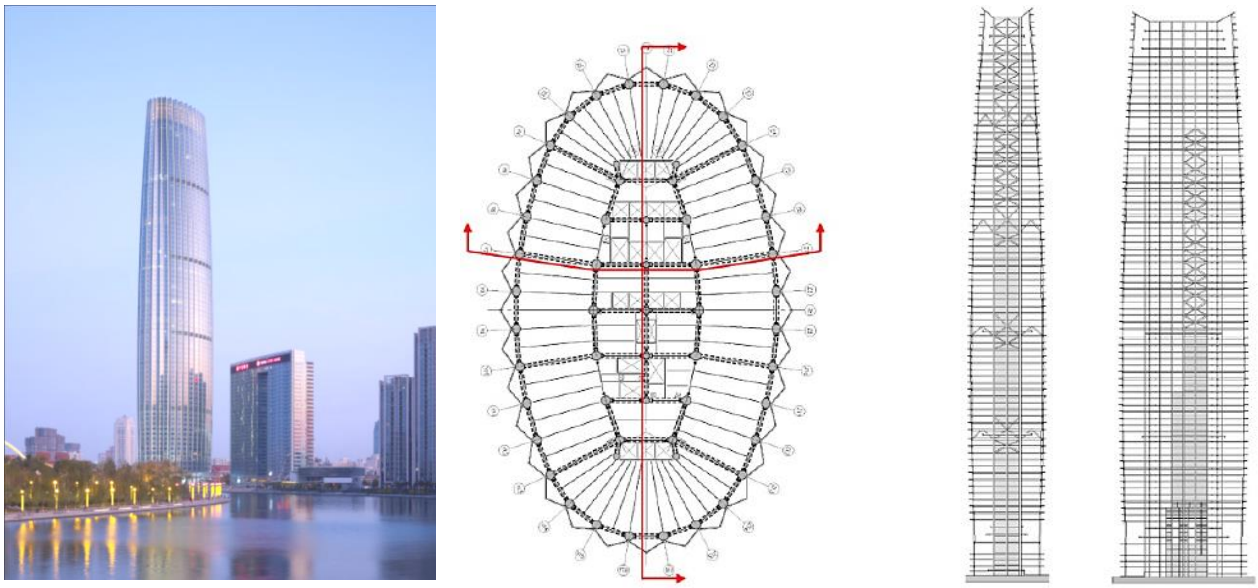

Figure 1.5 74-story Jinta Tower in Tianjin, China (figure adapted from Sarkisian and Mathias, 2012)

Besides the new construction projects listed in Appendix A, there have also been retrofit projects that employed steel plate shear walls. One example is the Veterans Administration Medical Center in Charleston, South Carolina. The decision to use steel shear walls instead of concrete walls was based on the need to minimize the disruption of services in the hospital, which justified the higher cost of using steel shear walls instead of concrete shear walls. The designers pointed out that wall stiffness requirements governed the design and prevented the use of thinner walls (Baldelli 1983). This is indeed an issue of the thin unstiffened steel shear wall systems and was also mentioned in Design Guide 20 (AISC 2007). Oregon State Library is an example of retrofit of reinforcement concrete moment frame with steel plate shear walls. The steel plate shear wall was chosen because book relocation could be avoided during steel construction. Bolted splices were used to minimize the risk of fire from welding in the library (Robinson and Ames 2000). Steel shear walls have also been used to strengthen steel moment frames that were damaged during the 1994 Northridge earthquake. An example is a two-story structure in San Fernando Valley that was designed by Degenkolb Engineers (described in Design Guide 20). The main reason to select steel shear walls was the high available stiffness to required space ratio as compared to concrete shear walls and steel braced frames, and the possibility of keeping the building occupied during construction.

Installation of buckling-restrained braces in the roof

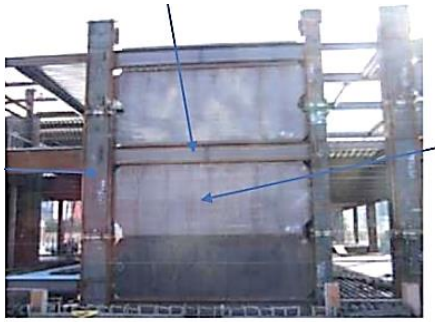

1/4” to 3/8” Plate

Figure 1.6 55-story Los Angeles Convention Center Hotel (tower rendering photo courtesy of Gensler; construction photos adapted from Lee et al.,2010)

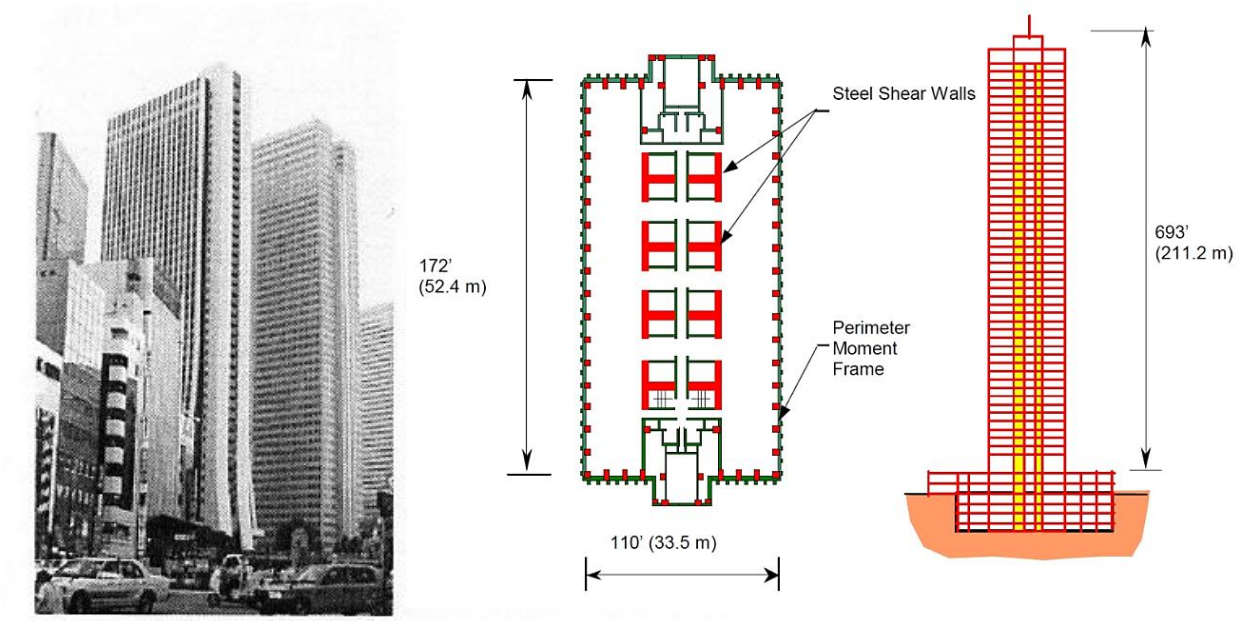

Figure 1.7 53-story Shinjuku Nomura Building in Tokyo, Japan (Photo courtesy of P.Becker; figure adapted from Astaneh-Asl, 2001)

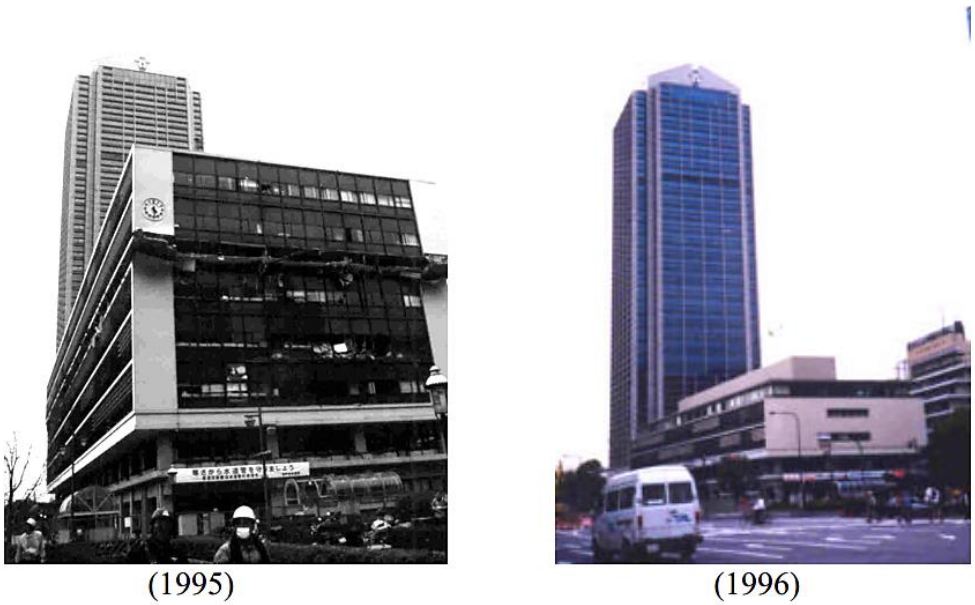

Figure 1.8 35-story Kobe building (in the background) survived the Kobe earthquake; City Hall Office building (in the foreground) lost top 3 floors (Photos courtesy of A.Astaneh-Asl and M.Kanada)

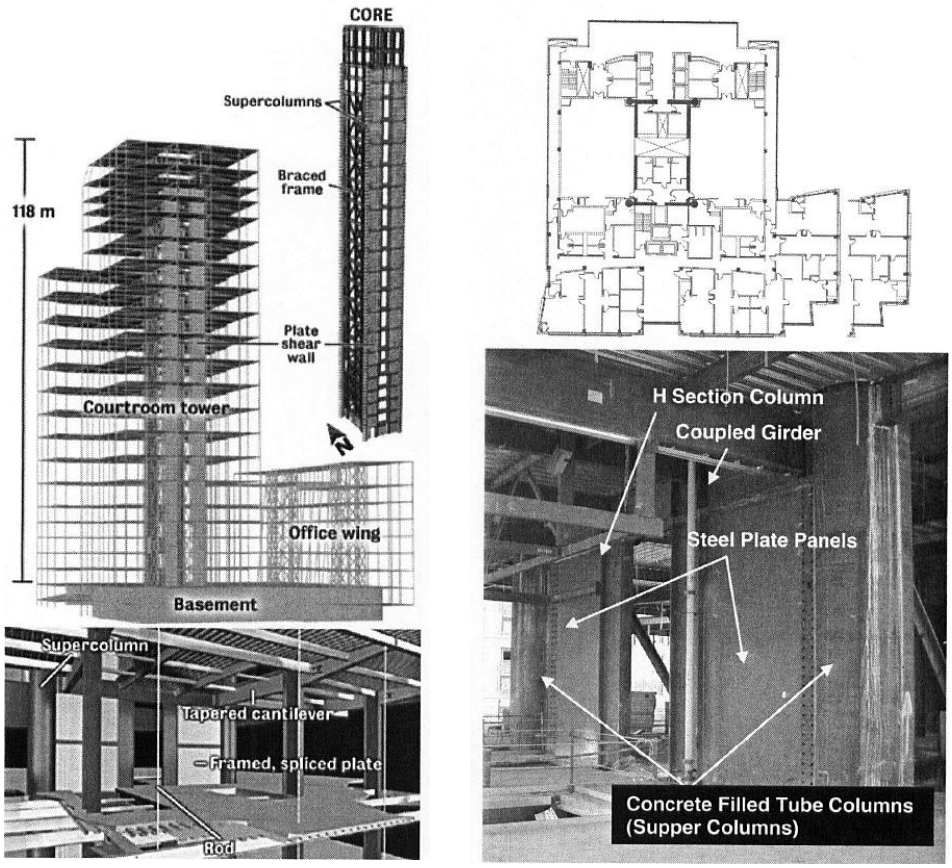

Figure 1.9 24-story U.S. Courthouse Building, Seattle, WA. (photo courtesy of Magnusson Klemencic Associates)

Figure 1.10 7-story ING building – mid-span splice and base connections (photo courtesy of Louis Crepeau and Jean-Benoit Ducharme, Groupe Teknika, Montreal, Canada)

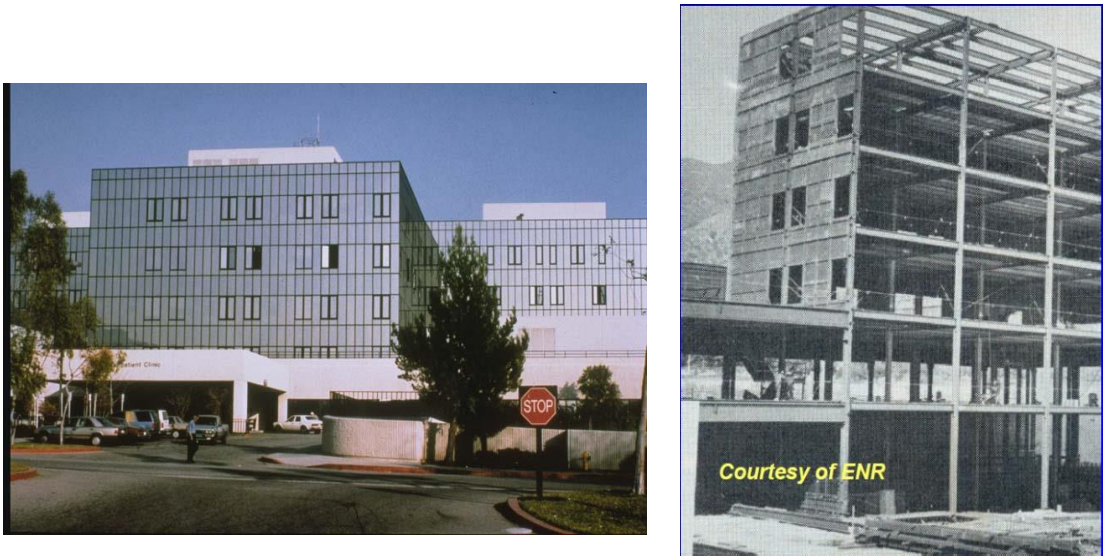

Figure 1.11 6-story Olive View Hospital in Sylmar, California (photo courtesy of NOAA and ENR)

Figure 1.12 6-story Canam Manac Group headquarters expansion (photo courtesy of Richard Vincent, Canam Manac Group, St. George, Quebec, Canada)

Figure 1.13 Residential building with steel plate shear wall in Atherton, California (photo courtesy of M.Eatherton, GFDS Engineers, San Francisco)

Figure 1.14 Installation of new steel plate shear walls in the 1937 Oregon State Library (photo courtesy of KPFF Consulting Engineers, Portland, OR)

1.4 Motivation

While possessing the above-mentioned advantages with a wide range of applications, the current unstiffened steel plate shear wall system has a number of issues associated with its design, construction, inspection, and performance under service-level and ultimate loads that prevent widespread use of this potentially versatile lateral force-resisting system. The main disadvantages of using *unstiffened* steel plate shear walls, currently designed following the AISC Seismic Provisions (AISC 2010; AISC 2016), are given below and shown in Figure 1.15:

(1) The post-buckling tension field action of the infill plate creates relatively large lateral forces on the boundary columns, causing large bending moments and additional axial forces in the columns. Large column sections are almost always required as a result of the capacity design process to provide sufficient stiffness and strength as the boundary elements and to avoid excessive column bending as shown in Figure 1.1(c) earlier. This is a major drawback affecting the cost effectiveness of the current system;

(2) In the current system, the steel shear infill plate is connected to the boundary columns as well as to the boundary beams using fillet *field-welds*. The relatively large amount of vertical field welds results in higher costs and the potential problem of burning of the infill plate during the upward field welding (Eatherton 2006);

(3) The design of column depends on the choice of infill wall. The thicker the wall and the stronger the steel material used for the wall, the heavier the column will be since the columns in the current steel shear wall system have to be designed to resist the *expected* strength of the tension field action of the infill wall under capacity design philosophy. Also, in the current system, the column section has to be a wide-flange with its flange connected to the steel infill panel;

(4) After designing the wall to resist the applied shear, in the current steel shear wall system, the wall thickness cannot be increased freely to satisfy the drift requirements without increasing the size of the column. To solve the problem, typically, more moment connections have to be used in the frames outside the steel plate shear wall to increase the lateral stiffness of the system. These moment connections are often expensive, leading to significantly higher construction costs;

(5) Tests and analyses of steel shear walls (e.g., Shi and Astaneh-Asl 2008; Timler and Kulak 1983; Zhao and Astaneh-Asl 2008) have shown that unstiffened steel plate shear walls can buckle along their compression diagonal at relatively small drifts in the order of 0.005 radians. Almost all of the past research on unstiffened steel plate shear wall system have focused on understanding and improving the post-buckling performance, ductility, and energy-dissipation capacity of the system under ultimate loads – with little or no attention paid to the elastic buckling of the wall that often occurs under relatively small shear force. The elastic buckling of the thin infill plates under service wind or small and frequent earthquakes limits the wider application of unstiffened steel shear walls in buildings of high importance. Concerns include the unpleasant elastic buckling sound under service loads, lower initial stiffness, and small yielding drift ratio (Lee et al. 2010; Nie et al. 2012). Although there are a few examples that consider service-level performance according to the performance-based design philosophy (Lee et al. 2010), the AISC Seismic Provisions imposes no explicit drift requirements under service conditions;

(6) The use of the complete joint penetration (CJP) field-welded beam-to-column connections in the current steel plate shear wall system results in higher construction and inspection costs;

(7) Past cyclic tests of the unstiffened steel shear walls (e.g. Timler and Kulak 1983) have shown that the corners of the infill plate, where there is a gap between the horizontal and vertical fin plates, could fracture due to the relatively large cyclic strain concentrations at the corners. To prevent the corner fracture, researchers have recommended adding welded strap plates to fill the gap between the horizontal and vertical fin plates (Tromposch and Kulak 1987), providing corner cut-outs (Schumacher et al. 1999), or incorporating special corner brackets and connecting the horizontal and vertical fin plates away from the corner(Choi and Park 2008). All these methods add to the design and construction efforts, increasing the cost of fabrication;

(8) The use of welded beam-to-column connections in the current system often results in undesirable yielding in the column panel zones, and in many cases, requires *doubler- plates* to strengthen the column web, which adds to the fabrication costs;

(9) The use of currently available welded moment connections, where the flange of the beam is perpendicular to the column web, in most cases, requires *continuity plates* be added to the column web of the panel zone. This is yet another labor-intensive element that adds to construction costs; and

(10) Current seismic design codes require that the *strong-column–weak-beam design philosophy* be satisfied for the boundary moment frame in the current steel plate shear wall system to prevent the formation of plastic hinges in the columns. Satisfying this requirement often results in larger columns than what is required by the strength and drift limit, resulting in increased costs.

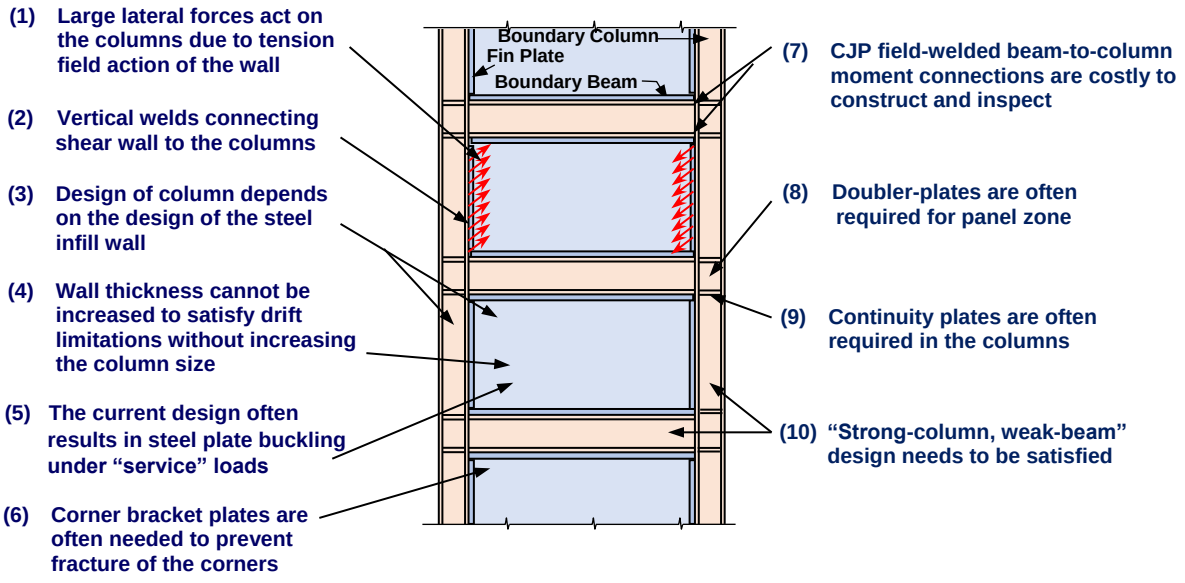

Figure 1.15 Disadvantages of the current unstiffened Steel Plate Shear Wall

1.5 Objectives

The main aim of this study is to propose and develop a new steel plate shear wall system that can address the issues and disadvantages of the current AISC steel plate shear wall system identified in Section 1.4. This research project intends to offer the structural engineering community a new lateral force resisting system that is versatile, ductile, and cost effective, satisfying all or most of the *Performance Criteria* for a high-performance lateral force resisting system listed below.

Performance Criteria for High-Performance Lateral Force Resisting Systems

1) The system should possess sufficient strength and stiffness to remain essentially elastic under *service-level* earthquakes and wind loads;
2) The system should have sufficient strength, ductility, and energy-dissipation capacity to resist *factored lateral forces* resulting from medium and large earthquakes;
3) The system should have sufficient stiffness to satisfy the drift limitations under both *service-level* and *ultimate factored* loads;
4) The system should have minimal or no *residual drift* after earthquakes and high winds;
5) The system should have an *optimal level of post-yielding strain-hardening* to ensure the *P*-delta effects do not become significant under high seismic or wind loads;
6) The system should have relatively long *"low-cycle fatigue"* life and should not develop fracture in essential components that would severely deteriorate system performance;
7) The system components other than the primary energy-dissipation element, such as the boundary columns and beams in a steel plate shear wall system, should remain *essentially elastic* throughout the cyclic loading;
8) The connections should have ductile steel fuses and enable all other elements of the connection such as welds and bolts to remain elastic;
9) The system should be easy and economical to fabricate and erect, requiring as little field-welding and complex field-inspection as possible;
10) The system should be flexible enough to be used in both new construction and retrofit of existing buildings;
11) The configuration of the system should enable "modular" fabrication and construction;
12) After a major earthquake, the damage to the system should be easily observable and repairable, and the structural system should also be able to limit the damage to the non-structural elements after a major earthquake event;
13) The structural system should be easy and cost-effective to demolish and recycle at the end of its life; and,
14) All of the above criteria should be satisfied in a sustainable manner by reducing the amount of material, energy, and labor costs, and with reduced environmental impacts.

While it is certainly difficult to satisfy all the items listed above, this dissertation proposes an innovative steel plate shear wall system that consists of a new steel moment connection in pursuit of an improved version of the steel plate shear wall system that can satisfy most, if not all, of the above mentioned high-performance criteria.

1.6 Overview and Organization of Dissertation

To achieve the above-mentioned research objective, a series of analytical studies were carried out to develop and evaluate the proposed new steel shear wall system.

To better understand the knowledge gap and gather useful information for the research objectives, a review of relevant literature is presented in Chapter II. First, benchmark studies on steel plate shear walls and the current code provisions are summarized, followed by an extensive review of recent experimental and analytical studies that directly or indirectly provide methods and concepts to solve the disadvantages of SPSWs identified in Chapter I. Then, the available analytical method for design and analysis of the current steel plate shear wall system is reviewed to provide tools for developing simplified design equations and analytical models for the proposed new system. The last part of Chapter II includes brief reviews of some currently available design approaches for steel plate shear wall system, such as the ASCE/AISC approach, performance-based plastic design, and displacement based design.

Chapter III describes the main features and behavior of a new "Gusset Plate Moment Connection(GPMC)". First, preliminary recommendations of the geometric parameters of the new connections is proposed based on some early development efforts of this study using shallow beam sections. Then, additional sets of nonlinear finite element parametric studies are presented on typical beam-to-column sub-assemblies on a wider range of beam and column sections. Both welded and bolted versions of the proposed GPMCs are included. Potential issues of the new GPMC are discussed, followed by solutions and modifications on the connection material, detailing, and design methods to alleviate those issues. Calibration of moment-rotation hinge properties is also performed for use in Chapter V where the system performance is evaluated on the global level. Finally, Chapter III provides an interim design procedure for the proposed new GPMC, which is based on the results of the analytical studies and the existing moment connection design theories and concepts.

Chapter IV introduces the proposed new High-Performance Steel Plate Shear Wall (HPSPSW) system which uses the new Gusset Plate Moment Connection developed in Chapter III. The basic components and key features of the new HPSPSW are introduced first and supported by nonlinear finite element parametric studies with both monotonic and cyclic analyses included. Then, several collapse mechanisms available for the steel plate shear wall systems and plate girders are reviewed, followed by analytical derivations based on plate girder theories to establish the critical buckling, ultimate shear capacity, and initial stiffness of the infill plate of the proposed HPSPSW system. The validity and reliability of the derived equations are verified by extensive nonlinear finite element parametric studies. A simple equivalent brace model is then proposed to capture the yielding point and ultimate strength of the infill panel. Hysteretic properties are also defined based

on available models developed for the current SPSW system. The last part of Chapter IV provides design equations for the selection of the infill plate thickness and side stiffener sections.

Chapter V investigates the system performance of a series of 3-, 9- and 20-story realistic prototype buildings that conform to the SAC buildings described in the FEMA 355C document using the simplified analytical models developed and calibrated in Chapters III and IV. Chapter V proposes two seismic design procedures representing code-based and performance-based design approaches. A set of enhanced performance objectives is selected based on the literature and the current knowledge about the new HPSPSW system. The performance of the prototype building designs following the proposed design procedures are evaluated using response history analysis with ground motions representing the *service-*, *design- based-* and *maximum-considered-level* hazards. In addition, a comparison between the proposed new HPSPSW system and the current AISC SPSW system is conducted to better understand the characteristics of the two versions of SPSW systems. Chapter V also provides several recommendations to improve the proposed design procedures for enhancing system performance in the future.

Finally, Chapter VI summarizes the major findings of this dissertation, including the innovative concepts of the High-Performance Steel Plate Shear Wall System and the Gusset Plate Moment Connection, simplified analytical equations and models as well as the design procedures for the proposed new connection and system. At the end of Chapter VI, topics and areas are suggested for future research.

Chapter II

Literature Review

2.1 Introduction

Important benchmark studies on steel plate shear walls (SPSWs) are summarized in this chapter, followed by the various new and modified configurations of steel plate shear walls that have been investigated through the years, directly or indirectly, to solve the drawbacks of the current SPSW system. For the purpose of further development of the proposed HPSPSW system, simplified analytical models for the SPSWs and available design procedures for the system are also briefly reviewed.

2.2 Benchmark Studies of Steel Plate Shear Walls

In early applications of the steel plate shear wall system, relatively thick plates or closely spaced stiffeners were often used to prevent buckling and to utilize the shear yielding capacity of the steel plate. Takahashi et al. (1973) published one of the earliest test results on steel plate shear walls, where the steel plate shear wall system was investigated as an alternative to concrete shear walls (Takahashi et al. 1973). Although incorporating stiffeners resulted in higher shear strength, stiffness, ductility, and energy-dissipation capacity of the system, the addition of the stiffeners has been criticized for being a relatively labor-intensive, time-consuming, and costly fabrication process that resulted in a wider footprint for the wall. In recent years, and particularly in North America, much of the research and development activities have focused on the post-buckling behavior of the unstiffened thin steel infill walls. Many benchmark research projects summarized

below have shown that unstiffened steel plate shear walls are capable of providing relatively large displacement ductility, stable hysteresis behavior, and desirable energy dissipation capability.

Basler and his colleagues (1961) proposed a theory for calculating the shear capacity of steel plate girders, which served as the basis of several analytical models developed later for the unstiffened steel plate shear wall system (Basler 1961; Basler and Thuerlimann 1961; Basler et al. 1960). Starting in the early 1980s, the post-buckling strength of steel plate shear walls was investigated at the University of Alberta, where Thorburn et al.(1983), Timler and Kulak (1983) and Tromposch and Kulak(1987) tested several single and multi-story specimens under quasi-static cyclic load, and proposed the use of a strip model to compute the post-buckling shear strength of the steel plate shear walls (Thorburn et al. 1983; Timler and Kulak 1983; Tromposch and Kulak 1987). The initial strip model proposed by Thorburn et al. (1983) was found to be capable of predicting the overall force-displacement response well but tended to overestimate the elastic stiffness. Based on test results, Timler and Kulak (1983) modified the tension field action equation proposed by Thorburn et al.(1983) for multi-story systems and included the effect of flexural stiffness of the columns (Figure 2.1).

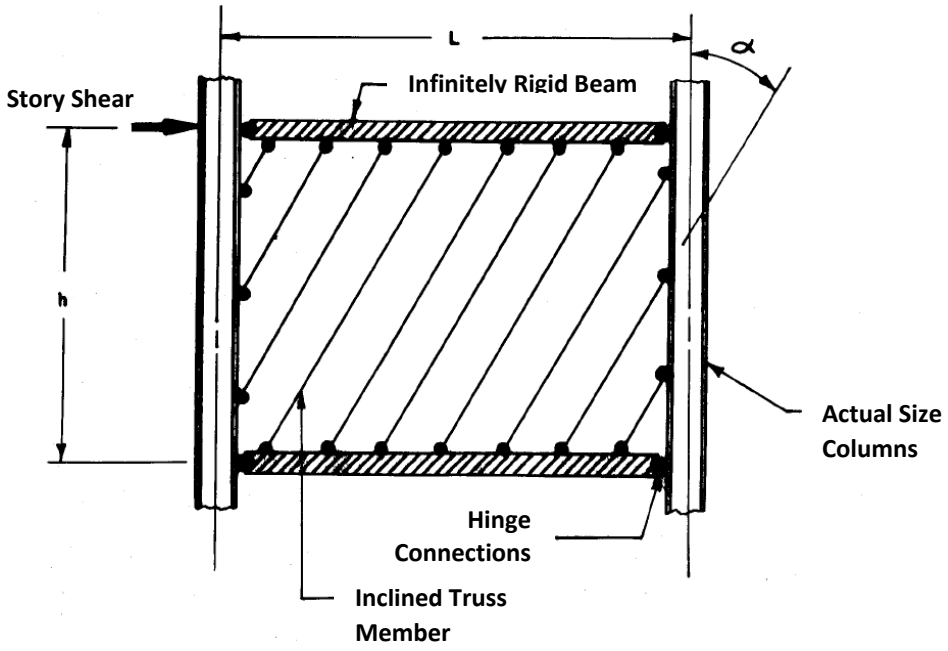

Figure 2.1 Strip model for a plane frame proposed by Timler and Kulak (1983)

Tromposch and Kulak (1987) tested a similar specimen as the one tested by Timler and Kulak(1983) but with some modifications based on findings of the previous study. They developed a new hysteresis model based on the work by Mimura and Akiyana (1977) as shown in Figure 2.2. In addition, their parametric studies indicated that frames with fixed beam-to-column connections could dissipate as much as three times more energy as that dissipated by frames with simple beam-to-column connections.

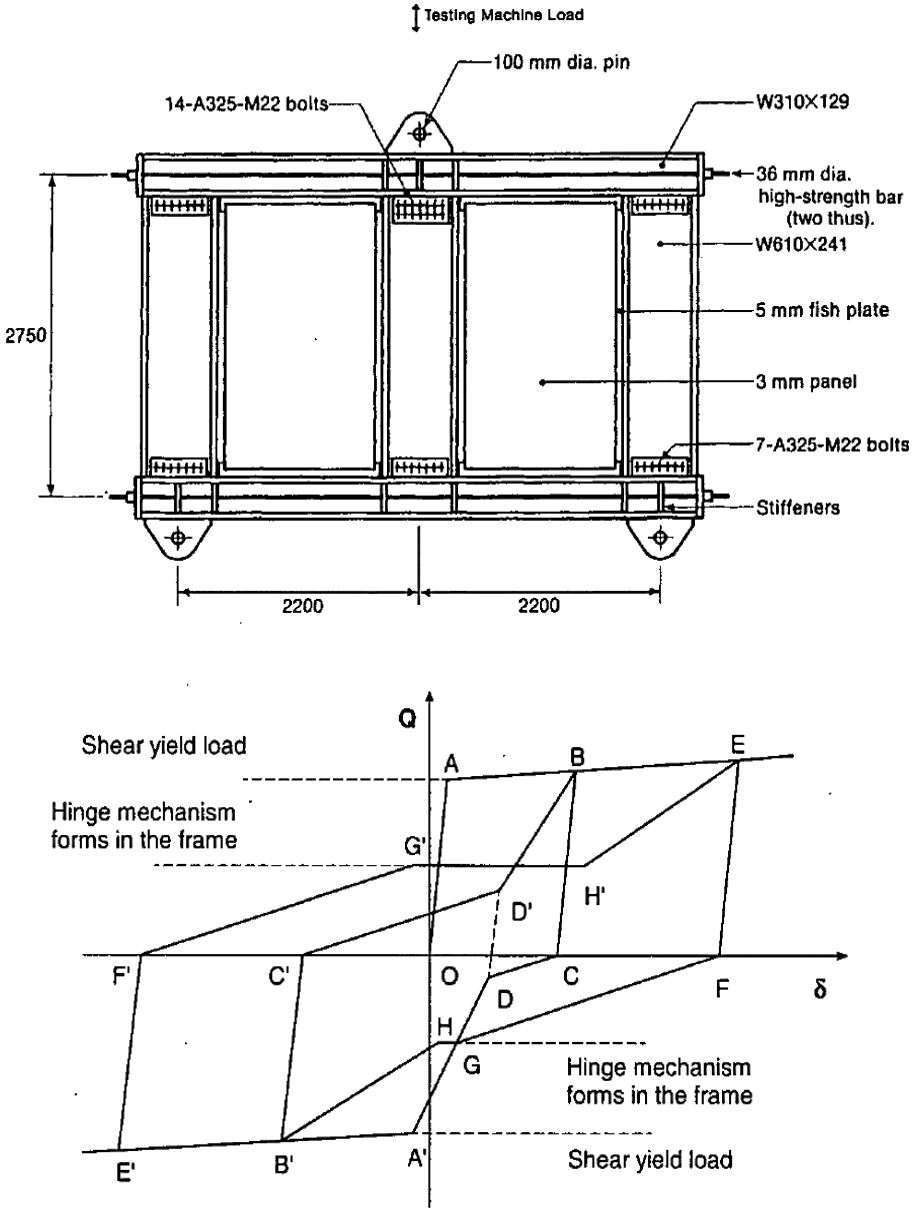

Figure 2.2 Specimen and proposed hysteretic model by Tromposch and Kulak (1987)

The strip model was verified and improved by cyclic tests and analytical work of many other researchers (Behbahanifard et al. 2003; Berman and Bruneau 2003; Caccese et al. 1993; Chen 1991; Driver et al. 1998a; Elgaaly 1998; Kharrazi et al. 2010a; Kharrazi et al. 2010b; Lubell 1997; Sabouri-Ghomi et al. 2005); it formed the basis of the current design method in the North American design codes such as CAN/CSA S16-01(CSA 2001), FEMA 450 (FEMA-450 2003), AISC-341-10 (AISC 2010c) and the recently released AISC-341-16 (AISC 2016). Numerical examples of seismic design of steel plate shear walls in both low- and high-seismic applications are provided in AISC Design Guide-20 (AISC 2007).

Caccese et al.(1993) conducted tests for a series of three-story quarter-scale specimens to study the effects of different parameters on the behavior of SPSWs. They recognized the difference in the governing limit state for thin and thick infill plates – the former is governed by yielding of infill plates and the latter is governed by the instability of columns (Caccese et al. 1993). Unlike the findings reported by Timler and Kulak(1983), they demonstrated that the rigidity of the beam-to-column connections had a minor effect on the overall load-displacement behavior with slightly larger influence on more slender specimens. This was explained by the fact that the welds joining infill plates to surrounding beams and columns were continuous which lead to rigid moment connection behavior even without using the actual rigid beam-to-column connections.

In the same year, Elaggaly et al.(1993) developed two analytical models for the SPSW system as shown in Figure 2.3 – one being a finite element model and the other model being a simplified strip model using a series of bilinearly elastic perfectly plastic strips (buckling strength of the steel plate panels was neglected). They reported that these two models were able to predict the test behavior of three specimens accurately. The strip model was further extended to predict the behavior of the specimens under cyclic loads by introducing strips oriented in both directions (Figure 2.3 left). Column instability due to yielding or buckling was found to be one of the main factors that limits the ultimate capacity of the system (Elgaaly et al. 1993).

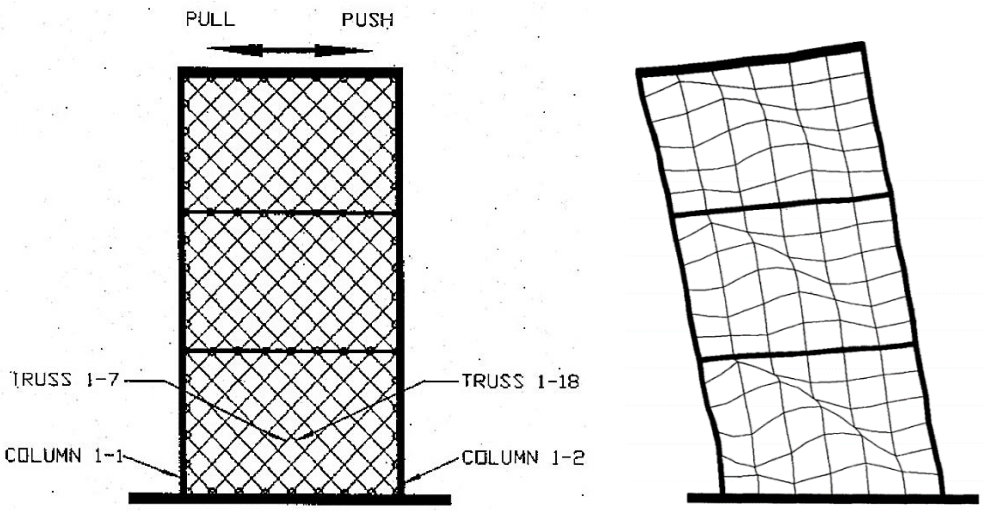

Figure 2.3 The double strip model for hysteretic behavior (left), the finite element model (right) developed by Egaaly et al.(1993)

Lubell and his colleague tested two single panel specimens and one four-story specimen under fully reversed cyclic quasi-static loading(Lubell 1997; Lubell et al. 2000). The importance of sufficient boundary elements was clearly demonstrated by comparing the deformation of columns and the roof beam of the two single panel specimens (Figure 2.4). They found that the infill plates significantly reduced the rotational demand on the beam-to-column connections by providing a redundant lateral force resisting mechanism. The simplified strip model was again reported to be

adequate in predicting post-yield strength, but not the elastic stiffness. Lubell et al.(2000) pointed out that the Canadian code provision at that time, CAN/CSA-S16.2-M94 (CSA 1994), may not be adequate for multi-story steel shear wall frames since it fails to incorporate the effects of 1) large overturning moments of multi-story frames, 2) infill panel aspect ratio, and 3) the undesirable yielding sequences of the system components.

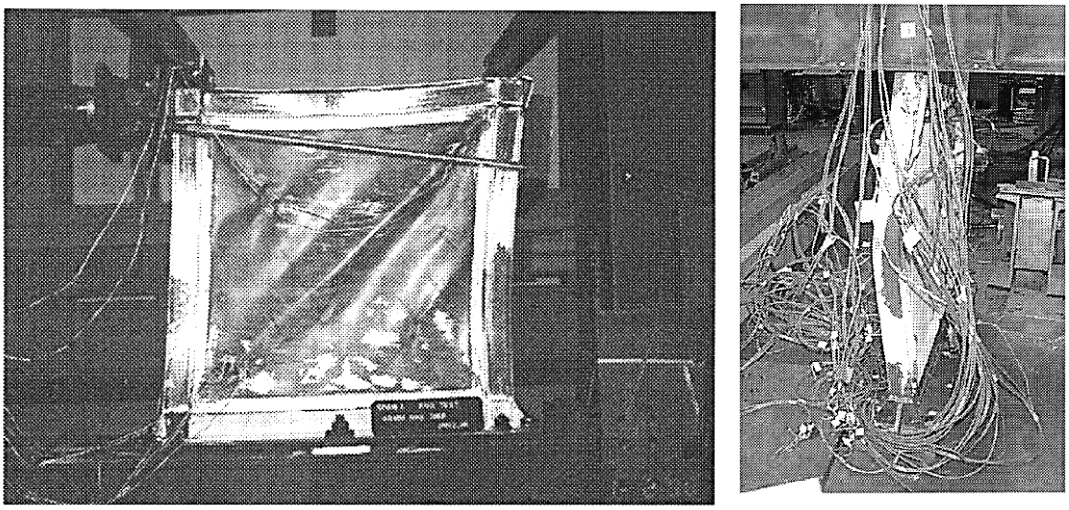

Figure 2.4 Bending of boundary beam and column of specimen SPSW1 at the end of test (left) and North column buckled shape for the 4-story specimen (right) by Lubell et al.(1997, 2000)

Driver et al. (1997) tested a large-scale four-story specimen including gravity effects under cyclic loading (Figure 2.5). It was reported that the structure was still able to hold 85% of the ultimate strength even when local buckling of column flange below the first story and several tears in the first-story plate and fracture of the complete penetration welds at the base plate had occurred (Driver 1997; Driver et al. 1998b). This observation is a good example that shows the redundancy of the steel plate shear wall system. They also found that most of the energy was dissipated by the plates with limited yielding in the moment beam-to-column connections, and that the first-story plate absorbed most of the damage. The strip model was found to be adequate for predicting ultimate strength but underestimated the initial stiffness. A revision of the hysteretic model proposed by Tromposch and Kulak (1987) was also proposed, in which the contributions from the moment frame and the infill panels were explicitly separated.

Schumacher et al. (1997) studied four infill plate-to-boundary element connection details (Figure 2.6). The load-displacement responses of all four specimens had similar force-displacement and energy-dissipation behavior regardless of the plate-to-boundary detailing. Tears were concentrated in the corner region of specimens B, C, and Modified B, but the deterioration of connection capacity was gradual and stable under increased load. Significant tearing was delayed in specimen Modified B compared to specimen B. Specimen A was found to be the least susceptible to tearing; however, it was regarded as impractical for actual construction considering the level of fabrication precision required (Schumacher et al. 1999).

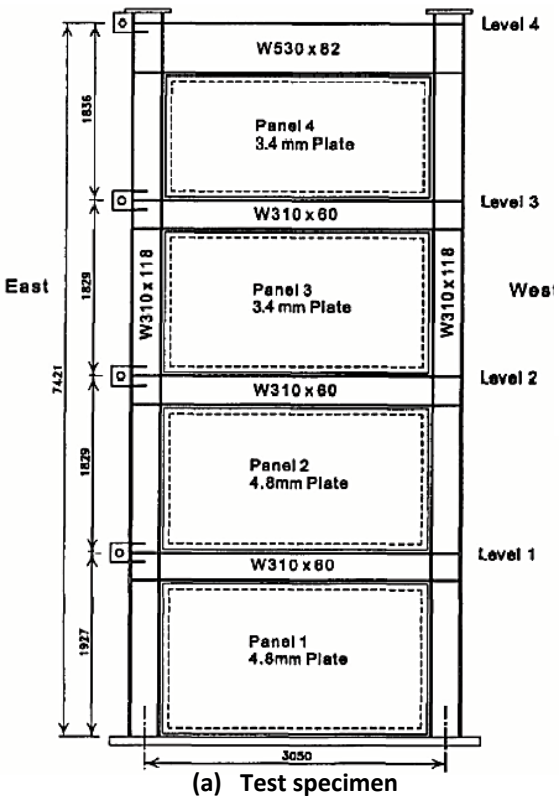

(a) Test specimen

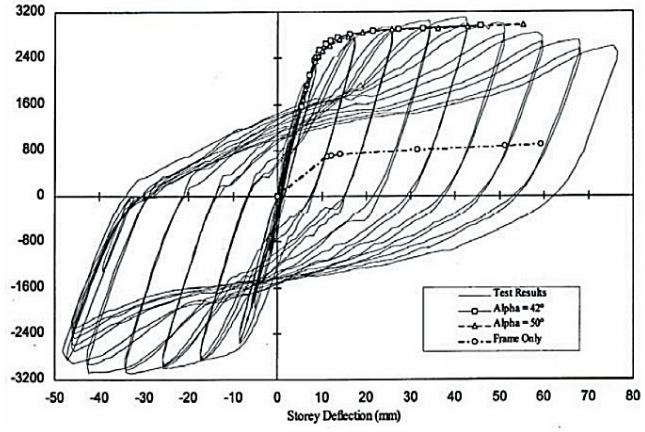

(b) Comparison of strip model to the test result

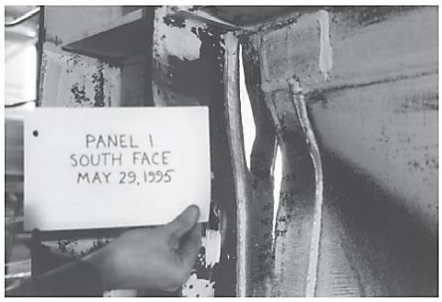

(c) Tears at top corner of first-story panel (photo courtesy of Robert Driver, University of Alberta, Edmonton, Canada)

Figure 2.5 Test specimen and results of the four-story steel plate shear wall specimen by Driver et al. (1997)

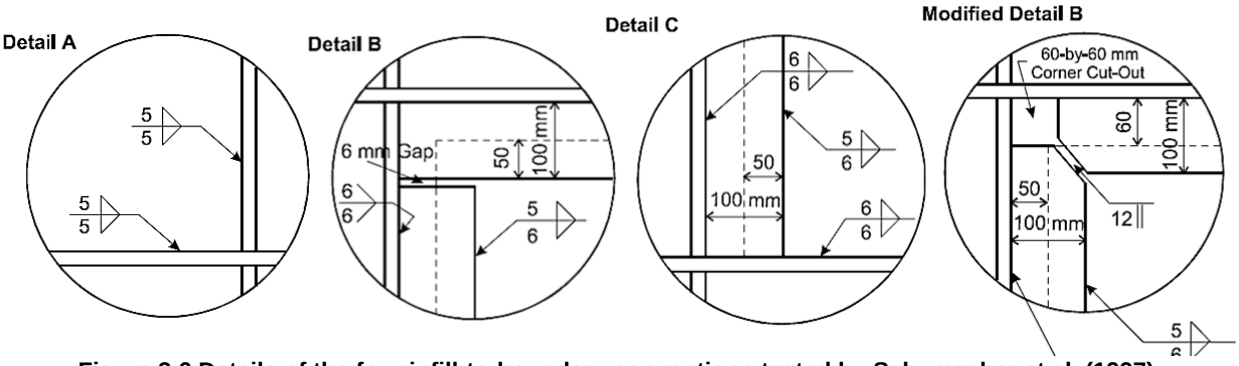

Figure 2.6 Details of the four infill-to-boundary connections tested by Schumacher et al. (1997)

Some examples of other important experimental studies include:

In an effort to solve the adverse effects of tension field action on the columns, a new steel plate shear wall system was developed and used by Skilling, Ward, Magnussen and Barkshire, now as Magnusson Klemencic Associates, a structural engineering firm in Seattle. This innovative system was used in at least one tall building. In this system, one boundary column is a relatively large concrete-filled tube composite section easily capable of resisting lateral forces of the tension field

forces applied to it. The other boundary column of this innovative system is a wide flange section that is designed to resist the seismic forces only without carrying any gravity loads. During the seismic event, this wide flange column under the tension field forces yields and becomes an energy dissipating component of the system. Zhao and Astaneh-Asl studied and cyclically tested two half-scale specimens of the system (Figure 2.7) and established that the system has relatively high strength, stiffness, ductility, and energy dissipation-capacities, reaching larger than 0.03 radian inter-story drift and up to 15 inelastic cycles. Both specimens with different splice locations were shown to perform satisfactorily (Zhao and Astaneh-Asl 2004b; Zhao and Astaneh-Asl 2008). Astaneh-Asl also developed seismic design procedures for this and traditional steel plate shear walls(Astaneh-Asl 2001; Astaneh-Asl 2002b).

Figure 2.7 The steel plate shear wall with composite column specimens at the end of the test by Zhao and Astnaeh-Asl (2004b)

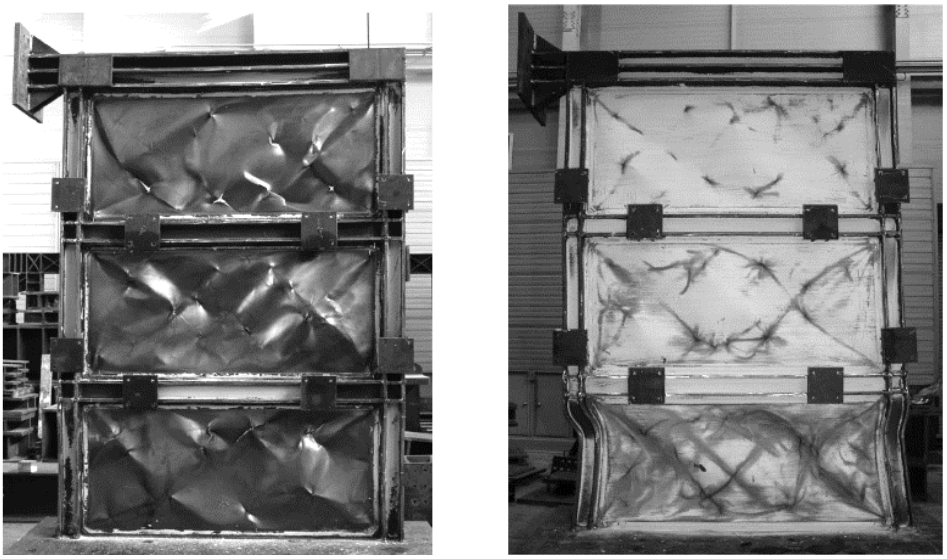

Figure 2.8 Deformed shapes of FSPW specimens at the end of test for specimen (a) FSPW2 and (b) FSPW3 tested by Choi and Park (2008)

Through the test of five single-bay three-story specimens, the system behavior and ductility behavior were classified to be shear-dominate for steel shear wall system with thin infill plate and flexure-dominate for thick infill plate by Choi and Park. By testing another set of SPSW specimens with ductile details (examples shown in Figure 2.8), they reported higher displacement ductility and energy-dissipation capability of the shear dominated steel shear wall specimens compared to concentrically braced frames (CBF) and moment resisting frames (MRF). It was found that the shear strength and energy dissipation capacity of the steel plate walls increased in proportion to the width of the infill steel plate, the overall displacement ductility increased with the ratio of the flexural capacity to the shear capacity, and the maximum inter-story drift ratio increased with the compactness of the column section. Different infill-to-boundary connections details were also studied and advantages and disadvantages of each alternatives were discussed (Choi and Park 2008; Choi and Park 2009; Park et al. 2007).

The behavior of steel plate shear wall with reduced beam section connections and composite floors was studied by Qu et al. (2008) through a two-phase experimental program on a full-scale two-story specimen. The buckled panels due to progressively increasing ground motions in Phase I were replaced by new panels before applying additional shakings in Phase II. The study verified the reparability and redundancy of the SPSW system such that the repaired specimen can survive a subsequent earthquake without severe boundary frame damages or overall strength degradation, and could achieve story drifts up to 5.2% (Qu et al. 2008).

Two-phase pseudo-dynamic tests on a two-story steel plate shear wall system conducted at the National Center for Research on Earthquake Engineering in Taiwan (Figure 2.9) showed that the SPSW specimens could withstand three earthquakes without significant wall fracture or overall strength deterioration, but with reduced energy-dissipating capacity when subjected to the same ground motions again in Phase II. The horizontal restrainers used in Phase I design were found to be effective in improving the serviceability of the steel plate shear wall systems. The use of strip model and equivalent brace model was also reported to be adequate in predicting global system response provided that the boundary elements are properly designed based on capacity design principle (Lin et al. 2010).

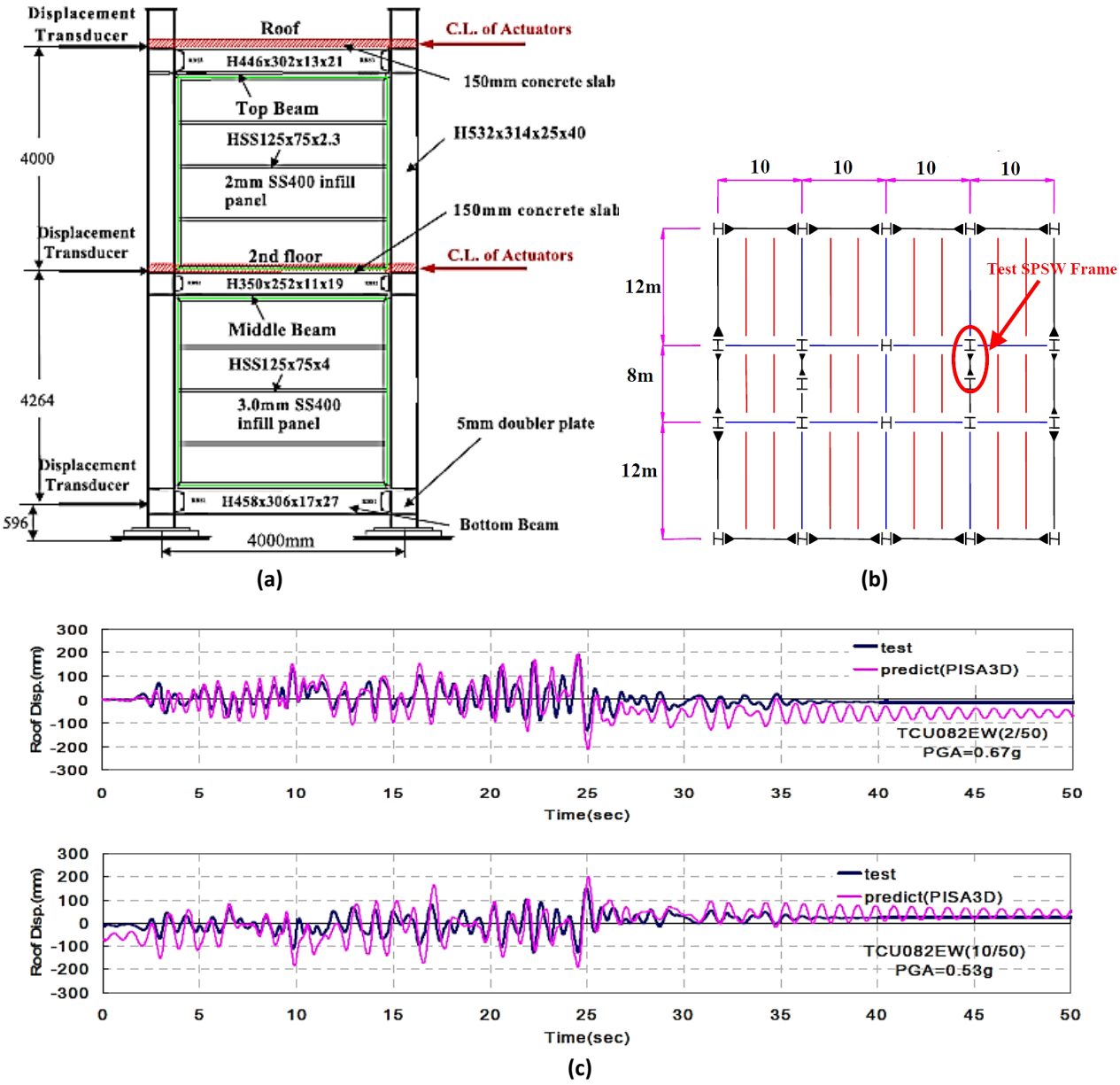

Figure 2.9 Pseudo-dynamic test by Lin et al. (2010) (a) Test specimen (b) Assumed floor framing, and (c) Comparison of predicted and tested roof displacement time history

Examples of some important analytical studies include but not limited to the following:

Zhang and Guo (2014) established a reduction coefficient for the shear capacity of the system considering the pre-compression effect from boundary columns (Zhang and Guo 2014). Habashi and Alinia (2010) examined the wall frame interaction for the system. They concluded that with practical steel plate shear wall dimensions (Length/Height < 2), if the system is designed as per the AISC Design Guide 20 rules, the frame behavior is independent of the infill wall; therefore the shear capacity of the system can be calculated by simply adding frame and the infill wall capacities (Habashi and Alinia 2010). Hosseinzadeh and Tehranizadeh (2014) reviewed the code-designed

SPSW system and found that the boundary frames are effective in resisting story shear only at a few of the lower stories, while a substantial portion of the story shear is taken by the infill plates at the upper stories. They also found that about 70 to 80% of the compressive axial force in the boundary columns results from plate tension field action (Hosseinzadeh and Tehranizadeh 2014). Shi and Astaneh-Asl (2008) investigated the design of steel plate shear wall system using different design philosophies. They found that the plate girder design procedures applied to steel plate shear walls can predict the shear strength of the walls reasonably well and can lead to more economical designs (Shi and Astaneh-Asl 2008). Bruneau and his research associates studied the plastic design method of SPSPWs and many other code-based design aspects of the steel plate shear walls, such as the capacity design of the boundary columns and boundary beams (Berman and Bruneau 2003; Berman 2011; Berman and Bruneau 2008; Purba and Bruneau 2015b; Qu and Bruneau 2009). Kharmale and Ghosh (2013) proposed a performance-based plastic design method for steel plate shear walls with rigid beam-to-column connections (Kharmale and Ghosh 2013). The strain rate and *P*-delta effects were considered by Bhowmick et al. (2009). They found that the loading rate increases flexural demand mostly at the base of the steel plate shear wall but imposes limited influences on the inelastic seismic demands for a suite of spectrum compatible earthquake records for Vancouver. They also pointed out the conservative nature of the current National Building Code of Canada stability factor approach to include the *P*–delta effects for steel plate shear walls, and that *P*–delta has small effects on seismic demand estimations (Bhowmick et al. 2009). Research efforts have considered other design methods, such as the capacity spectrum method (Shao et al. 2008) and the design of the system based on inelastic drift demand (Ghosh et al. 2009). Baldvins et al. recently proposed a set fragility functions for steel plate shear walls for use in the performance-based design applications (Baldvins et al. 2012).

2.3 Recent Studies

Despite the many advantages of steel plate shear wall (SPSW) systems established in the past research as presented above, issues and challenges were also reported for the current design of unstiffened steel plate shear wall system. The ten issues for the current SPSW system identified earlier in Chapter I can be grouped into three major categories: issues related to (1) tension field forces acting on the columns, which affects the detailing and design of the system; (2) the beam-to-column connection; and (3) the design criteria, especially the service-level requirements, of the system. The following is a summary of research projects that have attempted to address directly or indirectly one or more issues identified in Chapter I.

2.3.1 Reduction or Elimination of Tension Field Action

In an effort to reduce or eliminate the forces applied to the columns by steel infill panels, research has focused on both *passive* and *active* strategies. The *passive* method reduces the tension field forces acting on the column either by restraining the infill steel plate and delaying the buckling

and formation of the tension field, or by weakening the tension fields or plate material to reduce the magnitude of tension field forces. In the *active* method, the steel infill panel is prevented from transferring the tension field forces to the boundary columns by actively separating the wall from the column and connecting the infill wall to the boundary beams only. The use of composite column sections as the boundary columns, such as the one tested by Zhao and Astaneh-Asl (2004b, 2008) and discussed earlier, can also be an effective method for preventing column bending due to the tension field forces. Because this approach aims at increasing the boundary constraints instead of reducing or eliminating tension field forces, it was not included in this section but in Section 2.2 as one of the benchmark studies on steel plate shear wall system.

2.3.1.1 Passive Solutions

Historically, attaching welded stiffeners to one or both sides of the steel infill plates was the most popular method to prevent the early elastic buckling of thin steel plates and development of tension fields. Takahashi et al. (1973) may have conducted one of the first published projects on stiffened shear walls. They found that increased number of stiffeners changes the pinched hysteresis loops to bulkier shapes that corresponding to higher energy-dissipation capacity (Takahashi et al. 1973). Although unstiffened thin steel plate shear walls are more popular in North America, stiffened steel shear walls are still well received in other countries, e.g., Japan and China. Stiffeners can protect shear walls against overall buckling, limit the out-of-plane deflections, increase the elastic buckling strength, and spread yielding throughout the plate. Since the stiffened steel shear wall is not the focus of this study, only some of the recent research conducted on stiffened steel shear wall is summarized here.

Alinia and Dastfan (2007) carried out an extensive parametric study on the effects of stiffeners. It was concluded that a stiffener rigidity ratio (defined as EI_s/bD, where I_s is the second moment of area of stiffeners, b is panel width, D is the flexural rigidity of isotropic plate and E is the modulus of elasticity) of approximately 30 seemed to be optimal and could lead to both sufficient rigidity and deformability. In addition, unilateral stiffeners parallel to the shear direction (i.e., horizontal stiffeners only) were found to be more effective than bilateral stiffeners (both vertical and horizontal stiffeners) (Alinia and Dastfan 2007). Later more cases were studied based on their previous work. They defined the optimal stiffener arrangement as the arrangement that enables the critical stresses of stiffened plates to be equal to that of the individual subpanels (Alinia and Shirazi 2009). Sabouri-Ghomi and Sajjadi (2012) showed that the addition of stiffeners increased the system's energy dissipation capacity by 25% and the shear stiffness by 51.1%. The plate–frame interaction (PFI) theory proposed by them earlier to predict the behavior of steel plate shear walls with and without stiffeners was verified satisfactorily (Sabouri-Ghomi and Sajjadi 2012). In the study conducted by Nie et al. (2013), the shear capacities of stiffened steel plate shear walls with and without openings were investigated. Stiffened steel plate shear walls were shown to possess high strength, ductility, and energy-dissipation capability. Openings reduced the strengths and

stiffness as expected, but stiffeners around openings were reported to be effective in recovering the stiffness and in enhancing the stability (Nie et al. 2013).

In addition to the traditional stiffening method, one of the most efficient recently developed passive solutions has been to add a concrete wall to the steel plate, effectively creating a composite wall (Zhao and Astaneh-Asl 2004a).The concrete wall delays the buckling of the wall and development of the tension field. The concept of composite shear walls (concrete cover on top of the steel infill plate configuration) was first studied at the University of California, Berkeley (Astaneh-Asl and Zhao 2000; Zhao and Astaneh-Asl 2004a; Zhao 2007; Zhao and Astaneh-Asl 2003; Zhao and Astaneh-Asl 2006a; Zhao and Astaneh-Asl 2006b) (Figure 2.10). A seismic design procedure was also developed for the composite steel shear walls (Astaneh-Asl 2002a). This study has motivated many later studies on the various analysis and design issues of the composite shear wall configuration (Ahmadi and Arabzadeh 2013; Arabzade et al. 2011; Arabzadeh et al. 2011; Rahai and Hatami 2009).

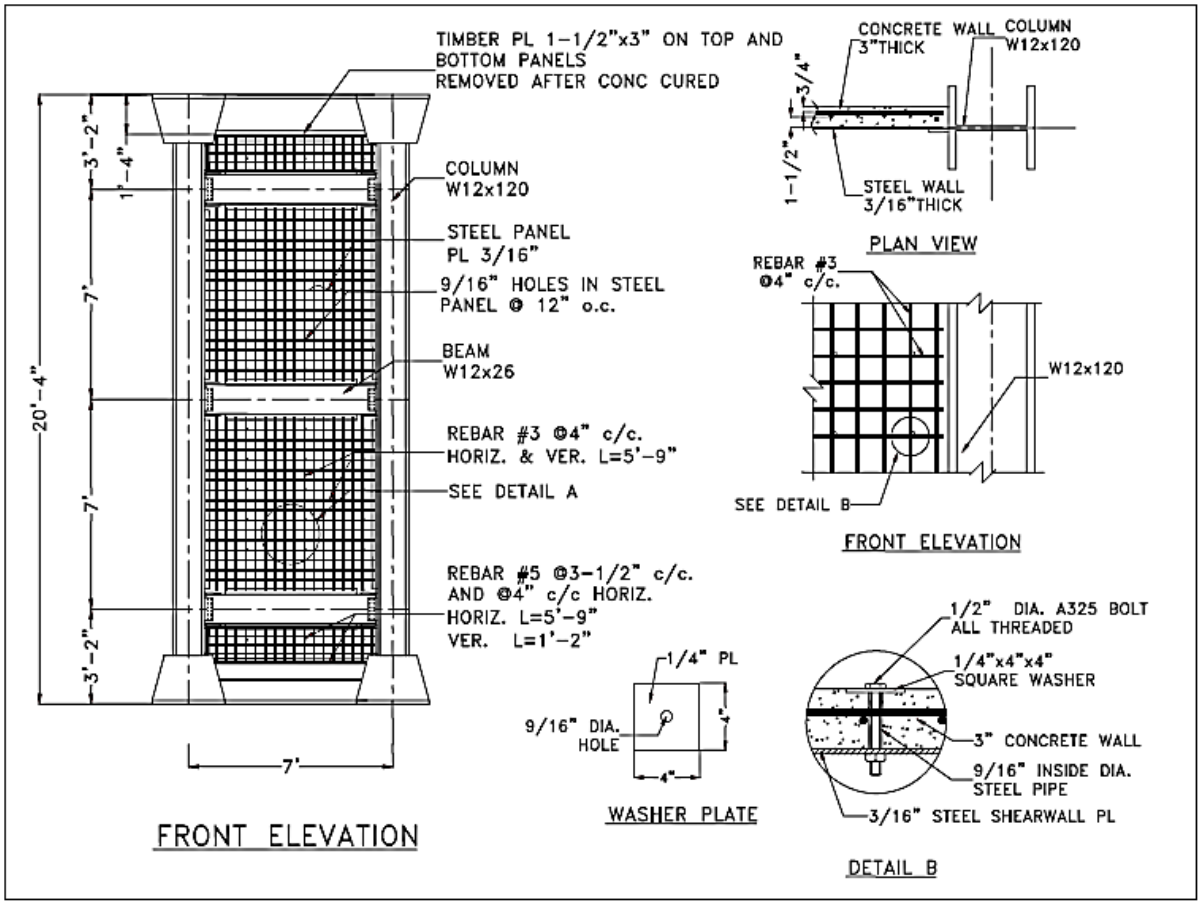

Figure 2.10 Details of composite shear wall specimen tested by Zhao and Astaneh-Asl (2004a)

Another solution has been to add buckling-restraining braces to the steel infill plate to prevent its buckling before yielding in shear (Li et al. 2010; Nie et al. 2012; Tsai et al. 2007; Tsai et al. 2010). As shown in Figure 2.11, the major forms of existing buckling restrainers published in the literature include:

(a) channels welded to the infill plate but with a gap left between the restrainer and the boundary beam (Lee et al. 2010; Nie et al. 2012);
(b) square tubes bolted on both sides of the infill plate using enlarged bolt holes to allow the relative movement of the infill plate and the buckling restrainers (Li et al. 2010; Tsai et al. 2007; Tsai et al. 2010); and
(c) a concrete cover plate similar to that in a composite shear wall but with enlarged bolt holes so that the concrete cover could slide freely relative to the steel plate (Guo et al. 2009).

Recently, a new type of buckling restrained shear wall was proposed by Jin et al., which consists of steel plate with inclined slots sandwiched between two external concrete panels and can be viewed as a series of buckling restrained braces placed in parallel (Jin et al. 2016). Note: introduction of the inclined slots changes the basic load carrying mechanism of the steel plate.

Weakening of the infill plate is another approach to reduce the tension field forces acting on the columns. This can be achieved by creating a regular pattern of circular perforations (Figure 2.12), e.g., (Roberts and Sabouri-Ghomi 1992; Vian 2005; Vian et al. 2009), or by using low-yield point (LYP) steel plates, e.g., (Nakagawa et al. 1996; Vian et al. 2003). The research of perforated steel shear wall was first initiated due to the concern for utility passage, but later it was realized that the perforations could reduce the shear capacity of the infill plate (Roberts and Sabouri-Ghomi 1992), and, promote more uniform panel stress distributions, thus indirectly reducing the deformation demands on the columns (Chan et al. 2011). Design recommendation for perforated SPSWs was proposed based on finite-element analysis (Purba and Bruneau 2009). Recently, however, it was found that perforations in the infill plates may not necessarily reduce the net force and deformation demands on the columns; although the perforation consistently reduces the axial force demands, it increases the contribution of frame action in the system and results in an increase in the moment demands for upper stories. In addition, column demands were found to be sensitive to the perforation pattern provided (Moghimi and Driver 2014).

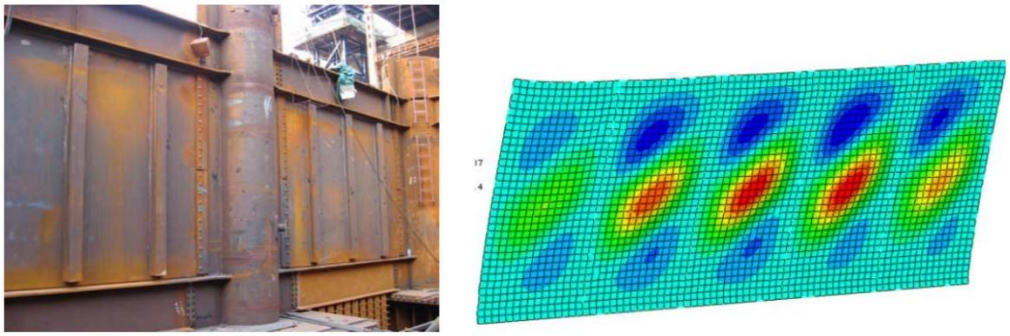

(a) Buckling restrained SPSW Type I: channel stiffener with a gap between end of stiffeners to the boundary beams by Lee et al. (2010)

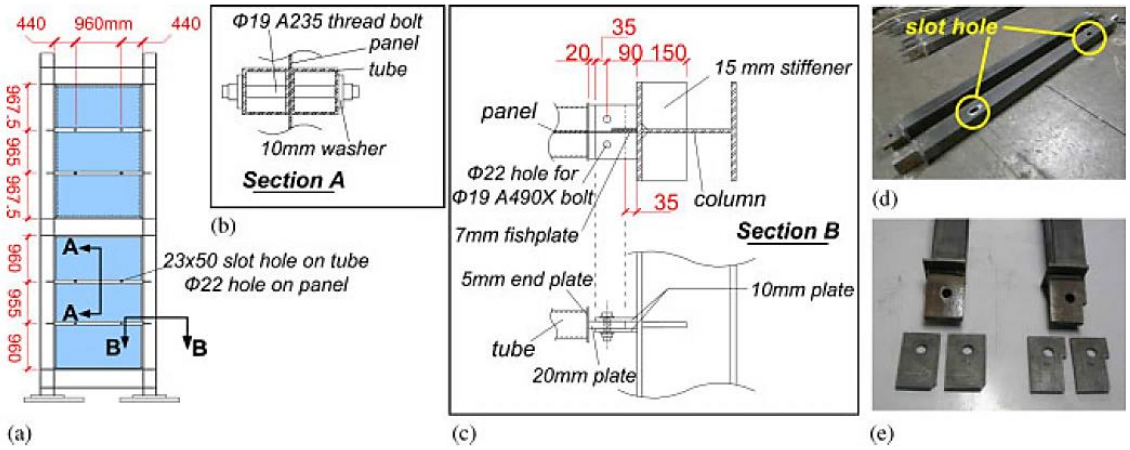

(b) Buckling restrained SPSW Type II: infill panel sandwiched between rectangular tubes on both sides with enlarged bolt holes by Tsai et al. (2010)

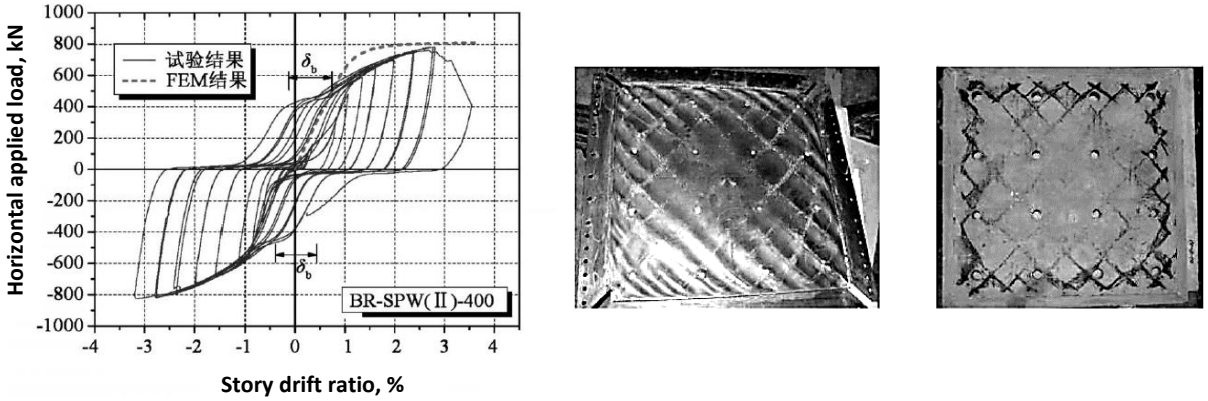

(c) Buckling restrained SPSW Type III: infill panel sandwiched between concrete panels on both sides with enlarged bolt holes by Guo et al. (2009)

Figure 2.11 Three types of buckling-restrained SPSW systems

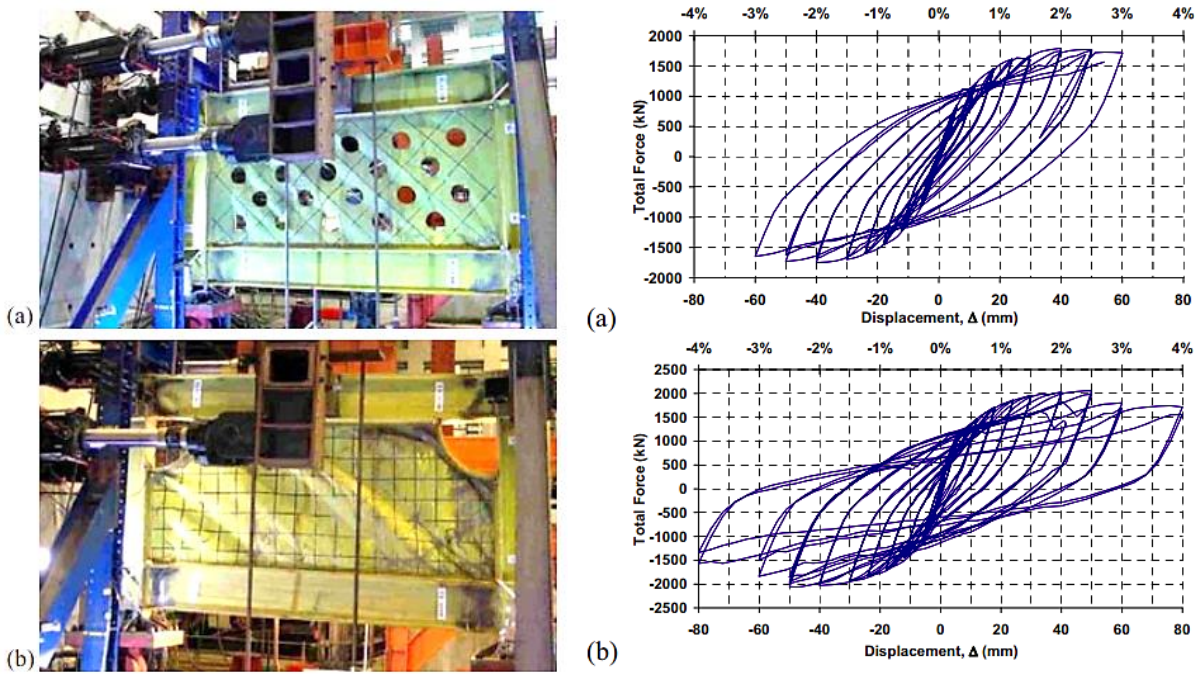

Figure 2.12 Deformed shapes of perforated specimens tested by Vian et al. (2009) and their hysteresis responses (from top: specimen P, CR)

Low-yield steel (LYS) was first developed by Nippon Steel in Japan, and its application in SPSW system was first studied by Nakashima and his colleagues in the early 1990s (Nakagawa et al. 1996; Nakashima 1995; Nakashima et al. 1995; Nakashima et al. 1994). A typical test specimen and its hysteresis behavior are shown in Figure 2.13. The main advantages of LYS include its low-yield strength, high ductility, and energy-dissipation capability, lower strain rate dependency, longer low-cycle fatigue life, and improved weldability (Saeki et al. 1998). Vian et al. (2003) tested an SPSW with reduced yield strength steel (F_y=165MPa) and concluded that SPSW with LYS could be a viable alternative to the traditional unstiffened SPSWs where the reduced yield strength and thickness of the plates lead to lower stiffness and earlier onset of yielding and higher energy dissipation. The LYS walls were considered capable of alleviating the over-strength problem on the adjacent framing members (Vian et al. 2003). More information on the behavior of LYP steel shear wall under in-plane load with different width-to-thickness ratios and the beam-to-column connections can also be found in the work of Chen and Jhang (Chen and Jhang 2006; Chen and Jhang 2011). Construction of fragility curves of SPSW system using LYS also demonstrated that employment of relatively thicker LYP steel infill plates in seismic design and retrofit of steel moment frames could lead to lower damage potential and better seismic performance (Zhang and Zirakian 2015).

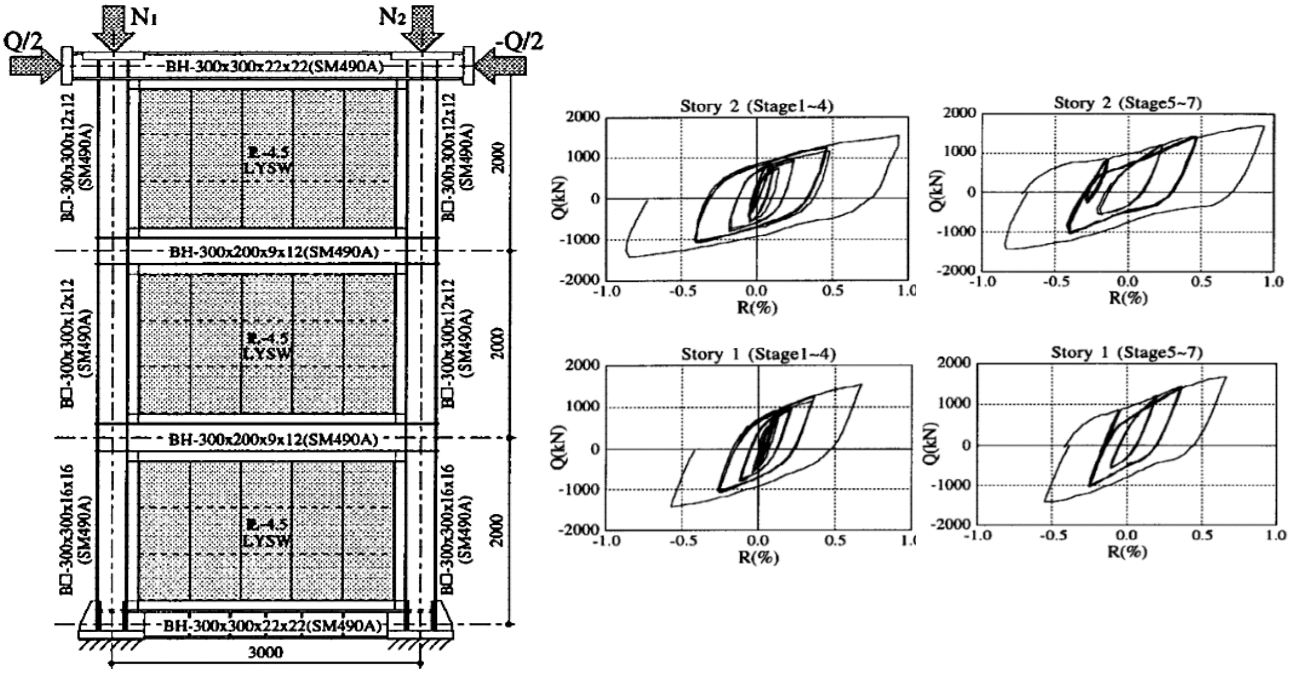

Figure 2.13 Test specimen using low-yield point steel by Nakagawa et al. (1996) and their hysteresis responses

Researchers have also tried to change the load carrying mechanism in the infill plate by providing vertical slits or by cutting out specific patterns on the wall (Figure 2.14). The use of a series of slits on the infill panel enables the formation of a series of flexural links in between the slits and allows the system to provide a fairly ductile response without the need of substantial stiffening (Chen et al. 2012; Hitaka and Matsui 2003). The behavior and design of slit-panel frame were also investigated (Cortes and Liu 2011a; Cortes and Liu 2011b). The ring-shaped steel plate shear wall (RS-SPSW) proposed by Egorova et al. (2014) has a special cut pattern that helps resist out-of-plane plate buckling through the mechanics of how a circular ring deforms into an ellipse. The RS-SPSW system was found to exhibit full hysteretic behavior and possess significantly improved stiffness relative to thin unstiffened SPSW (Egorova et al. 2014).

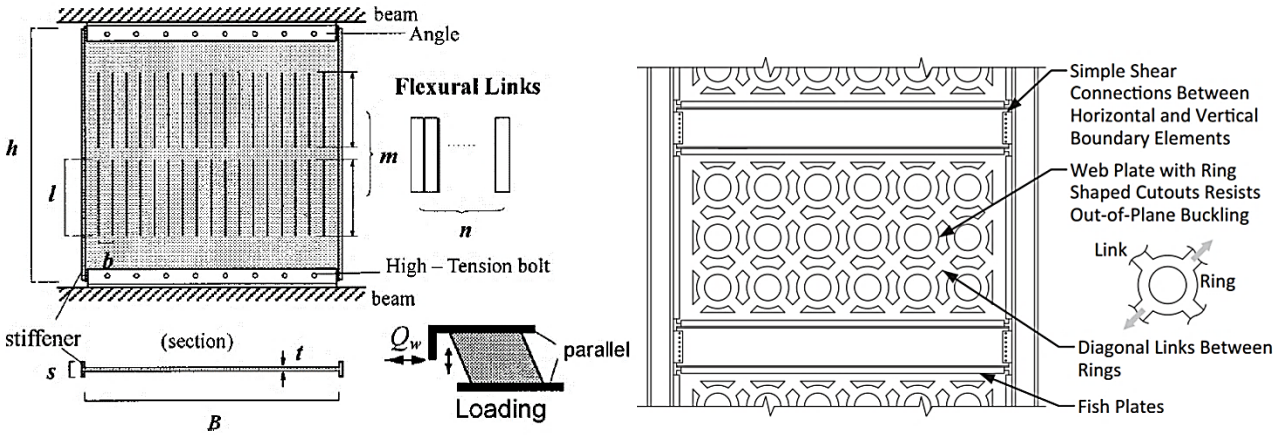

(a) SPSW with slits by Hitaka and Matsui (2003) **(b) Ring-shaped SPSW by Egorova et al. (2014)**

Figure 2.14 Types of SPSW that has a changed load-carrying mechanism

Application of the above-mentioned passive methods can successfully reduce the lateral forces acting on the columns but does not eliminate them. They often require additional material and labor, resulting in increased construction time and cost.

2.3.1.2 Active Solutions

The *active* solution to prevent the infill panel from transferring the tension field forces to the boundary columns has been to weld the infill panel to the boundary beams only (Choi and Park 2009; Clayton et al. 2015; Guo et al. 2011; Vatansever and Yardimci 2011; Xue and Lu 1994). This is a more intuitive and simpler solution compared to the *passive* methods discussed in the previous section.

Xue and Lu (1994) were likely the first to propose the method to reduce the demand on the framing members adjacent to an SPSW by connection of the infill panel to the beams only. In their work, a three-bay, 12-story, frame–wall structure was studied analytically. The structure had moment resisting frames in the exterior bays and steel plate shear walls in the middle bays. Minimal differences in lateral stiffness were reported between the frames with moment and shear beam-to-column connections. Compared with fully connected infill panels, the infill panels in the P-G system (shear beam-to-column connection with infill plate connected to the girder only) participated early in resisting the lateral load, which caused more nonlinear behavior in the infill panels but maintained more elasticity in the boundary frame. Xue and Lu (1994) recommended the P-G configuration due to the advantages of a symmetric distribution of story shears in columns, less bending in columns, and reduced demand on the beam-to-column connections.

Another test relevant to the concept of connecting the infill plate to the beams only and not to the columns is the specimen FSPW4 by Choi and Park (2009) where they studied a series of different infill-to-boundary element connection configurations. Specimen FSPW4 shown in Figure 2.15 had the infill plate welded to the beams, and the vertical edge of the infill plate was partially welded to the column flange to avoid premature failure at the edge. Fractures initiated at the corners where the infill plate was partially welded to the column flange since no stiffeners were provided for the free edge of the panel. Despite this detailing problem, the overall performance of the FSPW4 specimen exhibited excellent deformation capacity equivalent to that of its fully-connected infill plate counterpart.

Analytical models to establish the elastic buckling capacities were proposed based on the finite-element parametric studies on single-panel SPSWs with slots at two vertical edges (Guo et al. 2007; Miao et al. 2007).

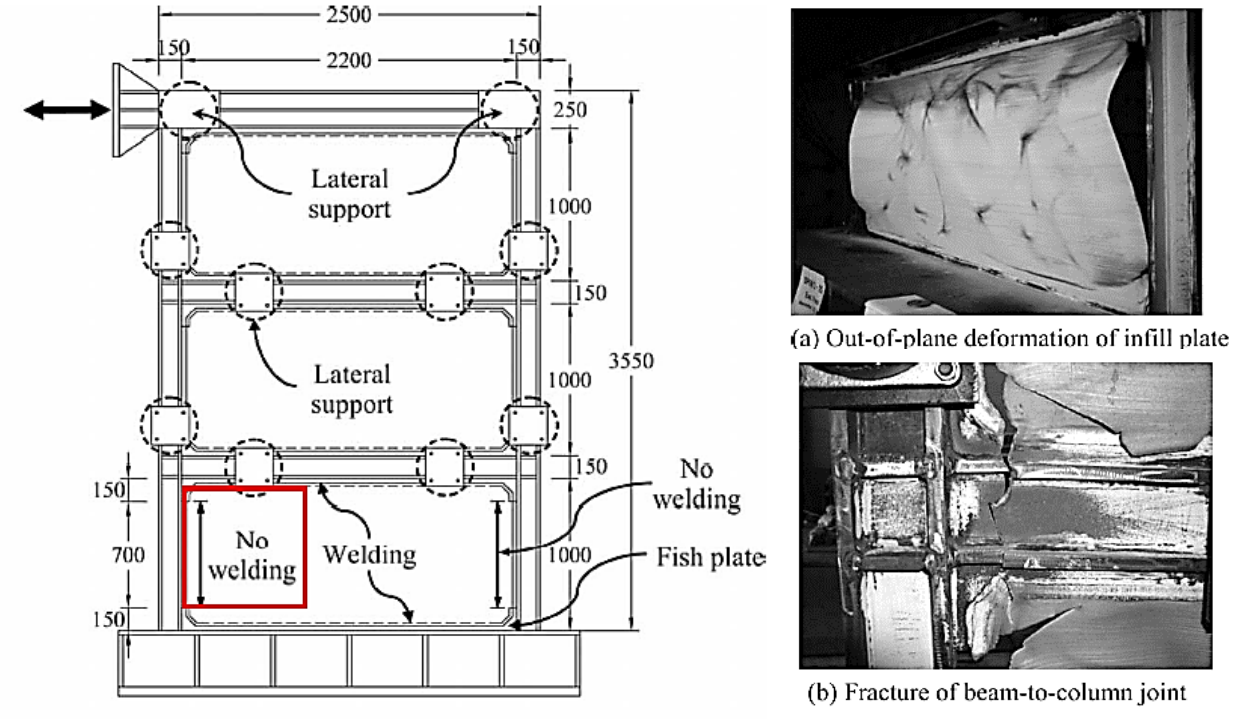

Figure 2.15 Details of specimen FSPW4 and its failure modes by Choi and Park (2009)

Vatansever and Yardimci (2011) tested and compared the cyclic behavior of a fully-connected (SW-A-H) and beam-only connected (SW-B-H) one-bay one-story specimens in comparison with a pure boundary frame system (BF-H). With an emphasis on retrofit applications, they adopted some unconventional details. The beam-to-column connections were semi-rigid header plate connections. Self-drilling screws instead of welding were used to connect the thin infill plate to the beams (Figure 2.16). In the tests, some nonlinearity due to bearing failure of the screw connections appeared before yielding of infill plate but had insignificant influence on the overall behavior. Large net section fractures occurred, but no significant strength degradation resulted from these fractures. They found that fully-connected SW-A-H specimen was superior in terms of its energy-dissipation capacity and strength. However, they argued that the beam-only connected specimen SW-B-H is a viable alternative compared to the fully-connected configuration as they showed significant performance improvement compared to the frame-only specimen BF-H. This is especially true for retrofitting applications where labor and material savings due to fewer connections of infill panel to boundary elements are preferred.

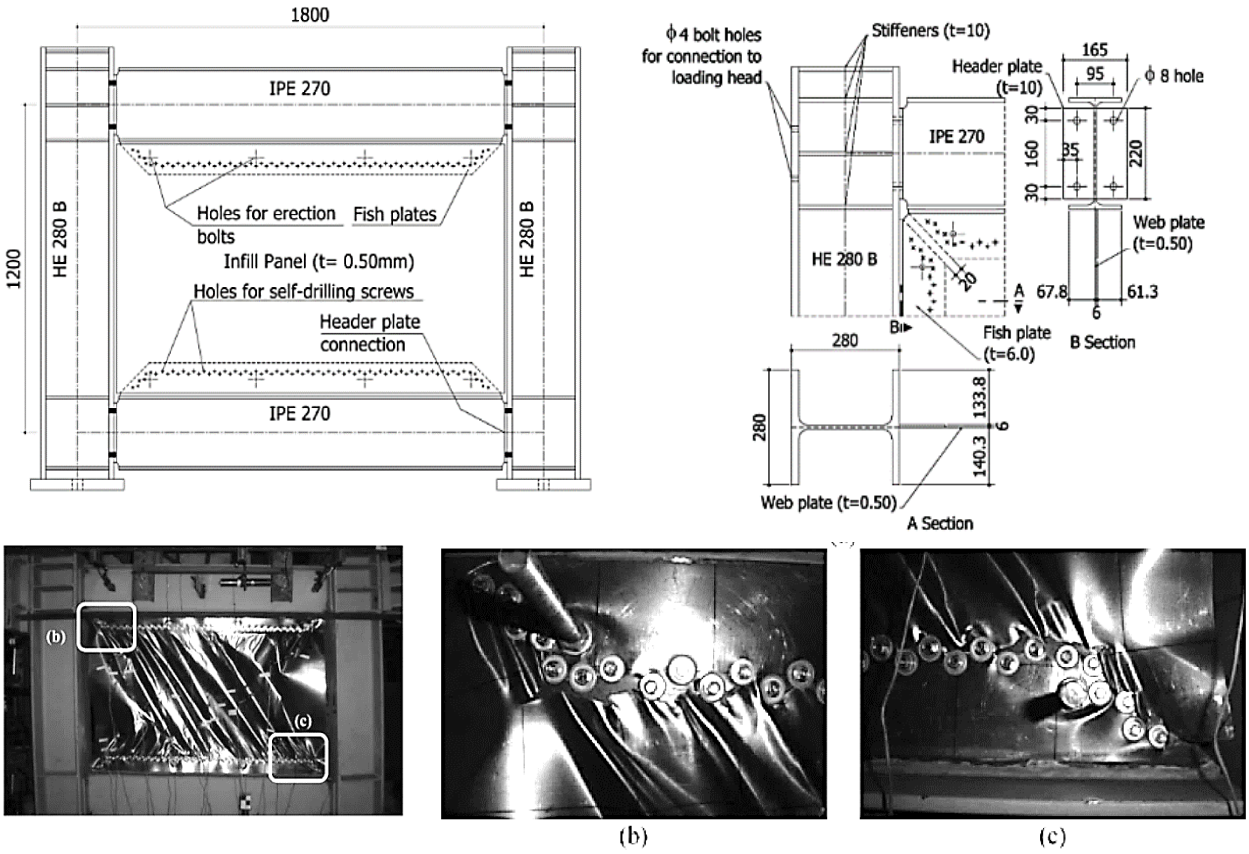

Figure 2.16 Details of specimen SW-B-H and its failure modes by Vatansever and Yardimci (2011)

The behavior of steel plate shear walls connected to beams only was also studied by Guo et al. (2001) with pin-connected beam-to-column connections; in 2013, they studied composite steel plate shear wall connected to beams only using a similar test set-up (Figure 2.17). The experimental results illustrated that both steel and composite shear walls with steel panels connected to beams only exhibited good ductility and high energy-dissipation capacity. From the SPSW test, they found that providing minimum required stiffeners on the free edges of the infill panel increased the energy-dissipation capacity but with no obvious improvement on the load-carrying capacity and ductility. The analytical parametric studies showed that specimens with low height-to-thickness ratio were able to dissipate more energy (Guo et al. 2011). They also confirmed the benefit of reinforced concrete (RC) panels in resisting the out-of-plane buckling of the steel plate and in increasing the energy-dissipation capacity – even with the infill plate connecting to the beam only (Guo et al. 2013). However, in their test setup, only the infill panel was tested with the help of very large pin connected test columns. In these tests, possible beam-to-column connection modifications were not considered, and the frame action may not have been very accurately represented.

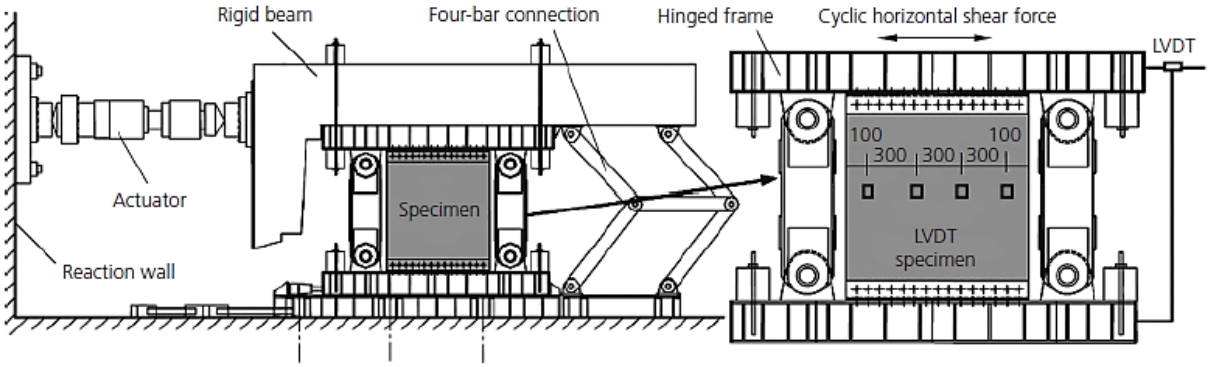

Figure 2.17 Details of test set-up by Guo et al. (2013)

Recent work by Clayton et al. (2015) is an application of infill panel connected to the beam only in self-centering steel plate shear walls. This initial investigation was followed by studies on fully connected self-centering SPSWs (Clayton et al. 2012; Clayton et al. 2013). In a self-centering SPSW, the thin steel panels are the primary lateral load resisting elements while the post-tensioned beam-to-column connections provide re-centering capabilities. The benefits of releasing the web plate from the columns were well recognized by Clayton et al.: 1) the elimination of the distributed lateral load on the columns; 2) the simplification of design since location of maximum moment on the column can be assured; 3) the release of net horizontal strain in the web plate due to frame expansion; 4) the reduction of localized out-of-plane deformation at the ends of web plate-to-boundary element connection; 5) the savings of steel due to reduced column demands can be significant, especially for taller buildings, and 6) the savings in labor cost for web plates installation can be considerable. A design procedure for the beams and post-tensioned connection in a fully connected self-centering SPSWs was proposed earlier (Dowden and Bruneau 2014).

In addition, in Wang et al.(2015)'s comparative study on SPSWs with different construction details and materials using finite-element simulations, the steel shear walls connected to the beam only showed advantages of less likelihood of fracture in the infill panel and in the corner welds, effectiveness in eliminating the tension field forces acting on the columns, good ductility behavior and being comparatively more economical than the other details (Wang et al. 2015). These advantages to some extent compensate for the slightly lower load-carrying capacity and energy-dissipation capacity of the SPSW connected to the beam only.

Given that there are no additional fabrication costs, the *active* method is certainly more cost effective and worth further investigation than *passive* methods. Existing research on the infill wall connected to the boundary beams only primarily regards this system as an alternative infill plate to boundary element connection method compared to the traditional SPSW system where the infill panels are connected to both the beams and columns. Most of the analytical and experimental

studies have focused on the behavior of a single panel with idealized boundary conditions. While being initially promising and potentially cost-effective, a holistic study on the performance, design, and detailing of the steel shear walls connecting to the beam only as a system has not yet been conducted.

2.3.1.3 Infill-to-Boundary Element Connection

Continuous connections along the boundary beams and columns assure better continuity and uniformity of stress path, increases the rigidity of the beam-to-column connection (Caccese et al. 1993), and provide more redundancy to the SPSW system. However, some construction difficulties were observed and reported in the literature.

Past cyclic tests of the unstiffened steel shear walls (Timler and Kulak 1983) have shown that during the cyclic loading the corners of the wall plate fractured due to the relatively large cyclic strain concentrations at the corners where there is a gap between the horizontal and vertical fin plates. To prevent the corner fracture, researchers have recommended adding welded strap plates to fill the gap between the horizontal and vertical fin plate(Tromposch and Kulak 1987), providing corner cut-outs (Schumacher et al. 1999), or incorporating special corner brackets and connecting the horizontal and vertical fin plates away from the corner (Choi and Park 2008). All these methods as shown in Figure 2.18 add to the effort and cost of fabrication.

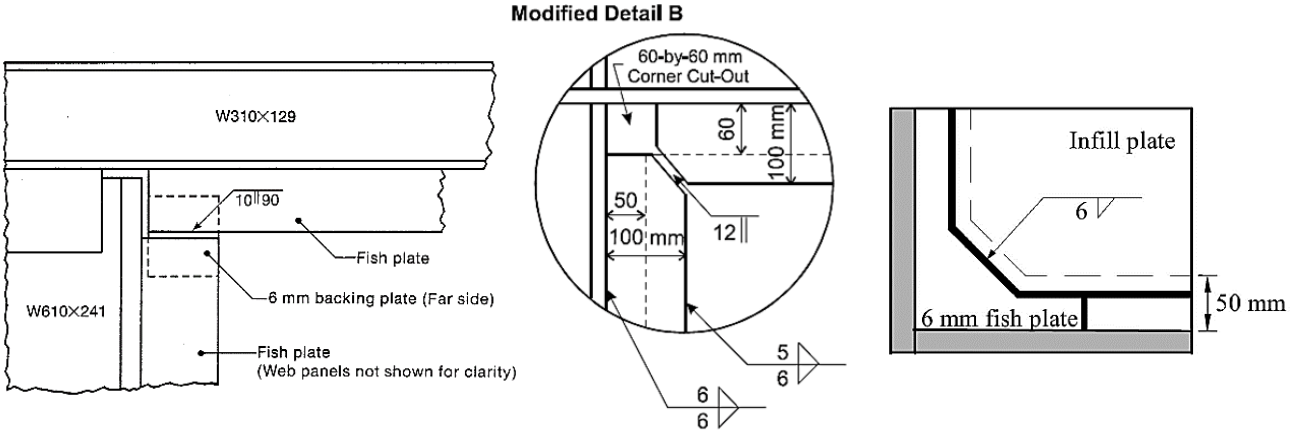

(a) welded strap plates filling the gap between horizontal and vertical fin plates by Tromposch and Kulak (1987)

(b) special corner cut-outs by Schumacher et al.(1999)

(c) special corner brackets to move away the interface between horizontal and vertical fin plates by Choi and Park (2008)

Figure 2.18 Illustration of corner details proposed by different researchers

The significant amount of vertical field welds connecting the infill panels to the boundary columns also results in higher costs. The potential problem of burning of the infill plate during the upward field welding has been reported (Eatherton 2006). Difficulties were also encountered in constructing the infill-to-column connection at the column splice location. Sometimes, relatively large holes had to be cut in the infill plates to provide space and access to the column splice

connection. Figure 2.19 is an example of the column splice details for the 55-story LACCH building designed by Nabih Youssef Associates (Youssef et al. 2011). This detail may affect the continuity of the tension fields, leading to a behavior not as strong and ductile as expected.

Very few research had addressed the potential modular construction possibilities of this system. Modular detailing with mid-height splices was adopted in the work of steel shear wall system with composite columns and coupling beams (Zhao and Astaneh-Asl 2004b) and proved to be a viable option. Driver and Moghimi (2011) investigated the modular components with repetitive fabrication processes, but it was specifically for low- and moderate-seismic regions (Driver and Moghimi 2011). Three different concepts were proposed, and the one with mid-height continuous splices was considered as the most promising configuration in terms of practicality and economics (Figure 2.20).

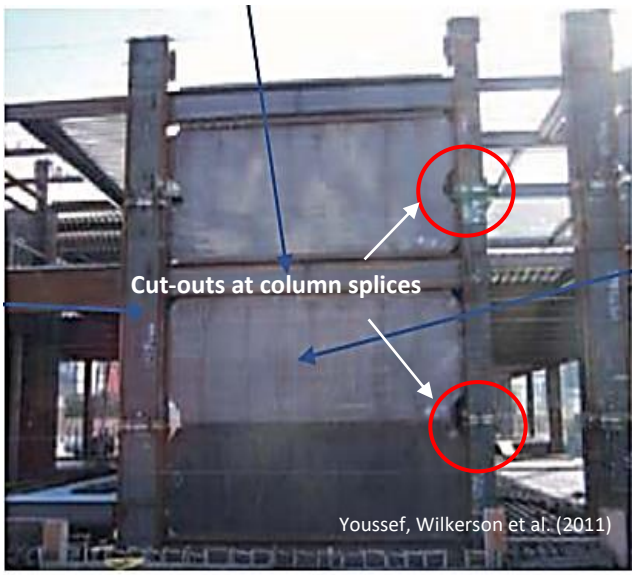

Figure 2.19 Illustration of cutouts at column splice location in the actual construction (photo from Youssef et al.,2011)

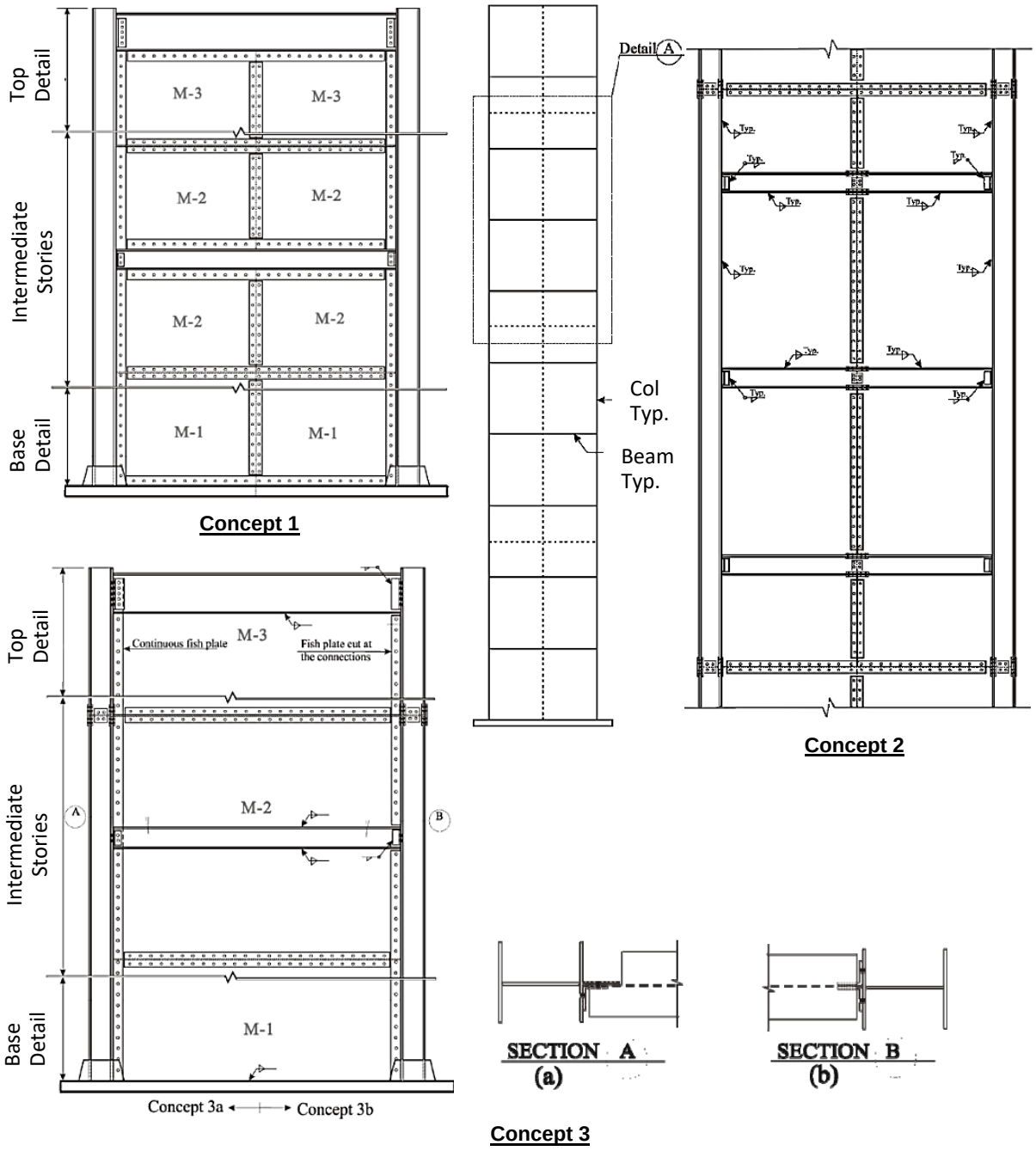

Figure 2.20 Proposed concepts for modular SPSWs in low- and moderate-seismic regions by Driver and Moghimi (2011)

2.3.1.4 Limitations on Design Choices

As mentioned in Chapter I, due to the application of tension field action forces to the columns, the choice of column and infill plate are dependent on each other: in the current steel shear wall system, after designing the infill walls and the columns to resist the applied lateral force, the wall thicknesses cannot be increased to satisfy the drift requirements (either ultimate or service level) without increasing the size of the columns. To solve the problem, typically more moment connections have to be used in the frames outside the steel plate shear wall to increase the lateral stiffness of the system (AISC 2007). These moment connections are often expensive, leading to significantly higher construction costs. In addition, the capacity design approach requires use of heavier columns for thicker or stronger infill walls in order to provide sufficient boundary constraints and avoid mid-height hinges. This is the major reason leading to the design of SPSWs using composite columns, especially for tall buildings (Nie et al. 2012; Zhao and Astaneh-Asl 2008). In the current system, the column section has to be a wide-flange, if not composite columns, with its flange connected to the steel shear infill wall to allow the column to bend about its strong axis under lateral forces. This is the case for all tested SPSWs regardless of the difference in configurations. This aspect again restricts the design flexibility of the system, especially when SPSWs are used in combination with moment frames in the perpendicular direction and in retrofit applications. Use of capacity design procedures, e.g., (Berman and Bruneau 2008), can resolve some, but not all, of the limitations on design choices due to tension field action. A new SPSW system or configuration might be a better approach to fundamentally solve these design concerns.

2.3.2 Beam-to-Column Connection

For the beam-to-column connection used in the SPSW system, the 2010 AISC Seismic Provisions only requires ordinary moment connections(AISC 2010b). However, except for a few early tests, all subsequently tested SPSW specimens used moment beam-to-column connections, some even being the special reduced beam section connections. This choice is probably due to energy dissipation and system redundancy considerations; Tromposch and Kulak (1987) showed that frames with fixed beam-to-column connection could dissipate as much as three times more energy than the system using similar frames but with simple connections. However, note that their test also showed a robust rotation capacity of the bolted shear beam-to-column connections. In addition, Caccese et al.(1993) found that the rigidity of beam-to-column connections had a minor effect on the overall load-displacement behavior of the system.

Some past studies have recommended the use of special moment connections in steel plate shear wall systems (Qu et al. 2008; Vian et al. 2009). This recommendation has been incorporated into the design of a few steel plate shear wall systems. Higher ductility and energy-dissipation capacity resulting from incorporation of special moment connections in the boundary frame of a steel plate shear wall system is a desirable property; however, the beam-to-column connections should not be relied upon as the main source of energy-dissipation in a steel shear wall system, let alone the

current pre-qualified special moment connections (AISC 2010b; AISC 2016a), which have relatively high construction and inspection cost. This is primarily due to the use of Complete Joint Penetration field welds and the required field inspections using ultrasonic testing for these welds.

The potential savings gained by replacing the special moment connection by some other simpler and more cost-efficient beam-to-column connections should be more widely recognized and developed. Since the SPSW system is essentially a dual system, the study of steel shear walls should not be restricted to the use of traditional moment connections. The exercise of using post-tensioned (PT) beams is an example of improvement of the performance and economy of the system by expanding the beam-to-column connection type of the SPSW system to other innovative connections. Apparently, separating the infill wall from the column eases the infill-to-boundary element connection and allows a wider range of beam-to-column connections to be used. Use of simple shear connection (Cortes and Liu 2011a; Xue and Lu 1994) and bolted plate moment connection(Caccese et al. 1993; Vatansever and Yardimci 2011) in the SPSW system should be re-visited, and development of new beam-to-column connections that fit the steel shear wall system should be encouraged.

2.3.3 Service Level Design Requirements

Tests and analysis of steel shear walls (Shi and Astaneh-Asl 2008; Timler and Kulak 1983; Zhao and Astaneh-Asl 2008) have shown that unstiffened steel plate shear walls can buckle along their compression diagonal at a relatively small drift values in the order of 0.005 to 0.01 radians. Almost all of the past research on steel plate shear wall system have focused on studying and improving the post-buckling performance, ductility, and energy dissipation capacity of the system under ultimate loads with little or no attention paid to the investigation of the elastic buckling of the wall that often occurs under relatively small shear force. The elastic buckling of the thin infill plates under service wind, or small and frequent earthquakes limits the wider application of unstiffened steel shear walls in buildings of high importance (e.g. the 74-story Jinta Tower in Tianjin, China). Concerns include the unpleasant elastic buckling sound under service loads, lower initial stiffness, and low yielding drift ratio (Lee et al. 2010; Nie et al. 2012). Although there have been examples that consider service-level performance according to the performance-based design philosophy (Lee et al. 2010), the U.S. Seismic Design Provisions (AISC, 2010 and AISC, 2016) imposes no explicit requirements on the building performance under serviceability conditions. Given the easy-to-buckle nature of thin unstiffened steel plates, satisfactory performance at the service level should be required for the steel plate shear wall system or evidence should be provided that the design procedure for the traditional SPSW system; new SPSW configurations could automatically satisfy the service-level performance goals.

2.4 Modelling of Steel Plate Shear Walls

2.4.1 Overview

Currently, the SPSW is modeled using the following methods: 1) strip model, 2) orthotropic membrane model, and 3) full finite-element model. Compared to the orthotropic modeling approach, which only works well for loading in one direction, and the full finite-element method, which is relatively time consuming and normally used in research to analyze system sub-assemblies that consist several panels, the strip model with appropriate hysteretic material properties for the strips (essentially a series of truss elements) is usually the preferred modeling approach for cyclic pushover or time history analysis for a multi-story buildings using a steel plate shear wall system. As a design tool, the strip model is relatively straightforward and can generally provide reliable results. However, especially in the preliminary design iterations, it can still be time-consuming because of the interaction between the strip inclination angle and the size of the boundary elements. An equivalent brace model, which replaces the infill plate to a single diagonal brace, is suggested by the Canadian seismic code for initial sizing of the infill plate. In the following, emphasis will be given to review of the simpler and more engineer-friendly analytical models, i.e., the strip model and the equivalent brace model.

2.4.2 Strip Model

Wagner first determined the angle of inclination for flat aluminum sheet metal girders in 1931 under the assumption that the web plate is very thin and the flanges are capable of carrying the lateral load from the tension field without distorting enough to disrupt the tension field distributions(Wagner 1931). Based on this work, Thorburn et al. (1983) re-derived the relationships of the angle of inclination and shear strength equations for the steel plate shear wall system neglecting the energy due to buckling of the plate as well as the shear within the framing members. At the same time, the strip model was developed, in which the infill plates are modeled by a series of pin-ended, tension-only strips. In the same year, Timler and Kulak refined the formulations, adding the bending strain energy of the boundary elements (mainly the boundary columns) to the formulation(Timler and Kulak 1983). The form of the equation has been adopted in the Canadian and U.S. seismic design codes (CAN/CSA S16-01, FEMA 450, AISC-341-05). Thorburn et al. (1983) also established the relationships for a partial tension field where the boundary column is assumed to be infinitely flexible. Many studies have reported reasonable match of the test results and the strip model results, e.g., (Behbahanifard et al. 2003; Caccese et al. 1993; Driver 1997; Elgaaly et al. 1993; Lubell 1997).

Elgaaly et al.(1993) used both finite-element models and strip model to predict the experimental results by Caccese et al.(1993). An empirically derived, hysteretic stress-strain relationship was derived for the strips (oriented in both directions) in order to capture the hysteretic cyclic behavior of thin steel plate walls. Kharrazi et al. (2008) proposed a modified plate-frame interaction model

for the analysis of shear and bending deformations and the resulting force-displacement relationship in an SPSW. A trilinear shear force-displacement diagram was proposed to include the point of buckling of the infill plate (Kharrazi et al. 2008). If the critical shear buckling is neglected for very thin panels, the derived equations for panel strength, stiffness and yield displacement reduces to those proposed by Thorburn et al.(1983).

The above mentioned early strip model involved equally spaced tension-only truss elements, normally with perfectly plastic or bilinear material properties. Later, several modified strip models were proposed, including the use of supplemental degradation elements (Driver et al. 1998a), multi-directional strip model (Rezai et al. 2000), compression strut and deterioration strip (Shishkin et al. 2009) or semi-empirical material and hysteretic models to better match with the available test data. Two of the modified strip models are illustrated in Figure 2.21. Other modification of strip models focused on the improvement of material properties of the strip elements (Choi and Park 2010; Driver et al. 1998a; Elgaaly et al. 1993; Elgaaly and Liu 1997; Purba and Bruneau 2015a; Sabouri-Ghomi and Roberts 1992; Webster 2013). Most of the hysteretic models mentioned herein were developed based on the force-deformation behavior of the entire web panel, except that Choi and Park (2010)'s and Webster(2013)'s models, which were developed based on the stress-strain behavior of a single finite-element of the panel.

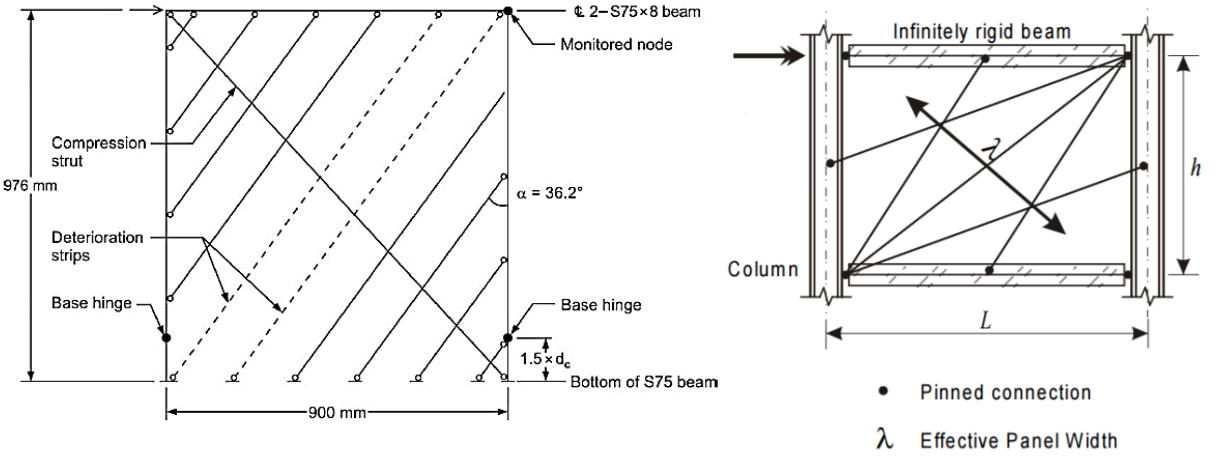

(a) Strip model with compression strut and deterioration strips by Shishkin et al.(2009)

(b) Multi-directional strip model by Rezai et al.(2000)

Figure 2.21 Examples of modified strip model

The material model proposed by Choi and Park (2010) was essentially based on an empirical relationship of the web plate elements observed from finite-element analysis. They have made several simplifications of the key points of the hysteretic model, including the tensile reloading stiffness and the two pivot points. The system model utilizing this material model for the strips appears to perform well in matching several test results. Webster (2013) also developed a new hysteresis model for the steel shear wall based on stress-strain responses observed in finite element

analysis. This model was shown to have some improvements in predicting the boundary column demands and story drifts compared with the existing *Hysteretic* material model in OpenSees analysis software (Filippou et al. 1983; McKenna et al. 2010). The deterioration model recently proposed by Purba and Bruneau (2015a) was developed for evaluating collapse performance of the SPSW system following the FEMA P695 methodology(FEMA-P695 2009). Their model was statistically quantified and calibrated based on a review of 36 SPSW specimens. More details of the hysteretic material models will be discussed in Chapter IV where an analytical model is proposed for the new steel plate shear wall system developed by the author.

Note that due to the significantly increased number of time steps and interactions in a nonlinear time history analysis, complicated material models do not always work well due to greater required computational effort and convergence issues. Simple models like the simple tension-only material model appear sufficient and provide a reasonable match to the dynamic test results (Lin et al. 2010), which may justify the use of simpler analytical models in response history analyses.

2.4.3 Equivalent Brace (EB) Model

The equivalent brace (EB) model was first proposed and recommended by Thorburn et al.(1983) for preliminary design purposes and is included in the Canadian standard CAN/CSA-S16. The inherent assumption of EB model is that all tension strips develop the same strain and can be replaced by a single diagonal truss member. The properties of the equivalent brace are related to the properties of the infill plate by matching the shear strength and stiffness of the equivalent brace to the original steel shear wall. Due to its simplicity, the EB model has also been commonly used in the analysis of SPSWs, e.g. (Tsai et al. 2010). However, certain phenomena cannot be captured by the EB model such as the tension field effects on the columns and the compression resistance of the panel near the corners. These concerns will be less of an issue if the infill panels are connected to the beam only since the column is no longer subjected to the distributed lateral tension field forces. The application of EB model for the proposed high-performance steel plate shear wall system will be discussed in Chapter IV.

2.4.4 Plate Girder Formulations

Plate girder analogy is commonly used to explain the load-resisting mechanism of a steel plate shear wall. There have been arguments that steel plate shear walls are different from plate girders mainly due to the difference in the strength and stiffness of the boundary elements in the two systems – the flange in a plate girder and the column in an SPSW. It was pointed out that in plate girders, the stiffnesses of boundary elements (the flange) are generally neglected due to their low in-plane stiffness, but the column stiffness in an SPSW significantly affects the angle of inclination of the diagonal tension field and its associated shear strength (Berman and Bruneau 2004). By isolating the infill panels from the boundary columns, the infill panel behavior is believed by the

author of this dissertation to be closer to that of a plate girder since the stiffness of the side stiffeners to be used on the two free vertical edges of the infill panel would be closer to that of a plate girder flange. This is especially true if the side stiffeners used are flat rectangular plates, i.e., they act similarly to the flanges of plate girders. Therefore, some of the important formulations for plate girders that are applicable to the new steel shear wall system developed in this dissertation are revisited to investigate possible application to the newly developed system.

The first ultimate load method capable of predicting the shear strength of conventional plate girders was proposed by Basler and his colleagues in 1960 (Basler 1961; Basler et al. 1960). They assumed that the flanges of plate girders were so flexible that they could not take the lateral load of the tension field. The failure mechanism was assumed to be the combination of the shear buckling of the web plate plus the membrane stress field. If neglecting the web plate buckling contribution, the formulation becomes very close to the partial tension field model proposed by Thorburn et al.(1983).

Evans, Porter and Rockey (1978 and 1987) pointed out that solutions based on Wagner's work were not suitable for applications in civil engineering for two reasons: the significant distortion of the flange would affect the extent and nature of the web plate membrane field, and it might be too conservative. In their assumed collapse model, the flanges of plate girders take a certain portion of the lateral loading imposed by the inclined tension field by forming plastic hinges. The ultimate failure mechanism is a result of combined effect of web buckling (simply supported plates) and tension field yielding plus the development of the plastic hinges in the flanges (Evans et al. 1978; Porter et al. 1987; Rockey et al. 1978). More details of these plate girder formulations will be discussed in Chapter IV.

2.5 Design of Steel Shear Wall System

Several main design approaches for the steel plate shear wall system are briefly reviewed in this section, including the code-based strength design, performance-based plastic design, displacement-based design and design of the system using inelastic fuse philosophy.

2.5.1 Code-Based Strength Design

The basic design philosophy provided in the Canadian and U.S. seismic design codes are primarily strength-based: the infill walls are initially sized to carry the entire code-specified lateral forces, a capacity design concept is then applied for selecting the boundary beams and columns, and the system is checked in later stages against the drift limitations before moving on to connection designs. Design Guide 20(AISC 2007) contains detailed examples that implements the code-design procedure.

Bruneau and his research associates proposed a plastic design method for the SPSW system, and studied many other code-based design aspects of the steel plate shear walls, such as the capacity design method for the boundary column, how to avoid in-span hinges in the boundary beams and the method to reduce the system over-strength by using the balanced design concept (Berman and Bruneau 2003; Berman 2011; Berman and Bruneau 2008; Purba and Bruneau 2015b; Qu and Bruneau 2009). By using the proposed plastic and capacity design methods, it was shown that the behavior of the SPSW system could be improved.

Currently, no explicit requirement for the service-level performance is included in the AISC Seismic Provisions (AISC 2016). Engineers are allowed to select and verify the service-level performance goals under the performance-based design guidelines, such as the guideline by the PEER Tall Building Initiative (PEER 2010) and Los Angles Tall Building Structural Design Council (LATBSDC 2015).

2.5.2 Performance-Based Plastic Design

Since the code-based design focuses on strength, inelastic displacement demands are not directly considered. Kharmale and Ghosh (2013) have pointed out several limitations of the strength-based design:

(1) The strength-based approach does not explicitly include the inelastic behavior, which is incorporated implicitly by the response modification factor, *R*;
(2) These design guides do not provide specific design equations to attain the specified desirable yielding mechanism (Purba and Bruneau 2011), especially for the boundary beams and columns in the SPSW system; and
(3) These standards do not provide enough leeway for designers to choose a specific yielding hierarchy or failure mechanism.

Kharmale and Ghosh (2013) proposed a performance-based plastic design method for steel plate shear walls with rigid beam-to-column connections, where a specific ductility demand and a preferred yield mechanism are chosen as the performance target (Kharmale and Ghosh 2013). Before this work, Ghosh et al. (2009) proposed a ductility or displacement-based design methodology for SPSW systems with simple beam-to-column connections. They considered the target displacement ductility ratio and pre-selected yield mechanism with inelastic energy balance concept in the formulation. Plastic design is performed to detail the frame members and connections to achieve the target ductility ratio and yield mechanism (Ghosh et al. 2009). These studies all have roots in the performance-based plastic design (PBPD) concept, which was first developed at the University of Michigan (Goel and Chao 2008). In this method, the design base shear for a selected hazard level is determined by matching the work needed to push the structure monotonically up to the target drift to the work required by an equivalent single-degree-of-freedom (SDOF) to achieve the same state. There are several applications of the PBPD method in different

systems, two examples are the application in moment resisting frames (Lee et al. 2004) and eccentrically braced frame (Chao and Goel 2005).

2.5.3 Direct Displacement-Based Design

Another performance-based design concept is termed the direct displacement-based design (DDBD) approach. It has been advocated as a more rational and relevant approach compared to traditional strength-based design methods (Kowalsky et al. 1995; Moehle 1992; Priestley 1993; Shibata and Sozen 1976). This method was first introduced by Priestley in 1993. Subsequently, considerable research of this method was conducted in Europe, New Zealand, and North America. The fundamental philosophy of DDBD is that "structures should be designed to achieve a specified performance level, defined by strain or drift limits, under a specific level of seismic intensity" (Priestley et al. 2007). The idea of incorporating a specific ductility/drift goal is very similar to that in the PBPD methods. Applications of this approach in many structural systems are available; examples include frame buildings such as Concentrically Braced Frame (Salawdeh and Goggins 2016), wall buildings, bridges, seismically isolated structures and systems using passive energy-dissipation devices (Lin et al. 2003). A review of limitations and performances of different displacement-based design methods are provided in (Sullivan et al. 2003). However, as Chopra and Goel (2001) pointed out, the DDBD that uses elastic design spectra for equivalent linear systems based on the secant stiffness or its variations tends to underestimate the deformation and ductility demands, and may lead to an erroneous impression that the allowable plastic rotation constraint has been satisfied (Chopra and Goel 2001). In their paper, the inelastic design spectra method is promoted.

Since both the PBPD and DDBD design approaches involve the use of the equivalent SDOF system and, more importantly, modification of design lateral forces, it is difficult to incorporate these approaches into the strength-based design frameworks. While being more rationale and performance-oriented, these two methods will not be directly applied in the developed design procedure for the new high-performance steel plate shear wall system proposed and developed in this dissertation.

2.5.4 Design of Dual System

The steel plate shear wall system can be viewed as a dual system consisted of the steel infill wall and the surrounding moment frame. The infill plate can also be viewed as a structural fuse instead of a pure lateral force-resisting element. Vargas and Bruneau proposed a general procedure for designing new or retrofitted structures with metallic fuses, which should be disposable and easy to repair, while the main structure is designed to remain elastic or have only minor inelastic deformations. The proposed procedure was based on a parametric study of several nonlinear SDOF systems subjected to synthetic ground motions. A range of stiffness and strength ratios of the fuse to the surrounding frame were also suggested in their work (Vargas and Bruneau 2009a; Vargas

and Bruneau 2009b). Segovia and Ruiz (2016) also studied the best values of the stiffness ratio and strength ratios, but based their study on parametric studies on an 8-story building consisted of Buckling Restrained Braces in a moment frame (Segovia and Ruiz 2016). The recommended ranges of stiffness and strength ratios are of comparable magnitude with the values suggested by Vargas and Bruneau (2009a). A similar elastic stiffness ratio between the moment frame system and the whole structure is obtained based on the study of low- to medium-rise regular reinforced concrete moment resisting braced frames (RC-MRBFs) with hysteretic energy dissipation devices mounted on chevron steel bracing (Tena-Colunga and Nangullasmú-Hernández 2015). These design recommendations for dual systems have been found useful for the new high-performance steel plate shear wall system developed in this dissertation and will be discussed further in Chapter V.

2.6 Concluding Remarks

This chapter reviewed three main components of the steel plate shear wall (SPSW) system: the system configuration and behavior, analytical modeling, and the design approaches for the system. Benchmark research on SPSW was reviewed followed by a discussion of recent research efforts in solving the issues of the unstiffened SPSWs – including both active and passive methods to eliminate or reduce the tension field action acting on the columns, the use of more cost-effective beam-to-column connections, and the need for more explicit service level performance goals.

With the purpose of developing the proposed new SPSW system, reviews of the modeling and design approaches focused on those factors that are relevant and useful for the proposed new system. In particular, the strip model and equivalent brace model for SPSWs were reviewed in detail, as are several plate girder collapse mechanisms.

A number of design approaches, including strength-based code design and performance-based and displacement-based design, were reviewed and briefly discussed. Although the above-mentioned design approaches may not be fully utilized in the later proposed system design procedure, some important concepts of these methods still shed some light on the decision-making process.

Chapter III

Gusset Plate Moment Connection

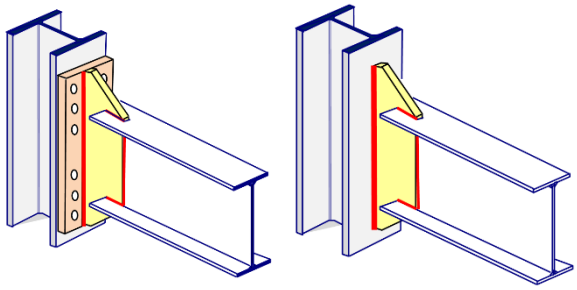

This Chapter presents the development effort of the new Gusset Plate Moment Connection (GPMC). The concept of GPMC was initially inspired during the process of developing the High-Performance Steel Plate Shear Wall (HPSPSW) System that aims to resolve the performance issues of the current Steel Plate Shear Wall system identified in Chapter I. A cost-effective and well-behaved moment connection is desired to maximize the economy of the steel plate shear wall system. Fabrication costs are particularly considered in the early conceptual development. After analyses of the High-Performance Steel Plate Shear Wall (HPSPSW) system produced very promising results on its seismic performance, it was decided to develop this moment connection as a ductile moment connection for use in other systems, especially in steel moment frames, independent of steel shear wall systems. Initial studies on the effects of various geometric parameters on the behavior of the proposed Gusset Plate Moment Connections (mainly for shallow beam sections that can be used in steel shear wall systems) can be found in Appendix C and in Qian and Astaneh-Asl (2016c). This chapter aims to (1) provide a summary of the key features of the proposed new GPMC connection; (2) investigate the effects of various design parameters on the behavior of the GPMC using typical moment frame beam sections; (3) examine a simplified connection modeling method; and (4) propose a design procedure for the new GPMC.

3.1 Introduction

Steel moment frames are widely used in buildings subjected to lateral loads due to wind and earthquakes. Many different types and details of moment connections are available based on the severity of the imposed loads. In the U.S., moment connections are categorized into (a) Wind and Low Seismic Applications and (b) High-Seismic Applications (has a higher ductility demand).

The 1994 Northridge earthquake caused damage to a large number of field-welded steel moment connections in modern steel buildings in Los Angeles, and led to extensive research activities that

facilitated significant changes in the design of steel moment connections. As summarized by Mahin (1998), the efforts after the 1994 Northridge earthquake to modify and retrofit damaged pre-Northridge field-welded steel moment connections were aimed at relocating the plastic hinge in the girder away from the face of the column, where most of the observed damages were located (e.g., at the beam-to-column connection groove welds or the areas of the beam and/or column adjacent to the welds). A survey of moment frame buildings affected by the 1994 Northridge earthquake was done by Bonowitz and Youssef (1994). To force the plastic hinge to form in the beam instead of in the connections, two main approaches were chosen: (1) strengthening the connection, and (2) reducing the beam section. The repair and retrofit efforts following the "strengthening" approach included adding cover plates to beam flanges, adding side plates to beams, connecting beam flanges to the columns using vertical fins or haunches, or adding knee braces (Anderson and Duan 1998). The beam-weakening approach focused on the reduction of the area of the beam flanges by cutting the width of the flange (Englehardt et al. 1997), or by drilling holes in them (Yang and Popov 1995).

Reviews of the approaches and testing programs for the modification of the existing welded steel moment frame connections can be found in FEMA-267 (1995), FEMA-289 (1997), and FEMA 355D-E (2000). The main goal of moving the plastic hinge away from the column face was to prevent premature fracture that is likely to occur at the column face due to: potential weld defects, stress concentrations at the weld access holes, high levels of restraint and the associated tri-axial tension state, stress concentrations due to column flange bending, and uncertain column flange through-thickness properties (Engelhardt and Sabol 1998). Moving the plastic hinge away from the column towards the mid-span of the beam, however, increases the plastic hinge rotation demands (a ductility concern) as well as the bending moments acting on the column face (a strength concern for the welds). The increased bending moments acting on the column face compared to the beam plastic hinge may result in significant demands on the column panel zone; in most cases this would require the use of horizontal continuity plates, which is relatively costly (Mahin 1998). The increased bending moment acting on the column creates larger shear forces in the panel zone, which sometimes requires the use of doubler plates, another costly strategy.

In 2000, the SAC Joint Venture on behalf of the Federal Emergency Management Agency (FEMA) released the findings and recommendations of this research effort in a series of Recommended Design Criteria documents. These reports addressed the issue of seismic performance and design of moment-resisting steel frame structures (FEMA-355A 2000; FEMA-355B 2000; FEMA-355C 2000; FEMA-355D 2000; FEMA-355E 2000; FEMA-355F 2000), and a series of recommendations were made to improve the connection design and performance in high-seismic applications. During the period of 1994–2000, while efforts were underway to find solutions to the problem of unsatisfactory seismic performance of welded steel moment connections, bolted moment connections, especially top-and-bottom bolted plate moment connections (Astaneh-Asl 1995) gained popularity; many welded steel moment connections in buildings under construction were converted to this type of bolted connection.

The SAC project also resulted in the development of several "Prequalified Steel Moment Connections"(AISC 2010b), which were validated by analysis and tests. The prequalified connections have necessary strength, stiffness, and, especially, the rotational ductility to be used by designers without any further testing. Figure 3.1(a) shows the welded steel moment connection widely used in the US. before the 1994 Northridge earthquake. The connection is now called the Pre-Northridge connection. Figures 3.1(b), 3.1(c), and 3.1(d) are examples of pre-qualified post-Northridge moment connections that are currently used in *High Seismic Applications.* Many of the popular welded flange steel moment connections shown in Figure 3.1 require the use of field Complete Joint Penetration (CJP) welds, which require onsite ultrasonic sound testing to assure their integrity, a costly and time-consuming fabrication detail.

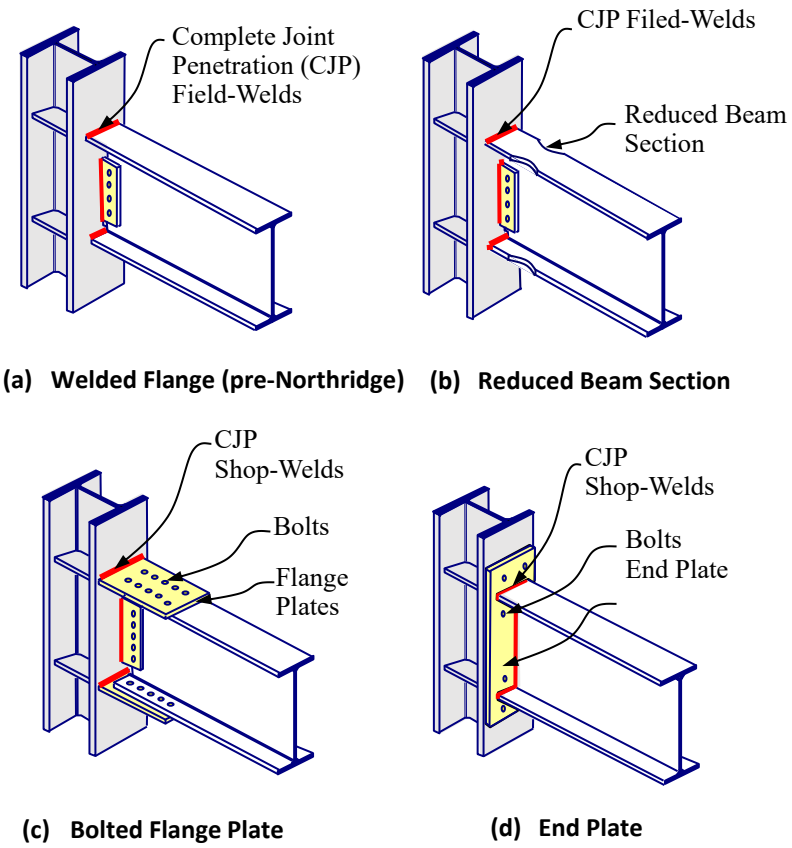

Figure 3.1 (a) Pre-Northridge low ductility steel moment connection, (b) through (d) examples of post-Northridge ductile Pre-qualified moment connections

The new GPMC proposed and developed in this dissertation targets a new economical and high-performance special steel moment connection that reduces or, in many cases, even eliminates the costly fabrication details, such as the field CJP welds, doubler plates, and continuity plates, while still maintaining the satisfactory stiffness, strength and ductility performance of the connection. The remainder of this chapter introduces the main components and characteristics of the proposed GPMC in details, followed by parametric studies conducted to quantify connection behavior and

provide input to design procedure development. Then, a rotational hinge model proposed for the GPMC is discussed. The last part of this chapter provides a design procedure for the new GPMC.

3.2. The Proposed New Gusset Plate Moment Connection (GPMC)

3.2.1 Main Components

Figure 3.2 shows the main elements of the new Gusset Plate Moment Connection (GPMC). The connection has two versions: welded and bolted. In the welded version, the gusset plate is shop-welded to the column flange, and the beam is then field-welded to the gusset plate. The field-welds are either fillet or Partial Joint Penetration (PJP) welds. For some very heavy beams, these welds would be Complete Joint Penetration (CJP) welds. In the bolted version, the "Tee" shaped gusset connection can be either fabricated by shop-welding a flange plate to the gusset plate to form a "T" section, or the "T" shaped gusset connection can be directly cut from a hot rolled W or WT section. The flange of the "T" will be referred to as the "gusset flange" in the remainder of this chapter. The "T" shaped gusset is proposed to be shop-welded to the beam, and the gusset flange is bolted to the column flange in the field.

Both the welded and bolted versions of the proposed new GPMCs have five separate elements: (1) Gusset Plate, (2) Beam, (3) Column, (4) Gusset-to-Column Connection, and (5) Beam-to-Gusset Connection. These elements will each be discussed in detail in the following sections.

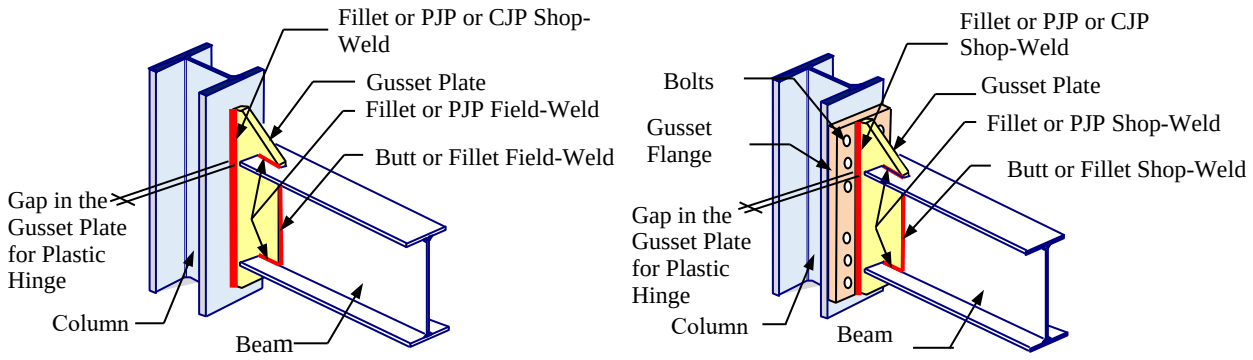

(a) Welded Version of the New Gusset Plate Moment Connection

(b) Bolted Version of the New Gusset Plate Moment Connection

Figure 3.2 (a) Welded, and (b) bolted versions of the new Gusset Plate Moment Connection

3.2.1.a. Gusset Plate

The gusset plate in the new GPMC is a vertical flat plate in the plane of the column and beam web. It is mainly subjected to bending and shear and a small amount of axial force. The plastic hinge formation is expected to occur primarily due to in-plane yielding of the gusset plate. The gusset

plate is designed to yield within a pre-designated area – the area between the face of column flange and end of the beam (Figure 3.2) – and this area is the only inelastic region of the connection. The gusset plate, being the only element of the connection that yields and dissipates energy, acts as a "fuse," and protects all other elements of the joint such as the beam, column, welds, and bolts, which are designed to remain essentially elastic during the seismic events.

The gusset plate is designed to have sufficient bending capacity to resist the moments due to all load combinations required by applicable building codes (ASCE 2010; ASCE 2016; IBC 2015). The plastic hinge area of the gusset plate is designed to be ductile enough to accommodate the rotation demand of the connection. The gusset plate is also designed to have sufficient rotational stiffness to keep the story drifts under the limits specified by the seismic design codes (AISC 2010c; AISC 2016). The main parameters in the design of gusset plates are its depth and thickness, the gap between the end of the beam and the face of the column, and the material of the gusset plate. The effects of these variables on the strength, stiffness, and ductility of the proposed GPMC will be discussed later in this chapter.

3.2.1.b. Beam

With the gusset plate acting as the ductile fuse in this connection, the beam is expected to remain essentially elastic during the seismic event, one of the main advantages of the proposed new connection compared to other steel moment connections; this includes all prequalified connections currently in use as all of them have the plastic hinge form in the beam. The beam in the proposed GPMC is designed to satisfy the gravity load strength demand and the lateral load stiffness demands.

3.2.1.c. Column

Again, because the gusset plate acts as the ductile fuse and is located close to the column face, similar to the beam, the column is expected to remain essentially elastic with only limited column web yielding. Here, the column is subjected to the plastic moment capacity of the gusset plate instead of the beam. The smaller plastic moment capacity of the gusset plates compared to that of the beam (as will be shown later is about 60~80% of beam plastic moment capacity) often leads to minimum yielding of the column web and thus reduces the need for doubler plates for most cases. Also, in the proposed connection, there is no direct connection between the beam flange and the column flange; therefore, it is less likely that stress concentration, distortion and kinking of the column flanges, or column web local yielding, column flange local buckling and web crippling due to concentrated beam flange force will occur as is the case in other welded flange moment connections. In the proposed GPMC, rarely is there a need for continuity plates in the column web. Figure 3.3 shows a comparison of an exterior beam-to-column connection using a typical welded flange connection and the proposed GPMC. At the same drift ratio, the welded flange moment connections, either with or without continuity plates, show larger column web yielding and deformation at the beam-to-column connection region compared to the GPMC. This simple

comparison demonstrates, theoretically, that there is a reduced demand for doubler plates and continuity plates in a GPMC. In this case, the column is designed to remain elastic and resist the combined effects of gravity and lateral loads as well as to provide stiffness to the frame.

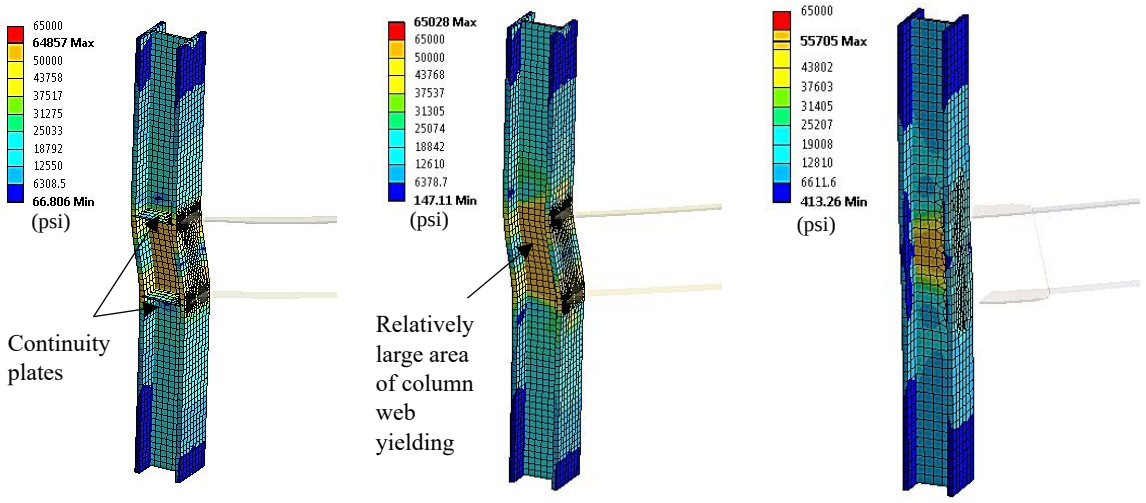

(a) Welded flange connection with continuity plate **(b) Welded flange connection without continuity plate** **(c) GPMC designed for nominal yielding strength of beam without continuity plate**

Figure 3.3 Comparison of the column deformation and column web yielding between the welded flange beam-to-column connection and the proposed GPMC (drift ratio = 0.04, scale factor = 5)

Note that the requirements for doubler plates and continuity plates in the current seismic design code (AISC 2010c; AISC 2016) are closely related to the beam flange-to-column flange connection and the moment demand at the column face: (1) the beam flange applies concentrated force, causing stress concentration in the web of the column behind the column flange, which in turn lead to column web local yielding and crippling; (2) the shear in the panel zone depends on the moment couple at column face projected by the plastic hinge capacity brought in by the beam flanges; and (3) the thickness of the column web continuity plate also depends on the width and thickness of the adjacent beam flanges.

Without the direct connection of the beam flange to the column flange, and also the "weak gusset" design philosophy, the above listed issues in current moment connections and the corresponding requirements are no longer compulsory. While the above reasoning explains how the use of doubler plates and continuity plates can be minimized or eliminated in most cases for welded GPMC, the need for these two elements shall not be completely ruled out. For both welded and bolted option, column web failure might still occur if the column web is much weaker than the in-coming gusset plate. Therefore, checking the adequacy of the column is still included in the proposed design procedure for the new GPMC.

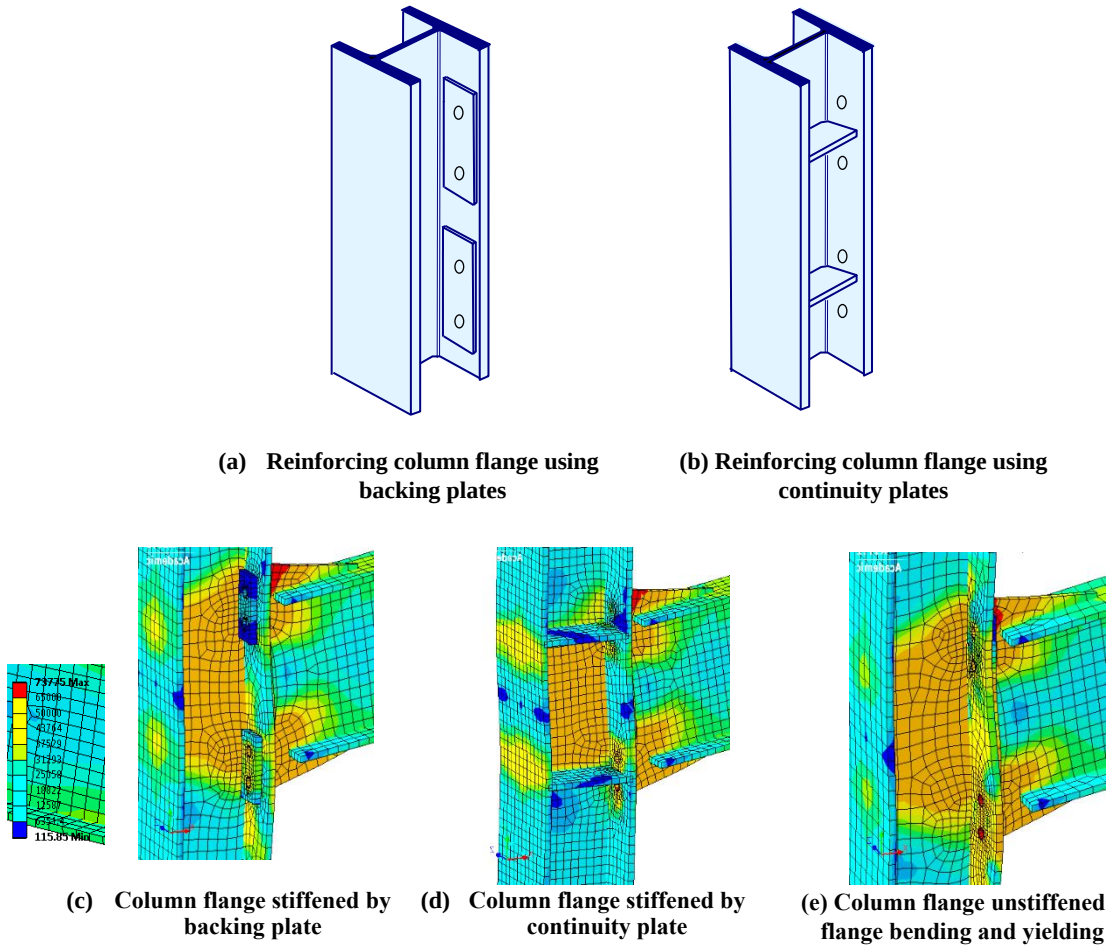

(a) Reinforcing column flange using backing plates

(b) Reinforcing column flange using continuity plates

(c) Column flange stiffened by backing plate

(d) Column flange stiffened by continuity plate

(e) Column flange unstiffened – flange bending and yielding

Figure 3.4 Illustration of a simple column flange strengthening method (drift ratio = 0.04, scale factor = 5)

For the bolted GPMCs, the flexibility of the column flange together with the gusset flange plays an essential role in the ultimate failure modes of the connection. Because column flange bending could occur in relatively thin column flanges, similar to the case of an end-plate moment connection, some form of reinforcement might be required. One of the common ways to reinforce flexible column flanges has been the use of continuity plates, which also helps to increase the ductility of the panel zone. A simpler reinforcing technique is available: adding bolted backing plates; see Figure 3.4(a).

To compare the effect of adding the backing plate and continuity plate, a simple exercise was done on a W21×83 beam-W14×112 column with a 4-bolt gusset flange connection. The thickness of the backing plates used was 1 in, which is close to the column flange thickness. This thickness may not be optimal and is used here for demonstration purposes only. After adding the backing plate, the level of deformation of column flange was reduced [Figure 3.4(c)], and, more importantly, yielding of the column flange in the originally unreinforced design [Figure 3.4(e)] was almost eliminated. Adding backing plates is a straightforward and less-costly solution, according to Horne and Morris (1982) p. 187, as – "such stiffeners require minimal fabrication." In addition, the

backing plate method is applicable for both new and retrofit constructions due to the simplicity and minimum welding requirement. A third case using the continuity plate is also provided as a reference [Figure 3.4(d)]. The thickness of the continuity plate is equal to that of the beam flange and located at the same level as the beam flange. In this case, the column local in-ward bending was significantly relieved, and the column flange yielding problem was also solved. This analysis demonstrates that both reinforcing methods can be effective and using continuity plates is not the one and only method to resolve the problem of local column flange bending.

3.2.1.d. Gusset-to-Column Connection

The gusset plate to column connection in the proposed GPMC can be either welded or bolted as shown in Figure 3.2. In the welded version, the welds can be either fillet welds or PJP welds. Complete Joint Penetration (CJP) welds might be needed if a relatively thick gusset plate is used. However, the proposed fabrication sequence is such that the gusset plate is welded to the column in the shop, assuring better quality control and reducing the cost of fabrication. More importantly, the cost of field ultra-sonic testing required for field-CJP welds for other moment connections can be reduced by performing these tests in the shop. The welds simply need to be sufficient to develop the expected strain hardened capacity of the gusset plate material next to it.

For the bolted option, the gusset flange plus gusset plate assembly can be either fabricated in the shop, using fillet, PJP, or CJP welds, to form a “T” section or be cut from a rolled wide flange or a WT section. The beam plus gusset and gusset flange are then bolted to the column flange in the field, which is a relatively easy and low-cost operation. Appropriate gusset flange thickness and bolts should be used to resist the expected strain-hardened moment capacity of the gusset plate. The bolts and gusset flange thickness can be designed similar to a T-hanger. “Upset” bolts are recommended to avoid brittle fracture of bolts under combined tension and shear, which have been used for decades in bridge engineering as tension anchor rods. In these bolts, the shank of the bolt has a smaller diameter than the threaded part, resulting in tension yielding of the unthreaded shank area to be the ductile governing failure mode, preventing the threaded area to fail in a brittle manner.

3.2.1.e. Beam-to-Gusset Connection

In the configuration shown in Figure 3.2, the beam flange needs to be slotted, part of beam web needs to be cut, and the beam is then connected to the gusset plate by fillet or PJP welds or, in rare and large connections by CJP welds.

In the welded version shown in Figure 3.2(a), since the beam is welded to the gusset plate in the field, a gap will be left at the end of the slot, creating a net section in the beam. The bolted version, which connects the beam to the gusset plate in the shop, will not have the same net section issue. Unlike the case of HSS braces in Special Concentrically Braced Frames, where the brace itself is the inelastic ductile fuse and cannot have a net section failure mode, the beam in the welded GPMC

is an elastic element of the system and is thus much less critical, even with a net section at the end of the slot.

In the following parametric study, if not otherwise stated, the nominal yield-moment capacity, $M_{yb}= S_{bx} F_{yb}$, of the beam was conservatively designed to be greater than the "expected strain-hardened" plastic moment capacity of the gusset plate, i.e., $M_{prg} = C_{prg} R_{yg} F_{yg} Z_{gx}$. If the gusset plate is not too thick, the bending capacity of the net section of the beam, $F_{ub} Z_{bnet}$, will be greater than M_{yb}; thus, there is almost no possibility of fracture of the net section of the beam. Also, if one considers the relatively short length of the gusset plate plastic hinge, the bending moment along the net section of the beam would not be significantly larger than M_{prg}. By ensuring the net section capacity of the beam is larger than M_{prg}, in most cases net section fracture will not govern.

Figure 3.5 shows two other viable options for connecting the beam to the gusset plate. In these options, instead of having the slots in the top and bottom flanges of the beam, two slotted top and bottom flange plates are welded to the gusset plate in the shop and then the top and bottom flange plates are either field-bolted [Figure 3.5(left)] or field-welded [Figure 3.5(right)] to the beam flanges. Again as before, the components of these gusset-to-beam connections are designed to remain elastic throughout the cyclic loading and have a yield strength greater than the "expected, strain-hardened " plastic moment capacity of the gusset plate, M_{prg}. The details shown in Figure 3.5 were originally presented by Astaneh-Asl, Cochran, and Sabelli for gusset plate connections of Steel Special Concentrically Braced Frames (Astaneh-Asl et al. 2006).

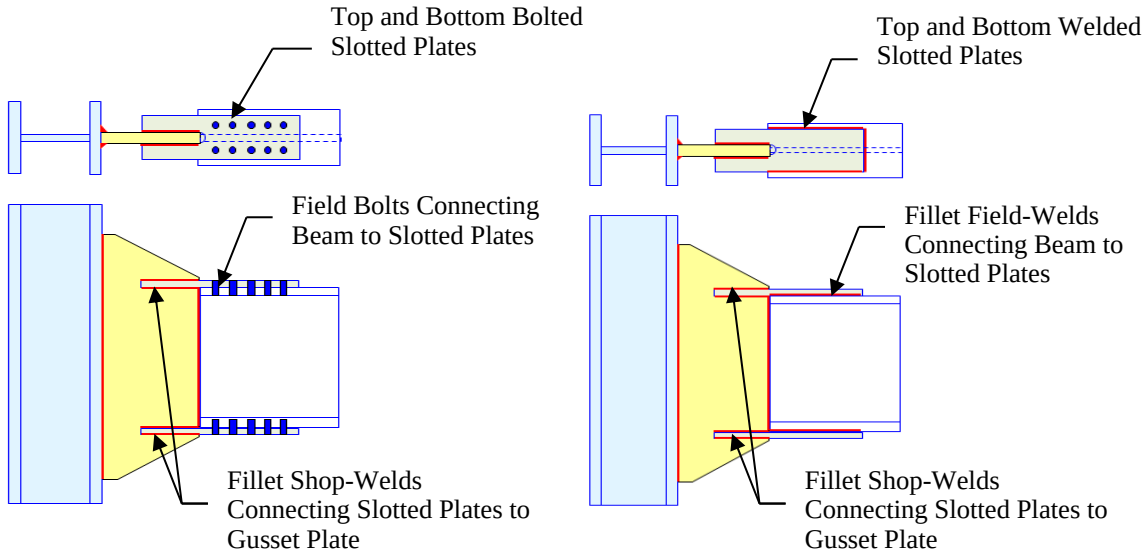

Figure 3.5 Two viable alternatives for beam-to-gusset plate connection details

3.2.2 Design Philosophy

The design philosophy for the proposed GPMC is similar to that of a Reduced Beam Section (RBS) prequalified connection: to provide a plastic hinge fuse that is weaker than the plastic moment capacity of the beam at a pre-determined location to protect all other components of the system from yielding, buckling, and fracture. What makes the proposed GPMC so advantageous is that this "fuse" is no longer in the beam but in a separate gusset plate element, making the "strong-column–weak-beam" criteria no longer required. Instead, "strong-column–weak-gusset" and "strong-beam–weak-gusset", or to be simpler, "strong-frame–weak-gusset" philosophy becomes a viable alternative, providing much more leeway to the designers for the selection of beams and columns (Table 3.1). Since the beams and columns in moment frames are usually controlled by the stiffness requirements to limit drift, their strengths are normally much larger than what is required by equivalent lateral forces. Therefore, although gusset plates would have smaller moment capacities, satisfying the strength requirements will not be an issue in most cases. At first sight, the new GPMC looks very similar to a stiffened end-plate moment connection, which also has triangular plates extending above the beam depth. However, the gap between the beam and the column face in the GPMC and the fact that the plastic hinge forms in the gusset plate instead of in the beam, is a key factor that makes the GPMC fundamentally different from a stiffened end-plate moment connection.

As mentioned before, the approach to move the plastic hinge away from the column face is mainly to avoid premature connection failure; this may increase the rotational ductility demand for the plastic hinge as well as increase the bending moment strength demands at the column face. In the proposed GPMC, the plastic hinge fuse is in the gusset plate between the end of the beam and face of the column. Due to the simple connection detail and less complicated stress paths, the proposed GPMC is less likely to suffer premature connection failure while it imposes less demand on the column.

Table 3.1 Differences between the new GPMC and commonly used existing moment connections

Moment connection type	Is the beam directly welded to the column?	Plastic hinge location	Need to satisfy "strong-column–weak-beam" criteria
Gusset Plate Moment Connection (GPMC)	No	In the gusset plate	No (but the need to satisfy "strong-frame–weak gusset" criteria)
Stiffened End-Plate (EP) Connection	No	In the beam	Yes
Moment Connection with Top and Bottom Brackets	Yes	In in the beam	Yes
Reduced-Beam Section (RBS) Connection	Yes	In the reduced area region in the beam	Yes
Bolted-Flange Plate (BFP) Moment Connection	No (but the flange plate is welded to the column)	In the beam	Yes
Welded Unreinforced Flange-Welded Web (WUF-W) Moment Connection	Yes	In the beam	Yes

3.2.3 Advantages

The main features and advantages of the proposed GPMC are summarized below:

- Plastic hinge forms in the gusset plate, providing sufficient strength and rotational stiffness and ductility;

- "Strong-column–weak beam" criterion does not need to be satisfied: instead, "strong frame (strong beam and strong column)–weak-gusset" criteria should be satisfied to ensure plastic hinge forms and remains in the gusset plate, while the column, the beam and all welds, bolts and connection elements remain essentially elastic;

- Continuity plates in the column are not needed in most cases as there is no direct connection between the beam flange and the column flange, reducing the possibility of localized deformation of column flange and column web crippling and buckling;

- Column web doubler plates are not needed in most cases since with the "strong frame - weak gusset" design philosophy, yielding in the column web is very limited;

- The beam does not need to be compact with *b/t* ratio of "high-ductility" since the beam is designed to remain essentially elastic;

- The CJP groove welds in this connection are fabricated and tested by ultrasonic sound in the shop. This is an advantage compared to the other currently available steel welded moment connections, where the CJP welds are done and inspected in the field. Field CJP welds not

only result in additional costs but also pose restrictions on such field operations in low-temperature and windy days;

- With the gusset plate as a vertical flat plate, the proposed GPMC finds a broad range of applications in various gravity and lateral force-resisting systems. It is suitable for application not only in *special ductile steel moment frames* but also in *steel plate shear wall systems* and *dual systems* consisting of moment frames and concentrically braced frames. An example of an application in the new high-performance steel shear wall system proposed in this dissertation and Qian and Astaneh-Asl (2016b) is shown in Figure 3.6(a). Figure 3.6(b) shows a possible application in dual systems.

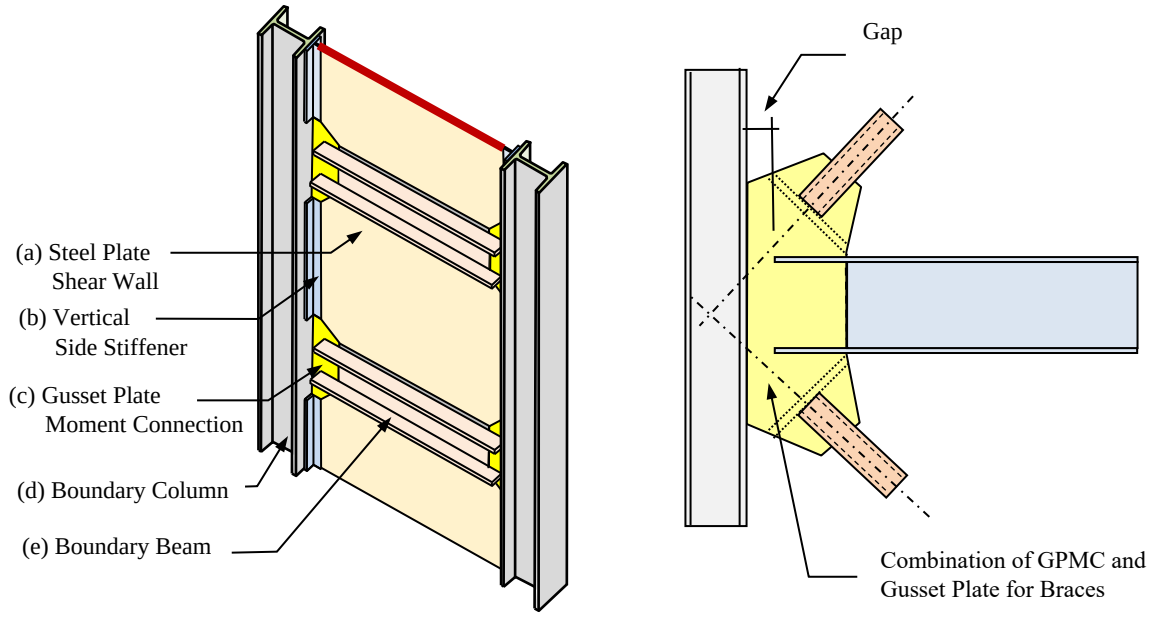

(a) Application in the New High-Performance Steel Shear Wall Developed by the Authors

(b) Application in a Dual System of Concentrically Braced Frame plus Moment Frame

Figure 3.6 Example applications of the new GPMC in other lateral force resisting systems

3.3 Behavior of the New Gusset Plate Moment Connection

3.3.1 Finite-Element Modeling

Four-node SHELL181 element in the ANSYS element library (ANSYS 2013) was used to model all components in the beam-to-column connection subassemblies. The material model for the steel material was plasticity with multi-linear kinematic hardening model with the equivalent stress-equivalent strain relationship defined by the Ramberg-Osgood relationship. Although fracture is

not explicitly included in the modeling, the fracture tendency was closely monitored by the magnitude of equivalent plastic strain (PEEQ).

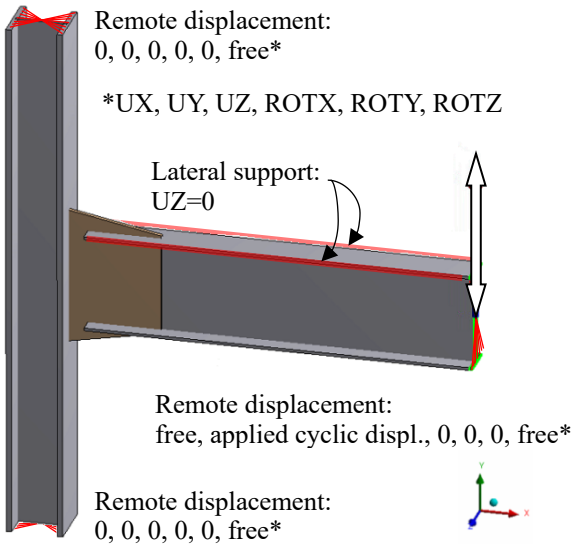

(a) Boundary conditions used in the parametric studies of GPMC

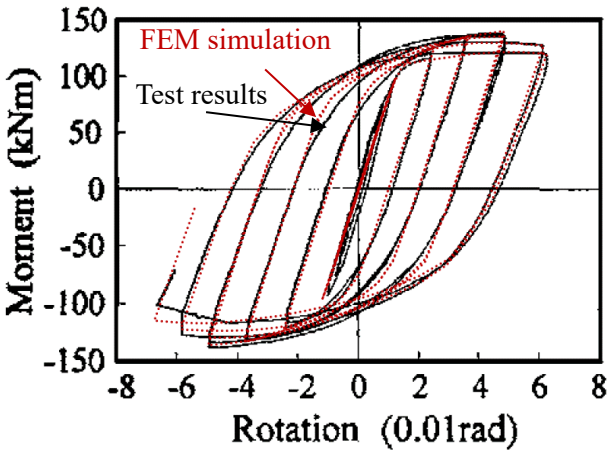

(b) Comparison of finite element and test result for an end-plate moment connection (Specimen S3 by Guo et al., 2006)

Figure 3.7 Boundary conditions used in the GPMC finite element model and the validation of finite element model using the stiffened extended end-plate moment connection test results

For the bolted GPMC, the bolts were modeled by simple *beam connections* in ANSYS with bilinear kinematic hardening material model matching the properties of the bolt material. The *beam connections* connect the edge of the bolt holes in the column flange (reference geometry) and the edge of the bolt holes in the gusset flange (mobile geometry). The beam connector is essentially a beam element (BEAM 188 in ANSYS element library) between the mobile/reference geometry. Effects of detailed bolt failure modes like shank tearing or nut stripping reported in many experimental studies (D'Aniello et al. 2016) were not included, nor the bolt slippage and bolt-hole elongation. Friction contact (coefficient of friction = 0.2) was assigned between the gusset flange and the column flange with the shell thickness effect considered. By using the simplified beam connector bolt model, the pretension effect, tensile, and shear capacity of bolts can be relatively well captured, which is considered sufficient to study the effects of bolt configuration and gusset flange thickness on the global connection behavior. Using simple beam connector model is also more computationally efficient for experimenting different connection configurations in the development process.

The boundary conditions adopted are shown in Figure 3.7(a). Geometrical imperfection for the connection subassembly was included using the first elastic buckling mode of the system (gusset plate buckling in the case of GPMC) with a peak magnitude equal to 0.1% of the beam length. A comparison between the hysteresis loop using the simplified bolt modeling technique and one

stiffened-end plate moment connection test result (Guo et al. 2006) is shown in Figure 3.7(b). The first buckling mode for chosen specimen is the buckling of beam flanges. Due to the simplification of the bolt modeling and the fact that nut was not explicitly modeled, the initial stiffness was slightly underestimated, but the overall behavior is reasonably close to the test result.

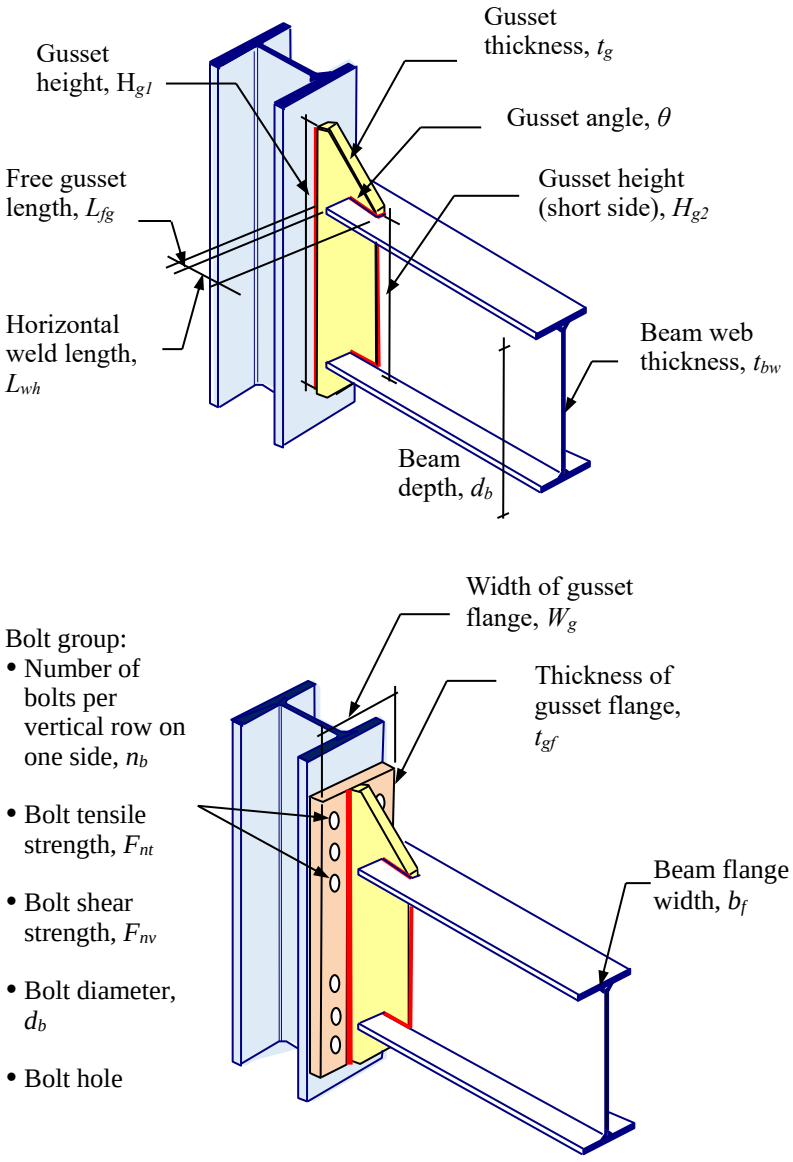

Figure 3.8 Main design parameters for the welded and bolted GPMC

For the studies summarized in the remainder of this chapter, typical beam and column sections that are commonly used and tested in the SAC projects (FEMA-355D 2000) were selected. A typical exterior beam-to-column subassembly was modeled assuming a floor height of 3.66 m (12 ft) and a beam span of 6.1 m (20 ft). The cyclic loading used in the inelastic analysis of the models conforms to the AISC moment connection testing requirements given in Chapter K of the AISC Seismic Provision (AISC 2010c). Figure 3.8 illustrates the critical design parameters that affect

the connection behavior. Except for the study on the design of gusset flange and bolts for bolted GMPC, other parameters were investigated using the welded GPMC configuration for ease of analysis. Lateral supports were provided along the top flange of the beam to represent the slab bracing effect, but the actual slab was not included at this stage nor its impact effects. The presence of slab could be beneficial to prevent the buckling of thin gusset plates. The exact effects are worth further research in the future.

If not otherwise stated, the gusset plate geometry (free gusset length, gusset plate thickness, and gusset plate geometry) follows the key findings of the preliminary studies of the connection detailed in Appendix C: (1) The gusset plates are designed to be weaker than the beam; (2) the gusset thickness, t_g, is equal to 1.25 times the beam web thickness, $t_{bw,}$; (3) the gusset height, H_{g1}, and the thickness should together provide the desired gusset plate strength; (4) the horizontal welds should be sufficient to avoid weld fracture and block shear rupture of the base metal; and (5) the free gusset length is between $4 \leq L_{fg}/t_g \leq 6$.

3.3.2 Effects of Strength and Thickness of Gusset Plate

To investigate how "weak" the gusset plate should be to act as a reliable inelastic fuse, several different designs of the proposed connection were analyzed. Six different cases were designed with three different gusset thicknesses (t_g = 1.0t_{bw}, 1.25$t_{bw,}$, and 1.5t_{bw}) and each thickness designed using two criteria to ensure that: the expected strain-hardened plastic moment capacity of the gusset plate, M_{prg}, is less than either the yield moment capacity of the beam, M_{yb}, or the plastic moment capacity of the beam, M_{pb}. Since the overall strength, M_{prg}, of the gusset plate is maintained as either M_{yb} or M_{pb} for each design, thicker gusset plates are associated with smaller gusset plate heights (M_{prg} can be established using t_g and H_{g1} for a rectangular cross-section). All geometry parameters are defined in Figure 3.8. The beam and column sections adopted in these analyses were W27×94 and W14×221, A992 Gr. 50 steel (F_{yb} = 345 MPa or 50 ksi). The gusset plates were all A572 Gr. 50 steel (F_{yg} = 345 MPa or 50 ksi). The properties of the sections are given in the AISC Manual of Steel Construction (AISC 2010a).

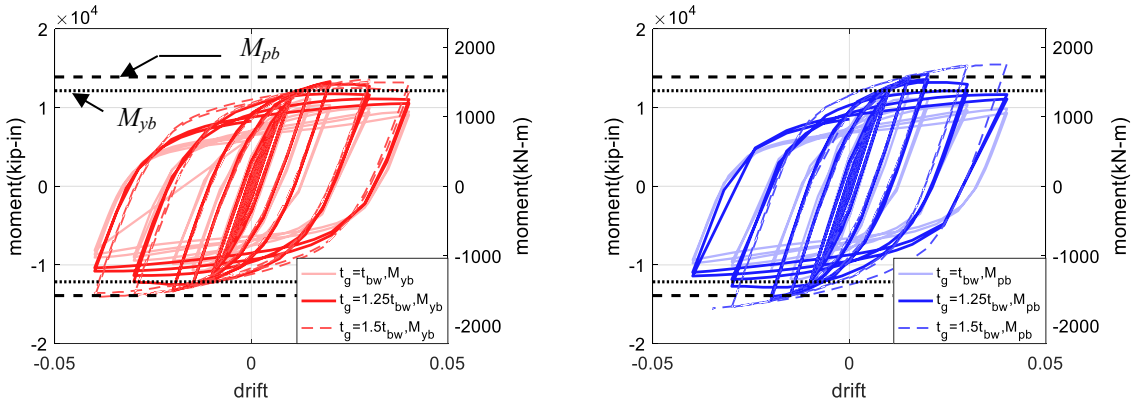

Figure 3.9 Comparison of hysteresis responses for different M_{prg} and t_g

Figure 3.9 shows the cyclic behavior of the connections with three different gusset plate thicknesses and the two design criteria. As shown in Figure 3.9(a), the connections were designed so that the "expected strain hardened" plastic moment capacity of the gusset plate, M_{prg}, is smaller than the yield moment of the beam, M_{yb}, i.e., $M_{prg} \leq M_{yb}$,. In Figure 3.9(b), the connections were designed so that $M_{prg} \leq M_{pb}$; note that the gusset plate designed to match M_{pb} is capable of achieving the load level of M_{pb} before buckling, and in general has a higher capacity for each drift level compared to gusset plates designed to match M_{yb}. Gussets designed to match M_{yb} are also capable of reaching the level of M_{pb} if certain strain hardening occurs before the drop of the strength due to buckling. The global behavior does not differ significantly between M_{pb} and M_{yb} designs, which may be because the difference between M_{pb} and M_{yb} for the wide flange shapes is only 10~15%.

Figure 3.10(a-c) shows von Mises stresses for the three connections with three gusset plate thicknesses designed to match the *yield moment* of the beam. Since the overall bending strength of the gusset plate was fixed to be equal to M_{yb}, with the thicker but shorter height gusset plate—see Figure 3.10(c)—significant yielding in the beam, or bucking or torsional out-of-plane deformations did not occur. Thicker gusset plates *did* cause more yielding in the column than the intermediate thickness [Figure 3.10(b)] or thin gusset plates [Figure 3.10(a)].

Figure 3.10(d-f) shows von Mises stresses for the three cases with three gusset plate thicknesses, where the gusset plates were designed to match the *plastic moment* of the beam. Similarly, the thicker but shorter gusset plate—see Figure 3.10(f)—yielded the beam and column more than the thinner gusset plates and did not experience buckling or twisting deformation. Based on a comparison Figures 3.10(a) to (d), (b) to (e) and (c) to (f), it is clear that cases designed based on M_{pb} indeed caused larger stresses in the beams and columns.

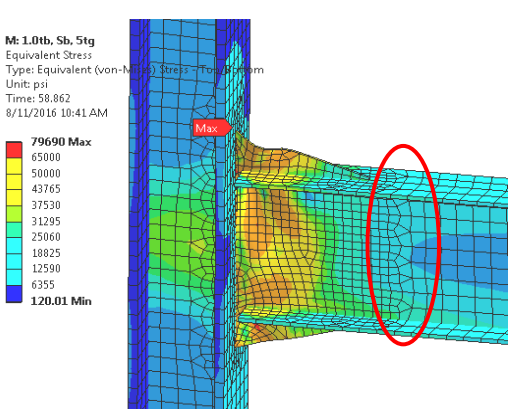

(a) t_g=1.0t_{bw} and $M_{prg} \cong M_{yb}$

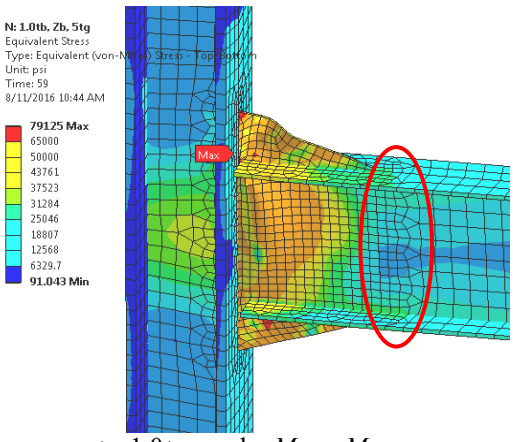

(d) t_g=1.0t_{bw} and $M_{prg} \cong M_{pb}$

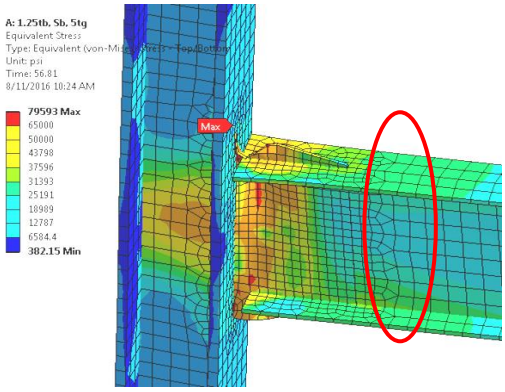

(b) t_g=1.25t_{bw} and $M_{prg} \cong M_{yb}$

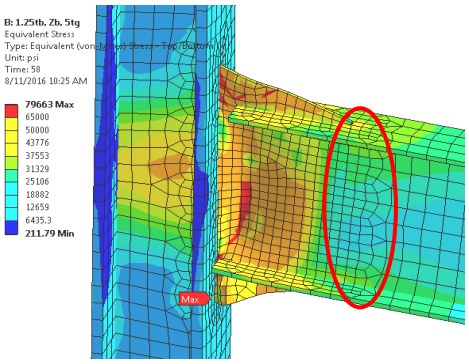

(e) t_g=1.25t_{bw} and $M_{prg} \cong M_{pb}$

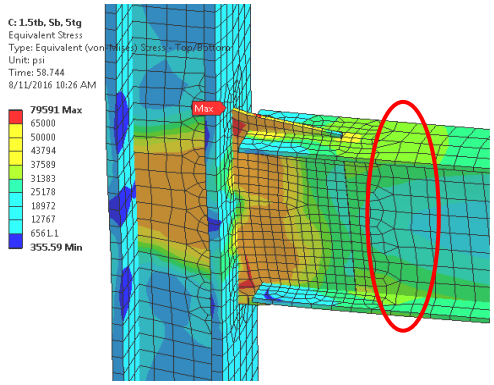

(c) t_g=1.5t_{bw} and $M_{prg} \cong M_{yb}$

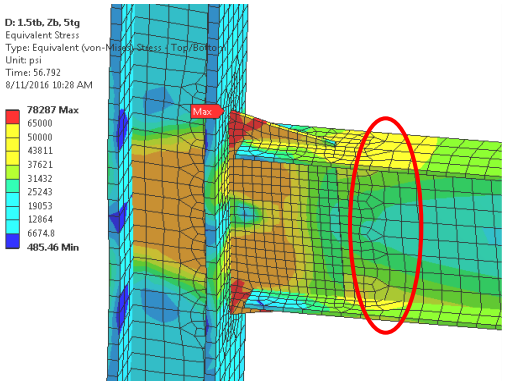

(f) t_g=1.5t_{bw} and $M_{prg} \cong M_{pb}$

Figure 3.10 Comparison of Von Mises stresses for different t_g for gusset plate designed to match the yield moment capacity, M_{yb} (a to c) and the plastic moment capacity M_{pb} (d to f) of beam (drift ratio = 0.04)

Regardless of the slightly different behavior of the analyzed cases, it was found that for all cases, significant plastic strain in excess of 0.15 could accumulate at about 0.015 ~ 0.03 drift ratios, either because of the lateral distortion of the gusset plate after buckling—see Figure 3.11(a,b,d,e)—or because of the high strain demand concentrated at the corners of the thicker gusset plates—see Figure 3.11(c,f). High equivalent plastic strains normally indicate a high probability of fracture initiating from these highly-strained areas. Modifications of the designs, which worked well for the shallow girders shown in Appendix C, seem necessary to assure better performance of deeper beam sections used in moment frames.

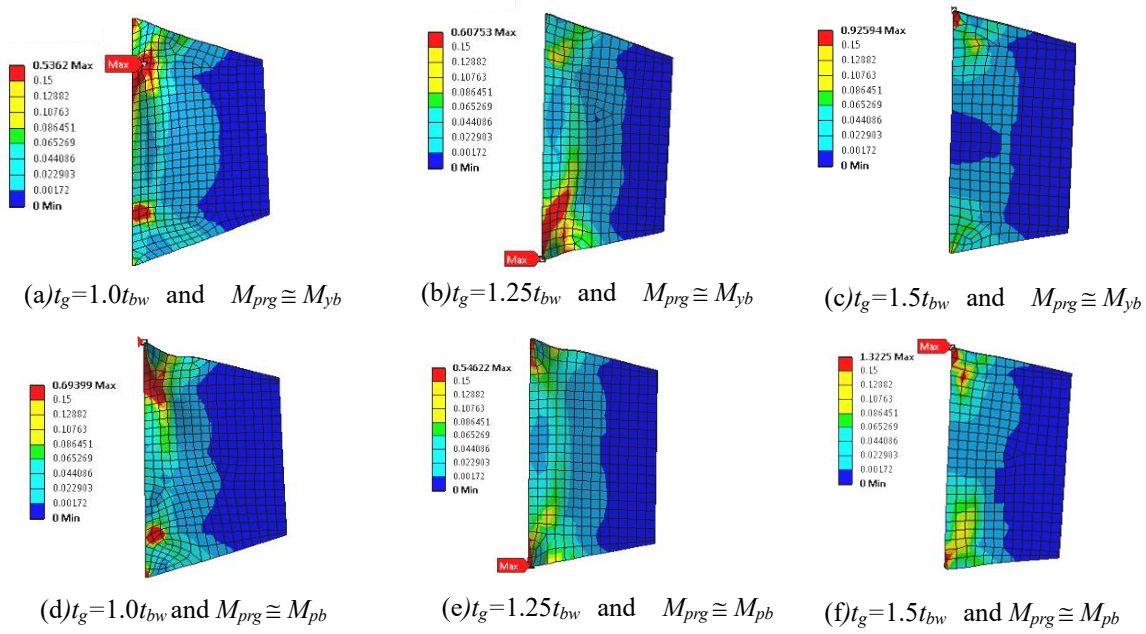

(a)t_g=1.0t_{bw} and $M_{prg} \cong M_{yb}$ (b)t_g=1.25t_{bw} and $M_{prg} \cong M_{yb}$ (c)t_g=1.5t_{bw} and $M_{prg} \cong M_{yb}$

(d)t_g=1.0t_{bw} and $M_{prg} \cong M_{pb}$ (e)t_g=1.25t_{bw} and $M_{prg} \cong M_{pb}$ (f)t_g=1.5t_{bw} and $M_{prg} \cong M_{pb}$

Figure 3.11 Comparison of peak equivalent plastic strain distributions for different t_g for gusset plate designed to match M_{yb} (a to c) and to match M_{pb} (d to f) (drift ratio = 0.04)

3.3.3 Effects of Free Gusset Length

Due to the nature of thin gusset plate oriented in the vertical direction, lateral instability is a primary concern that can have a notable effect cyclic behavior. It is well known that the *b/t* ratio controls the local buckling behavior of plates, which for the GPMC is the free gusset length to thickness, L_{fg}/t_g, ratio. Based on the preliminary parametric studies, a free gusset length to gusset thickness ratio of $4 \leq L_{fg}/t_g \leq 6$ was recommended; see Appendix C for details.

According to ANSI/AISC 360-10 (AISC 2010d), for a normal compression element in a connection under monotonic loading, buckling is not an issue if its slenderness ratio is smaller than 25. Assuming an effective length factor of 0.75, with a factor of 0.8 for the limiting slenderness ratio to account for cyclic effect, this slenderness requirement can be translated to a L_{fg}/t_g of 7.696 (calculated from $0.75 \cdot L_{fg}/t_g \leq 0.8 \cdot 25$), which indicates that the above-recommended range of free gusset length automatically satisfies this requirement.

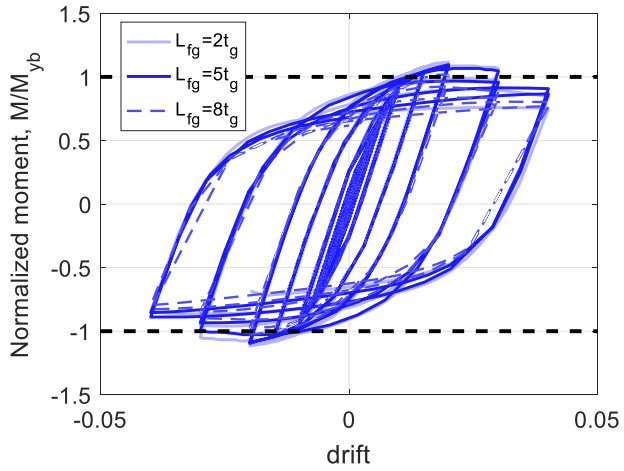

(a) Moment-drift hysteresis

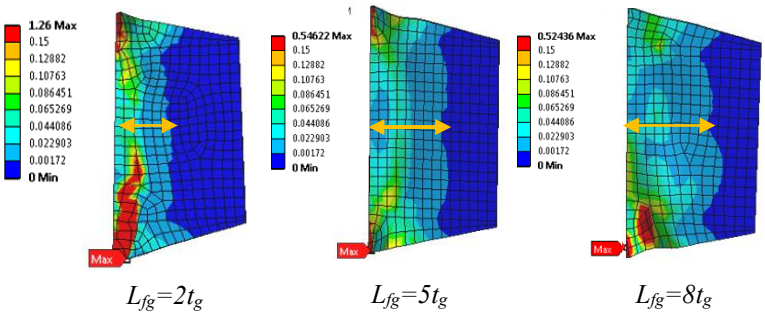

(b) Peak equivalent plastic strain distributions (drift ratio = 0.04)

Figure 3.12 Comparison of (a) moment-drift hysteresis and (b) equivalent plastic strain responses for using different free gusset lengths, L_{fg}

Another parametric study was conducted to further verify the recommended range for free gusset length with W27×94 beam and W14×221 column sections. The gusset plates were designed based on M_{yb} of the beam, with a gusset depth corresponding to a gusset thickness t_g equal to $1.25t_{bw}$. The horizontal welds were sufficient to avoid weld fracture and block shear rupture of the base metal. Three different free gusset lengths were analyzed, with a free gusset length L_{fg} equal to $2t_g$, $5t_g$, and $8t_g$. The $5t_g$ design represents a design that follows the preliminary design recommendation. This study included bottom flange lateral supports.

In general, the behavior agrees with the shallow beam parametric study: a shorter L_{fg} leads to higher local demand. Since all cases were designed to the same strength criteria, the global hysteresis curves are comparable [Figure 3.12(a)]. Note that the free gusset length directly affects the effective plastic hinge length, i.e., a short L_{fg} corresponds to a shorter hinge length and can result in significant strain demands at the re-entrant corners of the gusset plate [Figure 3.12(b)]. Using the same reasoning, the local strain at the gusset corners can be released slightly with longer L_{fg}, providing no significant lateral instability has happened. Therefore, if lateral support can be provided to the bottom flange of the girder, using a slightly larger L_{fg} but one that is less than $8t_g$ seems also acceptable.

3.3.4 Effect of Gusset Material

As shown in Section 3.3.2, for relatively deep and heavy girders, following the preliminary design recommendations, the resulting gusset plate would be in a less desirable shape with a very shallow slope. Relatively large plastic strains can develop even at a drift ratio of 1.5%, indicating a high probability of fracture and insufficient ductility. This section shows an attempt to resolve this issue.

According to the design criteria that the expected strain hardened moment capacity of the gusset plate is smaller than the yield moment of the beam, i.e., $M_{prg} = C_{prg} R_{yg} F_{yg} Z_{gx} \leq M_{yb} = F_{yb} S_{bx}$, if the gusset plate has a lower yielding strength F_{yg}, and small C_{prg} and R_{yg} value, larger or thicker gusset plates can be used without violating the "weak gusset" criterion. A thicker gusset plate is found to be beneficial because it can better distribute the stresses from the beam into a rectangular shaped stress block, which is close to the idealized stress distribution for a plasticized steel section. A thicker gusset plate with low-yield material is also more efficient in preventing lateral buckling due to a small slenderness ratio and a higher buckling threshold, i.e., a smaller b/t with larger t, and higher $\sqrt{(E/F_y)}$ limit with smaller F_y value. A36 and low-yield point (LYP) steel developed by the Nippon Steel Japan were therefore selected as potential candidates.

Four different GPMCs were designed for W27×94 beam and W14×221 column sections using three different materials, i.e. Gr.50, A36, and LYP100 steel: (1) Gr.50 steel (F_{yg} = 345 MPa or 50 ksi) using R_{yg} equal to 1.1 and a pre-defined t_g of $1.25t_{bw}$, (2) A36 steel (F_{yg} = 248 MPa or 36 ksi) using R_{yg} equal to 1.3 and a pre-defined t_g of $1.25t_{bw}$, (3) A36 steel using R_{yg} equal to 1.0 and a pre-defined H_{g1} equal to d_b+12 in., and (4) LYP100 steel (F_{yg} = 131 MPa or 19 ksi) using R_{yg} equal to

1.0 and a pre-defined H_{g1} of d_b+12 in.. The first two designs represent the preliminary design recommendation with the currently available material property, while the latter two cases represent possible perfectly made lower yield strength steel A36 and LYP100 steel having no variability of yield strength. The last two cases were designed with a maximum allowed height of H_{g1} equal to d_b+12 in., where the 12 in represents twice the thickness of typical 6-in. slab thickness. For the latter two cases, the resulting gusset thickness is about twice the beam web thickness. This was done because, with low yield strength, thicker gusset will be required to prevent the weld failure and shear rupture of plates limit states without unreasonably long horizontal weld length, L_{wh}. Generally, the resulting low-yield gusset plate will be larger than the Gr.50 gusset plates.

As shown in Figure 3.13, it can be observed that Gr.50-1.25t_{bw} design and A36-1.25t_{bw} design both suffered from lateral instability and experienced fairly large plastic strain. In contrast, no strength degradation due to gusset plate buckling occurred to A36-1.75t_{bw} and LYP-2.5t_{bw}. In addition, the strain level or the possibility of fracture was reduced effectively for A36 and LYP100 with R_{yg} being 1.0; the lower the yield point, the lower the peak plastic strain. The improvement is especially significant for low-yield steel LYP100, which has a much more ductile stress–strain relationship compared with the other two relatively higher strength materials.

Figure 3.14 compares the deformation and equivalent plastic strain distributions of the four cases where it can be seen that use of low-yield gusset material effectively reduced the magnitude of the strains and changed the location of high strain areas. For the design using A36 steel with gusset plate thickness of 1.75t_{bw}, though the magnitude of strain was still relatively high, the location of peak strain was changed to a more desirable location. Yielding at this location, compared to the corners of the gusset plate, is internal and is less likely to initiate crack or facilitate crack propagation. The design using LYP steel with a gusset thickness of 2.5t_{bw} again resulted in the most desirable condition, without any significant stress–strain concentrations.

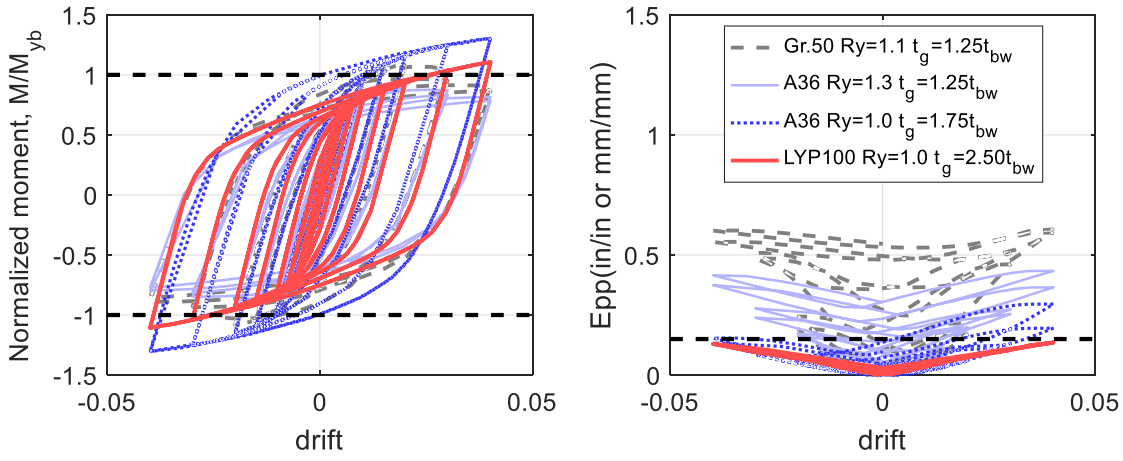

Figure 3.13 Comparison of (a) moment-drift hysteresis and (b) equivalent plastic strain (Epp) responses for using different gusset plate material

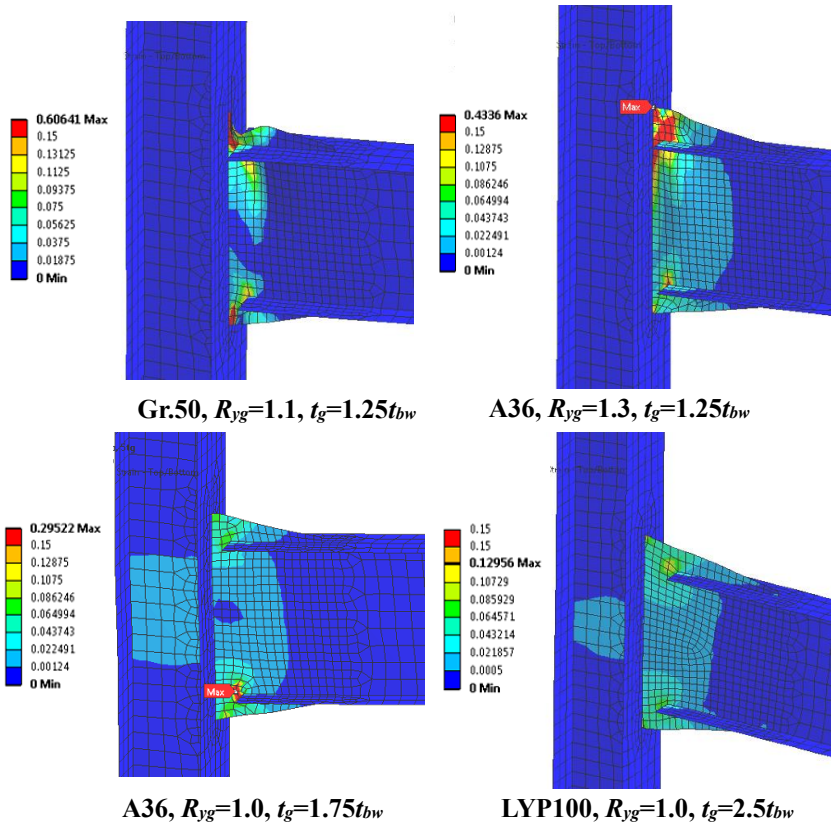

Figure 3.14 Comparison of peak equivalent plastic strain distributions for different gusset plate material (drift ratio = 0.04)

This study, demonstrates that for deeper beam sections, a thicker gusset plate with lower yield strength seems to be more effective and showed better behavior. The A36 steel did not improve the behavior significantly when considering the relatively high R_y value. If fabrication of low-yield steel ensures relatively low variation in material properties, then low-yield steel LYP100 is especially promising and could be applied to even deeper beam sections. Considering the fact that LYP steel was also shown to possess low-yield strength, enhanced hysteresis properties, lower strain rate dependency, longer low-cycle fatigue life, and improved weldability (Yamaguchi et al. 1998), it is a desirable material for metal energy-dissipation elements.

Further designs using a LYP gusset were done for beam-column sections of W21×83-W14×120, W27×94-W14×221, and W30×99-W14×176. All designs have t_g=1.25t_{bw}, $M_{prg} \leq M_{yb}$ and L_{fg}=5t_g. These three sections were chosen to represent different depths of commonly used wide flange girders but with the same beam web thickness so as to have a higher degree of comparability. Geometric properties of these sections can be found in the AISC Manual of Steel Construction (AISC 2010a).

In general, as shown in Figure 3.15 of a comparison moment-rotation hysteresis curves, regardless of the beam depths, the low-yield LYP100 gusset did not suffer from the buckling problem (no

strength degradation or un-symmetric hysteresis curves) as did the relatively higher strength Gr.50 gusset designs. The low-yield gusset plate also saw relatively low levels of plastic strains even under relatively large drift ratio, while the Gr.50 gussets could experience higher than 0.15 equivalent plastic strains at a drift ratio as low as 0.015. These parametric studies indicated that for shallow beams of up to 600 mm (24 in.) in depth used in short spans and steel plate shear wall system systems, Gr. 50 and A36 steel gusset plates can perform well. To avoid significant localized plastic strains and buckling of the gusset plate, use of low-yield steel is recommended for beam sections with a depth larger than 600 mm (24 in).

Note that for small angles of gusset slope, θ, as is the case for W21×83 and W30×99 Gr.50 beam, the two ends of the gusset plate will be subjected to relatively high stresses as most of the moments are decoupled to the two ends. This results in less likelihood of lateral instability but imposes significant strain demand at the upper and lower corners of the gusset plate; see Figure 3.16. By designing for all available wide flange sections listed in the AISC Manual of Steel Construction (AISC 2010a) (results shown in the commentary section for the proposed design procedure in Section 3.5.3), it was found that the resulting gusset slope tends to decrease for heavier sections with similar depth. In contrast, if lateral instability occurs, as was the case for Gr.50 gusset with the W27×94 Gr.50 beam, the lateral deformation of the gusset plate tends to create dragging forces that can cause tensile stresses in the compression zone of the gusset plate.

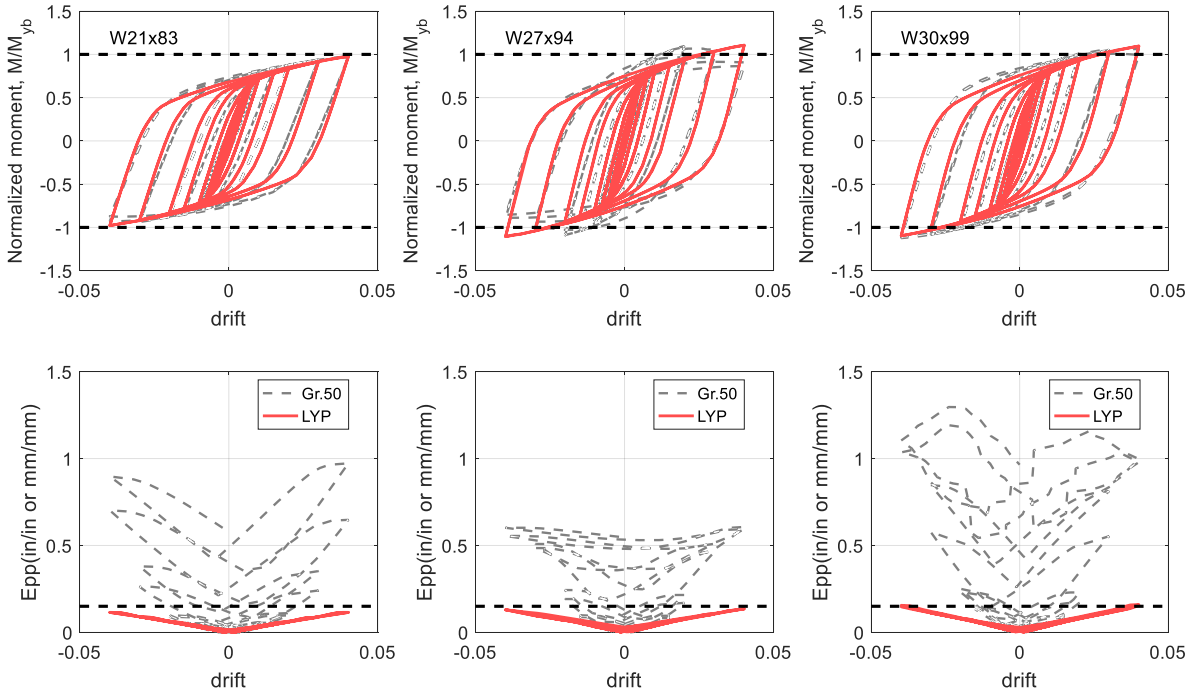

Figure 3.15 Comparison of (a) moment-drift hysteresis (b) equivalent plastic strain (Epp) responses for Gr.50 and LYP100 GPMC designs for different beam sections

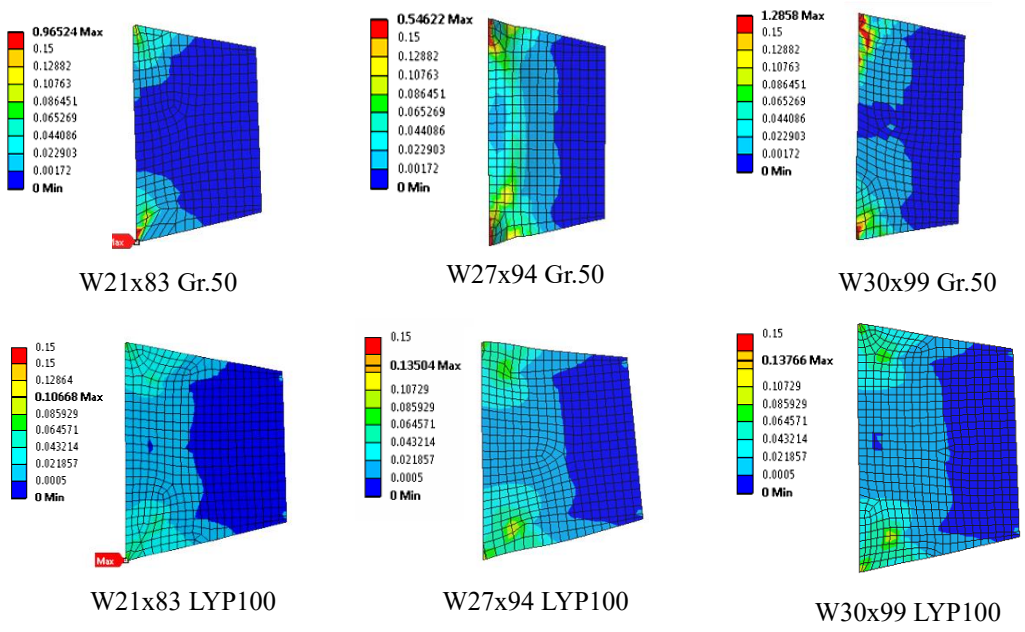

Figure 3.16 Comparison of peak equivalent plastic strain distributions for Gr.50 and LYP100 designs for different beam sections (drift ratio = 0.04)

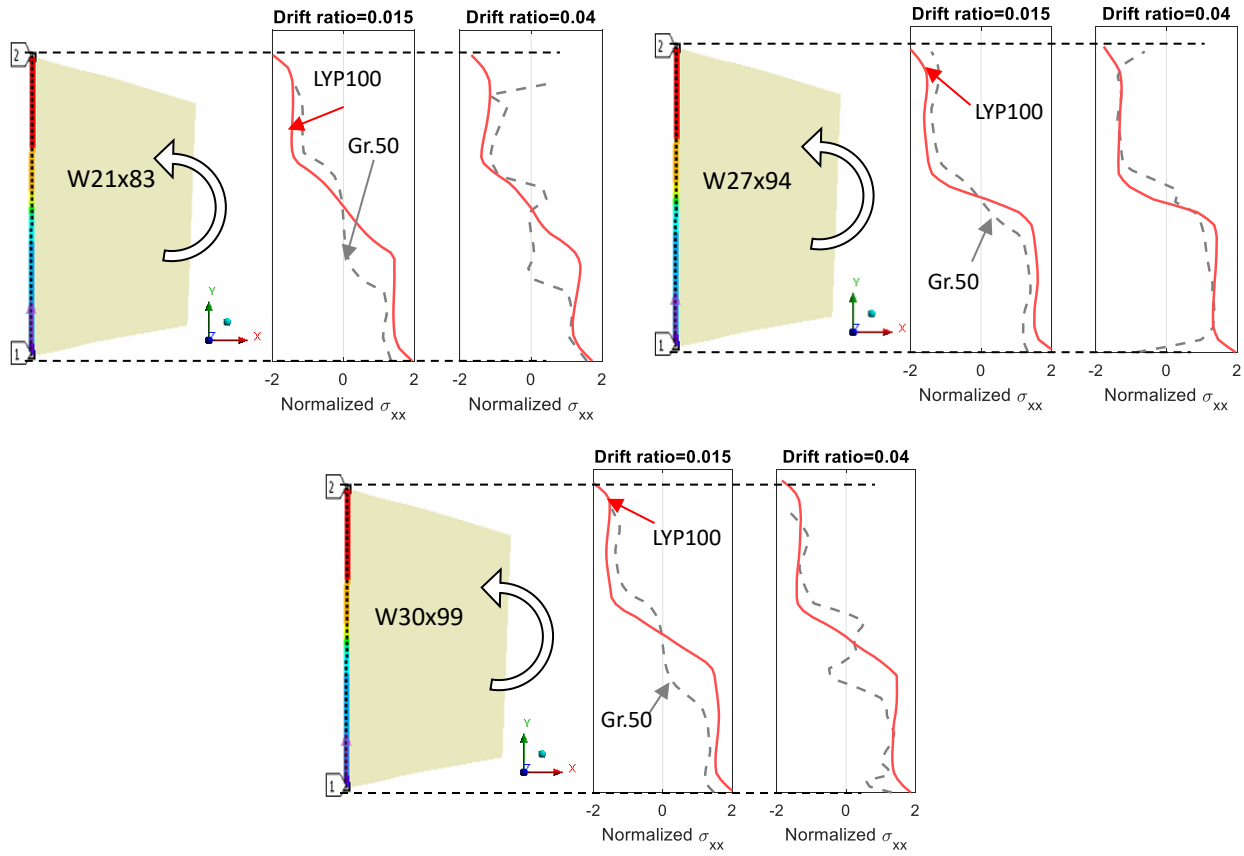

Figure 3.17 Comparison of normalized normal stresses for Gr.50 and LYP100 designs subjected to positive moment at 1.5% and 4% drift ratios

Both of these two phenomena appear to be able to be eliminated by using the low-yield LYP100 steel. Figure 3.17 shows the normal stress in the *x*-*x* direction (longitudinal direction of the beam) along the vertical edge of gusset plate at a drift ratio of 0.015 and 0.04 normalized with respect to the yield strength of the gusset plate, F_{yg}. Through the entire cyclic loading, LYP100 designs have more uniform stress distributions that are closer to the idealized rectangular stress blocks of the plasticized cross sections. This again shows why LYP100 designs exhibit desirable force-displacement behavior and relatively uniform yielding of the gusset plate with relatively small plastic strains. In this sense, the low-yield LYP100 gusset plate once again shows great potential to be used in the proposed new moment connection and can be used for all beam depths.

3.3.5 Use of Gusset Stiffener

In addition to using low-yield and more ductile gusset material, modifications to improve the connection behavior were also considered by adding transverse stiffeners to the gusset plate, which is a commonly used method for braced frames or trusses to prevent gusset plate edge buckling (Astaneh-Asl 2010; Astaneh-Asl et al. 2006).

Several cases were designed to study the effectiveness of adding edge stiffeners to the gusset plate in the new GPMC connection. Again, the gusset plates were designed according to the criteria that the expected strain-hardened plastic moment capacity of gusset plate does not exceed the *yield moment* of the beam, with a gusset thickness, t_g equal to $1.25t_{bw}$, and sufficient block shear rupture and weld strength. A36 steel is used for gusset plate in this study. Stiffening that extended to the middle of the horizontal welds with sizes of PL3 × 0.5625 (76.2 mm × 14.3mm) and PL5 × 0.75 (127 mm ×19.1 mm) were compared with the design without any stiffeners. The two stiffener sizes have a *b/t* ratio of 5.3 and 6.6, respectively.

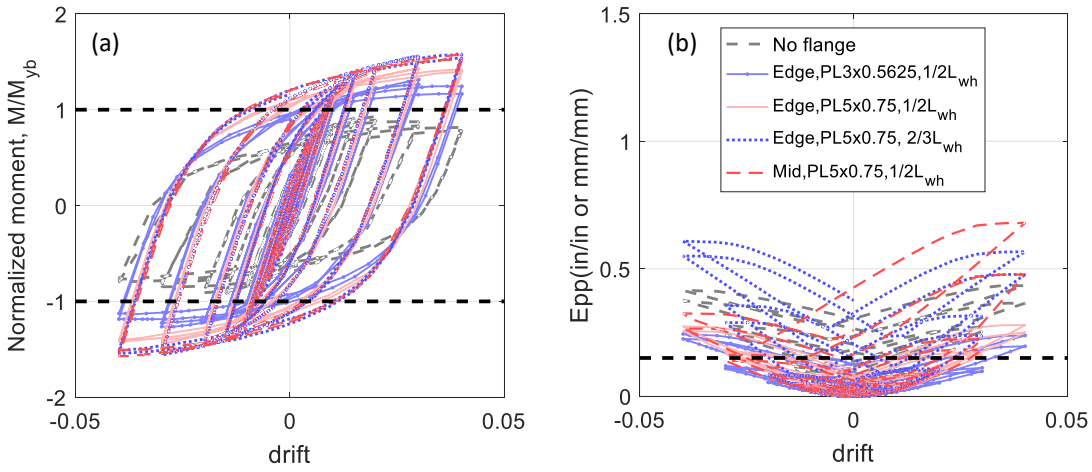

Figure 3.18 Comparison of (a) moment-rotation hysteresis and (b) equivalent plastic strain (Epp) responses for different gusset stiffener sizes, lengths and locations

Although the stiffener dimension of PL3 ×.5625 was insufficient [Figure 3.19(b2)], use of the PL5 × 0.75 seems to improve the behavior considerably. As expected, by adding the edge stiffeners, the strength of the connection increased [Figure 3.18(a)] as the stiffeners acted as flanges and contributed to the bending moment capacity of the gusset plate; however, the maximum equivalent plastic strain still exceeded 0.15 at a drift ratio of about 0.03 [Figure 3.18(b)], but compared to the non-stiffened cases, the level of strain was much reduced.

Different locations and lengths of stiffeners were also compared: (a) no stiffener; (b) PL5 × 0.75 stiffener at the edge that extends to the middle of the horizontal weld; (c) PL5 × 0.75 stiffener at the edge that extends to two-thirds of the horizontal weld; and (d) PL5 × 0.75 stiffener in the middle of the gusset plate. It was found that a longer stiffener or placing the stiffener in the mid-way of the gusset plate would more efficiently reduce the severity of out-of-plane buckling, resulting in an even higher strength of the connection and more yielding in the column web; see Figure 3.18(a) and Figure 3.19(c and d). Also, the location of maximum strain was shifted to the location where the beam ends. Although the shifting of maximum strain location had led to a higher absolute strain magnitude compared with shorter gusset edge stiffener, this location is more desirable: this location is less likely to contain fabrication flaws or imperfections that will facilitate crack initiation. Besides, it is more constrained and thus would inhibit fracture or connection failure after the crack initiation. In general, adding sufficient gusset stiffeners does improve the behavior of the connection, but is less effective than changing the gusset material to low-yield steel.

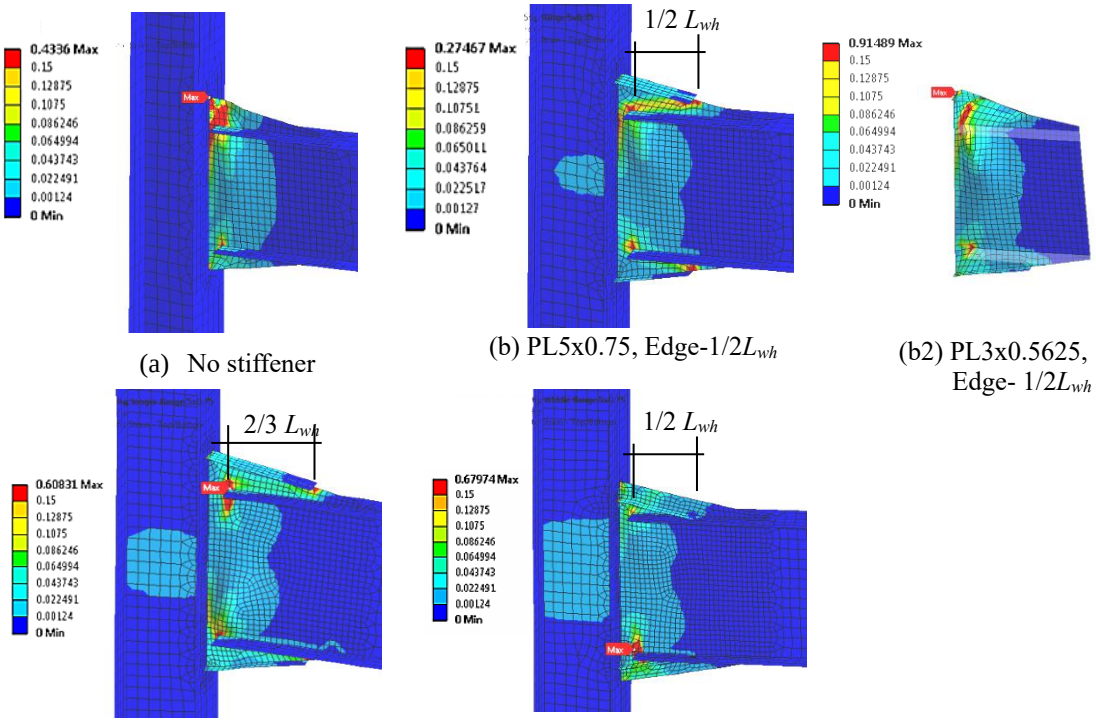

(a) No stiffener

(b) PL5x0.75, Edge-1/2L_{wh}

(b2) PL3x0.5625, Edge- 1/2L_{wh}

(c) PL5x0.75, Edge- 2/3L_{wh}

(d) PL5x0.75, Middle-1/2L_{wh}

Figure 3.19 Comparison of peak equivalent plastic strain distributions for different gusset stiffener sizes, lengths and locations (drift ratio = 0.04)

3.3.6 Bolted GPMC

So far, all parametric studies were carried out using the welded version. The behavior and design of bolted a GPMC are investigated in this section, with a focus on the design of bolts and gusset flange. For the designs analyzed in this section, the dimensions of the gusset plate were identical to the welded GPMC designs (Gr.50) for the three-typical beam-column sections described in Section 3.3.4. The variables were the number of bolts per vertical row on one side, n_b, bolt diameter, d_b, and gusset flange thickness, t_{gf}. The expected strain-hardened plastic moment capacity of the gusset plate, $M_{prg,}$, was used as the demand to design the gusset flange and the bolts.

Note that the tension zone of the connection behaves very similarly to that of a T-hanger; see Figure 3.20. Figure 3.21 shows three possible failure mechanisms for T-hanger type of connections (Astaneh-Asl 1985): (1) Case I-plate yielding due to plastic hinge formation, which occurs when gusset flange plate is relatively thin; (2) Case III- bolt yielding/ fracture in tension, which is likely to occur when the gusset flange plate is relatively thick; and (3) Case II-combined plate yielding and bolt yielding/fracture failure due to prying action, which occurs when the thickness of the gusset plate flange is intermediate. Therefore, due to similarities between the tension side of the bolted gusset plate and the T-hanger connections, the design of bolted GPMC was based on the design procedures of T-hangers given by Astaneh-Asl (1985). Several designs that do not satisfy the T-hanger requirements were also considered in order to illustrate the effects of each parameter. Gusset flange plate widths, W_g, were set to be equal to the beam flange width plus 50 mm (2 in.). Table 3.2 shows different cases designed for this study. Note that unlike the welded GPMC, which has no direct connection of the gusset plate to the column flange, the column side in the bolted GPMC needs to be checked against column flange flexural yielding and column web yielding, buckling, and crippling. Effects of weak column flange occurred in some of the analyzed cases.

Table 3.2 Parameters used for different bolted GPMC designs

Case	Beam Section	Column Section	Gusset Flange		Bolts		
			Gusset Flange Plate Thickness t_{gf}, mm(in)	Thickness Ratio [a] t_{gf}/t_g	Total Number per vertical row ($2n_b$)	Diameter, d_b mm (in)	Material
1	W21x83	W14x120	28.575(1.125)	1.80	4	31.75(1.25)	A490X[b]
2			28.575(1.125)	1.80	8	28.575(1.125)	A490X
3	W27x94	W14x211	25.4(1.0)	1.78	6	31.75(1.25)	A490X
4			31.75(1.25)	2.22	6	31.75(1.25)	A490X
5			25.4(1.0)	1.78	8	28.575(1.125)	A490X
6			25.4(1.0)	1.78	4	33.338(1.3125)	A490X
7	W30x99	W14X176	33.338(1.3125)	2.10	8	28.575(1.125)	A490X

a. The gusset plate thickness is the closest 1/16-in rounded down from 1.25 times the beam web thickness

b. Nominal tensile strength F_{nt} = 779MPa (113ksi), Nominal shear strength, F_{nv}=579MPa (84ksi)

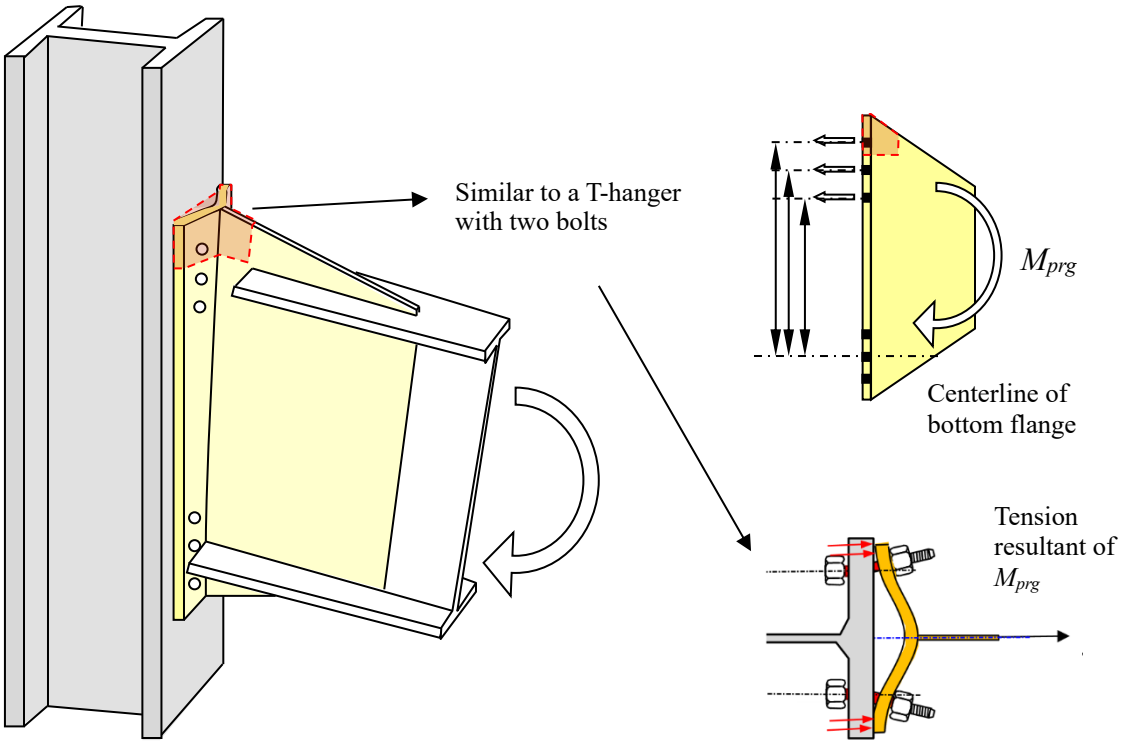

Figure 3.20 Analogy of the tension zone in a bolted GPMC to a T-hanger connection

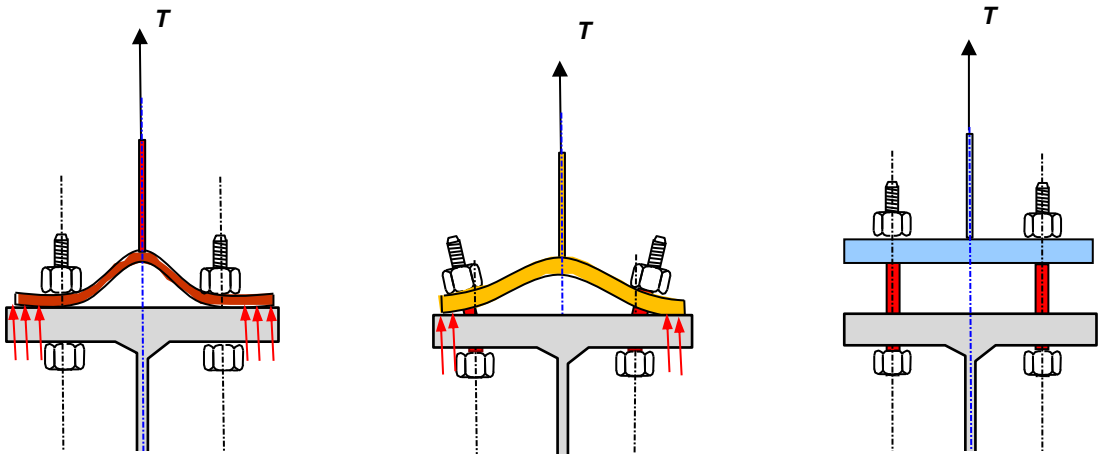

(a) Case I- Gusset Flange Yielding for Thin Gusset Flange

(b) Case II- Bolts and Gusset Flange Yielding for Intermediate Gusset Flange

(c) Case III - Bolts Yielding for Thick Gusset Flange

Figure 3.21 Possible failure modes of the gusset flange connection similar to T-hanger connections

Although not directly analyzed in this study, it is recognized that the bolts connecting the gusset plate to the column are under combined tension and shear forces. To avoid potential brittle fracture of bolts under cyclic loading, the use of "upset bolts" is recommended. In "upset bolts", the diameter of the shank is less than the diameter of the threaded part to force yielding of the unthreaded part of the bolt (i.e., the shank) to occur before fracture of the threaded parts to ensure ductility and avoid fracture.

Figures 3.22 – 3.24 and Table 3.3 show the hysteretic responses and stress/strain distributions of the seven bolted GPMC designs. The key observations from this parametric study are as follows:

1. The design procedure for T-hanger connections outlined in AISC Construction Manual (2010a) and Astaneh-Asl (1985) can be used effectively in design of bolted GPMC;

2. Following the T-hanger design procedure, the designs generally lead to a rigid or intermediate gusset flange;

3. Bolted GPMC is generally less stiff compared to the welded version; see Figure 3.23. This is likely to be due to the additional flexibility of the gusset flange plate and, to the lesser extent, bolt elongation. The stiffness of the bolted GPMC can vary depending on the relative thickness of the gusset flange plate and the strength of bolts;

4. The designs with less number of bolts, and relatively thin gusset flange, tend to show greater pinching in the cyclic behavior (e.g., Figure 3.22, case 6), which is undesirable;

5. Use of thicker gusset flange plate can reduce the level of prying action and impose smaller force on the bolts; see Figure 3.24 (case 4 &7). Use of thicker gusset plate flange plates can also result in increased rotational stiffness and better drift control, a desirable behavior;

6. If the gusset flange plate is rigid enough, most of the plastic deformation will be concentrated in the gusset plate, with similar deformation and drift at first cyclic buckling as its welded counterpart (Figure 3.23, W27×94, case 5, Bolted 8B). However, the level of strain concentration at the re-entrant corners of the gusset plate in the bolted gusset plate is lower than the welded version. This is likely to be due to the flexibility of the gusset flange plate, which releases some of the strain concentrations;

7. A weak column tends to release the stress/strain concentrations on the gusset plate itself. However, the forces in the bolts would be increased due to larger relative displacement between the gusset flange and the column flange, even when a relatively large number of bolts are used. The designs with W21×83 -W14×120 columns are examples of columns with insufficient flange thickness, as shown in Figure 3.24 (case 1 & 2), while designs with

W14×176 and W14×211 columns have relatively thick flanges, so no significant column flange deformation was observed;

8. The force demands on the bolts can be reduced by using a larger number of bolts or thicker gusset flange; however, if the gusset flange plate is too stiff (i.e., too thick), there can be more yielding in the column web compared to the case with thinner gusset flange plate. The gusset flange thickness following the T-hanger design procedure for W27×94-W14×211 columns with eight 29 mm (1-1/8 in.) diameter bolts and 25 mm (1 in.) gusset flange appears to result in a relatively desirable cyclic behavior; see Figure 3.24 (case 5);

9. Use of 4-bolt groups may be ineffective in engaging the entire gusset plate to yield and dissipate energy and may require relatively large bolts; see Figure 3.24 (case 1 & 6).

Note that here a failure mode of Case II and III (Figure 3.21) is recommended for the gusset flange-to-column flange connection. Case III may seem unfavorable since the brittle fracture of bolts is not a desirable failure mode. The use of "upset" bolts is proposed to prevent bolt fracture. In addition, if we consider the entire connection, there are limit states for all components and those limit states can be listed in a hierarchical order following the desirability. It was shown in this study that by using a relatively thick gusset flange, the inelastic deformation would be concentrated in the gusset plate itself with minimal gusset flange yielding and prying action, thus limiting the force being transferred to the bolts. In this case, although the controlling limit state for the gusset flange is the bolt yielding/fracture, this limit state for the entire connection will happen relatively late in the cyclic loading due to the "protecting mechanism" from the gusset plate yielding. Also, making the bolt group capacity greater than the expected strain-hardened moment capacity of the gusset plate can help to avoid bolt fracture.

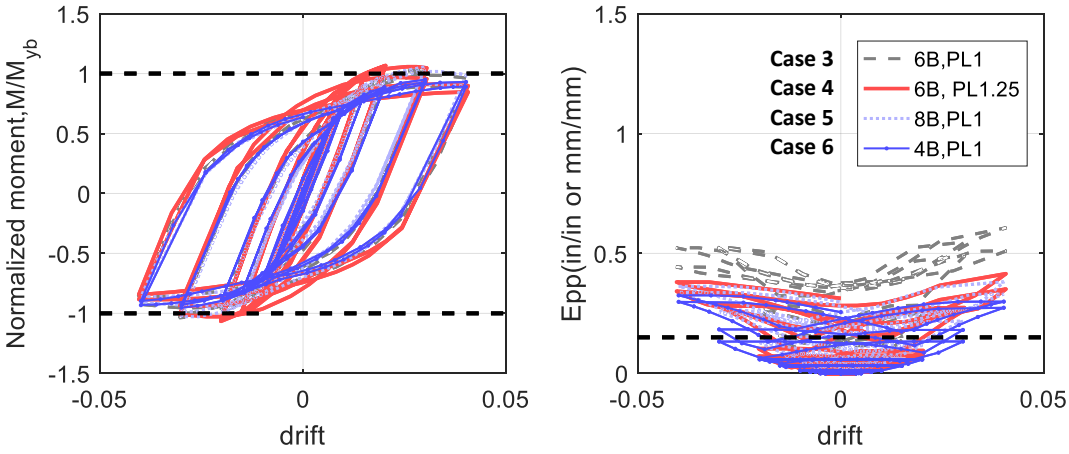

Figure 3.22 Comparison of (a) moment-drift hysteresis and (b) equivalent plastic strain (Epp) responses for bolted GPMCs with different number of bolts and gusset flange thicknesses for W27×94

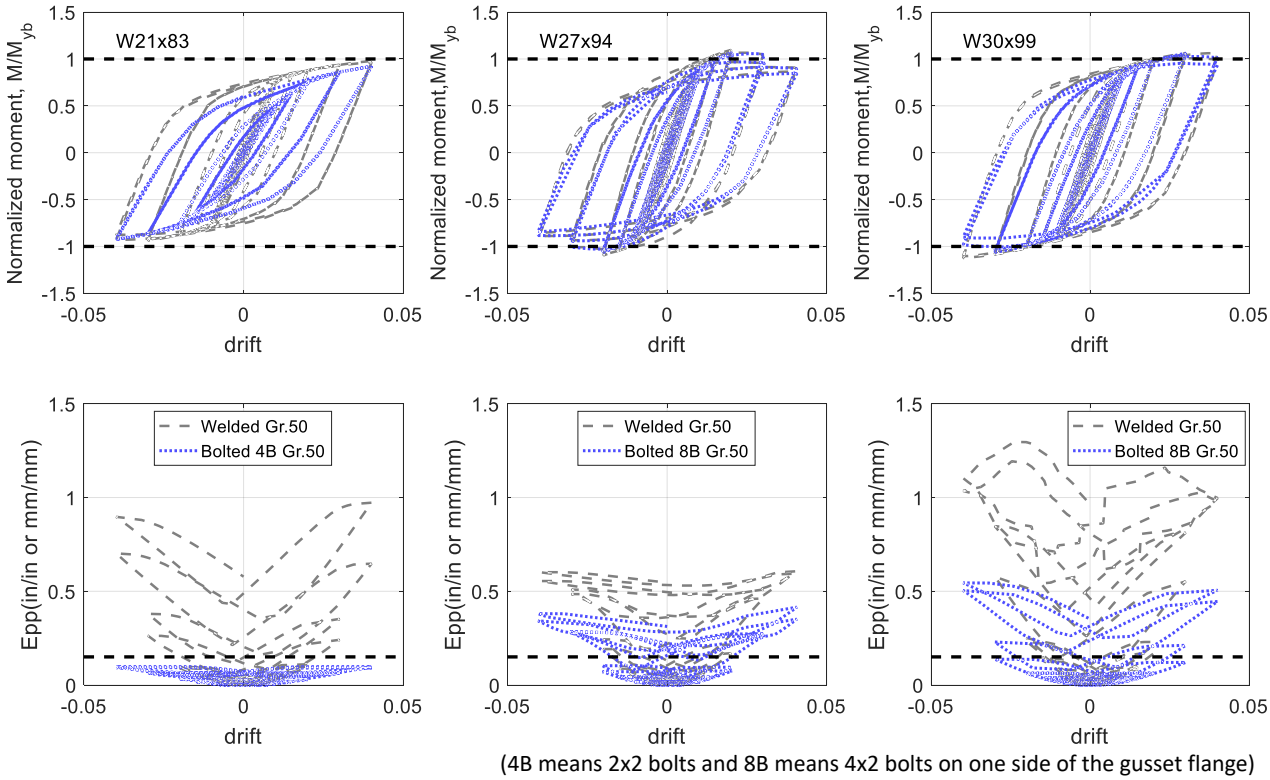

Figure 3.23 Comparison of (a) moment-drift hysteresis and (b) equivalent plastic strain (Epp) responses for different designs of welded and bolted GPMCs

Table 3.3 Behavior of different components for the seven bolted GPMCs designs

Case	Gusset flange yielding	Prying action	Column web yielding	Column flange deformation
1	some	slight	large	significant
2	some	slight	large	significant
3	slight	slight	slight	negligible
4	negligible	negligible	slight	negligible
5	some	slight	slight	negligible
6	significant	significant	slight	negligible
7	negligible	negligible	some	negligible

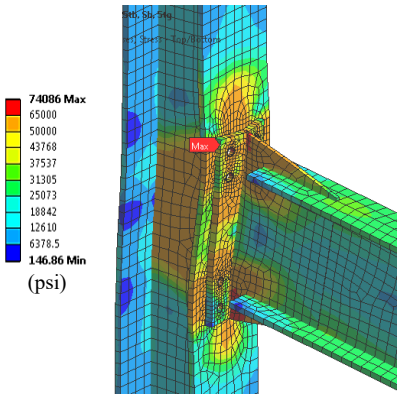

(1) W21x83-W14x120 Case 1

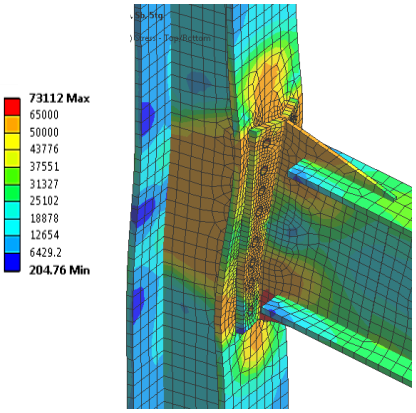

(2) W21x83-W14x120 Case 2

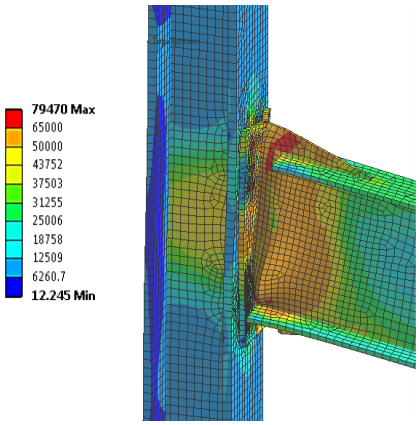

(3) W27x94-W14x211 Case 3

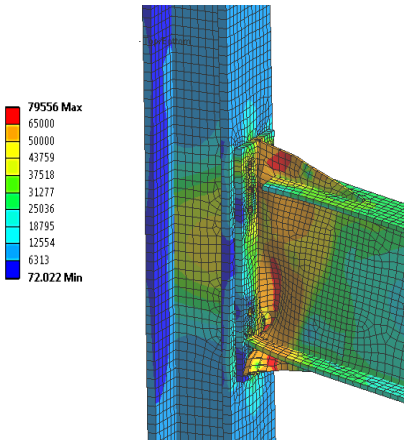

(4) W27x94-W14x211 Case 4

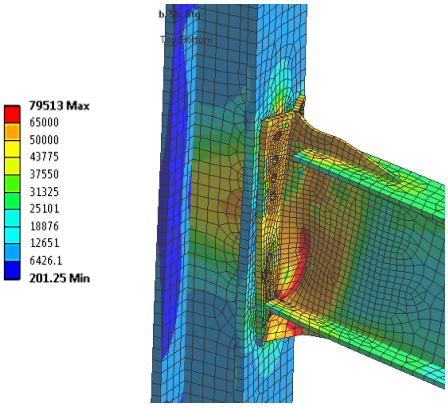

(5) W27x94-W14x211 Case 5

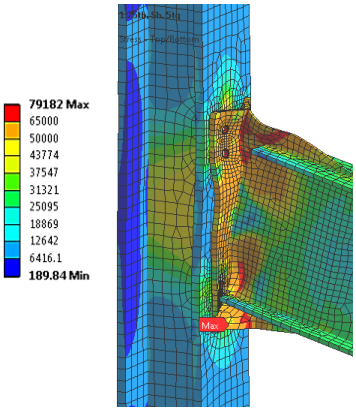

(6) W27x94-W14x211 Case 6

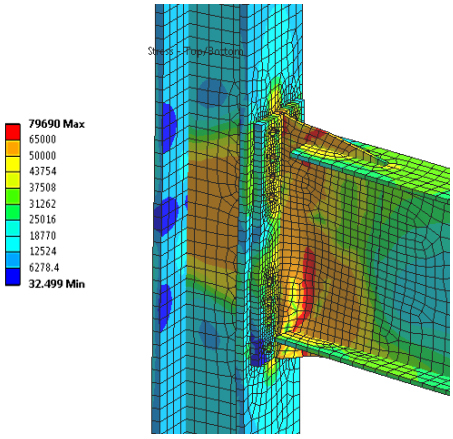

(7) W30x99-W14x176 Case 7

Figure 3.24 Comparison of deformations and Von Mises stresses for the seven bolted GPMCs designs (drift ratio = 0.04)

3.3.7 Other Design and Construction Considerations

3.3.7.1 Improving the Performance by Cut in the Beam Flange

As observed in the case study analysis herein, that with appropriately chosen material and proportioned gusset plate design, the location with maximum equivalent plastic strain (an indicator of fracture) is likely to occur at the end of the beam; see circled region in Figure 3.26. This location is internal and is less likely to cause sudden strength and stiffness loss after crack propagation. However, it is still desirable to reduce the absolute magnitude of the local stress/strain at this location. One way to reduce the local stress/strain is to cut the beam flange, considering (1) the shear lag effect on the beam flange (Figure 3.25); and (2) that the stress at the critical location depends on the beam flange force.

Figure 3.26 compares the GPMC with full beam flange and the case with beam flange cut by on a 30° angle. It can be seen that the maximum equivalent plastic strain value was effectively reduced by 20% (from 0.13 to 0.11) with a simple beam flange cut.

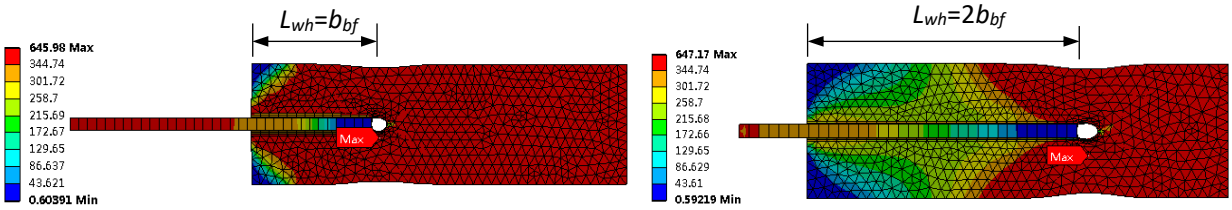

Figure 3.25 Illustration of shear lag effect as shown by the Von Mises stresses

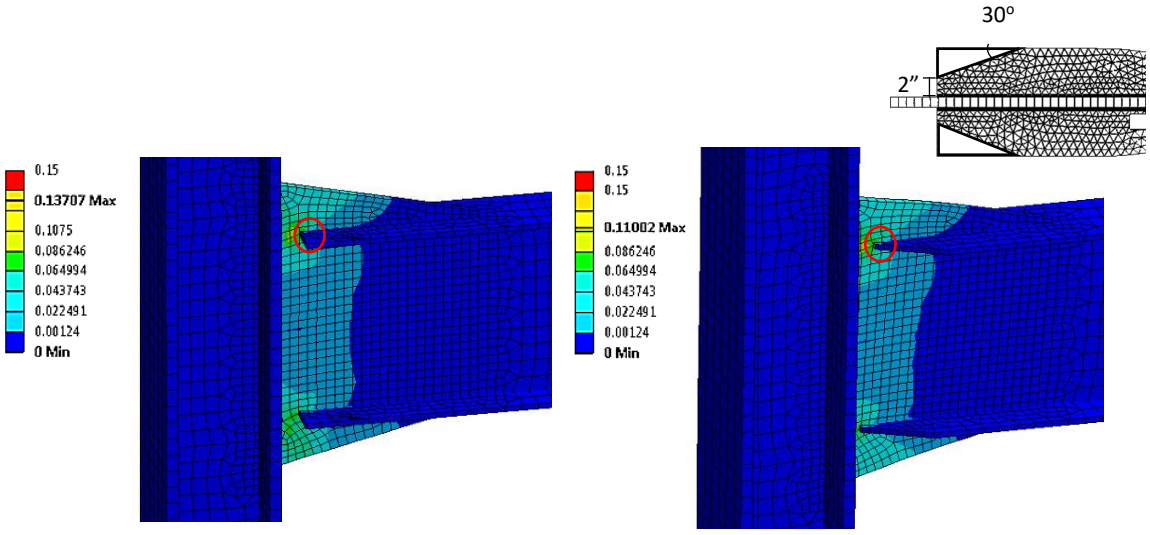

Figure 3.26 Comparison of peak equivalent plastic strain without and with beam flange cut (drift ratio = 0.04)

3.3.7.2 Lateral Stiffness and Drift Control

Since the gusset plate in the proposed connection is designed to be weaker than the beam and the column, similar to the RBS moment connection, elastic drift amplification may be required in the design process due to reduced lateral stiffness. The extent of drift amplification is investigated by pushover analyses of a one-bay one-story frame with W21×55, Gr. 50 beams and W14×120, Gr. 50 columns. Five different cases were studied, including: (1) elastic beam column frame with direct connection of the beam to the column; (2) elastic beam and column with a nonlinear GPMC designed to match the plastic moment capacity, M_{pb}, of the beam; (3) elastic beam and columns with a nonlinear GPMC designed to match the yield moment capacity, M_{yb}, of the beam; (4) elastic column with a nonlinear beam having RBS section at both ends with 35% cut in the beam flanges; and (5) elastic column with nonlinear beam having RBS section at both ends with 50% cut in the beam flanges. The first case will serve as a basis of the stiffness of an elastic frame with idealized moment connection.

Figure 3.27 shows the pushover curves of the five cases. Designing a GMPC according to M_{yb} of the beam in general leads to about 40% reduction in strength, but it does not suffer substantial stiffness reduction and has almost the same pushover curve as the RBS connection with 35% flange cut up to 4% story drift. The case with RBS (50% cut) shows slightly larger deviation from the baseline scenario compared to all other cases. From this simple pushover analysis, it appears that use of the GPMC would not cause significant stiffness reduction, or at least not more than the RBS connection. In lieu of more detailed analysis, we suggest the use of the drift amplification factors for RBS be applied to GPMCs. The effective elastic drifts may be calculated by multiplying elastic drifts obtained in a model that uses the gross beam sections by 1.1 for gusset plate with expected plastic moment strength reduced up to 60% of that of the beam, i.e., $R_{yg}F_{yg}Z_g = 0.6R_{yb}F_{yb}Z_b$. This 40% strength reduction corresponds approximately to a 50% reduction of beam flange width in a RBS (ANSI/AISC 358-10 p.9.2-16). Linear interpolation may be used for smaller gusset strength reductions.

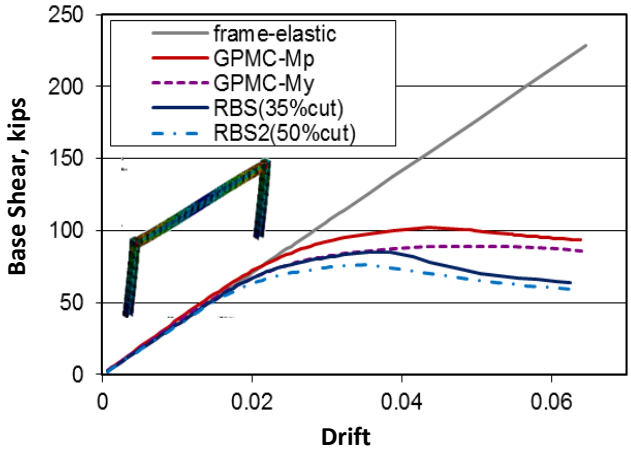

Figure 3.27 Comparison of pushover curves for different moment connection designs

3.3.7.3 Upper Limit of the Gusset Depth

If the proposed gusset plate moment connection is employed in industrial buildings, within steel plate shear wall frames, as part of a dual system of steel moment frames and concentrically braced frames, or when the frame panel is infilled with a wall panel, there is no limit on the depth of the gusset plate. However, when the proposed connection is used in office or residential buildings with steel deck-concrete slab floors, there might be some restrictions on the depth of the gusset plate such that it does not extend above the depth of concrete slab or other applicable architectural limit. This aspect is addressed in the proposed design procedure in Section 3.5.3. The effect of imposing this additional architectural limit on the connection behavior will be presented in the commentary section of the design procedure.

3.4. Modeling of the New Gusset Plate Moment Connection

3.4.1 Modeling of GPMC in Global Building Models

3.4.1.1 Introduction

Detailed finite-element analyses were carried out and results discussed in previous sections to obtain a better understanding on the connection behavior. On the global level, the connections often have to be captured by simpler models using either fiber section or rotational springs. Multi-scale modeling, which uses detailed shell/solid elements in the connection (critical) region and simple line elements for the members, should be conducted in future research to capture detailed connection behavior in a global setting under relatively low computational demand. At this stage, the conventional method of beam-to-column connection modeling technique will be adopted for easy implementation in global structural analysis software such as SAP2000, ETABS(CSI 2016), Perform 3D(CSI 2011), and OpenSees (McKenna et al. 2010). Here, the discussion is focused on the implementation in OpenSees, which provides a wide variety of choices of material and moment-rotation relationships. Due to the similarity in the modeling parameters for rotational hinges, the values suggested for OpenSees can be easily adapted to other nonlinear structural analysis software such as Perform 3D.

Based on the observations from Section 3.3, the proposed gusset plate moment connection is essentially a designated concentrated plastic hinge next to the column flange. For normal welded moment connections, the distributed plastic hinge formation can often be more easily captured using a *forcebeamcolumn* element with fiber section; see Figure 3.28d. It is more suitable to model the GPMC by a concentrated hinge (Figure 3.28a, b) or a finite length hinge (Figure 3.28c) model due to the known plastic hinge capacity and hinge location. A major drawback of concentrated plasticity model is that axial force-moment interaction cannot be captured. However, this is generally considered acceptable for beams in moment frames, for which the axial force level is not as critical as in columns.

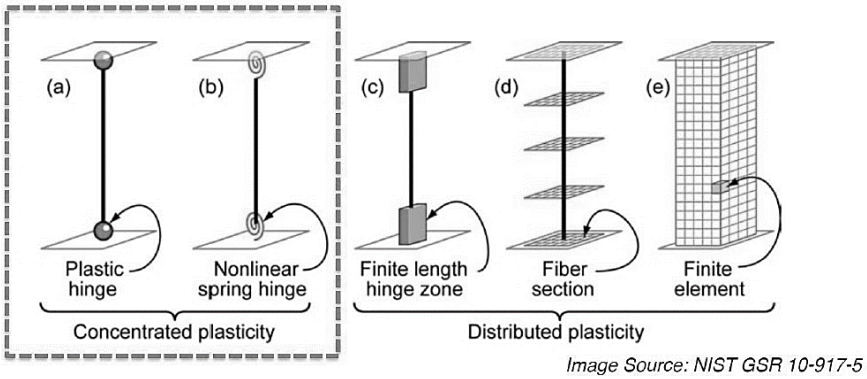

Figure 3.28 Different beam-column connection models

As shown in Section 3.3, the characteristics of the GPMC hysteresis loops depend on the beam depths and material of the gusset plate. The moment-rotation hysteretic relationship of the GPMCs using low-yield strength steel LYP100 (Figure 3.15) represents an ideal ductile GPMC connection behavior and will be used for the calibration process.

Due to the relatively small free gusset length compared to the hinge length in an RBS connection, the concentrated spring hinge model is considered suitable for the GPMC. In constructing the concentrated spring hinge model, an elastic *beamcolumn* element is created and connected with two *zero-length* rotational spring hinges on both ends; see Figure 3.28(b). Only the Young's modulus, the moment of inertia and area of the cross-section are needed to define the elastic *beamcolumn* element. To define the inelastic rotational hinge, a suitable material model that can describe the hysteretic characteristics of the plastic hinge behavior should be specified. Two types of material models were found to be suitable for modeling the GPMC with the *zero-length* rotational spring:

a. Uniaxial Steel02 material

This material model is based on the uniaxial Giuffre-Menegotto-Pinto (GMP) steel material model with isotropic hardening. The OpenSees *Steel02* material was developed by Filippou et al. (Filippou et al. 1983). The backbone curve of this material model is defined by the GMP model, and therefore the gradual yielding and Bauchinger effect can be captured. Only a few parameters need to be specified when using this model. However, it is not capable of capturing strength and stiffness degradation behavior and thus is only suitable for connections showing ductile behavior.

b. Uniaxial Bilin02 material using the modified Ibarra-Medina-Krawinkler (IMK) model

This material model uses the predictive equations developed by Lignos and Krawinkler (Lignos and Krawinkler 2009; Lignos and Krawinkler 2010). These equations relate the deterioration modeling parameters with geometric and material properties of the steel

components. They were developed based on multivariate regression analysis after extensive calibration of a recently developed steel component database of more than 300 steel specimens (Lignos et al. 2011; Lignos and Krawinkler 2007; Lignos and Krawinkler 2009). The backbone curve of this model is defined by a bilinear relationship and therefore cannot capture the gradual yielding of the material; however, it can capture the strength and stiffness degradation behavior of steel moment connections with and without composite slab action. Due to the inclusion of degradation features, this model is more complicated and requires many parameters to be specified.

Although the response history analyses in Chapter V will mainly use the *Steel02* material model, assuming a ductile behavior of the proposed GPMC moment connection, the use of IMK model is still discussed here for future reference. The following is a description of how to define the main parameters of these two material models.

3.4.1.2 Effective Yield Moment

To define a nonlinear moment hinge, typically only the effective yielding moment needs to be specified instead of defining separately the yield strength and plastic section modulus. A library containing all the section properties of the standard beam sections is usually available in most structural analysis software. For ease of implementation, the effective yielding moment of the GPMC can be defined by simply modifying the effective yielding strength of the input material properties while keeping the section properties the same as the incoming beam section. For example, for a GPMC with the expected plastic moment capacity ($R_{yg}F_{yg}Z_g$) equal to about 60% of that of the beam ($R_{yb}F_{yb}Z_b$), the input yielding strength, $R_{yg}F_{yg}$, will be equal to $0.6R_{yb}F_{yb}$ while assuming the section of the gusset plate is the same as the beam, i.e., $S_g = S_b$, $Z_g = Z_b$. It now becomes easy to modify the GPMC hinge model for different beam sections.

3.4.1.3 Stiffness Modification

As pointed out by Ibarra and Krawinkler (2005), the stiffness of the rotational springs should be modified to be "n" times larger than the rotational stiffness of the elastic element to avoid numerical problems and ensure all damping to be assigned to the elastic element. They recommended making the moment of inertia of the elastic element to be $(n+1)/n$ times greater than the actual moment of inertia of the elastic frame member so that the equivalent stiffness of the assembly becomes equivalent to the stiffness of the actual frame member (Ibarra and Krawinkler 2005), i.e.,

$$K_s = (n+1)K_{mem} \tag{3.1}$$

$$K_{bc} = \frac{n+1}{n}K_{mem} \tag{3.2}$$

The resulting strain hardening coefficient of the plastic hinge should also be modified as

$$\alpha_{s,s} = \frac{\alpha_{s,mem}}{1+n(1-\alpha_{s,mem})} \tag{3.3}$$

In the above equations, n is the amplification factor for the rotational spring stiffness, K_s is the modified stiffness of the rotational spring, K_{bc} is the modified stiffness of the elastic beam-column element, K_{mem} is the actual stiffness of the member, $\alpha_{s,mem}$ is the actual strain hardening coefficient of the member, and $\alpha_{s,s}$ is the strain hardening coefficient of the spring. When n is set to be a considerably large number, then the stiffness of the elastic beam-column element does not need to be modified since n+1 will be approximately equal to n. The stiffness modification was implemented in both Steel02 and IMK hinge model.

3.4.1.4 Ultimate-to-Yielding Moment Ratio (Strain Hardening Ratio)

The ultimate-to-yield moment ratio of any connection can be determined based on the properties of the selected gusset material or calibrated by experimental test results or finite element (FE) analysis results. If no test or FE results are available, this ratio is essentially the ratio of the expected ultimate strength to the expected yield strength of the gusset material, i.e., $R_{tg}F_{ug}/R_{yg}F_{yg}$. If the material model requires the definition of strain hardening ratio, the yielding drift ratio (rotation) and capping drift ratio (rotation) are needed in addition to the expected yield and ultimate moment of the connection to calculate this value. The capping point is defined as the point with maximum strength and beyond which the strength will start to drop. For the low-yield steel LYP100 GPMC, the strain hardening ratio is assumed to be 2%.

3.4.1.5 Other Parameters

a. Uniaxial Steel02 material

The material parameters that control the transition from elastic to plastic branches are chosen to have the following values: R0=10, cR1=0.925, and cR2=0.15, which were found to match the FE results well. More on the parameters of the *Steel02* model in OpenSees can be found in reference (OpenSeesWiki).

b. Uniaxial Bilin02 material using the modified Ibarra-Medina-Krawinkler (IMK) model

If the post-capping degradation behavior is not needed, the L_{mda} factor that defines the reference cumulative energy can be set to a large number, say, 1000, and all of the "*c*" exponent variables that defines the rate of strength deterioration to 1.0, and rate of cyclic deterioration variables "*D*" to 1.0. If the post-capping degradation behavior is included, the calibrated parameters for RBSs without composite action can be used (Lignos and Krawinkler 2010).

At this stage, no experiment has been conducted on the new GPMC; whether the degradation characteristics of a GPMC will match that of a typical welded flange steel connection is not yet available since the FE model can only reflect the strength/stiffness drop due to buckling but not fracture. Theoretically, directly application of the IMK model is not accurate. However, due to lack of enough information, the parameters calibrated by Lignos and Krawinkler (2009, 2011) are considered at this stage as an option to simulate the possible effects of degradation of the beam-to-column connection, assuming the degradation characteristics of the new GPMC are similar to those specimens used in developing the IMK model. More details of this model can be found in reference (OpenSeesWiki).

Figures 3.29 and 3.30 compare the calibrated OpenSees concentrated hinge model for the GPMC using the two chosen material types versus the FE results. Since the use of the LYP steel gusset plate leads to very ductile connection behavior, the non-degrading *Steel02* material is able to match the FE analysis results very well. Although the non-degrading IMK model could also match the FE analysis results fairly well, it tends to predict a smaller capping point for the LYP100 GPMC. It seems non-degrading IMK model might be a more suitable application for modeling the Gr.50 GPMC. Because the capping point of GPMCs depends heavily on the buckling of the gusset, and the capping points for different beam sections can be highly variant, it is expected that directly using the IMK model parameters calibrated for the RBS would be somewhat inaccurate. Without necessary experimental data at this stage, the IMK material can be employed as an option if a degradation feature is to be included. However, it is important to recognize that, in general, IMK model with cyclic degradation using the parameters calibrated for RBS (Lignos and Krawinkler 2010) would over-predict the level of stiffness and strength deterioration.

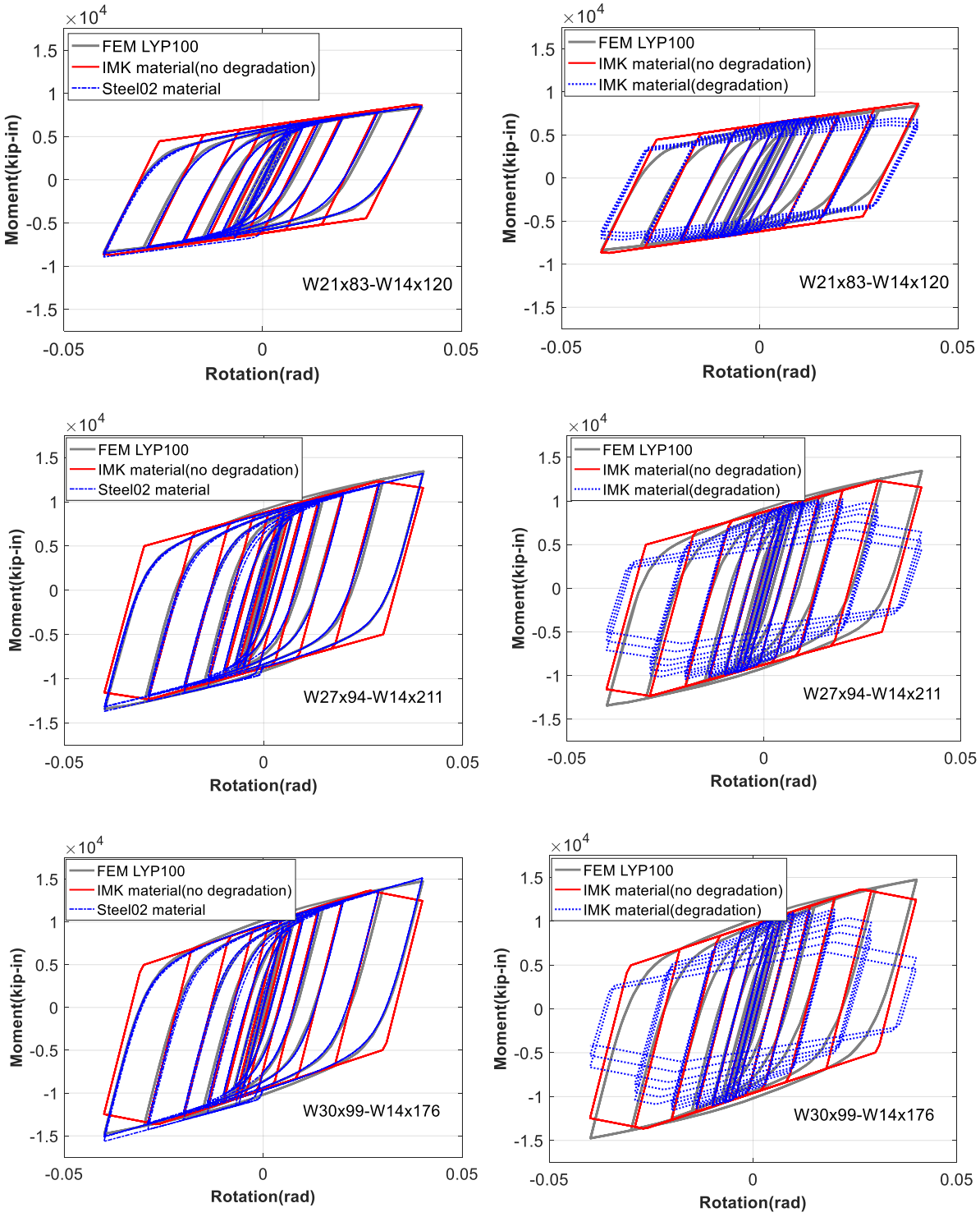

Figure 3.29 Comparison of FE results and concentrated hinge model in OpenSees for LYP100 GPMCs

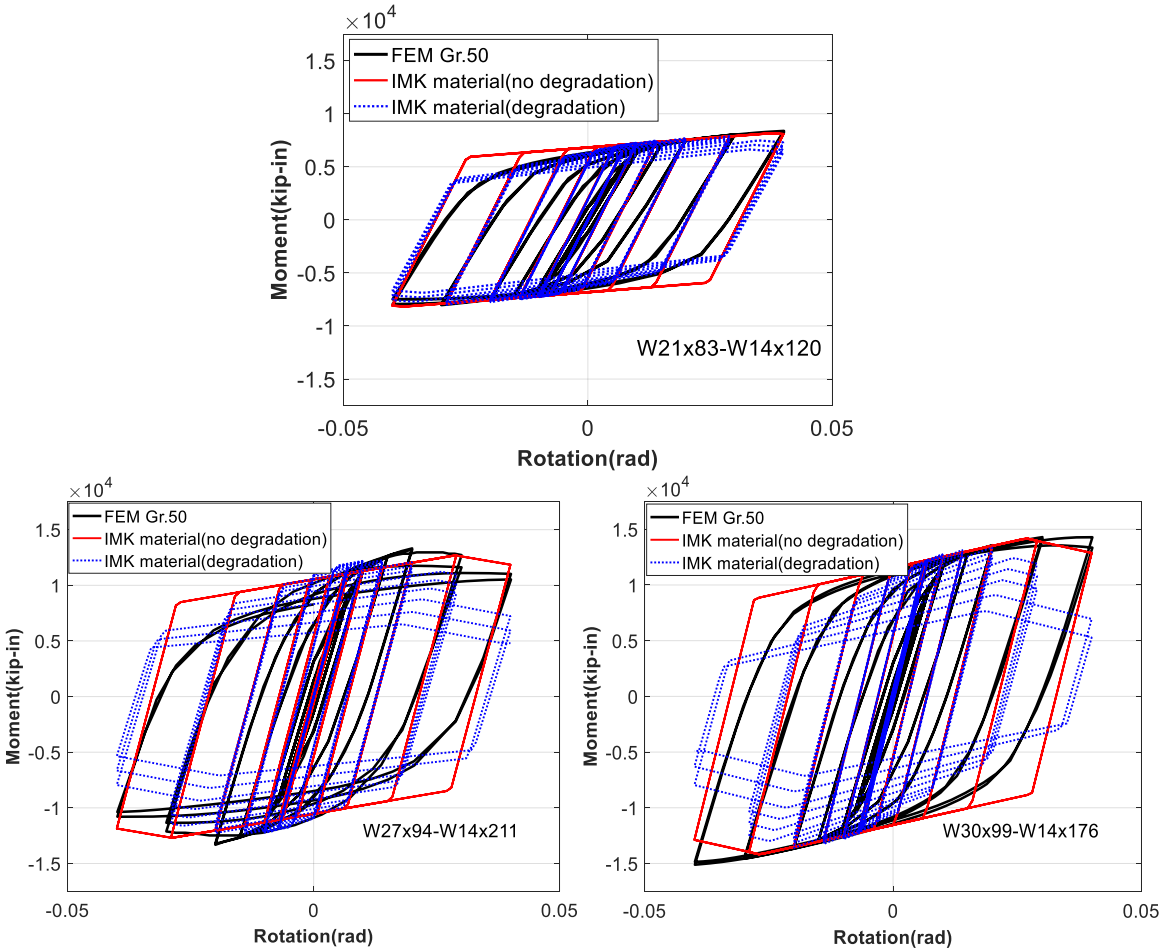

Figure 3.30 Comparison of FE results and concentrated hinge model in OpenSees for Gr.50 GPMCs

3.4.2 Equivalent Truss Model

As a simplified analysis and design tool, the equivalent truss model has been used by many researchers for the preliminary design of steel gusset plates, extended end-plate moment connections, and other connections. Astaneh-Asl (1989) proposed a simple method for the design of steel gusset plates where the gusset plate is represented by a series of radially positioned prismatic trusses (Figure 3.31). Both single member and multi-member scenarios were considered. The proposed method was found to predict the stresses in the gusset plates and the boundary welds reasonably well (Astaneh-Asl 1989). The truss analogy also has applications in moment connections. Popov and Stephen (1970) demonstrated that the well-established concept for designing the welded flange moment connections such that webs transfer shear, and the flanges transfer moment, may not be correct right at the connection region (Popov and Stephen 1970). Some theoretical evidence (Abel and Popov 1969) showed that right next to a rigid connection, a large portion of the shear is transferred from the web to the flanges. In 1996, Goel and his colleague

proposed the truss model for a steel moment connection as shown in Figure 3.32 (Goel et al. 1996). Based on the truss analogy based force transfer mechanism, they developed a new moment connection (Goel et al. 1996; Lee et al. 1997). Lee (2002) proposed an equivalent truss model in developing a seismic design procedure for rib-reinforced steel moment connections (Lee 2002). The FE results showed that the flexural stress profile is inconsistent with the linear stress profile predicted by a beam theory, and "reverse shear" phenomena was observed. The proposed equivalent truss model (Figure 3.33) was shown to better capture the stress distribution in the connection.

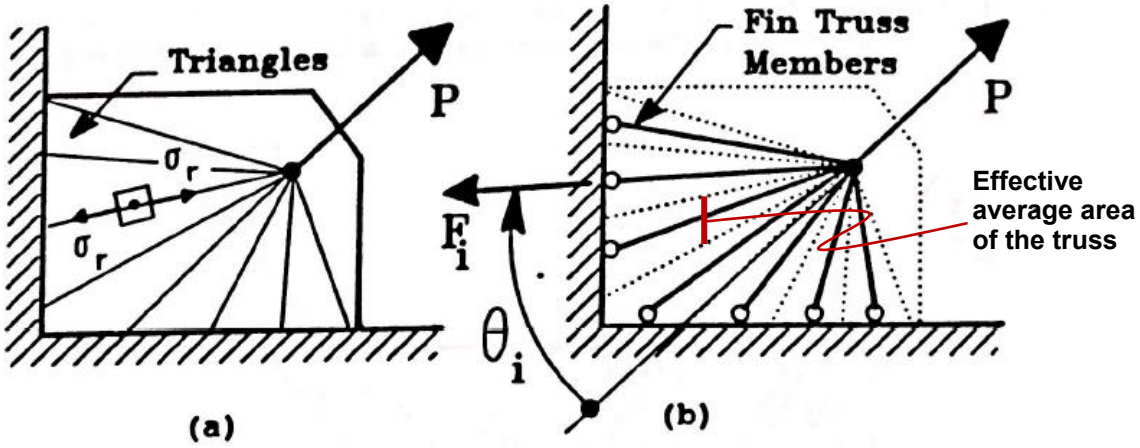

Figure 3.31 Simplified truss (wedge) analogy for design of gusset plate proposed by Astaneh-Asl (1989)

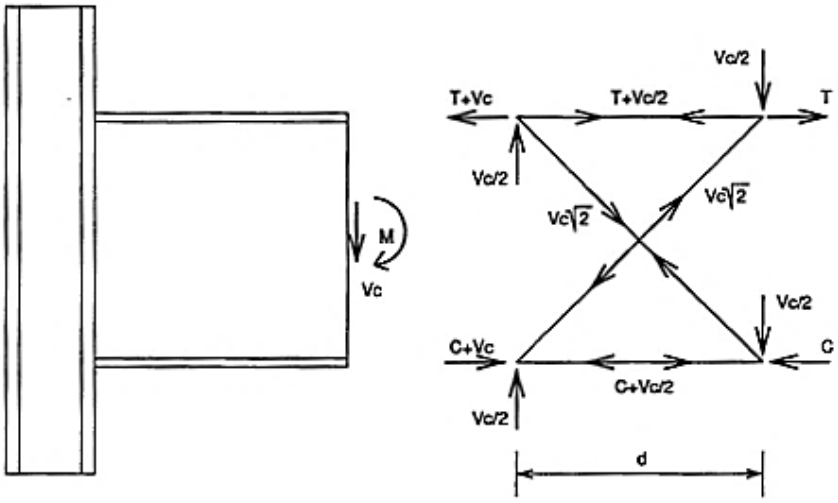

Figure 3.32 Truss analogy for moment connections proposed by Goel et al.(1996)

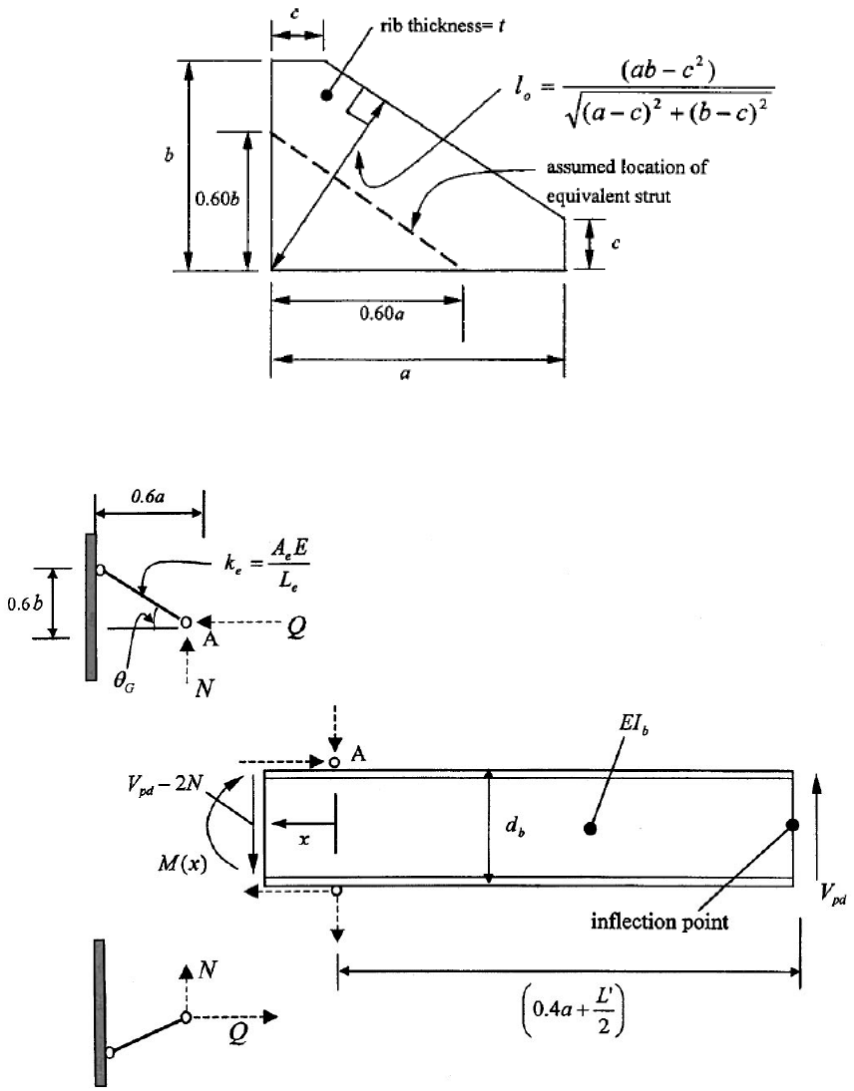

Figure 3.33 Truss analogy for rib-reinforced moment connection proposed by Lee (2002)

The truss analogy method is a relatively simple yet powerful tool that can be used to understand the force transfer mechanism and could possibly be used as an alternative analysis tool for steel connections. The following are some efforts in developing a truss analogy for the proposed GPMC.

In a GPMC, since the beam is not directly connected to the column, the force transferring mechanism is expected to be slightly different from that in a rib-reinforced moment connection. Instead of converting only the part of the gusset plate that extends outside the beam flange to an equivalent truss, which is similar to the truss analogy proposed by Lee (2002) for the rib-reinforced end-plate moment connection, it is considered more rational to replace the entire gusset plate with a series of trusses, as proposed in Astaneh-Asl (1989). Figures 3.34 and 3.35 show two possible truss analogies of the gusset plate. Here, for ease of comparison, the number of trusses used was the same as the number of nodes in the FE model. In design applications, the number of trusses

can be reduced to simplify the analysis. Each analogous truss member represents the gusset material corresponding to a wedge replaced by it, and the cross section of the truss is the average cross-sectional area inside the wedge; see Figure 3.31.

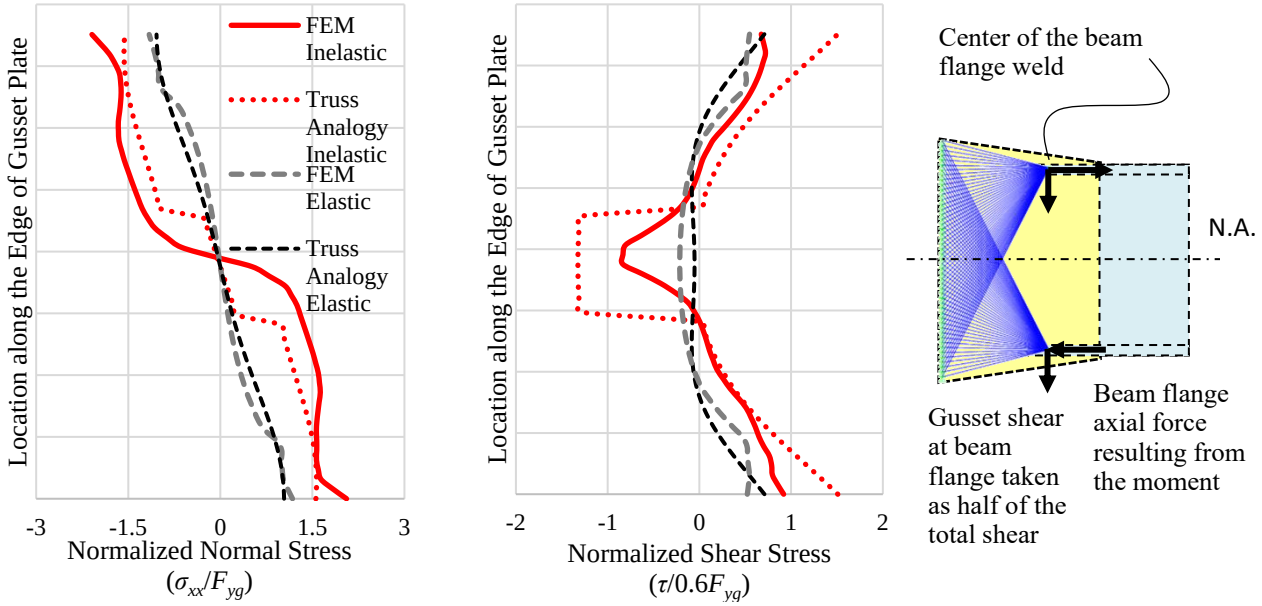

Figure 3.34 Simplified truss analogy for GPMC without considering the shear force distribution

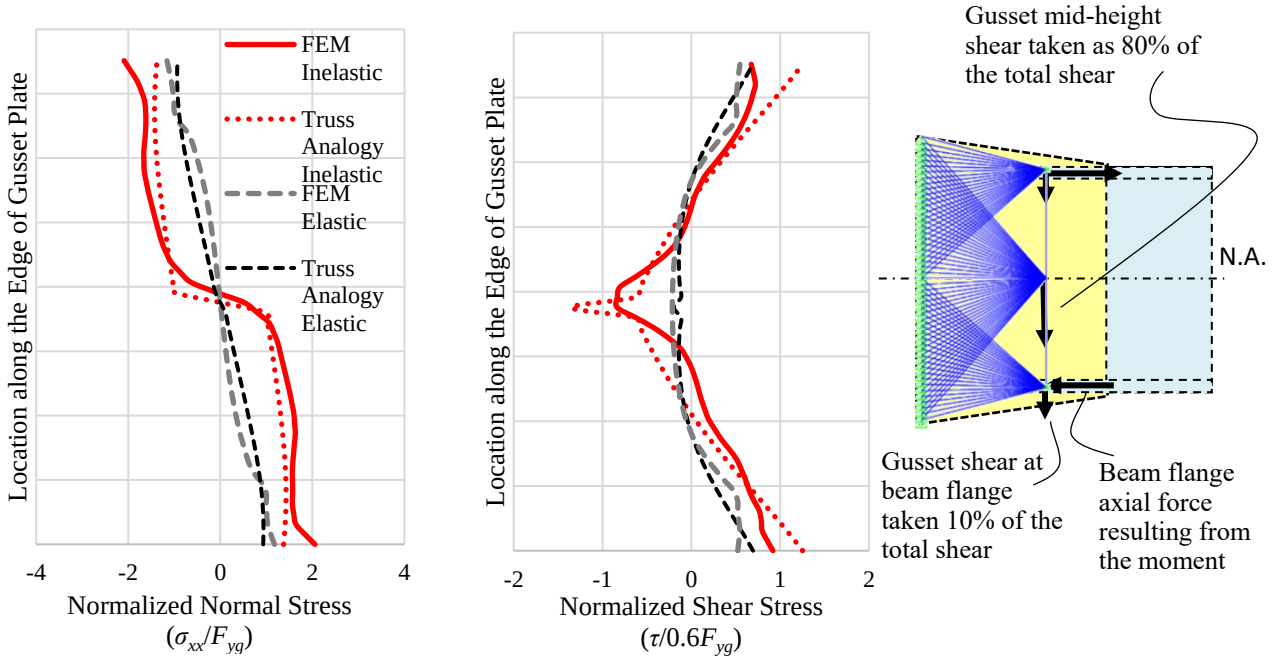

Figure 3.35 Simplified truss analogy for GPMC considering the shear force distribution

For the inelastic stage, tension and compression limits were assigned to each truss element to reflect the yielding of the gusset material. Two cases were considered: one did not include the shear force taken by the web inside a wide flange beam section, and the other did. The forces transferred by the beam flange and web were used as the applied force to the "truss" system of the GPMC. The nodes where forces are applied are located at the center of the gusset horizontal welds. The nodes were connected to each other by a rigid link so that the behavior of the analogous truss system mimics the behavior of nodes at the corresponding locations in a wide flange beam (plane section remains plane).

Figure 3.35 shows that this truss analogy can, in general, capture the basic shape of the normal and shear stress profile for the elastic (at a drift ratio of 0.001) and inelastic stage (at a drift ratio of 0.03). After including the more realistic shear force distribution as the applied force, assuming approximately 80% transferred by beam web, and 10% transferred by each beam flange, both normal and shear stress close to the neutral axis achieved a better match to the FE results.

Note: the above is just a preliminary attempt of the truss analogy. Several limitations still exist, and further refinement is needed for future work: (1) a fewer number of trusses is desired for preliminary design purposes; (2) the double counting problem should be resolved as in the current truss analogy some of the truss members intersect with each other; and (3) more rigorous parametric studies are desired to validate the general applicability of the proposed truss analogy to establish stresses in the gusset plate in the proposed GPMC.

3.5 Proposed Design Procedure for the New Gusset Plate Moment Connection

Based on the results of previous parametric studies and calibration/development of simplified models for the proposed GPMC, a proposed design procedure will be presented in this section. The design procedure was developed based on the pre-set performance criteria and follows the desirable limit state hierarchy defined below.

3.5.1 Performance Criteria

The desirable performance criteria for GMPC is as follows:

1. The inelasticity should occur primarily in the gusset plate, which means the gusset plate should be the inelastic "fuse" in the connection, and the plastic hinge in this beam-to-column connection forms in the gusset plate and remains there.
2. The column web within the joint is allowed to have some limited yielding.
3. The beam needs to remain essentially elastic with some limited local yielding allowed.
4. The connection should have sufficient plastic bending moment and axial capacity and shear strength to resist the combined effects of the gravity and lateral forces.

5. The connection should have sufficient rotational stiffness and ductility to ensure that the inter-story drift values remain under the limits allowed by applicable building codes.
6. All connectors (i.e., welds and bolts) should remain elastic throughout the cyclic event.
7. No fracture of any element of connection is allowed throughout the cyclic event.
8. Ductile failure modes such as yielding of steel should occur before the brittle failure modes like fracture of components.
9. All of the inelastic activities should occur in a controlled and predictable manner, and occur at designated locations.

3.5.2 Hierarchy of Limit States (Failure Modes)

The first step in developing design procedures is to identify all possible limit states (failure modes) of the system as well as its components. The next step is to group them into "ductile," "mildly ductile," and "brittle" categories. Then, the limit states are further placed in a hierarchical order such that ductile behavior always occurs before the mildly ductile limit states, and brittle limit states occur last. The limit states will differ slightly for different connection details as shown in Figures 3.2 and 3.5. Table 3.4 and Table 3.5 provide a hierarchical relationship that generally applies to all the different details of the proposed designs of the GPMC.

Table 3.4 Limit states for welded GPMC

Ductile
• Yielding of the gusset plate under combined shear and bending, and axial load if present
• Yielding of top and bottom flange plates (when applicable)
• Limited yielding of the column web
• Limited local yielding of the beam
Mildly Ductile
• Local buckling of the gusset plate
• Local buckling of the beam flange and the web
• Local buckling of the column flanges and the web
• Local buckling of top and bottom flange plates (when applicable)
• Bearing failure at bolt holes in the beam flange and in the top and bottom flange plates (when applicable)
• Limited yelding of the column panel zone
Brittle
• Block shear rupture of the gusset plate around the horizontal welds
• Shear rupture of the gusset plate near the vertical welds under gravity and lateral load effect
• Block shear rupture of the beam
• Block shear rupture of the top and bottom plate (when applicable)
• Net section fracture of the beam tension flange (when applicable)
• Fracture of any weld in the connection

Table 3.5 Limit states for bolted GPMC

Ductile
• Yielding of the gusset plate under combined shear and bending, and axial load if present
• Limited yielding of gusset flange plate under prying action effects
• Yielding of top and bottom flange plates (when applicable)
• Limited yielding of the column web
• Limited local yielding of the beam
Mildly Ductile
• Flexural yielding of the gusset and column flanges in the vicinity of the bolts
• Local buckling of the gusset plate
• Local buckling of the beam flange and the web
• Local buckling of the column flanges and web
• Limited yielding of column panel zone
• Shear yielding of the gusset flange plate
• Bearing failure at bolt holes in the gusset flange, beam flange and the top and bottom flange plates (when applicable)
Brittle
• Block shear rupture of the gusset plate
• Shear rupture of the gusset plate around the vertical welds under gravity and lateral load effect (applicable only when the gusset plate is welded to the gusset flange plate)
• Shear rupture of the gusset flange along bolt holes under gravity and lateral load effect
• Block shear rupture of the beam
• Block shear rupture of the top and bottom plate (when applicable)
• Fracture of bolts
• Fracture of any weld in the connection
• *Net section fracture of the beam flange (N.A. if follow the suggested construction sequence)

Particular attention should be paid to limit states that involve gravity loads, since if these limit states are reached, partial or full collapse of a part of the structure can occur. An example of such failure mode is a shear failure of the beam-to-column moment connections. If the shear capacity of the connection is lost, the end of the beam can drop due to the gravity load in the connection, resulting in collapse of the span. In the 1994 Northridge earthquake, however, the shear strength of the connection was sufficient, even after the failure of connections in bending (i.e., fracture of flange welds), and no span collapsed under gravity shear. Studies showed that after fracture of the flange welds in welded momnet connections in one of the buildings during the Northridge earthquake, the frame converted to a semi-rigid frame and developed less seismic forces and smaller drift, thus surviving the event without collapse (Astaneh-Asl et al. 1998).

3.5.3 Proposed Design Procedure

The proposed design procedure contains five major stages after selection of beam and column sections: (1) sizing the gusset plate, including selection of the gusset material; (2) determining the shear strength of the gusset plate; (3) confirming the "strong-frame–weak-gusset" criteria; (4) designing the beam-to-gusset connection; and (5) designing the gusset-to-column connection. As this design procedure is an intermediate product based on the current numerical analysis results and existing steel moment connection design theories and concepts, it is considered interim and accepts any necessary changes based on future experimental and analytical research and development efforts. All references to the code specifications applicable at the time of writing of this design procedure should be the adjusted to the most updated version at the time of use. Before presenting the step-by-step design procedure, several aspects are worth mentioning:

1. In the parametric study part in Section 3.3, most cases were designed to satisfy the criterion that the probable moment capacity of the gusset plate is smaller than the nominal yield capacity of the beam, i.e., $M_{prg} < M_{yb}$. When developing the design procedure, instead of using the conservative nominal yield moment capacity of the beam to avoid the net section issue, the limit states of net section fracture and gross yielding of beam are explicitly included;

2. Figure 3.36 shows that a typical flexural stress profile along the edge of the gusset plate where it is connected to the column is very close to, though not exactly, what the beam theory would predict: triangular at the elastic stage and almost rectangular after most fibers yield. Some edge effects of the gusset plate can be observed, but they were not as pronounced as that in a rib-stiffened moment connection per Lee (2002). Therefore, in the proposed design procedure, the plastic moment capacity of the gusset plate is calculated based on the rectangular stress distribution for a simple rectangular cross section;

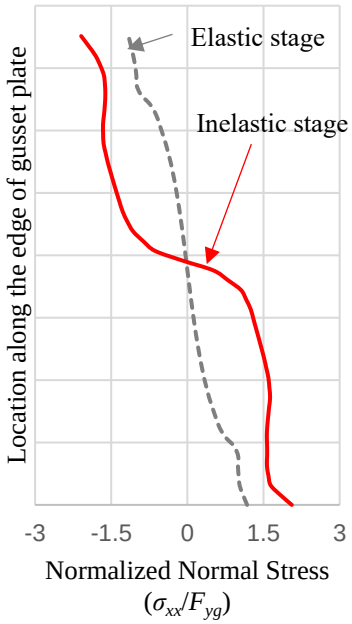

Figure 3.36 Typical stress distribution in the gusset plate at elastic and inelastic stage

3. For a proposed bolted GPMC, establishing the actual center of compression is much more complicated than simply assuming it to be at the center of the compression beam flange shown in Figure 3.20 (Abidelah et al. 2012; D'Aniello et al. 2017). However, the compression center is still assumed to be at the beam compression flange in the proposed design procedure because it is conservative and straightforward, and is consistent with the common practice for existing moment connection (AISC 2010b);

4. Since the column flange in a bolted GPMC under tension is experiencing a similar loading condition as the flange in a T-hanger type connection, similar checks should be used in determining the thickness of the T-hanger flange. For most cases of both bolted and welded GPMCs, it was found that the column web local yielding, column web buckling, and crippling limit state present for other moment connections will not govern. This is mainly because of the elimination of the concentrated beam flange force: the force transferred to the column from the gusset plate will be more uniform and result in a much larger bearing width, i.e., the t_{bf} parameter in all the related equations will have to be changed to $H_{g1}/2$. This elimination of concentrated beam flange force increases the column web capacity significantly. Therefore, the column side check in the proposed design procedure for the GPMC becomes significantly simpler compared to the end-plate moment connection procedure.

The step-by-step design procedure is presented below. The equations and figures are numbered for the design procedure separately from the equations in the main text, starting with a prefix "C-". The numbering of equations follows the numbering of steps.

Proposed Design Procedure for the GPMC

Stage I. DESIGN OF FRAME

The beams and columns should be designed before designing the connection. The beams and columns should be selected to satisfy the strength and drift requirements for all load combinations specified by the applicable building code, with the GPMC strength considered. High-strength beam and column material such as A992 Gr.50 or A913 Gr.50 or Gr.65 are recommended for moment frames using GPMCs. In lieu of more detailed analysis and similar to the design of RBSs, effective elastic drifts may be calculated by multiplying elastic drifts obtained in a model that uses the gross beam sections multiplied by 1.1 for gusset plates with expected plastic moment strength reduced up to 60% of that of the beam, i.e., $R_{yg}F_{yg}Z_g = 0.6R_{yb}F_{yb}Z_b$. This 40% strength reduction is approximately equivalent to 50% reduction of beam flange width in a RBS given in ANSI/AISC 358-10 (AISC 2010b). Linear interpolation may be used for smaller gusset strength reductions.

Stage II. DESIGN OF GUSSET PLATE

Step 2-1 Selection of gusset material

Common plate material such as A572 Gr.50, A36, and low-yield point steel can be chosen based on market availability. For deep and heavy beams, lower strength gusset material, including the low-yield point steel (LYP), is recommended.

Step 2-2 Determine gusset thickness

The thickness of the gusset plate should satisfy:

a. For Gr.50 or A36 gusset

$$1.0t_{bw} \le t_g \le 1.75t_{bw} \quad \text{(C-2-2a)}$$

b. For LYP100 gusset

$$1.5t_{bw} \le t_g \le 2.5t_{bw} \quad \text{(C-2-2b)}$$

where

t_g = the gusset plate thickness

t_{bw} = the beam web thickness

Thicker gusset thickness is recommended for lower yield strength. For LYP steel, the thickness can be up to $3.5t_{bw}$ as long as the performance criteria is satisfied, and the resulting plate thickness is reasonable. *See the commentary section of this design procedure on the effect of choice of gusset thickness on the resulting gusset angle and nominal gusset plastic moment capacity (all other parameters determined following the design procedure in this document).*

Step 2-3 Determine the required gusset plate plastic hinge capacity

(a) For GPMC <u>with</u> a net section at the gusset-beam interface

This case usually applies to the welded GPMC, where a slot in the beam flange is needed to connect the beam to the gusset plate in the field. The required plastic section modulus of the gusset plate should be determined by Eqn.(C-2-3a),

$$Z_g = \frac{0.9R_{yb}F_{yb}Z_b}{C_{prg}R_{yg}F_{yg}} \le \frac{0.75R_{tb}F_{ub}Z_{nb}}{C_{prg}R_{yg}F_{yg}} \quad \text{(C-2-3a)}$$

where

Z_{nb} = the plastic section modulus of the beam at the net section,

$$Z_{nb} = Z_b - t_g t_{bf} \cdot \left(d_b - t_{bf}\right) \quad \text{(C-2-3b)}$$

R_{yb} = the expected yield strength factor of the beam

R_{tb} = the expected ultimate strength factor of the beam

F_{yb} = the minimum specified yield strength of the beam

F_{ub} = the specified ultimate strength of the beam

Z_b = the gross plastic section modulus of the beam

C_{prg} = the strain hardening factor of the gusset plate, which is determined as

$$C_{prg} = \frac{F_{ug} + F_{yg}}{2F_{yg}} \quad \text{(C-2-3c)}$$

R_{yg} = the expected yield strength factor of the gusset plate

F_{yg} = the minimum specified yield strength of the gusset plate

F_{ug} = the specified ultimate strength of the gusset plate

With the presence of a slot, the limit states of net section fracture at the slot location as well as the plastic hinge formation in the beam should be considered in this case, i.e.,

a. Gross yielding of the beam:

$$M_{prg} = C_{prg}R_{yg}F_{yg}Z_g \le \phi M_{pb} = 0.9R_{yb}F_{yb}Z_b \quad \text{(C-2-3d)}$$

b. Net section fracture at the slot location

$$M_{prg} = C_{prg}R_{yg}F_{yg}Z_g \le \phi M_{nb} = 0.75R_{tb}F_{ub}Z_{nb} \quad \text{(C-2-3e)}$$

Equation (C-2-3a) is derived based on the above two limit states. In the above equations, the strength of gusset plate is designed such that the expected strain hardened moment capacity of the gusset, combined with the gravity load effect, should not cause any net section fracture at the slot location or yielding in the gross section of the beam. R_y, R_t, and φ factors should be considered to make the right-hand-side of Eqn. (C-2-3d) and (C-2-3e), the correct seismic capacities. The left-hand-side of these two equations should be the moment demand at the slot location caused by the plastic hinge formation in the gusset plate and the additional moment due to gravity shear. The

extra moment due to gravity shear is neglected in Eqn.(C-2-3a) due to the small free gusset length. More accurate moment demand at the slot location can be established using basic equilibrium.

This research found that for thin gusset plates causing small reduction of net area, the yielding limit state might govern over the net section fracture. The limit state of block shear rupture at the beam-to-gusset plate connection is not considered in this step but it will be included when designing the beam-to-gusset connection.

(b) For GPMC <u>without</u> a net section at the gusset-beam interface

This case will usually be applied to the proposed bolted GPMC, where the beam is welded to the gusset plate in the shop, and the gap at the end of the slot creating the net section can be eliminated. In this case, only the limit state of plastic hinge formation in the beam needs to be considered in establishing the required plastic section modulus for the gusset plate,

$$Z_g = \frac{0.9 R_{yb} F_{yb} Z_b}{C_{prg} R_{yg} F_{yg}} \qquad \text{(C-2-3f)}$$

Step 2-4 Determine the gusset height

The height of the gusset plate, together with the selected thickness should provide the required plastic modulus determined in Steps 2-3 above. The height of gusset plate, H_{g1}, is calculated using,

$$H_{g1} = \sqrt{\frac{4Z_{g\_req}}{t_g}} \le d_b + \Delta_{\lim} \qquad \text{(C-2-4)}$$

where

Z_{g_req} = the required plastic section modulus of the gusset plate determined in Step 2-3
$\Delta_{\lim}$ = the applicable architectural limit
d_b = the total depth of the beam

The height of gusset plate in Eqn. (C-2-4) is calculated using the plastic section modulus for a rectangular cross section. The height of gusset plate can be rounded down based on what is determined by Eqn. (C-2-4), but it is recommended to be not too small to avoid too much sacrifice in the strength of the connection. *See the commentary section of this design procedure on the effects of the architectural limit on the resulting gusset angle and nominal gusset plastic moment capacity (all other parameters chosen following the design procedure in this document).*

Step 2-5 Determine the free gusset length

The free gusset length, L_{fg}, is recommended to satisfy the following,

$$4t_g \le L_{fg} \le 7t_g \tag{C-2-5}$$

Step 2-6 Determine the shorter gusset height

The shorter height of gusset plate, H_{g2}, should simply be the beam depth plus 2 in. to accommodate welding

$$H_{g2} = d_b + 2'' \tag{C-2-6}$$

Stage III. CHECK ADEQUACY OF GUSSET PLATE SHEAR CAPACITY

Step 3-1 Check the shear capacity of gusset plate

The shear capacity of the gusset plate should be greater than the shear demand,

$$V_{gu} \le \phi V_{gn} \tag{C-3-1a}$$

where

ϕ = 0.9

V_{gn} = the nominal shear capacity determined by

$$V_{gn} = 0.6F_{yg}H_{g1}t_g \tag{C-3-1b}$$

V_{gu} = the shear demand in the middle of plastic hinge which can be calculated as

$$V_{gu} = \frac{2M_{prg}}{L_h} + V_{gravity} \tag{C-3-1c}$$

L_h = distance between plastic hinges, which can be established by the clear distance between column faces minus the free gusset length, L_{fg}

$V_{gravity}$ = beam shear force resulting from $1.2D+f_1L+0.2S$ (where f_1 is the load factor determined by the applicable building code for live loads, L, but not less than 0.5; D and S are the dead load and snow load respectively), kips(N)

Stage IV. CHECK ADEQUACY OF THE COLUMN IN THE JOINT

Step 4-1 Check strong-column weak-gusset relationship

The strong-beam–weak-gusset relationship is already ensured in the first stage. This step is to ensure the gusset plate is also weaker than the column by satisfying the following,

$$\mathrm{M}^{*}_{prg} \le \sum M^{*}_{pc} \tag{C-4-1a}$$

where

M^{*}_{prg} = the modified probable gusset plastic moment capacity at the intersection of the beam/column centerlines, i.e.,

$$M^{*}_{prg} = M_{prg} + (L_{fg}/2 + d_c/2)\cdot V_{gu} \tag{C-4-1b}$$

$\sum M^{*}_{pc}$ = the sum of the moments in the column above and below the joint at the intersection of the beam and column centerlines. It is determined by summing the projections of the nominal flexural strengths of the columns above and below the joint to the beam centerline with a reduction due to the axial force, P_{uc}, in the column, i.e.,

$$\sum M^{*}_{pc} = \sum \left[Z_c \left(F_{yc} - P_{uc}/A_{gc} \right) + V_c \cdot d_b/2 \right] \tag{C-4-1c}$$

V_c = the shear force in the column outside the joint
V_{gu} = the shear force in the gusset plate determined in Eqn. (C-3-1c)
Z_c = the plastic section modulus of the column
F_{yc} = the minimum specified yield strength of the column
A_{gc} = the gross section area of the column
P_{uc} = the factored axial force in the column due to the governing combined loads

Stage V. DESIGN GUSSET-TO-BEAM WELDED CONNECTION

Step 5-1 Design the horizontal weld length

Design the horizontal fillet weld length, L_{wh}, such that block shear rupture of the beam flange and gusset plate does not occur, and the welds can develop the force due to expected yielding of the beam flange. The length of the horizontal welds, L_{wh}, should satisfy,

$$L_{wh} = \frac{T_{y\_bf}}{0.9F_{yb}t_{bf}} \ge \frac{T_{y\_bf}}{0.9F_{yg}t_g} \tag{C-5-1a}$$

where

T_{y_bf} = the expected yield strength of the beam flange given by,

$$T_{y\_bf} = R_{yb}F_{yb}b_{bf}t_{bf} \tag{C-5-1b}$$

Eqn.(C-5-1a) is derived considering the following two limit states,

a. Block shear rupture of the beam flange

$$0.75(0.6F_{yb})(2t_{bf}L_{wh}) \geq T_{y\_bf} \quad \text{(C-5-1c)}$$

b. Block shear rupture of the gusset plate

$$0.75(0.6F_{yg})(2t_{g}L_{wh}) \geq T_{y\_bf} \quad \text{(C-5-1d)}$$

Step 5-2 Design the horizontal weld size

The weld size should be determined such that the weld can provide the required strength and satisfy the minimum weld size requirements of the AISC Specifications (AISC, 2010d; AISC, 2016c).

(a) For fillet welds, the weld size, *D*, is given by,

$$D = \frac{T_{y\_bf}}{1.273F_{EXX}L_{wh}} \geq D_{\min} \quad \text{(C-5-2a)}$$

where

D_{min} = the minimum fillet weld requirement in AISC Specifications (AISC, 2010d; AISC, 2016c)
F_{EXX} = filler metal classification strength of the weld specified in ASIC Specifications (AISC, 2010d; AISC, 2016c)

The first part of Eqn. (C-5-2a) ensures the limit state of weld fracture has a strength larger than the force due to the expected yield capacity of the beam flange, i.e.,

$$0.75 \cdot 0.6F_{EXX} \cdot \left(4 \cdot \frac{D}{\sqrt{2}}L_{wh}\right) \geq T_{y\_bf} \quad \text{(C-5-2b)}$$

(b) For Partial Joint Penetration (PJP) welds, the weld size, *S*, is given by,

$$S = \frac{T_{y\_bf}}{1.8F_{EXX}L_{wh}} \geq S_{\min} \quad \text{and} \quad S \leq S_{\max} \quad \text{(C-5-2c)}$$

where

S_{min} = the minimum PJP weld requirement in AISC Specification (AISC, 2010d; AISC, 2016c)
S_{max} = the maximum PJP size limit in AISC Specification (AISC, 2010d; AISC, 2016c) by

$$S_{\max} \leq t_{bf} - \frac{1}{8}" \quad \text{(C-5-2d)}$$

Again, the first part of Eqn. (C-5-2c) ensures the limit state of weld fracture has a strength larger than the force due to the expected yield capacity of the beam flange, i.e.,

$$0.75\cdot\left(0.6F_{EXX}\right)\cdot\left(4\cdot S\cdot L_{wh}\right)\geq T_{y\_bf} \qquad \text{(C-5-2e)}$$

Step 5-3 Design the weld connecting the beam web to gusset plate

Design the welds connecting the beam web to the gusset plate as standard "butt" weld or fillet weld following the procedures given in the AISC Specifications (AISC 2010d, AISC 2016c).

Stage VI. DESIGN GUSSET-TO-COLUMN CONNECTION

W. Welded Option

Step 6W-1 Design the welds connecting the gusset plate to the column

(a) If fillet welds are used, then the weld size, *D*, should be determined by the following

$$D=\frac{C_{prg}R_{yg}F_{yg}t_g}{0.636F_{EXX}}\geq D_{\min} \qquad \text{(C-6W-1a)}$$

where

D_{min} = the minimum fillet weld requirement in AISC Specifications (AISC, 2010d; AISC, 2016c)

The above equation ensures the weld connecting the gusset plate to the column flange can develop the strain hardened tension force by 1-in. strip of the gusset plate material by satisfying,

$$0.75\cdot 0.6F_{EXX}\cdot 2\cdot\frac{D}{\sqrt{2}}\cdot(1'')\geq C_{prg}R_{yg}F_{yg}(1'')t_g \qquad \text{(C-6W-1b)}$$

(b) If CJP welds are chosen, matching filler weld material should be used.

Step 6W-2 Check column web thickness

The column web should be thick enough to take the force transferred by the gusset plate. The following equation is recommended to be satisfied to avoid excessive column web local yielding, buckling and crippling

$$t_{cw}\geq\frac{F_{yg}}{F_{yc}}t_g \qquad \text{(C-6W-2)}$$

where

t_{cw} = the column web thickness

Note that for the welded GPMC, due to the relatively well distributed force transfer from the gusset plate to the column, the limit state of local column yielding, column web buckling, and column web crippling need not to be explicitly checked. If the column web is too thin, then doubler plates should be provided to satisfy Eqn. (C-6W-2).

Step 6W-3 Check column shear capacity

The applied shear force inside the column should not exceed its nominal shear capacity.

$$V_{cu} \le \phi V_{cn} \qquad \text{(C-6W-3a)}$$

where

V_{cu} = shear force in the column inside the joint given by,

$$V_{cu} = \frac{M_{prg}}{H_{g1}/2} - V_c \qquad \text{(C-6W-3b)}$$

V_{cn} = the nominal shear capacity of the panel zone, which can be calculated according to Section J in AISC 360-10 or a corresponding section in AISC 360-16 (AISC, 2010d; AISC, 2016c).

V_c = the shear force in the column outside the joint

Based on the analysis result, the stress distribution on the gusset plate cross section is almost rectangular; therefore, the point of reaction is assumed to be located at the center of the rectangular stress blocks, making the moment arm half of the gusset depth, i.e. $H_{g1}/2$. The first term on the right-hand-side of Eqn. (C-6W-3b) is equivalent to $M_{pr}/(d_b\text{-}t_{bf})$ in conventional welded flange moment connections. Although changing the moment arm from $(d_b\text{-}t_{bf})$ to $H_{g1}/2$ in Eqn. (C-6W-3b) will increase the level of shear demand in the column web, the reduction of the column face moment demand due to weak gusset design philosophy helps to keep a relatively low column shear demand. If the column shear capacity is not sufficient, then doubler plates should be provided to increase the column shear capacity by increasing the shear area, or continuity plates can be added to increase the shear capacity and ductility of the panel zone by providing stronger boundaries to the panel zone.

B. Bolted Option

For the bolted option, both the gusset flange side and the column side need to be designed/checked.

Gusset Flange and Bolt Design

Step 6B-1 Select the bolt group configuration

Select the bolt group configurations that fit the height of the gusset plate. Typical 3-in. bolt spacing, and 1.5-in. edge distance are recommended.

Step 6B-2 Determine the preliminary bolt diameter

The bolt diameter can be preliminarily designed by the expected tensile forces in the bolts according to the assumed simple equilibrium as shown in Figure 3.20. A bolt diameter slightly larger than that required in Eqn. (C-6B-2a) can be selected to avoid too many iterations that may be caused by development of prying action forces. The equation to establish the required bolt diameter, $d_{breq'd}$, is:

$$d_{breq'd} = \sqrt{\frac{2M_{prg}}{N\pi\phi_n F_{nt}\sum h_i}} \tag{C-6B-2a}$$

where

F_{nt} = nominal tensile strength of bolt given in the ASIC Specifications (AISC 2010d; AISC 2016c)
ϕ_n = effective strength factor of bolt rupture = 0.75
h_i = distance from the centerline of the beam compression flange to the centerline of the i^{th} tension bolt row
N = number of bolts per horizontal row, typically $N = 2$

Note that the center of compression may migrate during the cyclic loading; here, the center of compression is assumed be to at the beam compression flange for simplicity and conservatism.

Step 6B-3 Determine the required gusset flange thickness

Using the preliminary bolt diameter and the determined forces acting on the "equivalent hanger" part of the gusset flange (Figure 3.20), the applied tension per bolt can be established as follows,

$$T = \frac{1}{N}\frac{M_{prg}}{\sum h_i} \tag{C-6B-3}$$

N is the same as used in Step 6B-2. Then the gusset flange thickness can be designed according to the simplified T-hanger design procedure (AISC 2010a; Astaneh-Asl 1985). Iterate the bolt strength to obtain a reasonable gusset flange thickness.

Step 6B-4 Check the bolt shear rupture capacity

Check bolt shear rupture assuming the shear strength is provided by the bolts on the compression side only. The equation to check the bolt shear strength is,

$$V_{gu} \le \phi_n \left(n_{bc} F_{nv} A_{bolt}\right) \tag{C-6B-4}$$

Where

V_{gu} = shear force demand in the gusset plate defined in Eqn. (C-3-1c)

n_{bc} = number of bolts at the compression side, typically assumed to be half of the total number of bolts
A_{bolt} = nominal gross area of bolt
F_{nv} = nominal shear strength of bolt given in the AISC Specifications (AISC 2010d; AISC 2016c)

Step 6B-5 Check bolt-bearing/tear-out failure of the gusset flange and column flange
Check bolt bearing failure for the same compression-side bolts used in Step 6B-4. This check can be done using the standard method for checking the bearing strength at bolt holes as given in the AISC Specifications (AISC 2010d; AISC 2016c).

Column-Side Check
Step 6B-6 Check column flange flexural yielding
The column flange in a bolted GPMC experiences similar forces as the flange in a T-hanger connection. Therefore, column flange thickness should at least satisfy the minimum thickness required for a T-hanger flange due to prying action (AISC 2010a; Astaneh-Asl 1985). Some additional tolerance should be given to the column flange considering the axial force in it.

Step 6B-7 Check column web thickness
This check is the same as Step 6W-2.

Step 6B-8 Check column shear capacity
This check is the same as Step 6W-3. For the bolted configuration, the shear demand in Eqn. (C-6W-3b) should be modified as follows,

$$V_{cu} = \frac{M_{prg}}{H_{b-b}/2} - V_c \qquad \text{(C-6B-8)}$$

where

$H_{b\text{-}b}$ = the distance between the center of the tension and compression bolt groups.

The design flow chart is shown in Figure 3.37. Reference to the section number in the design procedure is provided in the bracket.

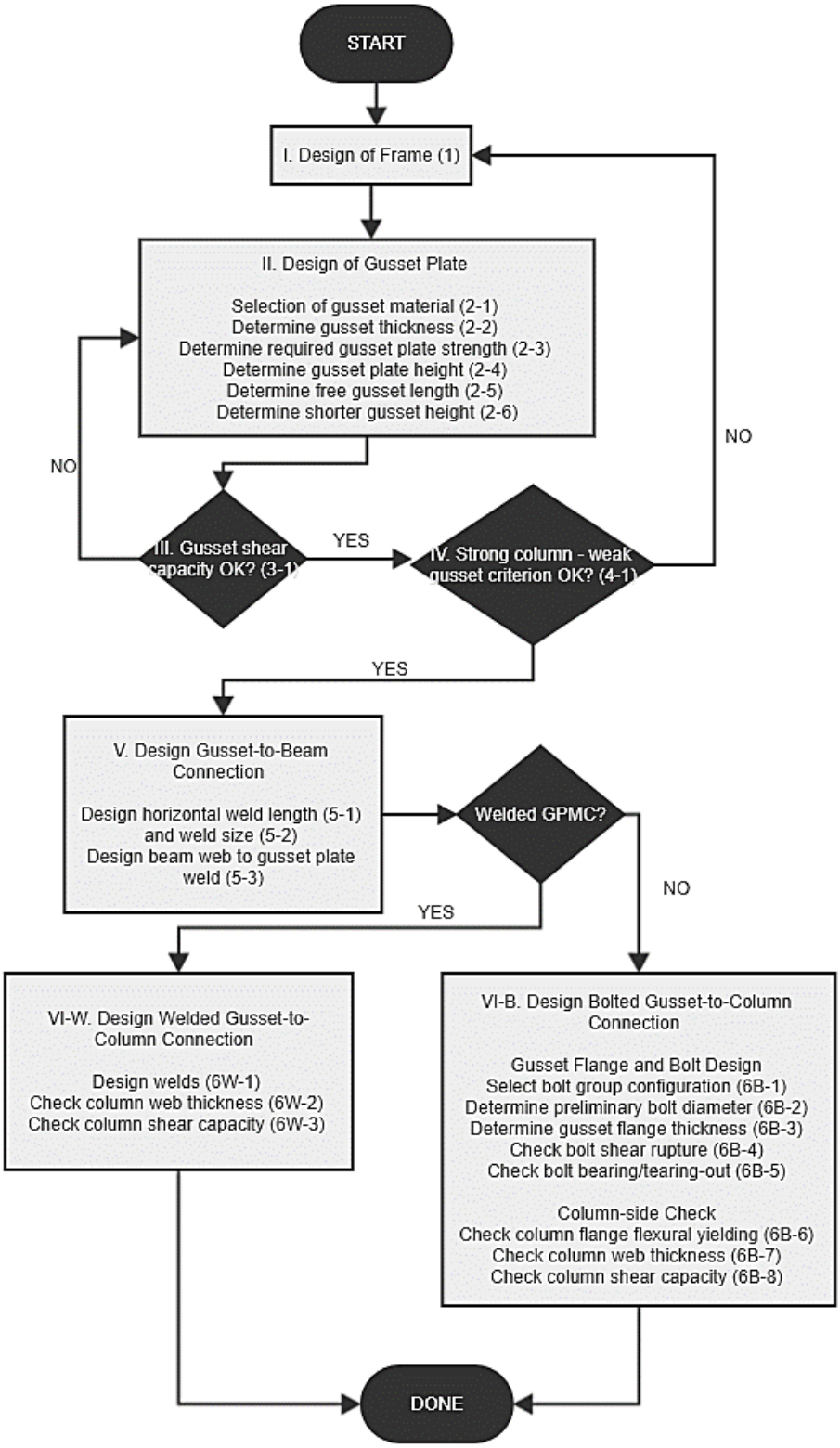

Figure 3.37 Design flowchart for welded and bolted GPMC

Commentary on the Proposed Design Procedure

In order to illustrate the resulting design following the proposed design procedure and to provide some design tips, designs were performed for wide flange beams ranging from W18×35 to W36×652 using different beam-gusset material combinations, gusset plate thicknesses, and whether or not architectural limits are imposed. Designs were performed up to Step 5-1 in the proposed design procedure to establish the main gusset strength and geometry. Without specific loading conditions, it was assumed that the gusset plate shear capacity and "strong-column–weak gusset" criteria can be satisfied for all cases. The gusset angle (θ) and expected gusset plate moment capacity ratio ($M_{peg}/M_{peb} = R_{yg}F_{yg}Z_g/R_{yb}F_{yb}Z_b$) were computed as a means of accessing the proportion as well as the strength of the resulting GPMC design. Each point in Figure C1-C5 represents the gusset angle or gusset/beam strength ratio for each beam section considered. The beam sections are ordered in accordance with the AISC section property tables (AISC 2010a), descending from W36×652 from the left to W18×35 on the right.

The legend in the figures refers to the beam material yield strength/gusset material yield strength per the imposed architectural limit. The architectural limit used here is 12 in. considering a 6-in-thick slab. For example, 65/50 Y means Gr.65 beam and Gr.50 gusset with the 6 in. architectural limit.

General observations to help in selection of the gusset material and thickness are as follows:

1. Regardless of the material choice and gusset thickness, the architectural limit tends to reduce the strength of gusset plate and the slope of the gusset, especially for heavy sections where the required gusset depth is usually much larger than what the architectural limits would allow. Imposing architectural limit could also result in more shallow gusset plate designs, which is not favorable for cyclic performance;
2. The average M_{peg}/M_{peb} ratio for Gr.50 (F_{yg}=50ksi) gusset plate is about 80%, for A36 (F_{yg} = 36ksi) gusset is about 60% and 55% for LYP100 (F_{yg} = 19ksi);
3. For the same beam-gusset material combination, the thickness of the gusset plate does not affect the gusset strength very much, but the thicker the gusset, the shallower the gusset plate will be. For gusset plates made of low-yield steel, thicker but shallower gusset plate were shown to behave well without any sign of gusset buckling or significant strain concentrations in the gusset plate;
4. High-strength beams will, in general, allow higher M_{peg}/M_{peb} if there is no architectural limit; if there is a limit, the gusset strength will suffer a larger reduction;
5. Heavy sections tend to be less well proportioned, i.e., heavy sections of the same depth have a smaller gusset slope;
6. The general observation is that this design procedure and GPMCs might work better for light sections for beams with similar depth and also for shallow beams. One may consider avoiding

the use of the beam sections and the corresponding gusset material that would result in very weak gusset plates (very small M_{peg}/M_{peb} ratio) following the proposed design procedure.

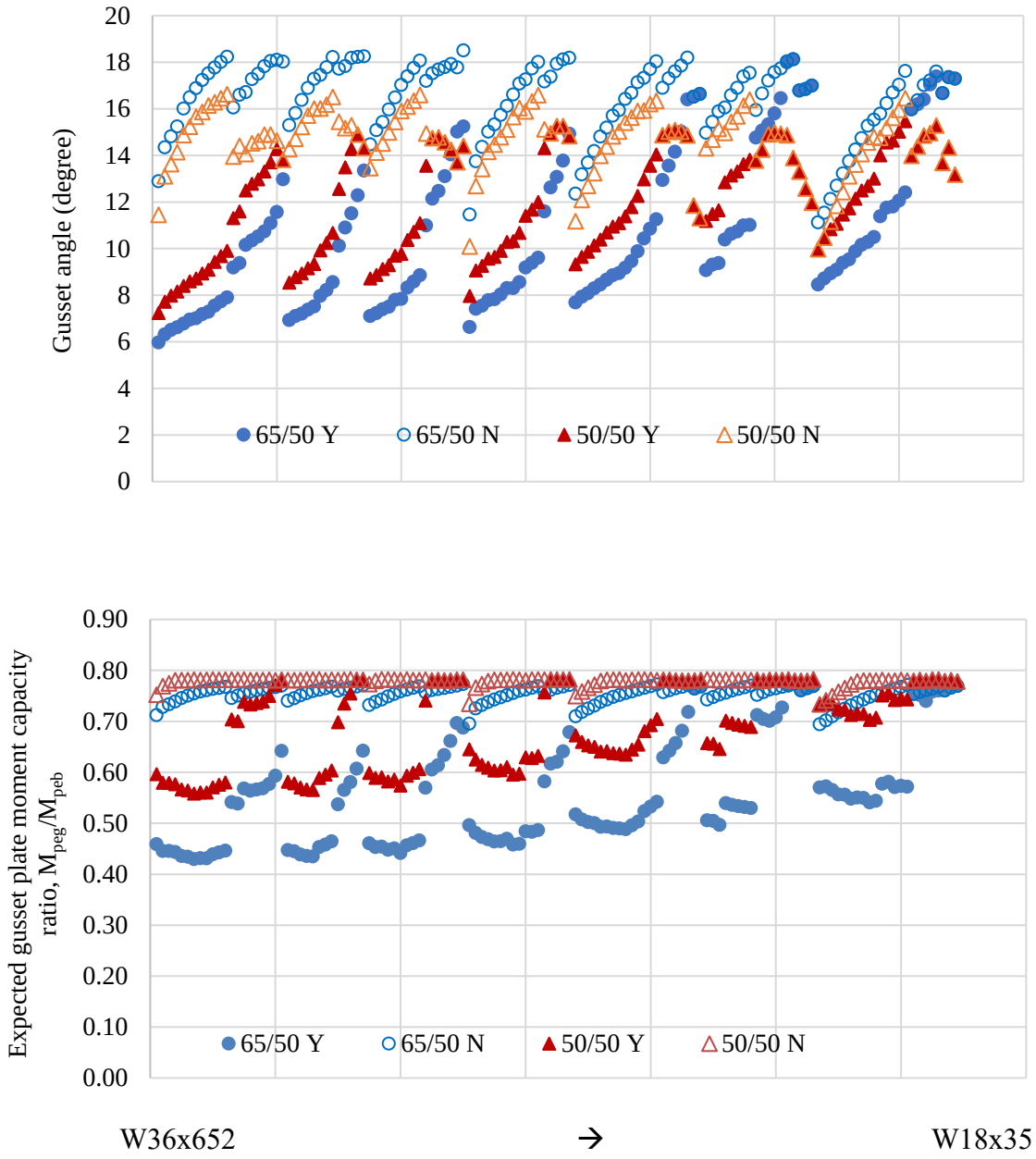

Figure C1 Effect of beam sections, frame material and architectural limit on gusset angle and expected gusset strength for Gr.50 gusset plate with t_g=1.25t_{bw}

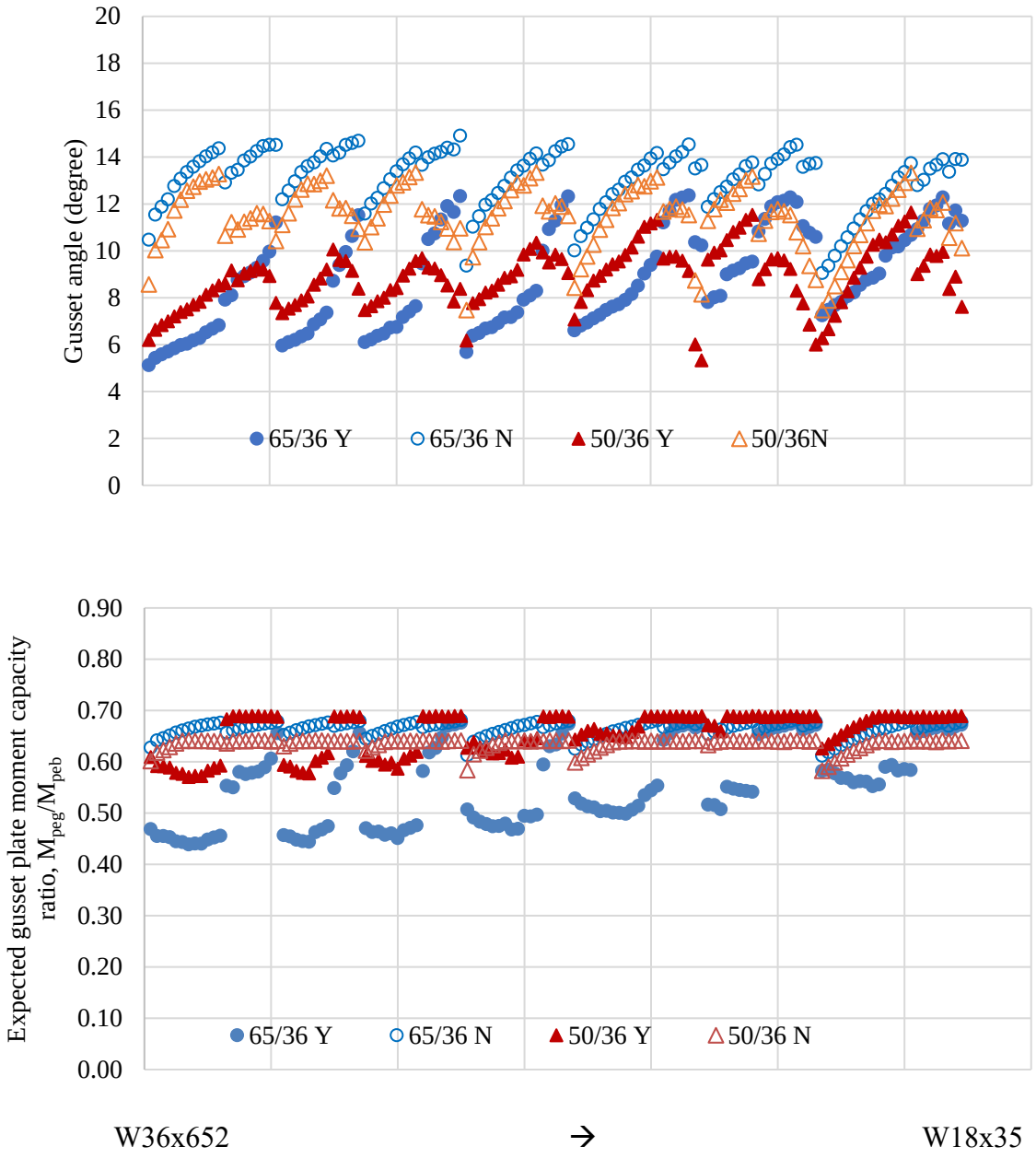

Figure C2 Effect of beam sections, frame material and architectural limit on gusset angle and expected gusset strength for A36 gusset plate with t_g=1.5t_{bw}

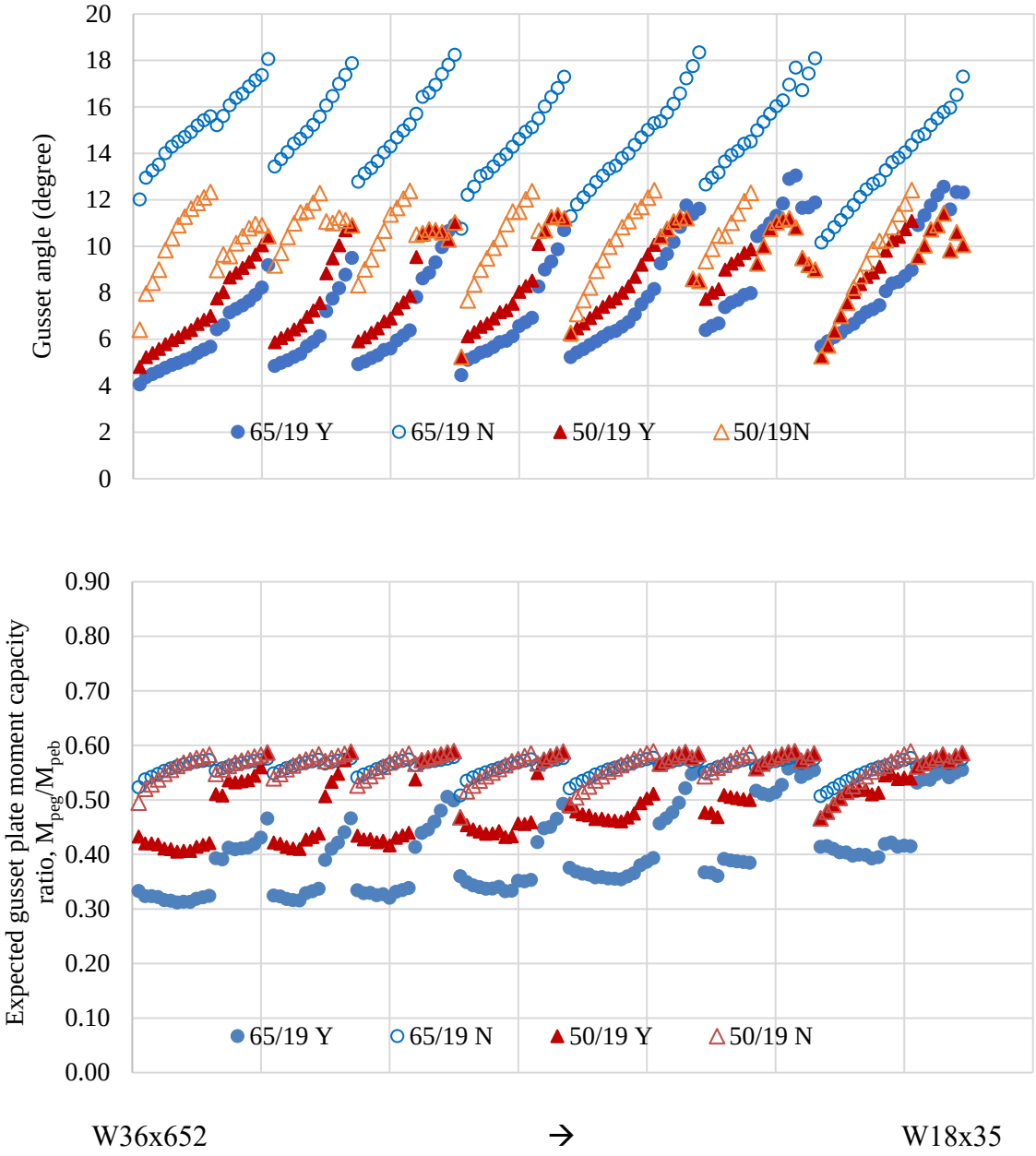

Figure C3 Effect of beam sections, frame material and architectural limit on gusset angle and expected gusset strength for LYP100 gusset plate with t_g=2.5t_{bw}

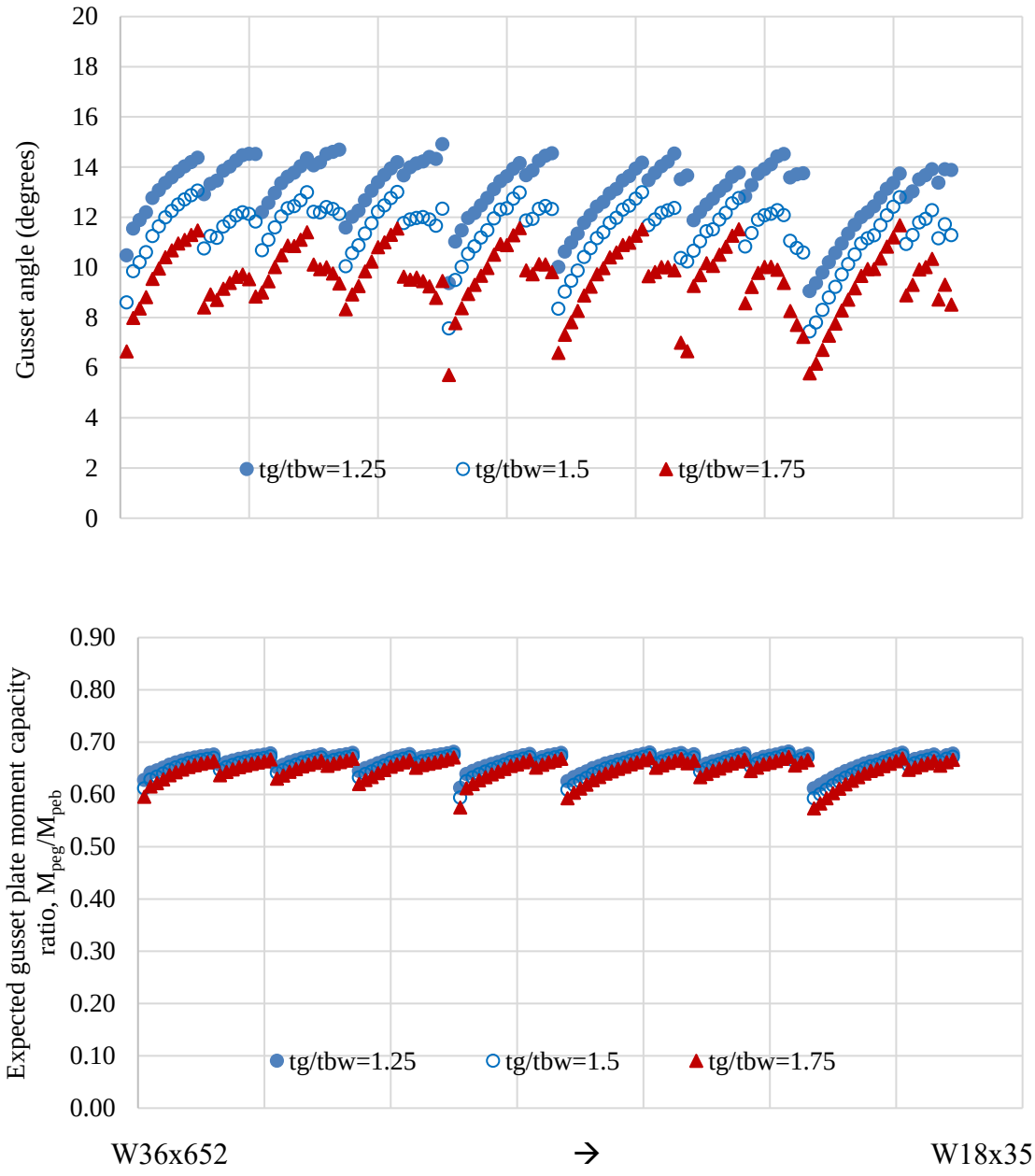

Figure C4 Effect of beam sections and gusset thicknesses on gusset angle and expected gusset strength for A36 gusset plate, Gr.65 beam without architectural limit

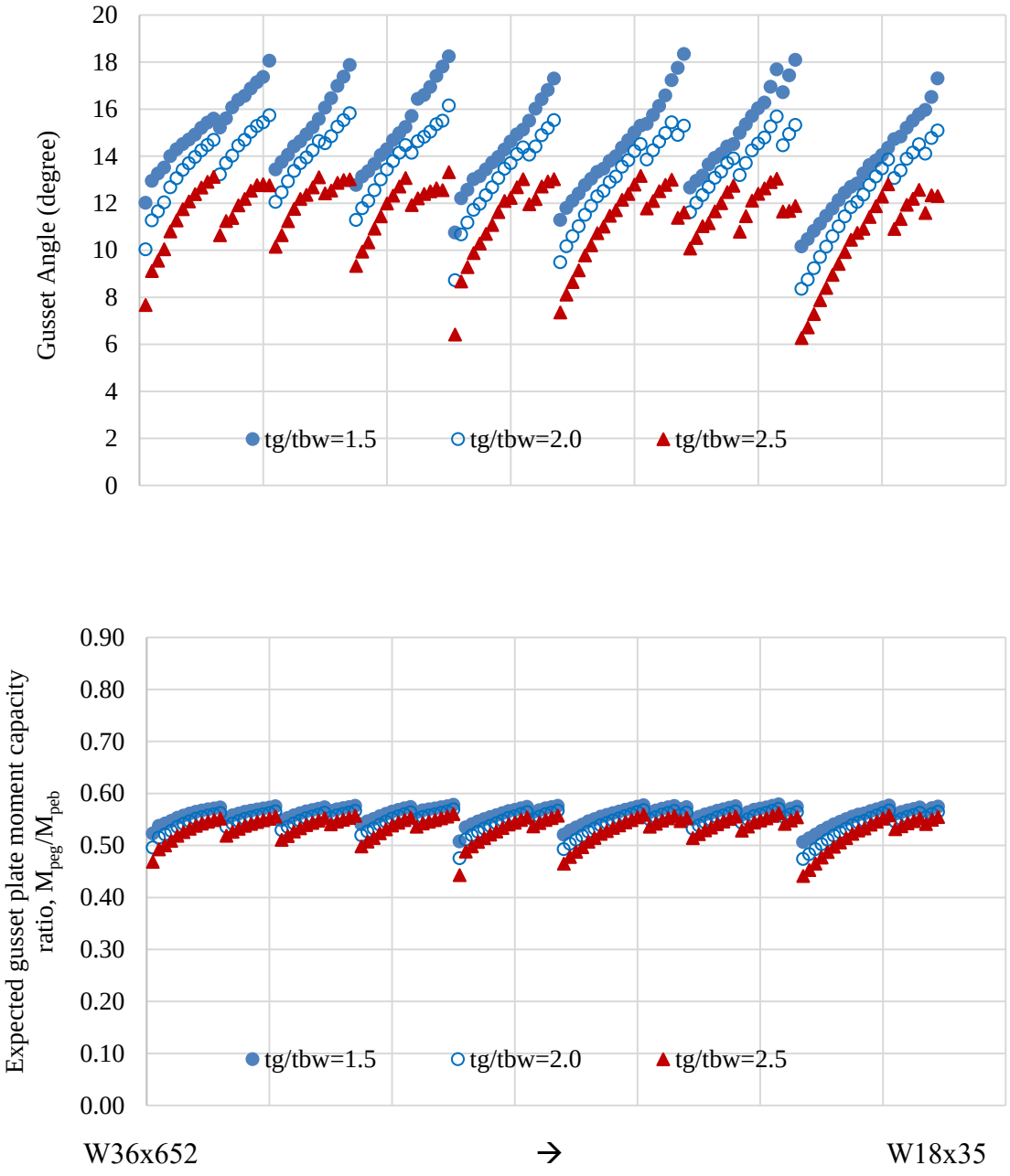

Figure C5 Effect of beam sections and gusset thicknesses on gusset angle and expected gusset strength for LYP100 gusset plate, Gr.65 beam without architectural limit

3.6. Concluding Remarks and Recommendations for Future Works

In this chapter, a new and potentially very economical steel moment connection that primarily utilizes the ductility of gusset plate – Gusset Plate Moment Connection (GPMC) – was introduced along with its key features, design philosophy, and advantages. The proposed connection is highly versatile and widely applicable; both welded and bolted versions are presented, with other beam-to-gusset plate connection methods. They can be adopted not only in special moment frames but also in steel plate shear wall systems and dual systems consisting of moment frame and concentrically braced frame.

Through extensive nonlinear finite element analyses, the behavior of the proposed connection with different gusset plate strengths with respect to the beam strength, gusset plate thicknesses, and free gusset lengths was studied, and results were discussed. In order to resolve the issue of strain concentration for deep beams, use of low-yield material gusset plate and different stiffener configurations were investigated. The effect of gusset flange thickness and bolt group design for the bolted GPMC was also examined. Other considerations such as the lateral stiffness reduction, reduction of incoming beam flange force by providing beam flange cut, and effect of architectural limits were discussed.

Calibration of concentrated hinge model to represent the behavior of the GPMC in OpenSees using the *Steel02* material was carried out. This concentrated hinge model can be adopted in the response history analysis of a global building model. Discussion of IMK material model in the concentrated hinge connection model was also provided for future reference if strength/stiffness degradation becomes essential in certain applications. A simple truss analogy was proposed in its preliminary form to provide an easy modeling and analysis tool for designers.

Lastly, using the results of the parametric studies and suggestions from the professional advisory panel and the design theory and concepts used in existing pre-qualified steel moment connections, an interim design procedure was developed and proposed for the new GPMC. The design procedure was developed based on the established performance criteria that ensure the brittle limit states occur after the ductile yielding of the gusset plate following the capacity-design principle. To aid engineers in choosing the appropriate gusset material and thickness, supplementary charts are provided on the resulting gusset plate angle and connection moment capacity for all available wide-flange beam sections following the proposed design procedure.

Clearly, the proposed GPMC is a potentially very economical high-performance connection. However, to better understand the actual behavior and to refine the interim design procedure, more research and development efforts are needed to make the connection another “prequalified” connections in the AISC Seismic Design Manual (AISC 2010b, AISC 2016a). Some future research and development needs are listed below:

1. Low-yield point (LYP) steel was found to be very promising for use in the proposed GPMC. However, since it is a relatively new material, the cost-effectiveness of adopting this material needs to be investigated;
2. For further development of bolted GPMC, more detailed models of bolts to include the effect of bolt-slippage, bolt-hole elongation, shank tearing, and nut stripping for the bolts would assist in further refinement of the proposed design procedure;
3. Actual cyclic testing of the proposed new GPMC should be performed to establish actual behavior, to further calibrate the numerical model, and to refine the proposed interim design procedure;
4. A cost comparison of the GPMCs and currently available moment connections is desired;
5. The truss analogy introduced in this chapter, even in its preliminary form, showed potential of being a useful and simple tool to establish gusset plate stresses. Future studies are needed to further advance the application of the truss analogy to the design of this new gusset plate design;

   and
6. The effect of slab on the behavior of the GPMC was not included in this dissertation, however, it is worthwhile investigating the positive/negative effects of floor slabs to understand the connection behavior in a more realistic setting.

Chapter IV

The High-Performance

Steel Plate Shear Wall

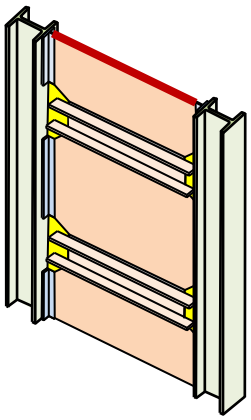

A new system, called the *High-Performance Steel Plate Shear Wall* (HPSPSW), developed at the University of California Berkeley, will be introduced in this chapter. The innovative HPSPSW system uses the new Gusset Plate Moment Connection (GPMC) introduced in Chapter III. This chapter will demonstrate how this proposed innovative system removes the disadvantages of the current steel shear wall systems identified in Chapter I and present a steel shear wall system that is both cost-effective and construction friendly, with superior performance. Equations for the angle of inclination of the tension field, shear strength and elastic stiffness of the system will be derived for use in the analysis and design. An equivalent brace (EB) model, a simple and feasible design and analytical tool, is proposed and validated by available FE and test results.

4.1 The Proposed High-Performance Steel Plate Shear Wall (HPSPSW)

4.1.1 Main Components

Figure 4.1 shows the main elements of the new *High-Performance Steel Plate Shear Wall* (*HPSPSW*) system:

a. **Unstiffened steel plate shear wall:** the unstiffened steel plate is designed to satisfy two levels of performance: (1) to resist the story shear under the ultimate factored load primarily by the strength and stiffness of the tension field action; and (2) to remain essentially elastic under the service wind and lateral seismic forces. North American seismic design codes (e.g., AISC 2010c, AISC 2016b, CSA 2011) only require that the steel plate be designed for the ultimate factored load; there is no specific requirements on the performance of the system under service loads. In the proposed new system, the infill steel plates are connected only to the boundary beams and not to the boundary columns. Separating the steel infill plate from the column frees the columns from the lateral forces of the tension field action and eases the construction and fabrication process. This is the main innovation and a major advantage of the new system over

the current steel plate shear wall system in the AISC Seismic Provisions (AISC 2010c, AISC 2016b);

b. **Vertical side stiffeners:** As shown in Figure 4.1, two vertical steel plates, T-sections, or other steel shapes, are shop-welded to the vertical sides of the infill steel plate and are next to but not connected to the columns. These side stiffeners are located between floors and play three essential roles: (1) they prevent lateral forces of the tension field action acting on the columns (strength), (2) they provide out-of-plane buckling restraint to the vertical edges of the steel infill plate (out-of-plane stiffness), and (3) theu provide in-plane boundary constraint to the tension field action and additional shear strength (in-plane stiffness and strength);

c. **Beam-to-column moment connections:** The beam-to-column connections in the new High-Performance Steel Plate Shear Wall (HPSPSW) system presented here is the new Gusset Plate Moment Connection (GPMC) (Qian and Astaneh-Asl 2016c; Qian and Astaneh-Asl 2016d) discussed in detail in Chapter III. The new connection utilizes highly ductile gusset plates to provide the necessary bending strength, rotational stiffness, required plastic rotation, and sufficient energy-dissipation capacity as demonstrated in past studies (Astaneh-Asl 1998; Astaneh-Asl 2010). Based on the extensive analytical studies performed, the new connection has proven to be highly ductile, easy to fabricate, and potentially cost effective. The proposed connection has a broad range of applications in steel and composite moment frames, and composite and steel shear walls (such as the new *HPSPSW* discussed herein), as well as in dual steel systems composed of special concentrically braced frames and moment frames (Astaneh-Asl et al. 2006). The GPMC can be used for seismic as well as wind and gravity resistance. The most significant advantage over the field-welded moment connections employed in the current steel plate shear wall is that the new connection does not incorporate Complete Joint Penetration (CJP) field-welds, which are not only relatively expensive to fabricate but require costly field-inspection using ultrasonic testing equipment and expert operators;

d. **Boundary columns**: The boundary columns in the *HPSPSW* are not connected to the steel shear wall between the floor beams, preventing the steel plate from applying lateral force to the columns. The columns can be steel [Figure 4.2(a-h)], composite [Figure 4.2(i,j)], or even reinforced concrete sections [Figure 4.2(k,l)], and there is no restriction on the column orientation. The role of the column in this system is similar to the role of the columns in concentrically braced frames: to carry axial loads along its length with some moment in the top and bottom connections; and

e. **Boundary beams:** in the new *HPSPSW* system, the boundary beams can be fillet-welded or bolted to the steel infill panel. If welds are used, welding can be done in the field or in the shop in the "modular" construction option of the new system. These welds are fillet welds, requiring only visual inspections and not ultrasonic testing in most cases (unless the weld size is too large then ultrasonic testing may be required). The beams in the new system do not need to be

wide flange shape as is the case in the current SPSW system; they can be angles, channels, or even simple flanges as long as they are strong enough to carry the gravity loads and the tension field forces imposed by the infill wall.

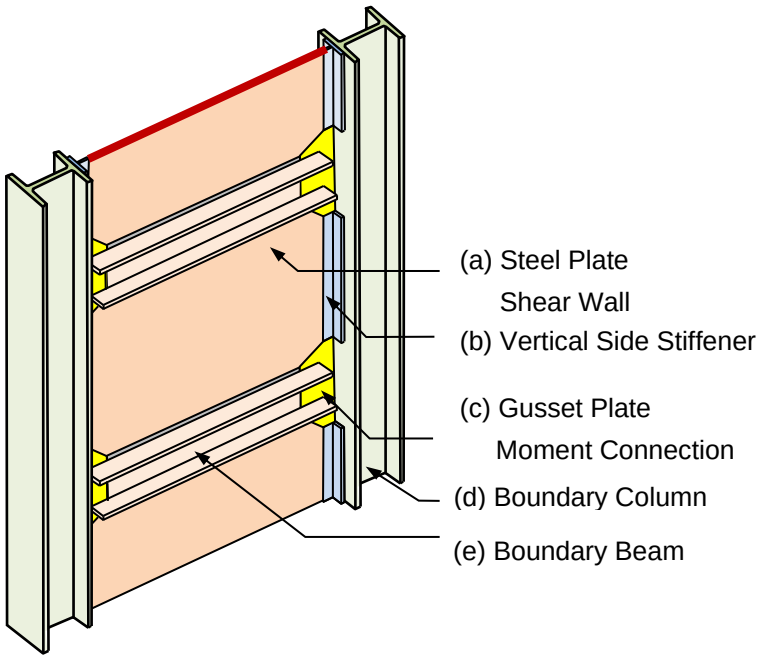

Figure 4.1 The main components of the new *High-Performance Steel Plate Shear Wall system*

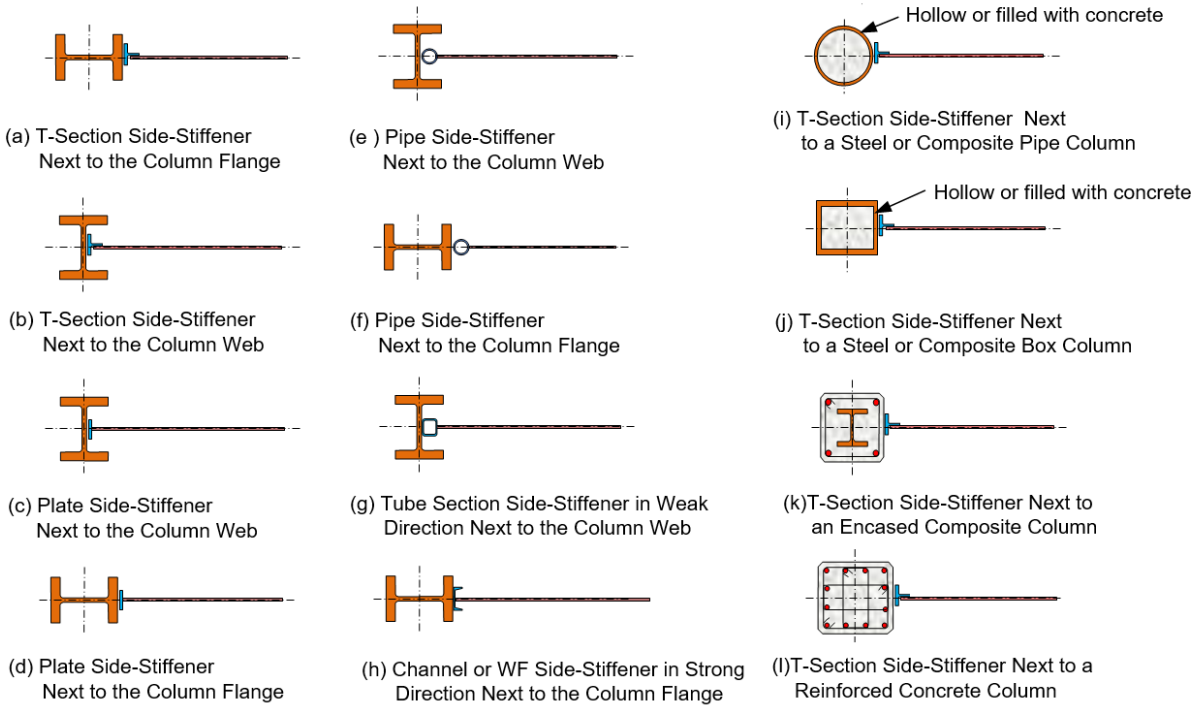

Figure 4.2 Different side-stiffener section and column section pairs for use in the *High-Performance Steel Plate Shear Wall* System (Qian and Astaneh-Asl, 2016b)

4.1.2 Advantages

The main advantages of the *HPSPSW* system using the new GPMCs are shown in Figure 4.3 and explained below:

(1) In the proposed system, the steel shear infill wall is not connected to the columns. As a result, the boundary columns are not subjected to any lateral forces created by the tension field action of the wall;

(2) Elimination of the vertical field welds connecting the steel infill plate to the column reduces costs and field work. The only field welds required are the welds connecting the beams to the gusset plates and the steel infill plate to the beams. Two horizontal welds eliminate the problem of possible burning of infill plate when doing upward welding, as described in Eatherton (2006), and can effectively reduce the construction effort;

(3) The design of columns will no longer be dependent on the wall thickness due to the separation of the steel plate from the column. The wall in the proposed HPSPSW can be of any thickness required by design based on the strength and drift limits for both ultimate and service level loads, while the column can be designed based on its own strength and stiffness requirements;

(4) The thickness of the shear wall can be selected independently of the column to satisfy drift requirements under the ultimate factored lateral loads;

(5) The thickness of the shear wall in the new system can be selected independently of columns to ensure that the wall will not buckle under the service and more frequent lateral loads;

(6) The gusset plate connections in the proposed system provide corner reinforcement for the steel shear wall plate, which is similar to the ductile corner welded bracket detail that was suggested to prevent localized fracture at the corners (Choi and Park 2008);

(7) No CJP *field* welds are needed, which are expensive to fabricate and require field inspection, are used in the new system. Most welds are fillet welds; some welds are PJP, and for large forces, *shop*-welded CJP welds are used;

(8) By using the new GPMCs, especially the welded option where the flanges of the beams are not directly connected to the column flange and the gusset plate is designed to be the "inelastic fuse," in most cases, the column panel zones remain essentially elastic, and there is no need to use costly doubler plates, another cost saving measure;

(9) Since the flanges of the beam in the new GPMC are not directly welded to the column flange, in most cases, there is no need for "continuity plates" for the columns due to the elimination of concentrated beam flange force, which is another cost saving measure; and

(10) Since the gusset plates are the inelastic fuses in the boundary frames of the new HPSPSW system, the beams, and the columns, as well as all weld lines and bolts, remain essentially elastic. Therefore, in this system, there is no need to satisfy the "strong-column–weak-beam" requirements. This can result in considerable cost savings in many applications, especially in low- and mid-rise buildings where the columns need not to be very large.

Note that advantages (1) to (5) are essentially due to disconnecting the shear wall from the column, and (6) to (10) are due to the use of the new GPMC. In addition to the above ten advantages of the

new *HPSPSW* system (Figure 4.3), there are two additional advantages: (1) the new system lends itself easily to "modular construction" and "prefabrication," as shown in Figures 4.4(a) and (b); and (2) the new system is not restricted for use in new construction, but it is also suitable for seismic retrofit of existing steel (e.g., pre-Northridge steel moment frame) and composite buildings, and even non-ductile reinforced concrete and timber buildings. This is because in the new system the steel shear wall is not connected to the columns; thus the columns can be any material and with any geometry and orientation. It was found that by adding the proposed steel shear wall system to only one bay of a pre-Northridge steel moment frame, the moment as well as the rotation demands on the moment connections were reduced so dramatically, that it was capable of surviving the pre-Northridge design earthquake. An example of retrofitted steel frame is shown in Figure 4.4(c).

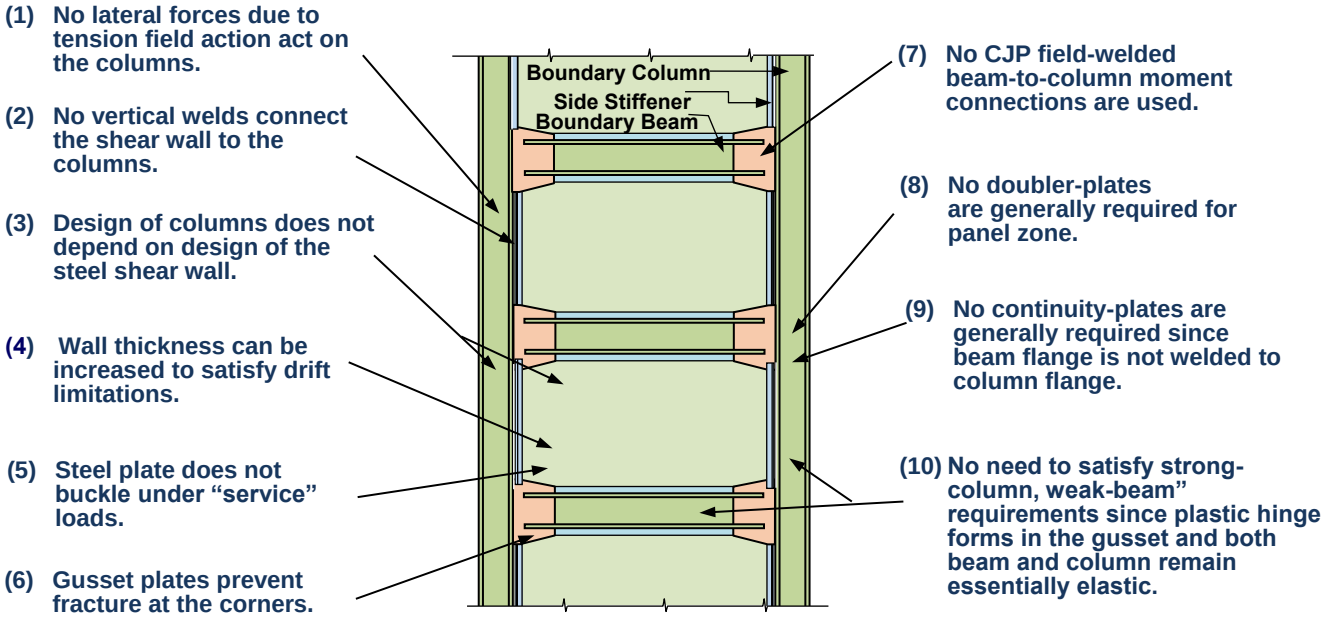

Figure 4.3 The new HPSPSW with its advantages

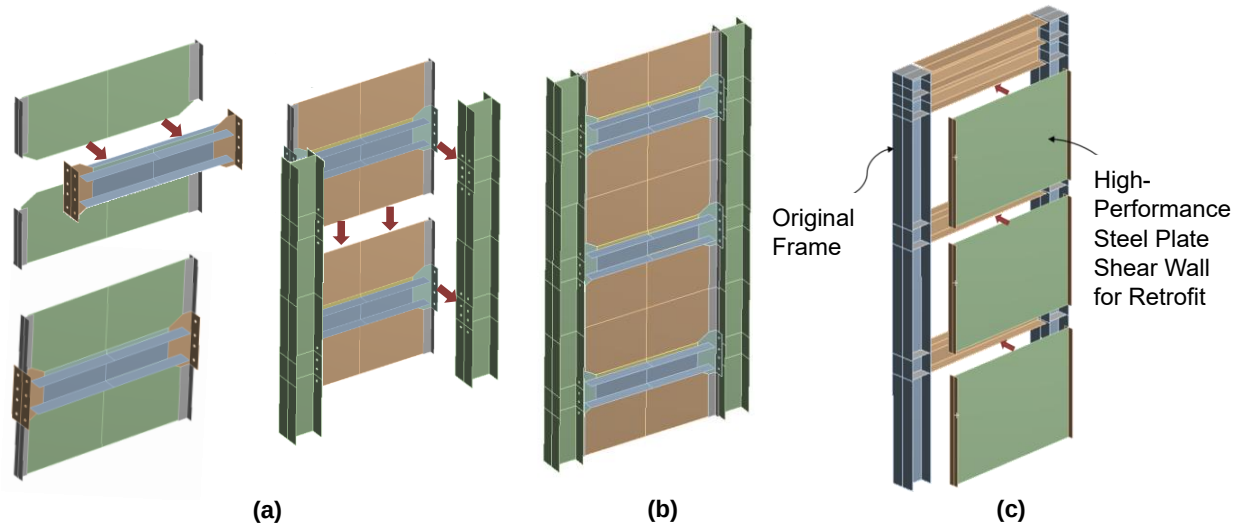

Figure 4.4 (a) Modular construction, (b) use of the new High-Performance Steel Plate Shear Wall system in new construction of buildings, and (c) use of the new system in retrofit of existing structures

4.1.3 Other Construction Configurations

In addition to the new gusset plate moment connection, other traditional and well-established steel connections such as shear and semi-rigid connections can also be used in the proposed new shear wall system without affecting the benefits due to the separation of the infill wall from the boundary column. Figure 4.5 shows some of the feasible alternative details. In addition to the proposed gusset plate beam-to-column connection [Figure 4.5(b)], other direct bolting, such as simple or semi-rigid connections [Figure 4.5(a, c, d, and e)], can also be used. Such freedom of choice of beam-to-column connection is possible because of the elimination of the need to connect the infill plate to both beams and columns.

Depending on the nature of the beam-to-column connections, the use of wide or narrow slotting is possible depending on specific project needs. Further research is recommended to study the performance of the proposed alternative configurations shown in Figure 4.5.

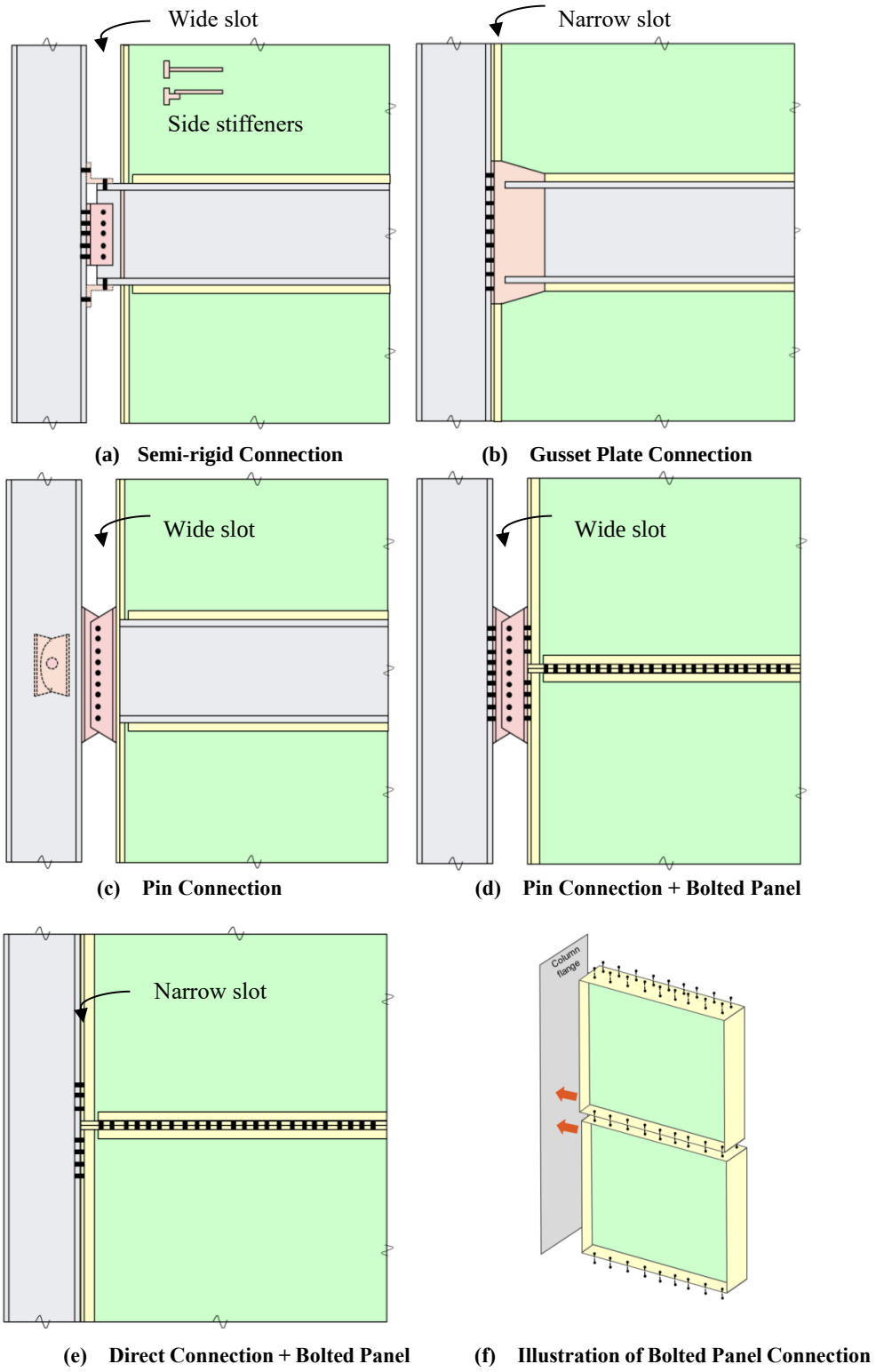

Figure 4.5 Other feasible details of the proposed High-Performance Steel Plate Shear Wall system

4.2 Performance of the New High-Performance Steel Plate Shear Wall System

4.2.1 Nonlinear Finite Element Analyses

In order to determine the performance of the new system, nonlinear finite element (FE) analyses of the system and its new gusset plate beam-to-column moment connections were conducted. Four-node SHELL181 elements from the ANSYS Shell element library were used to model all steel plate elements (ANSYS 2013). Mesh size was chosen based on mesh refinement analysis. Both material and geometric nonlinearities were considered. The initial imperfection that matches the lowest buckling mode shape for each infill panel was applied with a peak magnitude equal to 0.1% of the width of the panel. Again, Von Mises plasticity with kinematic hardening rule was used. The Ramberg-Osgood material model was used to define the equivalent stress-equivalent strain relationship since it can provide a much better match to the test backbone curve; see Figure 4.6. A total number of seven test specimens were chosen for the FE modeling validation, including single- and multi-story specimens and specimens with different construction details. Figures 4.6 – 4.8 compare the monotonic and cyclic analysis results of the FE models and the test results for three specimens [Park SC2T, SC4T and SC6T (Park et al. 2007)] that will be used extensively in the following parametric studies. It can be seen that generally the FE analyses results match the test results very well. More details on mesh refinement, comparison of different material models, the effect of various initial imperfections, and validation of the other four specimens are included in Appendix D1.

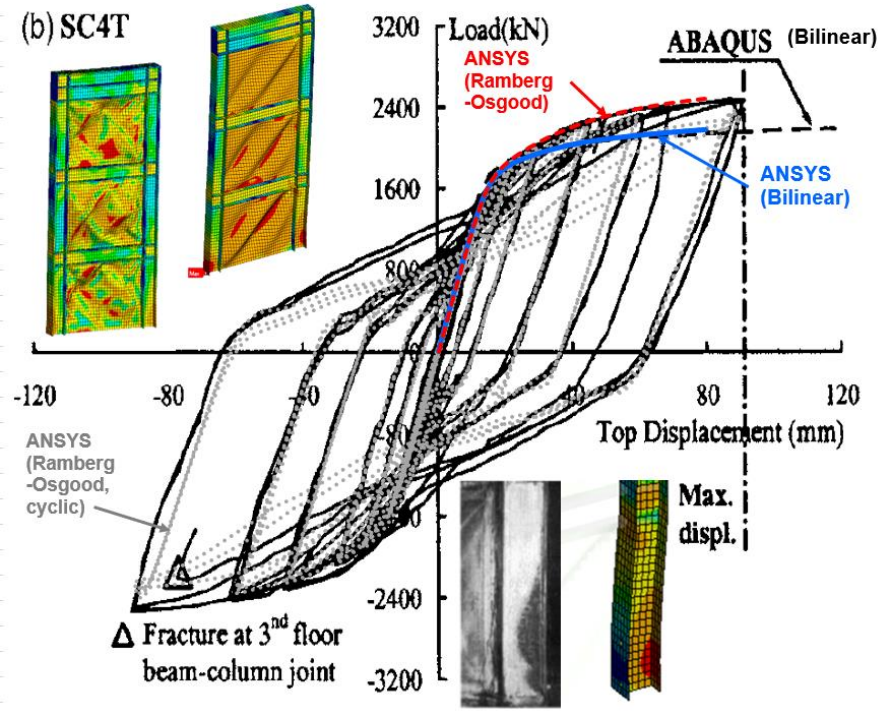

Figure 4.6 Validation of the FE model using SC4T specimen by Park et al. (2007) and comparison of Ramberg-Osgood and bilinear plasticity with strain hardening material model

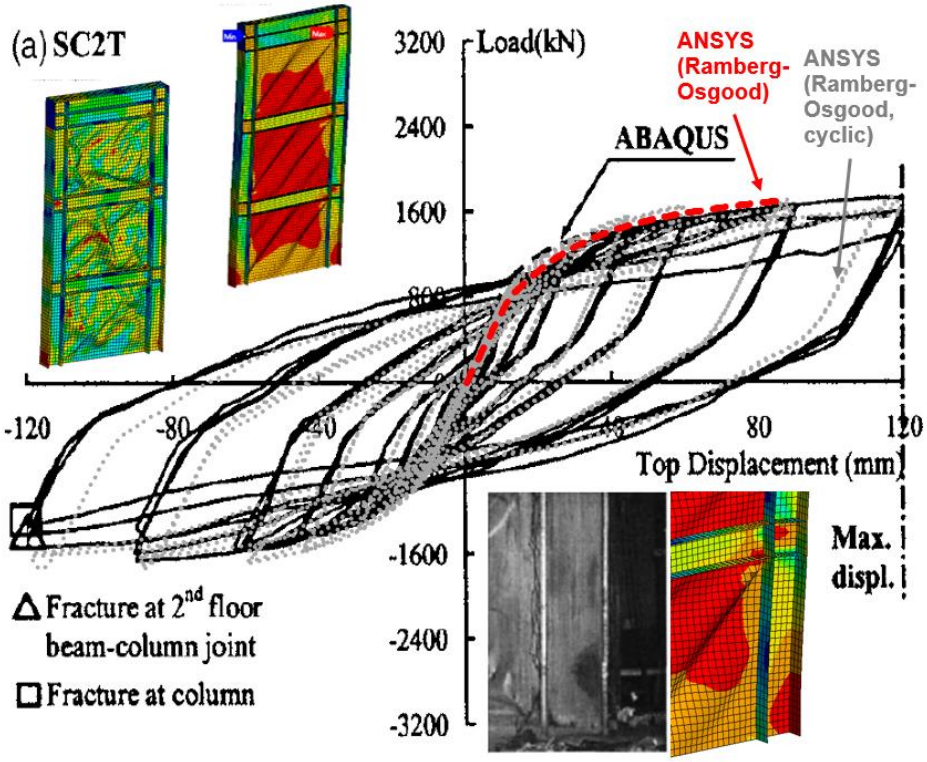

Figure 4.7 Validation of the FE model using SC2T specimen by Park et al. (2007)

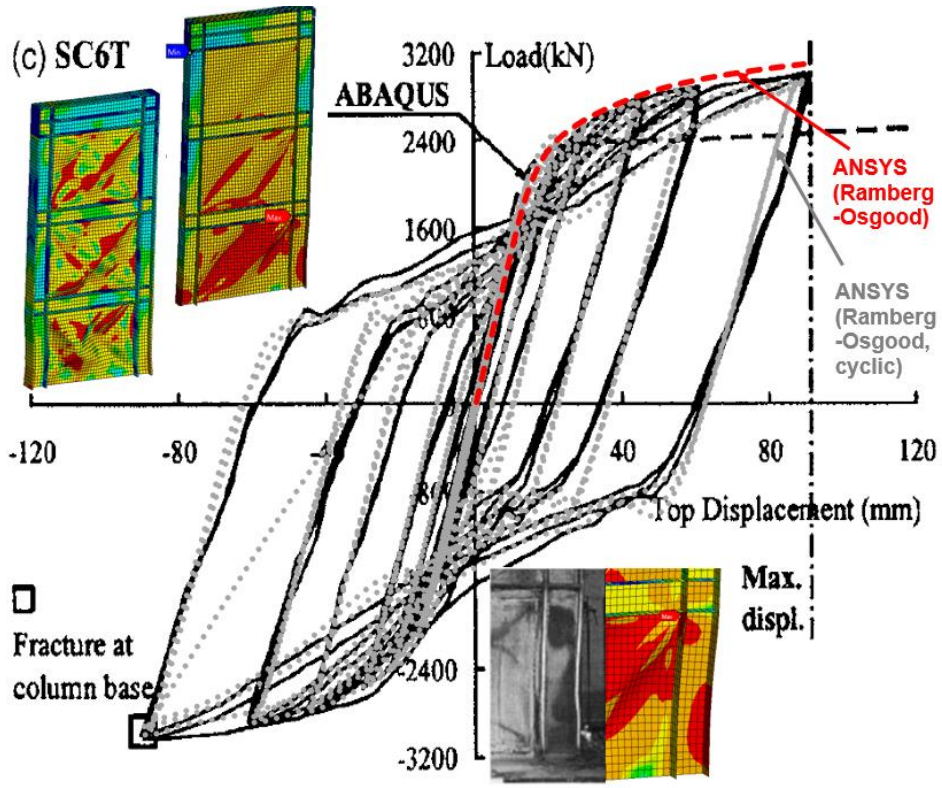

Figure 4.8 Validation of the FE model using SC6T specimen by Park et al. (2007)

4.2.2 Parametric Studies of the New HPSPSW System

To investigate the effectiveness of the proposed new shear wall system, extensive parametric studies were performed. Finite element models of steel shear walls representing the current system per AISC Seismic Provisions (AISC, 2010c) and the new high-performance system were built and subjected to monotonic and cyclic displacements. The analytical models consisted of two full typical stories and top and bottom half-stories of the typical shear wall with boundary columns and beams to impose a more realistic boundary condition for the two typical stories. The displacement history was applied at the section cut level of the top half-story as a remote displacement. Lateral supports were applied to the beam top flanges. The main parameters investigated were the effects of separating the columns from the steel shear walls, the use of the welded or bolted new gusset plate moment connections, and the use of different cross sections for the side-stiffeners.

4.2.2.1 Effectiveness of the Proposed System

Figure 4.9 compares the pushover curves for four cases. Three cases representing the proposed *HPSPSW* system were included, where the thicknesses of the steel shear walls and side stiffeners were varied. They were designed based on the dimensions of the Park SC4T specimen (Park et al. 2007). The fourth model was modified from the original test Specimen SC4T to the boundary condition of the current study. The fourth model represents the current AISC steel plate shear wall system, where the steel plate is welded to both the columns and beams, and the beam-to-column connections are traditional field-welded connections.

In this comparative case study, T-sections were used as side-stiffeners, with the stem of the T-section also acting as the vertical fin-plate used to weld the side-stiffener to the steel infill plate. The dimensions of the T-section used as side-stiffeners [i.e., flange width × depth × flange thickness × stem thickness (mm)] are shown in Figure 4.9 for each of the three cases of the new high-performance steel plate shear wall models. As shown in Figure 4.9, the proposed new *HPSPSW* system with the new gusset plate moment connection showed stable force-displacement behavior with well-defined yielding zone in the gusset plate as well as the infill plate tension field, a desirable behavior.

The analysis indicated that disconnecting the steel plate shear wall from the columns—as is done in the new *HPSPSW* system—resulted in two important effects:

(1) The columns developed much smaller bending moments and axial forces, and remained straight and essentially elastic; and
(2) There was a slight loss of shear capacity of the steel plate shear wall due to (a) the reduction in the width of the tension field area, and (b) to a lesser extent, a decrease in the shear forces resisted by the columns due to separation from the steel shear wall.

Reduction in the bending moment and axial force demands in the columns is the most important advantage of the new high-performance system, which eliminates the primary disadvantage of the current AISC steel plate shear walls, i.e., the lateral load applied to the columns by the steel shear wall makes the columns very heavy and expensive.

The relatively small reduction in shear capacity can be resolved very easily by selecting a slightly thicker steel plate for the infill wall or by using slightly stiffer and stronger side stiffeners: thicker plates will result in increased stiffness and shear strength; while the side stiffeners having larger bending stiffness and in-plane strength can lead to wider tension field and provide additional lateral resistance by forming plastic hinges. As shown in Figure 4.9, the resulting curves of the two cases with a thicker infill wall or stronger side-stiffener in are close to or even stronger and stiffer than the curve representing the current steel plate shear wall. This shows that both methods are cost effective as they do not increase labor costs significantly. Three additional benefits for implementing these two modification methods include: (1) enhancing the stiffness of the system to control drift; (2) delaying buckling of the wall under service loads; and (3) the fabrication and handling become easier and more cost effective especially when using thicker steel plates; "weld-burning" of thin plates can be avoided.

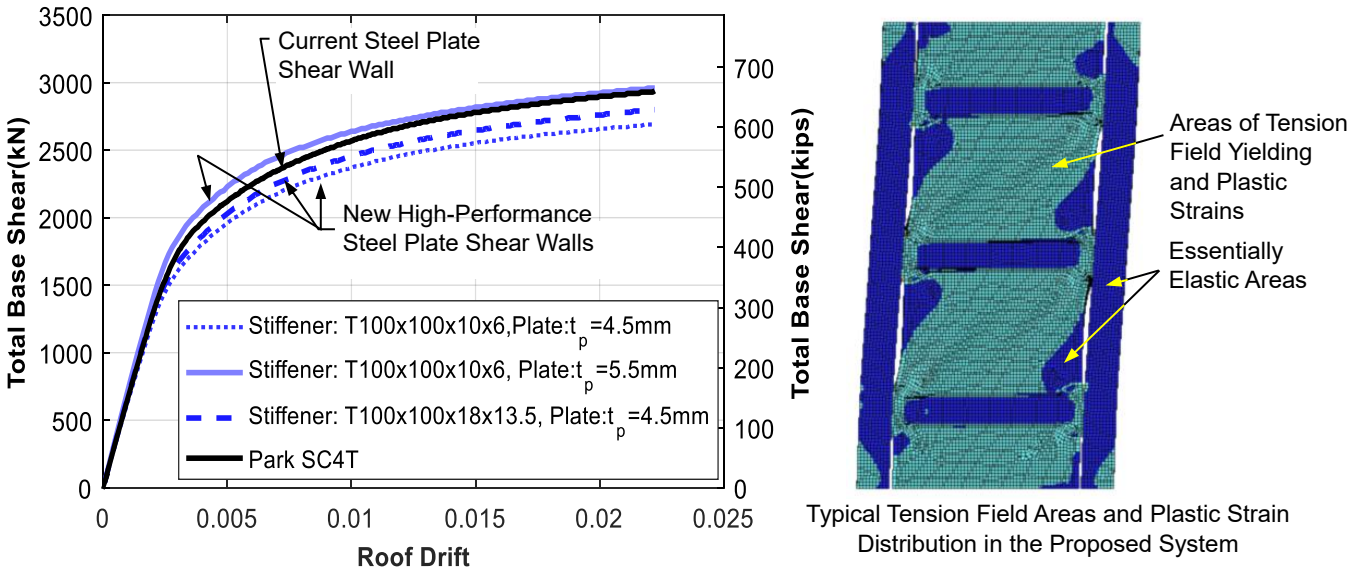

Figure 4.9 Comparison of pushover curves showing effectiveness of separating steel infill wall from the columns

4.2.2.2 Effectiveness of Gusset Plate Moment Connection

The beam-to-column connections in the new HPSPSW system consist of the proposed new GPMC system, designed to resist the shear force acting on them when the shear wall reaches its shear yielding capacity. More information on the design of gusset plates can be found in Chapter III. In

the design of gusset plates, a Whitmore angle of about 30° was used for the side slopes of the gusset plates as recommended by Astaneh-Asl (1998) for welded gusset plates. The 30° angle can be achieved because the beam sections in Park SC4T are relatively shallow and have large compactness. Both welded and bolted versions of the new GPMCs as shown in Figure 3.2 were considered. The main parameter varied in this analysis was the thickness of the gusset plate, being 2.0, 1.5 and 1.0 times the thickness of the beam web. Diffferent gusset plate thicknesses resulted in different plastic moment capacities and rotational stiffnesses for the beam-to-column connections in the six cases considered here.

Figure 4.10 shows the results of the pushover curves of six models of the HPSPSW system, again based on the Park SC4T specimen, with three different gusset plate thicknesses and a fourth model representing the current AISC design. As expected, the change in the gusset plate thickness mainly affected the behaviour of the boundary frame and had a minimal effect on the infill wall capacity; the pushover curves of steel shear wall alone for models with various gusset plate thicknesses were almost identical. Thus the separation of the steel shear wall from the boundary columns provides designers with more leeway in selecting the relative contribution of the shear wall and the boundary frame in resisting the shear.

For both welded and bolted versions of the new GPMC, thicker gusset plates resulted in a larger shear capacity of the frame due to greater frame action, but more yielding in the beams and columns. Thicker gusset plates tend to develop smaller peak plastic strains compared to thin gusset plates.

In general, the performance of the HPSPSW system with GPMCs was satisfactory, displaying a strength and stiffness equal to or greater than the welded moment connections used in the current AISC steel plate shear wall system. By changing the geometry and thickness of the gusset plate, there is considerable flexibility in fine-tuning the rotational stiffness and bending strength of the GPMC, allowing the pushover curves of the new HPSPSW system be modeled after the pushover curves of the current AISC shear wall configuration. Out of the three gusset plate thicknesses compared in this study, the gusset thickness that resulted in better overall (high stiffness and capacity) and local performance (less yielding in the beam and column, less stress/strain concentration) was equal to 1.5 times the thickness of the beam web. If the cyclic effect is included, the recommended value of 1.25 in Chapter III was found to be sufficient.

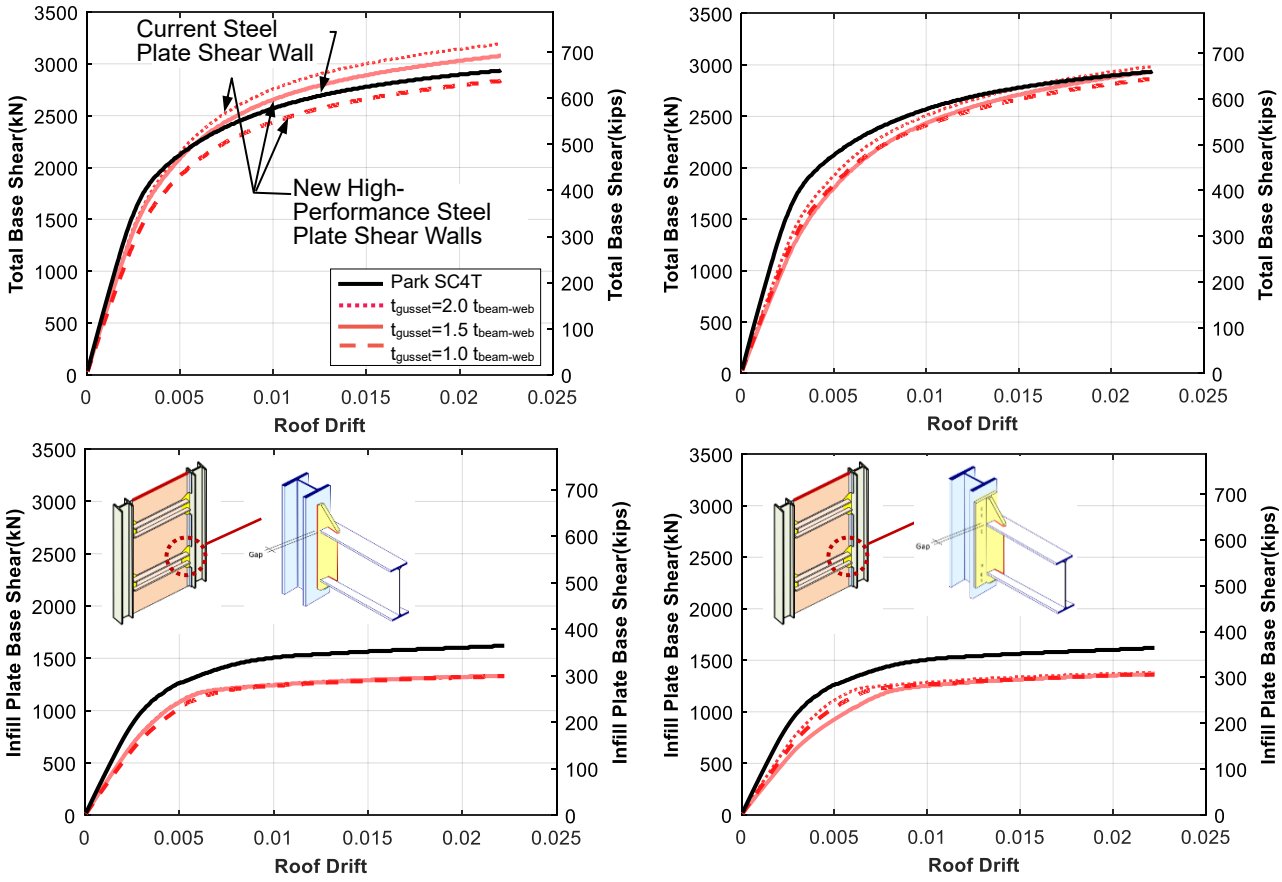

(a)Welded gusset plate moment connections shown in Figure 3.2(a) was used in the new system

(b) Bolted gusset plate moment connection shown in Figure 3.2(b) was used in the new system

Figure 4.10 Comparison of pushover curves showing effectiveness of using the new Gusset Plate Moment Connections

Figure 4.11 compares the von Mises effective stresses for two HPSPSW models using either welded or bolted GPMCs with the same gusset thickness (i.e., $t_g = 1.5t_{bw}$) at a roof drift ratio of 2.22%. The comparison demonstrates that the bolted version caused less yielding in the boundary elements, which is desirable. Bolted connections also allow better quality control and need less or no costly and somewhat weather-dependent field welding and field inspection. These advantages can compensate for the additional cost of bolt-hole drilling and material cost of the bolts. On the other hand, welded options are relatively easier to design. Therefore, both welded and bolted options are useful and can be selected based on specific project needs.

Figure 4.11 also shows that a clear plastic hinge and yield zone developed in the new GPMC. As designed, this yield zone, acts as a ductile fuse in the new GPMC and protects all other elements of the joint, including beams, columns, weld lines and bolts from yielding and fracture.

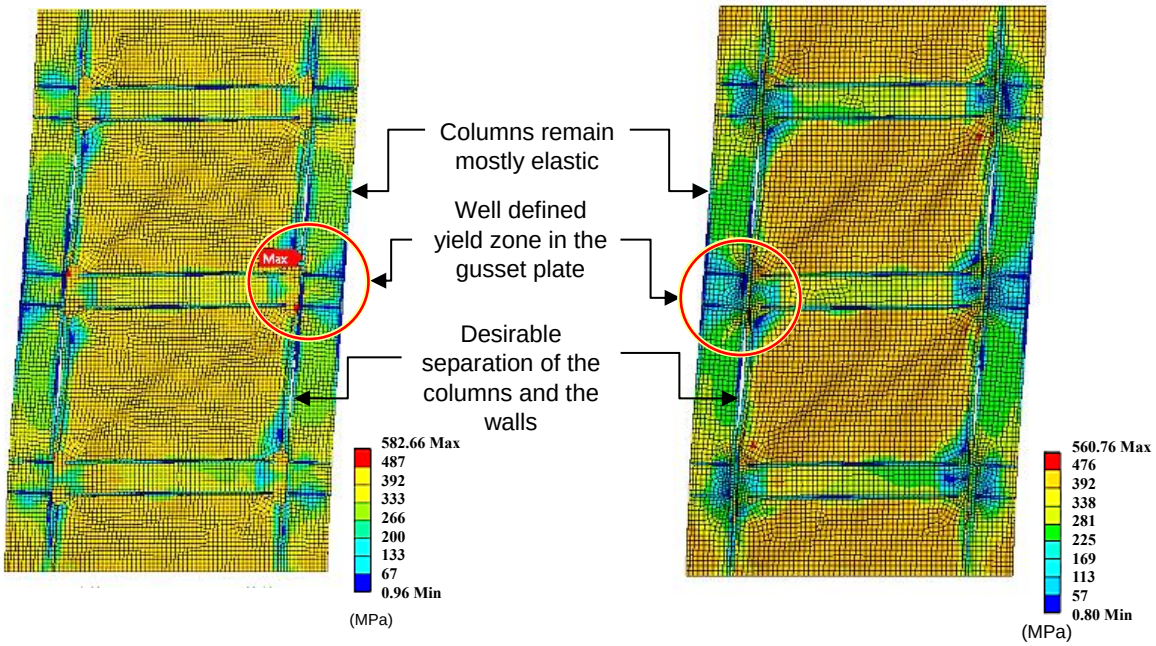

(a) Welded Gusset Plate Moment Connection with $t_g=1.5t_{bw}$

(b) Bolted Gusset Plate Moment Connection with $t_g=1.5t_{bw}$

Figure 4.11 Comparison of Von Mises stresses when welded (left) or bolted (right) new Gusset Plate Moment Connections are used in the HPSPSW system

4.2.2.3 Effect of Side Stiffeners

The side stiffeners in the proposed system are designed to perform three essential roles: (1) to provide out-of-plane bracing to the free vertical edges of the infill wall; (2) to delay elastic buckling of the infill plate beyond service load level; and (3) to contribute to the shear capacity of the infill wall by forming plastic hinges, which can be modeled using the commonly known collapse mechanism for plate girders (Evans et al. 1978; Porter et al. 1987; Rockey et al. 1978). Previously, the stiffeners considered for infill panels connected to the beam only (Choi and Park 2009; Guo et al. 2011) involved only small flat plates or header plates. Various feasible and easy-to-acquire structural shapes as side-stiffeners were considered in this study to determine their effects on the performance of the new system. Some examples of structural shapes that can be used as side-stiffeners were shown Figure 4.2. The behavior of various stiffener cross-sections in delaying or preventing local buckling of steel plates used in steel towers and piers of bridges was studied by the authors, and it was found that the plate stiffeners that are currently used in stiffening steel plates are not optimal and using other geometries may be more cost effective (Qian and Astaneh-Asl 2016a).

Figure 4.12(a) compares the pushover curves for the proposed *HPSPSW* system using five different cross sections as the side-stiffeners. The infill plates and frame sections were based on

the 3rd and 4th floor dimensions of the steel plate shear wall designed as an example in the AISC Design Guide 20 high seismic design (AISC 2007). The side-stiffener cross sections studied were pipe, flat plate, T-section cut from wide flanges (WT), wide flanges oriented in the strong direction with flanges parallel to the shear wall (WF_x), and wide flanges oriented in the weak direction with flanges perpendicular to the steel plate (WF_y).

Except for the WT-str and WF_y-str cases, all other side-stiffener cross sections were selected to have similar cross-section area (at almost equal cost) and a bending stiffness sufficient to restrain the out-of-plane deformation of the infill plate as well as to ensure a maximum critical infill wall shear buckling load capacity; see Section 4.3.1. The resulting stiffener sections based on this criterion were all relatively small. WT-str and WF_y-str side-stiffeners sections were designed to have larger in-plane plastic section modulus to compensate for the loss of the system shear capacity due to column detachment. All stiffener sections chosen are shown in Figure 4.13.

This study was limited to evaluating the effect of side-stiffeners only; the boundary frame and connections stayed the same. Figure 4.12 compares only the portion of base shear taken by the infill plate. It can be seen from Figure 4.12(a) that the shape of the stiffeners does not make a significant difference regarding the force-displacement relationship of the entire system if the sections are designed based on stiffener out-of-plane stiffness only, which is only a minimum requirement for the side stiffeners in the out-of-plane direction. Although the global force-displacement behavior turned out to be similar, not all the shapes experienced the same local deformation. The out-of-plane deformations are comparable since all sections were designed to have sufficient out-of-plane stiffness. However, due to the stability of the shapes themselves and their in-plane stiffness, Pipe, WT, and WF_y sections had less severe local in-plane deformation at their ends. Out of these three, the Pipe and WF_y sections tend to intrude into the useful space in the room along the edge of column and shear wall.

The WT-str and WF_y-str cases had higher in-plane plastic modulus and thus higher plastic moment capacity designed according to Section 4.3.5; as expected, they led to higher shear strength [Figure 4.12(b)]. This is a result of both the additional capacity brougth in by the plastic hinge formation of the side stiffeners and the enlarged yielding area of the infill plate with stronger boundary constraints (Figure 4.13). Furthermore, WT-str showed higher stiffness and strength compared with shape WF_y-str. This could be because, compared to wide flanges with similar area,the WT sections are more efficient in increasing the plastic capacity of the effective boundary constraint of the infill wall, thus leading to higher shear wall shear capacity.

Based on the above observations, WT sections are recommended to be used in the new high-performance steel shear wall system. They are more effective in contributing to the wall shear strength, less intrusive to the usable space and are widely available in a range of dimensions.

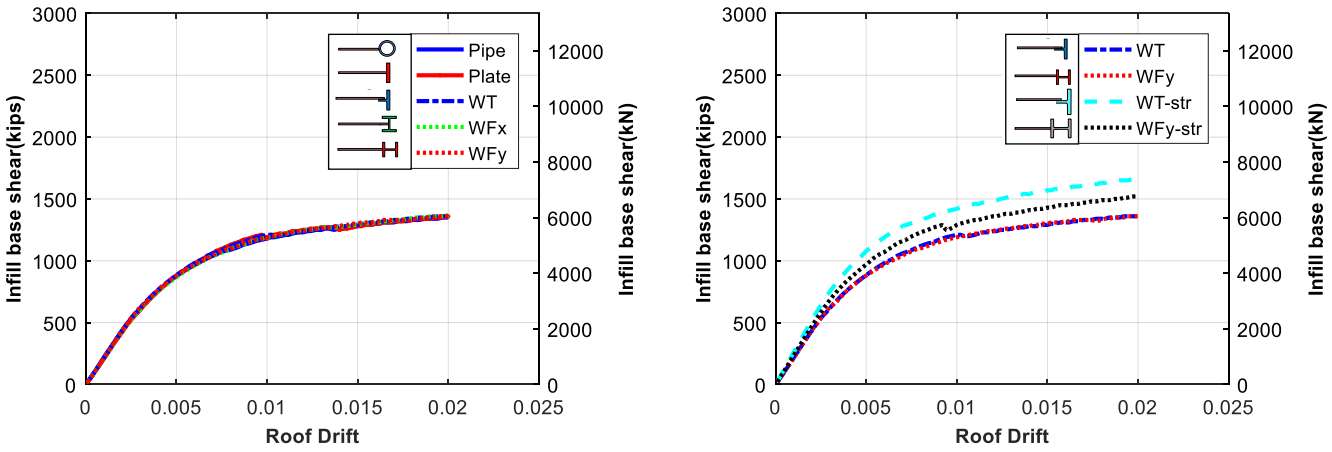

Figure 4.12 Comparison of pushover curves showing effects of different side-stiffeners

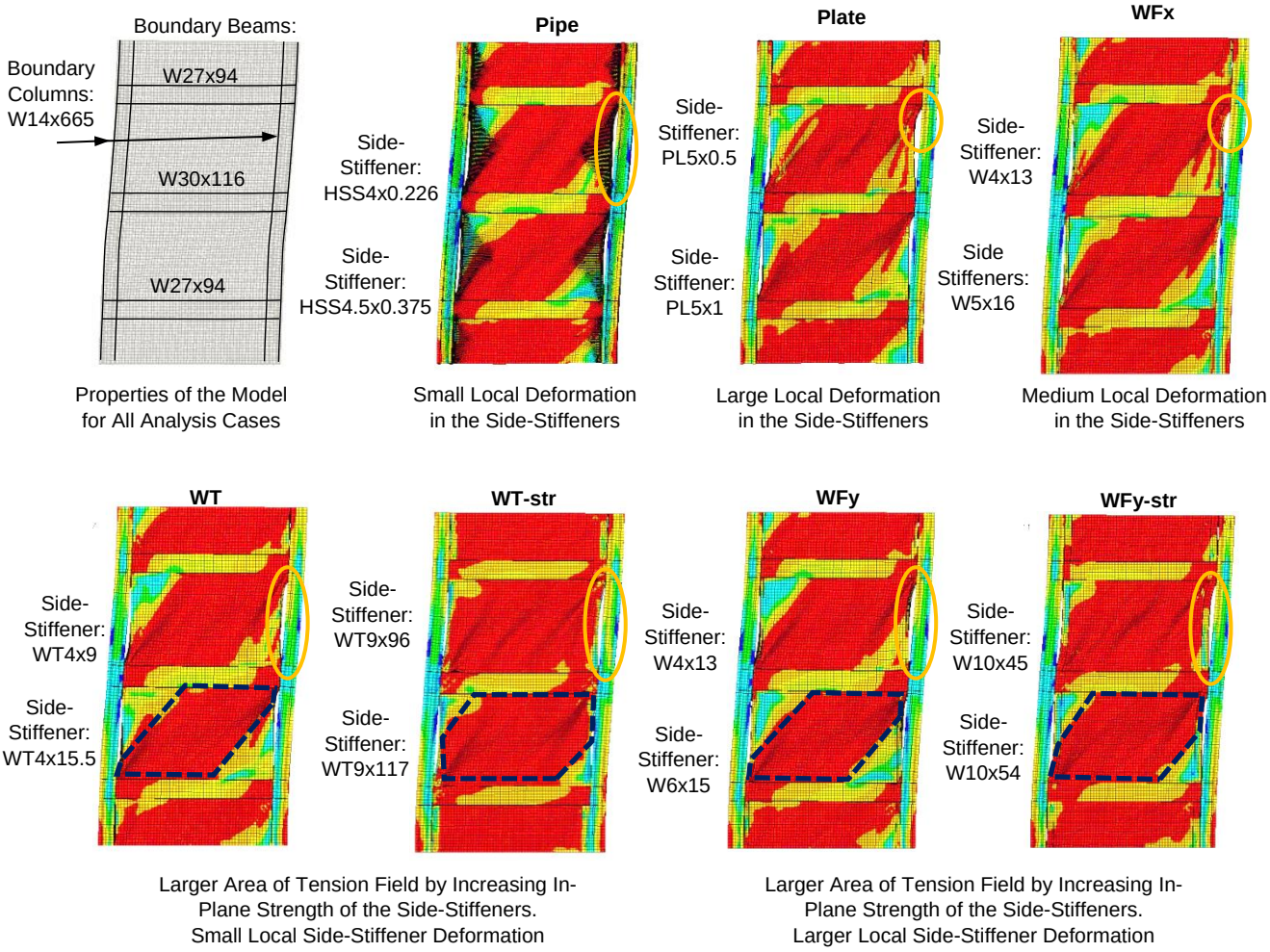

Figure 4.13 Comparison of Von Mises stresses showing effectiveness of various side-stiffeners

4.2.2.4 Hysteretic Behavior

Typical one-bay one-story panels were chosen to determine the hysteretic characteristics of infill wall connecting to the beam only. The panels had aspect ratios of 0.8 and 1.25 and slenderness ratios of 356 and 640, respectively. These parameters were chosen based on the commonly used dimensions of steel plate shear walls. According to Wang et al.(2015), the aspect ratios (L_p/h_p) of thin steel plate shear walls are in the range of 1.0–2.0, and the slenderness ratio(h_p/t_p) is around 20 ~400 (Wang et al. 2015). Note that the range of slenderness ratio could actually be larger. For example, the design of SPSW for high seismic application in AISC Design Guide 20 has an aspect ratio ranging from 1.15~1.8 and a slenderness ratio ranging from 500~2000.

Six different cases were analyzed; the key dimensions are shown in Table 4.1. For the side stiffeners, they were all T-sections determined according to the criterion to be discussed in Section 4.3.5. The infill panel height was 1600 mm, and the width varied with the aspect ratio. The beam section used was 400 ×200 × 6.5× 9 mm, and the column section was 300 ×200 × 8× 14 mm. The ratio of axial compression stress to yield strength of the column was maintained to be 0.2, which corresponds to a gravity axial force of 60 kN on each column. All cases were subjected to applied displacement under displacement controlled analysis. The loading history consisted of two cycles at 10, 20, 30, 40, 50, 60 mm roof displacement. The maximum story displacement corresponds to a drift ratio of 0.03. These models were slightly modified versions of the model used by Wang et al. (2015). The originally fixed bottom boundary beams were taken out, and the infill panel and base of the columns were directly fixed to the base. This way, the shear resisted by the infill panel and the total base shear can be separately monitored. The material properties used were the same as those presented in Wang et al.(2015).

Table 4.1 Dimensions and material used for single panel FE models under cyclic loads

Case	Infill f_{yp} (MPa)	Frame f_{yf} (MPa)	Stiffener f_{ys} (MPa)	Connection to column	Aspect ratio L_p/h_p	Slenderness ratio h_p/t_p	Side stiffeners(mm)*
1	240	380		Full	1.25	356	N/A
2	240	380		No	1.25	356	None
3	240	380	380	No	1.25	356	150x150x12x10
4	240	380	380	No	1.25	640	135x135x7.5x7.5
5	240	380	380	No	0.8	356	150x150x12x10
6	240	380	380	No	0.8	640	135x135x7.5x7.5

*Side stiffener dimensions are flange width × depth × flange thickness × stem thickness (mm)

Comparison between different infill panel designs

Figure 4.14 shows cyclic force-displacement curves for the entire system (dashed lines) and the steel shear infill panel only (solid lines). For Case 1, which represents the current system in the

AISC Seismic Provisions, plastic hinges formed early in the columns, causing shear capacity degradation for both the boundary frame and the infill panel; the system experienced higher residual strain compared to other two cases. Case 2 had the steel plate wall connected to the beam only, but no stiffeners were used to stiffen the vertical free edges of the infill plate. Even though the column was primarily loaded as a braced-frame column, the steel plate edges buckled early, and the hysteresis curves for the wall itself were pinched significantly with relatively low shear strength. However, there was no serious cyclic degradation as seen in Case 1 due to inward bending of columns due to tension-field actions. In Case 3, which represented the proposed system, the steel infill wall was connected to the beam only, and vertical edges of the steel infill plate were properly stiffened using T-shape stiffeners. With the contribution from the side stiffener, the stiffness and shear strength of Case 3 were comparable to the fully connected Case 1. Higher ductility and energy-dissipation capacity were achieved due to less cyclic degradation for Case 3. In addition, as expected, the column was subjected primarily to axial loads along the length and bending at the two ends.

Comparison between different aspect ratios and slenderness ratios

Four different steel plate shear walls with infill plate connected to the beam only (Case 3-6) were designed to have T-shaped side stiffeners with plastic moment capacity determined according to the criterion to be suggested in Section 4.3.5. Two different aspect ratios and slender ratios were used in order to obtain a more general view of the hysteresis characteristics of the system. Figure 4.15 shows the hysteresis curves of the four designs. As expected, thicker and wider infill panels possessed higher capacities.

From the normalized hysteresis curves shown in Figure 4.16 (base shear normalized by the maximum base shear, V/V_{max}), the general characteristics of the hysteresis behavior of the shear walls with different aspect ratios and slenderness ratios were very similar. The levels of pinching for all four cases were very close. This observation will be used to establish an empirical hysteresis model for a proposed simple EB model to be introduced in later sections. From the limited cases analyzed here, it appears that thicker panels tend to lead to higher *residual* equivalent plastic strains (Figure 4.17), while thin and wide panels tend to result in higher *maximum* equivalent plastic strains (Figure 4.18).

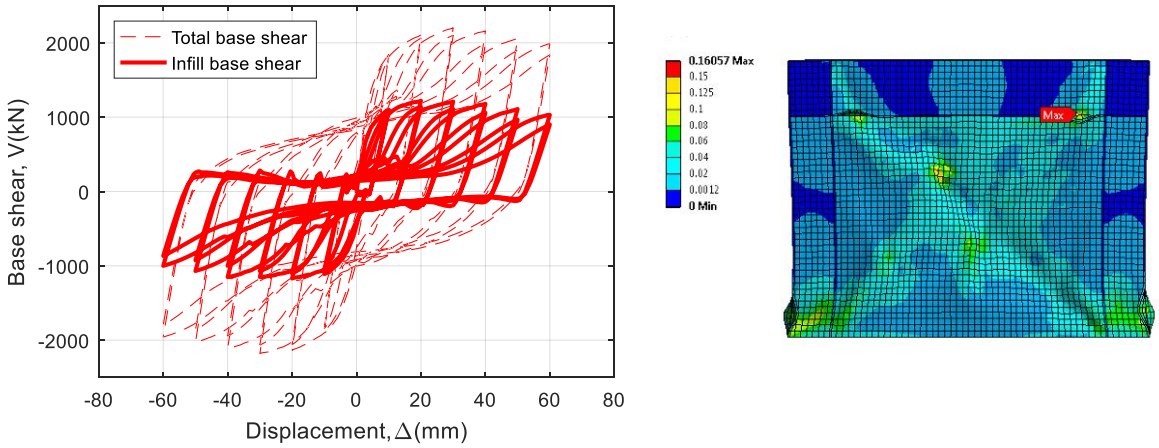

Case (1) Wall connected to the beams and the columns

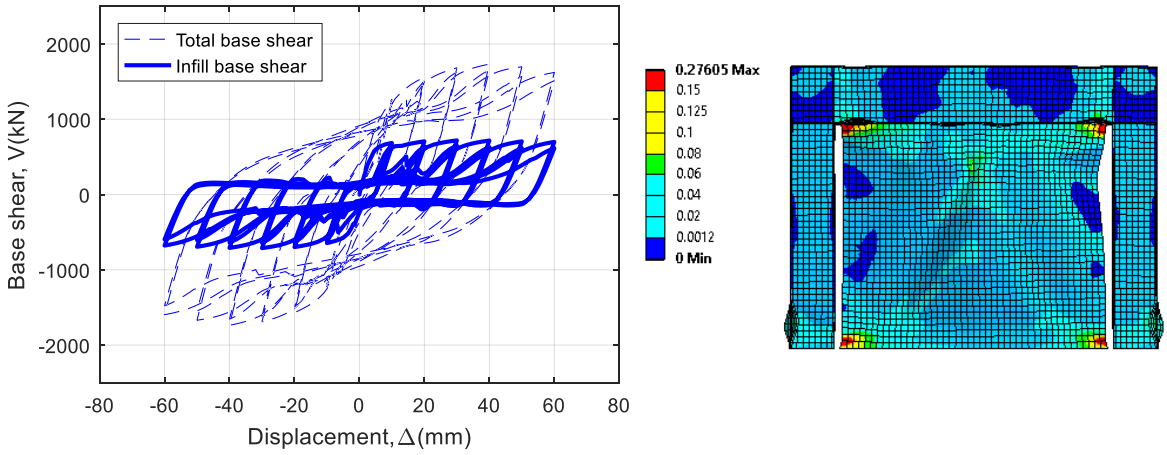

Case (2) Wall connected to the beams only. No side stiffeners

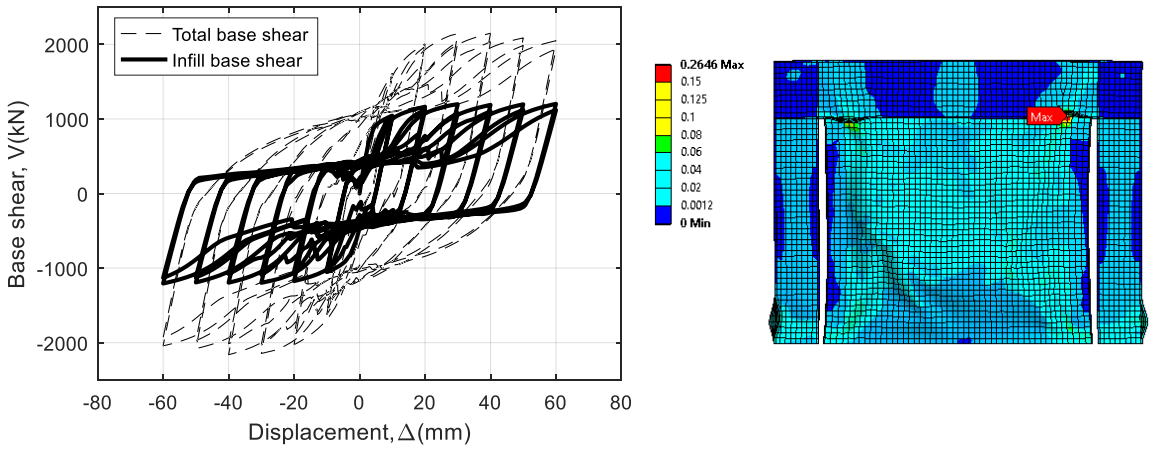

Case (3) Wall connected to the beams only. Side stiffeners used

Figure 4.14 Comparison of hysteresis curves and residual equivalent plastic strains for different infill panel connection details

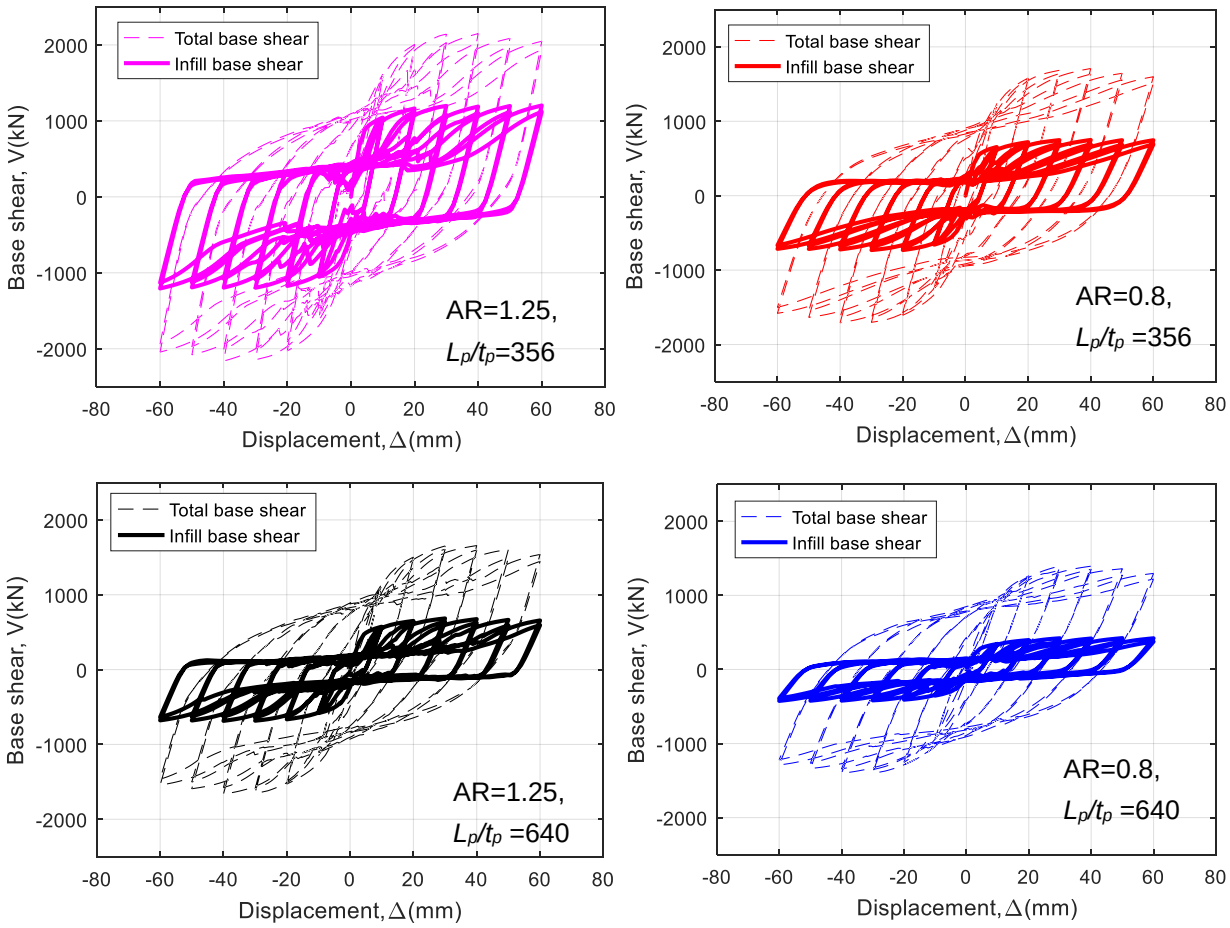

Figure 4.15 Comparison of hysteresis curves for steel shear wall with infill connected to beam only with side stiffeners for different aspect ratios and slenderness ratios

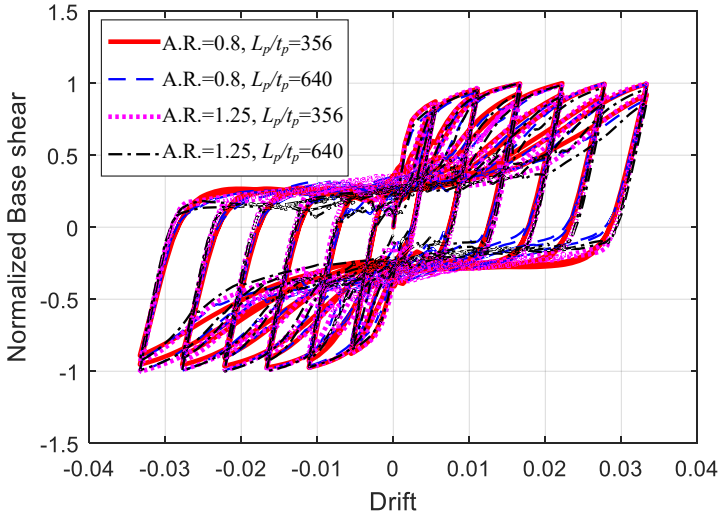

Figure 4.16 Normalized infill panel hysteresis curve for steel shear wall with infill connected to beam only with side stiffeners for different aspect ratios and slenderness ratios

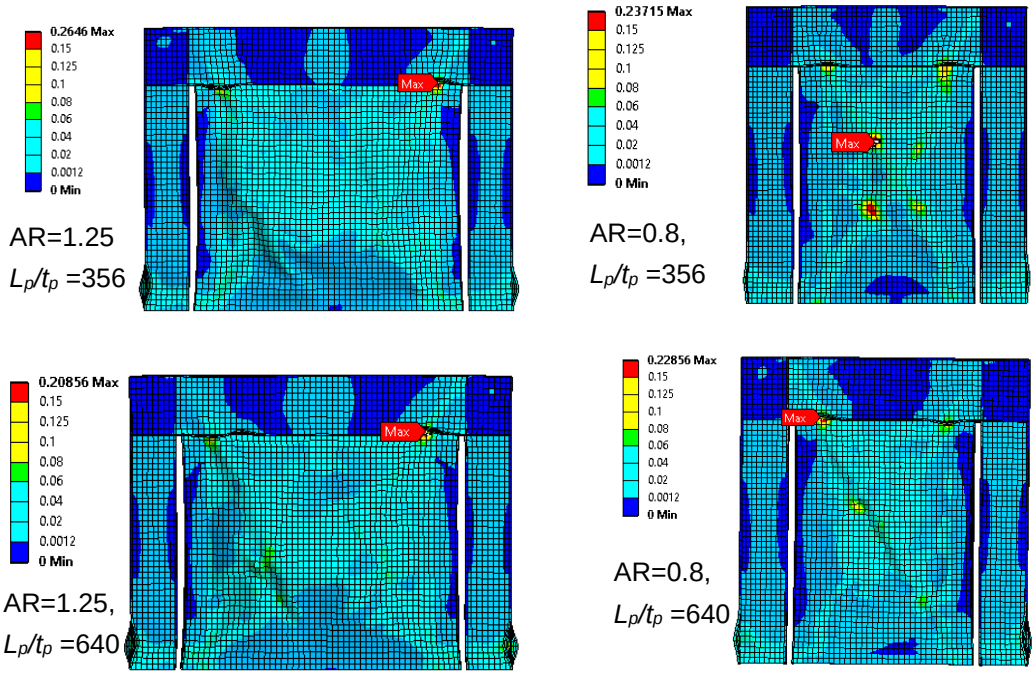

Figure 4.17 Comparison of residual equivalent plastic strain for steel shear wall with infill connected to beam only with side stiffeners for different aspect ratios and slenderness ratios

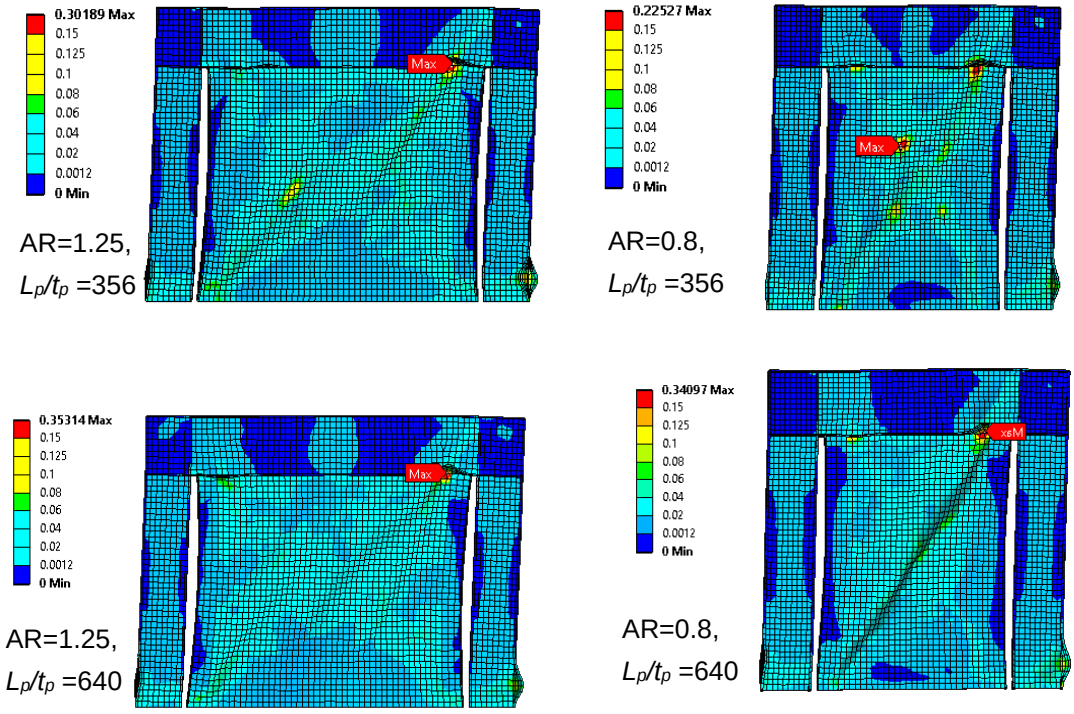

Figure 4.18 Comparison of maximum equivalent plastic strain for steel shear wall with infill connected to beam only with side stiffeners for different aspect ratios and slenderness ratios

4.3 Development of Analytical Equations and Equivalent Brace Model

4.3.1 Shear Buckling Capacity

It is well known that the boundary conditions affect the elastic shear buckling capacity of rectangular plates. Below is a brief review of the shear buckling coefficient in the literature, where the critical shear buckling stress can be obtained by Eqn. (4.1) with appropriate buckling coefficient k_s.

$$\tau_{cr} = k_s \frac{\pi^2 E}{12(1-\nu^2)(b/t)^2} \tag{4.1}$$

where b is the width of the panel, and t is the thickness of the panel, k_s is the buckling coefficient.

Simply Supported on Four Edges: Solutions were developed by Timoshenko (1910), Bergman and Reissner (1932), and Seydel (1933),

$$k_s = \begin{cases} 5.35 + 4/\alpha^2 & \alpha \geq 1 \\ 5.35/\alpha^2 + 4 & \alpha \leq 1 \end{cases} \tag{4.2}$$

where α is defined to be the panel length, a, to width, b, ratio.

Clamped on Four Edges: Southwell and Skan (1924) determined the buckling coefficient for an infinitely long rectangular plate with clamped edges as $k_s = 8.98$. Moheit (1939) further established the coefficient for a finite-length rectangular plate with clamped edges,

$$k_s = \begin{cases} 8.98 + 5.6/\alpha^2 & \alpha \geq 1 \\ 8.98/\alpha^2 + 5.6 & \alpha \leq 1 \end{cases} \tag{4.3}$$

Clamped on Two Opposite Edges and Simply Supported on the Other Two Edges: Cook and Rockey (1963) obtained solutions considering the anti-symmetric buckling mode that was not considered by the general solution by Iguchi (1938). The following expressions were obtained by polynomial fitting to the Cook and Rockey results in the book by Bulson (1970),

Long Edge Clamped

$$k_s = \begin{cases} 8.98 + 5.61/\alpha^2 - 1.99/\alpha^3 & \alpha \geq 1 \\ 8.98/\alpha^2 + 5.61 - 1.99\alpha & \alpha \leq 1 \end{cases} \tag{4.4}$$

Short Edge Clamped

$$k_s = \begin{cases} 5.34 + 2.31/\alpha - 3.44/\alpha^2 + 8.39/\alpha^3 & \alpha \geq 1 \\ 5.34/\alpha^2 + 2.31/\alpha - 3.44 + 8.39\alpha & \alpha \leq 1 \end{cases} \tag{4.5}$$

Effect of side stiffeners on the elastic buckling of a single panel was studied extensively by Alinia (2005), Alinia and Dastfan (2007a), Miao, Dong and Guo (2007) and Guo, Miao and Dong (2007).

Parametric studies were conducted in this section to investigate the effect of out-of-plane stiffness of the side stiffeners on the critical shear buckling capacity of the infill plate and to find a simple design equation for side stiffeners based on shear buckling capacity. Figure 4.19 shows the basic geometry of a steel shear wall with infill plate connected to the beam only and with rectangular side stiffeners. Although rectangular stiffeners were used in this study for simplicity, the conclusions can be applied for stiffeners with any structural shape.

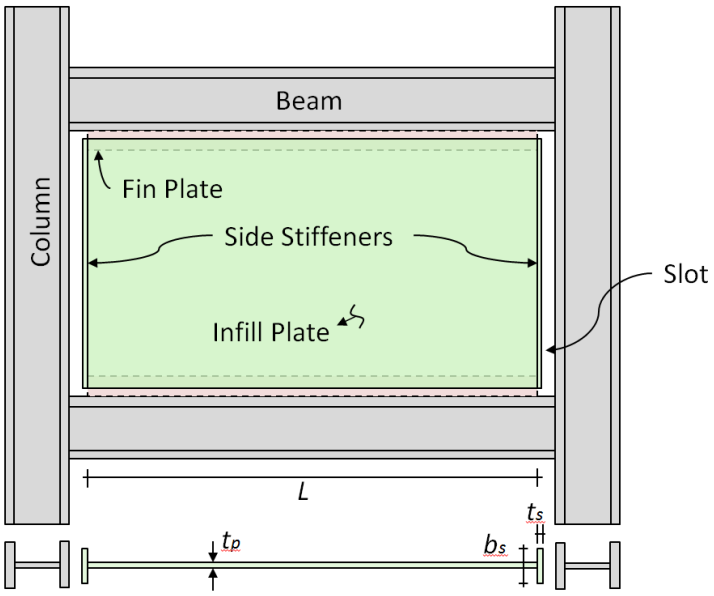

Figure 4.19 Infill panel connected to beam only with typical rectangular side stiffeners

In the parametric study, the infill panel geometry and material were kept the same while the width, b_s, and thickness, t_s, of the side stiffener plates were varied. Similar to the stiffeners for plate girders, the *thickness ratio*, defined as the stiffener thickness divided by the infill plate thickness, t_s/t_p, and the width-to-thickness ratio, b_s/t_s, of the stiffener were the parameters of interest. In addition, a parameter called the rigidity factor, β, is introduced, which is defined as,

$$\beta = \frac{EI_s}{DL_p} \tag{4.6a}$$

$$D = \frac{Et_p^{\,3}}{12(1-\upsilon^2)} \tag{4.6b}$$

where t_p is the thickness of the plate, E, v the Young's modulus and Poisson ratio of steel, L_p the width of the infill panel, D the flexural rigidity of the infill plate, and I_s is defined as the moment of inertia of the side stiffener about the axis parallel to the infill wall. The rigidity factor β shows the relative rigidity of the stiffener compared to that of the infill panel, which characterizes the ability of the stiffeners for restraining the out-of-plane deformation of the plate (Alinia and Dastfan 2007).

The parametric matrix included the stiffener-to-column flange width ratio, b_s/b_{cf}, being 0.08, 0.2, 0.4, 0.6, 0.8 and 1.0, and the stiffener-to-infill plate thickness ratio, t_s/t_p, ranging from 0 to 4.5 with 0.5 intervals. Three aspect ratios (A.R. = 1.0, 1.5 and 2.0) and three infill plate thicknesses (t_p = 2.5, 4.5 and 6.5 mm) were studied. The resulting stiffener stiffness ratio ranged from zero to about 1500. A total number of about 540 elastic buckling analyses were conducted.

Figure 4.20 shows the relationship between the normalized critical shear buckling load over the shear yielding capacity of the first three modes and the relative rigidity factor β. First, it was found that there is a general trend whereby the critical shear buckling capacity increases with increasing β under a certain critical value, beyond which the buckling capacity no longer increases.

To estimate the maximum elastic buckling capacity, the four-edge clamped solution, with k_s determined by Eqn.(4.3) seems to match the FE results better, while the four-edge simply supported solution with k_s determined by Eqn. (4.2) tends to underestimate the buckling capacity. Based on the general trend of the cases analyzed, it was found that the relationship between the normalized critical shear buckling load and the relative rigidity factor can be characterized by the following,

$$\frac{V_{cr}}{V_y} = \begin{cases} \left(\frac{\beta}{\beta_{cr}}\right)^x \left(\frac{V_{cr}}{V_y}\right)_0 & \beta \le \beta_{cr} \\ \left(\frac{V_{cr}}{V_y}\right)_0 & \beta \ge \beta_{cr} \end{cases} \tag{4.7a}$$

where $(V_{cr}/V_y)_0$ is defined as the idealized critical shear buckling to yield stress ratio as follows:

$$\left(\frac{V_{cr}}{V_y}\right)_0 = \frac{k_s \dfrac{\pi^2 E}{12(1-\nu^2)(\dfrac{h_p}{t_p})^2}}{0.6F_y} \tag{4.7b}$$

V_y is the shear yielding capacity of the infill plate, β_{cr} is the critical relative rigidity factor, and x is the exponential factor that controls the shape of the initial curved part.

It can be seen that as the infill plate thickness increases, this β_{cr} value increases. As discussed in Section 4.2.2.3, the out-of-plane stiffness of the side stiffeners is the minimum requirement and does not normally control the selection of side stiffeners.

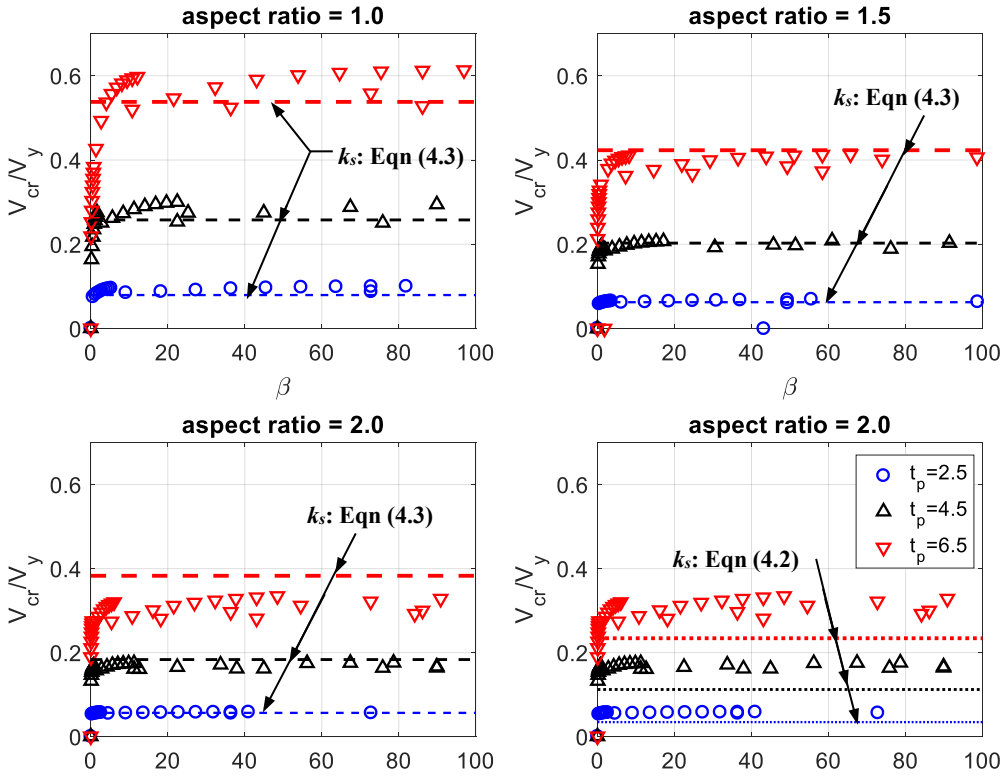

Figure 4.20 Normalized critical shear buckling capacity, V_{cr}/V_y versus relative rigidity factor, β

Therefore, although theoretical, exact values for x and β_{cr} can be established using regression analysis; for design purposes, a single β_{cr} value can be handy to select the out-of-plane stiffness of the side stiffeners. A conservative value of β_{cr} equal to 30 is recommended here, i.e.,

$$\beta_{cr} = 30 \tag{4.8}$$

Alinia and Dastfan (2007) also recommended an optimum rigidity ratio of 30 for the stiffener in stiffened steel shear walls so that both sufficient rigidity and deformability can be achieved.

Regarding the critical out-of-plane stiffness, I_s, the Chinese code on steel plate shear walls (JGJ 2015) has the following requirements (the notations are modified to be consistent with those defined herein),

$$\beta = \frac{(1-\nu^2)\,t_s\,b_s^3}{t_p^3 L_p} \geq 1 \qquad \text{and} \qquad t_s \geq t_p \tag{4.9}$$

This requirement is equivalent to a β_{cr} value of 1. The recommended β_{cr} value of 30 seems conservative if only elastic buckling is considered. But this criterion, as will be seen later, will normally not control over the criteria of the plastic moment capacity. The second requirement in Eqn. (4.9) says that if rectangular stiffeners are used, the stiffener thickness, t_s, should be larger or equal to the infill wall thickness, t_p. The same limit can be adopted for the proposed HPSPSW.

4.3.2 Angle of Inclination and Ultimate Capacity

4.3.2.1 Revisit of Steel Plate Shear Wall Solutions

An unbuckled web subjected to shear will develop equal tensile and compressive stresses inclined in approximately 45 and 135°. Wagner pointed out a new load-carrying mechanism in the form of an inclined tensile membrane field that develops to carry additional loading after plate buckling (Figure 4.21). Wagner first determined the angle of inclination for flat aluminum sheet metal girders in 1931, under the assumption that the web plate is very thin and the flanges can carry the lateral load from the tension field without distorting too much the tension field distributions (Wagner 1931).

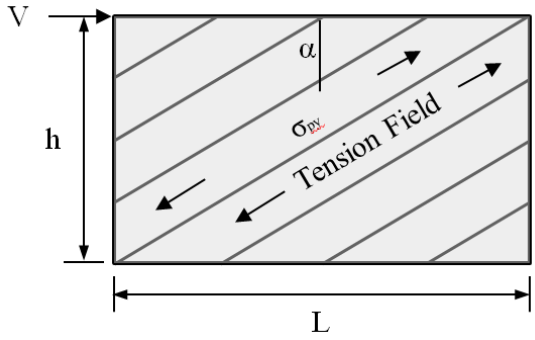

Figure 4.21 Analytical model assuming full tension field by Wagner (1931) and Thorburn et al. (1983)

Built upon the work of Wagner (1931), Thorburn et al. (1983) re-derived the relationships for steel shear wall system. They concluded that the formulation for the steel shear wall turned out to be the same as that derived by Wagner. The only energy contribution was taken as the energy absorbed by the axial forces within the system of the assumed uniform tension field, while the energy due to buckling of the plate as well as the shear within the framing members was ignored (Thorburn et al. 1983).

The resulting expressions for determining the angle of inclination of the tension field and shear capacity of the panel given by Thorburn et al. (1983) are as follows,

$$\alpha = \tan^{-1}\sqrt{\frac{1+\frac{t_p L_{cf}}{2A_c}}{1+\frac{t_p h_{bf}}{A_b}}} \tag{4.10a}$$

$$V_{sp} = \frac{1}{2} f_{yp} t_p L_{cf} \sin 2\alpha \tag{4.10b}$$

where α is the angle of inclination, t_p is the infill plate thickness, L_{cf} is the clear distance between columns, A_c is the area of the boundary column, h_{bf} is the clear distance between beams, A_b the area of the boundary beam and f_{yp} the yielding stress of infill plate.

In 1983, Timler and Kulak recognized the necessity of adding the bending strain energy of the boundary elements, especially the boundary columns. In addition to the strain energy due to the web plate tension field action, the work components they considered included the axial strain energy of the beams and columns, and the bending strain energy of the column (Timler and Kulak 1983). The resulting expressions, which are included in the AISC Seismic Provisions (AISC 2010c), are as follows. This solution could accurately predict a 45° inclination angle for infinitely rigid boundary elements.

$$\alpha = \tan^{-1}\sqrt{\frac{1+\frac{t_p L}{2A_c}}{1+t_p h\left(\frac{1}{A_b}+\frac{h^3}{360 I_c L}\right)}} \tag{4.11a}$$

$$V_{sp} = \frac{1}{2} f_{yp} t_p L_{cf} \sin 2\alpha \tag{4.11b}$$

where L is center to center distance between columns (same as L_{st} in AISC 341-10), h is story height (same as h_{st} in AISC 341-10), and I_c is the second moment of inertia of the boundary column.

As shown in Figure 4.22, Thorburn and his colleagues also established the angle of inclination by assuming a partial tension field for the case where the boundary column is flexurally infinitely flexible while the beam is infinitely rigid (Thorburn et al. 1983).

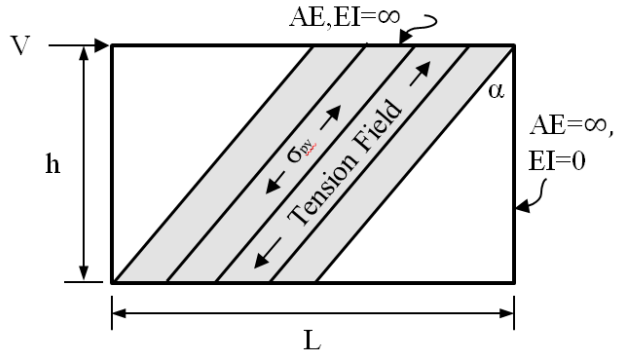

Figure 4.22 Analytical model assuming partial tension field by Thorburn et al. (1983)

In this case, the angle of inclination is no longer related to the boundary element properties but only to the aspect ratio of the infill panel.

$$\alpha = \frac{1}{2}\tan^{-1}\left(\frac{L}{h}\right) \tag{4.12a}$$

$$V_{sp} = \frac{1}{2} f_{yp} t_p L \tan\alpha \tag{4.12b}$$

Equation (4.12b) is also equivalent to

$$V_{sp} = \frac{1}{2} f_{yp} t_p L \left(1 - \frac{h}{L} \tan\alpha\right) \sin(2\alpha) \tag{4.12c}$$

In the original paper by Thorburn et al. (1983), the clear distance between the columns and the center-to-center distance between the columns was not clearly distinguished as evidenced by the slight inconsistency in Eqns. (4.12b) and (4.12c) compared to Eqns. (4.10b) and (4.11b), where the former uses the center-to-center distance and the latter uses the clear distance between columns. By eliminating the contribution of the boundary elements, the above expressions are inevitably conservative. For example, Eqn. (4.12a) predicted a 28° angle while the observed angles were 30–35° in an experimental test carried out recently (Vatansever and Yardimci 2011).

4.3.2.2 Revisit Plate Girder Solutions

There have been arguments that steel plate shear walls (SPSW) are different from plate girders due to the significant stiffness of the boundary columns compared to flanges in a plate girder (Berman and Bruneau 2004). Both the angle of inclination of the diagonal tension field in an SPSW and its associated shear strength depend on the stiffness of these boundary elements. In plate girders, the in-plane stiffnesses of boundary elements are usually neglected (Berman and Bruneau 2004). Then, after separating the infill panels from the boundary columns, as is the case for the proposed HPSPSW system, the infill panel behavior is believed by the author of this dissertation to be closer to that of a plate girder. This is because when compared with relatively rigid boundary columns, the stiffness of the side stiffeners will be much closer to that of a plate girder flange. Therefore, the solutions for plate girders are revisited to investigate possible application to the newly developed HPSPSW system.

The first ultimate load method capable of predicting the shear strength of the conventional plate girders was proposed by Basler and his colleagues (Basler 1961; Basler and Thuerlimann 1961; Basler et al. 1960). They assumed that the flanges of plate girders were so flexible that they could not take the lateral load of the tension field. The failure mechanism was assumed to be the combination of the shear buckling of the web plate plus the membrane stress or tension field (Figure 4.23). Stresses in the triangular wedges adjacent to the tension yield band were assumed to remain equal to the critical buckling shear stress.

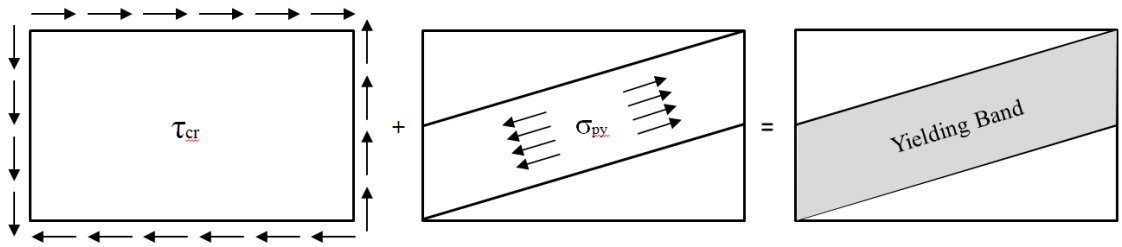

Figure 4.23 Ultimate collapse mechanism developed by Basler et al (1960, 1961)

Evans, Porter, and Rockey (1978, 1987) pointed out that the solutions based on Wagner's work were not very suitable for civil engineering applications since the significant distortion of the flange would affect the extent and nature of the web-plate membrane field. They also argued that Basler's solution was too conservative. In their assumed collapse mechanism (Figure.4.24), the flanges of plate girders would carry some portion of the lateral loads imposed by the inclined tension field up to the point of plastic hinge formation (Evans et al. 1978; Porter et al. 1987; Rockey et al. 1978). Failure would occur when the web yields as a result of combined effect of web buckling (simply supported plates) and tension field yielding and the development of the plastic hinges in the flanges (Figure 4.24). The same expression was obtained by both failure mechanism and equilibrium methods. Note that when *c,* the distance between two plastic hinges in the flange, is equal to zero, this solution is identical to the true Basler solution.

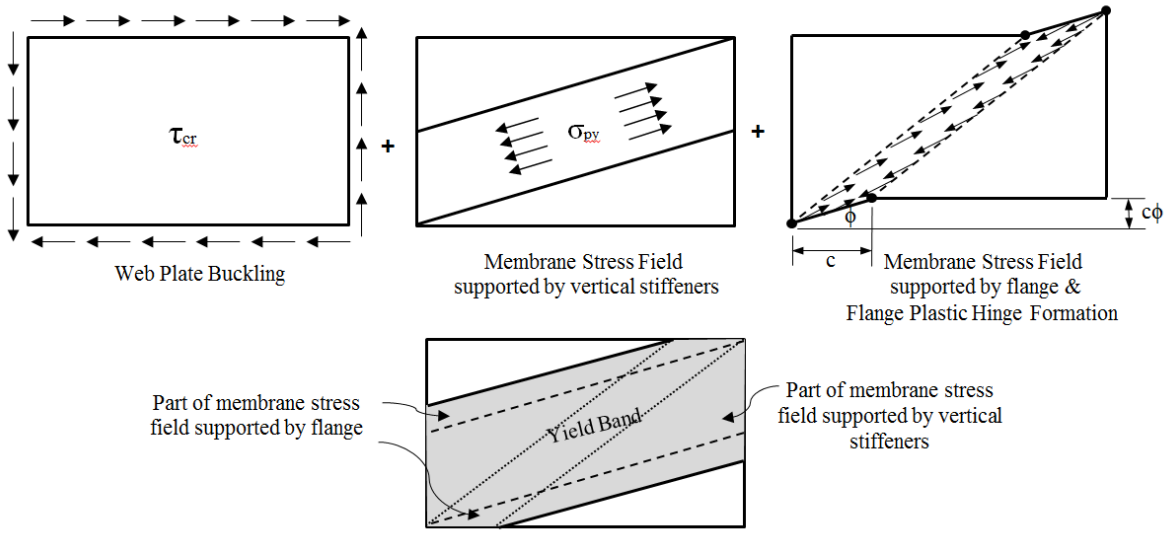

Figure 4.24 Ultimate collapse mechanism of symmetric plate girders under pure shear developed by Evans, Porter, and Rockey (1978, 1987)

The failure mechanism proposed by Porter, Evan and Rockey is considered to be a suitable and not extremely conservative model for the proposed steel shear wall system where the infill plate is connected to the beam only. Choi and Park (2009) was the first to apply this plate girder solution to a steel shear wall system. Based on the previously mentioned work by Porter, Evans, Rockey and Choi and Park (Choi and Park 2009; Evans et al. 1978; Porter et al. 1987; Rockey et al. 1978), the following is a summary of a rational way to determine the angle of inclination of the tension field as well as the ultimate shear strength of the steel infill wall in the proposed HPSPSW configuration.

4.3.2.3 Adapt Plate Girder Solutions to HPSPSW

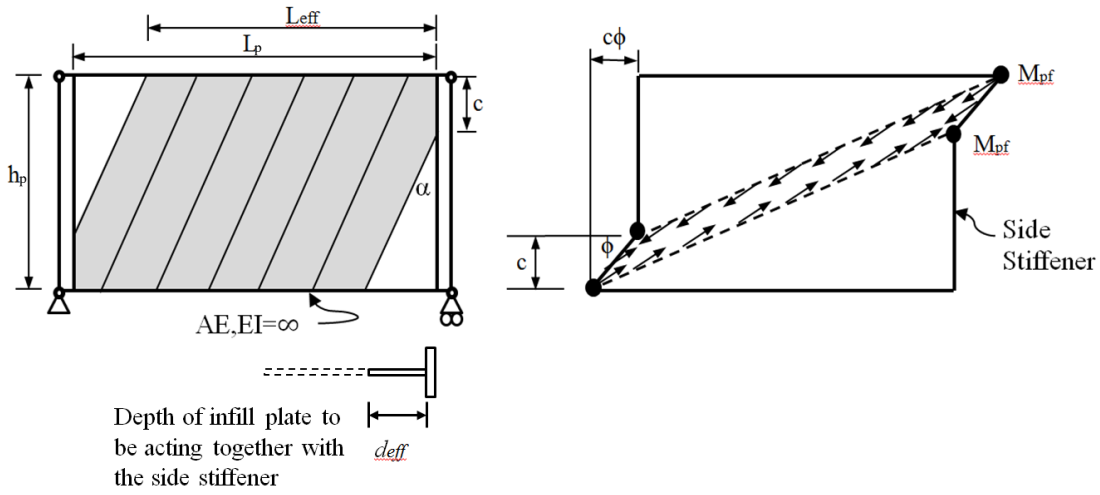

Figure 4.25 Analytical model for HPSPSW with steel shear wall connected to beam only based on the plate girder model by Evans, Porter, and Rockey (1978, 1987)

Figure 4.25 illustrates the analytical model of the proposed HPSPSW configuration, or any steel shear wall with the infill plate connected to the beam only, which is analogous to the plate girder flange-collapse mechanism. Either equilibrium or mechanism derivations would lead to the following equations of shear capacity of the infill panel. Here, use of the energy balance and principle of least work are presented. Similar to the previous steel plate shear wall solutions, the energy associated with buckling of the infill plate is ignored, assuming that the shear wall panel is thin and has relatively small buckling strength.

The overall shear capacity can be computed as the summation of the tensile capacities of the tension strips within the tension field. Here, instead of the full infill width of the infill plate, an effective tension field width L_{eff} should be used (Figure. 4.25).

$$V_{sp} = f_{yp} L_{eff} t_p \sin\alpha \cos\alpha \tag{4.13}$$

For infinitely flexible side stiffeners,

$$L_{eff} = L_p - h_p \tan\alpha \tag{4.13a}$$

For side stiffeners with some rigidity

$$L_{eff} = L_p - (h_p - c)\tan\alpha \tag{4.13b}$$

The infinitely flexible stiffener case can be considered as a special case for the more general expression in Eqn. (4.13b) where c is equal to zero. Applying the principle of least work, the angle of inclination can be derived. Details of the derivation can be found in Appendix D2.

As an alternative to solve the complex differential equations resulting from the least work calculation to determine the angle of inclination, a simplified equation for common panel aspect ratios of 1,1.5 and 2 was proposed by Choi and Park (2009) as follows,

$$\alpha = \alpha_0 + (45° - \alpha_0)\sqrt{(c/h_p)^3}$$
$$\alpha_0 = [0.65 - 0.04(L_p/h_p)]\tan^{-1}(L_p/h_p) \quad (4.14a)$$

It was found that for smaller and larger aspect ratios, slight modifications of the parameters will lead to a better match to the actual solution; see Figure. 4.26 versus Figure. 4.27. The modified parameters are as follows,

For aspect ratio = 2.5,

$$\alpha = \alpha_0 + (45° - \alpha_0)(c/h_p)^{1.95}$$
$$\alpha_0 = [0.65 - 0.04(L_p/h_p)]\tan^{-1}(L_p/h_p) \quad (4.14b)$$

For aspect ratio = 0.5,

$$\alpha = \alpha_0 + (45° - \alpha_0)(c/h_p)^{1.5}$$
$$\alpha_0 = [0.66 - 0.04(L_p/h_p)]\tan^{-1}(L_p/h_p) \quad (4.14c)$$

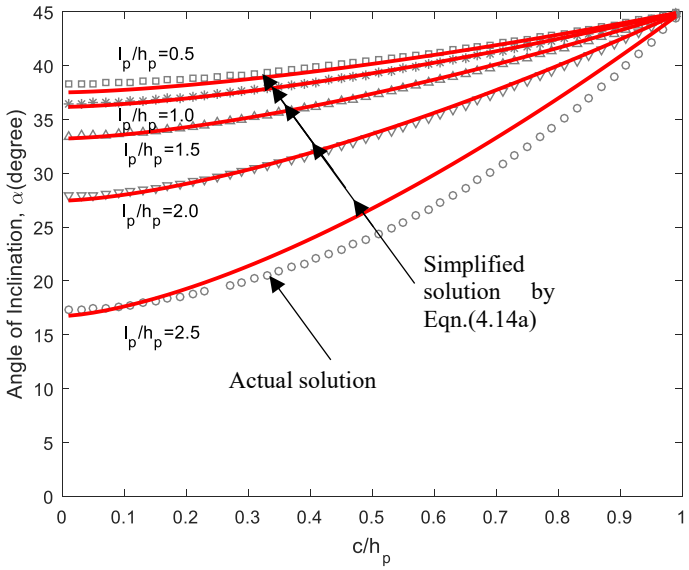

Figure 4.26 Relationship between the angle of inclination and the plastic hinge length ratio (c/h_p) using original parameters proposed by Choi and Park (2009)

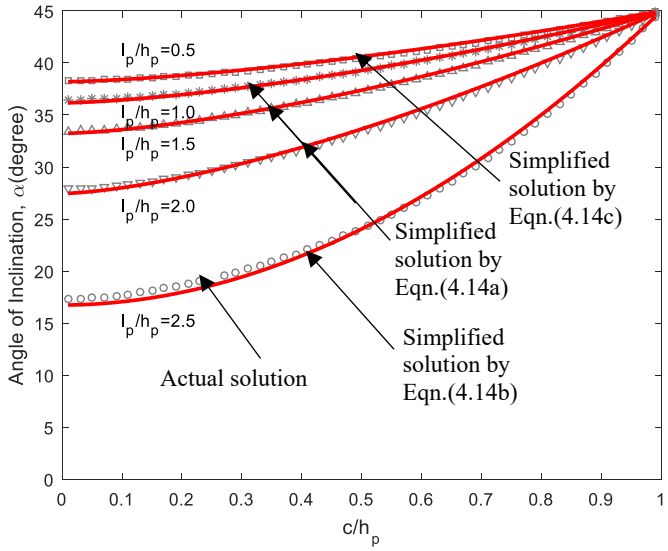

Figure 4.27 Relationship between the angle of inclination and the plastic hinge length ratio (c/h_p) using modified parameters

Using the angle of inclination obtained by Eqn. (4.14a, b, c), the shear capacity of the infill plate can be determined by considering the work conservation between work done by the external force and the internal strain energy. Detailed derivations can be found in Appendix D2.

The total shear capacity of the infill wall for the proposed HPSPSW system includes the strength of the infill panel and the plastic moment capacity of the side stiffeners. The final expression of the shear strength is as follows,

$$V_{sp} = \frac{4M_{pf}}{c} + f_{yp} L_{eff} t_p \sin\alpha \cos\alpha \tag{4.15a}$$

which can be simplified as

$$V_{sp} = \frac{1}{2} f_{yp} t_p [L_p - (h_p - 2c)\tan\alpha]\sin 2\alpha \tag{4.15b}$$

where α is the angle of inclination determined from Eqn. (4.14), and,

$$c = \frac{2}{\sin\alpha}\sqrt{\frac{M_{pf}}{f_{yp} t_p}} \tag{4.16}$$

In calculating M_{pf}, the bending capacity of the effective side stiffener should be used. Typically, a section of the infill plate is assumed to act with the side stiffener (Figure 4.25), which is similar to the flange in plate girders. As proposed by Rockey and Skaloud (1972), the depth of infill plate in the effective side stiffener section can be calculated as

$$d_{eff} = 30t_p(1-\frac{2\tau_{cr}}{\tau_{yw}}) \tag{4.17}$$

Since the shear buckling capacity of the infill panel is assumed to be negligible, the depth can be simply taken as $30t_p$. Iterations would be needed to obtain c and α. Although this method is summarized based on the work by Porter et al. (1987) and Choi and Park (2009), the original formulation was proposed by Porter and his fellow researchers; therefore, in the following comparison, this method will be referred to as Porter's work.

Note that Eqn. (4.15b) is actually an intermediate solution between the full tension field and complete partial tension field solutions. When fully restrained, $c = h_p$, and when rearranged, the expression of the V_{sp} will become close to the full tension field solution in Eqn. (4.11b). The second term is the contribution by the side stiffener,

$$V_{sp} = \frac{1}{2} f_{yp} L_p t_p \sin(2\alpha) + \underbrace{\frac{1}{2} f_{yp} h_p t_p \tan\alpha \sin(2\alpha)}_{stiffener} \tag{4.15c}^{1}$$

When there is no side stiffener, c equals to zero, and V_{sp} will approach the complete partial tension field solution given in Eqn. (4.12c) earlier,

$$V_{sp} = \frac{1}{2} f_{yp} t_p L_p \left[1-\frac{h_p}{L_p}\tan\alpha\right]\sin(2\alpha) \tag{4.15d}^{1}$$

Although the above analogy is not exact since the angle of inclination will be different in an infill wall connected to beam-only configuration in a HPSPSW system and fully connected configuration in traditional SPSW system, the above discussion demonstrates that the V_{sp} in Eqn. (4.15b) is a reasonable solution.

In actual application of the above equation to determine the ultimate shear capacity in design or analysis, appropriate R_y and C_{pr} factors can be included to account for the actual yield stress and strain hardening effect of the infill panel material respectively. Therefore, Eqn. (4.15b) can be modified as

$$V_{sp} = \frac{1}{2} C_{pr} R_y f_{yp} t_p [L_p - (h_p - 2c)\tan\alpha]\sin 2\alpha \tag{4.18}$$

[1] The numbering of Eqns. (4.15c) and (4.15d) did not follow usual sequence because they are simply another way of expressing Eqns. (4.15a) and (4.15b) instead of new equations.

4.3.3 Elastic Stiffness

The elastic stiffness is essential in determining the natural frequency and other elastic responses for a system. This section provides a review of existing models and presents the derivation of new equations to establish the stiffness of the infill wall of the HPSPSW system.

4.3.3.1 Revisit of Steel Plate Shear Wall Solutions

For the fully connected traditional steel plate shear walls, Sabouri-Ghomi et al. (2005) presented a procedure to derive the elastic stiffness of the infill panel. They assumed full tension field in the steel shear wall panels and equated the work done by the applied lateral force to the strain energy due to the infill panel tension field only (Sabouri-Ghomi et al. 2005). If the buckling capacity is ignored for thin infill panels, the resulting expression for the stiffness is

$$K_{w\_SG} = \frac{Et_p}{4}\frac{L_{cf}}{h_{bf}}\sin^2(2\alpha) \tag{4.19a}$$

This expression is the same as the results obtained by Thorburn et al. (1983). Sabouri-Ghomi et al. (2005) further argued that because the angle of inclination does not have a significant influence on the stiffness, one can assume $\alpha = 45^o$ and the equation simplifies to:

$$K_{w\_SG} = \frac{Et_p}{4}\frac{L_{cf}}{h_{bf}} \tag{4.19b}$$

Note that in the original work of Sabouri-Ghomi et al. (2005), they also suggested two modification factors C_{m1} and C_{m2} with their limits being $0.8 < C_{m1} < 1$ and $1 < C_{m2} < 1.7$ to be used in the numerator and denominator in Eqn. (4.19b), respectively. Since the researchers did not provide a clear procedure in selection of specific values for these modification factors, they will be neglected in the following parametric studies. However, it is recognized that directly applying Eqn. (4.19b) will result in a slightly larger predicted shear stiffness values. This will be addressed in the interpretation of the results.

For the complete partial tension field mechanism shown in Figure 4.22 associated with infinitely flexible boundary columns, Thorburn et al. (1983) derived the shear stiffness by using the geometric relation between the story drift and the elongation of the tension field strips. The equivalent story stiffness for the tension zone given by Thorburn et al. (1983) is as follows,

$$K_{w\_T} = \frac{Et_p}{4}\frac{L_{cf}}{h_{bf}}\sin(2\alpha)\tan(\alpha) \tag{4.20a}$$

where $2\alpha = \tan^{-1}(L_{cf}/h_{bf})$

Using trigonometric relationships, this is equivalent to

$$K_{w\_T} = \frac{Et_p}{4}\frac{L_{cf}}{h_{bf}}\left(1-\frac{h_{bf}}{L_{cf}}\tan\theta\right)\sin^2(2\theta) \tag{4.20b}$$

where θ is the angle of the diagonal equal to $\tan^{-1}(L_{cf}/h_{bf})$. Note here the infill panel dimension, L_{cf} and h_{bf} are used instead of the centerline-to-centerline distances, L and h, as derived in the original paper. This is done to be consistent with the other models.

4.3.3.2 Revisit of Plate Girder Solutions

In a more recent study by Guo et al. (2011), they presented two tests on the steel plate shear wall connected to the beam only and showed a simplified brace model to represent the shear wall. In their formulation, the ultimate capacity was obtained by curve fitting to relate the ultimate capacity to the height-to-thickness ratio, aspect ratio, shear yield stress, and width and thickness of the infill panel. They derived the elastic shear stiffness by idealizing the infill panel as a member with rectangular cross section fixed at both ends. The overall deformation was considered as a combination of shear and flexural deformations (Guo et al. 2011). The resulting shear stiffness is:

$$K_{w\_G} = \frac{Et_p}{\frac{1}{\left(\frac{L_{cf}}{h_{cf}}\right)^3}+\frac{2(1+\nu)k}{\left(\frac{L_{cf}}{h_{bf}}\right)}} \tag{4.21}$$

where k = correction coefficient considering non-uniform shear stress distribution on the cross section. For rectangular cross-section, k = 1.2.

Apart from this formulation based on basic mechanics of beam deformation, the plate girder collapse mechanism is also considered in this project. If an elastic – perfectly plastic relationship is assumed for the infill panel, then the yield point for the system corresponds to a status that the plastic hinges of the side stiffeners has just formed without any plastic rotations, and the infill panel has yielded in the shaded region shown in Figure 4.25. Under this assumption, the following shows the derivation of the shear stiffness of the HPSPSW following the procedure used for the fully connected traditional SPSW system.

First, the strain energy of the infill panel can be obtained by Eqn. (4.22a). Note that here only the strain energy of the yielded area of the infill panel is included given the assumption that there is no plastic rotation of the side stiffener plastic hinges has occurred,

$$W_I = \frac{V^2[L_p h_p - (h_p - c)^2\tan\alpha]}{2Et_p\left[L_p-(h_p-c)\tan\alpha\right]^2\sin^2\alpha\cos^2\alpha} \tag{4.22a}$$

Similarly, the external work done by the applied shear force, V, for a displacement of, Δ, is

$$W_E = \frac{1}{2} V \Delta \tag{4.22b}$$

By equating the two terms in Eqn. (4.22a) and Eqn. (4.22b) and defining the stiffness as K equals to V/Δ, we can obtain the shear stiffness as follows,

$$K_{sp} = \frac{E t_p \left[L_p - (h_p - c)\tan\alpha \right]^2 \sin^2\alpha \cos^2\alpha}{[L_p h_p - (h_p - c)^2 \tan\alpha]} \tag{4.23a}$$

If we take a closer look at Eqn. (4.23a), it is easy to recognize that the initial stiffness in Eqn. (4.23a) is an intermediate solution between the full tension field solution given by Eqn. (4.19) and complete partial tension field solution given by Eqn. (4.20). When fully restrained, which implies c equals to h_p, the expression of the stiffness in Eqn. (4.23a) is rearranged and will become close to the full tension field solution in Eqn. (4.19a),

$$K_{sp} = \frac{E t_p}{4} \frac{L_p}{h_p} \sin^2(2\alpha) \tag{4.23b}$$

When there is no side stiffener, i.e., $c = 0$, Eqn. (4.23a) will approach the complete partial tension field solution,

$$K_{sp} = \frac{E t_p \left[L_p - h_p \tan\alpha \right]^2 \sin^2\alpha \cos^2\alpha}{[L_p h_p - h_p^2 \tan\alpha]} \tag{4.23c}$$

It can be further simplified to the same format as that in Eqn. (4.20b)

$$K_{sp} = \frac{E t_p}{4} \frac{L_p}{h_p} \left(1 - \frac{h_p}{L_p} \tan\alpha \right) \sin^2(2\alpha) \tag{4.23d}$$

Although the above analogy is not exact due to the difference in the angle of inclination, it still shows the K_{sp} given by Eqn. (4.23a) is a reasonable solution.

The shear stiffness contributed by the side stiffener can also be added to the pure wall shear stiffness assuming they are two columns fixed on both ends. This assumption results in a value of shear stiffness of the stiffeners, K_s, equals to $24EI_s/h_p^3$, with I_s being the moment of inertia of the side stiffener about an axis perpendicular to the infill wall. But since h_p is normally a large number compared to I_s, the shear stiffness for stiffeners is negligible for most of the practical cases.

4.3.4 Parametric Study for Validation of Proposed Equations

In order to verify the proposed equations and compare various analytical solutions discussed in the previous section, a parametric study was performed. In the following comparison, the four solutions for the ultimate strength proposed by Wagner (1931), Porter et al. (1987), Thorburn et al.(1983), and Timler and Kulak (1983) will be referred to as W, P, T, TK, respectively. The four solutions for stiffness by the author based on the collapse mechanism proposed by Porter et al.(1987), Sabouri-Ghomi et al.(2005), Thorburn et al.(1983), and Guo et al.(2011) will be referred to as P, SG, T, and G, respectively.

The FE analysis model is a simple one-bay one-story specimen with infill wall connected to beam only. The height of the panel in the parametric studies was equal to 1000 mm, and the width varied with the aspect ratio. SHELL181 elements were used to model the infill panel, the boundary elements, and the side stiffeners. To make it easier to identify the yield point and ultimate capacity, a bilinear kinematic hardening material model was used with a yield strength equal to 50 ksi (345 MPa) with a relatively small hardening modulus of 1450 MPa (hardening ratio of 0.7%). The beam and column sections were the same for all cases with an I-shaped beam (200 × 200 × 16 × 16) and column (250 × 250 × 20 × 20 in mm). The main variables were the aspect ratio, L_p/h_p equal to 0.75, 1, 1.5, and 2, thickness of infill plate, t_p , equal to 2.5, and 4.5 mm, the stiffness of side stiffeners with the width b_s fixed to 100 mm, and the thickness t_s varied being 0, 10, and 25 mm. Cases with panel aspect ratio of 0.75 were also included since sometimes relatively narrow shear walls are needed.

Figure 4.28 shows the widening of tension field with increasing stiffness of the side stiffeners, which verifies the assumption of Porter's solution in which the contribution of boundary flanges to the ultimate shear capacity is recognized.

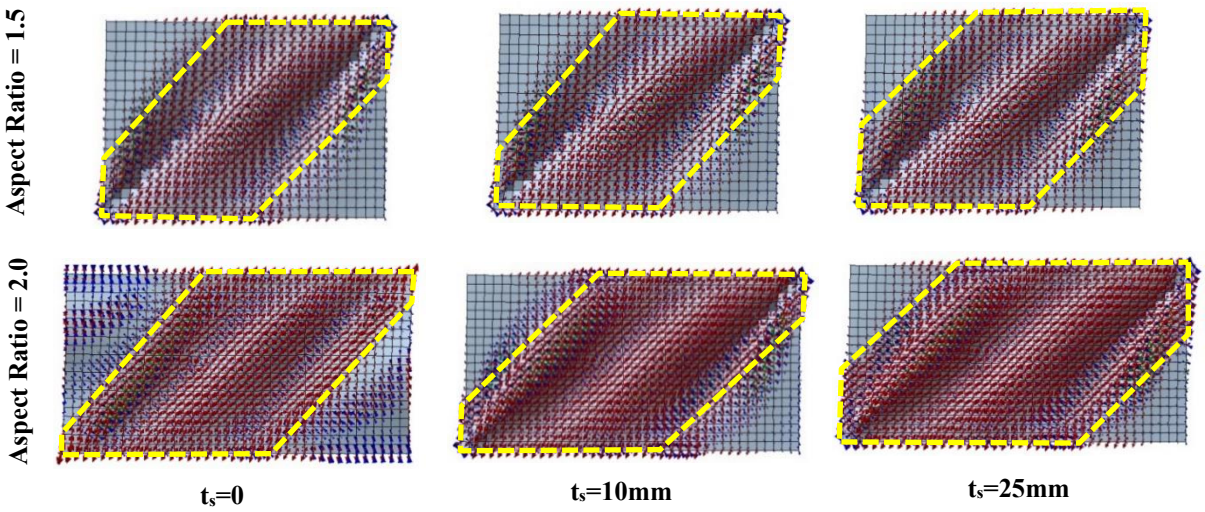

Figure 4.28 Plot of principle stresses showing the expansion of tension field with stiffer and stronger side stiffeners

Table 4.2 lists the results obtained by nonlinear FE analysis for the various analytical models with the corresponding equation number shown below the name. Table 4.3 lists the ratio of analytical equation prediction divided by the simulation results. The FE results were obtained through evaluating the pushover curves for the infill wall (including the contribution from the side-stiffeners). The angle of inclination was obtained by calculating the average of the angles of the principal stress vectors output in the yielded area; see shaded area in Figure 4.28.

The equations used to calculate the analytical solutions are also provided in Table 4.2. The material yield strength, f_{yp}, used in the analytical equations was the minimum specified yield stress of 345 MPa (50 ksi). This was done because the hardening ratio in the FE analysis material was set intentionally to be small.

As far as the closeness of predicted solutions to the FE simulation results, Porter's solution was optimal considering both the prediction of the angle of inclination of the tension field and the shear capacity of the infill panel. It predicted slightly lower shear capacity for thinner infill plate but higher values for thicker plates. On the average, there is slight under-estimation for the shear capacity, but this conservatism is acceptable for design purposes.

The recommended effective boundary concept was used to replace the properties of boundary columns (i.e., A_c, I_c) in Timler and Kulak's solution. It was found that the TK solution was also able to predict the angle of inclination relatively well, but over-predicted the shear capacity of the panel; this is probably because the axial energy of equivalent section of side stiffeners, which consisted of the plate stiffener and a portion of the adjacent infill plate, is not as big as that of a similar T-shape boundary column. Note that the use of the effective boundary concept is important, especially if one wants to directly use Timler and Kulak's solution, or the current AISC equation for the HPSPSW shear wall configuration. Neglecting the contribution by the portion of infill plate adjacent to the rectangular stiffener in computing A_c, I_c could lead to a very poor match to the numerical simulation with an average ratio of analytical to numerical results of 0.359.

As far as Thorburn's partial tension field solution, it was overly conservative as expected and reported in the past experimental study (Vatansever and Yardimci 2011).

Overall, all analytical equations for predictions of shear stiffness showed a less satisfactory match with the FE simulation results. This could be because the assumed energy equivalence considering only the tension field does not represent the actual behavior, where complex elastic buckling and partial yielding of the infill panel occur.

As shown in Table 4.3, use of the full tension field solution greatly overestimated the initial stiffness, but the level of overestimation may be reduced if the C_{m1} and C_{m2} modification factors are applied. The complete partial tension field solution (K_{w_T}) and the solution using basic flexural and shear theory (K_{w_G}) both had slightly higher average predictions than the FE analysis results.

K_{w_G} seems better in terms of the level of scattering. Overall, the initial stiffness derived from the plate girder collapse mechanism in Eqn. (4.23a) appears to work the best among the available analytical solutions; note that Eqn. (4.23a) tends to underestimate the stiffness for panels, especially for panels of small aspect ratio.

The complete partial tension field solution (K_{w_T}) had an acceptable average prediction of the elastic stiffness, but there was relatively large standard deviation of the predictions. It tends to underestimate the stiffness for panels with small aspect ratios and overestimate panels with large aspect ratios.

Table 4.2 Comparison of results by FE analysis and different analytical solutions on predicting V_{sp}, α and K_{sp}

aspect ratio	t_p	t_s	**Vsp_FEA**	Vsp_W (4.10b)	Vsp_P (4.15b)	Vsp_T (4.12b)	Vsp_TK (4.11b)	**α_FEA**	α_W (4.10a)	α_P (4.14)	α_T (4.12a)	α_TK (4.11a)	**K_FEA**	K_P (4.23a)	K_SG (4.19b)	K_T (4.20a)	K_G (4.21)
0.75	2.5	0	**150.38**	320.40	149.32	107.81	245.93	**23.80**	48.93	24.56	18.43	24.75	**3.22E+04**	2.27E+04	9.38E+04	2.31E+04	5.37E+04
0.75	2.5	10	**236.20**	318.59	198.79	107.81	251.40	**24.74**	40.04	26.94	18.43	25.51	**3.90E+04**	2.60E+04	9.38E+04	2.31E+04	5.37E+04
0.75	2.5	25	**257.20**	313.64	214.63	107.81	257.97	**26.20**	37.93	27.68	18.43	26.45	**4.26E+04**	2.72E+04	9.38E+04	2.31E+04	5.37E+04
0.75	4.5	0	**329.41**	579.52	342.79	194.06	516.24	**27.47**	42.26	26.54	18.43	31.23	**5.52E+04**	4.57E+04	1.69E+05	4.16E+04	9.67E+04
0.75	4.5	10	**448.80**	563.91	466.56	194.06	525.65	**27.60**	37.80	29.66	18.43	32.27	**7.14E+04**	5.54E+04	1.69E+05	4.16E+04	9.67E+04
0.75	4.5	25	**498.80**	552.08	524.00	194.06	519.10	**28.45**	35.75	30.98	18.43	31.54	**9.02E+04**	6.03E+04	1.69E+05	4.16E+04	9.67E+04
1	2.5	0	**251.20**	422.80	226.93	178.63	355.33	**34.30**	50.70	28.50	22.50	27.70	**5.66E+04**	4.21E+04	1.25E+05	5.00E+04	8.06E+04
1	2.5	10	**322.40**	427.17	283.90	178.63	355.73	**31.80**	41.10	30.20	22.50	27.80	**5.36E+04**	4.61E+04	1.25E+05	5.00E+04	8.06E+04
1	2.5	25	**378.52**	420.36	301.70	178.63	360.31	**32.70**	38.50	30.80	22.50	28.30	**7.13E+04**	4.76E+04	1.25E+05	5.00E+04	8.06E+04
1	4.5	0	**468.20**	775.64	493.99	321.53	721.20	**32.70**	43.90	29.90	22.50	34.10	**9.24E+04**	8.16E+04	2.25E+05	9.00E+04	1.45E+05
1	4.5	10	**607.59**	758.99	631.67	321.53	723.16	**34.10**	38.90	32.30	22.50	34.30	**1.42E+05**	9.37E+04	2.25E+05	9.00E+04	1.45E+05
1	4.5	25	**674.40**	742.71	694.02	321.53	710.37	**33.10**	36.50	33.30	22.50	33.10	**1.46E+05**	9.99E+04	2.25E+05	9.00E+04	1.45E+05
1.5	2.5	0	**426.60**	620.46	403.10	346.20	585.41	**32.30**	53.20	33.80	28.20	32.40	**7.68E+04**	9.07E+04	1.88E+05	1.35E+05	1.33E+05
1.5	2.5	10	**503.90**	644.87	469.79	346.20	574.71	**32.30**	42.70	34.80	28.20	31.30	**1.12E+05**	9.52E+04	1.88E+05	1.35E+05	1.33E+05
1.5	2.5	25	**589.90**	635.60	490.16	346.20	573.10	**33.30**	39.60	35.10	28.20	31.20	**1.13E+05**	9.69E+04	1.88E+05	1.35E+05	1.33E+05
1.5	4.5	0	**796.00**	1163.22	825.97	623.15	1133.78	**33.00**	46.30	34.60	28.20	38.40	**1.64E+05**	1.70E+05	3.38E+05	2.43E+05	2.39E+05
1.5	4.5	10	**955.20**	1151.97	981.97	623.15	1123.14	**33.80**	40.80	36.00	28.20	37.40	**2.10E+05**	1.84E+05	3.38E+05	2.43E+05	2.39E+05
1.5	4.5	25	**1044.30**	1129.10	1050.79	623.15	1099.62	**33.90**	37.90	36.70	28.20	35.40	**2.13E+05**	1.91E+05	3.38E+05	2.43E+05	2.39E+05
2	2.5	0	**672.50**	810.19	596.40	533.05	820.17	**34.50**	55.00	36.60	31.70	36.00	**1.37E+05**	1.46E+05	2.50E+05	2.50E+05	1.83E+05
2	2.5	10	**733.29**	862.09	668.28	533.05	800.41	**34.30**	44.10	37.20	31.70	34.10	**1.51E+05**	1.51E+05	2.50E+05	2.50E+05	1.83E+05
2	2.5	25	**812.99**	852.34	690.08	533.05	791.94	**35.20**	40.60	37.40	31.70	33.30	**1.43E+05**	1.52E+05	2.50E+05	2.50E+05	1.83E+05
2	4.5	0	**1210.50**	1543.57	1181.83	959.50	1540.82	**33.90**	48.10	37.10	31.70	41.50	**2.52E+05**	2.69E+05	4.50E+05	4.50E+05	3.30E+05
2	4.5	10	**1299.90**	1545.61	1348.03	959.50	1524.25	**35.30**	42.30	38.10	31.70	39.50	**2.72E+05**	2.84E+05	4.50E+05	4.50E+05	3.30E+05
2	4.5	25	**1386.10**	1519.62	1420.55	959.50	1493.66	**35.60**	39.10	38.60	31.70	37.10	**2.82E+05**	2.92E+05	4.50E+05	4.50E+05	3.30E+05

155

Table 4.3 Comparison of ratios of different analytical solutions over the FE analysis results on predicting V_{sp}, α and K_{sp}

			Prediction/ANSYS				Prediction/ANSYS				Prediction/ANSYS			
aspect ratio	t_p	t_s	Vsp_W	**Vsp_P**	Vsp_T	Vsp_TK	α_W	**α_P**	α_T	α_TK	**K_P**	K_SG	K_T	K_G
0.75	2.5	0	2.131	**0.993**	0.717	1.635	2.056	**1.032**	0.775	1.040	**0.706**	2.910	0.718	1.668
0.75	2.5	10	1.349	**0.842**	0.456	1.064	1.618	**1.089**	0.745	1.031	**0.666**	2.402	0.592	1.377
0.75	2.5	25	1.219	**0.834**	0.419	1.003	1.448	**1.056**	0.704	1.010	**0.638**	2.200	0.542	1.261
0.75	4.5	0	1.759	**1.041**	0.589	1.567	1.538	**0.966**	0.671	1.137	**0.828**	3.056	0.753	1.752
0.75	4.5	10	1.256	**1.040**	0.432	1.171	1.370	**1.075**	0.668	1.169	**0.776**	2.363	0.583	1.355
0.75	4.5	25	1.107	**1.051**	0.389	1.041	1.256	**1.089**	0.648	1.109	**0.669**	1.871	0.461	1.072
1	2.5	0	1.683	**0.903**	0.711	1.415	1.478	**0.831**	0.656	0.808	**0.744**	2.208	0.883	1.425
1	2.5	10	1.325	**0.881**	0.554	1.103	1.292	**0.950**	0.708	0.874	**0.860**	2.332	0.933	1.505
1	2.5	25	1.111	**0.797**	0.472	0.952	1.177	**0.942**	0.688	0.865	**0.667**	1.753	0.701	1.131
1	4.5	0	1.657	**1.055**	0.687	1.540	1.343	**0.914**	0.688	1.043	**0.883**	2.435	0.974	1.571
1	4.5	10	1.249	**1.040**	0.529	1.190	1.141	**0.947**	0.660	1.006	**0.660**	1.585	0.634	1.022
1	4.5	25	1.101	**1.029**	0.477	1.053	1.103	**1.006**	0.680	1.000	**0.685**	1.541	0.616	0.994
1.5	2.5	0	1.454	**0.945**	0.812	1.372	1.647	**1.046**	0.873	1.003	**1.181**	2.441	1.758	1.730
1.5	2.5	10	1.280	**0.932**	0.687	1.141	1.322	**1.077**	0.873	0.969	**0.850**	1.674	1.205	1.186
1.5	2.5	25	1.077	**0.831**	0.587	0.972	1.189	**1.054**	0.847	0.937	**0.858**	1.659	1.195	1.176
1.5	4.5	0	1.461	**1.038**	0.783	1.424	1.403	**1.048**	0.855	1.164	**1.035**	2.058	1.482	1.458
1.5	4.5	10	1.206	**1.028**	0.652	1.176	1.207	**1.065**	0.834	1.107	**0.876**	1.607	1.157	1.139
1.5	4.5	25	1.081	**1.006**	0.597	1.053	1.118	**1.083**	0.832	1.044	**0.899**	1.585	1.141	1.123
2	2.5	0	1.205	**0.887**	0.793	1.220	1.594	**1.061**	0.919	1.043	**1.065**	1.825	1.825	1.339
2	2.5	10	1.176	**0.911**	0.727	1.092	1.286	**1.085**	0.924	0.994	**0.997**	1.656	1.656	1.215
2	2.5	25	1.048	**0.849**	0.656	0.974	1.153	**1.063**	0.901	0.946	**1.065**	1.748	1.748	1.283
2	4.5	0	1.275	**0.976**	0.793	1.273	1.419	**1.094**	0.935	1.224	**1.069**	1.786	1.786	1.311
2	4.5	10	1.189	**1.037**	0.738	1.173	1.198	**1.079**	0.898	1.119	**1.045**	1.654	1.654	1.214
2	4.5	25	1.096	**1.025**	0.692	1.078	1.098	**1.084**	0.890	1.042	**1.037**	1.596	1.596	1.171
avg.			1.2597	**0.9571**	0.6229	1.1951	1.3523	**1.0307**	0.7863	1.0285	**0.8649**	1.9977	1.1081	1.3116
std.dev			0.1859	**0.0857**	0.1311	0.1982	0.2250	**0.0692**	0.1038	0.1003	**0.1647**	0.4359	0.4705	0.2144

156

4.3.5 Implications for Design

Based on the parametric study presented above, the collapse mechanism for plate girders proposed by Porter et al. (1987) is optimal for the new HPSPSW system with the infill wall connected to beams only. This section takes a closer look at Eqn. (4.15b) and Eqn. (4.23a) and discusses the design implications of those two equations.

4.3.5.1 Implication for Side Stiffener Design

Equation (4.15) is the general theoretical equation used to calculate the shear strength of the steel shear wall with an infill panel connected to the beam only. By re-arranging the equation, we obtain,

$$V_{sp} = \frac{1}{2} f_{yp} t_p L_p \sin 2\alpha - \frac{1}{2} f_{yp} t_p (h_p - 2c) \tan\alpha \sin 2\alpha \tag{4.24}$$

It is easy to see that the first term is identical to the expression for the steel shear walls connected to both the beams and columns in Eqn. (4.11b). The separation of the infill wall from the column causes loss of some boundary constraint and shear capacity, which is reflected in the second term where the reduction increases as c decreases. Therefore, in order to reduce the loss of shear capacity, one way is to force the second term to be as small as possible, which leads to the requirement

$$h_p \le 2c \tag{4.25}$$

Note that due to the difference in angle of inclination in the shear wall connected to both beams and columns and the shear wall connected to beam only, differences in the shear capacities remain, even making the second term zero. But Eqn. (4.25) is considered to be a reasonable and straightforward criterion for design the in-plane plastic moment capacity of the side stiffeners. Let h_p be equal to $2c$ and plug it back to Eqn. (4.16). By re-arranging the equation, we obtain a minimum required plastic moment capacity of the side stiffeners,

$$M_{pf,\lim} = \frac{h_p^2}{16} f_{yp} t_p \sin^2\alpha \tag{4.26a}$$

For preliminary design, the actual angle of inclination is unknown, then one can assume an angle of inclination of 30°, which results in a simpler criterion that depends only on the basic geometric dimension of the infill panel and its yield strength,

$$M_{pf,\lim} = \frac{h_p^2}{64} f_{yp} t_p \tag{4.26b}$$

The above criterion aims to minimize the reduction of shear capacity without making the side stiffeners too large. If one assumes α is 45°, the resulting $M_{pf,lim}$ will become impractical since it will lead to a side stiffener almost as big as a regular column.

4.3.5.2 Implication for Infill Wall Design

Figure 4.29 shows the variation of the normalized infill plate shear capacity versus the infill plate thickness for different aspect ratios under the assumption that the side stiffeners satisfy Eqn. (4.26b). It was found that the variation among various aspect ratios was very small. The slope of each line in Figure 4.29(a) is plotted in Figure 4.29(b) as a shear coefficient. It can be seen that this shear coefficient has a relatively small variation over the range of commonly used aspect ratios. It reaches a minimum value of 0.863 and increases with both smaller and larger aspect ratios. For extremely small aspect ratios, this coefficient becomes greater than one, which is outside the range of calibrated angle of inclination equation and not realistic.

Taking a conservative estimate from Figure 4.29(b); the following simplified equation can be used for design

$$V_{sp} = \eta \cdot \frac{1}{2} f_{yp} L_p t_p \tag{4.27}$$

where η can be obtained from Figure 4.29(b), or be taken conservatively as 0.86, which results in the expression

$$V_{sp} = 0.43 f_{yp} L_p t_p \tag{4.28}$$

Instead of the complicated expression in Eqn. (4.23a) that requires iterations, this simplified expression is much more straight-forward and is in a similar format with the theoretical shear capacity of the fully connected SPSW reproduced below,

$$V_{sp} = 0.5 f_{yp} t_p L_{cf} \sin(2\alpha) \tag{4.11b}$$

Note that the design equation of the fully connected SPSW provided in the AISC Seismic Provision (AISC 2010c) has a smaller coefficient due to consideration of the over-strength factor. The 0.42 factor in Eqn. (4.29) is simply the theoretical 0.5 in Eqn. (4.11b) divided by an over-strength factor of 1.2 (Berman and Bruneau 2003),

$$V_{sp} = 0.42 f_{yp} t_p L_{cf} \sin(2\alpha) \tag{4.29}$$

A similar over-strength factor can be applied to Eqn. (4.28), leading to the following design equation for the proposed new HPSPSW,

$$V_{sp} = 0.36 f_{yp} L_p t_p \tag{4.30}$$

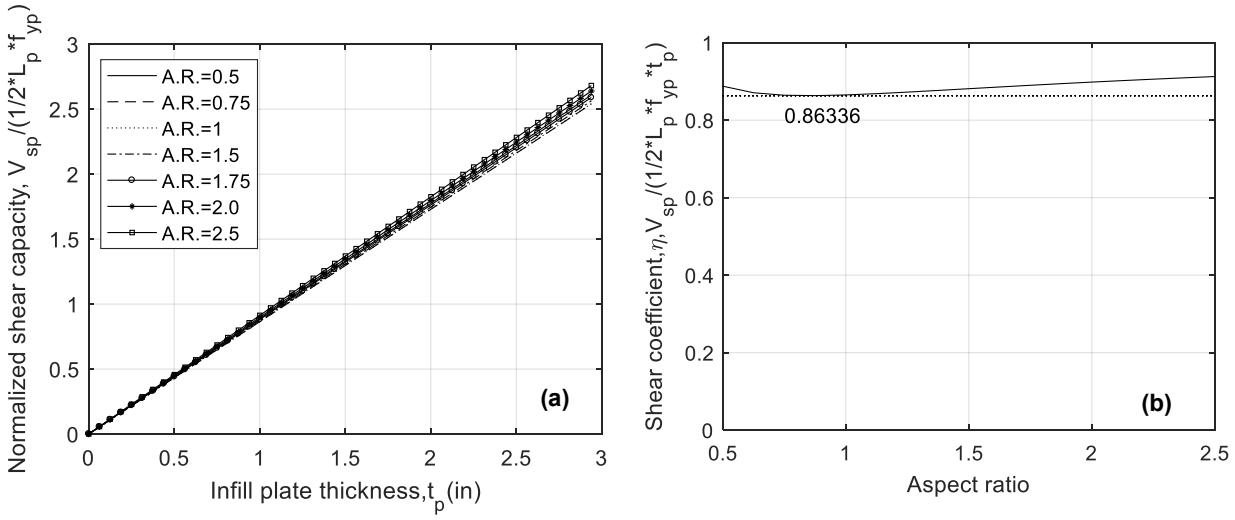

Figure 4.29 (a) Normalized shear capacity vs infill plate thickness (b) Shear coefficient, η, vs. aspect ratio

Another observation is that when the M_{pf} is fixed, the initial stiffness of the infill panel has a fixed ratio relative to $Et_p/4$ for different aspect ratios; see Figure 4.30(a). This property can be used when a certain stiffness ratio between the infill panel and the surrounding moment frame is desired. Accordingly, the theoretical yielding drift ratio, defined as $(V_{sp}/K_{sp})/h$, becomes a variable depending only on the aspect ratio and infill panel material; see Figure 4.30(b). This property can be used when a certain target ductility objective needs to be fulfilled. This property is also useful for designing for the boundary moment frame to control the yielding sequence of various components of the system.

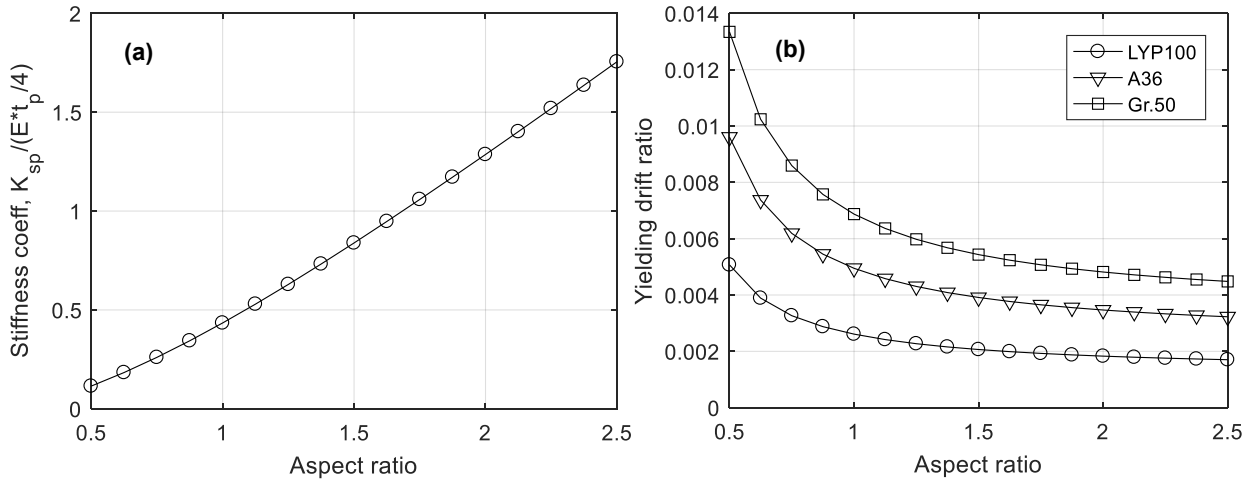

Figure 4.30 (a) Stiffness coefficient vs. aspect ratio and (b) yielding drift ratio vs. aspect ratio

4.3.6 Equivalent Brace Model for the New HPSPSW

4.3.6.1 Backbone Relationship

Equivalent brace (EB) model is a convenient tool that converts the complex 2D plate elements into the 1D beam or truss elements as long as the area and yield strength of the equivalent truss model can represent the overall force-displacement relationship of the system. As described in Thorburn et al. (1983), the steel shear walls in the Nippon Steel Building (completed in 1970), were replaced by a set of diagonal braces resistant to simultaneous tension and compression. The area of these braces was computed in a way that they provided the same stiffness as the steel shear wall by relating the shear deformation of the steel shear wall to the elongation of the equivalent brace. The analysis of the 53-story Shinjuku Nomura Tower also employed the same equivalent braces to model steel shear walls. These examples can be regarded as the early implementation of the EB model to represent steel shear walls in the analysis.

Although being capable of providing a satisfactory global force-displacement relationship, the EB model cannot capture the realistic anchor force demands imposed by the infill steel plate on the boundary columns. As a result, the actual force demands in the columns can be largely underestimated. In this sense, while still applicable as a preliminary design tool as suggested in the Canadian seismic code (CSA 2011), the EB model is less accurate if used as an analytical tool compared to the strip model proposed later for the fully connected steel plate shear wall system.

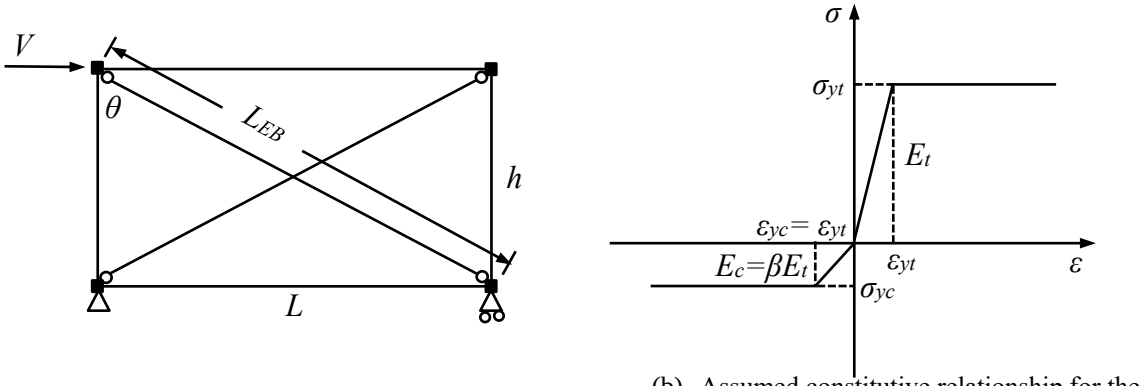

(a) Simplified equivalent brace (EB) model

(b) Assumed constitutive relationship for the Simplified equivalent brace (EB) model

Figure 4.31 Equivalent brace (EB) model

In contrast, if the infill plate is detached from the column, as is the case for the proposed HPSPSW system, it is believed that the simple EB model can be used as an analysis model for the new HPSPSW without substantial inaccuracies in predicting the component demands. It is worth noting that when replacing the continuous steel plate by equivalent braces, the beam is also subjected to unrealistic boundary conditions. This is considered acceptable due to the cancellation effect of

anchoring forces acting above and below the beams; the additional distributed force acting on the beam is relatively small and will not have a significant effect on system behavior. Even with the formation of in-span hinge in the beam, the effect will be relatively local. Special capacity design check of the roof beam and the base beam is, however, required to prevent under-design of these beams with anchor force acting on only one side of these beams.

To capture the system behavior in both directions under cyclic loads, equivalent braces in both diagonals are needed. Assume the tension and compression capacity ratio, γ, is approximately equal to the ratio of the critical shear buckling capacity and the tensile yielding capacity of the infill panel material,

$$\gamma = \frac{\sigma_{yc}}{\sigma_{yt}} \sim \frac{\tau_{cr}}{f_{yp}} \tag{4.31}$$

Assuming the yielding strain of the infill panel material in tension and compression are the same, then the equivalent brace area can be determined as follows,

$$A_{EB} = \frac{K_{spsw} L}{(1+\gamma) E \cdot \sin^3 \theta} \tag{4.32a}$$

If the shear buckling component of the infill panel can be neglected, the equivalent brace area can be simplified to:

$$A_{EB} = \frac{K_{spsw} L}{E \cdot \sin^3 \theta} \tag{4.32b}$$

The equivalent yielding strength of the equivalent brace, f_{yEB}, can be derived using the relation between yield strain, ε_y, and the yield displacement of the shear wall system, V_{u_spsw}/K_{spsw}, assuming an elastic perfectly plastic load-displacement relationship,

$$f_{yEB} = E\varepsilon_y = \frac{E V_{u\_spsw} \sin^2 \theta}{K_{spsw} L} \tag{4.33}$$

Derivations of Eqns. (4.32b) and (4.33) can be found in Appendix D2. Equations (4.32b) and (4.33) are the general expressions for the bilinear EB model for any assumed mechanism for the steel shear wall system. The area, A_{EB}, of the equivalent brace mainly controls the stiffness of the system, while the yield stress, f_{yEB}, controls the strength of the equivalent system. One only needs to plug

in the corresponding expressions of the shear strength, V_{u_spsw} and elastic stiffness, K_{spsw} of the original steel shear wall system to derive the properties of the equivalent brace.

If we plug the expression for the fully connected steel shear wall strength, Eqn. (4.11b), and stiffness, Eqn. (4.19a), expressions, into Eqns. (4.32b) and Eqn. (4.33), and approximate $L_{cf}/h_{bf} \sim L/h$, the corresponding area and yield stress become:

$$A_{EB} = \frac{t_p L}{2} \frac{\sin^2(2\alpha)}{\sin\theta \sin(2\theta)} \tag{4.34}$$

$$f_{yEB} = \frac{\sin(2\theta)}{\sin(2\alpha)} \frac{L_{cf}}{L} f_{yp} \tag{4.35}$$

In the above EB model, the L_{cf}/L ratio that represents 100% rigid-end zone offsets were adopted to represent the beam-to-column joints. Equations (4.34) and (4.35) are essentially the same as those derived in Thorburn et al. (1983).

Similarly, for the infill wall configuration in the proposed HPSPSW, if we plug in the expression of strength and stiffness in Eqns. (4.15b) and (4.23a) into Eqns. (4.32b) and (4.33), we obtain

$$A^*_{EB} = \frac{L t_p}{\sin^3\theta} \frac{\left[L_p - (h_p - c)\tan\alpha\right]^2 \sin^2\alpha \cos^2\alpha}{[L_p h_p - (h_p - c)^2 \tan\alpha]} \tag{4.36a}$$

If we re-arrange and simplify the above equation, we obtain,

$$A^*_{EB} = \frac{L t_p}{4} \frac{L}{h} \frac{\sin^2(2\alpha)}{\sin^3\theta} \frac{\left[L_p - (h_p - c)\tan\alpha\right]^2 / L}{[L_p h_p - (h_p - c)^2 \tan\alpha]/h} \tag{4.36b}$$

Notice that Eqn. (4.36b) can be decomposed into two parts,

$$A^*_{EB} = A_{EB} \cdot \underbrace{\frac{\left[L_p - (h_p - c)\tan\alpha\right]^2 / L}{[L_p h_p - (h_p - c)^2 \tan\alpha]/h}}_{\eta_{EB}} \tag{4.36c}$$

where A_{EB} is defined by Eqn. (4.34), and the second term η_{EB} is defined to be the area reduction factor.

The corresponding yield strength of the equivalent brace can be calculated as

$$f_{yEB}^{*} = \frac{1}{\eta}\frac{\sin(2\theta)}{\sin(2\alpha)}\frac{L_p - (h_p - 2c)\tan\alpha}{L} f_{yp} \tag{4.37}$$

Equation (4.37) can also be obtained by the following if not using Eqn. (4.33),

$$f_{yEB}^{*} = \frac{V_u / \sin\theta}{A_{EB}^{*}} = \frac{V_u / \sin\theta}{A_{EB}}\frac{1}{\eta_{EB}} \tag{4.37*}$$

Note that in the above equations, the minimum specified yield strength of the infill panel f_{yp} can be replaced by $C_{pr}R_y f_{yp}$ to account for the expected actual yield stress factor, R_y, and strain-hardening effect, C_{pr}, in the analysis models.

4.3.6.2 Review of Existing Hysteretic Models for SPSWs

To apply the EB model in nonlinear response history analysis, defining the elastic stiffness and ultimate strength is not sufficient. Hysteresis characteristics also need to be specified to capture the pinching and possible strength and stiffness degradations. In this section, several existing hysteretic models developed for the strip model for traditional SPSWs, where the infill panels are attached to both beams and columns, are reviewed first; then a model that can match the limited test results and the FE results of the proposed new HPSPSW system in Section 4.2.2.4 is developed.

The early versions of strip models involved equally spaced tension-only truss elements, normally with bilinear material properties. Later, several modified strip models were proposed, including the use of supplemental degradation elements (Driver et al. 1998), multi-directional strip model (Rezai et al. 2000), compression strut and deterioration strip (Shishkin et al. 2009) or semi-empirical material and hysteretic models to better match with the available test data. Several hysteretic material models were proposed in the literature, including the work by Roberts and Sabouri-Ghomi (1992), Driver et al. (1998), Elgaaly et al. (1993); Elgaaly and Liu (1997), Choi and Park (2010) and Webster (2013). Most of the above mentioned hysteretic models were developed for the entire web panel, with the exception of Choi and Park's and Webster's work, which were based on the responses of individual elements in the panel.

Choi and Park's proposed material model (Choi and Park 2010) was essentially based on the empirical relationship of the web-plate elements observed from FE analysis (Figure 4.32). They have made several simplifications of the key points of the hysteretic model: they assumed the tensile reloading stiffness to be 0.2Es, and the two pivot points to be $0.2f_{ts}$ and $0.5f_{cs}$. These simplifications seemed to be empirical without theoretical justification (Webster 2013). The

system model utilizing this material model for the strips appears to perform very well in matching several test results. Recognizing that the total capacities of many of the test specimens modeled in this work had relatively large contributions from the boundary elements, the assumptions and simplifications in the hysteretic model proposed by Choi and Park (2010) seemed to work well and had minimal influence on predicting the global response.

Due to the significantly increased number of time step and interactions in a nonlinear time history analysis, complex material models do not always work well because of the required large computational effort and likely convergence issues. Based on the limited dynamic testing of the steel plate shear wall systems and the effort to capture the dynamic responses, the tension-only material model provides a reasonable prediction of dynamic responses.

Lin et al. (2010) conducted a pseudo-dynamic test of a full-scale two-story steel plate shear wall using the hybrid simulation technique. Although the tension-only material developed and implemented in PISA3D showed a reasonable match to the test results(Lin et al. 2010), the model tended to underpredict the residual displacement and base shear (Figure 4.33). Note that in this model, the overall cyclic responses matched the test results even when the buckling capacities of the strips were ignored. This is likely to be due to the fact that the boundary frames were relatively heavy sections and contributed significantly to the system capacity. This can also be seen from the shape of the hysteresis curves, which is closer to that of a moment frame with only slight pinched component due to the buckling of infill panel. In this case, the buckling capacity of infill plates can be neglected for better computational efficiency.

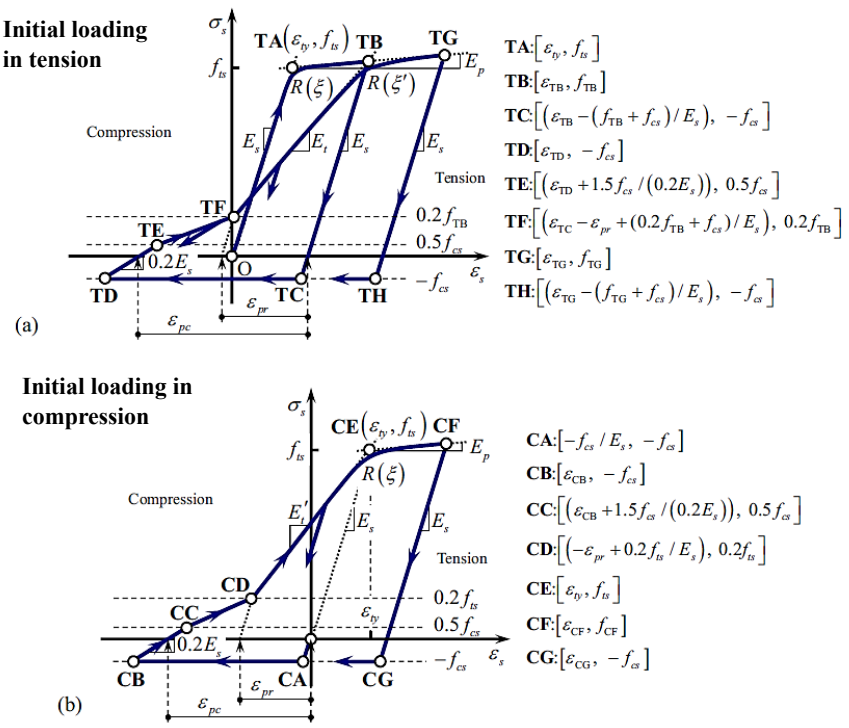

Figure 4.32 Hysteretic stress–strain relationship for strip elements proposed by Choi and Park (2010)

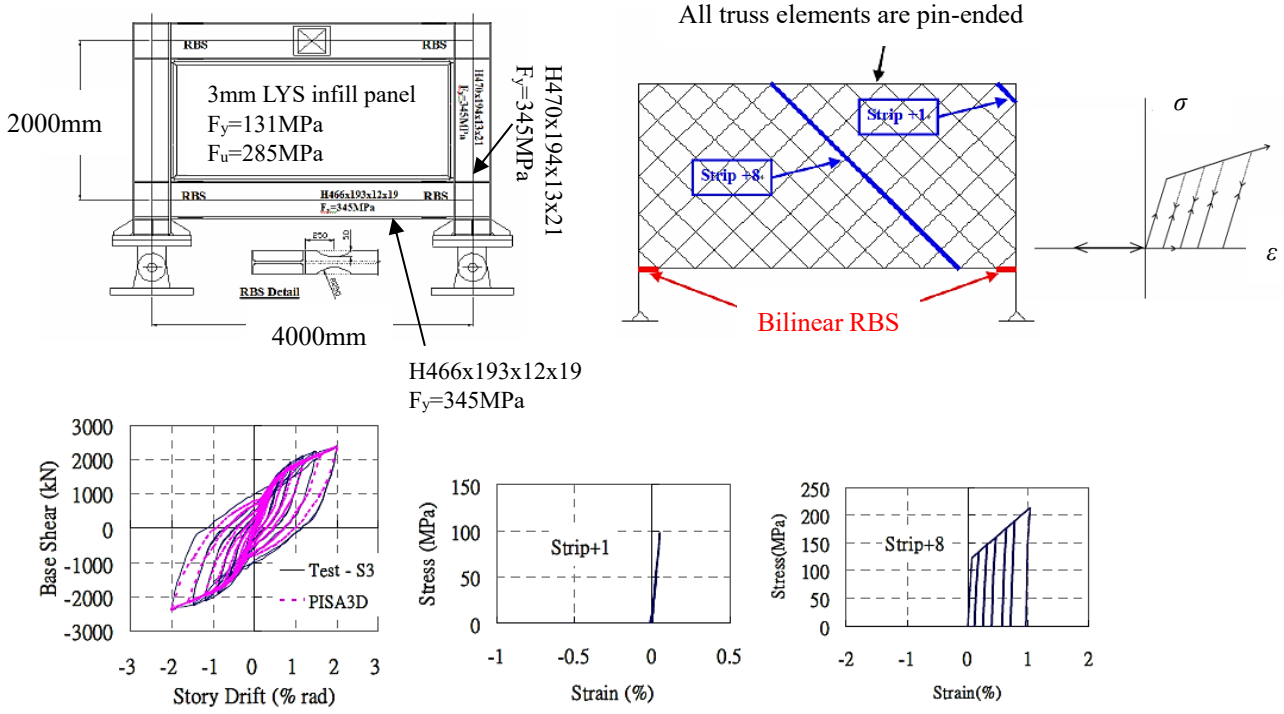

Figure 4.33 Hysteretic stress–strain relationship for strip elements used by Lin et al. (2010)

Webster (2013) noted that regardless of the size and geometry of the boundary elements, the inclination angle of the web plate tension field will ultimately migrate towards 45°. The difference in predicted demands on the columns using 45° and the angle determined from Eqn. F5-2 of the 2010 AISC Seismic Provisions (AISC 2010c) was shown to be negligible compared to the difference due to pushover and time history analyses. The effect of infill plate hardening was shown to have moderate effects on the vertical boundary element (VBE) demands. Webster also developed a new hysteresis model for the steel shear wall (Figure 4.34), which had some improvements in predicting the VBE demand and story drifts compared with the existing *Hysteretic* material model in OpenSees using a pinching factor for strain, PinchX, of 0.8, and a pinching factor for stress, PinchY, equal to 0.2.

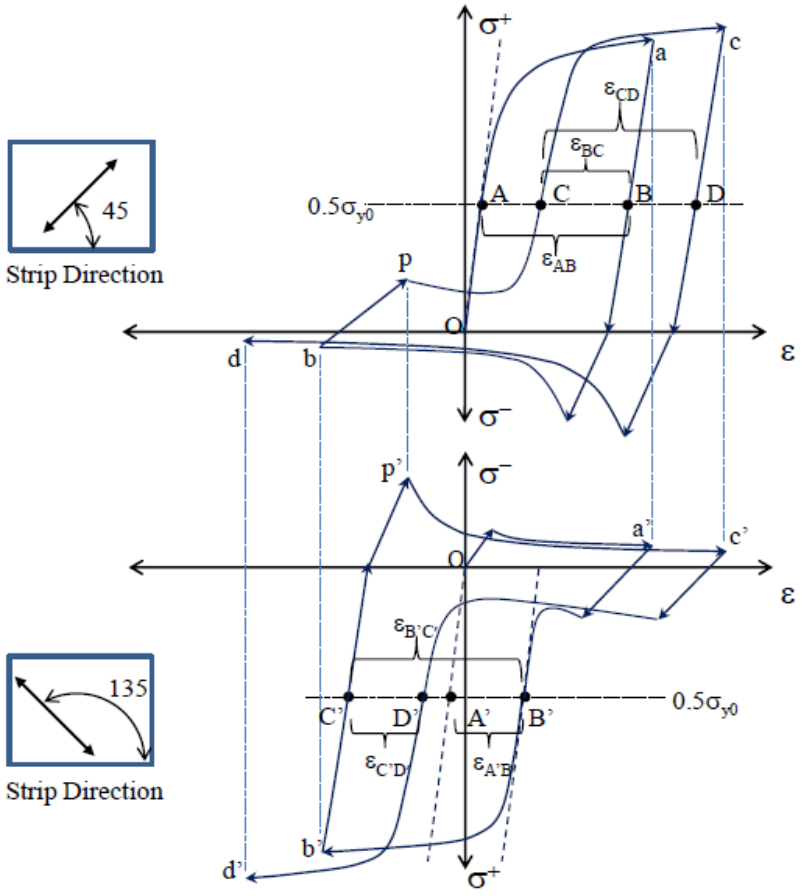

Figure 4.34 Hysteretic stress–strain relationship for strip elements proposed by Webster (2013)

A recent deterioration model for steel plate shear wall (SPSW) was developed by Purba and Bruneau for evaluating the collapse performance of the SPSW system following the FEMA P965 methodology (Purba and Bruneau 2015a; Purba and Bruneau 2015b). Their model was statistically quantified and calibrated based on a review of 36 SPSW specimens. The model was based on two

major deterioration sources: web plate tearing and flexural failure of boundary elements (Purba and Bruneau 2015a). They stated that other degradation sources such as shear failure or buckling of boundary elements could be avoided by using capacity design and compact sections, and therefore were not considered. The final proposed deterioration model is graphically shown in Figure 4.35. The parameters leading to the most conservative degradation behavior from all the calibration tests were adopted due to an insufficient number of specimens available for calibration. The compressive strength of the strip was excluded because the effect of the compressive strength was found to be insignificant in shake table tests as opposed to cyclic tests (Dowden and Bruneau 2014). Neglecting compression capacity was shown to impose insignificant effect on the dynamic responses as discussed in Lin et al. (Lin et al. 2010).

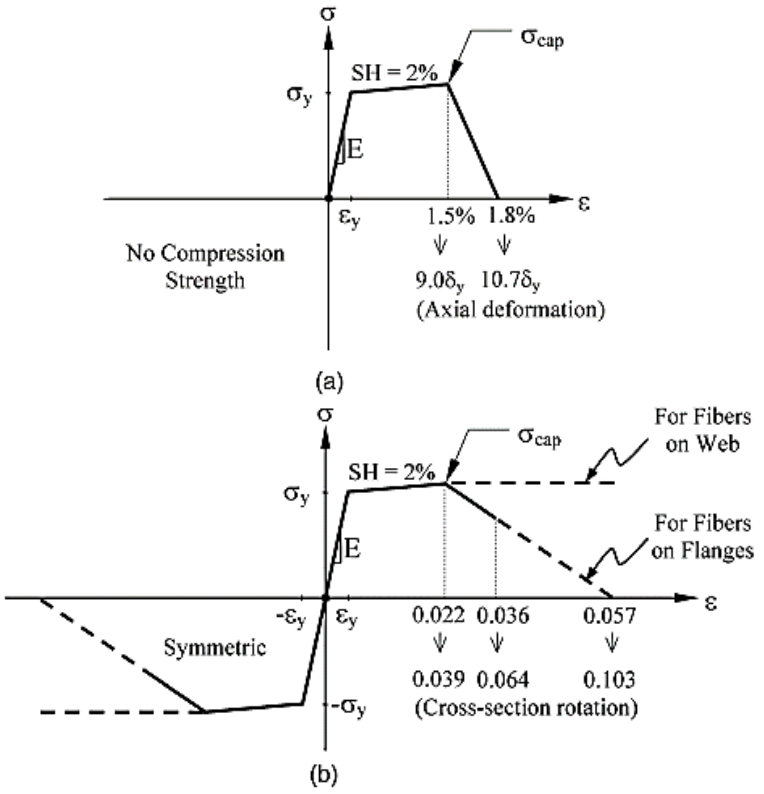

Figure 4.35 Deterioration model for steel plate shear wall strip model proposed by Purba and Bruneau (2015a)

According to their comparison results between the final proposed conservative model (worst case scenario) and the matching cases, the conservative model predicted rather significant deterioration and early degradation drift for some of the selected tests.

4.3.6.4 Define Equivalent Brace Model for the New HPSPSW

An extensive review of different hysteretic models and their effects on cyclic responses can be found in FEMA P440A (FEMA-P440A 2009). Complicated hysteretic models are not always necessary as they impose greater computational demands, and some features of the complex

hysteretic models only have minor effects on the dynamic response. Several important observations on the hysteretic behavior of an SPSW system have been pointed out in Purba and Bruneau (2015a):

(1) Up to the capping point (i.e., max strength point), shear stiffness during loading and unloading are similar between different cyclic loops. Moderate changes in stiffness are only observed after strength degradation occurs. They concluded that incorporating stiffness degradation is not critical;
(2) Strength degradation due to repeated cycles at the same displacement is relatively small;
(3) Strength degradation primarily occurs when increasing inelastic displacement passes the capping point. They concluded that cyclic envelope can be designated similar to the force-displacement backbone boundary; and
(4) They noted that the significant pinching behavior analogous to tension-only braces can be captured directly by modeling the wall using tension-only nonlinear strips.

Therefore, simple force-displacement backbone curve without cyclic degradation is sufficient to represent degradation models for the boundary element and infill plates.

Based on the theoretical derivations of elastic stiffness and shear strength, observations from the parametric cyclic simulations and above review of the models proposed for the current code-specified fully connected SPSWs, this section provides a summary of the definition of the equivalent brace (EB) model for the proposed HPSPSWs. A typical hysteresis model for the EB model is shown in Figure 4.36.

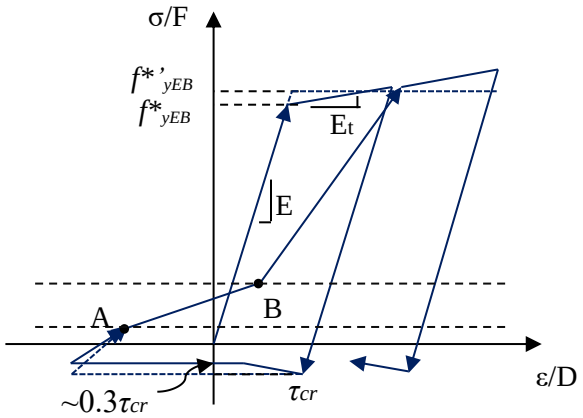

Figure 4.36 Typical hysteretic behaviour of an equivalent brace or strip

In Figure 4.36, f^*_{yEB} is the yield strength of the equivalent brace assuming bilinear behavior with hardening, and $f^{*\prime}_{yEB}$ is the modified yieldstrength of the brace assuming elastic-perfectly plastic behavior. To completely define the EB model, the following parameters need to be specified:

(1) **Area of the brace**: Eqn. (4.36c) can be used to establish the area of the equivalent brace, which mainly controls the stiffness of the system. Since normally the global models use line elements aligned along frame centerlines, it becomes crucial to differentiate the clear span length and centerline distance between columns and beams to correctly represent the actual shear wall stiffness and strength using the effective area and strength of the equivalent braces, i.e., L_p and L, h_p and h should be clearly distinguished when used in Eqns. (4.36c) and (4.37). This is not necessary if rigid offsets are modeled directly;

(2) **Material of the brace**: both the tension and compression capacities need to be specified plus the loading-reloading behavior or "pinch" factors:

a. **Yield stress**: If the software is capable of defining strain-hardening material with buckling, then f^*_{yEB} can be calculated according to Eqn. (4.37), and appropriate hardening ratio can be defined. In Eqn. (4.37), f_{yp} can be modified to $R_y f_{yp}$ if actual yield strength is needed. If a hardening model is not possible or a simple elastic-perfectly plastic model is desired, then a modified yield strength $f^{*\prime}_{yEB}$ can be defined by replacing f_{yp} in Eqn. (4.37) to $C_{pr} f_{yp}$ or $C_{pr} R_y f_{yp}$ to include the strain-hardening effect;

b. **Hardening ratio**: if hardening is desired in the model for a more graduate yielding of the system, then f^*_{yEB} that uses either f_{yp} or $R_y f_{yp}$ should be used as the yield stress with an appropriate hardening ratio, such as 2%, which is commonly used for structural steel;

c. **Buckling stress**: On the compression side, one reasonable simplification is to define the compression strength to be equal to the critical shear buckling capacity, τ_{cr}, of the infill panel with simply supported boundary conditions on all four sides [Eqn. (4.1) and (4.2)]. The actual compression strength would drop after the initial buckling, but since the compression capacity is much smaller than the tensile strengths, such a drop of the compression strength can be ignored in actual modeling. As mentioned in Lin et al. (2010), Dowden and Bruneau (2014), and Purba and Bruneau (2015a), the compression capacity does not affect the dynamic behavior noticeably and can be ignored. It is included here in case a better match to the quasi-static cyclic analysis results is desired;

d. **Residual stress after buckling**: this is assumed to be 0.3 of τ_{cr} if relatively thick plates are used, but this value may not be necessary for most cases. The buckling strength is suggested to be included if one needs to match the quasi-static cyclic test results;

e. **Loading – Reloading Point**: this parameter characterizes the shape of the hysteresis loop and the level of pinching. The definitions are slightly different in the two commonly used structural analysis software: Perform 3D (Perform-3D 2011) and OpenSees (McKenna et al. 2010):

In Perform 3D:

By examining the loading/reloading points for all the inelastic cycles for the four analyzed FE cases in Section 4.2.2.4, average values for the two pivot points A, B defined in in Figure 4.36 can be obtained empirically. Stress levels of Point A and Point B are

defined as the proportion of the tensile strength of the specific cycle, and their strain levels are defined as the percentage of the strain range of the specific cycle. Note that the for thinner infill panel, the hysteresis loops are slightly more pinched; this corresponds to smaller stress and strain factors for Point A, and a smaller stress factor and a larger strain factor for Point B. Note that the factors shown in Table 4.4 are obtained from the force-displacement relationship of the infill panel only. The responses of the entire system, i.e., infill + boundary frame, would not be very sensitive to the choice of the parameters within the given range. This is particularly true for the case when the boundary frame has a relatively large contribution to the lateral force resistance.

Table 4.4 Range of the stress and strain for the two critical points to define the reloading characteristic in Perform-3D

	Point A	Point B
Stress/tension strength	0.15 – 0.25	0.4 – 0.5
Strain/strain range	0.20 – 0.35	0.65 – 0.8

In OpenSees:
The *Hysteretic* material model developed by Fillipou et al. (1983) in OpenSees (Filippou et al. 1983) is chosen due to its robustness and flexibility to match a broad range of hysteresis shapes. The pinching parameters for the *Hysteretic* material model were calibrated from the limited tests and FE analysis results. It was found that the following parameters generally work well for the selected calibration specimens:

[1] Pinching factor for strain (deformation) during reloading PinchX to be 0.85
[2] Pinching factor for stress (force) during reloading PinchY to be 0.5
[3] Power used to determine the degraded unloading stiffness in $\mu^{-\beta}$, β to be 0.02
[4] Damage factor due to ductility to be 0.0
[5] Damage factor due to energy to be 0.0

Note that here the PinchY factor chosen is 0.5, which is larger compared to commonly used 0.2 value for the AISC SPSW configurations. This is because in the new HPSPSW, the side stiffeners also contribute to the infill panel capacities, leading to less pinched hysteresis loops.

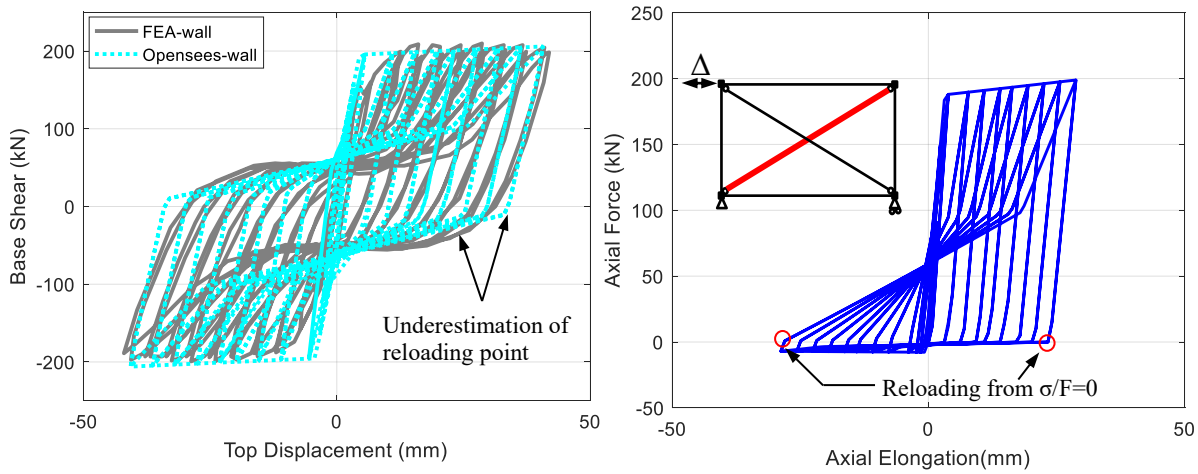

(a) Under-estimation of the reloading compression capacity

(b) Typical axial force – axial displacement relationship of the equivalent brace using *Hysteretic* material

Figure 4.37 Force-displacement relationship of the equivalent brace using *Hysteretic* material in OpenSees

Due to the definition of the *Hysteretic* material model in OpenSees, the infill panel capacity immediately after reloading of the system will be slightly underestimated even when the compression capacity is assigned to the equivalent brace; see Figure 4.37. Using a slightly larger PinchY factor could help to compensate for the energy loss due to this underestimation of the reloading compression capacity. This is not a problem in Perform 3D where the loading reloading points are explicitly specified.

The stiffness degradation factor, β, can be included to improve the matching with the quasi-static cyclic test results, but it is not essential for response history analysis since its effects on the dynamic responses for moderate and long-period systems are small, as mentioned in FEMA P440A, and the "differences in peak displacements between stiffness-degrading systems increase as the period of vibration decreases as the lateral strength decreases [(FEMA-P440A 2009), pg. 2-5].

f. **Degradation parameters**: degrading parameters are only needed when fairly large drift is expected, such as in an incremental dynamic analysis, and when significant strength degradation is expected after the capping point (point of maximum strength). For most of the cases, using the non-degrading parameters above will suffice. Since there is currently little experimental data on the proposed HPSPSW system, it is assumed here the EB model has similar degradation characteristics as calibrated by Purba and Bruneau (2015a) for the strip model for the current SPSW. It is worth noting that relatively large uncertainties exist for the capping and residual points among different specimens. Their

final proposed degradation material model is somewhat conservative and tends to predict earlier and faster deterioration.

i. **Capping point**: the capping point strain can vary from 0.015 to about 0.045 according to the different calibrated values given in Purba and Bruneau (2015a) for different specimens;
ii. **Residual point**: the ultimate strain can vary from 0.018 to about 0.05 according to the different calibrated values given in Purba and Bruneau (2015a) for different specimens, and no residual capacity is assigned. Relatively close capping strain and residual strain were used in their work, which seems appropriate for the strip model, where the strips can degrade one after another while the entire system degrades gradually. However, the inherent assumption for EB model is that the entire panel develops uniform strain. Using very close residual point to capping point would make the system degradation unrealistically fast and may cause convergence issues. Therefore, it is recommended to define a slightly larger residual strain than the values suggested for the strip model in Purba and Bruneau (2015a).

(3) Definition of the boundary frame:

There are many options available to model the boundary frame. The most commonly adopted methods include (1) model both the beam and column by a force-based *beamcolumn* element with a fiber section using the appropriate material model, or (2) model the column by force-based *beamcolumn* element while modeling the beam by elastic beam plus either two fiber hinges or two concentrated hinges on the two ends. For this dissertation, the second approach will be employed in the global structure model in the response history analysis. The inclusion of the GPMC by using concentrated hinges was discussed in Chapter III. Many models exist in the literature that aims to capture appropriately the moment connection behavior.(Ibarra et al. 2005; Lignos and Krawinkler 2007; Lignos and Krawinkler 2010; Purba and Bruneau 2015a). In cases where there is a lack of test results or simulation information available, the modeling parameters suggested in a number of guidelines and specifications such as FEMA (FEMA-356 2000), ASCE 41-13(ASCE 2013) as well as the on-going ATC-114 project (Hamburger et al. 2016) can be adopted. The ATC-114 document contains hysteretic relationships for use in performance-based analysis and modeling, and aims to support the development of updated building code criteria such as ASCE 7 and ASCE 41.

4.3.7 Validation of the Equivalent Brace Model

Due to the limited number of tests available for steel shear walls with an infill wall connected to the beam only, the calibration and validation of the proposed EB model were conducted based on the FE model described in Section 4.2.2.4, as well as three actual tests (Choi and Park 2009; Guo

et al. 2011) on a steel shear wall system with the infill wall connected to the boundary beam only. The Guo-S1 specimen and the Park FSPW4 specimen used a pure infill plate without any side stiffeners. They can be regarded as a special case of having a side stiffener that has negligible stiffness I_s and strength M_{pf}. The Guo-S2 specimen represents the case with relatively small rectangular side stiffeners. The basic dimensions of the specimens are shown in Figure 4.38. Both Perform3D and OpenSees, two of the most commonly used nonlinear structural analysis software, were used to test the performance of the proposed EB model.

4.3.7.1 Perform3D Model

Perform3D is a widely used nonlinear structural analysis software for nonlinear analysis of 3D structures (CSI 2011). It is used here as an additional test for the proposed EB model and to provide some references for structural engineers. The main response history analyses in Chapter V will be conducted using OpenSees.

To define the EB model that represents the infill panel, the *inelastic steel bar/tie/strut* element was used with the *buckling inelastic material* model in Perform3D. Table 4.5 summarizes the key parameters used to define the EB model, and the key parameters are defined in Figure 4.39. Note: Perform3D does not support trilinear relationships for buckling type materials. Therefore, the modified yield strength, $f^{*\prime}_{yEB}$ shown in Figure 4.36 was used to define the value of FU in this case. FA, FB, UA, and UB are the critical reloading points that define the pinching shape in Perform 3D [Figure 4.39(c)]. To define the backbone curve for the material for the equivalent brace material for non-degrading specimens (FE analysis cases and Guo-S1, S2), only FU and DX were specified, and a relatively large value of 0.5 was chosen for DX to avoid un-necessary convergence problems. For the degrading wall case (Park FSPW4), the degrading part parameters used were DL equal to 0.025, DR equal to 0.05, and FR/FU equal to 0.1. Slightly different values are considered acceptable since these values do not affect the global response significantly; the maximum axial strain for the equivalent brace is expected to be smaller than 0.02 for a story drift of 0.03 considering the relationship between the brace elongation and story drift.

The beam and columns were modeled by *frame member compound component*, consisting of an elastic end zone to represent the panel zone, inelastic fiber section with a length equal to 10% of the member length on each end, and an elastic section in the middle. A simple *non-buckling inelastic trilinear* material model was used to define the frame fiber section material. The yield strength and hardening ratio utilized for the frames were consistent with the specimen material properties. For the frame fiber hinges, the strength limits were calculated based expected yielding and plastic moment capacities of the corresponding frame section, and the strain limits were initially chosen based on the recommendation of Purba and Bruneau (2015a) and modified by trial and error to match the test results. For non-degrading case, only DU is needed and was set to equal to 0.025; for degrading cases (i.e., Park FSPW4), the strain limits used for the beams were 0.03

and 0.045 for DL and DX, respectively. The residual strength, FR/FU, was set to be 0.6. More studies are desired to establish generally applicable parameters for other HPSPSW specimens.

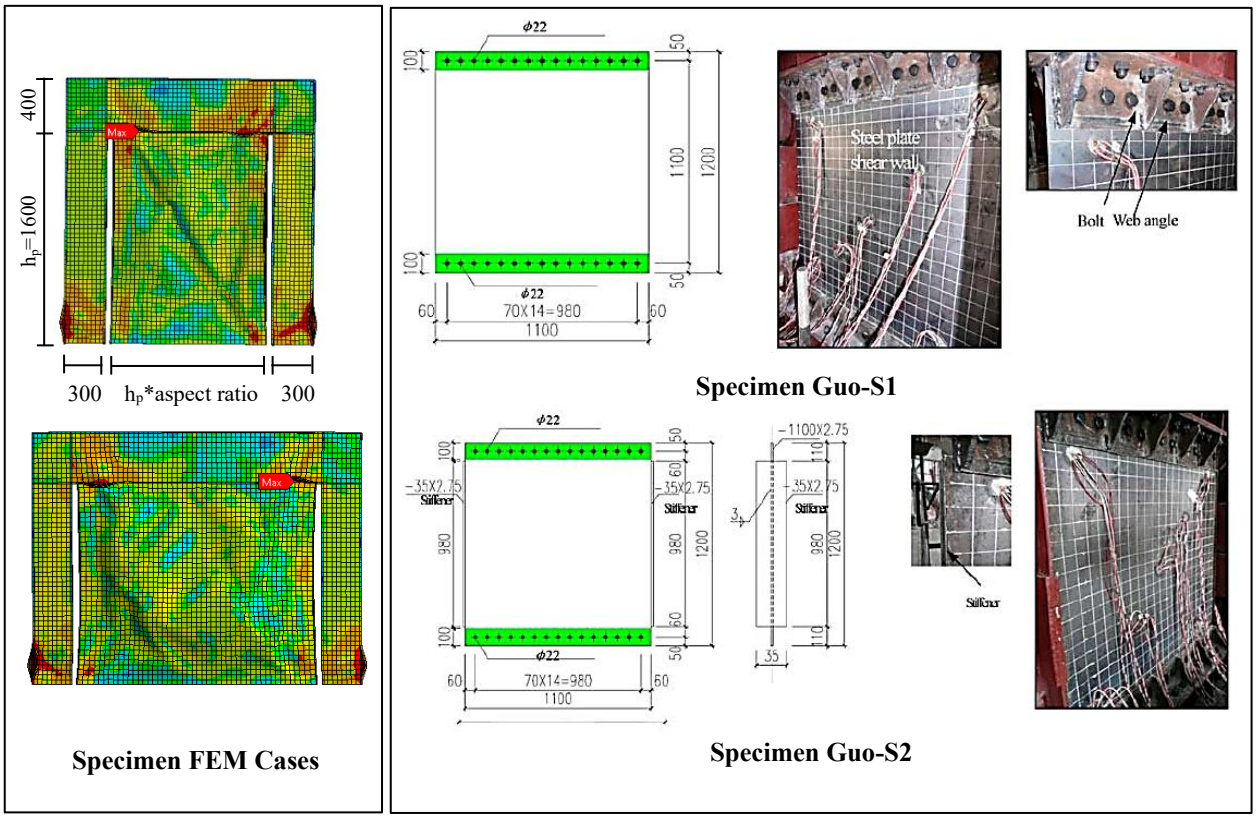

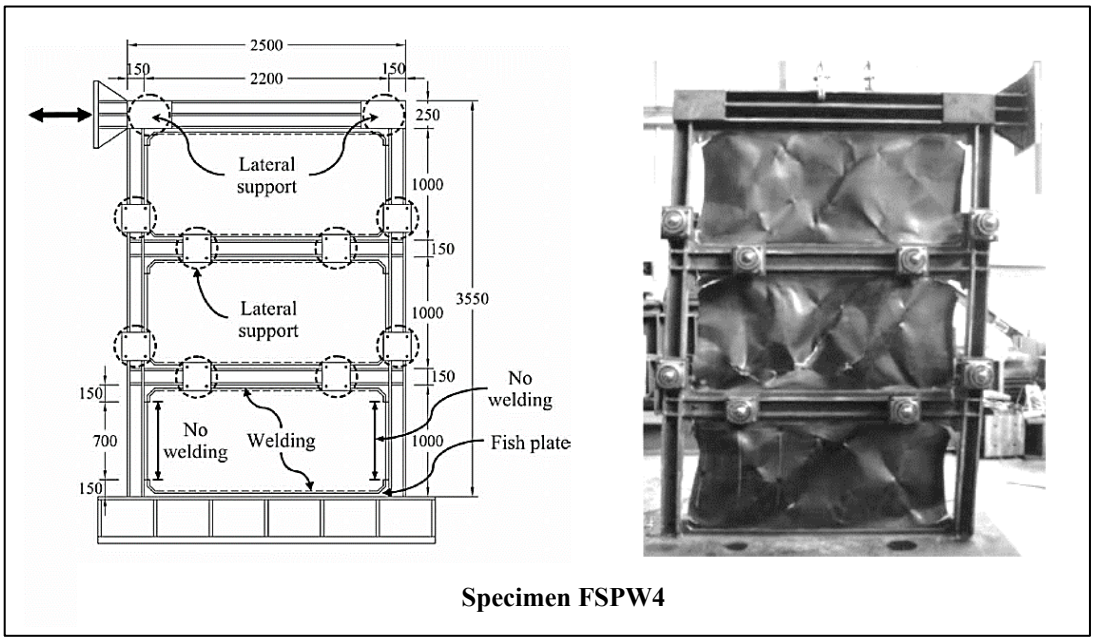

Figure 4.38 Specimens chosen to validate the proposed equivalent brace model

Table 4.5 Definition of the equivalent brace model in Perform 3D

Specimen		L_p/h_p	h_p/t_p	$f^*{}'_{yEB}$[a], FU (MPa)	A^*_{EB}[b] (mm^2)	τ_{cr}[c] (MPa)	FA	FB	UA	UB
FEA cases	3	1.25	356	470	3625	17	0.18	0.5	0.25	0.77
	4	1.25	640	390	2046	4	0.18	0.4	0.25	0.8
	5	0.8	356	519	2048	19	0.18	0.4	0.35	0.75
	6	0.8	640	524	1167	6	0.2	0.4	0.3	0.8
Park FSPW4	FL1	2.2	250	210	4071	18	0.2	0.4	0.2	0.8
	FL2	2.2	250	214	4225	19	0.2	0.4	0.2	0.8
	FL3	2.2	250	219	4334	22	0.2	0.4	0.2	0.8
Guo	S1	1.0	400	390	688	16	0.2	0.4	0.2	0.8
	S2	1.0	400	410	688	16	0.2	0.4	0.2	0.8

a. calculated by Eqn.(4.37) using $C_{pr}R_{yp}f_{yp}$

b. calculated by Eqn.(4.36c)

c. calculated by Eqn.(4.1) and (4.2)

Figures 4.41, 4.42, and 4.45 compare the performance among the chosen specimens and the EB models built in Perform 3D. Both the total cyclic response and the portion of load resisted by the infill panel are plotted whenever possible. It can be seen that the proposed EB model generally matches the FE simulation results well, especially the part resisted by the infill panel. Although the EB curves could not completely capture the smooth turns and gradual yielding of the FE analysis or test results, which is the nature of the simple bilinear material model adopted, it generally captured the ultimate strength, stiffness, and the overall pinched shape of the infill panel very well. Since stiffness degradation was not included in the EB material model, the unloading stiffness at later cycles for Guo-S1 and Guo-S2 was slightly overestimated.

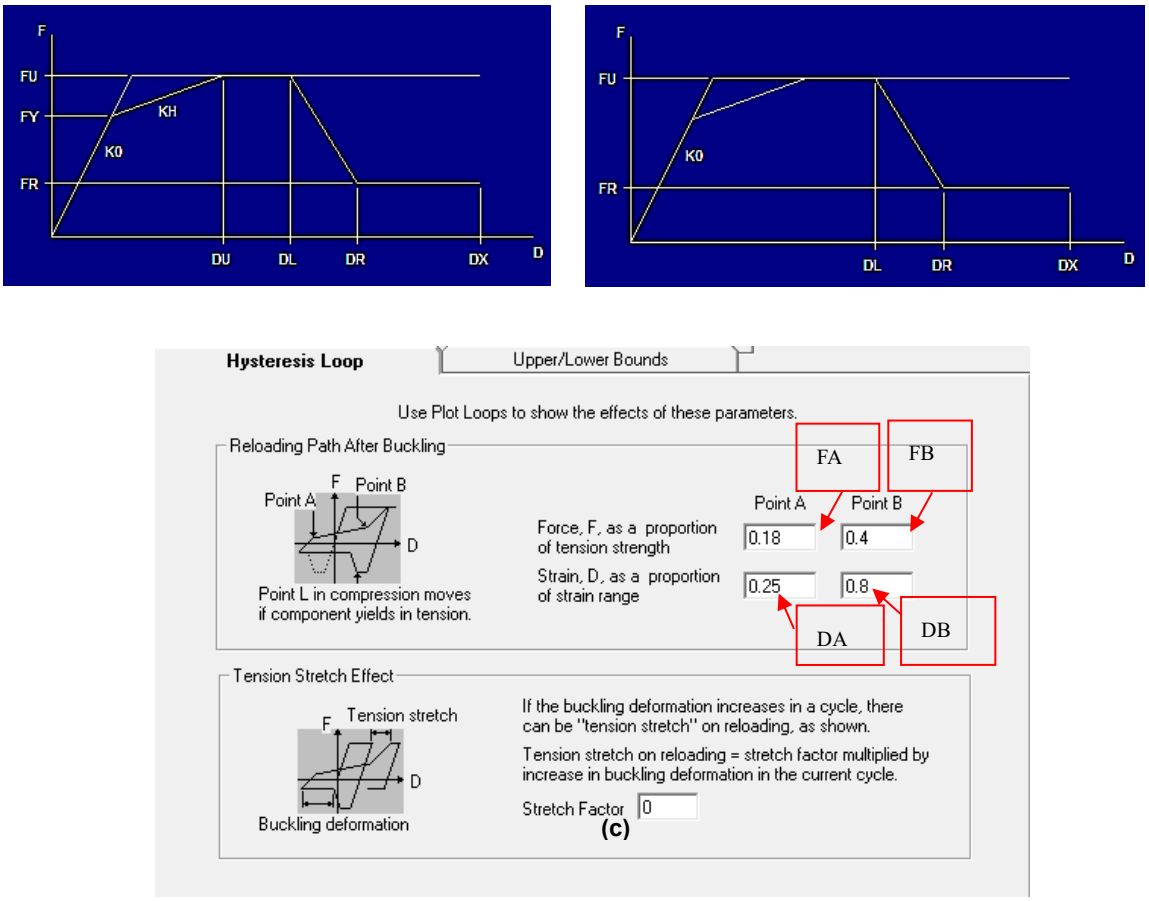

Figure 4.39 (a) simple *non-buckling inelastic trilinear* material for frame element (b) *buckling inelastic* material for equivalent brace (c) definition of hysteresis characteristics for equivalent brace (CSI, 2011)

4.3.7.2 OpenSees Model

In the OpenSees model, *corotational truss* element with *Hysteretic* material were selected to model the equivalent brace. $f^{*\prime}_{EB}$ and A^{*}_{EB} used were the same as used in the Perform 3D models. Negligible strain hardening was assigned from point 1 to point 2 in Figure 4.40 since $f^{*\prime}_{EB}$ already includes the strain-hardening effect. The strain limits used to define the material backbone curve in Figure 4.40 were 0.025, 0.05, -0.15 and -0.2 for $e2p, $e3p, $e2n and $e3n respectively. The residual strengths were set to be 0.6 in tension ($s3p/$s2p) and 0.3 in compression ($s3n/$s2n). Relatively large strain limit values were selected (the same as those used in the Perform3D model) because the final recommended values by (Purba and Bruneau 2015a) were found to be too conservative for the Park FPSW4 specimen considered here.

Since all the chosen specimens do not have a well-defined plastic hinge location like that in a RBS or a GPMC, *nonlinear/force-based beam-column* element with fiber section along the entire member length was adopted. As recommended in Kostic and Filippou (2012), the mid-point integration rule with four fibers in each flange and four fibers in the web shows excellent accuracy

and is computationally efficient (Kostic and Filippou 2012). In this study, five and ten fibers along the wide flange web direction were used in the flange and in the web, respectively. *Steel02* material (Giuffré-Menegotto-Pinto Model with isotropic strain hardening) available in OpenSees was used for modeling the frame fibers. For the case of Park FSPW4, material degradation was defined for the beams by using the *Hysteretic* material, with 0.035 capping strain and 0.065 ultimate strain established by trial and error. These values were slightly different from the values used in Perform3D, which may be probably caused by the different boundary frame modeling methods used in the two analysis software. Residual strength was set to be 0.6 of the capping capacity. Stiffness degradation factor of 0.2 was also included.

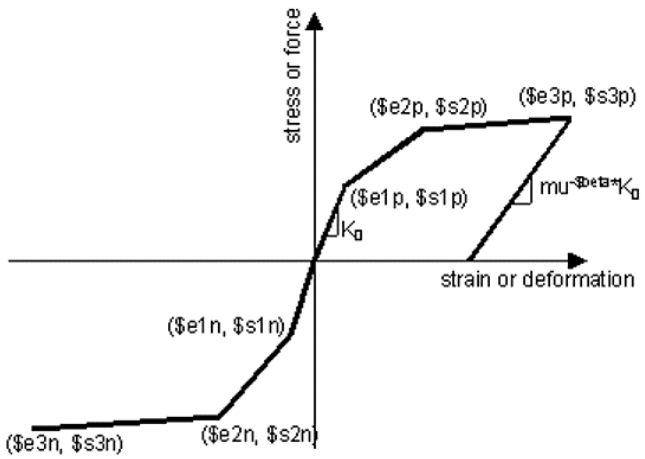

Figure 4.40 Definition of *Hysteretic* material in OpenSees

Designed according to the aforementioned material properties, the Equivalent Brace (EB) did not degrade at all, and the cyclic deterioration in the analysis results was mainly due to failure of the beam. This is consistent with test results where the main degradation was caused by the fracture of the second-story beam. The deterioration of hysteresis curve had a better match with the test results compared to the Perform 3D results.

Figures 4.43, 4.44, and 4.46 compare the performance among the chosen specimens and the EB model using OpenSees. Both the total cyclic response and the portion of load resisted by the infill panel were plotted. Again, the proposed EB model generally matched the FE analysis simulation and test results well, especially the part resisted by the infill panel. By changing the material model for the frame members from the trilinear model and concentrated fiber hinge in Perform3D to the *Steel02* material and fiber sections for the entire frame members in OpenSees, the overall match of the hysteresis curves improved significantly due to the inclusion gradual yielding and distributed plasticity. In addition, by adding the stiffness degradation factor in the EB material model, the unloading stiffness at later cycles for Guo-S1 and Guo-S2 were better matched.

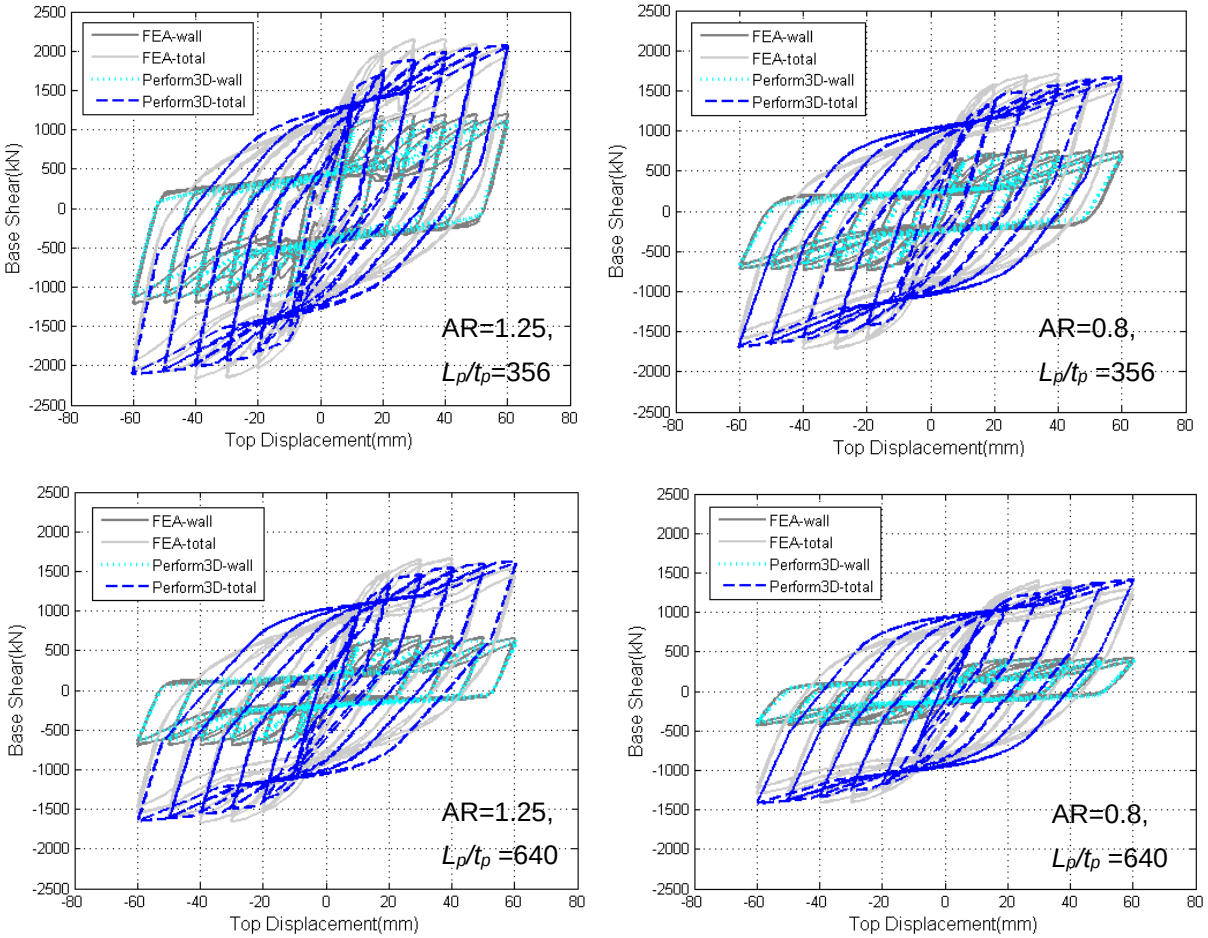

Figure 4.41 Equivalent brace model validation for specimen FE analysis cases using Perform-3D

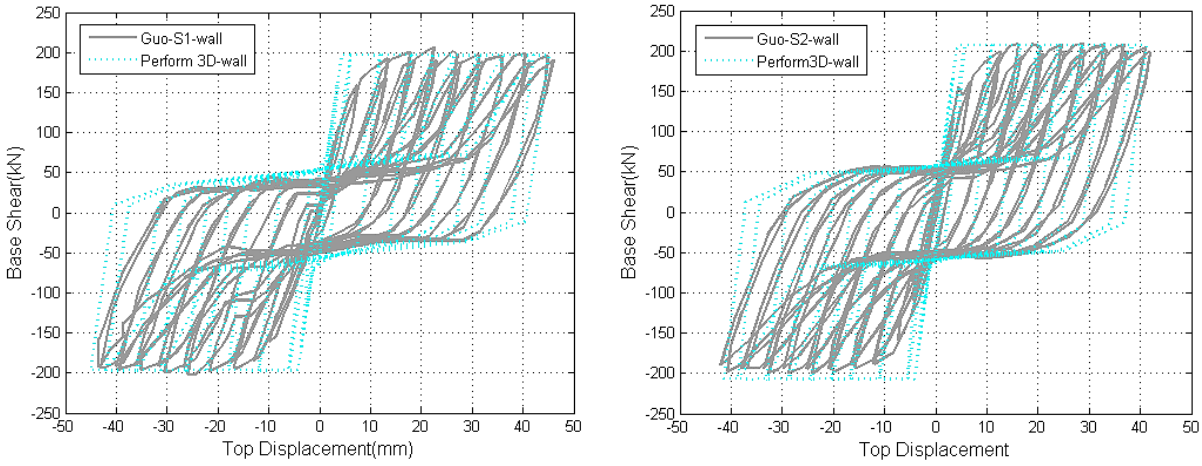

Figure 4.42 Equivalent brace model validation for specimen Guo-S1 and Guo-S2 using Perform-3D

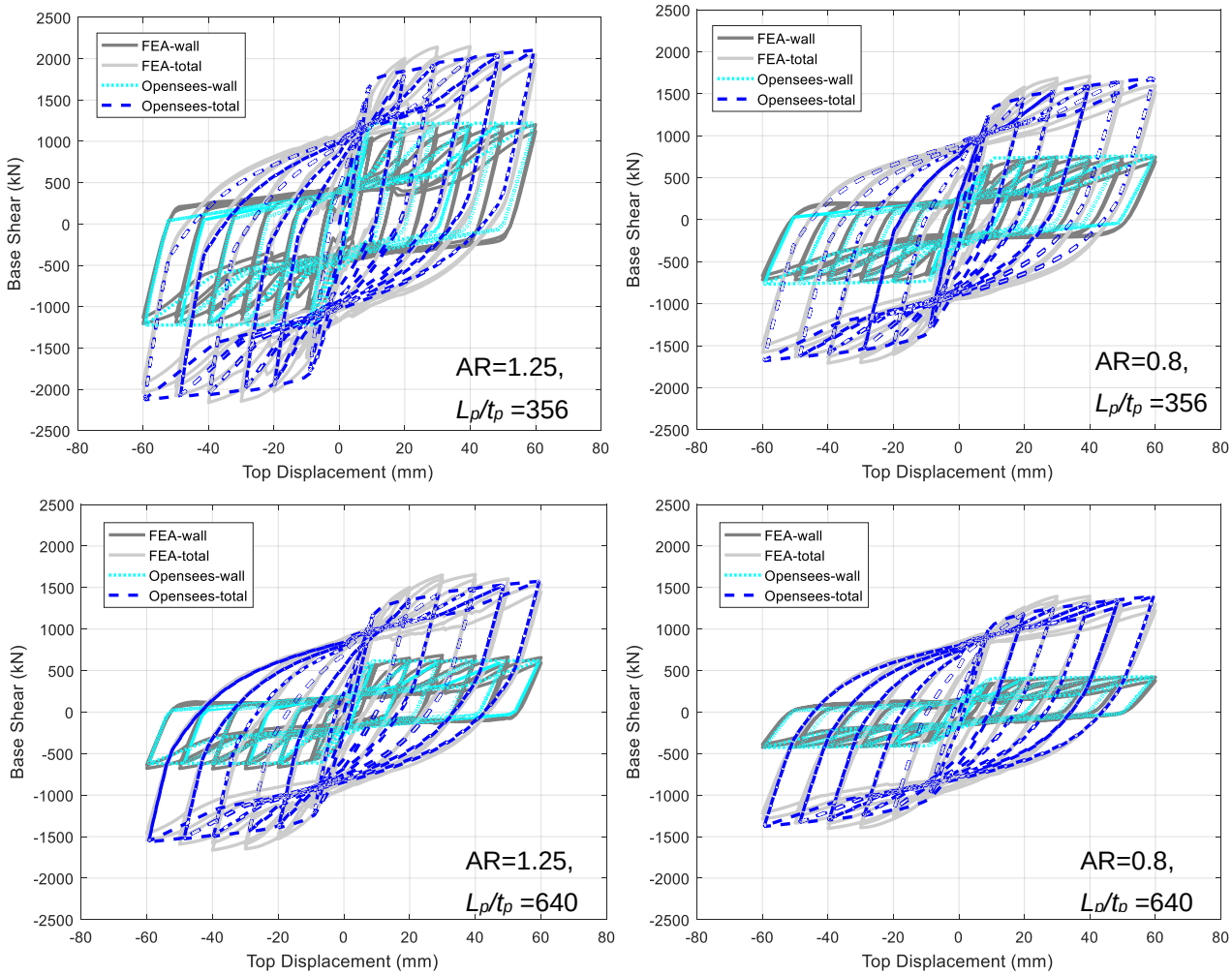

Figure 4.43 Equivalent brace model validation for FE analysis cases using OpenSees

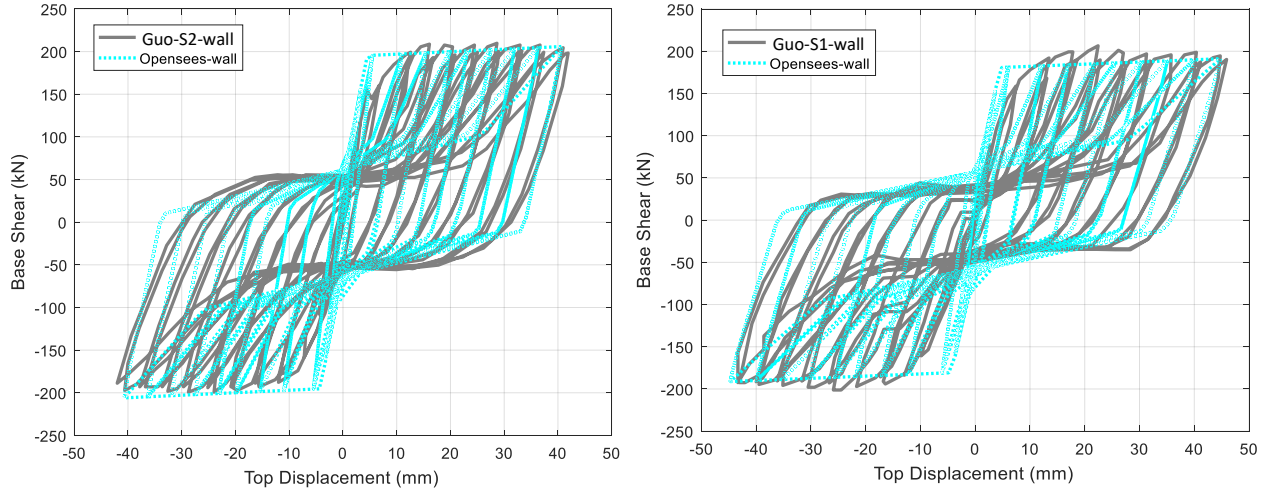

Figure 4.44 Equivalent brace model validation for specimen Guo-S1 and Guo-S2 using OpenSees

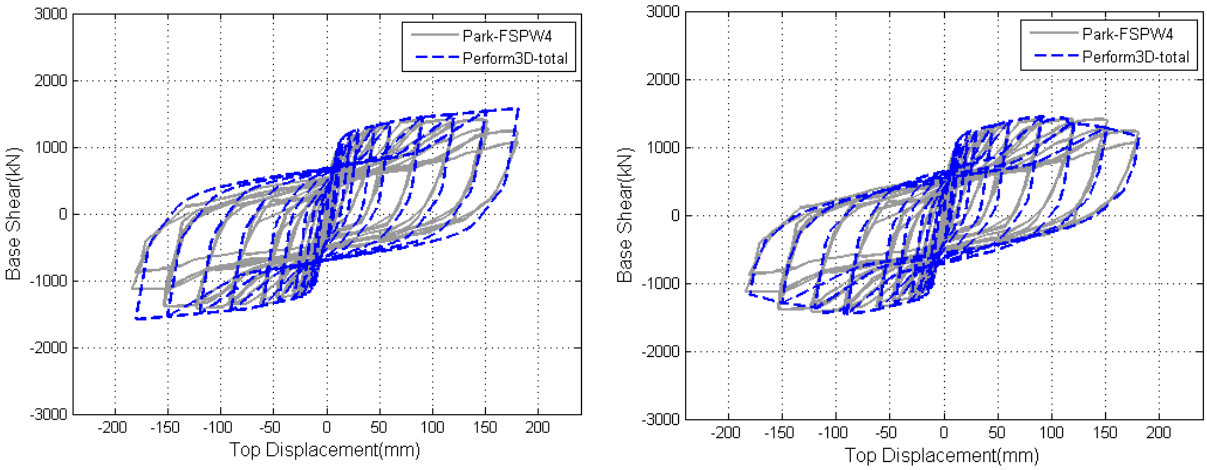

(a) Non-degrading material **(b) Degrading material**

Figure 4.45 Equivalent brace model validation for specimen Park-FSPW4 using Perform3D

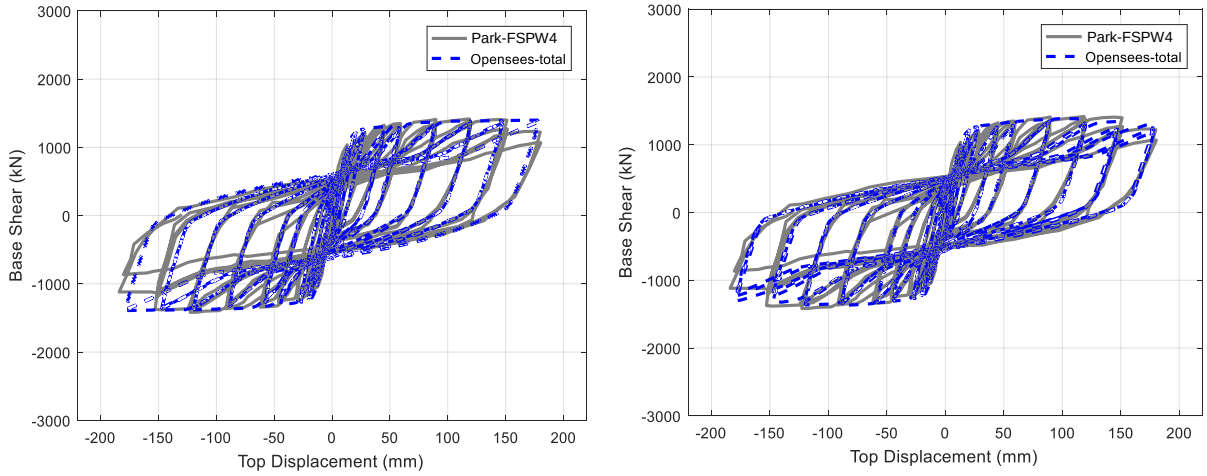

(a) Non-degrading material **(b) Degrading material**

Figure 4.46 Equivalent brace model validation for specimen Park-FSPW4 using OpenSees

4.4 Concluding Remarks and Recommendations for Future Works

A new steel shear wall system – the High-Performance Steel Plate Shear Wall (HPSPSW) – is proposed in this chapter. The infill wall in the new HPSPSW is attached to the beams only and installed with properly designed side stiffeners on the two vertical free edges of the infill wall. The innovative GPMC introduced in Chapter III is used in the HPSPSW system, replacing the expensive traditional welded flange moment connection. By introducing these two main features, this chapter demonstrated through nonlinear FE analyses how the new system can solve the ten design issues of the current code-designed SPSW identified in Chapter I as well as how an increase in economy, flexibility, and versatility of the system can be achieved. Additional advantages related to the repairability, retrofit applications and flexibility in modular constructions, as well as simplification in the design process, can also be achieved.

Theoretically derived equations are proposed for estimating the ultimate strength and stiffness of the infill panel, including the contribution from the side stiffener. This chapter also proposed a set of design recommendations for side stiffeners, as well as simplified design equations for the infill panel based on the study of the overall trend for panels with commonly used thicknesses and aspect ratios. Key design considerations for the infill panels are summarized, and important equations are reproduced on the next page.

A simple equivalent brace (EB) model with definitions of nonlinear hysteretic characteristics was also developed for use in the nonlinear response history analysis. The comparison of some test results and FE analyses results validated the effectiveness of the EB model in both Perform 3D and OpenSees.

This chapter focused on the design of an infill panel and its side stiffener only. The design of the entire system will be discussed in more detail in the next chapter.

Suggestions for future research include:

1. Although the currently adopted hysteretic properties for the EB model result in a reasonable match with the FE and test results, it is essentially empirical and is based on the model of the strip model for the current SPSW. More studies are desired to establish a hysteretic model that is more generally applicable based on more test results of the HPSPSW system; and
2. Axial force demand in the side stiffeners was not considered in the current study, but the side stiffeners are expected to take a certain amount of over-turning moment and may further reduce the column demand. This aspect is worth further investigation, and it may lead to some changes to the currently proposed EB model.

Design of Side Stiffener

In order to minimize the reduction in shear capacity due to partial tension field action, the plastic moment capacity of the side stiffener is recommended to be

$$M_{pf,\lim} = \frac{h_p^2}{64} f_{yp} t_p \tag{4.26b}$$

A less critical but important criterion is that the out-of-plane stiffness of the side stiffener should be sufficient such that the relative rigidity factor is

$$\beta_{cr} = 30 \tag{4.8}$$

In addition, it is also recommended that if single rectangular plate stiffener is used, the thickness of the stiffener be larger than that of the infill plate, i.e.,

$$t_s \geq t_p \tag{4.9}$$

Design of Infill Plate

The ultimate shear strength of the infill wall (including the capacity of the side stiffener) is

$$V_{sp} = \frac{1}{2} f_{yp} t_p [L_p - (h_p - 2c)\tan\alpha]\sin 2\alpha \tag{4.15b}$$

where

$$c = \frac{2}{\sin\alpha}\sqrt{\frac{M_{pf}}{f_{yp} t_p}} \tag{4.16}$$

M_{pf} is the plastic moment capacity of the effective side stiffener.

For aspect ratio = 1 to 2

$$\begin{aligned} \alpha &= \alpha_0 + (45° - \alpha_0)\sqrt{(c/h_p)^3} \\ \alpha_0 &= [0.65 - 0.04(L_p/h_p)]\tan^{-1}(L_p/h_p) \end{aligned} \tag{4.14a}$$

For aspect ratio = 2.5,

$$\begin{aligned} \alpha &= \alpha_0 + (45° - \alpha_0)(c/h_p)^{1.95} \\ \alpha_0 &= [0.65 - 0.04(L_p/h_p)]\tan^{-1}(L_p/h_p) \end{aligned} \tag{4.14b}$$

For aspect ratio = 0.5,

$$\begin{aligned} \alpha &= \alpha_0 + (45° - \alpha_0)(c/h_p)^{1.5} \\ \alpha_0 &= [0.66 - 0.04(L_p/h_p)]\tan^{-1}(L_p/h_p) \end{aligned} \tag{4.14c}$$

The stiffness contributed by the infill plate can be determined as

$$K_{sp} = \frac{Et_p\left[L_p - (h_p - c)\tan\alpha\right]^2 \sin^2\alpha\cos^2\alpha}{[L_p h_p - (h_p - c)^2 \tan\alpha]} \tag{4.23a}$$

Based on examination of typical infill panel strengths using side stiffeners that satisfy Eqn. (4.26b), the equation for shear strength in Eqn. (4.15b) can be simplified as,

$$V_{sp} = 0.43 f_{yp} L_p t_p \tag{4.28}$$

If an over-strength factor of 1.2 as used in AISC Seismic Provisions for the current SPSW system, the design equation becomes,

$$V_{sp} = 0.36 f_{yp} L_p t_p \tag{4.30}$$

Define Equivalent Brace

The equivalent area of the brace and equivalent yield stress are as follows,

$$A_{EB}^{*} = A_{EB} \cdot \underbrace{\frac{\left[L_p - (h_p - c)\tan\alpha\right]^2 / L}{[L_p h_p - (h_p - c)^2 \tan\alpha]/h}}_{\eta_{EB}} \tag{4.36c}$$

$$f_{yEB}^{*} = \frac{1}{\eta_{EB}} \frac{\sin(2\theta)}{\sin(2\alpha)} \frac{L_p - (h_p - 2c)\tan\alpha}{L} f_{yp} \tag{4.37}$$

where

$$A_{EB} = \frac{t_p L}{2} \frac{\sin^2(2\alpha)}{\sin\theta\sin(2\theta)} \tag{4.34}$$

Chapter V

Seismic Design of the High-Performance Steel Plate Shear Wall System

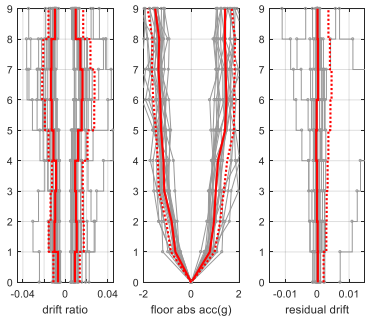

This chapter explores the system behavior utilizing the observations and the analytical models developed in the previous two chapters: the concentrated hinge model of the Gusset Plate Moment Connection and the equivalent brace model for the infill panel connected to the beam only with side stiffeners. Various system design considerations will be discussed, and two seismic design procedures will be proposed and evaluated based on response history analysis results. Lessons learned and suggestions for future work will also be discussed.

5.1 Modeling and Prototype Buildings

5.1.1 Prototype Buildings

Elevation and Plan Configurations: the SAC buildings described in the FEMA 355-C document (FEMA-355C 2000) were used as the basis of the prototype buildings studied in this chapter. The 3-, 9-, and 20-story SAC buildings were selected to represent the low-rise, mid-rise, and high-rise buildings that use steel shear wall as the primary lateral load-resisting system. The adopted elevation and plan configurations were similar to the SAC buildings. Because of the relatively large capacity of steel plate shear walls compared to moment frames, the floor plan was slightly modified to have a shorter width of 20 ft for the steel shear wall bays instead of the original uniform 30-ft bays for the SAC moment frame designs. For the 9- and 20-story buildings, typical floor height is 13 ft, except the first floor, which is 18 ft, and typical bay width is 20 ft, resulting in a typical floor aspect ratio of 1.54. For the 3-story building, the story height is 13 ft for all floors.

Based on the available literature, because of the cantilever action of tall steel plate shear wall systems and the capacity design requirements, the lower story columns can be relatively heavy. In one of the published work on evaluating the seismic behavior of AISC steel plate shear wall (SPSWs), the column sizes for the 20-story model were W36×800 or larger (Berman 2011). In

Purba and Bruneau's study on different design philosophies of SPSWs, even for a 10-story SPSW archetype, W36×798 first-story column would be required if the infill panel was designed to take 100% story shear (Purba and Bruneau 2014). Without utilizing composite columns or other supplemental structural elements (e.g., supplemental side moment frames, outriggers, coupled SPSWs connected by coupling beams, etc.), the shear wall design for taller buildings can be challenging. Therefore, to limit the discussion on more practical column sizes within the W14 sections of the wide flange rolled shapes, the 20-story prototype building was limited to the three-bay design option with one middle shear wall bay plus two side moment frames; the 3- and 9-story case study buildings were designed to have both the single bay and three bays options.

Building Functionality: the prototype buildings were assumed to be standard office buildings, which corresponds to a seismic importance category I defined in ASCE 7-10 (ASCE 2010).

Location: To be consistent with the Design Guide 20 high seismic design (AISC 2007), the prototype buildings were assumed to be located in downtown San Francisco on the corner of Montgomery and Market Streets (latitude: 37.789°, longitude: -122.402°). The soil category was assumed to be stiff soil (site class D with reference shear wave velocity = 180 to 360 m/sec). The spectral accelerations corresponding to short (0.2 sec), S_{DS} and long period (1 sec), S_{D1} are 1.13*g* and 0.853*g*, respectively.

Table 5.1 Summary of loading on the prototype building models

	Floor	Nodal seismic weight (kip)		SPSW nodal gravity force (kip)	Leaning column force (kip)
		1 bay	3 bay		
3-story	Roof	570.5	285.25	37.6	1235.6
	FL3 – FL2	527.5	263.75	43.2	1252.8
9-story	Roof	294.6	147.3	37.6	541
	FL9 – FL3	272.8	136.4	43.2	547.5
	FL2	277.8	138.9	43.2	551
20-story	Roof	-	53.6	37.6	182.3
	FL20 – FL3	-	51.0	43.2	186.7
	FL2	-	51.0	43.2	188.7

Loading: the seismic weight, dead and live loads are all consistent with the SAC buildings and slightly modified to fit the shorter (20 ft) steel shear wall bays. Since it was assumed that a beam in-span hinge would not form for properly capacity designed boundary beams, the distributed beam loads were simplified as nodal loads. The gravity loads were calculated for the load combination of (1.0DL + 1.0LL). The corresponding nodal seismic weight and nodal forces are summarized in Table 5.1. The loading was calculated based on the number of shear wall bays used:

for the 20- and 9-story building; a total number of six and four steel shear wall bays were employed in the north–south direction, respectively. For the 3-story building, only two steel shear wall bays were used to avoid unrealistically thin infill plate. A possible configuration of shear wall locations for the prototype building designs are illustrated in Figure 5.1.

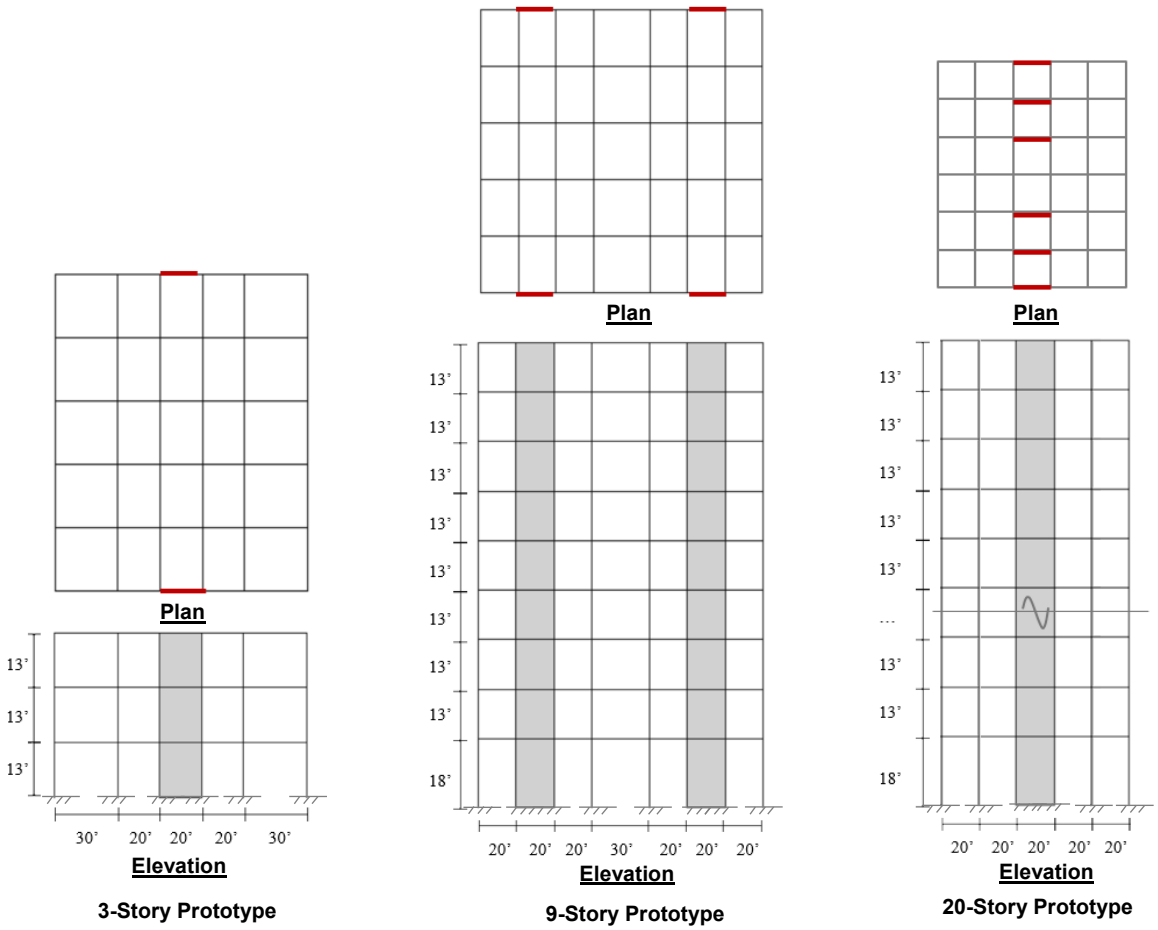

Figure 5.1 Plan and elevation view of the prototype buildings

5.1.2 Modeling and Specifications

5.1.2.1 Structural Model

This section includes modeling specifications that are applicable to both the current AISC Steel Plate Shear Wall (SPSW) and the proposed new High-Performance Steel Plate Shear Wall (HPSPSW) systems. More discussions on the SPSW is provided in Section 5.1.2.3. All analyses were performed in OpenSees (McKenna et al. 2010).

a. Infill wall

The steel plate for the code-designed AISC SPSW was modeled by a series of diagonally distributed strip elements, which is the common practice and code recommendation for SPSWs (AISC 2010; Driver et al. 1998; Thorburn et al. 1983; Timler and Kulak 1983). The steel plate plus side stiffeners in the proposed new HPSPSW were modeled with the equivalent brace (EB) model introduced in Chapter IV. Note that the EB model is also available for analyzing traditional SPSWs; however, as the anchor force of the infill plate on the boundary column is a crucial phenomenon that needs to be captured in this study, the strip model was adopted for the code-designed system.

b. Columns

Following the standard practice, a *force-based beam-column* element with fiber section was used to model the columns. This is because in columns, the axial force and bending moment interaction is critical and cannot be captured well by the concentrated hinge plus elastic element model. In addition, the distributed plasticity can also provide information on whether plastic hinge will form in places other than the two ends of the column, especially for the AISC code-designed SPSW system. On the element level, five Lobbato integration points along the length of the column were used, and on the cross-section level, five integration points in each flange and ten in the web long the web direction were used. Only one fiber was used along the beam flange and web thickness direction because more fibers in the out-of-plane direction are not needed for 2D models.

c. Beams

There are several methods available to model beams. Typically, the axial force level in the beams is not as high as that in the columns; therefore, the *elastic beam-column* element plus either concentrated hinge or fiber hinge at the two ends are common alternatives for using fiber section throughout the length of the beam. One advantage of using the rotation hinge model is that the moment-rotation behavior of the designated plastic hinge in the beam can be explicitly specified without the need to calibrate the material properties of the fibers. The properties of the rotational hinge for the proposed Gusset Plate Moment Connection (GPMC) were defined in Chapter III. All GPMCs were assumed to be made of low yield LYP100 steel (F_{yg} = 19ksi) with ductile behavior. According to the Design Procedure Commentary chart at the end of Chapter III, the expected moment capacities of the GPMCs for all designs were assumed to be 55% of the expected moment capacities of the beam.

d. Rigid Offset:

The rigid offset is often preferred for the centerline frame model to account for the additional stiffness and strength at the joint and to prevent unrealistic instability to happen during response history analysis. It has been demonstrated that depending on the inelastic modeling assumption, it is possible to reach contradictory conclusions about the seismic performance of the same moment frame design (Gupta and Krawinkler 1999; Krawinkler 2006): (1) Model M1, a basic centerline model, predicts collapse; (2) Model M2, which explicitly incorporates the strength and stiffness properties of panel zones, predicts story drifts approaching 15%; and (3) Model M2A which includes the effect of interior gravity columns, shear connections, and floor slabs, predicts a maximum story drift of 5% for all stories. These observations were based on assuming ductile

behavior of all components; these conclusions could be more dramatic if deterioration properties were included. In particular, the study shows that panel zones help to stabilize the responses for moment frames when they are included in the analytical model (FEMA-355C 2000).

In moment frames, because the main lateral force resistance is provided by the moment connections, it is expected that the panel zone or floor slab effect will affect significantly the beam rotation and nonlinear behavior. This effect, however, could be less critical in a braced frame or in a steel shear wall system since the beam-to-column connections are secondary load-resisting elements. Studies on SPSW systems (Lin et al. 2010; Purba and Bruneau 2015; Thorburn et al. 1983; Tsai et al. 2010) that used the strip model do not usually include this rigid offset explicitly.

The effect of various beam-to-column connection models is compared below to investigate whether the inclusion of rigid offset is necessary for the proposed HPSPSW models.

Different beam-to-column connection model

Four different models were considered: (1) simple centerline model with *forcebeamcolumn* element using fiber sections throughout the length of both beams and columns; (2) centerline model with *forcebeamcolumn* element using fiber sections for the columns, and elastic + zero length hinge (*Steel02*) for the beams; (3) centerline model with *forcebeamcolumn* element using fiber sections for the columns and elastic + zero length hinge (IMK hinge) for the beams; and (4) which is the same as (2) but with rigid offsets at the panel zone region. The rigid offsets were modeled as additional elements that extend from the centerline intersection to the edge of the panel zone and has ten times the area and moment of inertia of the connected members. All models used the same equivalent brace model for the infill wall and leaning columns to capture the P-Delta effect. Figure 5.2 illustrates the fiber model and the concentrated hinge model with and without rigid offsets.

The *Steel02* hinge model was supposed to represent the LYP100 GPMC, which on average has an expected moment capacity of 55% of the expected moment capacity of the beam. The IMK hinge is corresponding to the Reduced Beam Section (RBS) connection with an expected moment capacity of 80% of that of the beam. For cases without rigid-offsets, the difference between the clear span length and centerline distance between columns and beams become important when calculating the effective area and strength of the equivalent braces (i.e., L_p and L should be clearly distinguished when used in Eqns. 4.34, 4.36c, and 4.37).

Figure 5.3 shows that all three models had similar drift profile prediction in the elastic range. The *Steel02* hinge model had a lower connection moment capacity, and therefore yielded first and had the most uniform drift profile at a roof drift of 0.05. The fiber section model, which included the distributed plasticity and the highest strain-hardening ratio, predicted a slightly more concentrated drift at story six. The IMK hinge model that incorporated the strength and stiffness degradation predicted the largest drift concentration at the sixth story. However, as can be seen from the pushover analysis, the base shear capacity started to drop at a roof drift of 0.03, and the stiffness

deterioration was rather gradual compared to pure moment frames as demonstrated in Gupta and Krawinkler (1999). This slower global deterioration with degrading beam-to-column connections is likely due to the contribution by the infill wall. As far as the effect of the panel zone, since the main load carrying element in a steel shear wall system is the infill wall, compared to Model (2), the addition of rigid offsets in Model (4) made the structure slightly stiffer, with T_1 changing from 1.058 sec to 1.013 sec, and the drift profile at large roof drift level was also slightly more uniform. But this improvement is rather small. Considering the fact that panel zones are not actually rigid, Model (2) without rigid offset was adopted in the subsequent global system model for assumed ductile LYP100 GPMC behavior due to its simplicity and acceptable accuracy.

e. Leaning Column:

P-delta effects are widely known to affect the dynamic responses and can cause ratching behavior or dynamic instability (FEMA-P440A 2009). If the motion has a long strong-motion duration or if it can cause any story to enter negative tangent stiffness region, then the system becomes P-delta sensitive and the best possible analytical model should be employed. Leaning column, or a P-Delta column, is therefore necessary to account for the large deflection effects, especially when only the lateral resisting system is modeled. In the study herein, the mass of the gravity systems was converted to loads on leaning columns to capture P-delta effects. In a conservative manner, it was assumed that the interior gravity framing would not contribute to the lateral strength and stiffness of the steel shear wall system. The forces on leaning columns are summarized in Table 5.1.

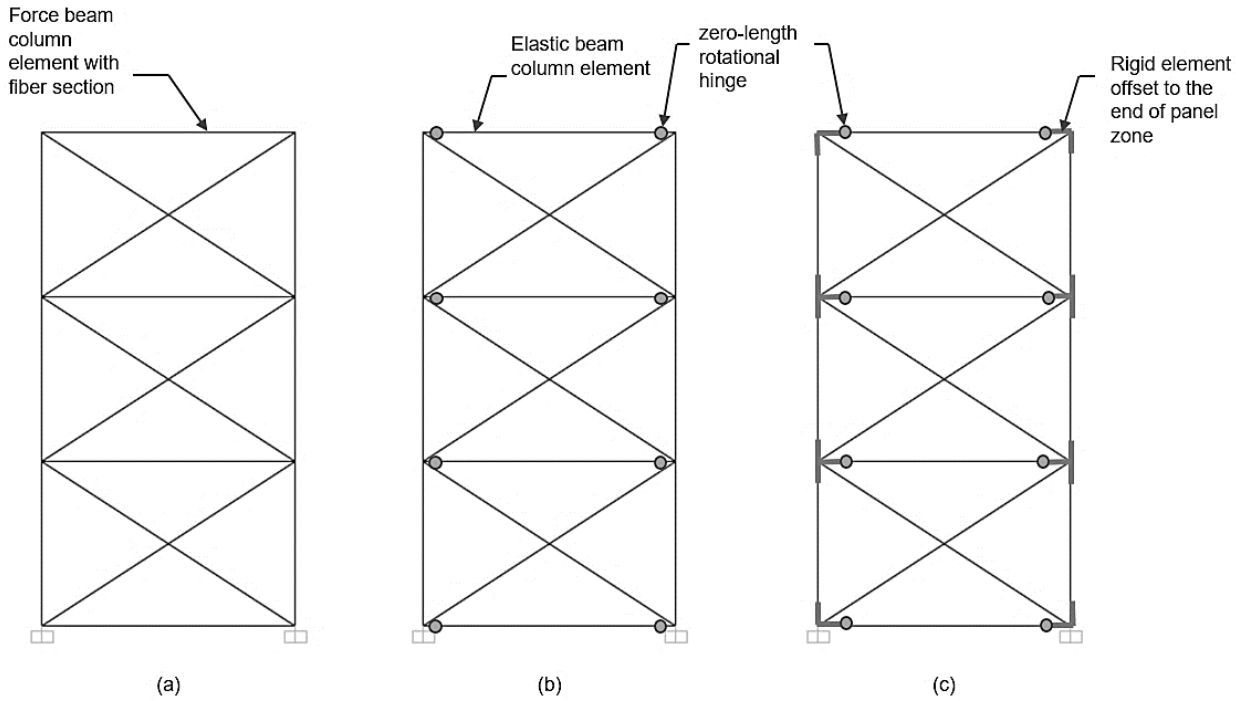

Figure 5.2 Different models for the moment frame surrounding the infill wall (leaning column not shown for clarity)

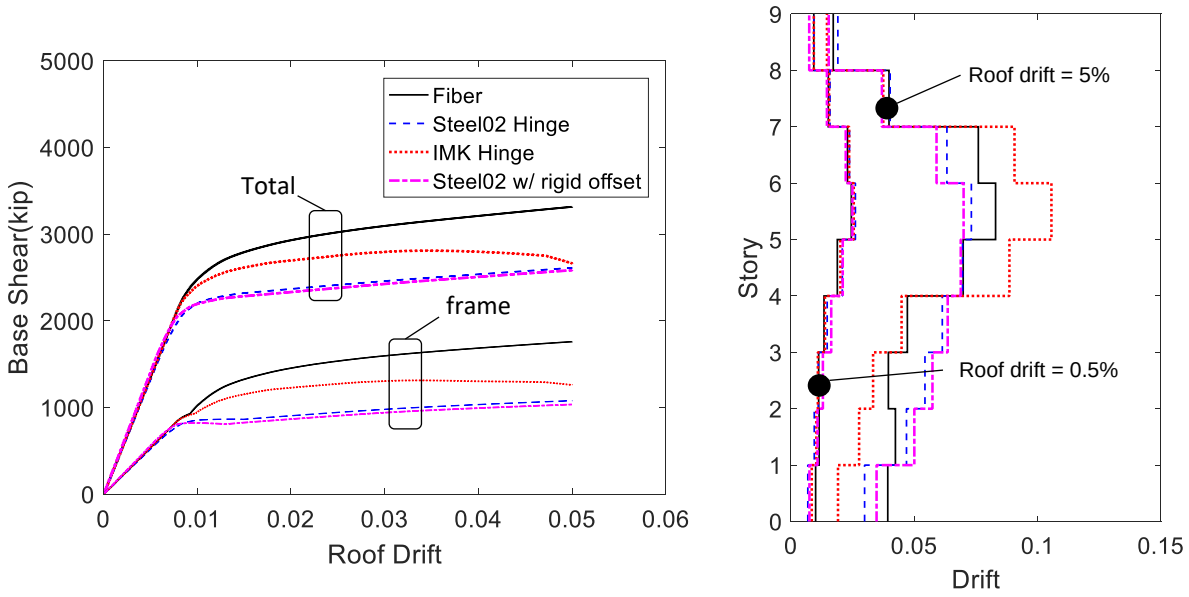

Figure 5.3 Comparison of pushover curves and drift profiles using different moment frame models

f. Slab Effects:

The slabs as non-lateral load-resisting components can contribute to the strength and stiffness of the system and may improve or worsen the seismic performance (FEMA-355C 2000). Composite actions of the floor beams are usually asymmetric, resulting in higher flexural strength and plastic rotations in the positive loading direction when slab is under compression compared to the negative direction. It was found that the composite action decreases the computer-based first-mode period, increases the over-strength factor, and could lead to a greater chance of a bottom weak-story mechanism; the effective strong column-weak beam ratio is smaller than one if including the slab effect. One approach to include the slab effect is to calculate the effective width of the slab and consider the effective slab plus beam as a composite section. Another approach would be to use specially calibrated plastic hinge models for the beam with composite actions like those proposed by (Elkady and Lignos 2014).

However, very few previous analytical studies on steel plate shear walls have explicitly included the slab effect. Models using only the out-of-plane support at the beam location can successfully predict the hysteresis responses and even pseudo-dynamic test results with composite floors [e.g. (Qu et al. 2008)]. Therefore, it seems reasonable not to include the slab effect in this comparative study and design procedure development. The slab effect on the steel plate shear wall system in general, regardless of the specific configurations, should be an area for future research.

g. Lumped Mass:

The seismic mass is assumed to be lumped at the nodes of the lateral force-resisting system. It was assumed the lateral floor mass is shared equally by all nodes of the lateral force-resisting frame. If moment frame is added outside the one-bay steel shear wall, they also share the story mass equally.

h. Damping:

Following the standard practice, Rayleigh damping was incorporated in this study. The Rayleigh

damping stiffness and mass proportional term were assigned to all the frame nodes. Since the major nonlinear components were explicitly modeled, a 2% Rayleigh damping ratio (ζ = 2%) was assumed. The first and third mode of the system was used to compute the stiffness and mass-proportional coefficients for all prototype building models. Notice that instead of the third mode, a higher mode can be selected in the calculation for taller buildings as suggested by Chopra (2007). The two selected modes for computing the Rayleigh damping coefficient should be such that they will result in reasonable damping ratios in all the modes contributing significantly to the response (Chopra 2007).

i. Added Free Vibration Duration:
To assess the residual drift at the end of the ground-motion excitations, an additional 5 sec was added at the end of each ground-motion time history to ensure that most structural vibration is damped out, and the obtained residual drift is not significantly affected by the local peaks.

5.1.2.2 Limitations of the Mathematical Model:

In summary, the main modeling assumptions include:

1. The seismic mass assigned to each node of the lateral force resisting frame was calculated by assuming the seismic mass is equally taken by the steel shear wall frame nodes and the moment frame nodes outside the shear wall bay if applicable;
2. For the proposed new HPSPSW, the steel infill panel plus side stiffeners were modeled by the EB model; for the AISC SPSW, the infill panels were modeled by the strip model. Strength deterioration was included.
3. Beams were modeled by elastic *beamcolumn* element plus zero-length rotation hinges, and columns were modeled by force-based *beamcolumn* elements with fiber sections. The frame members and beam-to-column connections were assumed to be ductile without strength degradation;
4. The diaphragm was assumed to be rigid, i.e., all nodes in the same story have the same horizontal displacement;
5. The base of the shear wall was assumed to be fixed to the ground (both the first-story column and the infill panel);
6. P-delta effects from the gravity columns were accounted for by leaning columns;
7. The effects of large deformation from the beam and column elements were included by using P-delta nonlinear geometric transformation of the column;
8. 2D frames were analyzed, and subjected to either the fault-normal or fault-parallel components of ground motions (component 1). No vertical accelerations were considered in this study;
9. 2% Rayleigh damping was assigned to the system with mass and tangent stiffness (last committed stiffness) proportional Rayleigh coefficients based on the first and the third period;
10. Five seconds was added to each ground motion to obtain the residual drift ratios.

Note: the mathematical model developed and used in this study is not comprehensive and is not intended to predict all possible behavioral characteristics of the steel shear wall system under the chosen excitations. Several, but not all, limitations are identified as follows:

1. The element and material model for the beams and columns did not capture the local buckling behavior of the structural sections;
2. Soil–structure interaction effects were not included;
3. Stiffness contribution from non-structural components, such as the concrete elevator core wall, façade, and exterior cladding, was not included;
4. Panel zones at the beam-column connection and composite action between the beam, metal deck, and floor slab were not included;
5. Possible additional 3D effects were not captured by using the 2D analysis models.

5.1.2.3 Modeling of the Code Designed (AISC) SPSW

This section presents several analyses to validate the strip model for the code designed (AISC) SPSWs, as well as a discussion of the effect of boundary condition for the system.

Validation of the strip model for SPSW

Specimens tested by Park et al. (2007) used to validate the finite element models in Chapter IV were used here again to validate the strip model. The material properties of the strips for different plate thickness was based on Park et al. (2007). Strain hardening of 1% was assigned. Hysteresis material model in OpenSees was used with a pinch factor for strain (PinchX) equals to 0.85, and a pinch factor for force (PinchY) equals to 0.5. It was found that this pair of pinching factors leads to a better match of the zero-drift capacity compared to a smaller pinchY factor; see Figure 5.4. Damage factor due to energy can be added if strength loss due to fracture of the infill plate is reported. It can be seen that in general the strip model and chosen hysteretic material properties can capture the shear wall behavior reasonably well.

Effect of boundary conditions

As shown in Figure 5.5 for the analyzed AISC SPSW, there can be two different scenarios: (1) only the column base is connected to the foundation (which will be referred to as BC2); and (2) both the column base and the first-story beam are anchored to the ground (which will be referred to as BC1). As for the proposed new HPSPSW, the infill wall is converted to a pair of equivalent braces. These two realistic boundary conditions have little effect on the modeling since for both conditions only the column base restraints need to be specified (Figure 5.5 top). However, for the code-designed system, whether the nodes on the bottom beam are pinned or free can make a significant difference in the predicted response.

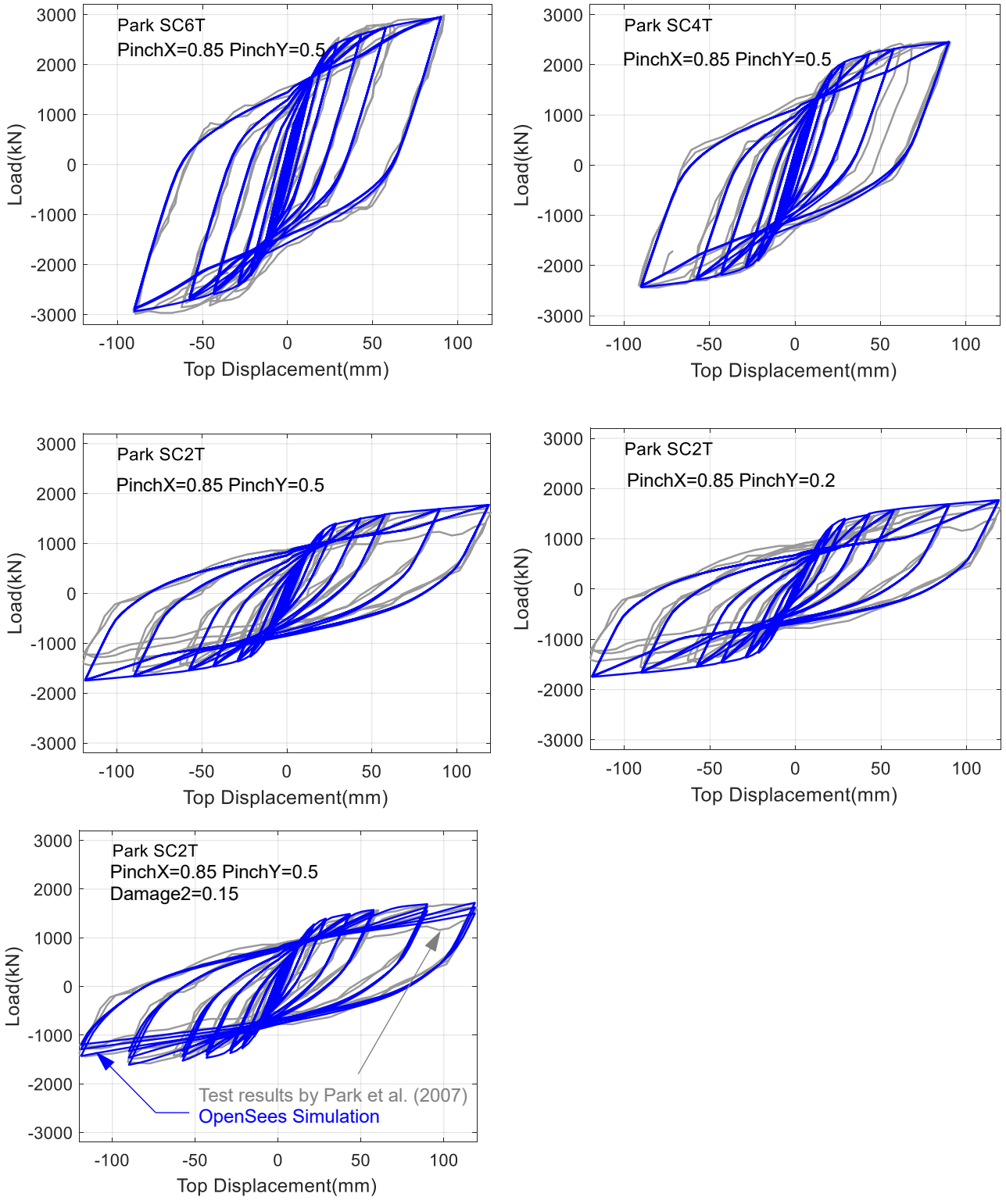

Figure 5.4 Validation of the strip model for SPSWs

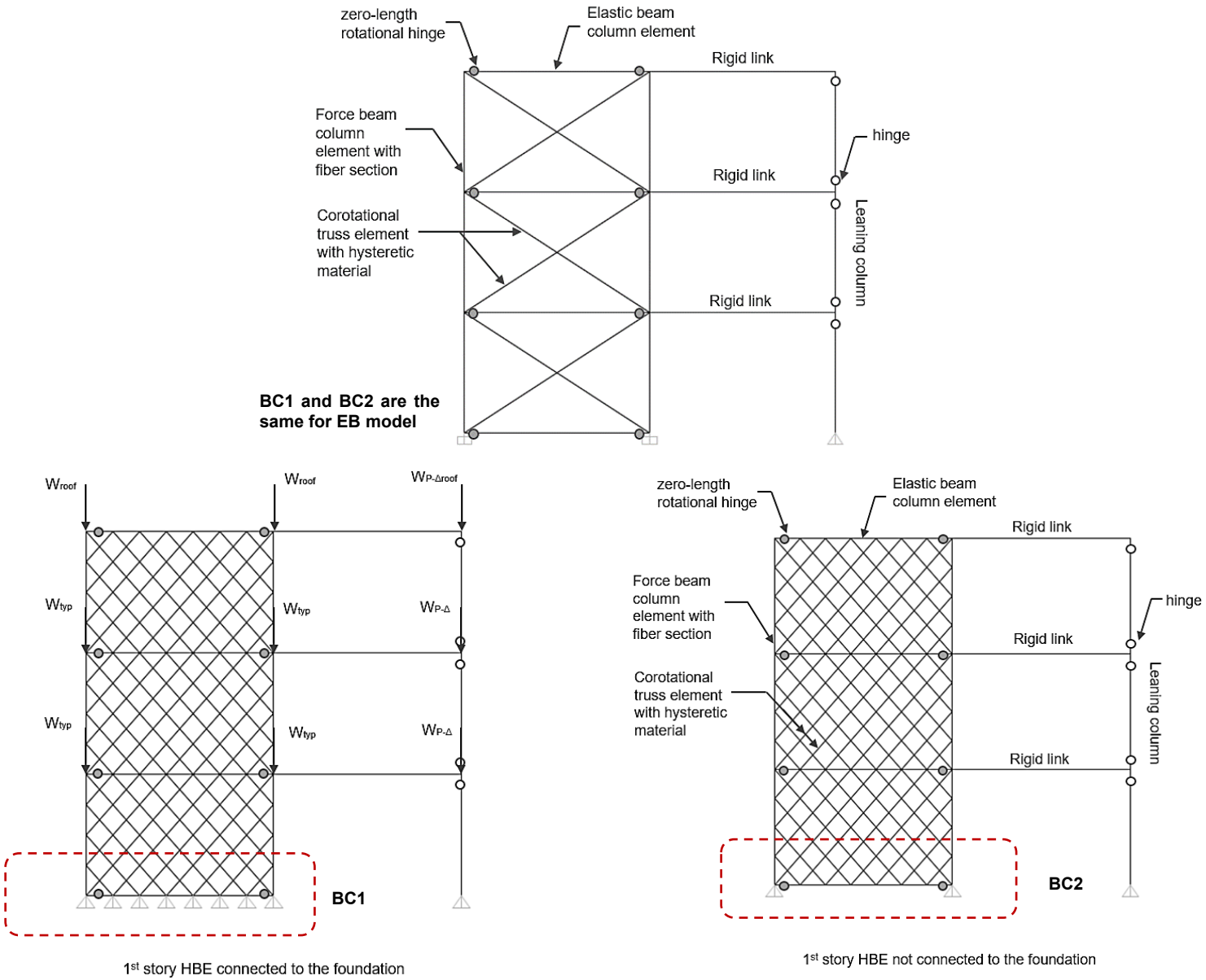

Figure 5.5 Illustration of the boundary conditions of the HPSPSW and AISC SPSW models

Figures 5.6 and 5.7 compare the key displacement and infill wall hysteresis responses of the AISC Design Guide 20 SPSW design using the two boundary conditions. It can be seen that BC1 is more rigid and more effective in limiting the story drift (especially the first-story drift). As BC2 sacrifices the drift in the first story, the upper story drifts are slightly lower compared to BC2. This can also be seen from the infill panel hysteresis curves.

As BC1 makes the bottom story much stiffer, it can attract more seismic inertia forces and lead to much higher column demand-to-capacity (D/C) ratio. While the axial force D/C ratio for the two boundary conditions are very similar (Figure 5.8), the bending moment D/C is quite different, especially for the lower stories. For both boundary conditions, the column bending phenomena due to the infill panel anchoring force is evident. But due to the fixed base condition, the first story column base in BC1 is under much larger bending moments. The beam hinge rotation demands shown in Figure 5.9 reflect the local response of the beam-to-column connection. The BC2 model shows larger first-story beam hinge rotation but slightly smaller larger upper floor rotations.

BC1 model was used in the comparison study to be consistent with the design assumption that the base of the infill plate is fixed to the ground.

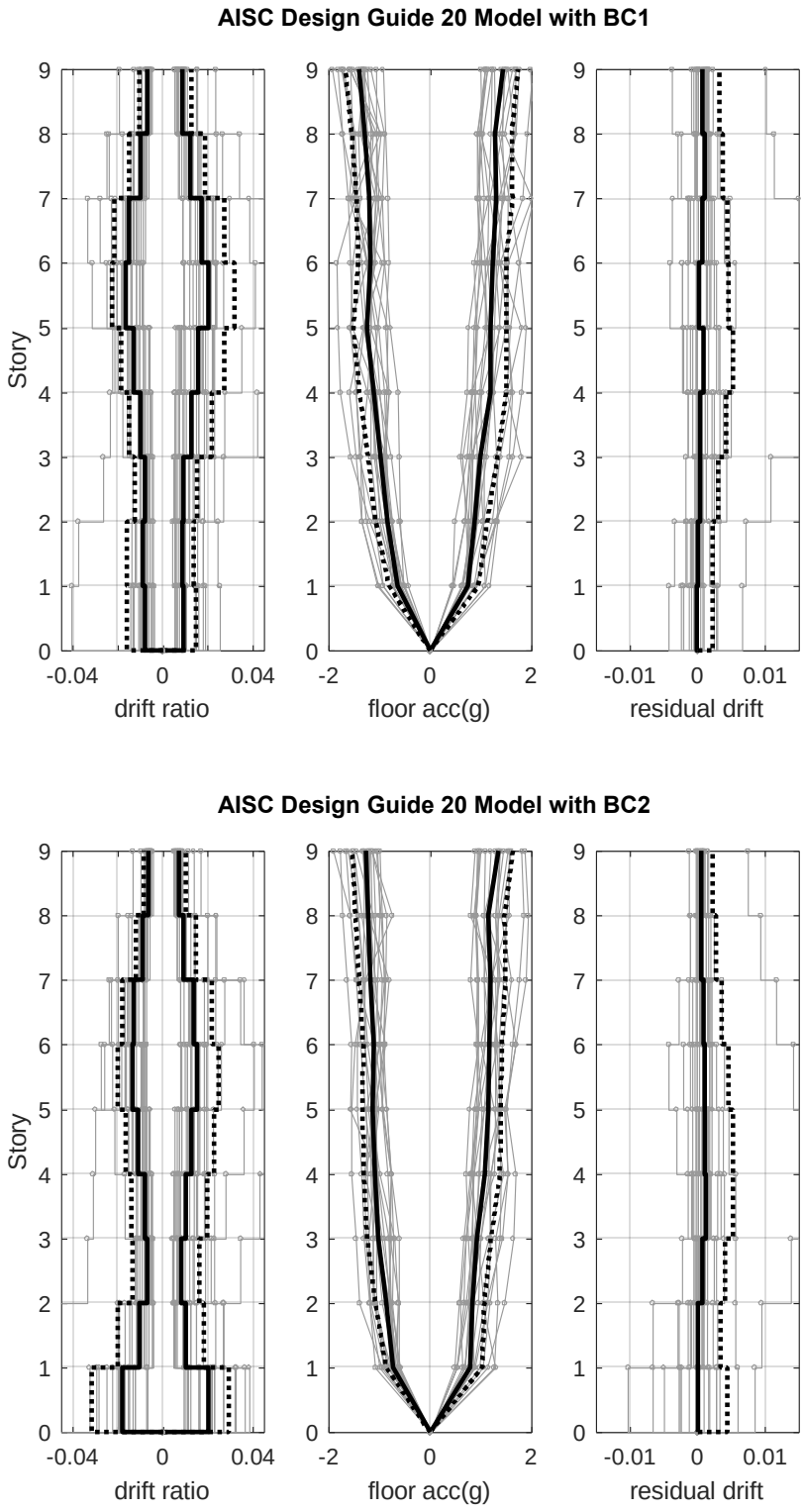

Figure 5.6 Comparison of story drift and acceleration responses for SPSW strip model with different base boundary conditions (2%-50 level hazard)

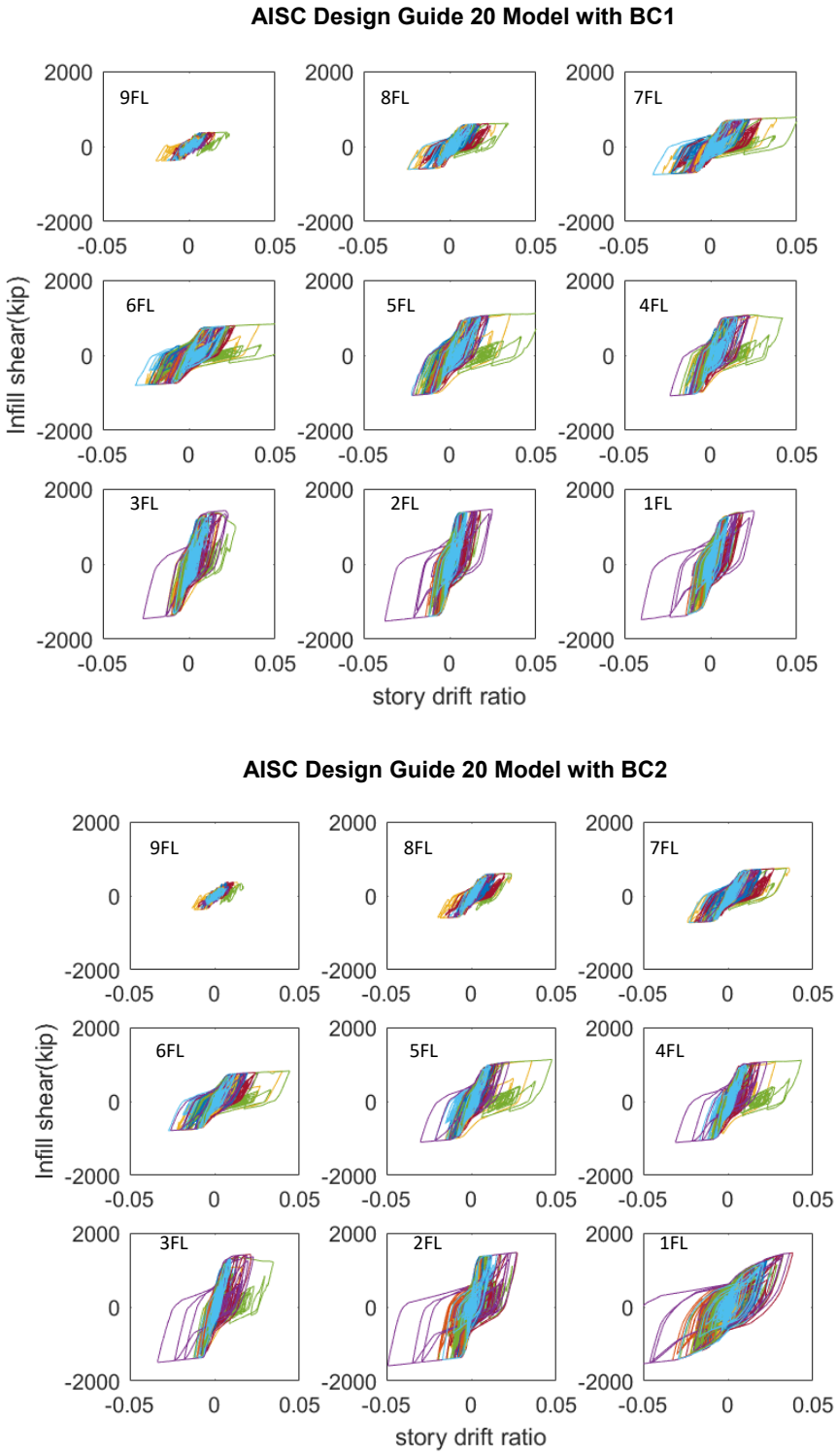

Figure 5.7 Comparison of infill plate hysteresis responses for SPSW strip model with different base boundary conditions (2%-50 level hazard)

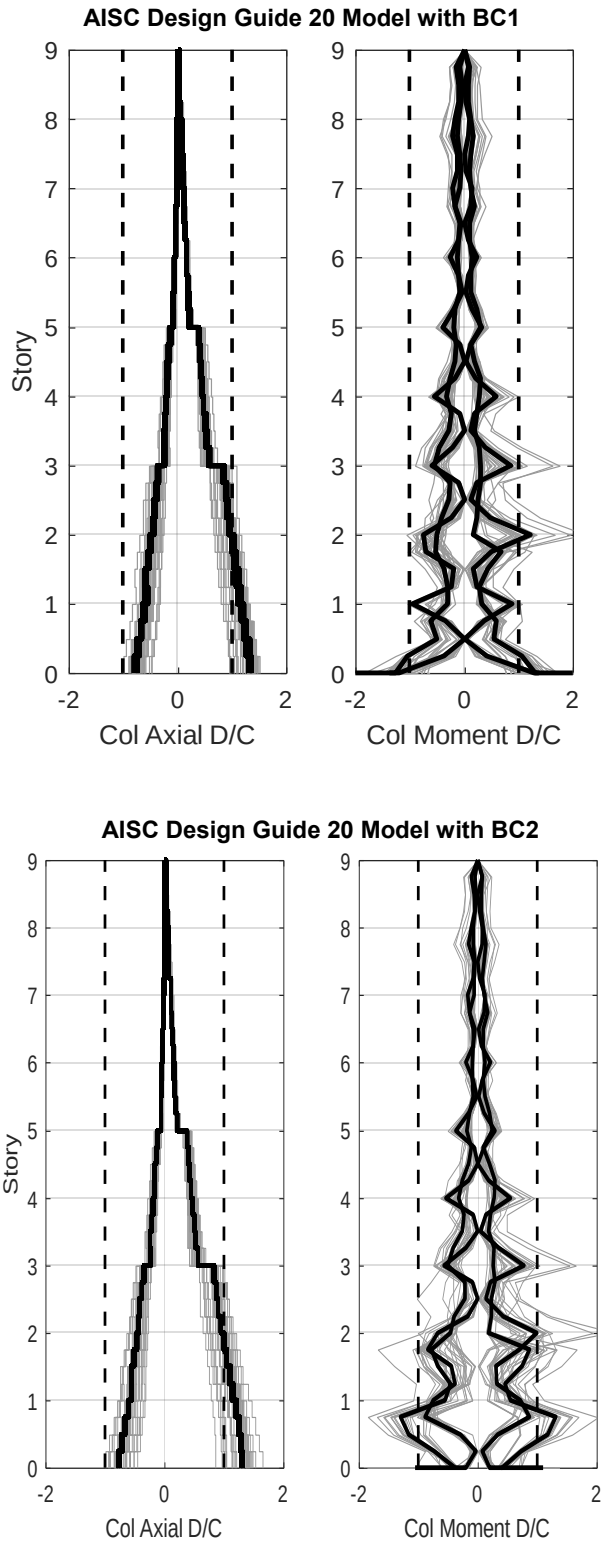

Figure 5.8 Comparison of column demand-capacity (D/C) responses for SPSW strip model with different base boundary conditions (2%-50 level hazard)

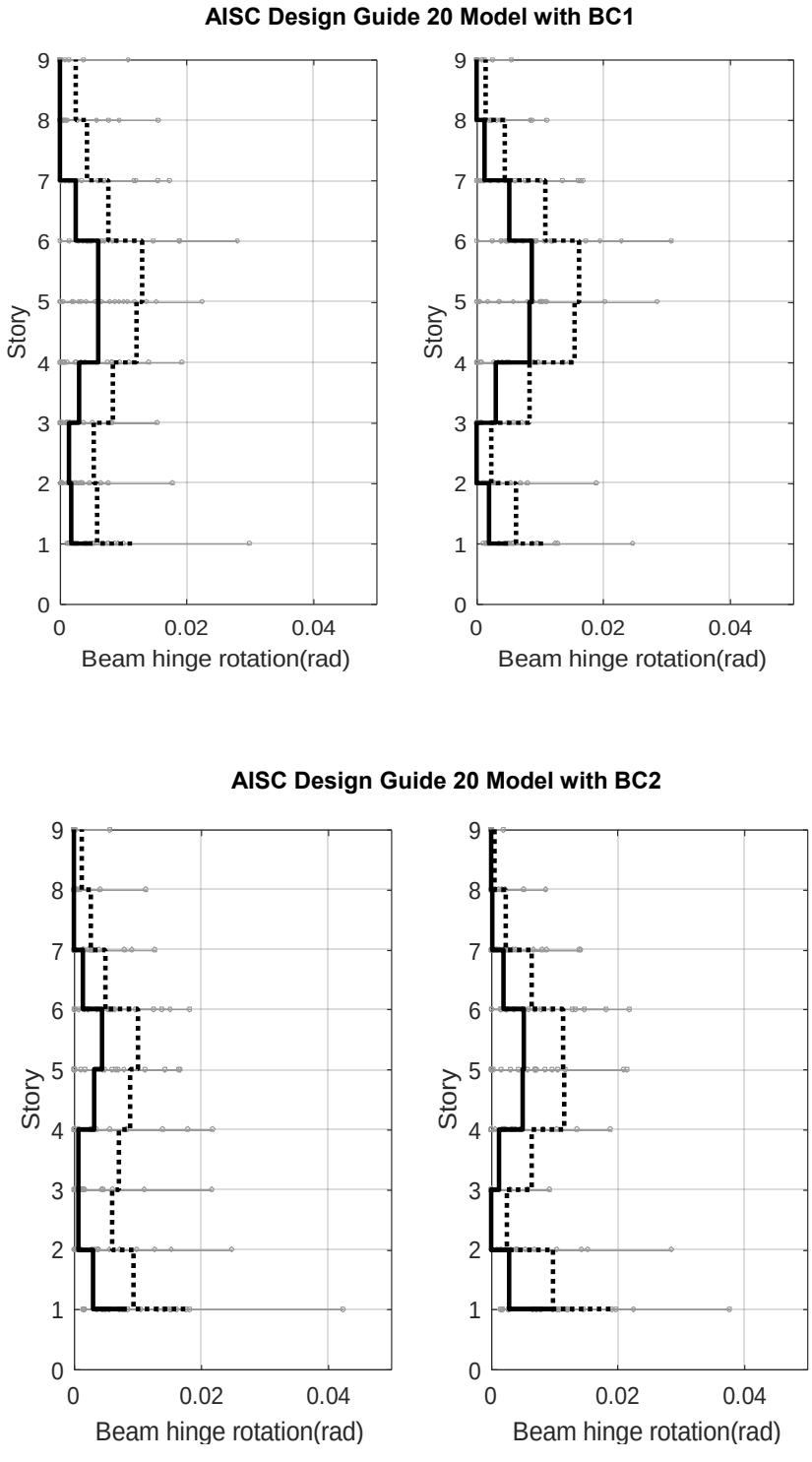

Figure 5.9 Comparison of beam hinge total rotation responses for SPSW strip model with different base boundary conditions (2%-50 level hazard)

5.1.3 Selection of Ground Motions

In this project, suites of earthquake events with 2% and 10% probability of exceedance in 50 years and 50% of exceedance in 30 years were selected. The first two levels represent the design based earthquakes (DBE) and maximum considered earthquakes (MCE), and the third level represents the service-level earthquake. Twenty three-component records were selected to match the uniform hazard spectrum (UHS) at each hazard level; see Figure 5.10. The basic information for the ground motions can be found in Appendix E1. The horizontal component 1 motions were applied to the prototype building models, resulting in a total number of 60 nonlinear response history analyses for each model. These ground motions were selected and scaled by J. Baker for a PEER tall building project (Lai et al. 2015), which is located near to the chosen prototype building site. According to the report by Lai et al. (2015), scaling was based on geomean of the two horizontal components for the selected probabilistic hazard spectrum. The geometric mean spectra matched the target uniform UHS between 0.8 and 8.4 sec. The fundamental natural periods for the 9- and 20-story designs fall within this range, but the 3-story prototype models have slightly shorter first mode period than 0.8 sec. But in order to keep the consistency of the chosen ground motions, the ground motions selected by the same criteria was also applied to the 3-story models. Details of ground motion selection criteria and methodology can be found in Lai et al. (Lai et al. 2015). It was noted that UHS was shown to lead to conservatively biased predictions of the mean response, but it is useful when simplicity and conservatism are desired (Haselton et al. 2012).

Although this project did not cover the entire process of the performance-based earthquake engineering (PBEE) framework, by using the ground motions representing different hazard levels, it is believed that the effect of the uncertainties in earthquake hazard due to nearby faults, magnitude-recurrence rates, fault mechanism, source-to-site distance, travel path, and site condition can be partly reflected in the analysis results. When more information is available based on the tested system behavior, i.e., fragility curves and loss functions, the complete PBEE evaluation of the system can be conducted to further evaluate and develop the new HPSPSW system first proposed herein.

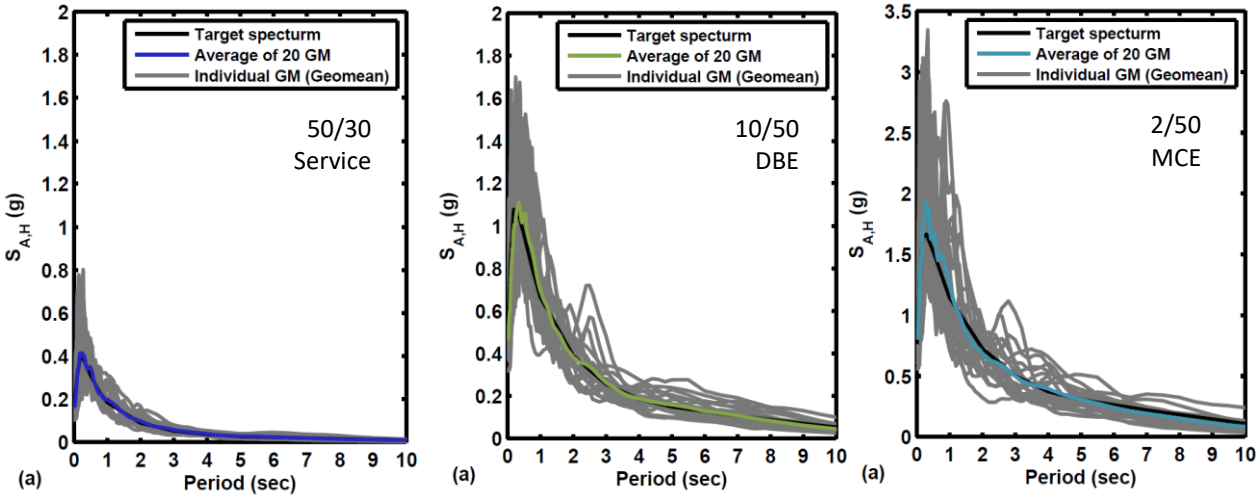

Figure 5.10 Target and selected ground motion spectrums (Adapted from Lai et al. 2015)

5.2 Code-Based Design Approach

5.2.1 Introduction

Since the proposed new HPSPSW system can be viewed as an improved version of the currently available steel plate shear wall system, it makes sense to use the current seismic design provisions at the time of writing to design the system: ASCE 7-10 and 2010 AISC Specifications and Seismic Provisions.

In this section, the prototype buildings will be designed using the existing code strength and stiffness requirements, followed by an evaluation of the performance of the designs using the selected ground motions at different hazard levels. The 9-story three-bay HPSPSW design will be compared with the Design Guide 20 high seismic design, which is considered the best representative of the current fully connected AISC SPSW following existing code provisions.

Berman (2011) designed and analyzed a series of code-designed SPSWs to evaluate their seismic performance. Purba and Bruneau (2014) also developed a series of designed SPSW archetypes for evaluation of SPSW behavior designed using two different approaches. These two studies covered a wide range of building heights, aspect ratios, and seismic weights. The frame designed by Berman (2011) seem to have un-proportional boundary beam and boundary column sizes with very light beams compared to heavy columns. The un-proportional design under-utilizes the moment frame action of the system. The designs in the Purba and Bruneau(2014)'s study contained some impractical infill plate thicknesses; they seem to be selected based on story shear demands without consideration of the actual plate availability. Deep boundary columns were used as a result of the capacity design philosophy (e.g., for a 10-story SW1020 design, the first- story column is W36×798). Though these archetype designs provided valuable information about the seismic behavior of the fully connected AISC SPSW system on the global level, the limitation of market availability of plate thickness and the feasibility to use deep columns should be considered if one wants to evaluate realistically system behavior as opposed to an academic exercise. Therefore, the Design Guide 20 was chosen as a more appropriate benchmark design of the current AISC SPSW system.

5.2.2 Design Procedure

The design procedure that conforms to the existing seismic codes with slightly adjusted usage of equations is outlined below and illustrated in Figure 5.11:

Design Steps:

1. Make initial assumptions about the number and dimensions of the HPSPSW frames.

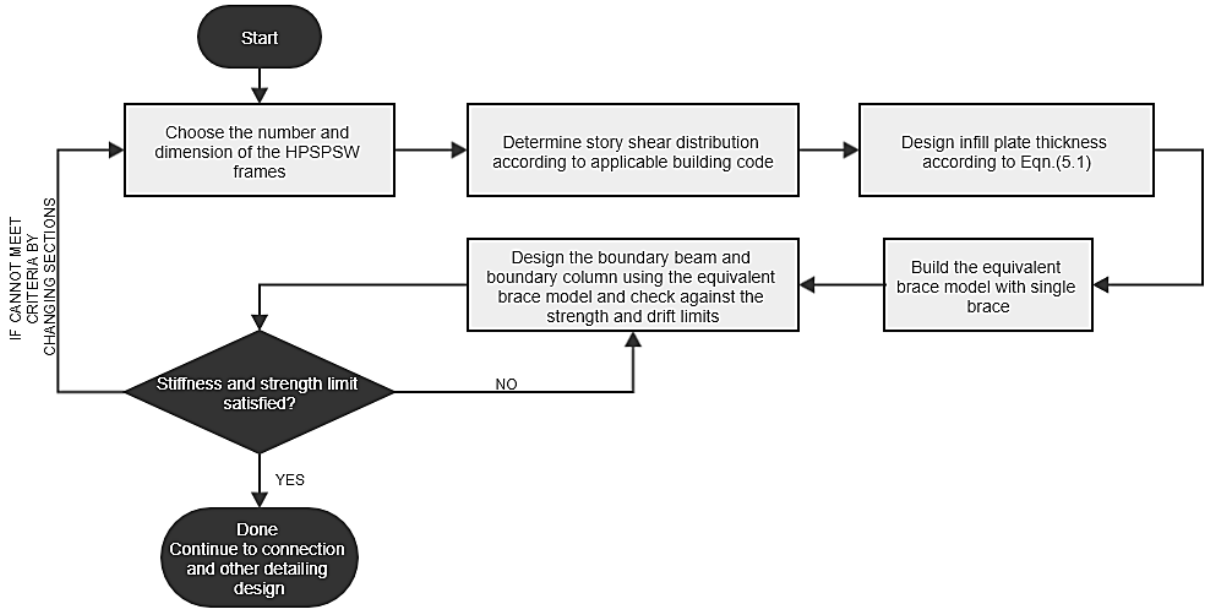

Figure 5.11 Proposed code-based seismic design procedure for the new HPSPSW system

2. Determine the seismic load distribution over the height of the building following the requirements in Chapter 11 and 12 of ASCE 7-10. Conservatively, the approximate periods based on the number of stories given in ASCE 7-10 is recommended in calculating the equivalent lateral forces. At this stage, unless specified, design factors R = 7, Ω_0 = 2, and C_d = 6 were selected, which are the values for the current SPSW system.

3. Determine the infill plate thickness using the following equation

$$t_p = \frac{V_{req'd}}{0.36 f_{yp} L_p} \tag{5.1}$$

where $V_{req'd}$ is the equivalent lateral forces determined in Step 2.

The inherent assumption here is that the infill plate should be able to take 100% of the design lateral force and the boundary frames provide the over-strength and system redundancy. According to Purba and Bruneau (2014), compared with SPSWs having infill wall designed to carry the total design story shear, SPSWs designed to have the infill wall taking only a portion of the lateral loads were found to have significantly larger interstory drifts and required smaller R, Ω_0, and C_d factors to rigorously satisfy the FEMA P695 performance criteria (Purba and Bruneau 2014). Therefore, in this project, it was chosen to stay with the current code requirement that the main lateral load-resisting element, i.e., the steel infill wall, should be able to carry the total design story shear. Some additional design considerations in infill plate thicknesses will be discussed in Section 5.2.3.2.

4. Calculate the equivalent brace (EB) properties as proposed in Chapter IV and construct the EB model with single brace only.

5. Design the boundary beam and boundary column using the EB model, which should then be checked against the strength and drift limits. The equivalent lateral forces should be re-computed using the analysis period of the single EB model in checking the drift limits.

   The EB model with a single diagonal brace should be used in this design step since the purpose is to ensure that the design can satisfy the inelastic drift requirement when the infill plate has buckled and the tension field has yielded. As the natural period of the system is expected to increase in the inelastic range, the actual analysis period using the single-brace EB model instead of the approximate period used in Step 2 should be adopted to re-compute the design lateral forces. This was done for determining the drift as allowed by ASCE 7-10 (ASCE 2010), recommended by Design Guide 20 (AISC 2007), and individual researchers (Berman 2011). Since the stiffness of a steel plate shear wall is in-between the stiffness of a brace frame and a moment frame, one might find it difficult to satisfy the drift limit using the design lateral forces based on the approximate period established in Step 2.

   Note that in most structural analysis software, the analysis period of EB model with single brace would be larger than EB model with an X-brace. The X-brace is needed in response history analysis where the frame is expected to deform in both directions; however, in modal analysis, using an X-brace EB model would lead to an overestimation of the system stiffness. This is because instead of using one tensile and one compression modulus of elasticity, common structural analysis software will use the tensile modulus of elasticity of both braces to compute the natural frequencies.

   The new equivalent lateral forces should be applied to the EB model in the direction that the brace is in tension. The resulting elastic drift multiplied by the drift amplification factor C_d equal to 6 should be checked against the drift limit in ASCE 7-10. In addition to satisfying the drift limit, the chosen beam and column sections should also satisfy all strength design limits, i.e., the demand capacity ratio should be smaller than one under all applicable load combinations, sections should be highly ductile members, and the strong-column–weak gusset criteria should be satisfied.

   Note that by using the proposed GPMC, this beam–column capacity ratio can be relaxed slightly. According to the study in Chapter III, a typical GPMC designed according to the proposed design procedure has an expected gusset plate plastic moment capacity equal to about 55% of that of the beam. So, without explicitly modeling the moment hinge in the analysis model, the resulting beam–column ratio should be allowed to be smaller than 1/0.55 = 1.81, instead of 1.0. However, to leave some margin of safety, the maximum beam–column ratio allowed for all the designs in this study was 1.4.

Besides the strength and stiffness checks using the results from the EB model, the beams should also be checked with one more scenario that is not captured by the EB model, i.e., capacity design the beams considering the effect of the tension field action.

6. Iterate Step 5, if necessary, repeat Steps 1–5, until all strength and stiffness requirements are satisfied.

5.2.3 Some Design Considerations

The proposed code-based design procedure outlines the most important decision-making steps for obtaining a reasonable HPSPSW design. This section offers some other design considerations that can be useful in selecting the infill plate and frame material and cross sections.

5.2.3.1 Stiffness and Strength Ratio

In the proposed HPSPSW, as well as well as the AISC SPSW, the steel infill plate can be viewed as a structural fuse instead of a pure lateral force-resisting element. It is desirable to have the infill plate to yield and dissipate energy before the surrounding moment frame. Due to the separation of the infill plate from the column in the proposed HPSPSW system, the replacement of damaged walls is already much easier than replacing the fully connected SPSW walls. It will be even more appealing if the yielding sequence of the wall and the frame can be achieved. The stiffness ratio, α, and strength ratios, γ, between the metallic fuse and the frame are used as the main parameters to control system behavior. Both parameters are defined in Figure 5.12 and Eqns. (5.2–5.4).

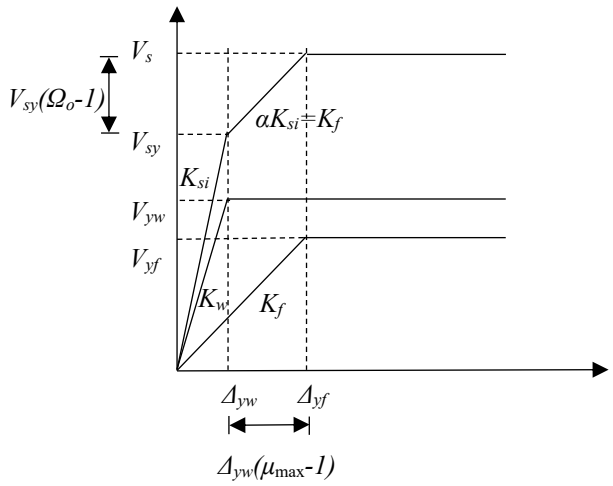

Figure 5.12 Definition of the stiffness ratio and ductility in a structural fuse system

$$\mu_{\max} = \frac{\Delta_{yf}}{\Delta_{yw}} \tag{5.2}$$

$$\alpha = \frac{1}{1+\frac{K_w}{K_f}} \tag{5.3}$$

$$\gamma = \frac{V_{yw}}{V_s} = \frac{1-\alpha}{1-\alpha+\alpha\mu_{\max}} \tag{5.4}$$

where V_{yf} is the yield strength of the frame, V_{yw} is the yield strength of the fuse, Δ_{yf} is the yield displacement of the frame, Δ_{yw} is the yield displacement of the fuse, K_w is the elastic stiffness of the fuse, and K_f is elastic stiffness of the moment frame.

Vargas and Bruneau (2009a) proposed a general design procedure for designing new or retrofitted structures with metallic fuses, which should be disposable and easy to repair while the main structure frame remains elastic or have only minor inelastic deformations. The proposed procedure was based on a parametric study of nonlinear single-degree-of-freedom (SFOF) systems subjected to synthetic ground motions (Vargas and Bruneau 2009a). They verified the design procedure by experimental tests on buckling-restrained braces and a ball-in-cone base isolation system. They found that the structural fuse contribution to the total base shear capacity increases with decreasing stiffness ratio, α, and yielding displacement ratio, μ_{max}. They recommended $0.25 \leq \alpha \leq 0.5$ and $\mu_{max} \geq 5$ to maximize the ductility and energy dissipation that can be provided by the structural fuse (Vargas and Bruneau 2009a; Vargas and Bruneau 2009b).

Segovia and Ruiz (2016) studied the best values of the stiffness ratio and strength ratios based on parametric studies of an 8-story building consisted of Buckling Restrained Braces (BRB) in a moment frame. A cost-efficiency index, defined as the ratio of the initial cost of the total system and the maximum design ductility, was chosen as the criteria to select the best design parameters. They recommended a stiffness ratio range of $0.25 \leq \alpha \leq 0.33$ and a range of 0.28–0.35 for the strength ratio, γ. They implemented the preferred stiffness and strength ratio in a direct displacement-based design procedure and showed that multiple performance objectives could be accomplished (Segovia and Ruiz 2016).

Tena-Colunga and Nangullasmú-Hernández (2015) studied the design parameters for low- to medium-rise regular reinforced concrete moment-resisting braced frames (RC-MRBFs) with hysteretic energy-dissipation devices mounted on chevron steel bracing. Nonlinear pushover analyses were performed on frame models ranging from five to twenty-five stories. They recommended that satisfactory global ductility capacity of the whole system can be achieved without significant inelasticity in the frame elements if: (a) $0.25 \leq \alpha \leq 0.5$, with α being the elastic stiffness ratios between the moment frame system and the whole structure; (b) $0.5 \leq \beta \leq 1.0$ with β being the elastic stiffness balances between the hysteretic device and the supporting braces; and (c) $\mu \leq 8$, with μ defined as the objective ductility. They observed that for 5-15 story models, α equal to 0.25 is the largest stiffness ratio, while the α value should increase as the building becomes taller (Tena-Colunga and Nangullasmú-Hernández 2015).

These studies are some examples of the preferred stiffness and strength relationship between the "fuse" element and the surrounding moment frame. The general trend for better system

performance in terms of cost efficiency for maximum ductility and energy dissipation are those with relatively stiff but weak structural fuse elements. However, whether these relationships can be achieved by the new HPSPSW system remains to be investigated.

Note that the strength and stiffness of the W-sections are correlated. The strength/stiffness ratios, i.e., plastic section modulus over second moment of inertia, of each wide flange sections are summarized in Figure 5.13, which is the same as given in Sullivan et al. (2006).

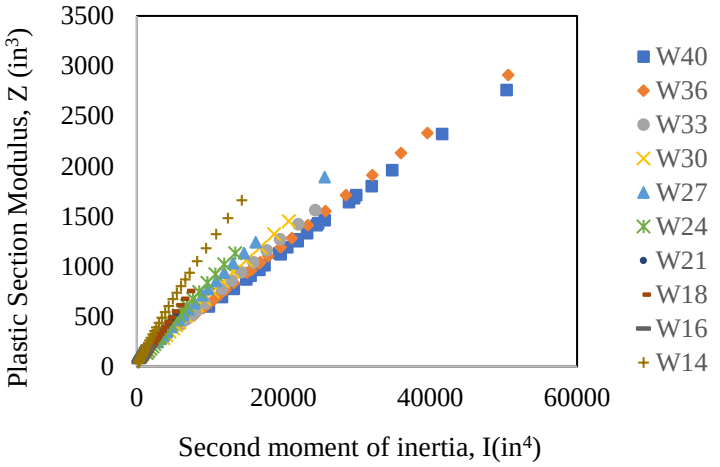

W group	Z/I, in^{-1}
W40	0.054
W36	0.057
W33	0.062
W30	0.068
W27	0.073
W24	0.083
W21	0.098
W18	0.107
W16	0.119
W14	0.130

Figure 5.13 Relationship of plastic section modulus and second moment of inertia for wide-flange sections

In addition, the strength and stiffness of the steel infill wall made of structural steel are also correlated. As shown in Chapter IV, the yield drift of the infill wall is independent of the plate thickness and is correlated with the infill plate material properties and the geometric aspect ratio.

With the correlation between the strength and stiffness for both the frame members and the infill wall, we found it challenging to satisfy the recommended stiffness ratio, α, and strength ratio, γ for the HPSPSW system. However, with the aim of increasing the infill wall stiffness, which increases with increasing thickness and aspect ratio, and at the same time reducing the yield drift of the infill wall, which reduces with decreasing material yield stress and increasing aspect ratio, one plausible method would be to use infill walls with a higher aspect ratio or lower yield strength steel. As the aspect ratio is normally controlled by the architectural constraint, selecting a proper infill wall material is a more feasible option. Higher strength frame members also contribute to increasing the frame yielding point and strength. Therefore, in all the prototype designs, the infill plates were A36 steel (more widely available compared to the low yield LYP100 steel), and the beams and columns were A572 Gr.65 steel.

5.2.3.2 Infill Panel Thickness

To allow relatively uniform and simultaneous yielding of infill walls for all stories, it is recommended to size the plate thickness as close as the applied design lateral forces. Sometimes the calculated plate thickness must be rounded up due to the limitation of available steel plate thicknesses. It is not recommended to significantly over-design the infill plates; rounding up by 1/16 or 1/8 of an inch can make a difference on the system behavior. Although the boundary moment frame in the proposed HPSPSW system is less sensitive to the infill plate thickness

because they do not need to be capacity-designed for the tension-field forces, it is still recommended to limit the rounding up amount.

That said, it is known that there can be difficulties in transportation, handling, and welding of thin plates, which are usually used for upper floors. In addition, thin infill plates could also raise a problem for mid-height splices. Because extremely thin plates have very low bearing capacity, using bolted splices are sometimes impossible; welded splices are also not an ideal alternative since thin steel plates are very easily burnt. Therefore, it is suggested here to limit the minimum thickness of infill plates to be 3/16 in.

5.2.4 Resulting Code-Based Designs

Tables 5.2–5.6 summarize the design sections and periods for the prototype buildings. As mentioned in Design Guide 20 (AISC 2007), the drift limitation may control the design, especially for taller buildings. It was found very difficult to satisfy the drift limit for the 20-story building with a single HPSPSW bay, which deforms like a cantilever under the ASCE7-10-based equivalent lateral forces. Supplemental moment frames were found necessary to reduce the drift. Therefore, only the three-bay configuration with one middle HPSPSW bay plus two side moment frame bays was designed for the 20-story building. For the 3- and 9-story buildings, both one bay and three bay configurations were considered. The designs were named in the form of *design method-number of stories-number of bays*. For example, C3-1 means code-based design three-story one-bay HPSPSW.

In general, either increasing the infill plate thickness or providing heavier or more moment frames can help satisfy the drift limit. Normally, for single bay designs, relatively heavy beam and column sections are needed to limit the drift if the infill plate thicknesses are kept close to values established by Eqn. (5.1). The infill plate thicknesses for design C3-1 were increased based on what is required by Eqn. (5.1) in order to provide a case with thicker wall but similar frame sections with design C3-3. In contrast, it can be seen that C9-1 has much heavier frame sections compared to C9-3 if maintaining the infill plate thicknesses the same as computed by Eqn. (5.1).

Table 5.2 Natural periods of the preliminary designs using code-based design procedure

Name of Design Case	# of stories	Bay Width (ft)	# of frames in loading direction	T_{approx}(s) by ASCE 7-10 Eqn.12.8-7	$T_{analysis}$(s) by single brace EB model	$T_{analysis}$(s) by X-brace EB model
C3-1	3	20	2	0.312	0.63	0.47
C3-3	3	20	2	0.312	0.64	0.48
C9-1	9	20	4	0.734	1.44	1.27
C9-3	9	20	4	0.734	1.40	1.21
C20-3	20	20	6	1.314	2.58	2.41

The beams, columns, and side stiffener sections for all design cases were A572 Gr.65 steel with minimum specified yield stress of 65 ksi; all infill plates were A36 steel with minimum specified yield stress of 36 ksi. The in-plane plastic section modulus requirement for the side stiffeners are only related to the story height, material, and infill plate thickness. Therefore, a table showing the required side stiffener sections corresponding to infill plate thicknesses and floor height, applicable to all building design cases was constructed and is shown in Table 5.3.

Table 5.3 Required side stiffener sections for different infill plate thicknesses and floor heights

t_p (in.)	Stiffener section for typical floor (13 ft)	Stiffener section for 1st floor (18 ft)
1/16	WT8X25	*
1/8	WT8X50	*
3/16	WT9X59.5	WT9X117
1/4	WT9X79	*
5/16	WT9X96	WT12X139.5
3/8	WT9X105.5	WT12X167.5
7/16	WT9X129	WT12X185

*not needed in the design cases considered in this project

Table 5.4 Code-based design sections for the 3-story prototype buildings

	Design Case C3-1			**Design Case C3-3**				
Story	t_p (in)	Shear Wall Column	Shear Wall Beam	t_p (in)	Shear Wall Column	Shear Wall Beam	Moment Frame Column	Moment Frame Beam
3	0.1875	W14X145	W27X117	0.125	W14X120	W27X94	W14X120	W27X94
2	0.25	W14X233	W27X146	0.1875	W14X233	W27X94	W14X132	W27X94
1	0.3125	W14X233	W24X146	0.25	W14X233	W27X94	W14X132	W27X94

Table 5.5 Code-based design sections for the 9-story prototype buildings

	Design Case C9-1			**Design Case C9-3**				
Story	t_p (in)	Shear Wall Column	Shear Wall Beam	t_p (in)	Shear Wall Column	Shear Wall Beam	Moment Frame Column	Moment Frame Beam
9	0.125	W14X426	W30X235	0.125	W14X211	W21X111	W14X145	W21X111
8	0.125	W14X426	W30X235	0.125	W14X211	W21X111	W14X145	W21X111
7	0.1875	W14X455	W30X235	0.1875	W14X283	W21X111	W14X159	W21X111
6	0.25	W14X455	W30X261	0.25	W14X283	W21X122	W14X159	W21X122
5	0.25	W14X455	W30X261	0.25	W14X283	W21X122	W14X159	W21X122
4	0.25	W14X605	W30X261	0.25	W14X370	W21X122	W14X176	W21X122
3	0.3125	W14X605	W30X261	0.3125	W14X370	W24X131	W14X176	W24X131
2	0.3125	W14X605	W30X261	0.3125	W14X370	W24X131	W14X176	W24X131
1	0.3125	W14X605	W30X261	0.3125	W14X370	W24X131	W14X176	W24X131

Table 5.6 Code-based design sections for the 20-story prototype building

Design Case C20-3					
Story	t_p (in)	Shear Wall Column	Shear Wall Beam	Moment Frame Column	Moment Frame Beam
20	0.125	W14X176	W27X94	W14X109	W27X94
19	0.125	W14X176	W27X94	W14X109	W27X94
18	0.125	W14X176	W27X94	W14X109	W27X94
17	0.125	W14X176	W27X94	W14X109	W27X94
16	0.125	W14X233	W27X94	W14X109	W27X94
15	0.1875	W14X233	W27X94	W14X176	W27X94
14	0.1875	W14X233	W27X94	W14X176	W27X94
13	0.1875	W14X233	W27X94	W14X176	W27X94
12	0.1875	W14X233	W27X94	W14X176	W27X94
11	0.1875	W14X233	W27X94	W14X176	W27X94
10	0.1875	W14X233	W27X94	W14X176	W27X94
9	0.1875	W14X233	W27X94	W14X176	W27X94
8	0.1875	W14X233	W27X94	W14X176	W27X94
7	0.1875	W14X257	W27X94	W14X211	W27X94
6	0.1875	W14X257	W27X94	W14X211	W27X94
5	0.1875	W14X257	W27X114	W14X211	W27X94
4	0.1875	W14X257	W27X114	W14X211	W27X94
3	0.1875	W14X257	W27X114	W14X211	W27X94
2	0.1875	W14X257	W27X114	W14X211	W27X94
1	0.1875	W14X257	W27X114	W14X211	W27X94

5.2.5 Comparison with AISC Design Guide 20 Design

In order to have a better understanding of the system response of the proposed HPSPSW designed using the code-based design procedure presented earlier, this section compares the key structural responses of the Design Guide 20 high seismic design (AISC 2007) and the case C9-3 design. The AISC Design Guide 20 design will be referred to as AISC-DG20 in the following discussions. The response parameters of interest include the peak interstory drift, residual story drift, absolute floor acceleration, and the beam–column connection rotation (or the beam hinge rotation), as well as column axial (P) and moment (M) demand capacity ratio and P-M interaction ratio. The former three response parameters represent the global behavior and are commonly used to assess the damage and loss, while the latter two parameters reflect the local element and connection responses.

5.2.5.1 General

Compared to the AISC-DG20 design, the C9-3 design has a much lighter frame but thicker infill plates and additional side stiffeners. AISC-DG20 is slightly stiffer and has a shorter natural period,

and is 20% heavier than C9-3 design. The revised 9 story-3 bay design PBD9-3 to be introduced in Section 5.3 is also 10% lighter than AISC-DG20.

Table 5.7 Comparison of general information of AISC-DG20 and HPSPSW C9-3 Design

Design	$T_{analysis}$(s) by single brace model or strip model	$T_{analysis}$(s) by X-brace model or double strip model	Weight of the structural system (lb)	W/W_{DG20}
AISC-DG20	1.20	1.03	265877	1.0
C9-3	1.40	1.21	219507	0.83
PBE9-3	1.35	1.15	235695	0.89

5.2.5.2 Peak Story Drift Ratio, Residual Drift and Floor Acceleration

As shown in Figures 5.14 – Figure 5.16, in general, the median peak story drift ratios for both AISC-DG20 and HPSPSW code-based designs were less than 1.5% at 10% when subjected to the 50-year-level ground motions and less than 2% under the 2% in 50-year-level motions. The 84th percentile responses for AISC-DG20 design can be maintained below 2% and 4% at 10/50 and 2/50 level hazards respectively, although a few motions had driven the first-story drift to be larger than 5% at 2/50 level hazards. Compared to AISC-DG20 responses, C9-3 drift profile at 10/50 hazard level, which corresponds to the design-level earthquake, was very uniform, indicating a first-mode deformed shape. The absolute values (median, 84th percentile, and maximum) of the drift responses of the code-designed HPSPSW system were much lower than AISC-DG20, where the AISC-DG20 design had almost formed a soft-story mechanism under one of the ground motions at 10/50 level. For the C9-3 design, the 84th-percentile peak story drift responses were maintained below 2% at 10/50 level, but a soft story had formed under several 2/50 level motions, leading to larger than 4% 84th percentile drift responses. This is likely due to the fact that after significant yielding of the infill panel at the high intensity level motions, the light boundary moment frames were not sufficient to resist the lateral forces. It could be also caused by the nature of the EB model, which has a simple bilinear backbone relationship; once the infill plate has yielded, it will lose almost all the lateral stiffness.

The lighter surrounding moment frame is also less effective in controlling residual drift, as indicated by the higher residual drifts for C9-3 design. It is widely known that due to the nature of tension field action, residual drift is inevitable. Therefore, keeping more elasticity in the moment frame is beneficial for the system's re-centering capability. It is likely that the two moment frames on the sides of shear wall bay of the AISC-DG20 design also contributed significantly to the lateral resistance in later stages after widespread yielding of the infill plate. As will be shown later in Section 5.3, after a slight modification of the lower floor column sections, the modified C9-3 design no longer suffered from the soft-story issue and could satisfy a series of enhanced design objectives. It is suggested that choosing slightly larger sections as required by the code-based design procedure would be beneficial for the collapse level performance.

The floor acceleration of design case C9-3 was, in general, higher than DG20, which could be because of the nature of the EB model, which has a sudden yielding point compared to the more gradual yielding behavior delivered by the strip model, and could cause "impact" type acceleration in the analysis model.

5.2.5.3 Hysteresis Curves of Infill Panels

The hysteresis curves of the infill panels are presented in Figures 5.17 and 5.18 to show the behavior of the infill panels, and can also be used to explain the large transient and residual story drift of the two systems. It can be seen that several ground motions drove the first-story panel of C9-3 far into the inelastic range, and the system did not return to the original position but oscillated around a position away from the original position. It appears that the middle stories of AISC-DG20 are relatively weak compared to other stories, indicating an S-shaped deformed shape of the system.

5.2.5.4 Beam Hinge Rotation

As shown in Figure 5.19 and 5.20, both AISC-DG20 and HPSPSW C9-3 designs resulted in insignificant moment connection rotations – less than 0.02 radian total beam hinge rotation at the 84^{th} percentile level under both 10/50 and 02/50 motions. The beam hinge rotations in design case C9-3 were very small even at 02/50 hazard level, which indicates the moment frame action in the shear wall bay was not effectively mobilized and the side moment frames provided most of the moment frame action. Another reason for the extremely small beam hinge rotation for design case C9-3 at 2%-50 year hazard level could be that a soft story formed at the first story, which concentrated most of the moment rotation demands at the first-story beam, while the other stories tended to move as a rigid body.

50/30 AISC-DG20

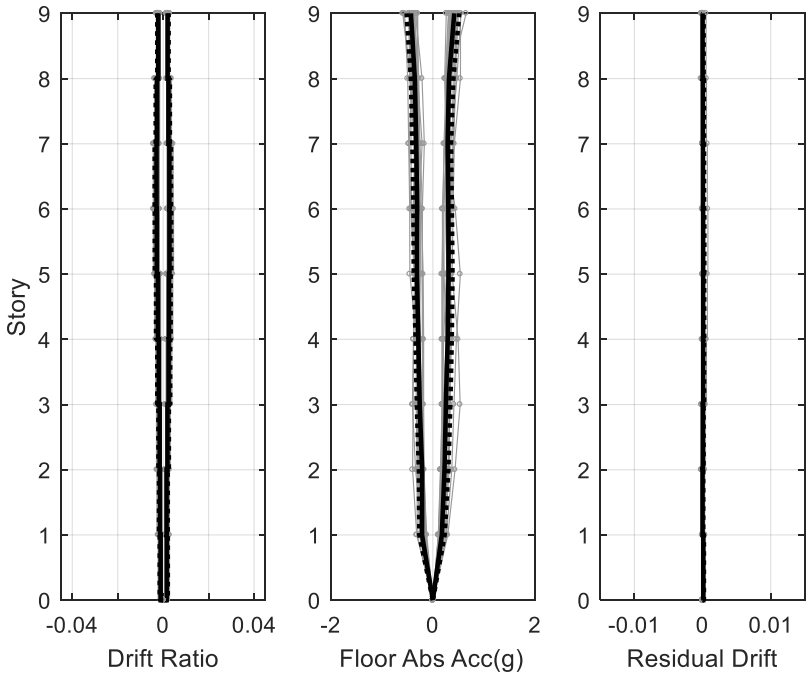

50/30 C9-3

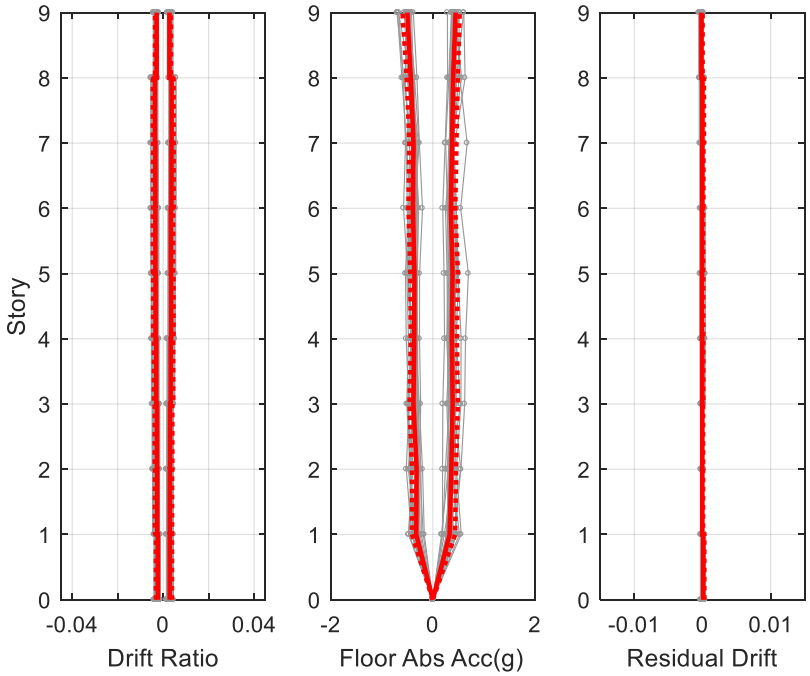

Figure 5.14 Comparison of story drift and floor acceleration responses of AISC-DG20 and C9-3 designs at 50/30 level hazard

10/50 AISC-DG20

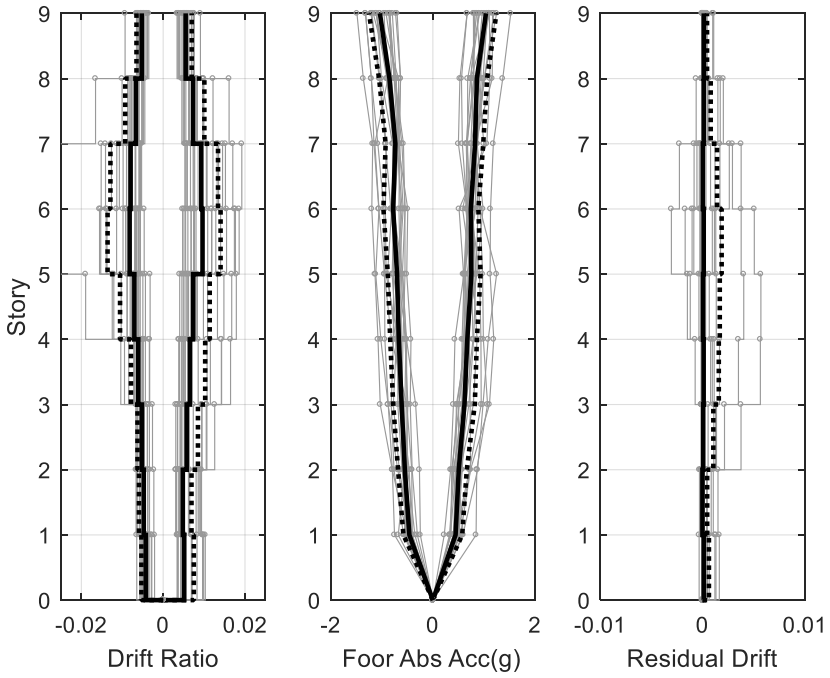

10/50 C9-3

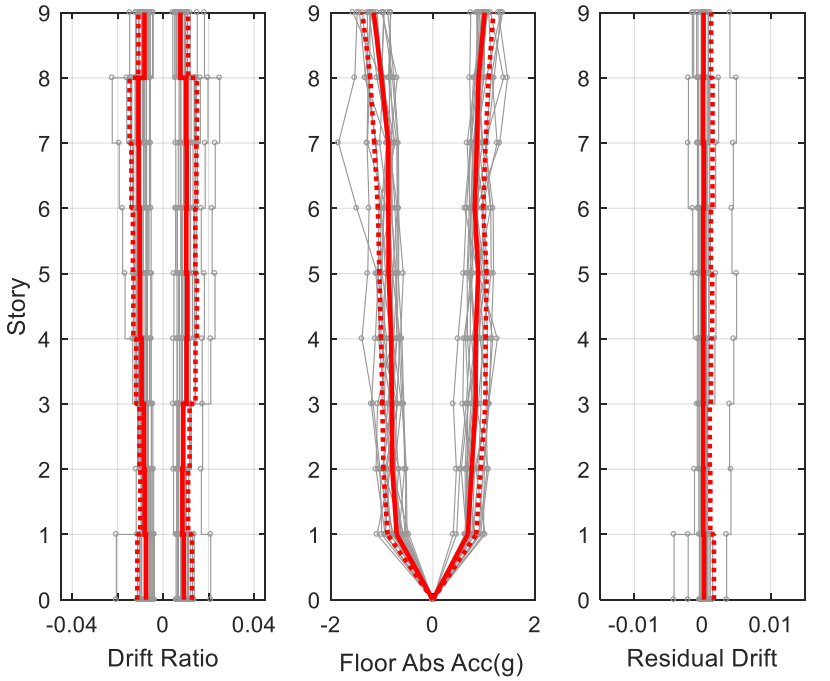

Figure 5.15 Comparison of story drift and floor acceleration responses of AISC-DG20 and C9-3 designs at 10/50 level hazard

02/50 AISC-DG20

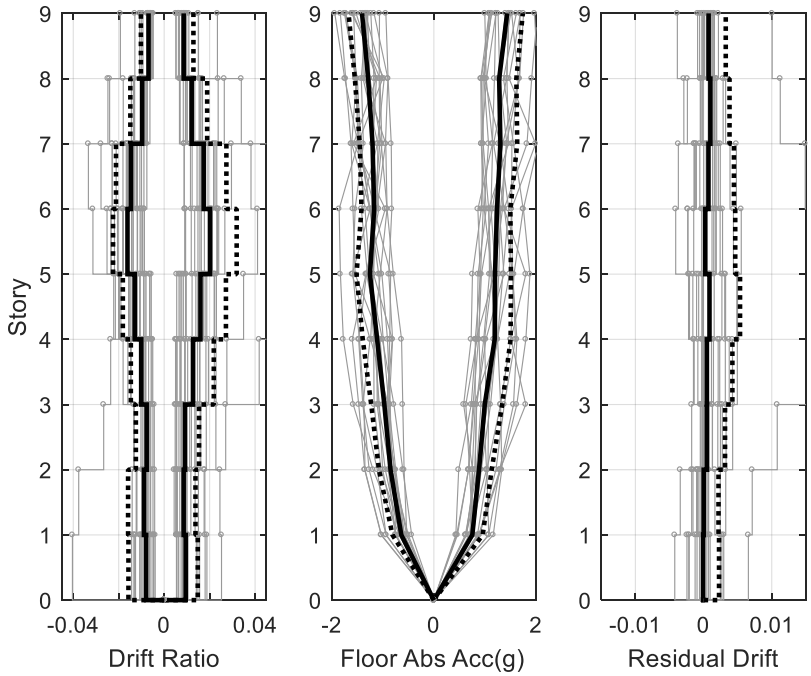

02/50 C9-3

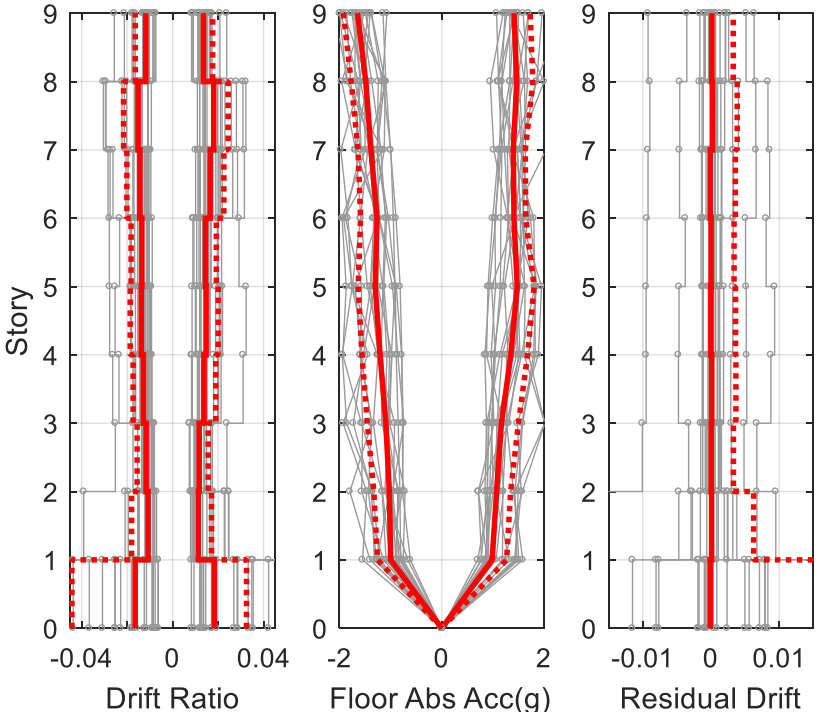

Figure 5.16 Comparison of story drift and floor acceleration responses of AISC-DG20 and C9-3 designs at 02/50 level hazard

10/50 AISC-DG20

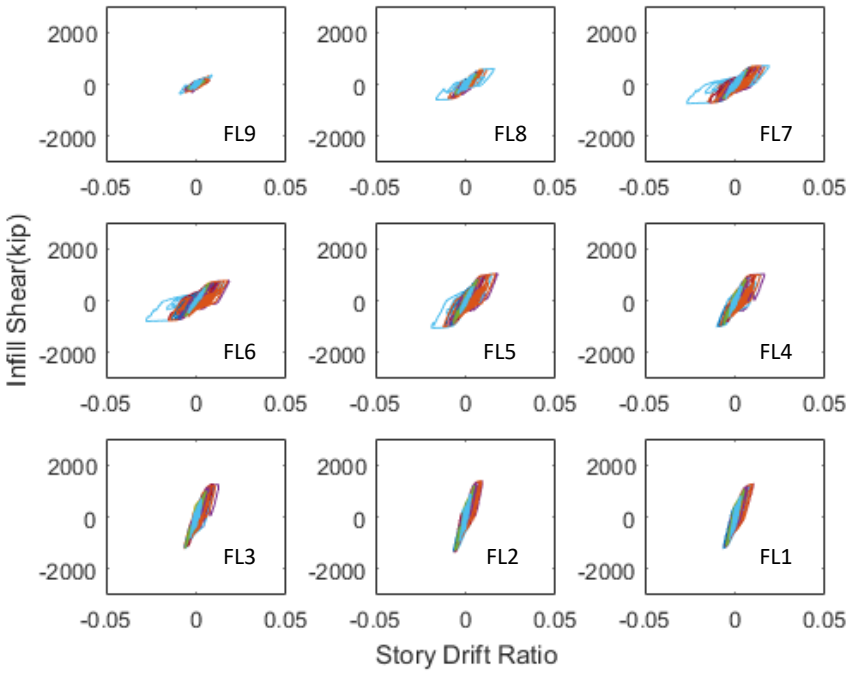

10/50 C9-3

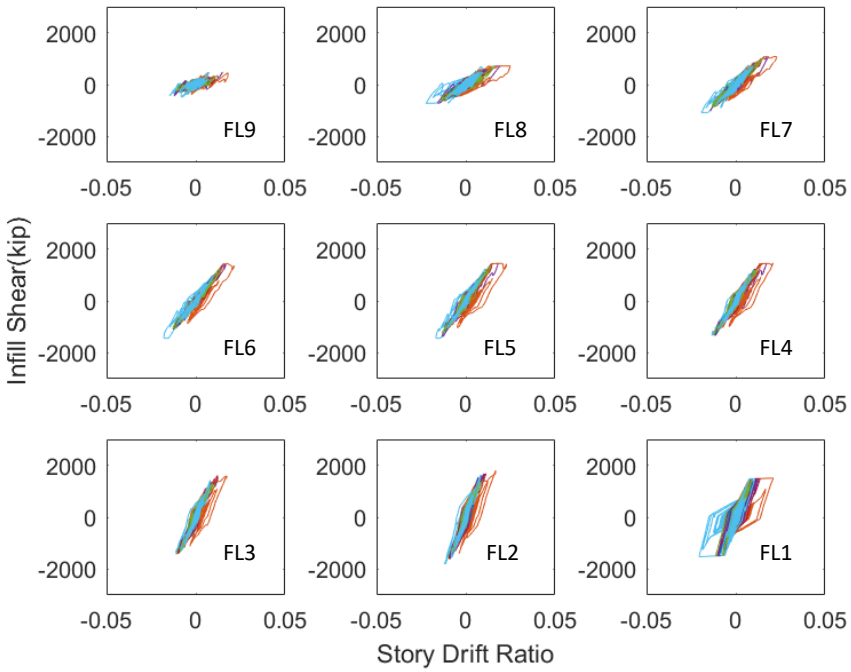

Figure 5.17 Comparison of infill plate hysteresis responses of AISC-DG20 and C9-3 designs at 10/50 hazard level

02/50 AISC-DG20

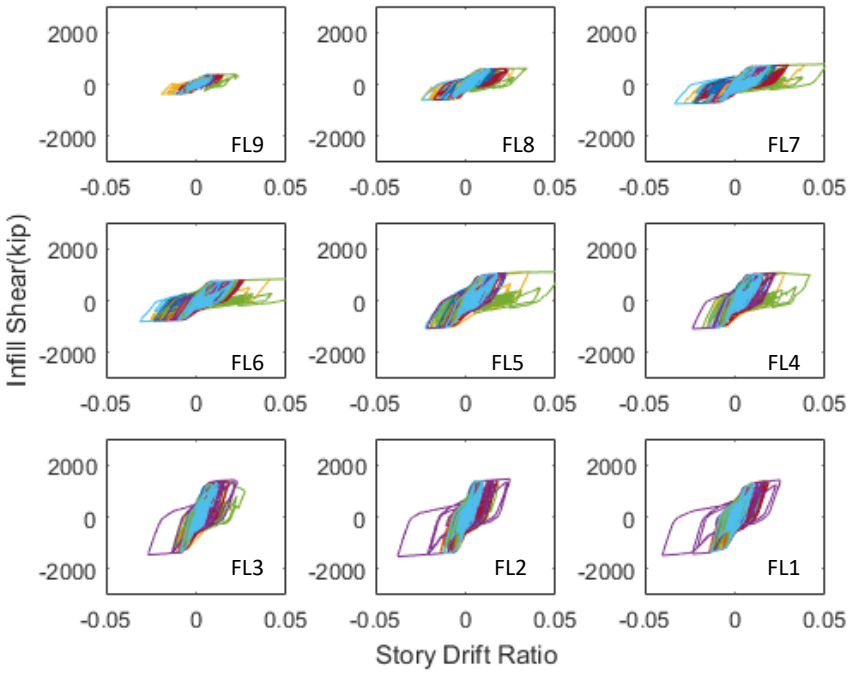

02/50 C9-3

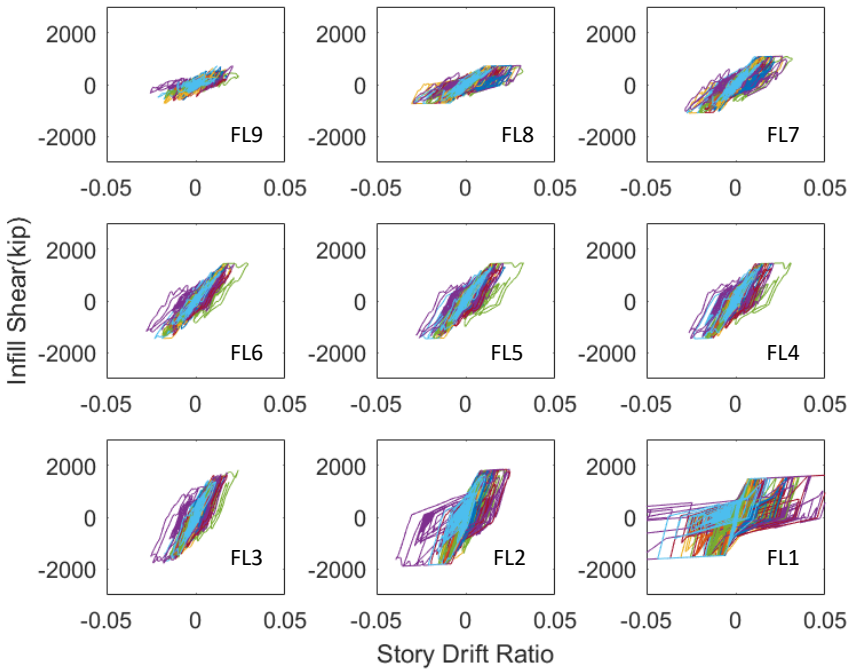

Figure 5.18 Comparison of infill plate hysteresis responses of AISC-DG20 and C9-3 designs at 02/50 hazard level

10/50 AISC-DG20

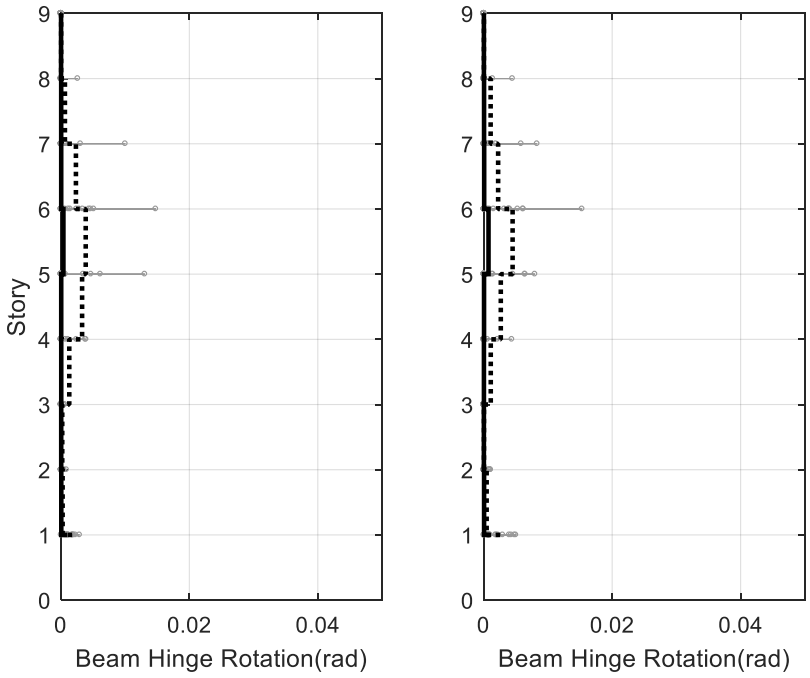

10/50 C9-3

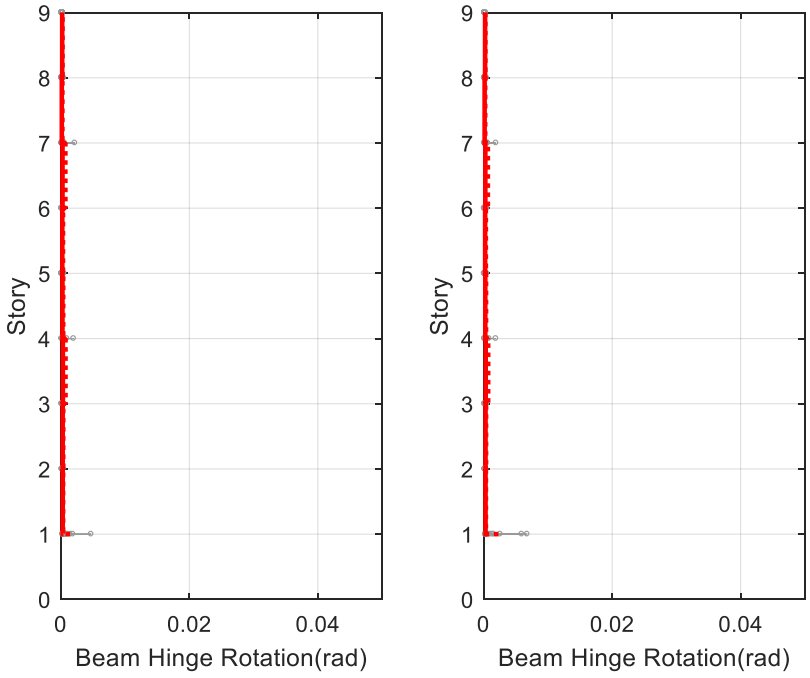

Figure 5.19 Comparison of beam-to-column connection rotation (beam hinge total rotation) responses of AISC-DG20 and C9-3 designs at 10/50 hazard level

02/50 AISC-DG20

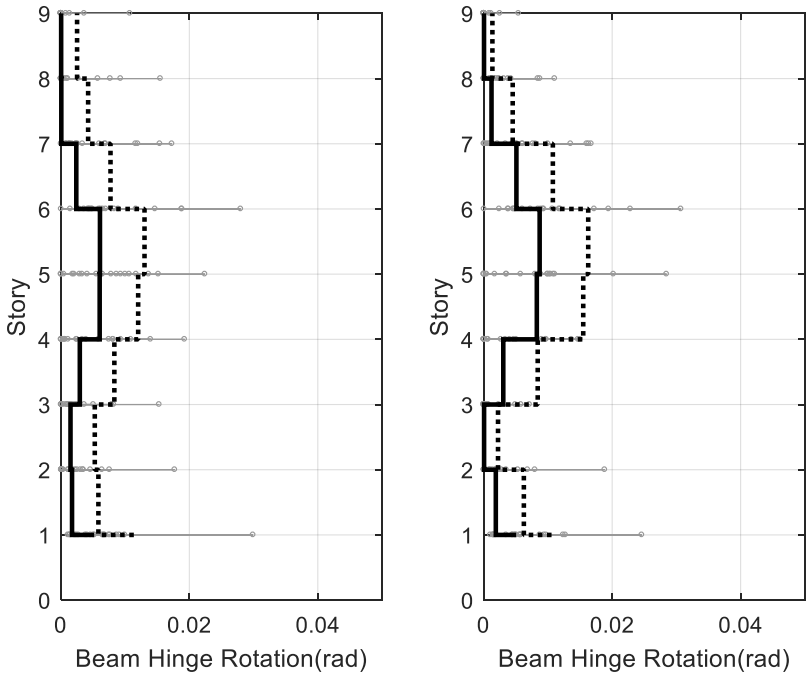

02/50 C9-3

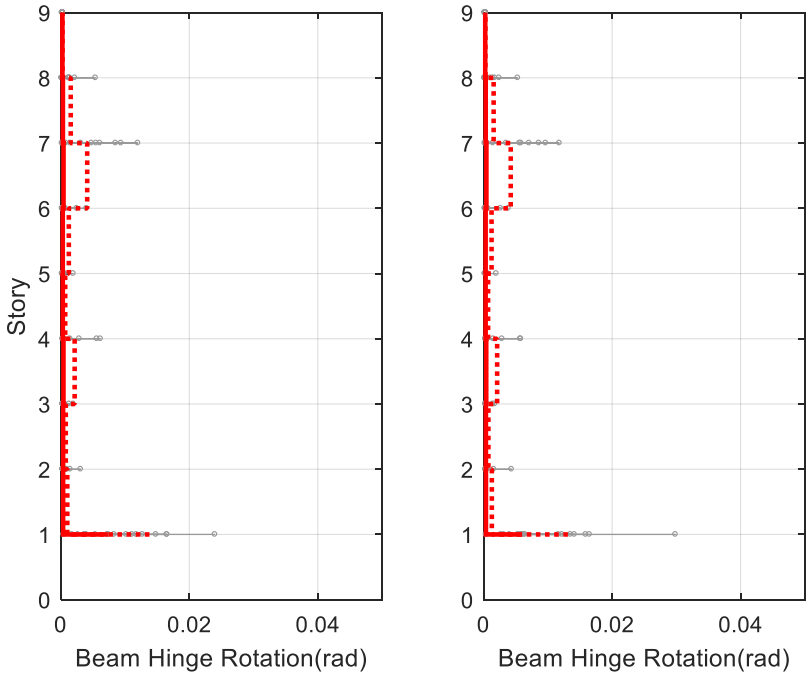

Figure 5.20 Comparison of beam-to-column connection rotation (beam hinge total rotation) responses of AISC-DG20 and C9-3 designs at 02/50 hazard level

5.2.5.5 Column Demand-to-Capacity (D/C) Ratios

The column demand-to-capacity (D/C) ratio can reflect the deformation mode of the system as well as the effect of tension field action on the boundary columns. Figures 5.21–Figure 5.23 show variation of the axial force (P_u/P_y) and bending moment (M_u/M_p) demand-to-capacity ratio as well as the P-M interaction ratio ($M_u/M_p + P_u/P_y$). P_u and M_u are the axial and moment demand obtained from the response history analysis, and P_y is the nominal yielding capacity of the section, calculated as P_y equal to $A_g F_y$, M_p is the nominal plastic moment capacity of the section, calculated as M_p equal to $Z_x F_y$. Note the P-M interaction ratio should be calculated by taking the maximum of the interaction ratio during the time history instead of summing up the maximums of the axial and moment demand capacity ratio. Expected yield strength, strain-hardening ratio, and φ factors were not used in creating the plots in order to provide a relatively direct representation of the results. These coefficients will not affect the shape of the plots but only the absolute values of the demand-capacity ratios. They will be addressed later when assessing the system performance.

It can be seen that the shear wall columns in the AISC-DG20 system were in general subjected to much higher axial and bending demands compared to its HPSPSW counterpart. The oval shape of moment demand capacity ratio is an obvious evidence of the tension field action effect acting on the column. The step increment of the axial force demand capacity ratio also shows this effect. The resulting P-M interaction ratios for AISC-DG20 exceeded two in the median level, and 2.5 at the 84th-percentile level under the 10/50 motions, and were even higher under the 2/50 motions. Such high P-M ratio indicates significant inelasticity in the column. Given that plastic hinge formation at the bottom of first-story column is allowed, it seems unacceptable to have the bottom three and even four columns to have an interaction ratio significantly greater than one. Note that even under the service-level motions, the column interaction ratios for AISC-DG20 were quite noteworthy, with the median ratio of the bottom three stories exceeding 0.6. In addition, the shape of the demand-to-capacity curves indicates that the capacities of the upper three-story columns were not effectively mobilized, while the bottom columns were under-designed.

In contrast, the C9-3 design demonstrated much more uniform demand-to-capacity distributions. Except for the first-story column, all other stories had both median and 84th-percentile interaction ratios smaller than one at 50/30 and 10/50 level hazards. Only the second-story column slightly exceeded one under the 02/50 level motions. The sudden increase of P-M interaction ratio for the first-story columns is mainly due to the increase in the moment demand caused by the fixed-base condition. As the columns are highly ductile, and the foundations will be designed using appropriate over-strength factor, the plastic hinge formation at the base of first-story columns is considered to be acceptable. Instead of changing the column sections, some simple measures, such as providing welded side plates to the column flange and/or web to the base of columns, can effectively increase the moment and axial strength of the base column, thus preventing severe buckling or yielding in the column. Note that these D/C ratio values are for the much lighter frame sections used in the C9-3 design. This comparison shows how effective it can be to relieve the columns from the tension field action by using the HPSPSW configurations. Design-wise, the C_m factor in calculating the second-order effect is 1.0 for columns with mid-height transverse forces, but it is only 0.6 for the case without mid-height forces. This can also explain why disconnecting the infill panel from the column is so effective.

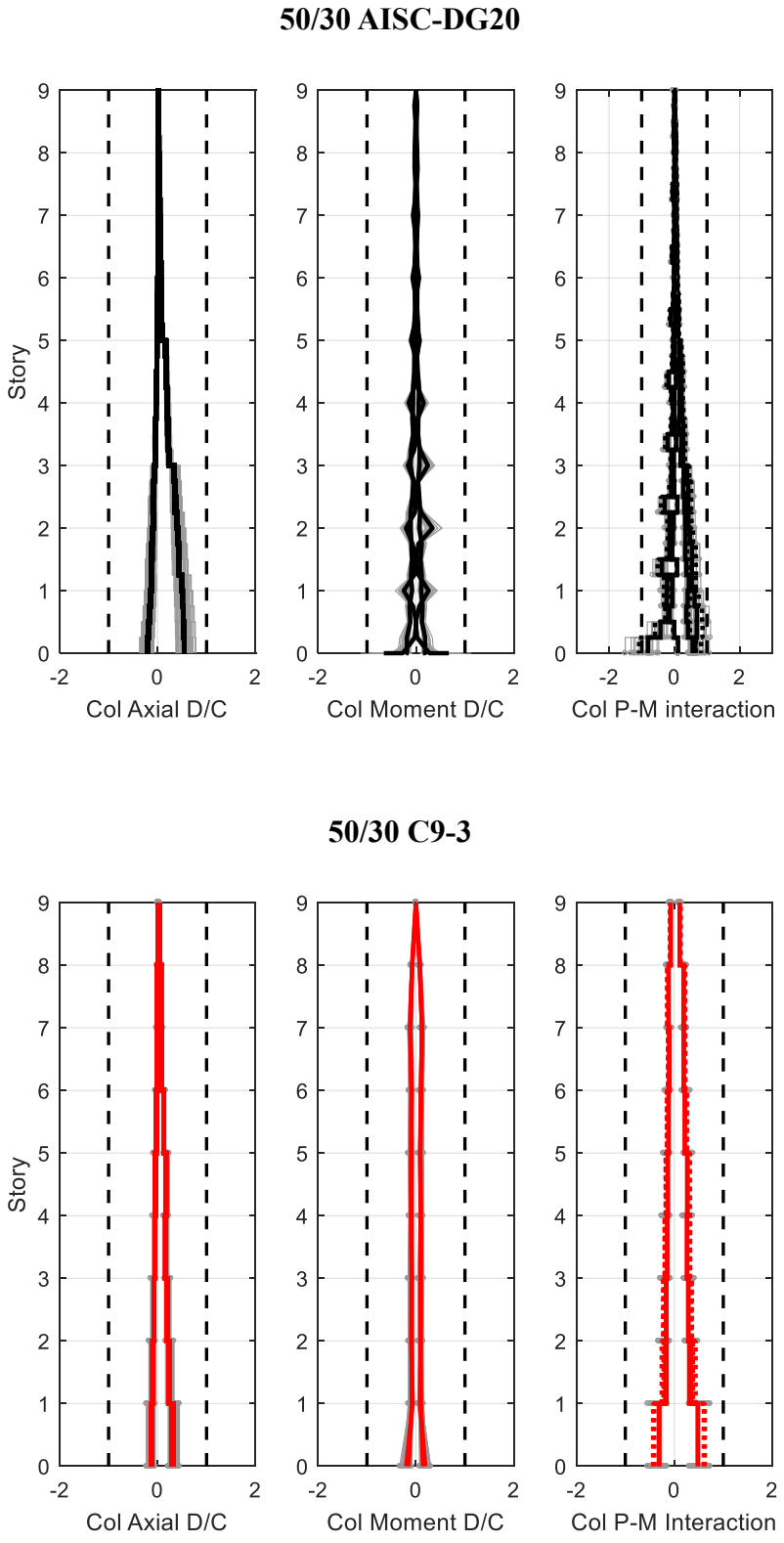

Figure 5.21 Comparison of shear wall column demand-capacity responses of AISC-DG20 and C9-3 designs at 50/30 hazard level

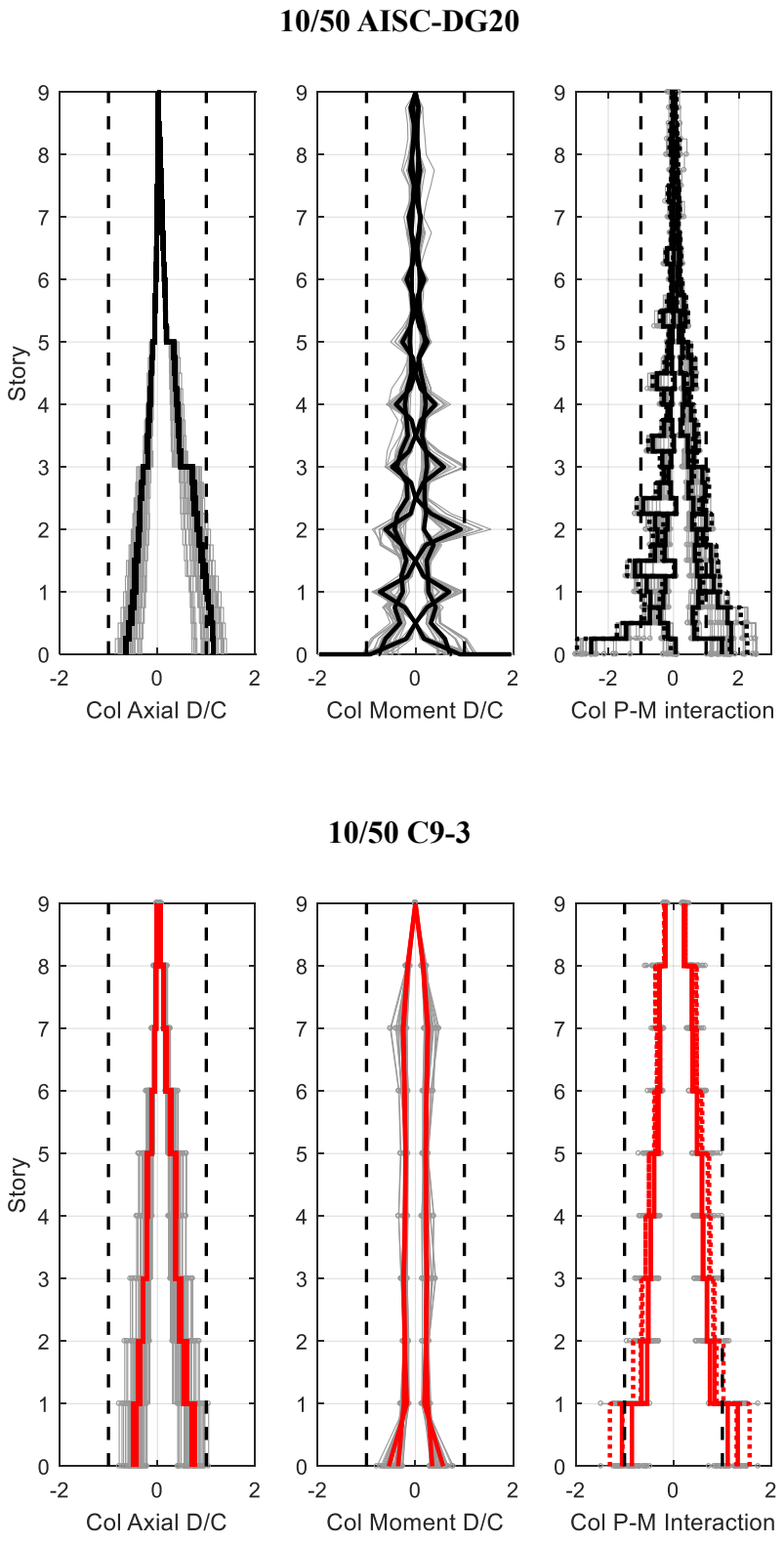

Figure 5.22 Comparison of shear wall column demand-capacity responses of AISC-DG20 and C9-3 designs at 10/50 hazard level

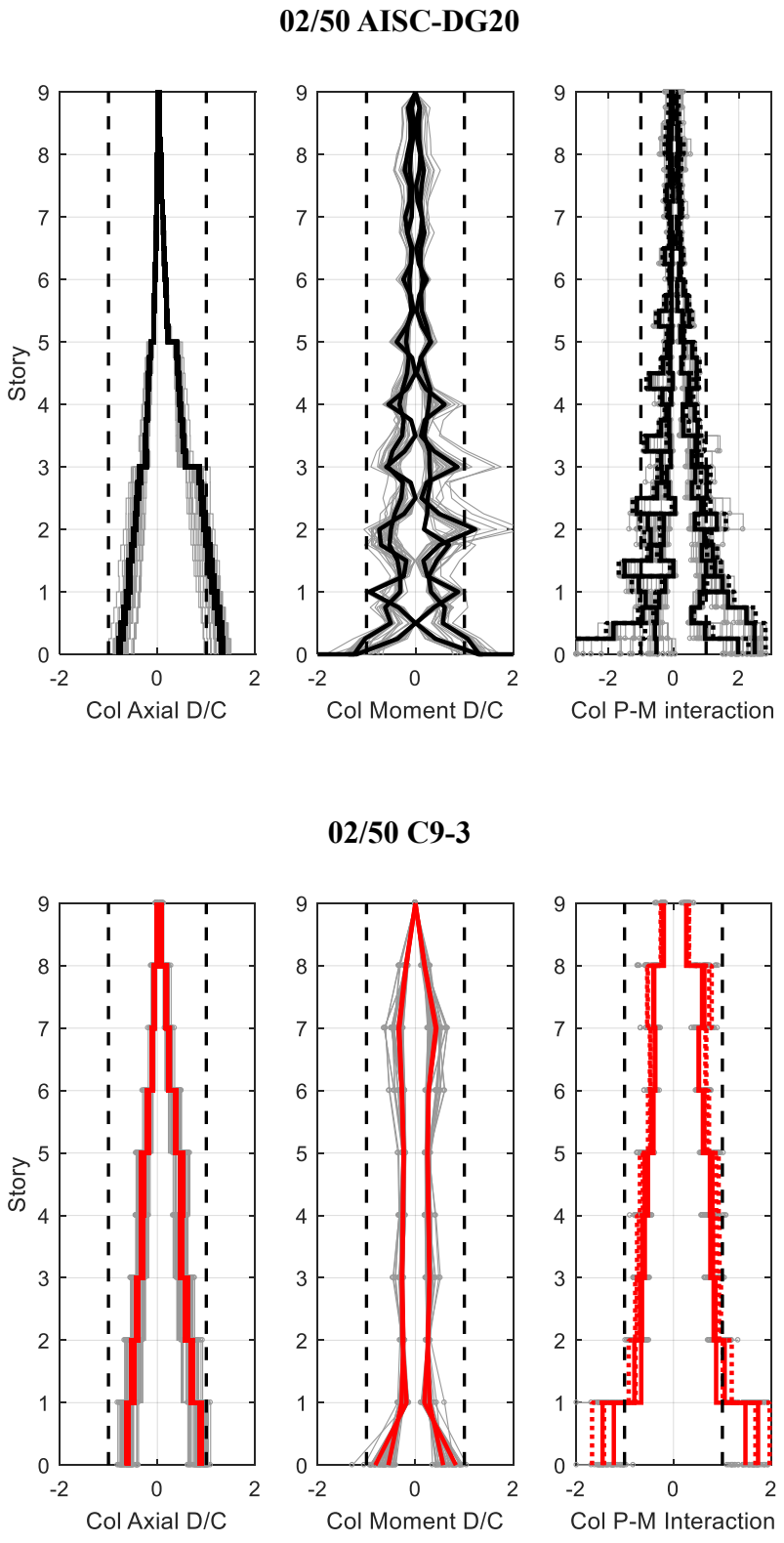

Figure 5.23 Comparison of shear wall column demand-capacity responses of AISC-DG20 and C9-3 designs at 02/50 hazard level

Notice that even when the AISC-DG20 design shear wall columns were significantly over-stressed, a soft-story mechanism did not form as suggested by the story drift responses. This could be because the columns underwent significant strain hardening after yielding (strength degradation was not included for the columns), which counteracted the softening effect of P-delta action. Another reason could be that the side moment frames in AISC-DG20 design outside the shear wall bay helped to prevent formation of a soft story formation. As will be seen in Section 5.3, when using larger side moment frames, the soft-story problem of C9-3 design is easily preventable.

5.2.6 Evaluation of Code-Based Design Responses

After a detailed analysis of the 9-story, three-bay design responses, this section evaluates all the designs done for the prototype buildings following the code-based design procedure aiming at establishing a more comprehensive understanding of the seismic behavior of the proposed HPSPSW system. Both median (μ) and 84th-percentile ($\mu+\sigma$) responses were considered.

5.2.6.1 Peak Story Drift Ratio and Residual Drift

Figure 5.24 shows that there is a trend for taller buildings to have smaller story drifts, especially the lower stories for single-bay designs. The 3-story designs normally have the largest drift at the second story, indicating a moment frame type (S-shaped) deformed shape; taller buildings exhibit more of a cantilever type deformed shape. The three-bay mid- and high-rise designs, i.e., C9-3 and C20-3, experienced a soft-story mechanism in the 18-ft first story. This behavior might be because (1) the first story is taller than other stories and prone to form a soft story, and (2) the beam and column sections selected are relatively small and could not provide enough lateral load resistance once the infill plate had yielded under 2/50 level motions. Note that the large 84th-percentile peak story drift and residual drift responses were mainly due to the several extreme motions that had driven the system near collapse. Three out of the twenty earthquakes collapsed C9-3, which is defined as when the maximum story drift exceeds 4% or the residual drift exceeds 1%, while four out of twenty motions collapsed C20-3. These correspond to a probability of 10% and 20% of collapse for C9-3 and C20-3, respectively. The median responses of these two designs, however, were all below 2% even at 2/50 level hazard. Apart from the two designs that suffered from a soft story under 2/50 motions, all the other designs had drift ratios within 2% and 4% at 10/50 and 2/50 hazard level, respectively. For all prototype code-based designs, the peak story drift ratios at the service level were under 0.5% and the residual drift ratios under 0.2% (Figure 5.25), which is a common limit for nonstructural damage and cosmetic repair, even when the systems were not specifically designed for this performance. The 84th-percentile residual drifts were all within 1% for both 10/50 and 02/50 level hazards, a drift limit requiring repair only but no demolition.

Figure 5.24 also shows the amplified story drift ratios in the design process, calculated as the elastic drift (δ_e) multiplied by the C_d factor, which is 6 for steel plate shear walls. It can be seen that the amplified elastic drifts under the ASCE7-10 equivalent lateral forces are, in general, higher than the median response history analysis responses. There is a slight under-estimation of drift level for low-rise buildings (especially the middle stories), and an over-estimation of drift responses for high-rise buildings. For the two 9-story designs, the amplified elastic drift profiles seem to approximately match the 84th-percentile drift responses from response history analysis. A period-dependent C_d value might enhance the performance and economy of the system of different heights. A simpler modification could be to use a slightly smaller C_d value, say, C_d = 5.5, for the new HPSPSW system – a value between the fully connected SPSW and braced-frame.

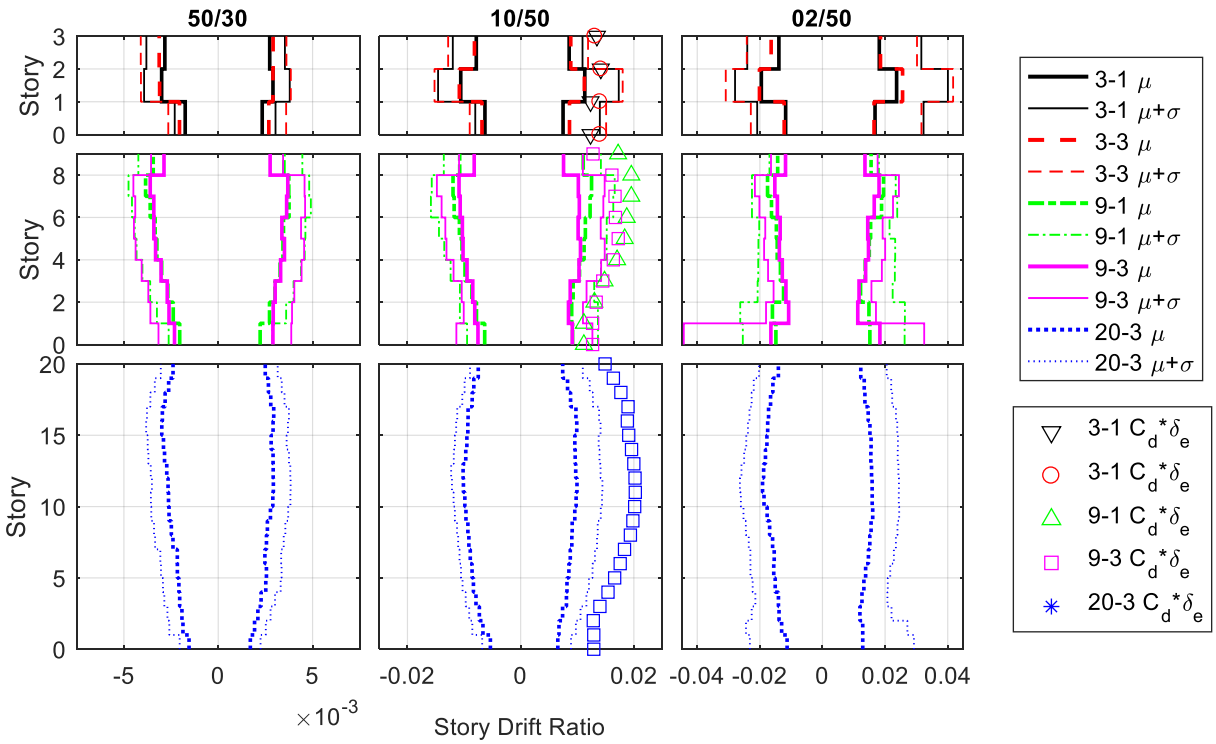

Figure 5.24 Peak story drift ratio profiles for the code-based designs

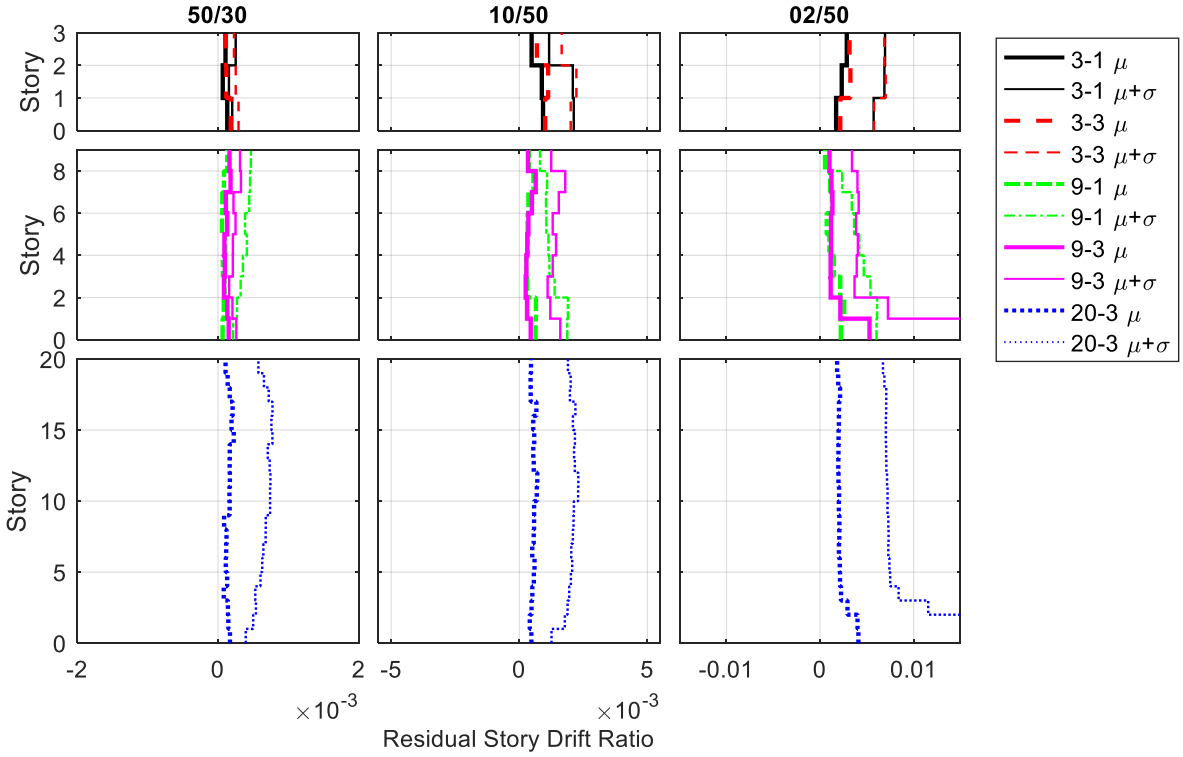

Figure 5.25 Residual story drift ratio profiles for code-based designs

5.2.6.2 Beam Hinge Rotation

Figure 5.26 shows that the connections of the shear wall boundary moment frame were subjected to smaller rotation demands in the taller buildings, which may be explained by the higher dominance of the cantilever action in the taller buildings. In general, the 3-bay designs, had less connection rotation demands compared to one-bay designs, which is likely because of the contribution from the side supplemental moment frames. The relative inactiveness of the upper stories for three-bay designs might be due to the contribution from the side moment frames: the shear wall bay deforms in the cantilever mode in the upper stories, while the side moment connections rotate and help to bring the structure back. The median total rotation of the connections for all designs were smaller than 0.02 even at 02/50 level ground motions, which means the moment connection is unlikely to suffer from severe strength or stiffness deterioration, thus requiring minimum repair.

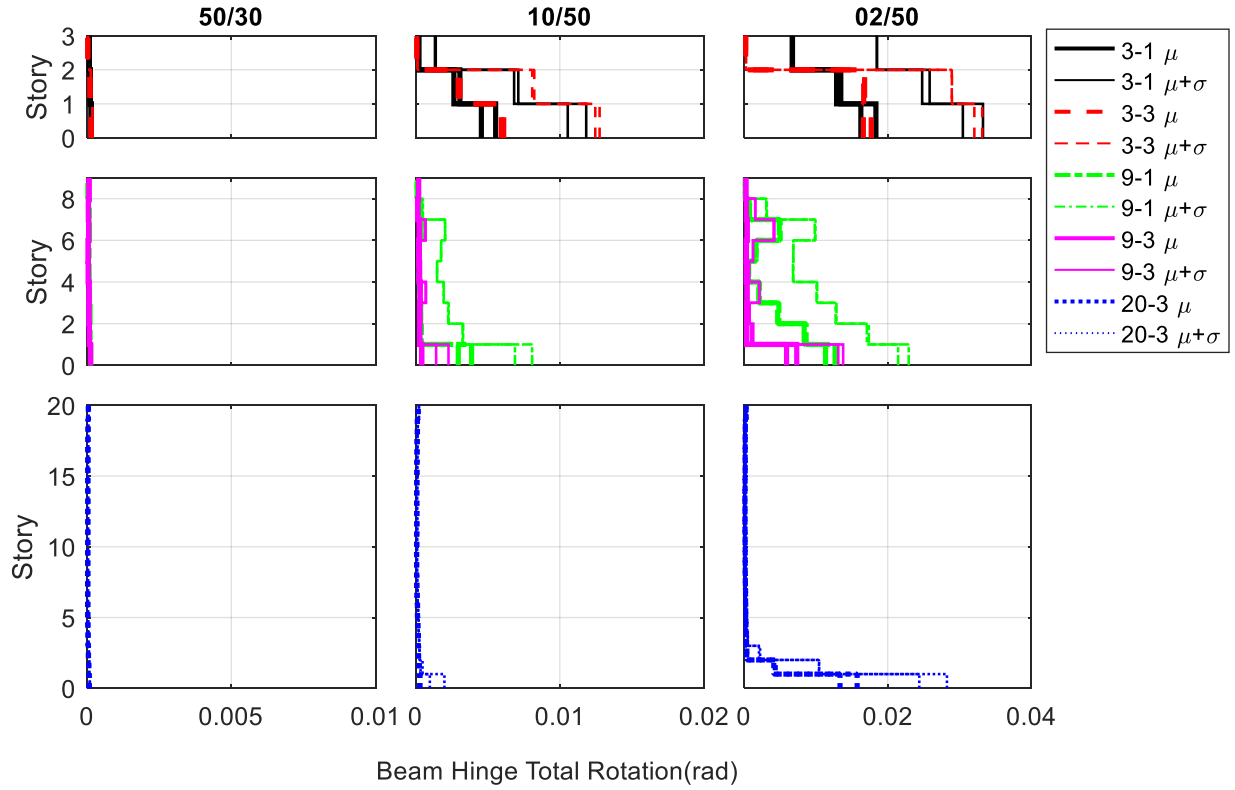

Figure 5.26 Beam hinge total rotation profiles for code-based designs

5.2.6.3 Column Demand-to-Capacity Ratio

The column demand-to-capacity (D/C) ratios presented in Figures 5.27–5.29 were calculated per Section 5.2.5.5. The bending moment D/C ratios for all designs were almost constant with the exception of the first-story column, where the fixed-base condition suddenly increased the moment demand. The constant moment D/C ratio profile is probably the result of yielding of the GPMC, which acts as a ductile fuse and limits the level of the moment that can be develop in the beam-to-

column connection. The axial force D/C ratio increased almost linearly from the top to bottom of the building. The thicker the infill wall, the larger the axial force D/C, which is as expected because part of the axial force in the column comes from the equivalent brace. Apart from the first story, the taller the building, the smaller is the overall P-M interaction ratio. This trend of higher demand on low-rise buildings was also reported for AISC SPSWs (Berman 2011) and Self-Centering SPSWs (Clayton et al. 2012).

At the 10/50 level hazard, which corresponds approximately to the design-based level earthquake, almost all the designs had first-story column yielding, i.e., a median P-M interaction ratio larger than one. At the 02/50 level hazard for most of the designs, the second and even the third story columns had a high probability of yielding, with either the median or 84th-percentile P-M interaction ratio larger than one. If plastic hinge formation at the base of first-story column is acceptable considering the ultimate collapse mechanism, upper story column yielding, even though the P-M interaction ratio is only slightly larger than one, may not be desirable. This indicates a need to increase the column capacity if better performance is desired. Strategies to improve the behavior will be discussed in detail in the next section when discussing the performance-based design of the HPSPSW system.

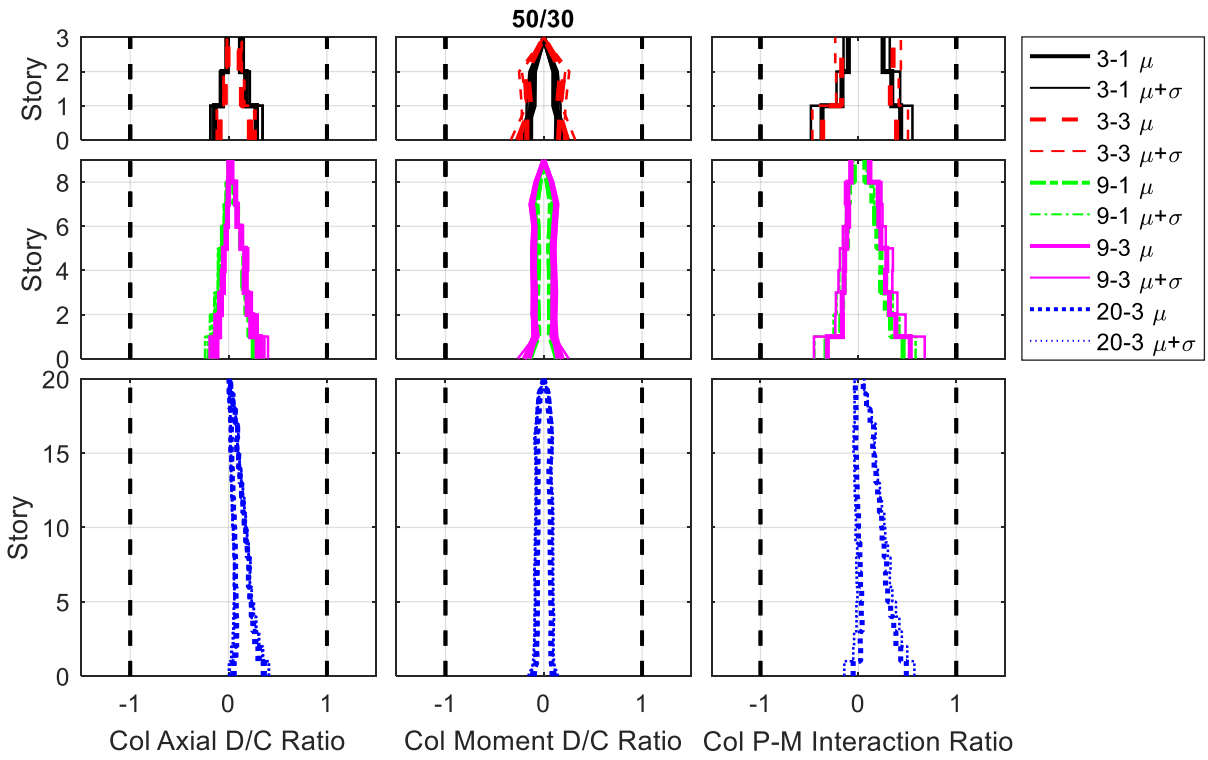

Figure 5.27 Column demand-capacity ratio profiles at 50/30 level hazard for code-based designs

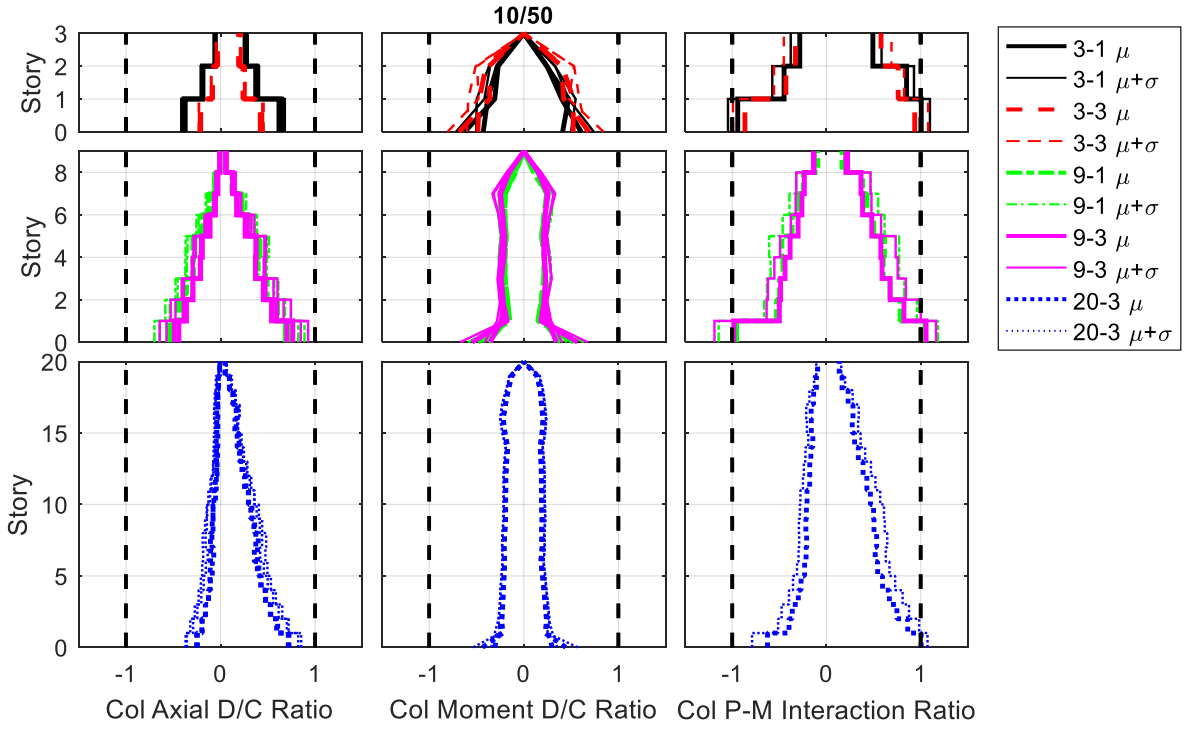

Figure 5.28 Column demand-capacity ratio profiles at 10/50 level hazard for code-based designs

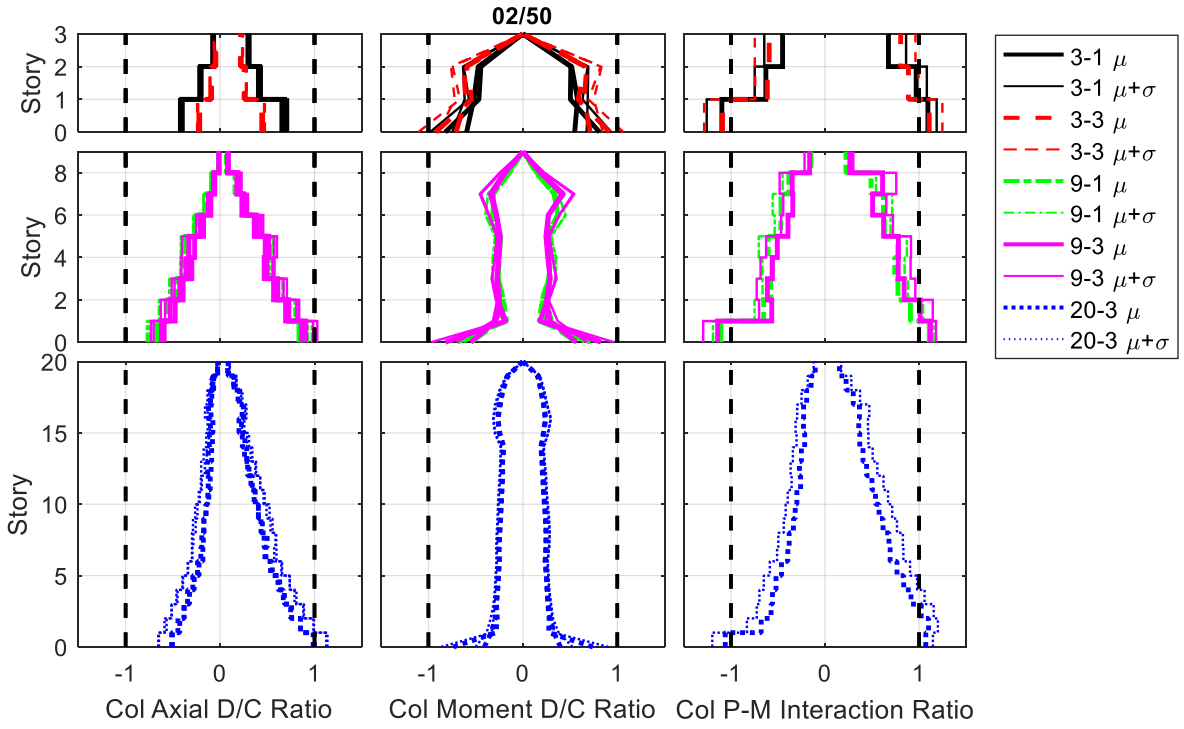

Figure 5.29 Column demand-capacity ratio profiles at 02/50 level hazard for code-based designs

5.2.6.4 Summary

Based on an evaluation of the five prototype designs following the proposed code-based design procedure, a summary of key observations are as follows:

1. The overall performances of the HPSPSW prototype designs are satisfactory but need improvement in several cases. The service-level drift responses are all below the limit requiring cosmetic repair, although none of the designs were specifically designed to meet this criterion. The design level responses for all designs were within common drift limit expected at this level. Relatively uniform drift profiles were achieved with no concern about the beam hinge rotation and column D/C ratio. At the maximum considered level, two out of the five designs suffered soft-story mechanisms shown by the 84th-percentile drift responses, which would require improvement if such behavior is considered unacceptable. A more organized check-list of the performance of these code-based designs will be conducted in the next section following defined performance objectives;

2. The separation of infill wall from the boundary column in the proposed HPSPSW system is very effective in reducing the column demands, as shown by the much lighter column sections used in HPSPSW designs and as observed from the comparison of the P-M interaction ratios for the AISC-DG20 and C9-3 designs. Although the global drift response of C9-3 design did not significantly improve compared to the AISC-DG20 design, the frames used in C9-3 are very light, therefore, the seismic performance of the system has the potential to be improved significantly;

3. In general, the HPSPSW designs based on the proposed code-design procedure can lead to a median story drift less than 2% at 10/50 level hazard and less than 4%, even 3% for 9- and 20-story buildings, at 02/50 level hazard if the data points indicating collapse are excluded. All designed systems have 10% or slightly higher probability of collapse. The 20-story design has the highest probability of collapse, although it has the least P-M interaction ratios in the shear wall boundary columns;

4. A weak-story mechanism is most obvious in the C9-3 and C20-3 designs, which have relatively light frame sections compared to their one-bay counterparts;

5. The beam-hinge rotations are all below 0.02 radians in the median level and 0.035 radians in the 84th-percentile level at all hazard levels;

6. In general, shorter buildings are subjected to higher connection rotation demand and column demands compared to taller buildings. A design factor correlated to the building height could be helpful to avoid under-design of low-rise frames;

5.3 Performance-Based Design Approach

5.3.1 Introduction

In the previous section, the performances of HPSPSW designed based on existing code requirements were evaluated. With the current trend of requiring better performance and clearer performance goals at each specific hazard level, this section investigates a performance-based design procedure for the proposed HPSPSW system.

5.3.2 Performance Objectives

The proposed performance-design approach has three main performance objectives, referred to as service- level (SL), design-level (DL) and maximum considered level (MCL) points. Service level includes small frequent earthquakes and service wind loads. The performance objectives are explained in detail as follows:

1. **Service Level**: at the service-level hazard (50% in 30 years) and wind loads, infill plate elastic buckling should be avoided, and limited damage should be imposed on the non-structural elements with only cosmetic repair required.

   According to the study by Baldvin et al.(2012), the median drift for cosmetic repair for steel shear wall systems is 0.4% (1/250), including the limit states of buckling of infill plate, initial yielding of infill plate, and initial local buckling and initial yielding of boundary beams and columns. This is slightly lower than the recommended drift limitation of 0.5% (1/200) by the Tall Buildings Initiative (TBI) (PEER 2010) for service-level earthquakes, which aims to provide some protection to non-structural elements and assures permanent drift is negligible. The Chinese code recommends a drift limit of 0.286% (1/350) for unstiffened steel plate shear walls under wind and frequent earthquakes(JGJ 2015). This is considered slightly conservative. Considering these suggested values, and the fact that the proposed HPSPSW will normally have thicker infill plates than the AISC SPSWs, a value of 0.5% widely used by the structural design community seems to be suitable for the proposed HPSPSW system.

   A reasonable quantifiable residual drift limit that can be used is 0.2% (1/500), which corresponds to the out-of-plumb limits for construction (ATC 2009). In Section 5.2.6, all HPSPSWs designed according to existing code requirements show residual drifts below 0.1%. Thus, it seems that 0.2% is a reasonable and probably conservative limit for residual drift check.

   At the service-level earthquakes and wind loads, the frame should remain elastic with negligible moment connection rotation, and the demand-to-capacity ratio of the column should be much less than one. Since the entire system is supposed to remain essentially elastic during the service-level motions, which corresponds to a “low-seismic” scenario, use of the nominal material property instead of actual expected properties can be justified when computing the capacity.

Due to the similarity in connection configuration and lack of test results for the new GPMC, the acceptance criteria stated for the welded top and bottom haunches in FEMA 356 (FEMA-356 2000) could be used as a probably conservative limit for the connection rotation. The service-level limit is considered correspond to the immediate occupancy (IO) level, which has a plastic rotation angle limit of 0.007 radians. In ASCE 41-13 Table 9-6, the acceptance criteria for this level is 0.014 (ASCE 2013), which is about twice the value specified in FEMA 356. This value (0.014) is considered slightly too large for moment connections in a steel shear wall system at the service level; the infill wall would have experienced serious buckling at a story drift of 0.014. Therefore, the smaller limit of 0.007 is adopted here.

2. **Design Level**: At the 10%-50 year level seismic hazard, or approximately the design-based earthquake (DBE), life safety must be ensured, and functionality should be maintained. Only repairable damage is allowed for both structural and non-structural elements.

   To ensure repairable damage to non-structural elements, story drift should be limited to the code-based limit, i.e., 2%. This is also the drift limit for unstiffened SPSW at design-level earthquake required by the Chinese code (JGJ 2015). The TBI does not include a specific drift requirement at design-level earthquakes, but only at the service- and maximum-considered levels. At 2% drift, conventional fully connected SPSWs may experience considerable yielding in the boundary columns; see Balvins et al. (2012). However, as the proposed new HPSPSW is better able to maintain the elasticity in the boundary elements and limit the inelasticity in the easily repairable infill walls, 2% is considered as an acceptable drift limit at the design level hazard for the new HPSPSW to limit damage, although it might be not suitable for conventional SPSWs. Without too many references in the literature, the residual drift limit at the design-based level is selected to be 0.5%, which is half of the commonly adopted 1% residual drift limit at the maximum-considered level.

   Some limited yielding in the GPMC used in the proposed HPSPSW is allowed as repair of beams requires much less effort than columns. Details and procedures for repair of some moment connections can be found in FEMA 352 (FEMA-352 2000). Similarly, the acceptance criteria for the welded top and bottom haunches is adopted, and the plastic rotation for the Life Safety (LS) limit for primary connections is considered a reasonable and conservative limit for the design-level connection rotation check. In ASCE 41-13 Table 9-6, the acceptance criteria for this level is 0.036 radians (ASCE 2013), which is the same as the LS acceptance criteria for secondary connections in FEMA 356.

   The columns should remain essentially elastic at this level. This can be quantified by checking that the demand-to-capacity ratio of the column to be smaller than one. A demand-to-capacity ratio of one or slightly higher is acceptable for the base of the first-story column. As recommended in both the Tall Building Initiative report and ASCE 41-13 (ASCE 2013; PEER 2010), expected material properties, instead of the minimum specified properties, can be used in establishing the capacity.

3. **Maximum Considered Level**: at this level (2%-50 year) of seismic hazard, collapse should be prevented, and damage should be limited. Some residual drift and yielding in the frame is allowed, but soft-story mechanism or fracture of the GPMC should be prevented.

   A target peak story drift limit for the maximum considered level chosen by Clayton et al. (2012) for the self-centering SPSW is 4%. This is higher than the 2.75% limit classified as the median drift that needs replacement of entire system for the conventional SPSW proposed by Baldvins et al. (2012). The Tall Building Initiative (TBI) suggests limiting the mean peak story drift to 3% and the maximum of any run to be less than 4.5% (PEER 2010). The TBI also recommends limiting the mean residual drift to 1% and the maximum residual drift of any run to 1.5%. Considering the high ductility of the steel shear wall system, the story drift limit for the 2%-50 year level is selected to be 4%, and residual drift limit is chosen to be 1%.

   To avoid fracture of the connection, the Collapse Prevention (CP) plastic rotation limit for welded top and bottom haunches in ASCE 41-13 Table 9-6 is adapted here, which is 0.048. This is the same as the CP acceptance criteria for secondary connection in FEMA 356 Table 5-6(FEMA-356 2000).

   The demand-to-capacity ratio for the columns at this level should still be below one, except at the base of the first-story column where plastic hinge formation in the column is allowed. Again, expected material properties will be used. As strain hardening is expected at this intensity level, the author of this dissertation proposes to include the strain-hardening factor, C_{pr}, defined in AISC Seismic Manual (AISC 2010c, AISC 2016b) in addition to the expected material properties in establishing the capacity.

   Note that the Tall Building Initiative (PEER 2010) states that for force-controlled elements, the demand should be obtained from statistical evaluation of nonlinear response history analysis. It states "… *where the computed demand for an action is not limited by a well-defined yielding mechanism, use 1.5 times the mean. Where the computed demand for an action is limited by a well-defined yield mechanism, use the mean plus 1.3 times the standard deviation obtained from the individual response history analyses but not less than 1.2 times the mean*" (PEER 2010, Section 8.6.1). These values are provided to account for the inadequate standard deviation value resulting from a small number of ground motions (less than 20). In this study, twenty ground motions were used, and thus the standard deviation can be considered accountable. In the following performance evaluation, both the median and the 84^{th}-percentile responses for the computed column demands without any amplification are compared with the proposed performance limits.

   One thing worth mentioning is that the columns inside a moment frame or a steel shear wall frame have a well-defined yield mechanism; normally, only the axial force action is considered force-controlled action. However, as ASCE 41-13 states, for "*steel columns with axial compressive forces exceeding 50% of the lower-bound axial compressive strength, P_{CL}, shall be considered force controlled for both axial loads and flexure and shall be evaluated using*

Eq.(9-12)", which is the P-M interaction equation. As observed in Section 5.2.5, the columns in the lower floors will, in general, exceed this 50% axial demand threshold. Therefore, instead of evaluating only the axial force demand-capacity ratio [e.g. (Berman 2011)], the P-M interaction ratio is selected as the primary parameter to evaluate column performance.

Table 5.8 summarizes the suggested performance objectives based on the available literature, common profession practices and current and best knowledge of the new system. If twenty or more ground motions are used, all the demand quantities obtained from the response history analysis to be checked against the following table should be mean plus one standard deviation (84th-percentile) responses unless otherwise justified. Otherwise, appropriate amplification of the mean responses or maximum responses should be used as required by documents like ASCE41, TBI, and LATBSDC (ASCE 2013; LATBSDC 2015; PEER 2010).

Table 5.8 Suggested performance objectives for the proposed HPSPSW system

Hazard Level	**Service Level and Wind (50% in 30 years)**	**Design Level (10% in 50 years)**	**Maximum Considered Level (2% in 50 years)**
General Objective	Immediate Occupancy and Fully Operational: Infill plate elastic buckling should be avoided and negligible damage should be imposed on the non-structural elements. Only cosmetic repair is required.	Life Safety and Repairable Damage: Only repairable damage is allowed for both structural and non-structural elements. Only significant yielding in the infill plate, which is easy to repair, and some limited yielding in the gusset plate moment connection are allowed. The columns and beams should remain essentially elastic.	Collapse Prevention: Some residual drift and yielding in the frame are allowed, but soft-story mechanism or fracture of the gusset plate moment connection should be prevented.
Peak Story Drift Ratio	0.5%	2%	4%
Residual Story Drift Ratio	0.2%	0.5%	1%
Beam-to-Column Connection Plastic Rotation	0.007	0.036	0.048
Column Demand-to-Capacity Ratio	<1.0 Use nominal capacity and φ factor	<1.0 other than base of the first story columns Use expected capacity and φ factor	<1.0 other than base of the first story columns Use expected capacity including strain-hardening and φ factor

The above performance objectives were chosen by the author of this dissertation based on the literature and best knowledge of the new system. However, these objectives are fairly general in

nature and just one possible set of performance objectives; the designers have the freedom to modify the suggested values depending on specific project needs.

5.3.3 Design Procedure

The key difference in the performance-based design procedure and the code-based design procedure is that the former will need iterations to satisfy specific performance objectives, while the latter only needs to satisfy a set of drift and strength requirements without the need to evaluate the actual performance of the resulting design through analysis. The following is a flow chart outlining the major steps in the performance-based design procedure.

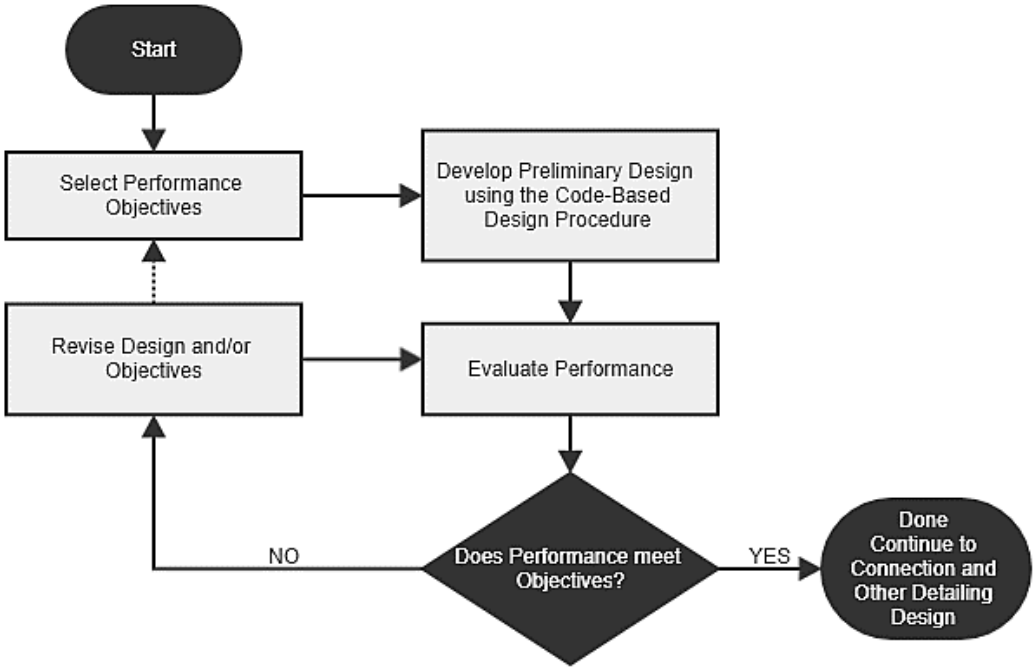

Figure 5.30 Performance-based design flow chart (modified from Hamburger, 2003)

Design Steps:

1. Define performance objectives depending on specific project needs. Suggested performance objectives are defined in Section 5.3.2 and summarized in Table 5.8.

2. Develop preliminary design. Preliminary design is a crucial starting point as it outlines the performance objectives that must be addressed in the final design. For the proposed HPSPSW, the code-based design procedure was used to develop the preliminary design. This is because the code-based designs were relatively well proportioned using the best knowledge of the new system and showed reasonably satisfactory performance (Section 5.2).

   Note: the first performance point defined in this dissertation was the service-level

earthquake having 50% exceedance in 30 years as defined in TBI report (PEER 2010). For some projects, the 50%-50 year hazard may be chosen as the first performance point. For certain locations, such as Los Angeles, the 50%-50 year hazard may be relatively high compared to the 10%-50 year hazard reduced by the *R* factor. With much higher ground motion intensities, it will be less likely that the first performance point objectives will be satisfied without specifically designing for them. In this case, the designers may wish to design the infill plate according to the 50%-50 year Uniform Hazard Spectrum in the preliminary design step instead of the reduced design based level forces ($V_{10/50}/R$). Note that the design story shear force should not be reduced by *R* factor at this level, i.e., use $V_{50/50}$ instead of using $V_{50/50}/R$.

3. Evaluate performance of the preliminary design. Performance capability should be evaluated against the chosen performance objectives, which serves as the primary basis for proposing necessary modifications of the design.

4. Modify the design until all the performance objectives determined in Step one are satisfied. If the performance objectives cannot be satisfied after multiple attempts that cover the practical upper and lower bound designs, the designer may go back to the preliminary design steps and modify the number and geometry of the HPSPSW bays. When justifiable, reasonable modification of the performance objective can be made.

5.3.4 Evaluation of Preliminary Design

As discussed above, code-based designs can serve as a good starting point for the preliminary design. Table 5.9 summarizes the maximum response parameters among all floors; Table 5.10 checks the maximum values plotted in Figures 5.24–5.29 against the performance objectives defined in Section 5.3.2; a value greater than one means the design requires modification. In the values presented in Tables 5.9 and 5.10, the beam-hinge total rotation was converted to plastic rotation, and the column P-M ratio was modified to include the expected material property and φ factor in order to be consistent with the performance criteria.

Table 5.10 shows that the preliminary designs can, in general, satisfy the deformation-controlled performance objectives such as peak story drift, residual drift, and connection rotation, except for cases C9-3 and C20-3, which formed a weak-story mechanism at the bottom floor. For all designs except C3-3, the median column D/C at 10/50 level exceeded 1.0 slightly (within 10%), with a higher exceedance at the 84th-percentile level. This indicates yielding in the shear wall boundary columns. At the maximum considered level, the P-M interaction ratios become even higher, indicating more severe yielding and plastic hinge formation in the columns. It is acceptable to have the maximum P-M interaction ratios occur at the base of the first-story column based on the proposed performance objectives considering the desired plastic mechanism. However, the P-M interaction ratio profile plots showed that in some designs, such as C3-1, C3-3, C9-3 and C20-3, the columns had yielded in stories other than the first story, and thus modification would be required. None of the designs had any issue with the beam-to-column connection rotations. Shorter buildings had larger connection rotation demands, but the maximum 84th-percentile plastic rotations were less than 0.03 even at the 2%-50 year level hazard.

Table 5.9 Maximum responses among all floors for code-based preliminary design

Design	Hazard	Peak story drift		Residual drift		Beam hinge plastic rotation		Column P-M	
		median	84th percentile	median	84th percentile	median	84th percentile	median	84th percentile
C3-1	50/30	0.30%	0.39%	0.01%	0.03%	0.000	0.000	0.39	0.50
	10/50	1.13%	1.73%	0.09%	0.21%	0.002	0.008	1.01	1.10
	02/50	2.37%	4.01%	0.29%	0.69%	0.014	0.029	1.10	1.26
C3-3	50/30	0.31%	0.41%	0.02%	0.03%	0.000	0.000	0.35	0.46
	10/50	1.13%	1.80%	0.11%	0.22%	0.002	0.009	0.94	1.08
	02/50	2.56%	4.17%	0.32%	0.70%	0.014	0.029	1.11	1.29
C9-1	50/30	0.39%	0.49%	0.01%	0.05%	0.000	0.000	0.41	0.53
	10/50	1.25%	1.66%	0.06%	0.19%	0.000	0.005	1.05	1.18
	02/50	1.95%	2.63%	0.26%	0.61%	0.009	0.020	1.11	1.19
C9-3	50/30	0.37%	0.46%	0.02%	0.03%	0.000	0.000	0.48	0.61
	10/50	1.09%	1.48%	0.06%	0.18%	0.000	0.000	1.06	1.19
	02/50	1.83%	4.43%	0.53%	2.35%	0.003	0.009	1.14	1.30
C20-3	50/30	0.30%	0.38%	0.02%	0.08%	0.000	0.000	0.44	0.51
	10/50	1.02%	1.44%	0.07%	0.23%	0.000	0.000	1.01	1.07
	02/50	1.91%	2.92%	0.41%	1.77%	0.012	0.025	1.10	1.20

Table 5.10 Evaluation of the code-based preliminary designs (maximum responses/performance objectives ratio)

Design	Hazard	Peak story drift		Residual drift		Beam hinge plastic rotation		Column P-M	
		median	84th percentile	median	84th percentile	median	84th percentile	median	84th percentile
C3-1	50/30	0.60	0.79	0.07	0.13	0.00	0.00	0.43	0.55
	10/50	0.57	0.87	0.19	0.42	0.05	0.22	1.02	1.11
	02/50	0.59	1.00	0.29	0.69	0.30	0.61	0.99	1.14
C3-3	50/30	0.63	0.82	0.09	0.15	0.00	0.00	0.39	0.51
	10/50	0.56	0.90	0.22	0.45	0.06	0.24	0.95	1.09
	02/50	0.64	1.04	0.32	0.70	0.29	0.61	1.00	1.16
C9-1	50/30	0.77	0.98	0.07	0.23	0.00	0.00	0.46	0.58
	10/50	0.63	0.83	0.13	0.38	0.01	0.13	1.06	1.20
	02/50	0.49	0.66	0.26	0.61	0.19	0.41	1.00	1.08
C9-3	50/30	0.74	0.92	0.09	0.16	0.00	0.00	0.53	0.68
	10/50	0.54	0.74	0.13	0.36	0.00	0.00	1.07	1.20
	02/50	0.46	1.11	0.53	2.35	0.06	0.20	1.03	1.17
C20-3	50/30	0.60	0.77	0.11	0.39	0.00	0.00	0.49	0.57
	10/50	0.51	0.72	0.14	0.46	0.00	0.00	1.02	1.08
	02/50	0.48	0.73	0.41	1.77	0.26	0.52	1.00	1.09

5.3.5 Modification of Preliminary Design to New Design

Modification of the preliminary designs were carried out based on the performance assessment. For designs that failed to meet the deformation performance objectives, major revisions to the frame sections or even the infill plate thicknesses were carried out. For other designs where only the column strength objectives were violated, only simple local modification of the column sections was needed. The following discusses the process of design revisions for C9-3 and C20-3.

5.3.5.1 Design C9-3

For this design, a soft-story mechanism occurs in the first story, where the story height is taller than other stories. The first trial modification was simply to increase the first-story column cross section, which was changed from W14×370 to W14×455 for the shear wall columns and W14×176 to W14×233 for the moment frame columns. This corresponds to approximately 25% increase in area, moment of inertia and section modulus. Since the main issue was at the maximum considered level, response history analysis was done only for the 2%-50 year level to evaluate whether further modifications were needed. After modifying the first-story column, the large 84th-percentile residual drift was effectively reduced, and the number of ground motions that resulted in collapse was also reduced from 3 to 2. However, with the deformation performance objectives satisfied, the column P-M ratio still indicated a need for further modification because the 84th-percentile P-M ratio for the lower three stories all exceeded the acceptable limit of one. Although the exceedance is not significant, yielding of column other than first-story column at the base was considered unacceptable. Therefore, a second revision was made, in which the column sections for all lower four floors were increased. For this second revised design, the second-floor columns achieved a P-M interaction ratio just below one at the 84th-percentile.

Figure 5.31 shows the drift and acceleration responses before and after design revisions for design case C9-3. Table 5.11 shows the change of frame sections for these design revisions. The change of peak story drift, floor acceleration, residual drift responses as well as the column demand-to-capacity ratios for the design revisions can be found in Appendix E2.

For this three-bay 9-story design, to resolve the drift problem only the column sizes were increased slightly. However, as can be seen in the next example, when the number of stories becomes larger, the revision process becomes complicated as the effects of higher modes become more pronounced.

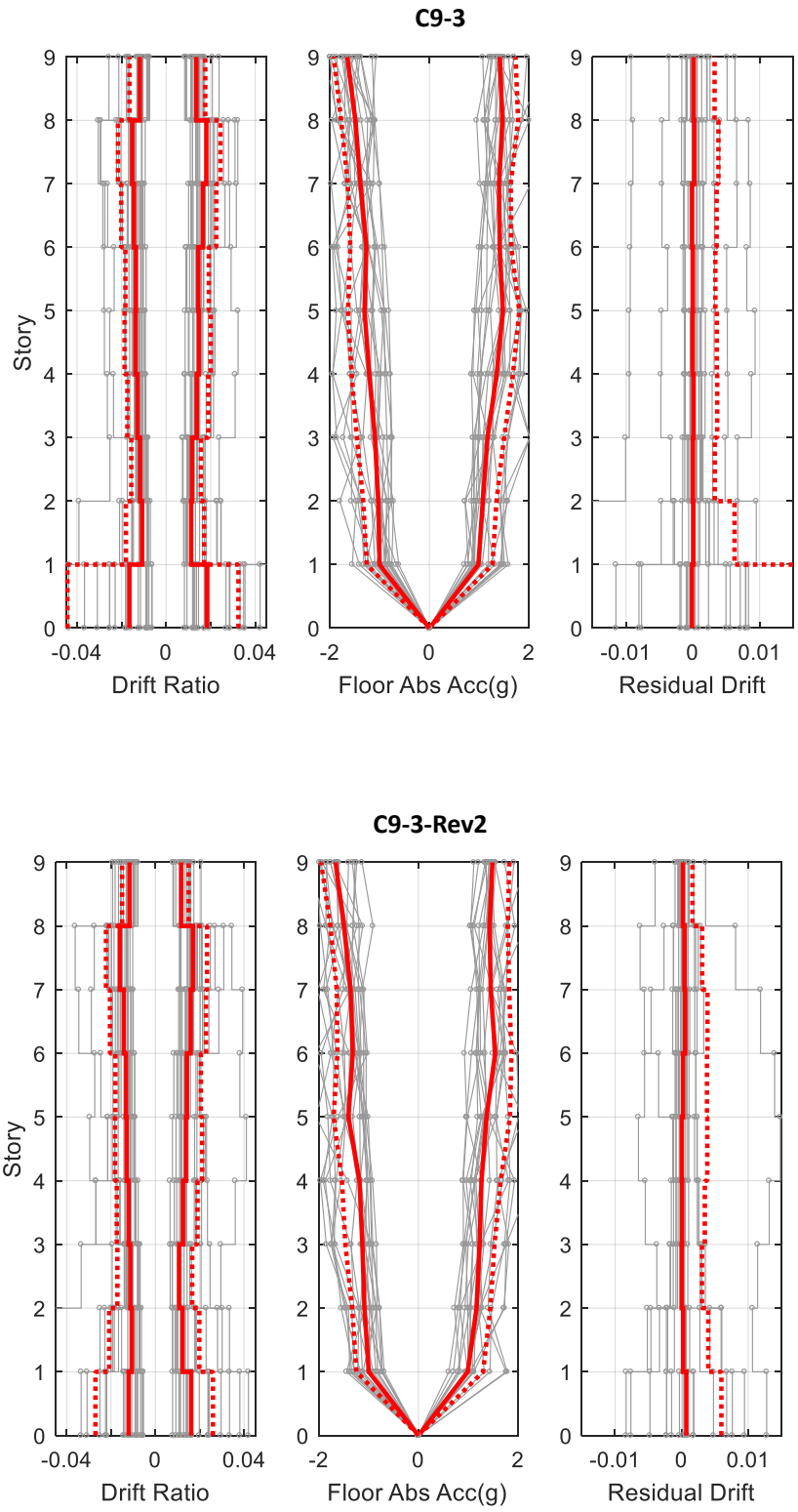

Figure 5.31 Drift and acceleration responses of C9-3 design before and after design iterations at 02/50 level motions

Table 5.11 Design Revisions for C9-3

	Design Case C9-3					Design Case C9-3-Rev1				
Story	t_p (in)	Shear Wall Column	Shear Wall Beam	Moment Frame Column	Moment Frame Beam	t_p (in)	Shear Wall Column	Shear Wall Beam	Moment Frame Column	Moment Frame Beam
6	1/4	W14X283	W21X122	W14X159	W21X122	1/4	W14X283	W21X122	W14X159	W21X122
5	1/4	W14X283	W21X122	W14X159	W21X122	1/4	W14X283	W21X122	W14X159	W21X122
4	1/4	W14X370	W21X122	W14X176	W21X122	1/4	W14X370	W21X122	W14X176	W21X122
3	5/16	W14X370	W24X131	W14X176	W24X131	5/16	W14X370	W24X131	W14X176	W24X131
2	5/16	W14X370	W24X131	W14X176	W24X131	5/16	W14X370	W24X131	W14X176	W24X131
1	5/16	W14X370	W24X131	W14X176	W24X131	5/16	W14X455	W24X131	W14X233	W24X131

Design Case C9-3-Rev2					
Story	t_p (in)	Shear Wall Column	Shear Wall Beam	Moment Frame Column	Moment Frame Beam
6	1/4	W14X283	W21X122	W14X159	W21X122
5	1/4	W14X283	W21X122	W14X159	W21X122
4	1/4	W14X455	W21X122	W14X233	W21X122
3	5/16	W14X455	W24X131	W14X233	W24X131
2	5/16	W14X455	W24X131	W14X233	W24X131
1	5/16	W14X455	W24X131	W14X233	W24X131

*upper three stories are not shown for clarity since no changes were made

5.3.5.2 Design C20-3

Figure 5.32 shows the changes in drift and acceleration responses of the revised designs for C20-3. Table 5.12 shows the revisions of the frame cross sections and infill plate thicknesses. More details of the change of drift and column demand-to-capacity responses can be found in Appendix E2. Similar to C9-3, the initial attempt was simply to change the first-story column section. However, almost no improvement was brought in by modifying the first-story columns. This may be because that as the building becomes taller, a single element will not affect the global responses as significantly as is the case in shorter buildings.

The second trial was to increase the column sections for the bottom seven floors using sections even heavier than the first trial, aiming for better force re-distribution along the height of the structure. However, while the column demand-to-capacity ratios saw an obvious decrease–mainly in axial force demand-capacity ratio because the bending demands on columns are mostly controlled by the GPMC capacity–the residual drift issue was not resolved.

Table 5.12 Design Revisions for C20-3

	Design Case C20-3					Design Case C20-3-Rev1				
Story	t_p (in)	Shear Wall Column	Shear Wall Beam	Moment Frame Column	Moment Frame Beam	t_p (in)	Shear Wall Column	Shear Wall Beam	Moment Frame Column	Moment Frame Beam
14	3/16	W14X233	W27X94	W14X176	W27X94	3/16	W14X233	W27X94	W14X176	W27X94
13	3/16	W14X233	W27X94	W14X176	W27X94	3/16	W14X233	W27X94	W14X176	W27X94
12	3/16	W14X233	W27X94	W14X176	W27X94	3/16	W14X233	W27X94	W14X176	W27X94
11	3/16	W14X233	W27X94	W14X176	W27X94	3/16	W14X233	W27X94	W14X176	W27X94
10	3/16	W14X233	W27X94	W14X176	W27X94	3/16	W14X233	W27X94	W14X176	W27X94
9	3/16	W14X233	W27X94	W14X176	W27X94	3/16	W14X233	W27X94	W14X176	W27X94
8	3/16	W14X233	W27X94	W14X176	W27X94	3/16	W14X233	W27X94	W14X176	W27X94
7	3/16	W14X257	W27X94	W14X211	W27X94	3/16	W14X257	W27X94	W14X211	W27X94
6	3/16	W14X257	W27X94	W14X211	W27X94	3/16	W14X257	W27X94	W14X211	W27X94
5	3/16	W14X257	W27X94	W14X211	W27X94	3/16	W14X257	W27X94	W14X211	W27X94
4	3/16	W14X257	W27X94	W14X211	W27X94	3/16	W14X257	W27X94	W14X211	W27X94
3	3/16	W14X257	W27X94	W14X211	W27X94	3/16	W14X257	W27X94	W14X211	W27X94
2	3/16	W14X257	W27X94	W14X211	W27X94	3/16	W14X257	W27X94	W14X211	W27X94
1	3/16	W14X257	W27X94	W14X211	W27X94	3/16	W14X311	W27X94	W14X257	W27X94

	Design Case C20-3-Rev2					Design Case C20-3-Rev3				
Story	t_p (in)	Shear Wall Column	Shear Wall Beam	Moment Frame Column	Moment Frame Beam	t_p (in)	Shear Wall Column	Shear Wall Beam	Moment Frame Column	Moment Frame Beam
14	3/16	W14X233	W27X94	W14X176	W27X94	3/16	W14X233	W27X94	W14X176	W27X94
13	3/16	W14X233	W27X94	W14X176	W27X94	3/16	W14X233	W27X94	W14X176	W27X94
12	3/16	W14X233	W27X94	W14X176	W27X94	3/16	W14X233	W27X94	W14X176	W27X94
11	3/16	W14X233	W27X94	W14X176	W27X94	3/16	W14X233	W27X94	W14X176	W27X94
10	3/16	W14X233	W27X94	W14X176	W27X94	3/16	W14X233	W27X94	W14X176	W27X94
9	3/16	W14X233	W27X94	W14X176	W27X94	3/16	W14X233	W27X94	W14X176	W27X94
8	3/16	W14X233	W27X94	W14X176	W27X94	3/16	W14X233	W27X94	W14X176	W27X94
7	3/16	W14X342	W27X94	W14X283	W27X94	3/16	W14X257	W27X94	W14X211	W27X94
6	3/16	W14X342	W27X94	W14X283	W27X94	3/16	W14X257	W27X94	W14X211	W27X94
5	3/16	W14X342	W27X94	W14X283	W27X94	1/4	W14X426	W27X94	W14X283	W27X94
4	3/16	W14X342	W27X94	W14X283	W27X94	1/4	W14X426	W27X94	W14X283	W27X94
3	3/16	W14X342	W27X94	W14X283	W27X94	1/4	W14X426	W27X94	W14X283	W27X94
2	3/16	W14X342	W27X94	W14X283	W27X94	1/4	W14X426	W27X94	W14X283	W27X94
1	3/16	W14X342	W27X94	W14X283	W27X94	1/4	W14X426	W27X94	W14X283	W27X94

Table 5.12 Cont'd

Design Case C20-3-Rev4					
FL	t_p (in)	Shear Wall Col	Shear Wall Beam	MF Col	MF Beam
14	3/16	W14X233	W27X94	W14X176	W27X94
13	3/16	W14X233	W27X94	W14X176	W27X94
12	3/16	W14X233	W27X94	W14X176	W27X94
11	3/16	W14X370	W27X94	W14X233	W27X94
10	3/16	W14X370	W27X94	W14X233	W27X94
9	3/16	W14X370	W27X94	W14X233	W27X94
8	3/16	W14X370	W27X94	W14X233	W27X94
7	3/16	W14X426	W27X94	W14X283	W27X94
6	1/4	W14X426	W27X94	W14X283	W27X94
5	1/4	W14X426	W27X94	W14X283	W27X94
4	1/4	W14X426	W27X94	W14X283	W27X94
3	1/4	W14X426	W27X94	W14X283	W27X94
2	1/4	W14X426	W27X94	W14X283	W27X94
1	1/4	W14X426	W27X94	W14X283	W27X94

*Upper six floors are not shown for clarity since no changes were made

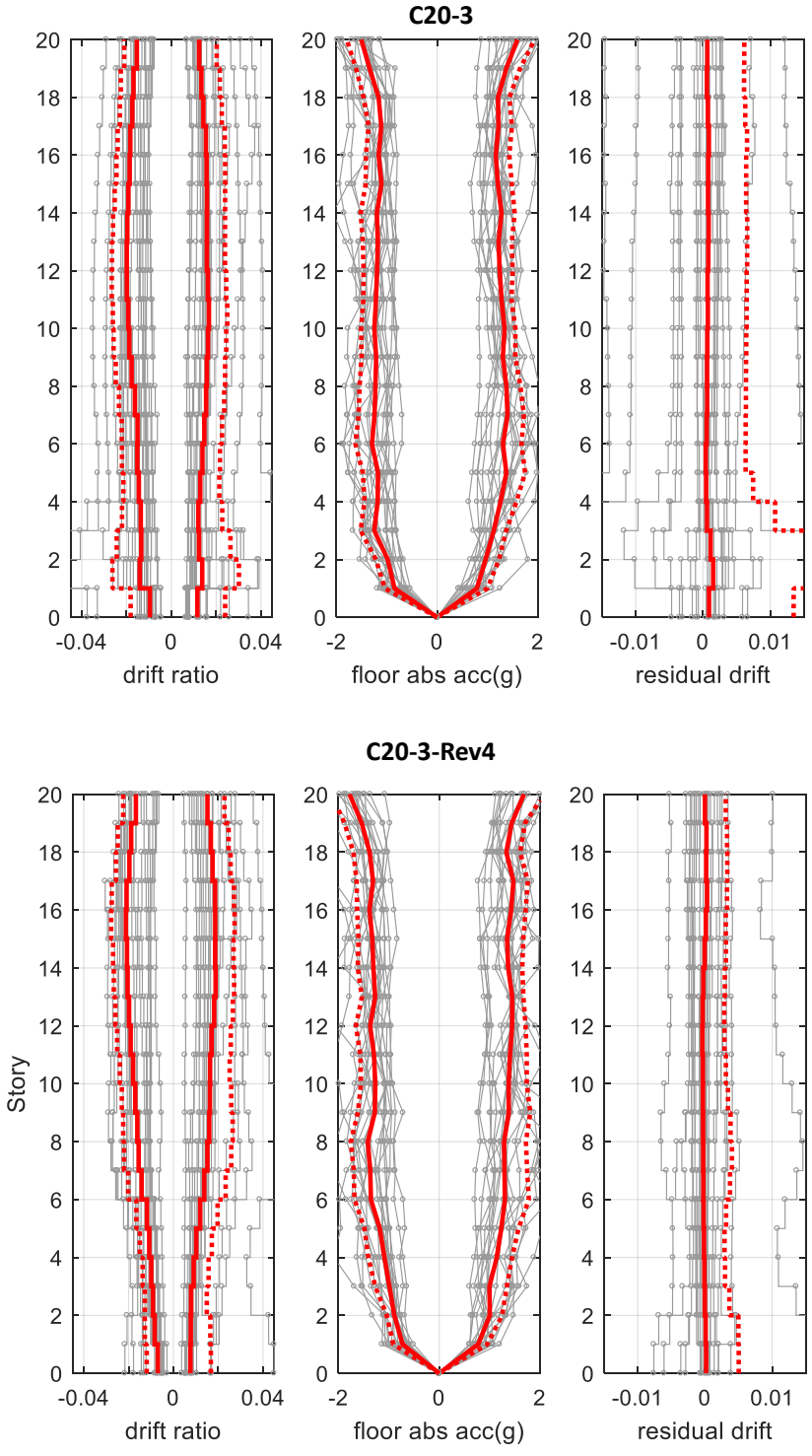

Figure 5.32 Drift and acceleration responses of C20-3 design before and after design iterations at 02/50 level motions

It was found that the large 84th-percentile residual drift was caused by several strong and long-period ground motions as can be seen from Figure 5.33. Those motions have a strong impulse that shifted the system from the original position and afterwards oscillated about the shifted center. The inability of the system to re-center is most likely due to significant yielding of the infill wall as shown in Figure 5.34. Therefore, it was decided that in addition to modifying the column sections, the infill plate thicknesses should also be increased to prevent severe residual displacements. The thicknesses of the infill walls of the lower five stories corresponding to the largest residual drift were increased. It was found the increase of plate thicknesses in the third revision (C20-3-Rev3) successfully prevented the formation of the soft-story mechanism of the lower floors. However, the weak stories were shifted up to approximately floors 6–8 when the infill plate thickness had been suddenly reduced. Based on this observation, the last revision made was to extend the floor with increased infill plate thickness to the sixth floor, and changed the column sections gradually. The final design met all the performance objectives on the mean plus one standard deviation.

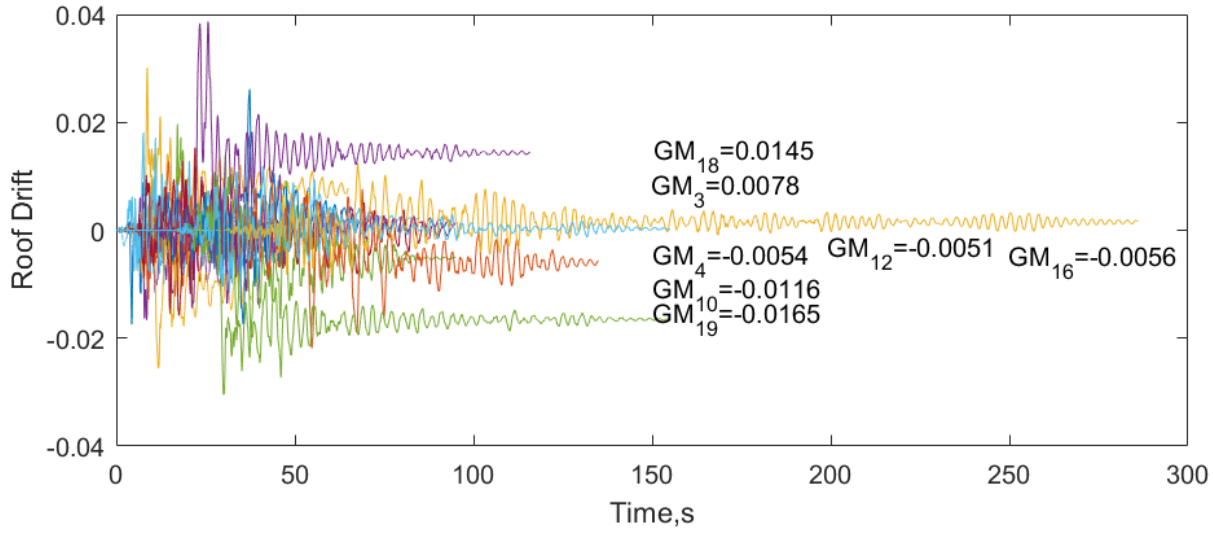

Figure 5.33 Time history of roof drift responses for C20-3 at 02/50 level motions

5.3.5.3 Other Preliminary Designs

Since other preliminary designs did not show major problems in satisfying the global drift criteria, simple local modifications of column sections were applied to ensure that the P-M interaction ratio for columns other than the base of the first-story column was smaller than one at the 84th-percentile level responses.

It is suggested that the increase in column sections should be slightly larger than what is indicated by the exceedance ratio. For example, if the 84th-percentile column P-M interaction ratio is 1.2, then it is better to increase the column strength and moment of inertia to 1.3 or 1.4 times larger. This is because heavier columns tend to decrease the natural period of the system, which will, in turn, attract larger seismic forces. No problem was found in the beam-to-column rotation demands. Therefore, no modifications were applied to the beam sections.

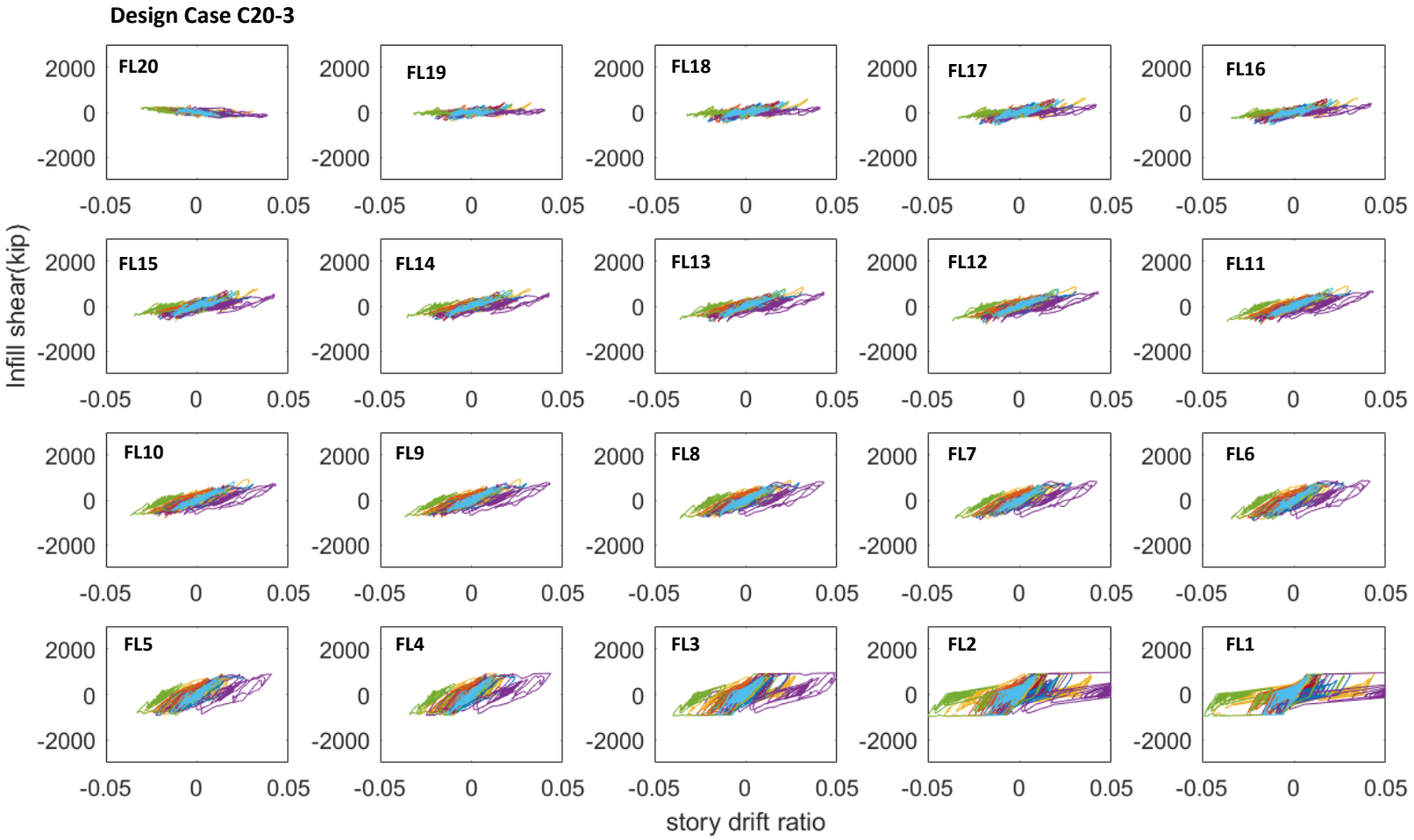

Figure 5.34 Infill plate hysteresis responses for C20-3 at 02/50

5.3.6 Resulting Performance-Based Designs

After the trial and error modification process, the new designs and their periods are summarized in the Tables 5.13–5.16. The side-stiffeners used are the same as specified in Table 5.3 based on the infill plate thickness, t_p.

Table 5.13 Natural periods of the performance-based new designs

Name	# of stories	Bay Width (ft)	# of frame in loading direction	T_{approx}(s) by ASCE Eqn.12.8-7	$T_{analysis}$(s) by single brace model	$T_{analysis}$(s) by X-brace model
PBD3-1	3	20	2	0.312	0.60	0.44
PBD3-3	3	20	2	0.312	0.62	0.46
PBD9-1	9	20	4	0.734	1.39	1.21
PBD9-3	9	20	4	0.734	1.35	1.15
PBD20-3	20	20	6	1.314	2.28	2.11

Table 5.14 Performance-based design sections for the 3-story prototype buildings

	Design Case PBD 3-1			**Design Case PBD 3-3**				
Story	t_p (in)	Shear Wall Column	Shear Wall Beam	t_p (in)	Shear Wall Column	Shear Wall Beam	Moment Frame Column	Moment Frame Beam
3	0.1875	W14X211	W27X117	0.125	W14X159	W27X94	W14X159	W27X94
2	0.25	W14X342	W27X146	0.1875	W14X311	W27X94	W14X176	W27X94
1	0.3125	W14X342	W24X146	0.25	W14X311	W27X94	W14X176	W27X94

Table 5.15 Performance-based design sections for the 9-story prototype buildings

	Design Case PBD 9-1			**Design Case PBD 9-3**				
Story	t_p (in)	Shear Wall Column	Shear Wall Beam	t_p (in)	Shear Wall Column	Shear Wall Beam	Moment Frame Column	Moment Frame Beam
9	0.125	W14X426	W30X235	0.125	W14X211	W21X111	W14X145	W21X111
8	0.125	W14X426	W30X235	0.125	W14X211	W21X111	W14X145	W21X111
7	0.1875	W14X455	W30X235	0.1875	W14X283	W21X111	W14X159	W21X111
6	0.25	W14X455	W30X261	0.25	W14X283	W21X122	W14X159	W21X122
5	0.25	W14X455	W30X261	0.25	W14X283	W21X122	W14X159	W21X122
4	0.25	W14X605	W30X261	0.25	W14X455	W21X122	W14X233	W21X122
3	0.3125	W14X605	W30X261	0.3125	W14X455	W24X131	W14X233	W24X131
2	0.3125	W14X730	W30X261	0.3125	W14X455	W24X131	W14X233	W24X131
1	0.3125	W14X730	W30X261	0.3125	W14X455	W24X131	W14X233	W24X131

Table 5.16 Performance-based design sections for the 20-story prototype building

	Design Case PBD 20-3				
Story	t_p (in)	Shear Wall Column	Shear Wall Beam	Moment Frame Column	Moment Frame Beam
20	0.125	W14X176	W27X94	W14X109	W27X94
19	0.125	W14X176	W27X94	W14X109	W27X94
18	0.125	W14X176	W27X94	W14X109	W27X94
17	0.125	W14X176	W27X94	W14X109	W27X94
16	0.125	W14X233	W27X94	W14X176	W27X94
15	0.1875	W14X233	W27X94	W14X176	W27X94
14	0.1875	W14X233	W27X94	W14X176	W27X94
13	0.1875	W14X233	W27X94	W14X176	W27X94
12	0.1875	W14X233	W27X94	W14X176	W27X94
11	0.1875	W14X370	W27X94	W14X233	W27X94
10	0.1875	W14X370	W27X94	W14X233	W27X94
9	0.1875	W14X370	W27X94	W14X233	W27X94
8	0.1875	W14X370	W27X94	W14X233	W27X94
7	0.1875	W14X426	W27X94	W14X283	W27X94
6	0.25	W14X426	W27X94	W14X283	W27X94
5	0.25	W14X426	W27X114	W14X283	W27X114
4	0.25	W14X426	W27X114	W14X283	W27X114
3	0.25	W14X426	W27X114	W14X283	W27X114
2	0.25	W14X426	W27X114	W14X283	W27X114
1	0.25	W14X426	W27X114	W14X283	W27X114

5.3.7 Evaluation of Performance-Based Design Responses

5.3.7.1 Evaluation against Performance Objectives

Similar to Tables 5.9 and 5.10, Tables 5.17 and 5.18 show the maximum responses over all floors and the evaluation checks against the design objectives. Even though the walls were not specifically designed to meet the service-level objective, all of the designs were able to limit the peak story drift within 0.5% and the residual drift within 0.2% at service-level ground motions for both median and 84th-percentile responses. This means these buildings have an 84% probability of meeting the no-repair performance objective in the 50/30 hazard level. Note that this level of performance objective was met even in the preliminary design cases.

The peak story drift and residual drift responses were also satisfactory at the 10%-50 year and 2%-50 year hazard levels. Some preliminary designs (C9-3 and C20-3) had issues at the maximum considered level (2%-50 year) with 84th-percentile residual drift exceeding the 1% limit. After modification, all design cases were able to limit both the median and 84th-percentile drift responses

below 2% and 4%, and residual drift responses below 0.5% and 1% at the 10%-50 year and 2%-50 year hazard level respectively. Performance-based designed 9- and 20-story buildings were even able to maintain the 84th-percentile peak story drift below 3% and residual drift below 0.5% at 2%-50 year level hazard.

The beam hinge rotation responses were satisfactory for all hazard levels. The low connection rotation demands validated the approach to replace the expensive fully rigid field-welded moment connections to the simpler and more economical GPMCs proposed and developed in this dissertation.

Table 5.17 Maximum responses among all floors for performance-based design

Design	Hazard	Peak story drift		Residual drift		Beam hinge plastic rotation		Column P-M	
		median	84th percentile	median	84th percentile	median	84th percentile	median	84th percentile
PBD 3-1	50/30	0.31%	0.41%	0.02%	0.02%	0.000	0.000	0.31	0.41
	10/50	1.07%	1.69%	0.08%	0.20%	0.003	0.009	0.85	1.02
	02/50	2.34%	3.90%	0.36%	0.81%	0.015	0.029	1.12	1.28
PBD 3-3	50/30	0.31%	0.41%	0.02%	0.03%	0.000	0.000	0.31	0.40
	10/50	1.12%	1.80%	0.09%	0.20%	0.002	0.009	0.76	0.94
	02/50	2.42%	3.94%	0.38%	0.71%	0.015	0.029	1.06	1.26
PBD 9-1	50/30	0.39%	0.50%	0.02%	0.03%	0.000	0.000	0.34	0.44
	10/50	1.22%	1.63%	0.07%	0.20%	0.000	0.004	1.00	1.15
	02/50	1.86%	2.53%	0.20%	0.53%	0.008	0.018	1.08	1.19
PDB 9-3	50/30	0.34%	0.44%	0.01%	0.03%	0.000	0.000	0.37	0.50
	10/50	1.03%	1.50%	0.05%	0.15%	0.000	0.000	1.00	1.13
	02/50	1.70%	2.70%	0.20%	0.58%	0.005	0.014	1.11	1.28
PBD 20-3	50/30	0.31%	0.39%	0.02%	0.04%	0.000	0.000	0.31	0.36
	10/50	1.06%	1.51%	0.10%	0.17%	0.000	0.000	0.71	0.88
	02/50	2.19%	2.84%	0.21%	0.52%	0.000	0.004	1.02	1.14

All performance-based designs were able to limit the shear wall column P-M interaction ratio below or equal to one at the median level. At the 84th-percentile level, only design cases PBD 3-3 and PBD 20-3 had a P-M interaction ratio below one at the 10%-50 year level. Almost all other designs had P-M interaction ratios above one for the 84th-percentile responses, indicating yielding in the column at the design and maximum considered level hazards. Note that straining-hardening factor, C_{pr}, as given in the AISC Seismic Provisions (AISC 2010c), was used in calculating the maximum considered level (MCL) column capacity. However, based on the definition of the C_{pr} factor, the resulting capacity does not represent the actual ultimate strength but an average strength between the yielding and ultimate capacity. Therefore, a P-M ratio exceeding one at the maximum considered level does not necessarily imply fracture. In addition, as the tabulated peak P-M interaction ratios often occurred during a very short period of time, after which the load would reverse and the system would unload. As will be shown later, all of the performance-based designs

had only the base of first-story column yielding, the slight exceedance at the 84th-percentile responses was considered acceptable, and therefore no further modifications were performed. However, if the designer is especially concerned about this design parameter, larger column sections could be adopted to bring the 84-percentile P-M interaction ratio below one. Further modification might be difficult for the 9-story one-bay configuration, noting that in the current PBD 9-1 design, the heaviest W14 section was used and built-up sections may be required for further increase of column sections.

Table 5.18 Evaluation of the performance-based designs (maximum responses/performance objectives ratio)

Design	Hazard	Peak story drift		Residual drift		Beam hinge plastic rotation		Column P-M	
		median	84th percentile	median	84th percentile	median	84th percentile	median	84th percentile
PBD 3-1	50/30	0.62	0.83	0.08	0.12	0.00	0.00	0.34	0.45
	10/50	0.54	0.85	0.16	0.40	0.08	0.25	0.86	1.03
	02/50	0.59	0.97	0.36	0.81	0.31	0.61	1.00	1.16
PBD 3-3	50/30	0.61	0.82	0.10	0.15	0.00	0.00	0.35	0.45
	10/50	0.56	0.90	0.17	0.40	0.06	0.24	0.76	0.94
	02/50	0.60	0.98	0.38	0.71	0.32	0.60	0.96	1.15
PBD 9-1	50/30	0.77	0.99	0.09	0.17	0.00	0.00	0.38	0.49
	10/50	0.61	0.82	0.13	0.41	0.00	0.12	1.00	1.16
	02/50	0.46	0.63	0.20	0.53	0.17	0.37	0.98	1.08
PBD 9-3	50/30	0.69	0.88	0.07	0.17	0.00	0.00	0.41	0.56
	10/50	0.52	0.75	0.10	0.31	0.00	0.00	1.00	1.14
	02/50	0.42	0.68	0.20	0.58	0.11	0.30	1.00	1.16
PBD 20-3	50/30	0.62	0.78	0.10	0.22	0.00	0.00	0.34	0.40
	10/50	0.53	0.75	0.21	0.33	0.00	0.00	0.72	0.89
	02/50	0.55	0.71	0.21	0.52	0.00	0.08	0.93	1.04

Again, the trend of higher drift demand for shorter buildings seems to be unrelated to the specific designs since a similar trend was observed for the code-based preliminary designs and also for the self-centered SPSW(Clayton et al. 2012) and current AISC SPSW(Berman 2011).

5.3.7.2 Peak Story Drift Ratio and Residual Drift

The drift profiles for the cases with only column section changes did not change significantly from their preliminary design counterparts. However, PBD 9-3 and PBD 20-3 designs, which were modified to avoid a weak bottom story, tended to be stiffer in the lower stories compared to their preliminary design version. Overall, as shown in Figures 5.35 and 5.36, all designs show relatively uniform peak story drift and residual drift distributions, without any significant deformation concentrations, indicating well-proportioned and well-mobilized systems, and satisfied all drift performance objectives.

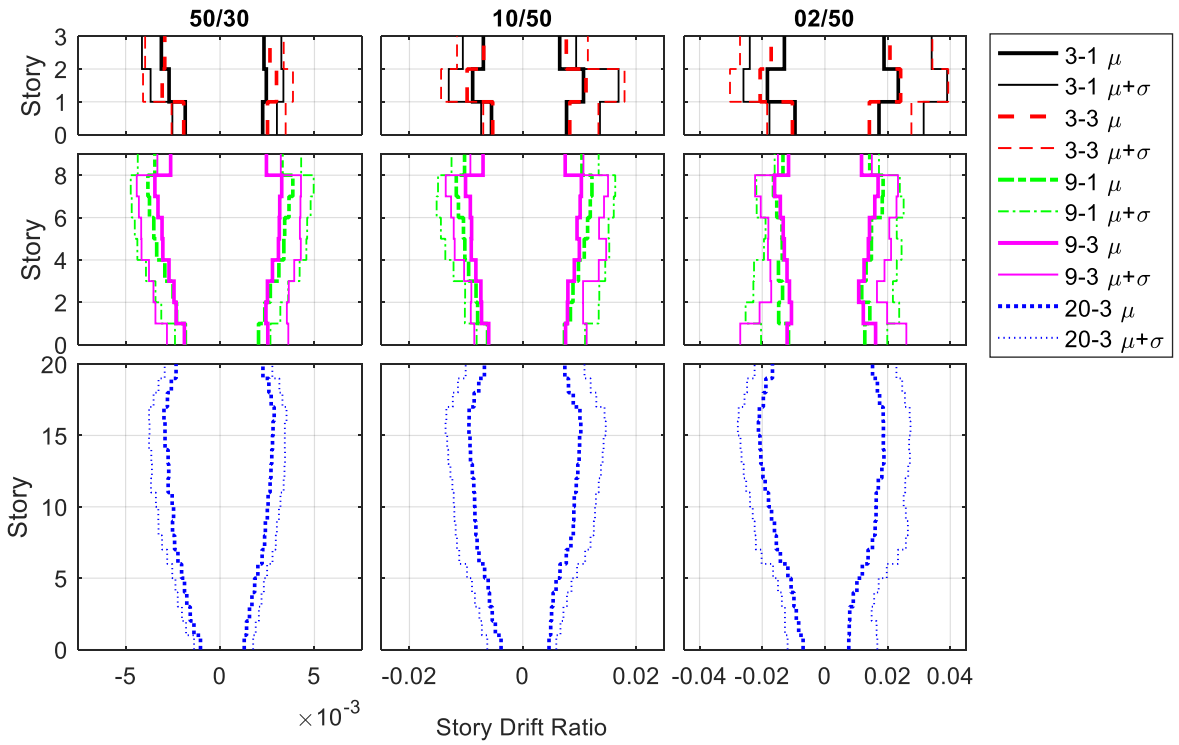

Figure 5.35 Peak story drift ratio profiles for the performance-based designs

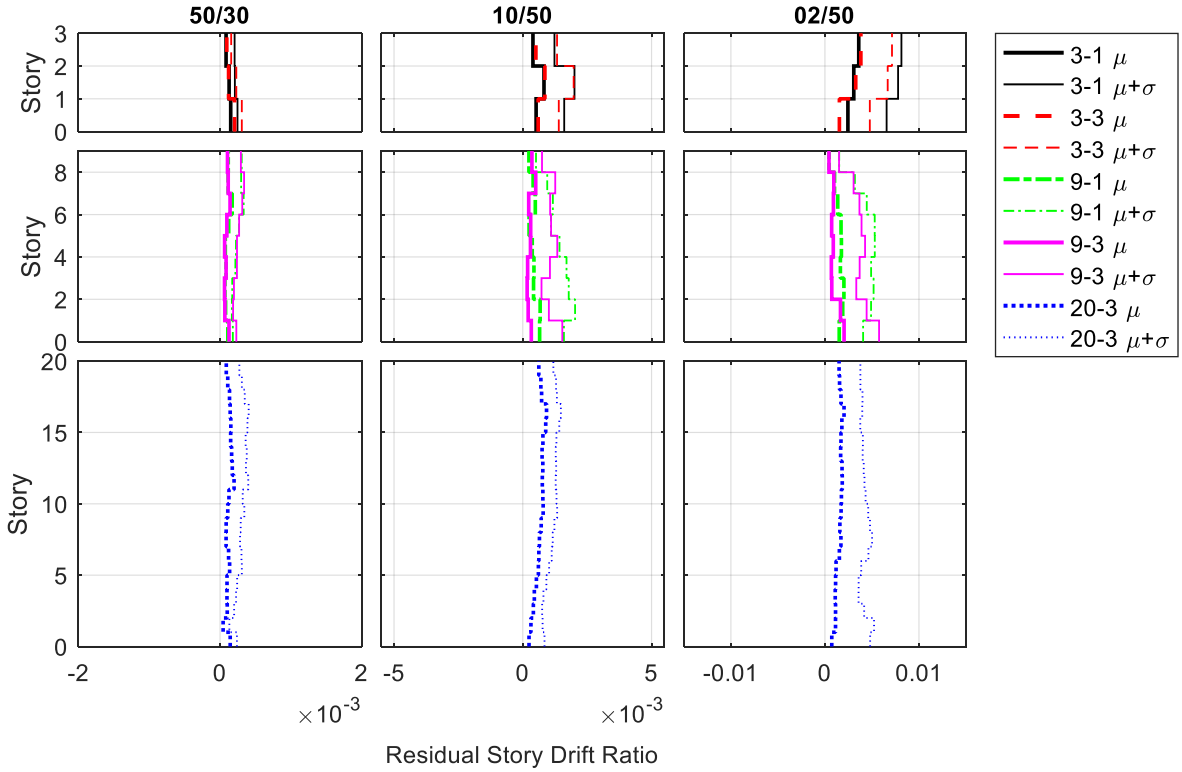

Figure 5.36 Residual story drift ratio profiles for the performance-based design

5.3.7.3 Beam Hinge Rotation

The beam hinge rotation representing the beam-to-column connection rotation responses were still far less than the performance objective limits (Figure 5.37). But several trends can be observed for both preliminary code-based and revised performance-based designs: (1) shorter buildings had larger connection rotation demands compared to taller buildings, which is closely associated with the story drift demands; and (2) the three-bay designs tended to impose less rotation demand on the shear wall bay, especially for upper stories; part of the story drift and connection rotation demands were taken by the outside moment frame bays (see Figure 5.38).

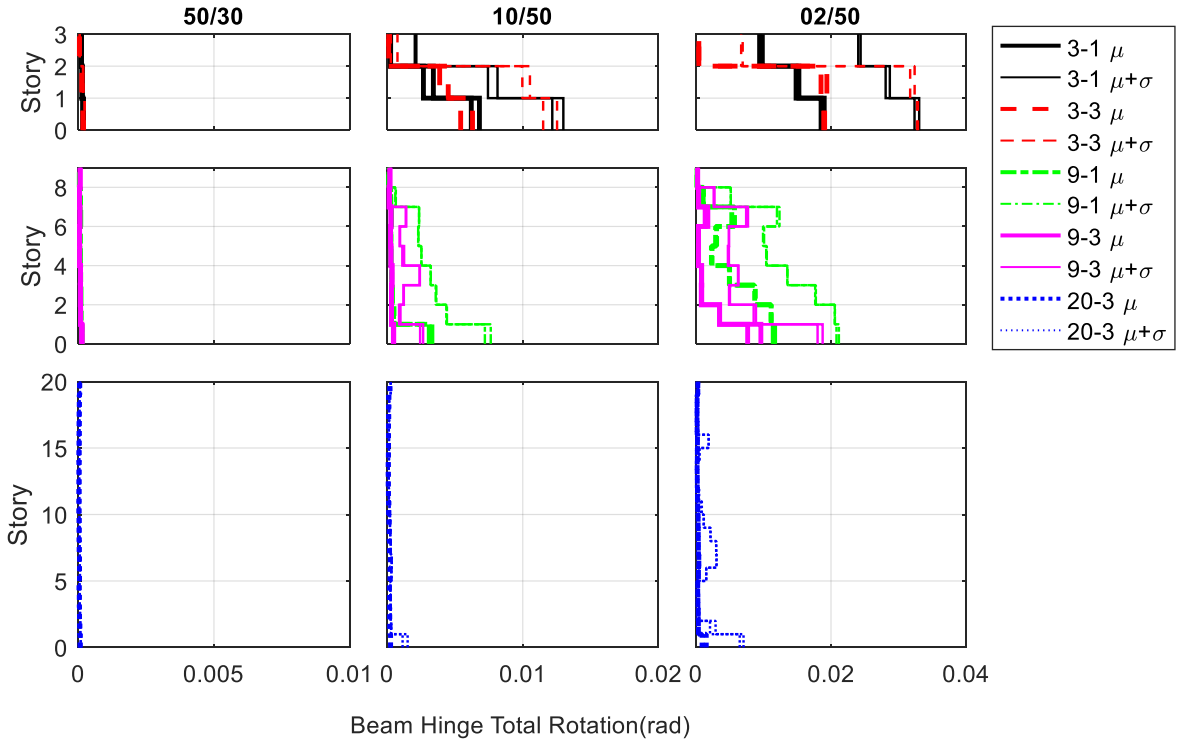

Figure 5.37 Beam hinge total rotation profiles for the performance-based designs

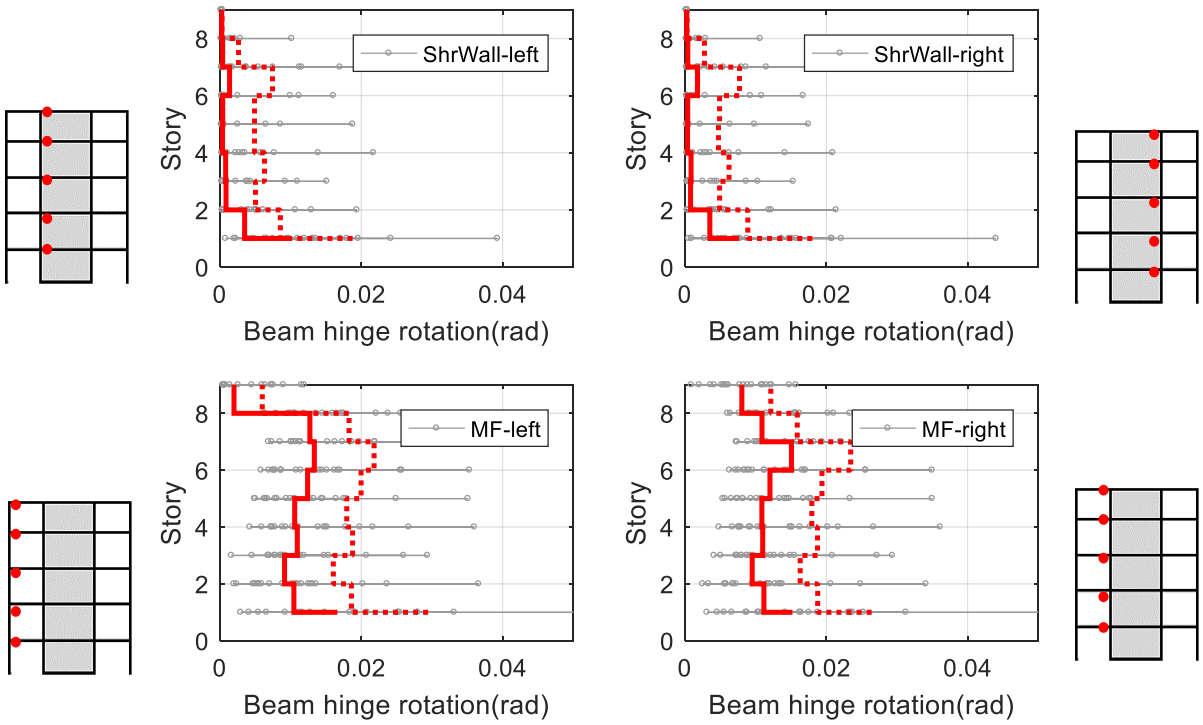

Figure 5.38 Typical beam hinge total rotation profiles for the shear wall bay and moment frame bay for C9-3-Rev1 at 2/50 level hazard

5.3.7.4 Column Demand-to-Capacity Ratios

As shown in Figures 5.40 and 5.41, all the revised new designs were able to limit the overall P-M interaction equal or below one at the median level for both 10/50 and 2/50 level hazards. All the plots show the nominal demand-to-capacity (D/C) ratio without applying the φ factor, expected yield stress factor, or the strain-hardening coefficients. For all designs, the location of the maximum P-M interaction occurred at the base of the first-story column. This is considered a desirable collapse mechanism. In addition, the P-M interaction ratio being larger than one is mainly caused by the sudden increase in the moment demand due to the fixed base condition of the first-story column. The axial force D/C for all cases was below one. As reported in Berman (2011), even when only considering the axial force D/C, more than half of the prototype designs experienced significant over-strength for 84th-percentile responses at the 2/50 level motions. With reasonable infill wall thicknesses and column sections, the slight exceedance of P-M ratio at the 84th-percentile level of the reported revised new designs was considered acceptable.

Apart from the performance evaluation, one thing is worth discussing here: compared with their three-bay design counterpart, it was more difficult for the one-bay designs to satisfy the drift and column strength requirements due to larger overturning moment from the cantilever action. Much heavier column sections had to be used with the first-story shear wall column being W14×730 for PBD 9-1 while W14×455 for PBD 9-3. For the 20-story prototype, it was not possible to satisfy the drift requirement using the heaviest W14 sections. Feasible designs can still be achieved using deep sections or composite columns, but they are outside the scope for this study, i.e., only use W14 columns. It is, therefore, recommended to use coupled steel shear walls or shear wall plus additional moment frames for taller buildings if there are similar constraints on column sections.

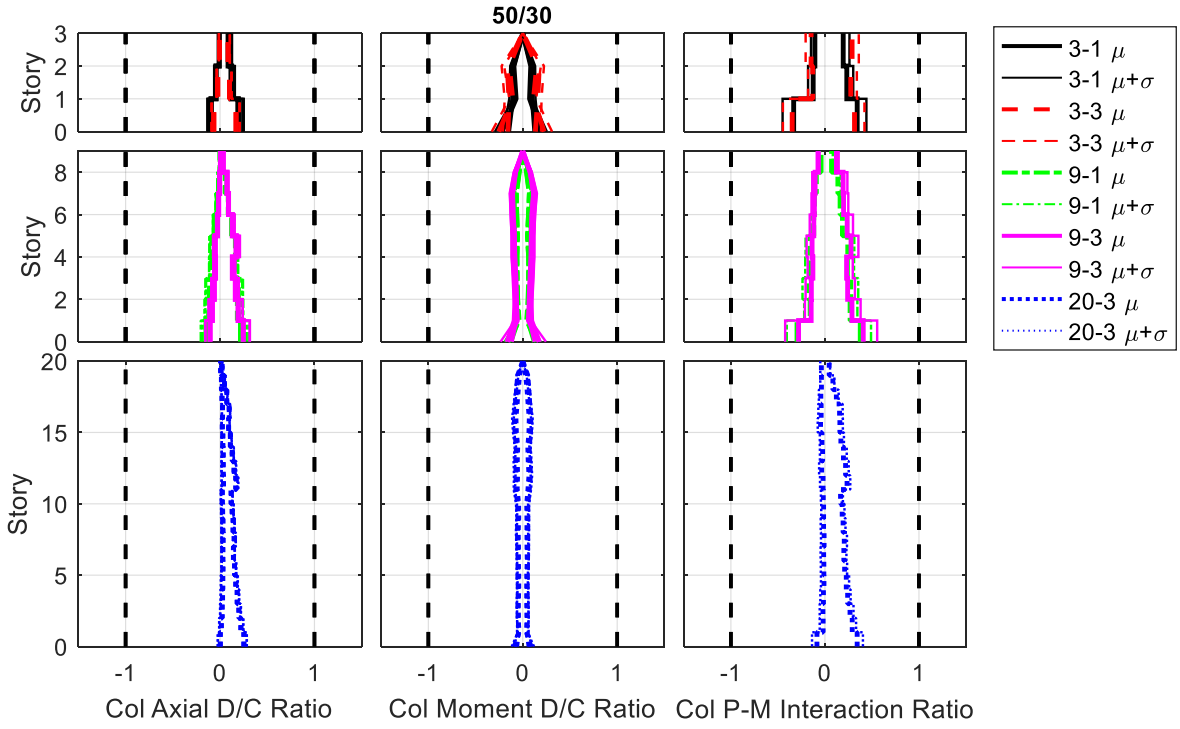

Figure 5.39 Column demand-capacity ratio profiles at 50/30 level hazard for performance-based designs

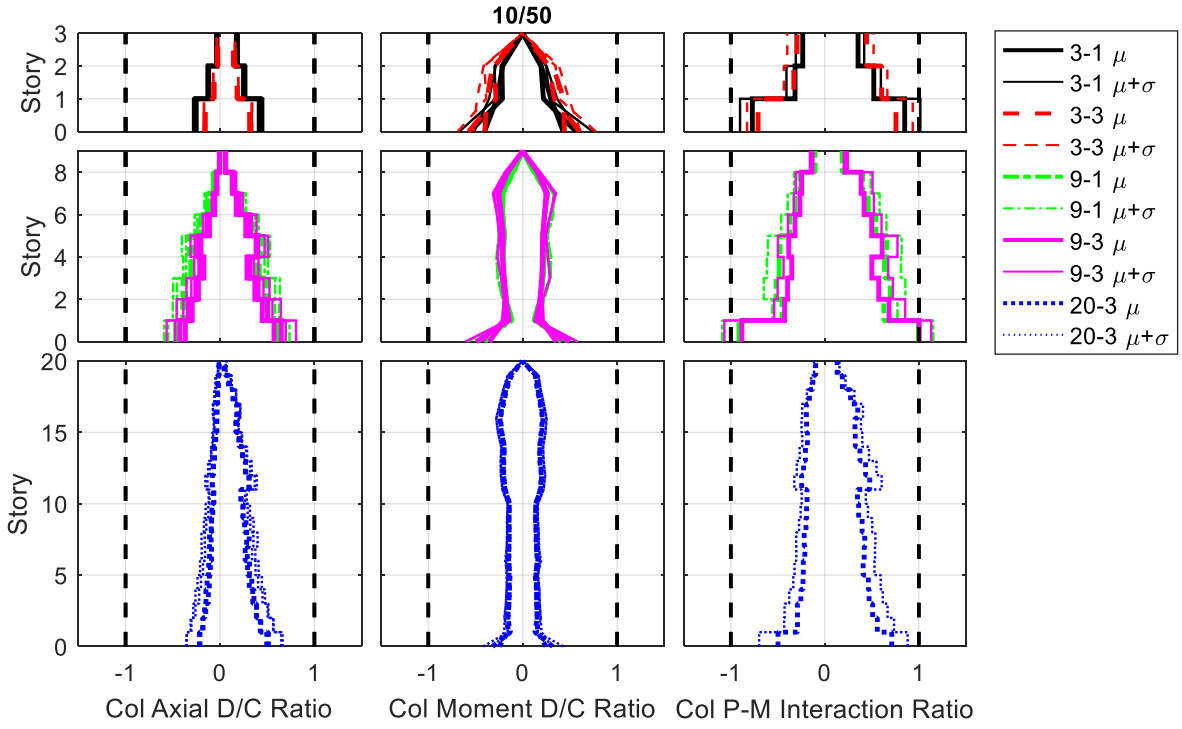

Figure 5.40 Column demand-capacity ratio profiles at 10/50 level hazard for performance-based designs

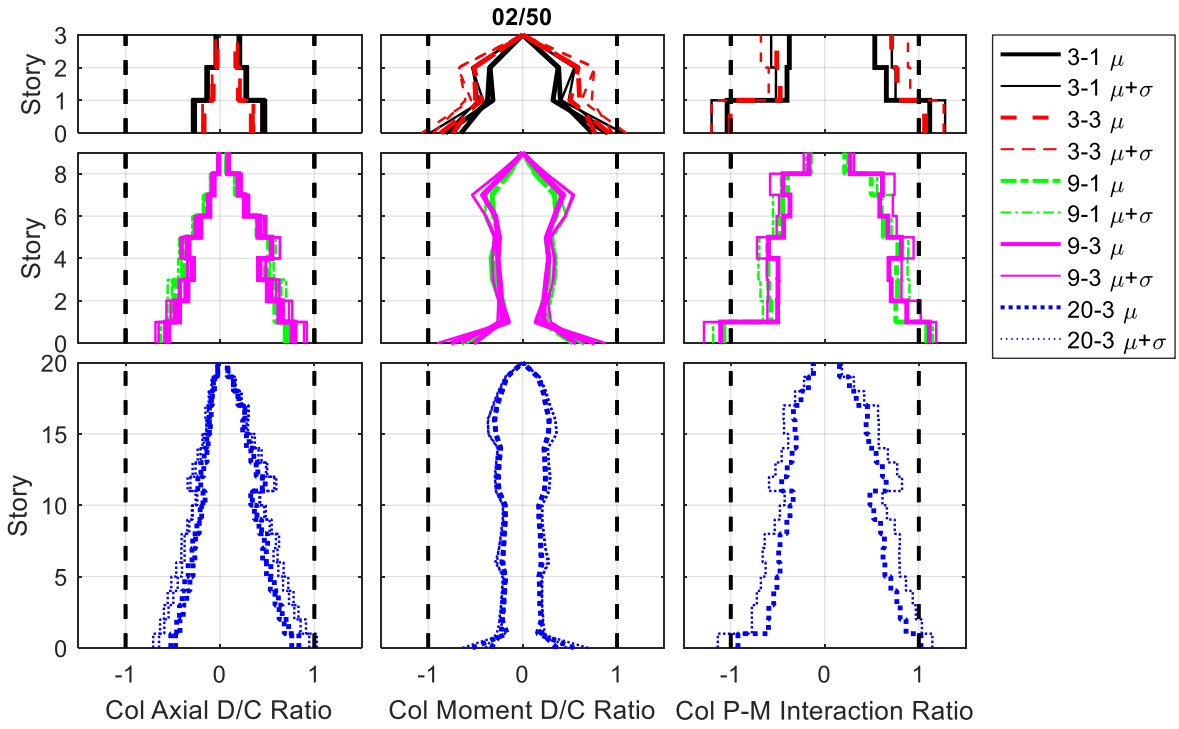

Figure 5.41 Column demand-capacity ratio profiles at 02/50 level hazard for performance-based designs

5.3.7.5 Collapse Probability

The reduction of collapse probability from the preliminary designs to the revised new performance-based designs can be seen from Table 5.19. The number of ground motions at 2% in 50 year level hazard that can cause collapse (defined as either the peak story drift ratio exceeds 4% or residual drift exceeds 1%) was very much reduced after the performance-based design revisions. Extremely severe drift responses (peak story drift larger than 10% or residual drift higher than 2%) were completely eliminated. Note that even after design revisions, the two single-bay designs still had a higher probability of collapse compared to their three-bay design counterpart. This is likely due to the lack of additional redundancy from the supplementary moment frames.

Table 5.19 Comparison of collapse probability of the preliminary code-based and the new performance-based designs

Design	# GM that caused collapse [a]	# GM that lead to >10% peak story drift	# GM that lead to >2% residual drift	Design	# GM that caused collapse [a]	# GM that lead to >10% peak story drift	# GM that lead to >2% residual drift
C3-1	4	-	-	PBD3-1	3	-	-
C3-3	2	-	-	PBD3-3	1	-	-
C9-1	3	-	-	PBD9-1	2	-	-
C9-3	3	1	2	PBD9-3	1	-	-
C20-3	4	-	4	PBD20-3	1	-	-

a. # GM that lead to >4% peak story drift or >1% residual drift

5.3.7.6 Stiffness and Strength Ratios

Section 5.2.3 discussed several design considerations about the relative stiffness and strength contributions from the infill plate and the surrounding moment frames. It was concluded that because the thin infill panel relies on the tension field action as the primary force resisting mechanism, the ideal strength and stiffness relationships could be difficult to achieve. In this section, the strength and stiffness ratios of the HPSPSW designs resulting from the code-based and performance-based design procedures are summarized to provide future researchers and designers with some additional information on the characteristics of this system.

Table 5.20 Comparison of weight, strength and stiffness ratios between the preliminary and performance-based designs

Design	Structural Weight (lb)	Strength Ratio[a]	Stiffness Ratio(roof)[b]	Design	Structural Weight (lb)	Strength Ratio[a]	Stiffness Ratio(roof) [b]
C3-1	37215	0.7377	0.9301	PBD3-1	44599	0.7012	0.9049
C3-3	52400	0.5360	0.7581	PBD3-3	60772	0.5085	0.7394
C9-1	210787	0.6160	0.9047	PBD9-1	218537	0.6034	0.8981
C9-3	219507	0.6168	0.5862	PBD9-3	235695	0.6050	0.5962
C20-3	389254	0.5854	0.2743	PBD20-3	464724	0.5921	0.3286

a. the strength ratio is computed by Eqn.(5.5)
b. the stiffness ratio here is defined as the stiffness of the infill wall to the stiffness of the entire system, i.e., K_w/K_t

The strength ratio in Table 5.20 was calculated using the following equation,

$$\frac{\sum_{i=1}^{N} V_{pi} h_p}{\sum_{i=1}^{N} V_{pi} h_p + \sum_{i=1}^{N}\sum_{j=1}^{n} M_{pbi,j} + \sum_{k=1}^{m} M_{pck}} \tag{5.5}$$

where V_{pi} is the infill plate shear capacity of the i^{th} story, h_p is the story height, $M_{pbi,j}$ is the plastic moment capacity of the the j^{th} GPMC at the i^{th} story, M_{pck} is the plastic moment capacity of the k^{th} first story column, n is the number of moment connection per story, m is the number of moment frame columns per story, and N is the number of stories.

The stiffness ratio was established by applying the same equivalent lateral force distribution on the two systems: the entire system with infill wall as diagonal braces and surrounding moment frames, and the system with the only infill wall and all beam-to-column connections are shear connections. The relative deformation resulting from the entire system and the system with infill wall only can be seen in Figure 5.42(a). The corresponding stiffness ratios of the wall over the entire system (K_w/K_t) in Figure 5.42 (b) were calculated as the ratio of the displacement of the entire system divided by the displacement of the system with infill wall only. It can be seen that for one bay HPSPSW configurations, more than 90% of the stiffness was contributed by the infill plates. With contributions from the supplemental moment frames on the two sides of the shear wall bay, the stiffness ratio of the three-bay configurations decreased. In addition, the stiffness ratio reduced with increasing building height regardless of the number of bays. This was especially the

case for the 20-story, where only about 30% of the upper stories stiffness was contributed by the infill wall. This small shear wall stiffness contribution is likely because of the cantilever mode of deformation for tall buildings, where the upper levels essentially rotate as a rigid body; see deformation shape in Figure 5.42 (a). Here the infill wall was no longer effective in controlling the drift, and the use of a supplementary moment frame became necessary. The preliminary designs show a similar trend as shown in Figure 5.42 for the performance-based designs.

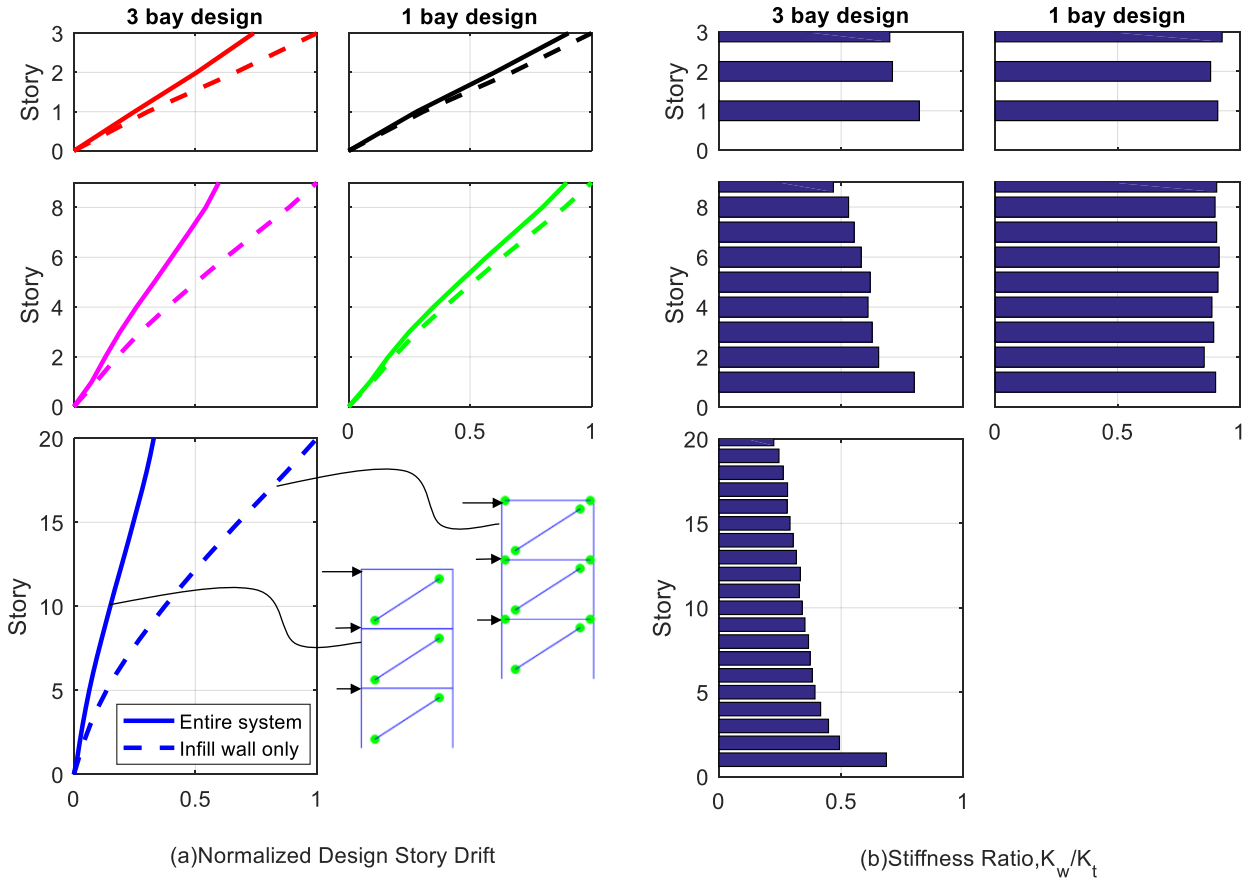

Figure 5.42 Normalized design story drift and corresponding wall-to-system stiffness ratio for the performance-based designs

The general observation is that following the design procedures proposed herein, the ideal strength and stiffness ratios cannot be achieved easily and economically. Comparing to the ideal strength ratio around 0.3, the design procedures will generally lead to an average strength ratio of 0.55~0.7. Stiffness ratio (K_w/K_t) for the one-bay configuration is about 0.9, while for three-bay configuration the stiffness ratio varies from 0.9 for low-rise buildings to 0.3 for high-rise buildings, which are larger than the ideal fuse-to-total stiffness ratio between 0.5 to 0.75 ($\alpha = K_f/K_t$ = 1- K_w/K_t = 0.25 ~ 0.5). Note that these results are for those designs using low-yield infill plate and high-strength frames. It is possible that this is due to both the system characteristics which has relatively fixed yielding drift and strength of the infill wall "fuse" element after fixing the aspect ratio and material, as well as the design procedure itself, which does not specifically aim at achieving certain stiffness or strength ratios.

Notice that the recommended stiffness and strength ratios were proposed to keep the boundary frames essentially elastic, which is not completely suitable for the proposed HPSPSW system or the AISC SPSW system, which allows inelastic behavior of the boundary frames to contribute together with the infill plate yielding to the system capacity. The HPSPSW system has the advantages of allowing lighter frames to be used without over-stressing them; frame yielding is acceptable as long as it does not affect the reparability of the system. Therefore, it may be worthwhile to develop a new set of preferred strength and stiffness ratios for steel plate shear wall systems by relaxing the level of elasticity in the boundary frames.

5.3.8 Lessons Learned

Modification of the preliminary designs that conform to the existing code requirements to the new designs that satisfy specific performance objectives led to the following observations and recommendations:

1) Following the code-based procedure, different designers may develop many different versions of preliminary designs.

    a. One recommendation is to use infill plate thicknesses and column sizes that change more gradually over the height of the building. Using too-uniform plate thicknesses may result in a weak-story mechanism in the lower floors (e.g., C20-3). Of course, a balance should be achieved considering the construction practicability at the same time.

    b. Another recommendation is to avoid using extremely light frame sections, even if they satisfy the drift limit following the equivalent lateral force procedure per ASCE 7-10. Incorporate a safety margin to avoid formation of a weak-story mechanism, which may require many iterations in the performance-design stage to eliminate. Some sort of amplification factor should be developed in future work to formalize the choice of this safety margin. If a safety margin isn't practical, modifications of the design parameters and process might be applicable, including using smaller R and C_d factors (this would require extensive studies to verify before implementation in actual design), and when designing the frame sections, using the design lateral forces corresponding to the approximate period for strength check while using the forces based on analysis period for a check on the stiffness;

2) There seems to be an under-estimation of column demands using the equivalent lateral force procedure per ASCE 7-10, which is amplified by the over-strength factor on the elastic model composed of a single diagonal equivalent brace and the surrounding moment frames. The under-estimation is especially noticeable for low-rise buildings;

3) The beam-to-column connection in the HPSPSW system seems to be relatively less of an issue since the addition of steel infill plate can effectively reduce the connection rotation demands;

4) In the trial and error modification process, if there is problem with either the peak story drift or the residual drift, it may require the use of thicker infill plates and stronger column sections simultaneously. If only the column demand-to-capacity ratio is an issue, most likely only change of column sections would suffice; and

5) Three-bay designs are more effective in controlling drift, especially for taller buildings. Compared to one-bay designs, three-bay designs in most cases can provide more redundancy to the system and can reduce the probability of collapse.

5.4 Concluding Remarks and Recommendations for Future Works

In this chapter, two seismic design procedures were proposed for the new high-performance steel plate shear wall (HPSPSW) system: a *code-based* design procedure that aims to satisfy the code stiffness and strength requirements at the design level and a *performance-based* design procedure that addresses multiple performance objectives at different seismic hazard levels. Without adding complicated design constraints, the performance-based design procedure can be regarded as an extension of the code-based method with additional revisions based on the response history analyses results. The two proposed design procedures were applied to a series of 3-, 9- and 20-story prototype buildings located in downtown San Francisco designed that incorporated the proposed new HPSPSW system in the design. Nonlinear response history analyses of the designed prototype buildings were performed in order to evaluate the system performance. A set of performance objectives was proposed based on the literature and the current knowledge about the new system.

It was found that the preliminary designs resulting from the code-based design procedure generally satisfied the deformation controlled performance objectives (story drift, residual drift, and connection rotation) at the median level, and for many cases, at the 84th-percentile level. All designs were able to satisfy the service-level performance goals even without explicit consideration in the design process. Two out of the five prototype designs experienced a soft-story mechanism at the 2%-50 year level hazard, which was likely to be due to the relatively light column sections chosen and the severe yielding of the infill plate due to the long and strong motions. Most of the code-based designs had a maximum median column P-M interaction ratio over all floors exceeding 1.0 at 10%-50 year level hazard, indicating column yielding and possibly plastic hinge formation. Column yielding other than the first story was observed in some of the code-based preliminary designs, indicating a need for improvement.

After revisions designed to satisfy all performance goals, the responses of the performance-based new designs satisfied the peak story drift, residual drift, and beam–hinge rotation objectives on the 84th-percentile level, and satisfied the column P-M interaction objective on the median level; there was less than 20% exceedance of P-M ratio performance goals on the 84th-percentile level responses. The performance-based designs also showed much less probability of collapse compared to the preliminary designs. The slight relaxation on the column strength objective is based on the argument that the maximum column yielding location is at the first-story column base, which is acceptable considering the plastic mechanism of the system. Following the performance-

based design approach, the designers have the freedom to continue the iteration process if enhanced seismic performance is desired.

The comparison with the AISC SPSW system using the Design Guide 20 high seismic design example shows that the proposed HPSPSW system effectively reduced the shear wall column demands, thus allowing much lighter and economical sections to be used. The revision process also demonstrated that the system provided more leeway for the designers to select the thickness of the infill plate and the column sections independent of each other in the sense that the engineer does not need to worry about changing the column section if he/she decides to increase the infill plate thickness. The use of GPMC also helped to control the level of the bending moment demand-to-capacity ratio in the columns. Much more uniform column demand-to-capacity ratio can be achieved, indicating better material-utilization ratio of the new system. The overall observation is that the new HPSPSW is more economical with enhanced global system performance compared to the current AISC SPSW system.

In addition, various modeling and design issues at the system level were discussed, and lessons learned were summarized. For example, compared with the current AISC SPSW, the new HPSPSW had fewer issues in satisfying the drift limit since thicker plates can be used without a need to increase column sections (as is the case with the AISC SPSW system). However, in general, if a single-bay steel shear wall is used—for both AISC and HPSPSW configurations—it will be difficult to satisfy drift requirements for tall buildings. It is recommended to add supplementary side moment frames, outriggers, or coupled steel shear walls to control drift. It was also found that the generally accepted ideal stiffness and strength ratios between the "fuse" element and the surrounding frames are not easily achievable for the HPSPSW system. But using a low-yield infill wall material and a high-strength frame material could aid in approaching the idealized ratios. Being able to use lighter frame sections, especially column sections, is an advantage of the proposed HPSPSW system, which makes the existing stiffness and strength ratios that aim to keep the frame elastic not completely applicable. Therefore, it may require future studies to find a new set of strength and stiffness ratios suitable for the HPSPSW system.

At last, improvements to the proposed design procedure were suggested, some of which would also be applicable for other steel shear wall configurations. Recommendations for future research are as follows,

1. The strain-hardening factor C_{pr} as defined in the AISC Seismic Provisions (AISC 2010c) was proposed to be included in the maximum considered level column checks in this dissertation. It is suggested conducting further discussion on the performance criteria for force-controlled elements at maximum considered level, which factors such as C_{pr}, R_y, R_t, φ should be included, and under what circumstances they should be included;

2. The boundary columns seemed to be slightly under-designed following the proposed preliminary design procedure; this may be improved by developing (1) a formalized safety margin, or (2) a period-dependent force amplification factor on column demands estimation using equivalent lateral force procedure;

3. It is desirable to investigate specific measures, instead of relying on engineering judgment, to ensure a more gradual change of infill plate thicknesses and frame sections over the height of the building;

4. Although challenging, it can be worthwhile to modify the design procedure to maximize the system ductility by developing a new set of ideal strength and stiffness ratios for the proposed HPSPSW system while maintaining the economic advantages of the new system. It can be beneficial to incorporate some displacement-based design concepts in the modified design procedure.

Chapter VI

Conclusions and Recommendations For Future Research

The research presented in this dissertation focused on development of a new High-Performance Steel Plate Shear Wall (HPSPSW) system aimed at solving the design issues associated with current AISC steel plate shear wall (SPSW) configurations that prevent their widespread use. Three fundamental issues of the current SPSW system include: (1) the steel shear wall applies large lateral forces to the columns, making the columns very large, heavy, and expensive; (2) the complete joint penetration (CJP) field-welded moment connections used in the current system are not cost effective, requiring field-welding and onsite ultrasonic testing, and (3) the infill wall is susceptible to buckling under wind load and small frequent earthquakes. The proposed new High-Performance Steel Plate Shear Wall (HPSPSW) system addresses two of those issues: (1) the infill plate is separated from the boundary columns and connected to the beams only, with side stiffeners added to the two vertical free edges of the infill plate; and (2) the innovative Gusset Plate Moment Connection (GPMC) developed and proposed as part of this dissertation replaces the conventional field-welded flange moment connections. As demonstrated herein, the new system is shown to resolve all ten issues related to the current SPSW system, with two additional advantages: the new system can be more easily adopted in the retrofit of structures and lends itself to modular construction and prefabrication.

This dissertation contains a detailed description of the main development efforts for the new high-performance system: (1) from a comprehensive literature review on the existing technologies and efforts in improving the performance of the SPSW to the concept development of the GPMC and the HPSPSW system; (2) from detailed parametric studies on the component and sub-assemblage level using finite-element (FE) methods and basic principles to the evaluation of system performance on the global level with the aid of response history analyses; and (3) from derivation of design and analysis equations for system components, development of simplified analysis

models to the proposal of generally applicable design procedures and recommendations. Each chapter presents conclusions and discussions for the specific topic of the dissertation. The following sub-sections highlight the most important findings for each stage, followed by recommendations for future research.

6.1 Conclusions

6.1.1 The Gusset Plate Moment Connection

With the need to replace the expensive welded flange steel moment connection used in the current SPSW system, several new moment connection concepts that are simpler, potentially cheaper and fit well into a SPSW system were proposed. The final selected concept is the gusset plate moment connection (GPMC), which utilizes the ductility of gusset plate as the main ductile energy dissipation element inside the beam-to-column connection while the beams and columns remain essentially elastic. The proposed GPMC is highly versatile with both welded and bolted versions and other beam-to-gusset plate connection methods available, and is widely applicable not only in special moment frames but also in steel shear wall systems and dual systems. The entire connection configuration was proposed to minimize the field CJP welds, doubler plates, and continuity plates for potential savings in terms of the time and costs of fabrication.

Extensive nonlinear FE analyses showed that if designed with appropriate gusset plate strength, thickness, free gusset length, gusset flange thickness and bolt strength (see recommended design values provided in Chapter III), the GPMC can achieve the desirable "strong-frame–weak-gusset" behavior, whereby the gusset plate will yield as a fuse and dissipate energy with only limited yielding in the column web and beam, and minimum bending in the column flange. Therefore, the proposed new GPMC reduces the need for column web reinforcement using doubler plates and continuity plates. This "strong-frame–weak-gusset" behavior can suspend the "strong-column–weak beam criteria for special moment frames, leading to greater leeway for designers, also leading to cost savings.

It was found that common Gr.50 or A36 can be used for shallow and stocky beams. Low-yield point (LYP) gusset plate material was shown to be ductile, promising, and especially effective in resolving strain concentration issues for deep beams. Other design aspects were also discussed, including the use of stiffeners, the lateral stiffness reduction due to "weak gussets," the use of a beam flange cut to reduce the incoming beam flange forces, and the effects of architectural limits.

Because of the stable behavior of GPMC using LYP steel, *Steel02* material in OpenSees captured sufficiently the hysteresis behavior of the connection for use in the global concentrated rotation hinge models. Further testing and calibration of the connection behavior would be necessary to include strength/stiffness degradation behavior of the GPMC using Gr.50 or A36 steel.

An interim step-by-step design procedure following the format for pre-qualified moment connection standard (AISC 2010b) was proposed. The procedure concentrates all information gained from the parametric studies and the design principles of the existing pre-qualified steel moment connections. Desirable performance criteria and limit-state hierarchy were adopted as the basis to develop the procedure. Both welded and bolted versions of the GPMC were included. Supplementary charts were also provided to aid engineers in selecting gusset plate material and geometry.

6.1.2 The High-Performance Steel Plate Shear Wall

Incorporating the new GPMC into the SPSW system, and separating the infill wall from the boundary columns, a new steel shear wall system – the High-Performance Steel Plate Shear Wall (HPSPSW) – was developed in Chapter IV. Nonlinear FE analyses verified that columns using the new HPSPSW configuration can be successfully relieved from the tension field action of the infill wall without causing other undesirable behavior. Both the GPMC and infill wall partial tension field action contribute to the lateral force resistance and energy dissipation, protecting other elements in the system and enabling them to remain essentially elastic. The slight reduction in the shear stiffness and strength of the system due to the detachment of the wall from the columns can be recovered either by increasing the thickness of the infill wall or by providing stronger side stiffeners on the two vertical edges of the infill plate. T-shaped side stiffeners were found to be the most efficient and practical among various shapes studied.

These findings indicated that the new HPSPSW solves the issues related to the tension field action anchor force, and is cost-effective, flexible, and versatile. The selection of infill wall thickness and the column sections are no longer strongly dependent on each other, thus thicker walls can be used for drift or service performance goals, and lighter columns with a variety of cross sections, materials, and orientations of the strong axis of the columns become possible. In addition, elimination of the two vertical welds connecting the infill wall to the boundary column increases the reparability, ease of retrofit, and modular construction of the proposed new HPSPSW system.

Besides enhanced behavior, the system also sees benefits in terms of design and analysis. The equivalent brace (EB) model has existed for some time and has been used for steel shear wall systems, but due to its inability to capture the distributed tension field forces acting on the boundary elements, it was mainly restricted to a preliminary design tool, and the strip model is the dominant analysis tool. However, as no tension field forces act on the columns in the HPSPSW system, the EB model deserves new attention in analysis. The collapse mechanism proposed for plate girders was adapted to the HPSPSW system, leading to a series of equations to estimate the strength and stiffness of the infill panel, as well as several design implications on the design of the infill wall and its side stiffeners.

Using this information, a simple EB model with nonlinear hysteretic characteristics defined was developed for the new system. The corotational truss element with hysteretic material model in OpenSees and Perform 3D structural analysis software were calibrated to represent the EB model for different infill wall designs. The model was validated against the limited available tests and FE analysis results and was considered sufficient at this stage to be adopted in nonlinear response history analyses. Further modifications and calibrations are desired upon the availability of more test results for the new HPSPSW system.

6.1.3 System Design and Performance

Chapter V extended the study of local beam-to-column connections and HPSPSW system sub-assemblies to system performance using realistic site and prototype buildings. Simplified models for the GPMC and the infill wall connected to the beam-only established in previous chapters were adopted in the global model using OpenSees.

Two seismic design procedures were proposed for the new HPSPSW system: a prescriptive code-based procedure and a performance-based procedure that aimed at achieving multiple performance objectives at different hazard levels. The code-based procedure was incorporated into the performance-based procedure in the first step to initiate preliminary design. A set of enhanced performance objectives was proposed based on the literature and the current best knowledge of the proposed new HPSPSW system.

Applying these two design procedures to a series of 3-, 9-, and 20-story prototype buildings that conform to the SAC building geometry and loading specifications, it was found that the preliminary designs resulting from the code-based design procedure satisfied the deformation controlled performance objectives (i.e., story drift, residual drift, and connection rotation) at the median level, and at the 84-percentile level for many cases. All designs satisfied the service-level performance goals even without explicit consideration in the design process. Some of the designs, especially the three-bay designs, which had relatively light frame sections, may experience a soft-story mechanism at the maximum considered level (2%-50 year) hazard. Column yielding other than of first story was also observed in some of the code-based designs, indicating a need for further improvement.

After design revisions following the performance-based design process, the performance of the revised designs met all deformation-controlled performance objectives at the 84-percentile level, and satisfied the column P-M interaction objective for the median responses with no column yielding other than the base of the first-story column, which is considered an acceptable mechanism. The designers have the freedom to continue the iteration process in the performance-based procedure if more enhanced seismic performance is desired.

The comparison with the Design Guide 20 high seismic design (AISC 2007) again validated the effectiveness of the proposed HPSPSW system with the new GPMC in solving the serious over-stress problem of the boundary columns in the current AISC SPSW system. The demand-to-

capacity ratio in the columns of the HPSPSW system is much more uniform over the height of the building, indicating a better material utilization ratio of the new system. The design iteration process was also simplified significantly due to the independence of the choice of infill thickness and column sections in the proposed HPSPSW system. The overall observation is as follows: compared to the current AISC SPSW system, the new HPSPSW will be more economical (about 10% lighter in structural weight plus additional savings resulting from its ease of fabrication) with enhanced global system performance.

Several issues of the general steel shear wall system, including the AISC SPSW and the proposed new HPSPSW, were discussed. Examples include the difficulty in achieving the ideal stiffness and strength ratios proposed for frame structures with metallic fuses between the infill wall and the boundary frame, while keeping the economic light column sections in the HPSPSW system. Some possible improvements of the proposed seismic design procedures were recommended.

6.2 Future Research

As summarized above, this dissertation has provided a relatively comprehensive description of the development efforts for a new innovative steel moment connection, the Gusset Plate Moment Connection, and a new steel plate shear wall system, the High-Performance Steel Plate Shear Wall System, including the initial concept proposal, parametric studies on the detailed local sub-assembly level, development of design equations and simplified analytical models, as well as system design procedure evaluated by nonlinear response history analyses. The proposed concepts were shown to be promising; however, as this research is the very first study on two completely new systems, further studies are necessary to develop and further understanding of the capabilities and limitations of the two systems. The following are some recommended future research areas:

6.2.1 Experimental Work

Experimental monotonic and cyclic testing of the proposed GPMC and the HPSPSW should be a major research effort. The tests are essential to verify the effectiveness of the proposed concepts, validate the design procedure, and capture problems like fracture or fatigue that are not explicitly included in the current FE models so that necessary revision of the detailing or concept can be conducted if unexpected failure modes occurs. The following is a possible testing program for the system:

1. First, cyclic testing of the new and promising GPMC needs to be performed to establish its actual behavior, to calibrate the numerical model further, and to refine the design procedure. At least one bolted and one welded GPMC designed using the interim design procedure should be tested using the cyclic moment-rotation histories as specified in the AISC Seismic Provisions. If possible, more specimens with varied gusset plate material properties (e.g., one Gr.50, one A36, and one with LYP steel) and/or different gusset-to-beam connection configurations (e.g., one slotted beam connection, and one bolted top and

bottom plates connection) should be tested. A possible beam-to-column test set-up is shown in Figure 6.1(a);

2. With enough confidence, more cyclic tests following the pre-qualification procedure are desired to make the GPMC connection a new pre-qualified moment connection to be included in the AISC Prequalified Connections standard (AISC 2010b, AISC 2016a). This step is not a compulsory element in the testing program for the HPSPSW system, but it is suggested as an additional track for the GPMC itself as a pure moment connection; and

3. After obtaining enough information on the cyclic behavior of the GPMC, experimental tests are needed to verify the behavior of the entire HPSPSW system. Typical half-scale two-story one-bay specimens representing the bolted and welded versions of the HPSPSW should be tested. The test set-up shown in Figure 6.1(b) used for studying the composite shear wall behavior by Zhao and Astaneh-Asl (2004a) at University of California at Berkeley can be adopted and either quasi-static cyclic tests or hybrid tests be conducted. The hybrid simulation may require more effort, but it would provide more information and insights on the dynamic responses of the system resulting from both the analytical and experimental substructures.

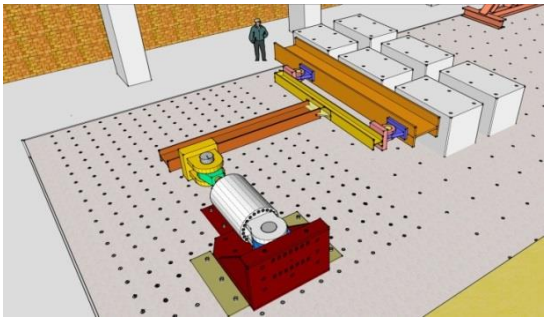

(a) A Beam-to-Column Specimen inside the Test Set-up

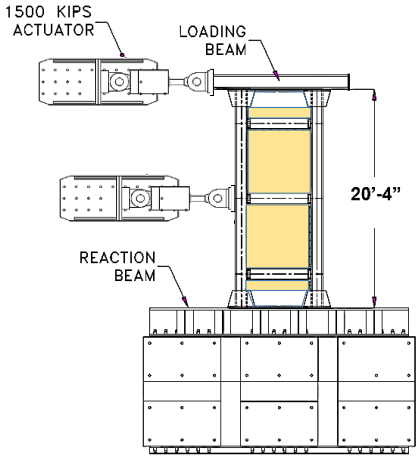

(b) Plan View of the potential HPSPSW Test Set-up

Figure 6.1 Possible specimen set-up in the proposed test program

6.2.2 Analytical Work

Upon the availability of experimental results, an update of the currently proposed analytical models is desired, and more parametric studies should be conducted using the updated model to assess aspects of the connection or system design that are not included in this dissertation:

1. Upon availability of the test results, validation and necessary revision of design concepts, fabrication details, analytical model, and design procedures should be carried out. Whether

significant fracture in certain parts would occur and whether such fracture will lead to significant stiffness or strength deterioration are areas of interest. Difficulties encountered in fabrication of specimens should be noted and used to make necessary modifications on the detailing;

2. For further development of the proposed bolted GPMC, several improvements on the analytical models can be implemented: use of more detailed models of bolts to include the effect of bolt-slippage, bolt-hole bearing elongation, shank tearing, and nut stripping for the bolts would be beneficial; the effect of slab should be investigated in the future research to have a more realistic connection behavior;

3. The truss analogy model for the gusset plate inside the GPMC is worth further development and has the potential to become a simple yet reliable design tool;

4. Multi-scale modeling that uses a combination of detailed shell/solid elements in the critical regions of the connection and simple line elements for the members would be a fruitful area for future research to provide an additional analysis tool that can capture detailed connection behavior in a global setting but at a reasonably low level of computational effort;

5. To understand better the economic aspects of the proposed concepts, a cost comparison between the GPMCs (bolted or welded, with or without using LYP steel) and the currently available moment connections, as well as between the HPSPSW and the current AISC SPSW, is desired upon availability of actual fabrication and test results. Fabrication costs should be included in addition to the structural weight (the latter was considered in the current study);

6. Although the currently adopted hysteretic properties for the equivalent brace (EB) model of the infill wall may result in a reasonable match with the FE and test results, it is essentially empirical and was developed based on the hysteretic formulations proposed for the strip model of the current SPSW. More studies are desired to establish a hysteretic model that is more generally applicable based on the test results of the HPSPSW system;

7. Axial force demand in the side stiffeners was not considered in the current study, but the side stiffeners are expected to take a certain amount of over-turning moment and may further reduce the demand on the columns;

8. By connecting the infill plate to beams only in the proposed HPSPSW system, the infill plate installation can be delayed, and the portion of gravity load supported by the infill plate due to column shortening can be very much reduced, but not completely eliminated. An interesting study would be to examine the effectiveness of a slotted bolted plate-to-boundary beam connection shown in Figure 6.2 to prevent gravity loads being transferred to the infill panel. Note Figure 6.2 is just a simple illustration, the orientation of the slotted

bolt holes does not need to be vertical and they should be designed such that the connection can transfer the tension field forces but not the gravity forces;

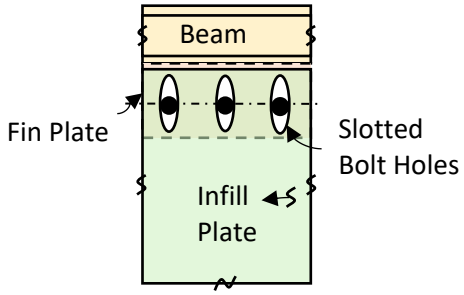

Figure 6.2 A possible slotted bolted plate-to-boundary beam connection to prevent gravity load to be transferred to the infill plate

9. The current study considered the boundary columns to be W14 sections because they are most commonly used in real construction. In some cases, deep columns, which were used in a number of analytical studies for AISC SPSWs, might be necessary. The system behavior using deep columns would be an interesting and useful topic to investigate;

10. Thicker infill walls can be effective in reducing the story drift under wind and frequent earthquakes. However, high floor accelerations due to high initial stiffness can be a driving force for post-earthquake non-structural element loss for buildings using stiff lateral force-resisting systems, such as concrete or steel shear walls. For most structural systems, designers are required to choose whether the displacement or acceleration related damages are more crucial for the specific projects. It would be beneficial to study whether there can be a simple combination of steel plate shear walls and dampers that can reduce both drift and acceleration demands at the same time. One possibility might be using composite shear wall with viscous material sandwiched between the concrete cover and the steel plate, thus resembling a stiffened wall damper;

11. The seismic design procedures proposed in this dissertation for the new HPSPSW system can be further improved to resolve issues observed in the seismic evaluation process. Some examples are: (1) a period dependent factor to solve the under-estimation of low-rise column demands would be beneficial not only for the HPSPSW system but also for the AISC SPSW system, (2) a rational way to enforce gradual change of plate thickness and frame sections along the height, and (3) incorporation of displacement-based design concept into the design procedure to further enforce uniform drift distribution for the system; and

12. With more information available from actual tests of the proposed system, fragility curves and lost functions based on future research, a complete performance-based earthquake engineering evaluation of the system can be performed to further evaluate the HPSPSW system's performance in terms of economical loss and downtime.

References

Abel, J., and Popov, E. (1969). "Static and dynamic finite element analysis of sandwich structures." *Second Conference on Matrix Methods in Structural Analysis, December*.

Abidelah, A., Bouchaïr, A., and Kerdal, D. (2012). "Experimental and analytical behavior of bolted end-plate connections with or without stiffeners." *Journal of Constructional Steel Research*, 76, 13-27.

Ahmadi, H., and Arabzadeh, A. (2013). "EVALUATING THE EFFECTS OF DISTANCE BETWEEN BOLTS ON THE BEHAVIOR OF COMPOSITE STEEL SHEAR WALL." *ASIAN JOURNAL OF CIVIL ENGINEERING (BHRC)*, 14(1), 145-159.

AISC (2005). *Seismic provisions for structural steel buildings. ANSI/AISC 341-05, American Institute of Steel Construction*, Chicago(IL).

AISC (2007). *Steel Design Guide 20: Steel Plate Shear Walls*, American Institute of Steel Construction, Chicago (IL).

AISC (2010a). *Manual of Steel Construction, 14th Edition, American Institute of Steel Construction*, Chicago(IL).

AISC (2010b). *Prequalified Connections for Special and Intermediate Steel Moment Frames for Seismic Applications. ANSI/AISC 358-10, American Institute of Steel Construction*, Chicago(IL).

AISC (2010c). *Seismic provisions for structural steel buildings. ANSI/AISC 341-10, American Institute of Steel Construction*, Chicago(IL).

AISC (2010d). *Specification for structural steel buildings. ANSI/AISC 360-10, American Institute of Steel Construction*, Chicago(IL).

AISC (2016a). *Prequalified Connections for Special and Intermediate Steel Moment Frames for Seismic Applications. ANSI/AISC 358-16, American Institute of Steel Construction*, Chicago(IL).

AISC (2016b). *Seismic provisions for structural steel buildings. ANSI/AISC 341-16, American Institute of Steel Construction*, Chicago(IL).

AISC (2016c). *Specification for structural steel buildings. ANSI/AISC 360-16, American Institute of Steel Construction*, Chicago(IL).

Alinia, M. (2005). "A study into optimization of stiffeners in plates subjected to shear loading." *Thin-walled structures*, 43(5), 845-860.

Alinia, M., and Dastfan, M. (2007a). "Cyclic behaviour, deformability and rigidity of stiffened steel shear panels." *Journal of Constructional Steel Research*, 63(4), 554-563.

Alinia, M. M., and Dastfan, M. (2007b). "Cyclic behaviour, deformability and rigidity of stiffened steel shear panels." *Journal of Constructional Steel Research*, 63(4), 554-563.

Alinia, M. M., and Sarraf Shirazi, R. (2009). "On the design of stiffeners in steel plate shear walls." *Journal of Constructional Steel Research*, 65(10–11), 2069-2077.

Anderson, J. C., and Duan, X. (1998). "Repair/Upgrade Procedures for Welded Beam to Column Connections, Report No.PEER-98/03."Earthquake Engineering Research Center, University of California Berkeley.

ANSYS (2013). *ANSYS Mechanical APDL Theory Reference, Release 15*, ANSYS Inc. Canosburg, PA.

Arabzade, A., Moharami, H., and Ayazi, A. (2011). "Local elastic buckling coefficients of steel plates in composite steel plate shear walls." *Scientia Iranica*, 18(1), 9-15.

Arabzadeh, A., Soltani, M., and Ayazi, A. (2011). "Experimental investigation of composite shear walls under shear loadings." *Thin-Walled Structures*, 49(7), 842-854.

ASCE (2010). *Minimum Design Loads for Buildings and Other Structures, ASCE/SEI Standard 7-10, American Society of Civil Engineers*, Reston, Virginia.

ASCE (2013). *Seismic Evaluation and Retrofit of Exisiting Buildings, ASCE/SEI Standard 41-13, American Society of Civil Engineers*, Reston, Virginia.

ASCE (2016). *Minimum Design Loads for Buildings and Other Structures, ASCE/SEI Standard 7-16, American Society of Civil Engineers*, Reston, Virginia.

Astaneh-Asl, A. (1985). "Procedure for Design and Analysis of Hanger-type Connections." *Engineering Journal, AISC*, 22(2), 63-66.
Astaneh-Asl, A. (1989). "Simple methods for design of steel gusset plates." *Steel Structures, ASCE Structures Congress, May*, J.S.B.Iffland, ed., ASCE, 345-354.
Astaneh-Asl, A. (1995). "Seismic Design of Bolted Steel Moment-Resisting Frames." *Steel Technical Information and Product Services (Steel TIPS) Report*Structural Steel Educational Council (www.steeltips.org) , CA.
Astaneh-Asl, A. (1998a). "Seismic behavior and design of gusset plates." *Steel Technical Information and Product Services (Steel TIPS) Report*Structural Steel Educational Council, (www.steeltips.org), CA, 45.
Astaneh-Asl, A. (1998b). "Seismic Behavior and Design of Gusset Plates." S. S. E. Council, ed.CA.
Astaneh-Asl, A. (2001). "Seismic Behavior and Design of Steel Shear Walls - SEAONC Seminar " *SEAONC Seminar* Structural Engineers Association of Northern California November 7, 2001, San Francisco
Astaneh-Asl, A. (2002a). "Seismic behavior and design of composite steel plate shear walls." *Steel Technical Information and Product Services (Steel TIPS) Report*Structural Steel Educational Council (www.steeltips.org) , CA, pp.45.
Astaneh-Asl, A. (2002b). "Seismic behavior and design of steel shear walls." *Steel Technical Information and Product Services (Steel TIPS) Report.* Structural Steel Educational Council, (www.steeltips.org), CA, pp.45.
Astaneh-Asl, A. (2010). *Gusset Plates in Steel Bridges - Design and Evaluation* Structural Steel Educational Council, (www.steeltips.org), CA.
Astaneh-Asl, A., Cochran, M., and Sabelli, R. (2006). *Seismic Detailing of Gusset Plates for Special Concentrically Braced Frames.* , Structural Steel Educational Council, (www.steeltips.org) , CA.
Astaneh-Asl, A., Modjtahedi, D., Mcmullin, K., Shen, J.-H., and D'Amore, E. (1998). "Stability of damaged steel frames in Los Angeles." *Engineering Structures*, 20(4-6), 433-446.
Astaneh-Asl, A., and Zhao, Q. H. (2000). "Seismic studies of an innovative and traditional composite shear walls." *6th ASCCS International Conference on Steel-Concrete Composite Structures*Los Angeles, CA, pp.6.
ATC (2009). "Guidelines for seismic performance assessment of buildings: ATC-58 50% draft." Rep. No.58, Applied Technology Council (ATC), Washington, DC.
Baldelli, J. A. (1983). "Steel Shear Walls for Existing Buildings." *AISC Eng. J.*, Second Quarter, 70-77.
Baldvins, N. M., Berman, J. W., Lowes, L. N., Janes, T. M., and Low, N. A. (2012). "Fragility functions for steel plate shear walls." *Earthquake Spectra*, 28(2), 405-426.
Basler, K. (1961). "Strength of plate girders under combined shear and bending." *Proc. A.S.C.E.87(ST7)*, 30.
Basler, K., and Thuerlimann, A. (1961). "Strength of plate girders in bending." *Journal of the Structural Division*, 87(6), 153-184.
Basler, K., Yen, B., Mueller, J., and Thurlimann, B. (1960). *Web buckling tests on welded plate girders*, Fritz Engineering Laboratory, Lehigh University.
Behbahanifard, M. R., Grondin, G. Y., and Elwi, A. E. (2003). "Experimental and numerical investigation of steel plate shear wall." *Structural engineering report*, 254.
Bergman, S., and Reissner, H. (1932). "Uber die Knickung von rechteckigen Platten bei Schubbeanspruchung (in German)." *Z. Flugtech Motorluftschiffahrt*, 23, 6.
Berman, J., and Bruneau, M. (2003). "Plastic analysis and design of steel plate shear walls." *Journal of Structural Engineering*, 129(11), 1448-1456.
Berman, J. W. (2011). "Seismic behavior of code designed steel plate shear walls." *Engineering Structures*, 33(1), 230-244.
Berman, J. W., and Bruneau, M. (2004). "Steel plate shear walls are not plate girders." *ENGINEERING JOURNAL-AMERICAN INSTITUTE OF STEEL CONSTRUCTION*, 41, 95-106.

Berman, J. W., and Bruneau, M. (2005). "Experimental investigation of light-gauge steel plate shear walls." *Journal of Structural Engineering*, 131(2), 259-267.
Berman, J. W., and Bruneau, M. (2008). "Capacity design of vertical boundary elements in steel plate shear walls." *ENGINEERING JOURNAL-AMERICAN INSTITUTE OF STEEL CONSTRUCTION INC*, 45(1), 57-71.
Bhowmick, A. K., Driver, R. G., and Grondin, G. Y. (2009). "Seismic analysis of steel plate shear walls considering strain rate and –delta effects." *Journal of Constructional Steel Research*, 65(5), 1149-1159.
Bonowitz, D., and Youssef, N. (1994). "SAC Survey of Steel Moment-Resisting Frame Buildings Affected by the 1994 Northridge Earthquake." *Technical Report 95-06: Surveys and Assessment of Damage to Buildings Affected by the Northridge Earthquake of January 17, SAC Joint Venture*, 169.
Bruneau, M., Uang, C., and Sabelli, R. (2011). "Section 2.7 - Material Models. In Ductile Design of Steel Structures, 2nd Edition.".
Bulson, P. S. (1970). *Stability of Flat Plates*, American Elsevier, New York.
Caccese, V., Elgaaly, M., and Chen, R. (1993). "Experimental study of thin steel-plate shear walls under cyclic load." *Journal of Structural Engineering*, 119(2), 573-587.
Celebi, M. (1997). "Response of Olive View Hospital to Northridge and Whittier Earthquake." *Journal of Structural Engineering, ASCE*, 123(4), 389-396.
Chan, R., Albermani, F., and Kitipornchai, S. (2011). "Stiffness and strength of perforated steel plate shear wall." *Procedia Engineering*, 14, 675-679.
Chao, S.-H., and Goel, S. C. (2005). "Performance-based seismic design of EBF using target drift and yield mechanism as performance criteria." *Ann Arbor*, 1001, 48109-42125.
Chen, R. (1991). "Behavior of unstiffened thin steel plate shear walls, Ph.D. Thesis " Ph.D., University of Maine.
Chen, S.-J., and Jhang, C. (2006). "Cyclic behavior of low yield point steel shear walls." *Thin-Walled Structures*, 44(7), 730-738.
Chen, S.-J., and Jhang, C. (2011). "Experimental study of low-yield-point steel plate shear wall under in-plane load." *Journal of Constructional Steel Research*, 67(6), 977-985.
Chen, Y., Ning, Y., and Jiang, L. (2012). "Experimental study on seismic behavior of frame-steel plate shear wall with slits." *Journal of Building Structures*, 7, 017.
Choi, I.-R., and Park, H.-G. (2008). "Ductility and energy dissipation capacity of shear-dominated steel plate walls." *Journal of structural engineering*, 134(9), 1495-1507.
Choi, I.-R., and Park, H.-G. (2009). "Steel plate shear walls with various infill plate designs." *Journal of structural engineering*, 135(7), 785-796.
Choi, I.-R., and Park, H.-G. (2010). "Hysteresis model of thin infill plate for cyclic nonlinear analysis of steel plate shear walls." *Journal of structural engineering*, 136(11), 1423-1434.
Chopra, A. K. (2007). *Dynamics of Structures: Theory and Applications to Earthquake Engineering, 4th e.d.*, Prentice Hall, Upper Saddle River, NJ.
Chopra, A. K., and Goel, R. K. (2001). "Direct displacement-based design: use of inelastic vs. elastic design spectra." *Earthquake Spectra*, 17(1), 47-64.
Chopra, A. K., and McKenna, F. (2016). "Modeling viscous damping in nonlinear response history analysis of buildings for earthquake excitation." *Earthquake Engineering & Structural Dynamics*, 45(2), 193-211.
Clayton, P. M., Berman, J. W., and Lowes, L. N. (2012). "Seismic Design and Performance of Self-Centering Steel Plate Shear Walls." *Journal of Structural Engineering*, 138(1).
Clayton, P. M., Berman, J. W., and Lowes, L. N. (2013). "Subassembly testing and modeling of self-centering steel plate shear walls." *Engineering Structures*, 56(0), 1848-1857.
Clayton, P. M., Berman, J. W., and Lowes, L. N. (2015). "Seismic performance of self-centering steel plate shear walls with beam-only-connected web plates." *Journal of Constructional Steel Research*, 106(0), 198-208.

Commerce, J. o. (1984). "Vancouver Steel Plate Shear Wall Design Follows Japanese Approach."
Cook, I. T., and Rockey, K. C. (1963). "Shear Buckling of Rectangular Plates with Mixed Boundary Conditions." *Aeronaut. Q.*, 14.
Cortes, G., and Liu, J. (2011a). "Analysis and design of steel slit panel frames (SSPFs) for seismic areas." *Engineering Journal-Chicago*, 48(1), 1.
Cortes, G., and Liu, J. (2011b). "Experimental evaluation of steel slit panel–frames for seismic resistance." *Journal of Constructional Steel Research*, 67(2), 181-191.
CSA (1994). *Limit state design of steel structures, CAN/CSA-S16.2-M94*, Canadian Standard Association,Toronto, Ontario
CSA (2011). *Limit state design of steel structures, CAN/CSA-S16-11*, Canadian Standard Association,Toronto, Ontario
CSI (2011). *Perform-3D Nonlinear Analysis and Performance Assessment for 3D Structures - User Guide, Version 5*, Computers & Structures Inc., Berkeley, California
CSI (2016). *CSI Analysis Reference Manual For SAP2000, ETABS, SAFE and CSiBridge*, Computers & Structures Inc., Berkeley, California
D'Aniello, M., Cassiano, D., and Landolfo, R. (2016). "Monotonic and cyclic inelastic tensile response of European preloadable GR10. 9 bolt assemblies." *Journal of Constructional Steel Research*, 124, 77-90.
D'Aniello, M., Tartaglia, R., Costanzo, S., and Landolfo, R. (2017). "Seismic design of extended stiffened end-plate joints in the framework of Eurocodes." *Journal of Constructional Steel Research*, 128, 512-527.
Dowden, D., and Bruneau, M. (2014). "Analytical and experimental investigation of self-centering steel plate shear walls." *Technical Report MCEER-14-0010*, Multidisciplinary Center for Earthquake Engineering Research, State Univ. of New York at Buffalo, Buffalo, New York.
Driver, R. G. (1997). "Seismic behaviour of steel plate shear walls." Department of Civil and Environmental Engineering, University of Alberta.
Driver, R. G., Kulak, G. L., Elwi, A. E., and Kennedy, D. L. (1998a). "FE and simplified models of steel plate shear wall." *Journal of Structural Engineering*, 124(2), 121-130.
Driver, R. G., Kulak, G. L., Kennedy, D. L., and Elwi, A. E. (1998b). "Cyclic test of four-story steel plate shear wall." *Journal of Structural Engineering*, 124(2), 112-120.
Driver, R. G., and Moghimi, H. (2011). "Modular construction of steel plate shear walls for low and moderate seismic regions." *Structures Congress, Structural Engineering Institute, American Society of Civil Engineers, Las Vegas, NV*, 758-769.
Eatherton, M. (2006). "Design and construction of steel plate shear walls." *Proceedings of the Eighth US National Conference on Earthquake Engineering*San Francisco, California, USA.
Eatherton, M., and Johnson, K. (2004). "High-End Residence using Steel Plate Shear Walls in Woodside, California." *SEAOC 2004 Convention: 75th Anniversary Celebration*Monterey, CA, 19-29.
Egorova, N., Eatherton, M. R., and Maurya, A. (2014). "Experimental study of ring-shaped steel plate shear walls." *Journal of Constructional Steel Research*, 103(0), 179-189.
Elgaaly, M. (1998). "Thin steel plate shear walls behavior and analysis." *Thin-Walled Structures*, 32(1–3), 151-180.
Elgaaly, M., Caccese, V., and Du, C. (1993). "Postbuckling behavior of steel-plate shear walls under cyclic loads." *Journal of Structural Engineering*, 119(2), 588-605.
Elgaaly, M., and Liu, Y. (1997). "Analysis of thin-steel-plate shear walls." *Journal of Structural Engineering*, 123(11), 1487-1496.
Elkady, A., and Lignos, D. G. (2014). "Modeling of the composite action in fully restrained beam-to-column connections: implications in the seismic design and collapse capacity of steel special moment frames." *Earthquake Engineering & Structural Dynamics*, 43(13), 1935-1954.
Engelhardt, M. D., and Sabol, T. A. (1998). "Reinforcing of steel moment connections with cover plates: Benefits and limitations." *Engineering Structures*, 20(4-6), 510-520.

Englehardt, M. D., Winneberger, T., Zekany, A. J., and Potyraj, T. J. (1997). "Experimental investigation of dogbone moment connections." *Engineering Journal, AISC*, 35(4), 128-139.

Evans, H., Porter, D., and Rockey, K. (1978). *The collapse behaviour of plate girders subjected to shear and bending*, IABSE, International Association for Bridge and Structural Engineering, Zürich, Schweiz.

FEMA-267 (1995). "INTERIM GUIDELINES: Evaluation, Repair, Modification and Design of Steel Moment Frames." *prepared by the SAC Joint Venture for the Federal Emergency Management Agency*Washington, DC.

FEMA-289 (1996). "Connection Test Summaries (SAC-96-02)." *prepared by the SAC Joint Venture for the Federal Emergency Management Agency* Washington, DC.

FEMA-352 (2000). "Recommended Postearthquake Evaluation and Repair Criteria for Welded Steel Moment-Frame Buildings,." *prepared by the SAC Joint Venture for the Federal Emergency Management Agency*Washington, DC.

FEMA-355A (2000). "State of the Art Report on Base Metals and Fracture." *prepared by the SAC Joint Venture for the Federal Emergency Management Agency*Washington, DC.

FEMA-355B (2000). "State of the Art Report on Welding and Inspection." *prepared by the SAC Joint Venture for the Federal Emergency Management Agency*Washington, DC.

FEMA-355C (2000). "State of the Art Report on Systems Performance of Steel Moment Frames Subject to Earthquake Ground Shaking." *prepared by the SAC Joint Venture for the Federal Emergency Management Agency*Washington, DC.

FEMA-355D (2000). "State of the Art Report on Connection Performance." *prepared by the SAC Joint Venture for the Federal Emergency Management Agency*Washington, DC.

FEMA-355E (2000). "State of the Art Report on Past Performance of Steel Moment-Frame Buildings in Earthquakes." *prepared by the SAC Joint Venture for the Federal Emergency Management Agency*Washington, DC.

FEMA-355F (2000). "State of the Art Report on Performance Prediction and Evaluation of Steel Moment-Frame Buildings." *prepared by the SAC Joint Venture for the Federal Emergency Management Agency*Washington, DC.

FEMA-356 (2000). "Prestandard and Commentary for the Seismic Rehabilitation of Buildings." *prepared by the American Society of Civil Engineers for the Federal Emergency Management Agency*Washington, DC.

FEMA-450 (2003). "NEHRP recommended provisions for seismic regulations for new buildings and other structures " *FEMA Report No.450.* Building Seismic Safety Council for Federal Emergency Management Agency, Washington, D.C.

FEMA-P440A (2009). "Effects of strength and stiffness degradation on seismic response." *FEMA Report No.P440A*Applied Technology Council for Federal Emergency Management Agency, Washington, D.C.

FEMA-P695 (2009). "Quantification of Building Seismic Performance Factors." *FEMA Report No.P695.* Applied Technology Council for Federal Emergency Management Agency, Washington, D.C.

Filippou, F. C., Popov, E. P., and Bertero, V. V. (1983). "Effects of Bond Deterioration on Hysteretic Behavior of Reinforced Concrete Joints."Report EERC 83-19, Earthquake Engineering Research Center, University of California, Berkeley.

Fujitani, H., Yamanouchi, H., Okawa, I., Sawai, N., Uchida, N., and Matsutani, T. (1996). "Damage and performance of tall buildings in the 1995 Hyogoken Nanbu earthquake." *67th Regional Conference (in conjunction with ASCE Structures Congress XIV)*, Council on Tall Buildings and Urban Habitat, Chicago, 103-125.

Ghosh, S., Adam, F., and Das, A. (2009). "Design of steel plate shear walls considering inelastic drift demand." *Journal of Constructional Steel Research*, 65(7), 1431-1437.

Goel, S. C., and Chao, S.-H. (2008). *Performance-based plastic design: earthquake-resistant steel structures*, International Code Council.

Goel, S. C., Stojadinović, B., and Lee, K.-H. (1996). *A new look at steel moment connections*, Research Report UMCEE 96-19, Department of Civil Engineering, University of Michigan, Ann Arbor, Michigan.
Guo, B., Gu, Q., and Liu, F. (2006). "Experimental behavior of stiffened and unstiffened end-plate connections under cyclic loading." *Journal of Structural Engineering*, 132(9), 1352-1357.
Guo, L., Rong, Q., Ma, X., and Zhang, S. (2011). "Behavior of steel plate shear wall connected to frame beams only." *International Journal of Steel Structures*, 11(4), 467-479.
Guo, L., Rong, Q., Ma, X., and Zhang, S. (2013). "Analysis of composite steel plate shear walls connected with frame beams only." *Proceedings of the ICE-Structures and Buildings*, 166(9), 507-518.
Guo, Y., Dong, Q., and ZHOU, M. (2009). "Tests and analysis on hysteretic behavior of buckling restrained steel plate shear wall." *Journal of Building Structures* 30(1), 10.
Guo, y., Miao, y., and Dong, q. (2007). "Elastic Buckling Behavior of Stiffened Steel Plate Shear Walls Slotted at Two Edges." *Progress in Steel Building Structures*, 9(3), 5.
Gupta, A., and Krawinkler, H. (1999). "Seismic demands for performance evaluation of steel moment resisting frame structures (SAC Task 5.4.3). Technical Report No.132." John A. Blume Earthquake Engineering Center, Stanford University, Stanford, California.
Habashi, H. R., and Alinia, M. M. (2010). "Characteristics of the wall–frame interaction in steel plate shear walls." *Journal of Constructional Steel Research*, 66(2), 150-158.
Hamburger, R. O., Deierlein, G., Lehman, D., Lowes, L., Shing, B., Lindt, J. v. d., Lignos, D., and Hortacsu, A. (2016). "ATC-114 Next-Generation Hysteretic Relationships for Performance-based Modeling and Analysis." *2016 SEAOC Convention.* Maui, Hawaii, 73-85.
Haselton, C. B., Whittaker, A. S., Hortacsu, A., Baker, J. W., Bray, J., and Grant, D. N. (2012). "Selecting and scaling earthquake ground motions for performing response-history analyses." *Proceedings of the 15th World Conference on Earthquake Engineering*.
Hertzberg, R. W., Vinci, R. P., and Hertzerg, J. L. (2012). "Deformation and Fracture Mechanics of Engineering Materials, 5ed."
Hitaka, T., and Matsui, C. (2003). "Experimental study on steel shear wall with slits." *Journal of Structural Engineering*, 129(5), 586-595.
Horne, M. R., and Morris, L. J. (1982). *Plastic design of low-rise frames*, The MIT Press.
Hosseinzadeh, S. A. A., and Tehranizadeh, M. (2014). "Behavioral characteristics of code designed steel plate shear wall systems." *Journal of Constructional Steel Research*, 99(0), 72-84.
Ibarra, L. F., and Krawinkler, H. (2005). *Global collapse of frame structures under seismic excitations*, Pacific Earthquake Engineering Research Center Berkeley, CA.
Ibarra, L. F., Medina, R. A., and Krawinkler, H. (2005). "Hysteretic models that incorporate strength and stiffness deterioration." *Earthquake Engineering & Structural Dynamics*, 34(12), 1489-1511.
IBC (2015). *2015 International Building Code*, Country Club Hills, III: International Code Council.
Iguchi, S. (1938). "Die Kninckung der rechteckigen Platte durch Schubkräfte." *Ing. Arch.*, 9, 1.
JGJ (2015). *Technical specification for steel plate shear walls, JGJ/T 380-2015*, China Architecture & Building Press, Beijing (in Chinese).
Jin, S., Ou, J., and Liew, J. R. (2016). "Stability of buckling-restrained steel plate shear walls with inclined-slots: theoretical analysis and design recommendations." *Journal of Constructional Steel Research*, 117, 13-23.
Kharmale, S. B., and Ghosh, S. (2013). "Performance-based plastic design of steel plate shear walls." *Journal of Constructional Steel Research*, 90(0), 85-97.
Kharrazi, M. H., Ventura, C. E., and Prion, H. G. (2010a). "Analysis and design of steel plate walls: analytical model." *Canadian Journal of Civil Engineering*, 38(1), 49-59.
Kharrazi, M. H., Ventura, C. E., and Prion, H. G. (2010b). "Analysis and design of steel plate walls: experimental evaluation." *Canadian Journal of Civil Engineering*, 38(1), 60-70.
Kharrazi, M. H. K., Prion, H. G. L., and Ventura, C. E. (2008). "Implementation of M-PFI method in design of steel plate walls." *Journal of Constructional Steel Research*, 64(4), 465-479.

Kostic, S. M., and Filippou, F. C. (2012). "Section Discretization of Fiber Beam-Column Elements for Cyclic Inelastic Response." *Journal of Structural Engineering*, 138(5).
Kowalsky, M. J., Priestley, M. N., and Macrae, G. A. (1995). "Displacement-based design of RC bridge columns in seismic regions." *Earthquake engineering & structural dynamics*, 24(12), 1623-1643.
Krawinkler, H. (2006). "Importance of good nonlinear analysis " *The Structural Design of Tall and Special Buildings* (15), 515-531.
Lai, J., Wang, S., Schoettler, M., and Mahin, S. (2015). "Seismic Evaluation and Retrofit of Exisiting Tall Buildings in California: Case Study of a 35-Story Steel Moment-Resisting Frame Building in San Francisco." *PEER Report No.2015/14*, University of California, Berkeley 301.
LATBSDC (2015). "An Alternative Procedure for Seismic Analysis and Design of Tall Buildings Located in the Los Angeles Region (2014 Edition with 2015 Supplements)."Los Angeles Tall Buildings Structural Design Council (LATBSDC), Los Angeles, CA.
Lee, C.-H. (2002). "Seismic design of rib-reinforced steel moment connections based on equivalent strut model." *Journal of Structural Engineering*, 128(9), 1121-1129.
Lee, K.-H., Goel, S. C., and Stojadinović, B. (1997). *Boundary effects in welded steel moment connections*, Research Report UMCEE 97-20, Department of Civil Engineering, University of Michigan, Ann Arbor, Michigan.
Lee, S.-S., Goel, S. C., and Chao, S.-H. (2004). "Performance-based seismic design of steel moment frames using target drift and yield mechanism." *13th world conference on Earthquake Engineering*.
Lee, S., Wang, D., Liao, Y., and Mathias, N. (2010). "Performance based seismic design of a 75 story buckling restrained slender steel plate shear wall tower." *Structures Congress, ASCE*. Orlando, Florida.
Li, C. H., Tsai, K. C., Lin, C. H., and Chen, P. C. (2010). "Cyclic tests of four two-story narrow steel plate shear walls. Part 2: experimental results and design implications." *Earthquake Engineering & Structural Dynamics*, 39(7), 801-826.
Lignos, D., Krawinkler, H., and Whittaker, A. (2011). "Prediction and validation of sidesway collapse of two scale models of a 4-story steel moment frame." *Earthquake Engineering & Structural Dynamics*, 40(7), 807-825.
Lignos, D. G., and Krawinkler, H. (2007). "A database in support of modeling of component deterioration for collapse prediction of steel frame structures." *Structural Engineering Research Frontiers*, 1-12.
Lignos, D. G., and Krawinkler, H. (2009). "Sidesway collapse of deteriorating structural systems under seismic excitations, Rep.No.TB 172."The John A. Blume Earthquake Engineering Research Center, Stanford University, Stanford, CA.
Lignos, D. G., and Krawinkler, H. (2010). "Deterioration modeling of steel components in support of collapse prediction of steel moment frames under earthquake loading." *Journal of Structural Engineering*, 137(11), 1291-1302.
Lin, C.-H., Tsai, K.-C., Qu, B., and Bruneau, M. (2010a). "Sub-structural pseudo-dynamic performance of two full-scale two-story steel plate shear walls." *Journal of Constructional Steel Research*, 66(12), 1467-1482.
Lin, C.-H., Tsai, K.-C., Qu, B., and Bruneau, M. (2010b). "Sub-structural pseudo-dynamic performance of two full-scale two-story steel plate shear walls." *Journal of Constructional Steel Research*, 66(12), 1467-1482.
Lin, Y. Y., Tsai, M. H., Hwang, J. S., and Chang, K. C. (2003). "Direct displacement-based design for building with passive energy dissipation systems." *Engineering Structures*, 25(1), 25-37.
Lubell, A. S. (1997). "Performance of unstiffened steel plate shear walls under cyclic quasi-static loading." University of British Columbia.
Lubell, A. S., Prion, H. G., Ventura, C. E., and Rezai, M. (2000). "Unstiffened steel plate shear wall performance under cyclic loading." *Journal of Structural Engineering*, 126(4), 453-460.

Mahin, S. A. (1998). "Lessons from damage to steel buildings during the Northridge earthquake." *Engineering structures*, 20(4), 261-270.
McKenna, F., Scott, M., and Fenves, G. (2010). "Nonlinear finite-element analysis software architecture using object composition." *Journal of Computing Civil Engineering*, 24(1), 95-107.
Miao, y., Dong, q., and guo, y. (2007). "Elastic Buckling Behavior of Steel Plate Shear Walls Slotted at Two Edges " *Steel Construction* 22(9), 4.
Mimura, H., and Akiyana, H. (1977). "Load-Deflection Relationship of Earthquake-Resistant Steel Shear Walls with a Developed Diagonal Tension Field." *Transactions of the Architectural Institute of Japan* 260(October).
Moehle, J. (1992). "Displacement-based design of RC structures subjected to earthquakes." *Earthquake spectra*, 8(3), 403-428.
Moghimi, H., and Driver, R. G. (2014). "Column demands in steel plate shear walls with regular perforations using performance-based design methods." *Journal of Constructional Steel Research*, 103(0), 13-22.
Moheit, W. (1939). "Schubbeulung rechteckiger Platten mit eingespannten Rändern, Thesis." Technische Hochschule Darmstadt, Leipzig, Germany.
Nader, M., and Astaneh-Asl, A. (1998). "Dynamic Behavior of Flexible, Semi-rigid and Rigid Steel Frames." *Engineering Structures*, 20(4-6), 261-270.
Nakagawa, S., Kihara, H., Torii, S., Nakata, Y., Matsuoka, Y., Fujisawa, K., and Fukuda, K. (1996). "Hysteretic behavior of low yield strength steel panel shear walls: experimental investigation." *Proceedings of the 11th WCEE, Elsevier, CD-ROM, Paper*(171).
Nakashima, M. (1995a). "Reconnaissance Report on Damage to Steel Building Structures Observed from the 1995 Hyogoken-Nanbu (Hanshin/Awaji) Earthquake." Steel Committee of Kinki Branch, Architectural Institute of Japan (AIJ).
Nakashima, M. (1995b). "Strain-hardening behavior of shear panels made of low-yield steel. I: Test." *Journal of structural Engineering*, 121(12), 1742-1749.
Nakashima, M., Akazawa, T., and Tsuji, B. (1995). "Strain-hardening behavior of shear panels made of low-yield steel. II: model." *Journal of Structural Engineering*, 121(12), 1750-1757.
Nakashima, M., Iwai, S., Iwata, M., Takeuchi, T., Konomi, S., Akazawa, T., and Saburi, K. (1994). "Energy dissipation behaviour of shear panels made of low yield steel." *Earthquake engineering & structural dynamics*, 23(12), 1299-1313.
Nie, J.-G., Zhu, L., Fan, J.-S., and Mo, Y.-L. (2013). "Lateral resistance capacity of stiffened steel plate shear walls." *Thin-Walled Structures*, 67(0), 155-167.
Nie, J., Fan, J., Liu, X., and Huang, Y. (2012). "Comparative Study on Steel Plate Shear Walls Used in a High-Rise Building." *Journal of Structural Engineering*, 139(1), 85-97.
OpenSeesWiki "Modified Ibarra-Medina-Krawinkler Deterioration Model with Bilinear Hysteretic Response (Bilin Material)." <http://opensees.berkeley.edu/wiki/index.php/Modified_Ibarra-Medina-Krawinkler_Deterioration_Model_with_Bilinear_Hysteretic_Response_(Bilin_Material)>. (August, 2017).
OpenSeesWiki "Steel02 Material - Giuffré-Menegotto-Pinto Model with Isotropic Strain Hardening." <http://opensees.berkeley.edu/wiki/index.php/Steel02_Material_--_Giuffr%C3%A9-Menegotto-Pinto_Model_with_Isotropic_Strain_Hardening>. (August, 2017).
Park, H.-G., Kwack, J.-H., Jeon, S.-W., Kim, W.-K., and Choi, I.-R. (2007). "Framed steel plate wall behavior under cyclic lateral loading." *Journal of structural engineering*, 133(3), 378-388.
PEER (2010). "Guidelines for Performance-Based Seismic Design of Tall Buildings (as part of the Tall Buildings Initiative) " *Report PEER-2010/05*, Pacific Earthquake Engineering Research Center, University of California, Berkeley, CA.
Popov, E. P., and Stephen, R. M. (1970). "Cyclic loading of full-size steel connections." *Technical Report UCB/EERC-70/03, Earthquake Engineering Research Center, University of California, Berkeley*.

Porter, D., Rockey, K., and Evans, H. (1987). "The collapse behaviour of plate girders loaded in shear." *The Structural Engineer*, 53(8), 313-325.
Priestley, M., Calvi, G., and Kowalsky, M. (2007). "Direct displacement-based seismic design of structures." *2007 NZSEE conference*.
Priestley, M. N. (1993). "Myths and fallacies in earthquake engineering—conflicts between design and reality." *Bulletin of the New Zealand National Society for Earthquake Engineering*, 26(3), 329-341.
Purba, R., and Bruneau, M. (2009). "Finite-element investigation and design recommendations for perforated steel plate shear walls." *Journal of structural engineering*, 135(11), 1367-1376.
Purba, R., and Bruneau, M. (2011). "Case study on the impact of horizontal boundary elements design on seismic behavior of steel plate shear walls." *Journal of Structural Engineering*, 138(5), 645-657.
Purba, R., and Bruneau, M. (2014). "Seismic Performance of Steel Plate Shear Walls Considering Various Design Approaches. Technical Report MCEER-14-0005." Multidisciplinary Center for Earthquake Engineering Research, State Univ. of New York at Buffalo, Buffalo, New York.
Purba, R., and Bruneau, M. (2015a). "Seismic Performance of Steel Plate Shear Walls Considering Two Different Design Philosophies of Infill Plates. I: Deterioration Model Development." *Journal of Structural Engineering*, 141(6), 04014160.
Purba, R., and Bruneau, M. (2015b). "Seismic Performance of Steel Plate Shear Walls Considering Two Different Design Philosophies of Infill Plates. II: Assessment of Collapse Potential." *Journal of Structural Engineering*, 141(6), 04014161.
Qian, X., and Astaneh-Asl, A. (2016a). "Behaviour and Seismic Design of Stiffeners for Steel Bridge Tower Legs and Piers." *World Congress on Civil, Structural, and Environmental Engineering (CSEE'16)*Prague, Czech Republic, 8.
Qian, X., and Astaneh-Asl, A. (2016b). "Development of a high-performance steel plate shear wall system." *Int. Journal of Earthquake and Impact Engineering, Inderscience Publishers*, 1(1), 57-80.
Qian, X., and Astaneh-Asl, A. (2016c). "Development of a New Steel Moment Connection." *World Congress on Civil, Structural, and Environmental Engineering (CSEE'16)*Prague, Czech Republic, 8.
Qian, X., and Astaneh-Asl, A. (2016d). "Introducing a New Ductile and Economical Steel Moment Connection." *2016 SEAOC Convention, October 12-15* Maui, Hawaii, 8.
Qu, B., and Bruneau, M. (2009). "Capacity design of intermediate horizontal boundary elements of steel plate shear walls." *Journal of Structural Engineering*, 136(6), 665-675.
Qu, B., Bruneau, M., Lin, C.-H., and Tsai, K.-C. (2008). "Testing of full-scale two-story steel plate shear wall with reduced beam section connections and composite floors." *Journal of structural engineering*, 134(3), 364-373.
Rahai, A., and Hatami, F. (2009). "Evaluation of composite shear wall behavior under cyclic loadings." *Journal of Constructional Steel Research*, 65(7), 1528-1537.
Rezai, M., Ventura, C. E., and Prion, H. G. (2000). "Numerical investigation of thin unstiffened steel plate shear walls." *12th World Conference on Earthquake Engineering*, 1-4.
Roberts, T. M., and Sabouri-Ghomi, S. (1992). "Hysteretic characteristics of unstiffened perforated steel plate shear panels." *Thin-Walled Structures*, 14(2), 139-151.
Robinson, K., and Ames, D. (2000). "Steel Plate Shear Walls - Library Seismic Upgrade." *Modern Steel Construction*, 40(1), 56-60.
Rockey, K., Evans, H., and Porter, D. (1978). "A design method for predicting the collapse behaviour of plate girders." *ICE proceedings*, Thomas Telford, 85-112.
Rockey, K., and Skaloud, M. (1972). "The ultimate load behaviour of plate girders loaded in shear." *The Structural Engineer*, 50(1), 29-47.
Sabouri-Ghomi, S., and Roberts, T. (1992). "Nonlinear dynamic analysis of steel plate shear walls including shear and bending deformations." *Engineering Structures*, 14(5), 309-317.

Sabouri-Ghomi, S., and Sajjadi, S. R. A. (2012). "Experimental and theoretical studies of steel shear walls with and without stiffeners." *Journal of Constructional Steel Research*, 75(0), 152-159.
Sabouri-Ghomi, S., Ventura, C. E., and Kharrazi, M. H. (2005). "Shear analysis and design of ductile steel plate walls." *Journal of Structural Engineering*, 131(6), 878-889.
Saeki, E., Sugisawa, M., Yamaguchi, T., and Wada, A. (1998). "Mechanical properties of low yield point steels." *Journal of materials in civil engineering*, 10(3), 143-152.
Salawdeh, S., and Goggins, J. (2016). "Performance based design approach for multi-storey concentrically braced steel frames." *Steel and Composite Structures*, 20(4), 749-776.
Sarkisian, M. P., and Mathias, N. J. (2012). "Testing as a Validation tool for tall, non-prescriptive buildings in China." *Structures Congress 2012, American Society of Civil Engineers*, p.848-859
Schumacher, A., Grondin, G. Y., and Kulak, G. L. (1999). "Connection of infill panels in steel plate shear walls." *Canadian Journal of Civil Engineering*, 26(5), 549-563.
Segovia, V. A., and Ruiz, S. E. (2016). "Direct Displacement-Based Design for Buildings with Hysteretic Dampers, using Best Combinations of Stiffness and Strength Ratios." *Journal of Earthquake Engineering*, 1-24.
Seydel, E. (1933). "Über das Ausbeulen von rechteckigen isotropen oder orthogonalanisotropen Platten bei Schubbeanspruchung." *Ing. Arch.*, 4, 169.
Shao, J.-h., Gu, Q., and Shen, Y.-k. (2008). "Seismic performance evaluation of steel frame-steel plate shear walls system based on the capacity spectrum method." *Journal of Zhejiang University-Science A*, 9(3), 322-329.
Shi, Y., and Astaneh-Asl, A. (2008). "Lateral Stiffness of Steel Shear Wall Systems." *Structures Congress, ASCE, April 24-26.* Vancouver, Canada, pp.10.
Shibata, A., and Sozen, M. A. (1976). "Substitute-structure method for seismic design in R/C." *Journal of the structural division*, 102(ASCE# 11824).
Shishkin, J. J., Driver, R. G., and Grondin, G. Y. (2009). "Analysis of Steel Plate Shear Walls Using the Modified Strip Model." *Journal of Structural Engineering*, 135(11), 1357-1366.
Southwell, R. V., and Skan, S. (1924). "On the Stability Under Shearing Force of a Flat Elastic Strip." *Proc. R. Soc.*, A105.
Sullivan, T., Calvi, G., Priestley, M., and Kowalsky, M. (2003). "The limitations and performances of different displacement based design methods." *Journal of Earthquake Engineering*, 7(spec01), 201-241.
Sullivan, T. J., Calvi, G. M., and Priestley, M. N. (2006). *Seismic design of frame-wall structures*, IUSS Press.
Takahashi, Y., Takemoto, Y., Takeda, T., and Takagi, M. (1973). "Experimental study on thin steel shear walls and particular bracings under alternative horizontal load (preliminary report)." *IABSE, Symp. On Resistance and Ultimate Deformability of Structures Acted on by Well-defined Repeated Loads*Lisbon, Portugal.
Tena-Colunga, A., and Nangullasmú-Hernández, H. (2015). "Assessment of seismic design parameters of moment resisting RC braced frames with metallic fuses." *Engineering Structures*, 95, 138-153.
Thorburn, L. J., Kulak, G. L., and Montgomery, C. (1983). "Analysis of steel plate shear walls."
Timler, P., and Kulak, G. L. (1983). "Experimental study of steel plate shear walls." Department of Civil Engineering, University of Alberta, Edmonton, Alberta, 112.
Timoshenko, S. (1910). "Einge Stabilitatsprobleme der Elastizitatstheorie." *Z. Math. Phys.*, 68, 337.
Tromposch, E., and Kulak, G. L. (1987). *Cyclic and static behaviour of thin panel steel plate shear walls*, Department of Civil Engineering, University of Alberta, Edmonton, Canada.
Troy, R. G., and Richard, R. M. (1979). "Steel Plate Shear Walls Resist Lateral Load, Cut Costs." *Civil Engineering, ASCE*, 49, 3.
Tsai, K., Lin, Y., and Lin, C. (2007). "Seismic responses and design of steel plate shear wall." *Progress in Steel Building Structures*, 9(5), 19-25.

Tsai, K. C., Li, C. H., Lin, C. H., Tsai, C. Y., and Yu, Y. J. (2010). "Cyclic tests of four two-story narrow steel plate shear walls—Part 1: Analytical studies and specimen design." *Earthquake Engineering & Structural Dynamics*, 39(7), 775-799.

Vargas, R., and Bruneau, M. (2009a). "Analytical response and design of buildings with metallic structural fuses. I." *Journal of Structural Engineering*, 135(4), 386-393.

Vargas, R., and Bruneau, M. (2009b). "Experimental Response of Buildings Designed with Metallic Structural Fuses. II." *Journal of Structural Engineering*, 135(4).

Vatansever, C., and Yardimci, N. (2011). "Experimental investigation of thin steel plate shear walls with different infill-to-boundary frame connections." *Steel and Composite Structures*, 11(3), 251-271.

Vian, D. (2005). "Steel plate shear walls for seismic design and retrofit of building structures." *Report MCEER-05-0010, MCEER*. Buffalo, NY.

Vian, D., Bruneau, M., Tsai, K., and Lin, Y.-C. (2009). "Special perforated steel plate shear walls with reduced beam section anchor beams. I: Experimental investigation." *Journal of Structural Engineering*, 135(3), 211-220.

Vian, D., Lin, Y.-C., Bruneau, M., and Tsai, K.-C. (2003). "Cyclic performance of low yield strength steel panel shear walls." *The Sixteenth KKCNN Symposium on Civil Engineering, Kolon Hotel, Gyeongju, Korea, December*, 8-10.

Wagner, H. (1931). "Flat sheet metal girders with very thin webs, Part I-General theories and assumptions." *National Advisory Committee for Aeronautics, Technical Memo*(604).

Wang, M., Yang, W., Shi, Y., and Xu, J. (2015). "Seismic behaviors of steel plate shear wall structures with construction details and materials." *Journal of Constructional Steel Research*, 107(0), 194-210.

Webster, D. J. (2013). "The Inelastic Seismic Response of Steel Plate Shear Wall Web Plates and Their Interaction with the Vertical Boundary Members." Doctor of Philosophy Doctor of Philosophy Dissertation University of Washington.

Xue, M., and Lu, L.-W. (1994). "Interaction of infilled steel shear wall panels with surrounding frame members." *Proceedings of 1994 Annual Task Group Technical Session, Structural Stability Research Council: reports on current research activities*.

Yamaguchi, T., Takeuchi, T., Nagao, T., Suzuki, t., Nakata, Y., Ikebe, T., and Minami, A. (1998). "Seismic control devices using low-yield-point steel." *Nippon Steel Technical Report No.77*(0), 65-72.

Yang, T. S., and Popov, E. P. (1995). "Experimental and analytical studies of steel connections and energy dissipators, UCB/EERC-95/13."Earthquake Engineering Research Center, University of California Berkeley.

Youssef, N., Wilkerson, R., Fischer, K., and Tunick, D. (2010). "Seismic performance of a 55-storey steel plate shear wall." *The Structural Design of Tall and Special Buildings*, 19(1-2), 139-165.

Youssef, N., Wilkerson, R., and Tunick, D. (2011). "Thin Steel Plate Shear Walls: Performance Based Design " *Steel Tips*.

Zareian, F., and Medina, R. A. (2010). "A practical method for proper modeling of structural damping in inelastic plane structural systems." *Computers & Structures*, 88(1–2), 45-53.

Zhang, J., and Zirakian, T. (2015). "Probabilistic assessment of structures with SPSW systems and LYP steel infill plates using fragility function method." *Engineering Structures*, 85(0), 195-205.

Zhang, X., and Guo, Y. (2014). "Behavior of steel plate shear walls with pre-compression from adjacent frame columns." *Thin-Walled Structures*, 77(0), 17-25.

Zhao, Q., and Astaneh-Asl, A. (2004a). "Cyclic behavior of traditional and innovative composite shear walls." *Journal of Structural Engineering*, 130(2), 271-284.

Zhao, Q. H. (2007). "Seismic behavior of composite shear wall systems and application of smart structures technology." *International Journal of Steel Structures*, 7(1), 69-75.

Zhao, Q. H., and Astaneh-Asl, A. (2003). "Cyclic behavior of steel and composite shear wall systems." *STESSA-2003, Behavior of Steel Structures in Seismic Areas, June*Naples, Italy, pp.6.

Zhao, Q. H., and Astaneh-Asl, A. (2004b). "Cyclic behavior of an innovative steel shear wall system." *13th World Conference on Earthquake Engineering, August 1-6.* Vancouver, Canada, 15.
Zhao, Q. H., and Astaneh-Asl, A. (2006a). "Cyclic Behavior of Steel and Composite Shear Walls." *100th Anniversary Earthquake Conference Commemorating the 1906 San Francisco Earthquake*San Francisco, CA.
Zhao, Q. H., and Astaneh-Asl, A. (2006b). "Experimental and Analytical Studies of Cyclic Behavior of Steel and Composite Shear Wall Systems." *Report No. UCB/CEE-STEEL-06/01*, Department of Civil and Environmental Engineering, University of California, Berkeley, pp.222.
Zhao, Q. H., and Astaneh-Asl, A. (2008). "Experimental and Analytical Studies of a Steel Plate Shear Wall System." *Structures Congress, ASCE, April 24-26.* Vancouver, Canada, pp.10.

Appendix A

List of Constructed Buildings with Steel Shear Wall System as The Main Lateral Force Resisting System

The list on the next few pages summarizes the constructed buildings that use steel shear wall system as the primary lateral load resisting system in one or more directions in the descending order of building height. Brief description and researcher/designers' comments are also included for each building. The list is considered extensive but not exhaustive.

Building Name/Location	# of Stories	Description	Designers/Researchers' Comments
Jinta Tower *Tianjin, China*	**74**	Currently the first high-rise building built with SPSWs in China; dual system consisting of an interior SPSW core and perimeter moment resisting frame linked by outriggers and belt trusses; vertical boundary elements are concrete-filled tubes (CFTs); the SPSWs were designed to resist both wind and seismic loads under serviceability and ultimate conditions; vertical stiffeners were designed to prevent plate buckling under gravity and to restrain out-of-plane deformation	The structural system was selected after considering various alternatives given the slenderness of the building(1:8 aspect ratio)(Sarkisian and Mathias 2012); under stability considerations, the steel panels had to be connected to beams and columns just after several stories of the framing were erected, vertical stiffeners were used to prevent possible plate buckling under gravity load and reduction of shear buckling capacity; the stiffened SPSWs welded to the boundary elements were chosen over the unstiffened SPSW bolted to the boundary mainly due to its higher stiffness at serviceability condition, higher initial yielding capacity and less unpleasant buckling sound(Nie et al. 2012)
Los Angeles Convention Center Hotel (LACCH) *Los Angeles, USA*	**55**	Consists of un-stiffened thin SPSWs within fully welded WUF-W moment frames, coupled with mid-height outriggers and cap trusses calibrated with buckling restrained braces	Performance based design was utilized; buckling of infill panels was encouraged as the "first-order energy dissipation mechanism of the system"; boundary columns turned out to be huge due to enormous demands including lateral and vertical forces from the infill panels, the moment frame flexural demands and the support of gravity floor framing (Youssef et al. 2010; Youssef et al. 2011)
Shinjuku Nomura Building *Tokyo, Japan*	**53**	Consists of moment perimeter frames and a series of T-shaped stiffened steel plate shear wall units (Figure 1.7); the walls have horizontal stiffeners on one side and vertical on the other side	According to the Engineering News Record (ENR) article, "contractor rejected a steel braced building core as too expensive" as compared to a steel shear wall; Construction contractor found the bolted steel panel-to-boundary element connections quite challenging
Kobe City Hall Tower *Kobe, Japan*	**35**	Dual system consisting of steel moment frames and stiffened steel shear walls starting from the 2nd floor; concrete shear wall in basement and composite walls over two stories as transition	Withstood the 1995 Kobe earthquake with minor damage, i.e., local buckling of sub-panel (Fujitani et al. 1996; Nakashima 1995); permanent roof drift of 225mm in the N-plane and 35mm in the W-plane; soft stories may have formed between 24-28th floors

280

Building Name/Location	# of Stories	Description	Designers/Researchers' Comments
Hyatt Regency Hotel *Dallas, Texas, USA*	**30**	Consists of steel braced frame in the longitudinal direction and steel shear walls in the transverse direction; the steel shear walls (1in thickness throughout) were designed to take about 60% of the tributary gravity loads	It is an example of efficient application of steel shear wall in areas with low seismicity but high wind loads; designers claimed they had saved 1/3 steel by using steel shear wall as the gravity load carrying element (Troy and Richard 1979); only 0.0025 drift was found under design wind load
Saitama-Shintoshin National Government Building (also known as the Saitama Wide-Area Joint Agency Buildings) *Japan*	**26 & 31**	Prefabricated stiffened low yield point (LYP100) steel wall units connected to boundary elements using friction bolts; designed to remain elastic under wind load but to yield under design earthquakes; the walls were placed in a checkerboard pattern to reduce the bending effect in the walls	Drift values decreased about 30% as a result of using low yield point steel infill panels, and less overall bending behavior was observed
U.S. Federal Courthouse *Seattle, USA*	**24**	Lateral load resisting core with four concrete filled tubes connected by unstiffened steel shear wall and coupling beams in one direction and a steel-braced frame in the other direction	Special ductile beam-to-column connections were developed using rebars to reduce the high cost of full-joint-penetration traditional moment connections; about 2% gross square footage was saved by using steel instead of concrete shear walls; significant savings were achieved due to the light weight of steel shear walls (18 percent lighter than equivalent concrete shear wall); according to the steel erector for that project, steel shear wall reduced the construction time and was easier to assemble than equivalent special concentrically braced frames(AISC 2007)
Hill-side Condominium Building using SPW *Mexico*	**22**	Consists of nearly identical architectural layout as a previous built building using steel moment frame and concrete shear walls located on the same hillside site; the steel shear wall was designed according to the CAN/CSA S16.1 requirements since this system had not covered by the applicable Mexican design code at that time (Reglamento de Construcciones del Distrito Federal, i.e., Policies for Construction in the Federal District)	The previous building had ductile steel frames combined with concrete shear walls around the elevator cores, but the construction of concrete shear walls could not match the pace of the steel frames; the later constructed building with SPW was built on schedule, significantly faster and at a lower cost compared to its twin building using concrete shear wall

281

Building Name/Location	# of Stories	Description	Designers/Researchers' Comments
Nippon Steel Building *Tokyo, Japan*	**20**	Completed in 1970 and is believed to be the first major building using steel shear wall system; the structural system is a combination of moment frame and steel shear wall units in an H-shape configuration in the longitudinal direction & only SPW in the transverse direction	SPW system was designed to resist lateral loads through shear yielding without forming any buckling in the steel plates; channels were used as stiffeners in both horizontal and vertical directions on both sides of the steel panels
ING building *Ste-Hyacinthe, Quebec*	**7**	Consists of central core of steel shear walls with full height (80-ft) walls prefabricated in the shop; some walls were fabricated in half-width segments and connected through vertical welded seam on site	SPW system was selected because of faster construction and a gain of floor space
Olive View Hospital *Sylmar, California, USA*	**6**	Consists of reinforced concrete shear walls in the first two stories and steel shear walls in the upper four stories; steel shear walls were designed to have critical buckling load of the entire stiffened panel and the sub-panels higher than the design loads; the building was part of California Strong Motion Instrumentation Program (CSMIP) and had records of 1987 Whittier and 1994 Northridge earthquakes	Tension field action was not used in the design and was considered as a 'second line of defense' mechanism in the event of high insensitive earthquakes; with insignificant structural damages in the upper stories using SPW, severe damages were found in non-structural elements after 1994 Northridge earthquakes, which was considered as an indicator of extreme stiffness of the structure(Celebi 1997)
Canam Manac Group headquarters expansion, *Saint Georges Quebec, Canada*	**6**	Consists of steel shear wall in the shear core; 0.19 in thick infill plates were used throughout	SPW system was selected due to simplicity in construction details which contributed to the cost effectiveness of the system
Low-rise residential buildings *Atherton and San Mateo County, California, USA*	**1, 2**	Belongs to low-rise residential buildings that have sizeable open floor plans for which an engineered framing system is required. The areas of the buildings are 17,000ft^2 in Atherton, California and 9000 ft^2 in San Mateo County(Eatherton and Johnson 2004)	The buildings were designed with steel shear walls because they were found to less costly than the moment frame alternative and allowed faster construction by having shop fabricated steel shear wall modules(Eatherton 2006)

282

Appendix C

Preliminary Parametric Study of the Gusset Plate Moment Connection (GPMC)

Since the development of high-performance steel plate shear wall (HPSPSW) and GPMC were started from a prototype steel shear wall design, the preliminary parametric studies for the GPMC were conducted using the beam and column sections employed in a steel plate shear wall system. The beam was relatively shallow and heavy compared to what is typically used in steel moment frames. Then, the study was extended to include deeper sections of up to W-30's. In this appendix, the preliminary parametric studies using shallow beam sections are presented.

C1.1 Prototype Connection Sub-assembly

A typical exterior beam-to-column sub-assembly was modeled using the dimensions of the beam (200x200x16x16 mm) and column (250x250x20x20 mm) sections of the SC4T specimen (Park et al., 2007). The loading history was based on ATC-24 loading protocol for step-wise increasing cyclic tests. The boundary condition and loading history are shown below. Out-of-plane constraints were applied at the cut boundaries of the beam and column, as well as along the beam top flange.

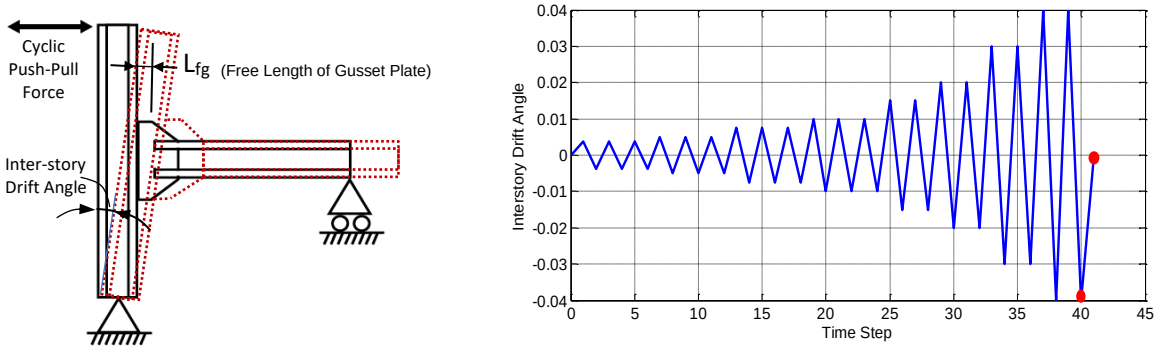

Figure C1.1 Details of test set-up showing the boundary condition for the connection subassembly and the loading history

C1.2 Effects of Various Parameters

The following sections provide a summary of the effects of different design parameters on the behavior of the proposed GPMC connection.

C1.2.1. Welded vs. Bolted Gusset Plate Moment Connection

As shown in Figure C1.2, the welded version of the proposed new Gusset Plate Moment Connection exhibited stable and stocky hysteresis with good energy dissipation capacity; while the bolted version of the GPMCs showed stable but somewhat pinched hysteresis. The bolts in these studies were not pre-tensioned to represent the condition that might occur during later cycles when the pre-tensioning is lost due to bolt elongation under cyclic loading.

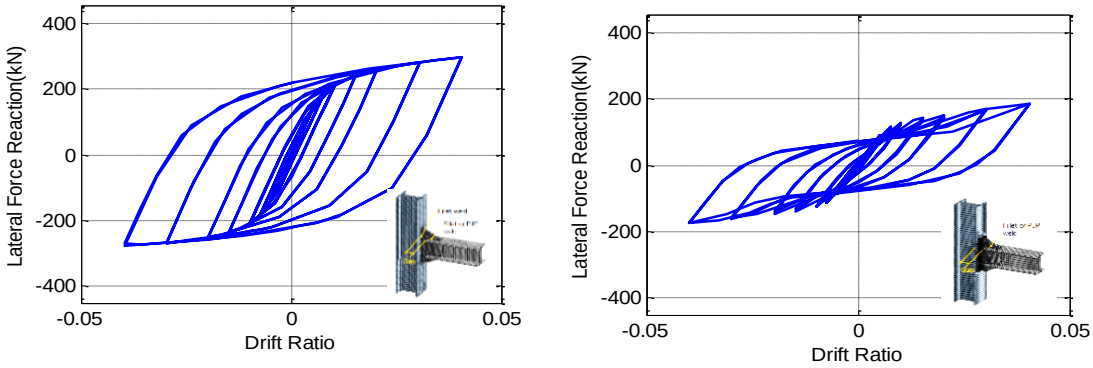

(a) Welded Option, $t_g = t_{bw}$

(b) Bolted Option, $t_g = t_{bw}$
(Note: bolt not pre-tensioned)

Figure C1.2 Comparison of welded vs bolted GPMC

It should be noted that unlike the reinforced concrete elements where pinching of the hysteresis loops is primarily due to cracking, crushing and spalling of concrete, which is not recoverable, in bolted Gusset Plate Moment Connection, the pinching of hysteresis loops is mainly due to the prying action of the gusset flange plate welded to the gusset plate and bolted to the column flange. Such pinching is stable and creates a "semi-rigidity" effect that increases ductility, reduces stiffness and can be beneficial in some cases in reducing the inertia forces attracted to the structure (Nader and Astaneh-Asl 1998).

Bolted connections normally have better quality control, and they can be done in the field under almost any weather condition with a minimal quality control and inspection efforts. Therefore, they are kept as one of the major configurations of the proposed GPMC. The analysis also showed that bolted gusset plates impose less strength demand on the beam and column.

C1.2.2. Effect of the Geometry of Gusset Plate

The geometry of the gusset plate was found to affect the stress distribution and location of the maximum equivalent plastic strain (denoted by yellow dots in Figure C1.3), which, is an indicator of the location of possible fracture initiation. The plot of Von Mises equivalent stresses showed that the yielded region in the gusset plate is roughly in the form of two intersected bell shapes around the roots of the gusset-to-beam flange connection, and this agrees with the commonly known Whitmore area behavior in welded gusset plates (Astaneh-Asl 1998a; Astaneh-Asl 2010).

Various geometries were considered for the gusset plate in the preliminary study. Six of these geometries are shown in Figure C1.3, which are rectangular (denoted as Rect 1 and Rect 2), the original gusset (denoted as Orig), trapezoidal (denoted as Trap 1 and Trap 2) and the curved geometry (denoted as Curve 1). Gusset geometry Trap 2 exhibited the most desirable behavior with the peak stress and strain occurring inside the gusset plate surrounded by less yielded elements. It was found that the straight edge perpendicular to the column flange (Orig, Trap 1) or to the beam

flange (Rect 1, Rect 2 and Curve 1) should be minimized to avoid excessive stress concentration at these exterior edges.

Case Trap 2 is the most desirable because its maximum stress point during the cyclic loading was inside the gusset plate surrounded by almost elastic or less stressed elements. When an element of the gusset plate yields but urrounded by elastic elements, the chances that the element will reach fracture strains is relatively low since the yielding is constrained. However, if the yielded element is at the edge of the gusset plate, it can continue yielding unrestrained – if in tension, fracture may be initiated (especially when unexpected material property or fabrication flaws exist), and if in compression, edge buckling of the gusset plate will be easier to occur, both undesirable.

The angles of the top and bottom edges of the gusset plate for the analyzed beam and column section were approximately between 20 to 30 degrees, as is the case in the gusset plates used in braced frames. However, such angles were later found to be difficult to achieve for deeper beam sections under other design constraints.

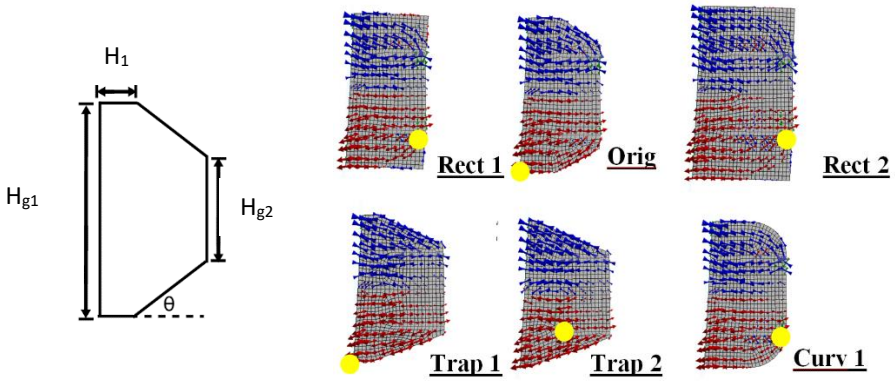

Figure C1.3 Effect of gusset plate shape on the location of maximum equivalent plastic strain

The effect of different geometry parameters shown in Figure C1.1 and C1.3 can be further seen through the following contour plots. The variables used in generating the contour plots are as follows (mm/degrees):

- Shorter gusset height: H_{g2}= [230, 240] (corresponding to 10mm and 20mm wide fishplate)
- Horizontal gusset edge length: H_1= [20, 50, 95] (1/12, 5/24, 19/48 of beam depth)
- Gusset angle: θ = [15, 20, 25, 30, 35] (degrees)
- Free gusset length: L_{fg} = [0.3, 0.4, 0.475, 0.6] (of beam depth)

Monotonically increasing displacements were applied to the beam-to-column connection sub-assembly as shown in Figure C1.1 and the peak Von Mises stresses, equivalent plastic strains and maximum base shears were monitored – lower stress or strain demand is desired along with larger shear capacity.

From the contour plots, a band of desired performance can be identified; this is especially obvious when the free gusset length L_{fg} is fixed (highlighted in Figure C1.4). Figure C1.5 shows that with increasing free gusset length, the region of low equivalent stress or equivalent plastic strain are

reduced and are shifted to the left (smaller angle). For very small horizontal gusset edge width H_1, the band of desired performance does not show a clear pattern, but for larger horizontal gusset edge width, the desired band generally lies in the highlighted region. As an example, in Figure C1.4, 'Trap 2' (H_{g2}=230mm, H_1= 20mm, and θ = 22.3°) in Figure C1.3 falls inside the band while 'Trap 1' (H_{g2}=230mm, H_1=50mm, and θ =25.8°) is located slightly off the boundary of this band. Though the parametric matrix is not large enough to include every possibility, the following 'design band' obtained from monotonic pushover analyses of the beam-to-column sub-assembly could provide valuable insight on the gusset plate geometry design: the wider the gusset horizontal edge width and the smaller the free gusset length is, the larger the gusset angle should be in order to minimize the stress/strain demand while maintaining a high capacity. But the gusset angle is best to be within 15 ~ 30 degrees.

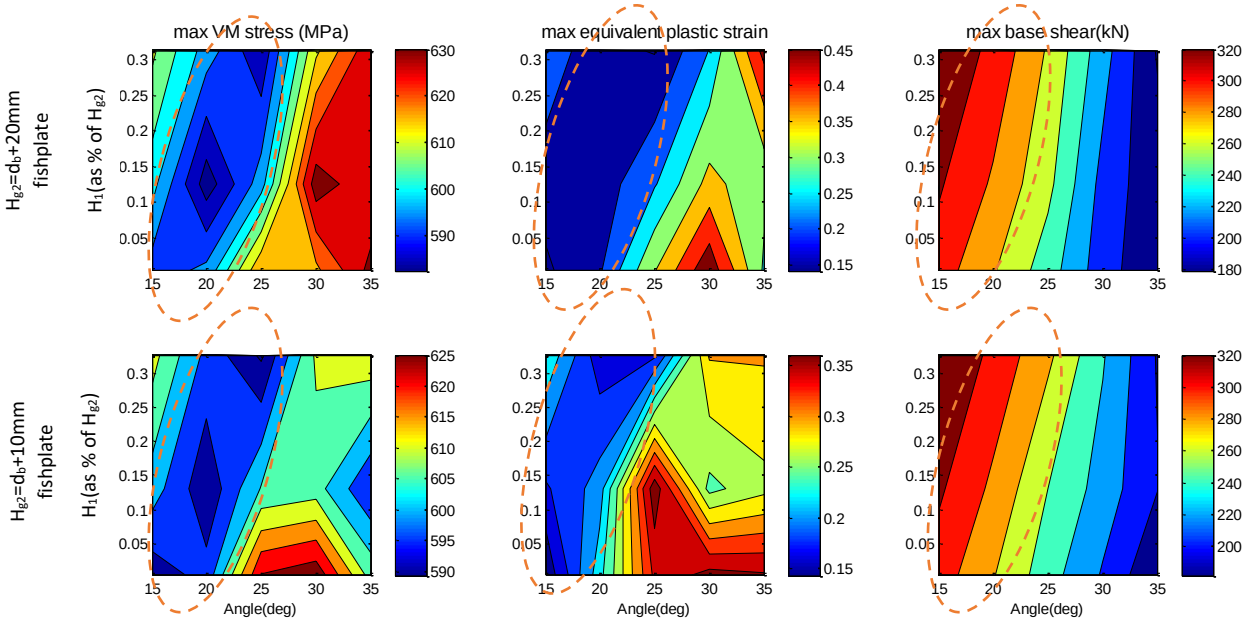

Figure C1.4 Contour plot for max Von Mises stress, max equivalent plastic strain and max shear capacity for the gusset plate moment connection with fixed free gusset length (L_{fg}=0.475d_b) showing effect horizontal gusset edge width vs. gusset angle

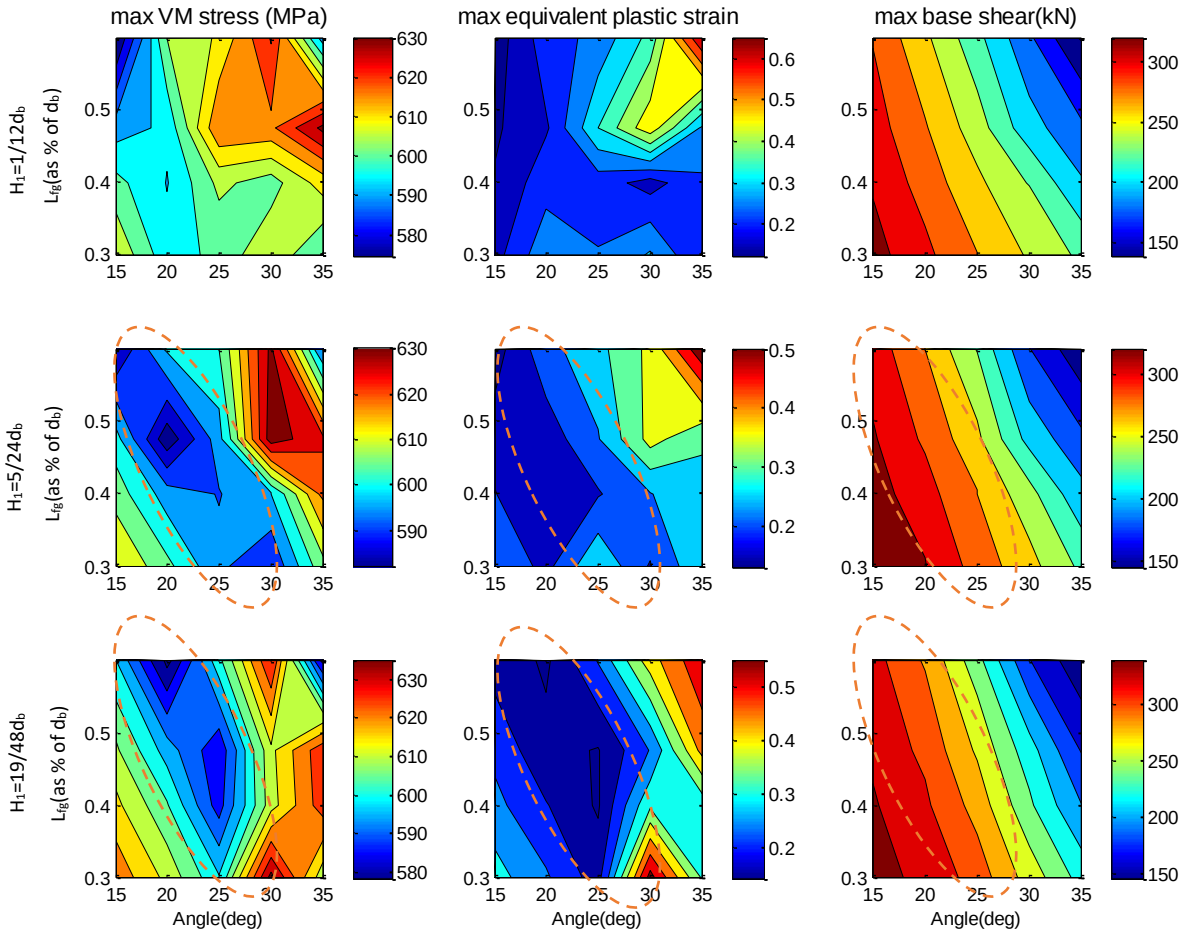

Figure C1.5 Contour plot for max Von Mises stress, max equivalent plastic strain and max shear capacity for the gusset plate moment connection with fixed shorter gusset height (H_{g2}=240mm) showing effect of free gusset length vs. gusset angle

C1.2.3. Effects of the Thickness of the Gusset Plate

Figure C1.6 shows the peak von Mises stress distributions for three cases under cyclic loading at a drift ratio of 4%, where the thickness of the gusset plate was 1.5, 1.25 and 1.0 times the thickness of the web of the beam.

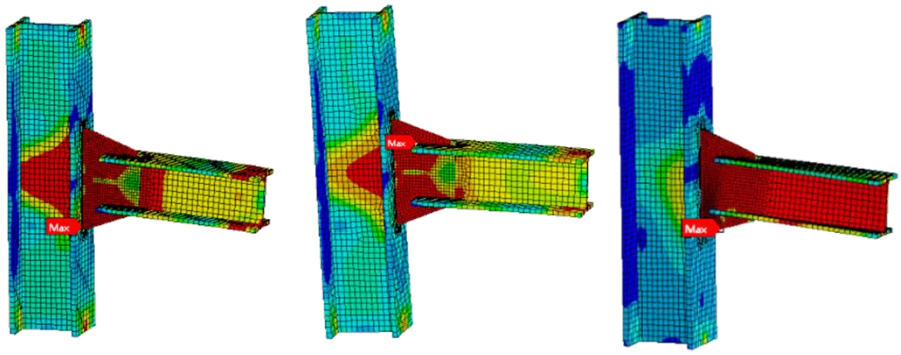

(a) t_g=1.5t_{bw} $L_{fg} \cong 6t_g$ **(b)** t_g=1.25t_{bw} $L_{fg} \cong 6t_g$ **(c)** t_g=1.0t_{bw} $L_{fg} \cong 6t_g$

Figure C1.6 Effect of gusset plate thickness on equivalent stress distribution (red: yielding)

For all cases, the gusset plate, as expected, yielded and formed a hinge. For thicker gusset plate (i.e. t_g=1.5t_{bw}), the column panel zone, as well as the beam just outside the gusset plate, had considerable yielding, Figure C1.6(a). For thin gusset plate, (i.e. t_g=1.0t_{bw}), the column panel zone had very small areas yielded. However, the entire length of the beam web had yielded, Figure Figure C1.6 (c), which is likely to be caused by twisting of the beam due to gusset lateral instability as lateral bracing was assigned to only the beam top flange. The best behavior was that of the case with intermediate thickness (i.e. t_g=1.25t_{bw}), where both the column panel zone and the beam had only limited yielding, Figure C1.6 (b).

In summary, thick gusset plate can provide larger capacity but could cause larger yielding in the column web and the beam; thin gusset plates impose less demand on the column but are susceptible to lateral instability (twisting of the gusset plate and un-symmetrical hysteresis curves). To obtain a balanced global and local behavior, the thickness of the gusset plate (t_g) is recommended to be 1.25 times the beam web thickness (t_{bw}).

C1.2.4. Effects of the Free Gusset Length

The free gusset length, L_{fg}, is defined as the distance between the end of the beam flanges to the face of the column flange. Figure C1.7 shows the cyclic hysteresis loops for three cases of gusset free length equal to $L_{fg} \cong 4t_g$, $L_{fg} \cong 6t_g$ and $L_{fg} \cong 9t_g$ and for two different thicknesses of gusset plate, t_g =1.25t_{bw} [Figure C1.7 (a)] and t_g =1.0t_{bw} [Figure C1.7 (b)].

It was found that as the free gusset length decreases, regardless of the thickness of the gusset plate, the overall shear capacity of the beam-to-column connection increased and there was less out-of-plane deformations of the gusset plate. By using a small magnitude of L_{fg}, which is a case close to the directly welded beam-to-column connection with triangular stiffening plates, the column web will be subjected to larger force transferred from the gusset plate.

Figure C1.8 shows the von Mises effective stresses for three cases: same beams and columns, same gusset geomery and thickness, but different free gusset length values ($L_{fg} \cong 4t_g$, $L_{fg} \cong 6t_g$ and $L_{fg} \cong 9t_g$). With larger L_{fg} and small gusset plate thickness, the connection is likely to suffer from lateral

instability and could even cause twisting of the beam and result in significant yielding of the beam web [Figures C1.8 (b) and C1.8 (c)]. From the preliminary parametric studies, we recommend the free length of the gusset plate, L_{fg}, to be 4 to 6 times the thickness of the gusset plate.

In addition to controlling the L_{fg} and t_g values to prevent the degradation of the behavior due to out-of-plane deformation of the gusset plate, it is recommended that sufficient lateral supports be added to the beam lower flange when possible to prevent any potential issues caused by out-of-plane deformation of the gusset plate.

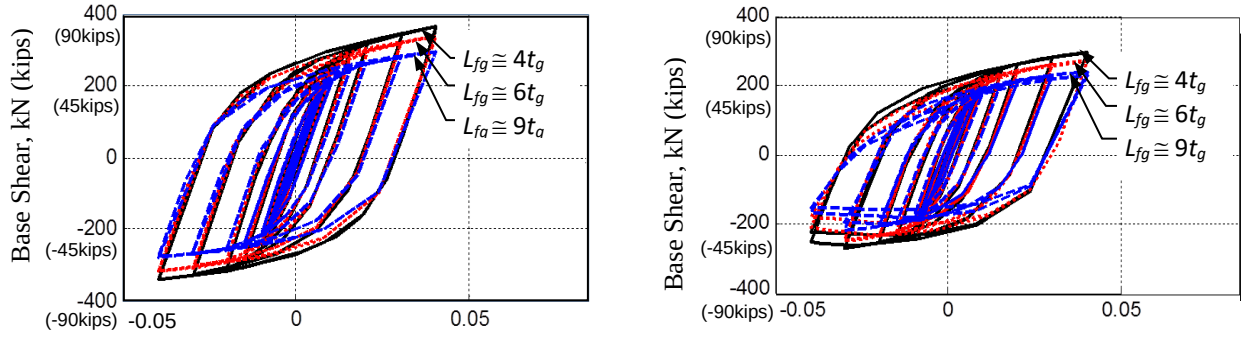

(a) t_g=1.25t_{bw} **(b) t_g=1.0t_{bw}**

Figure C1.7 Effect of thickness and free gusset length on the hysteresis responses

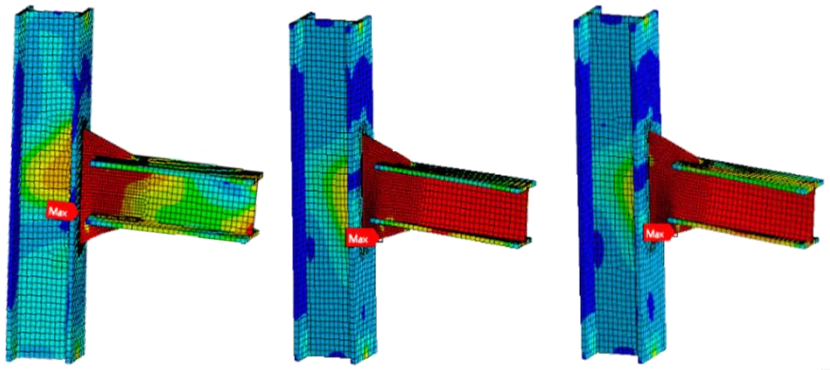

(a) $L_{fg} \cong 4t_g$ t_g=1.0t_{bw} **(b) $L_{fg} \cong 6t_g$ t_g=1.0t_{bw}** **(c) $L_{fg} \cong 9t_g$ t_g=1.0t_{bw}**

Figure C1.8 Effect of free gusset length on von Mises effective stress distribution (red: yielding)

C1.2.5. Effects of Moment Capacity Ratio

The moment capacity ratio, defined as the plastic moment capacity of the connection divided by that of the beam, i.e., M_{pg}/M_{pb}, was found to have a negligible effect on the overall force-displacement behavior but can cause different yield mechanism in the system. For cases with $M_{pg}/M_{pb} < 1$, almost all inelastic deformation was concentrated in the gusset plate while the beam remained elastic, Figure C1.9(a). However, as expected for cases with $M_{pg}/M_{pb} > 1$, relatively large areas of the beam yielded, Figure C1.9(b). Yielding of the beam is undesirable and violates

the performance criteria set for the proposed GPMC connection. Therefore, to fully achieve the goal of the performance criteria, it is important to keep the plastic moment capacity ratio M_{pg}/M_{pb} below one. Regarding how 'weak' the gusset plate should be, a detailed discussion is provided in Chapter III, Section 3.3.2.

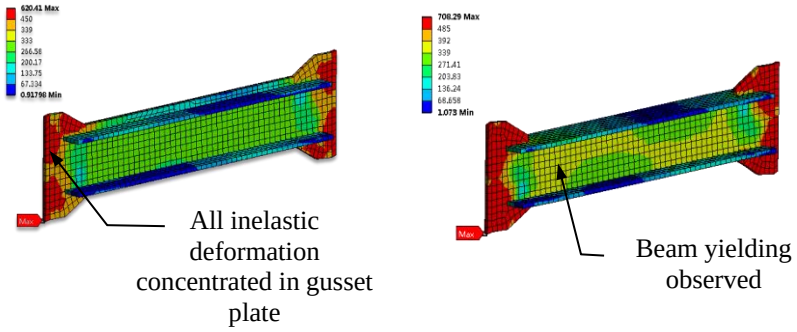

(a) M_{pc}/M_{pb}**=0.88 < 1.0** **(b)** M_{pc}/M_{pb}**= 1.24 > 1.0**

Figure C1.9 Effect of moment capacity ratio on the yielding behavior of gusset plate and beam

Appendix D1

Nonlinear Finite Element Modeling of Steel Plate Shear Walls

D1.1 Introduction to Prototype Specimens

Considering the importance of the test program in SPSW development history, the representativeness and diversity of specimens, as well as the simplicity for finite element modeling, a total number of seven test specimens in the literature were chosen to be simulated. One of them is the one-bay one-story SPSW2 specimen studied by Lubell (1997). Another three are half scale one bay three story specimens, i.e. SC2T, SC4T, and SC6T, tested by Park et al.(2007). The major difference in the three specimens is the infill plate thickness, which causes the overall behavior of the system to change from flexure dominant to shear dominant. The remaining three specimens simulated are one-story one-bay specimens tested by Vian et al.(2009) with perforations on infill panels (Vian et al. 2009). The selected specimen could cover cases for both single- and multi-story, flexural and shear dominant, well-proportioned design and insufficient design with weak boundary elements as well as modified infill plate design. Figure D1.2 shows the geometry layout of the case study specimens. Among the seven selected specimens, Park SC4T was used to test the mesh refinement and material models. Then the other specimens were modeled using the optimal choices based on the Park SC4T studies.

D1.2 Mesh

D1.2.1 Element Type

Four-node SHELL181 element from the ANSYS Shell element library was used (Figure D1.1). This element is well-suited for linear, large rotation and/or large strain nonlinear applications. It has six degrees-of-freedoms (UX, UY, UZ and ROTX, ROTY, ROTZ) with linear shape function and warping is supported. Change in thickness is accounted for in the analysis. Both full and reduced integration schemes are supported. In the Park SC4T specimen modeling, reduced integration with hourglass control was used with both bending and membrane stiffness.

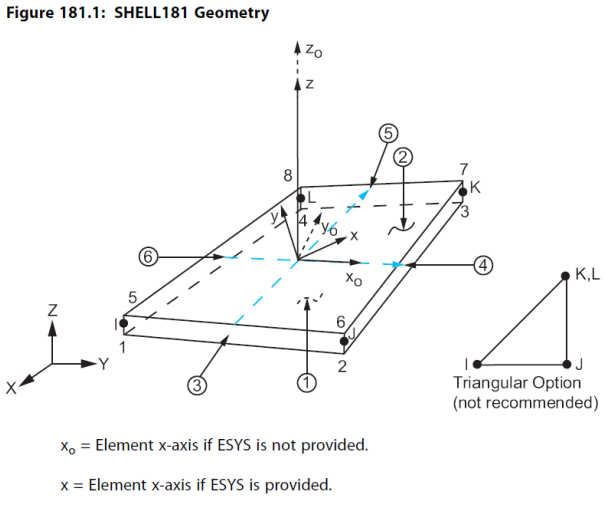

Figure D1.1 Illustration of SHELL181 element (ANSYS 2013, pp.842)

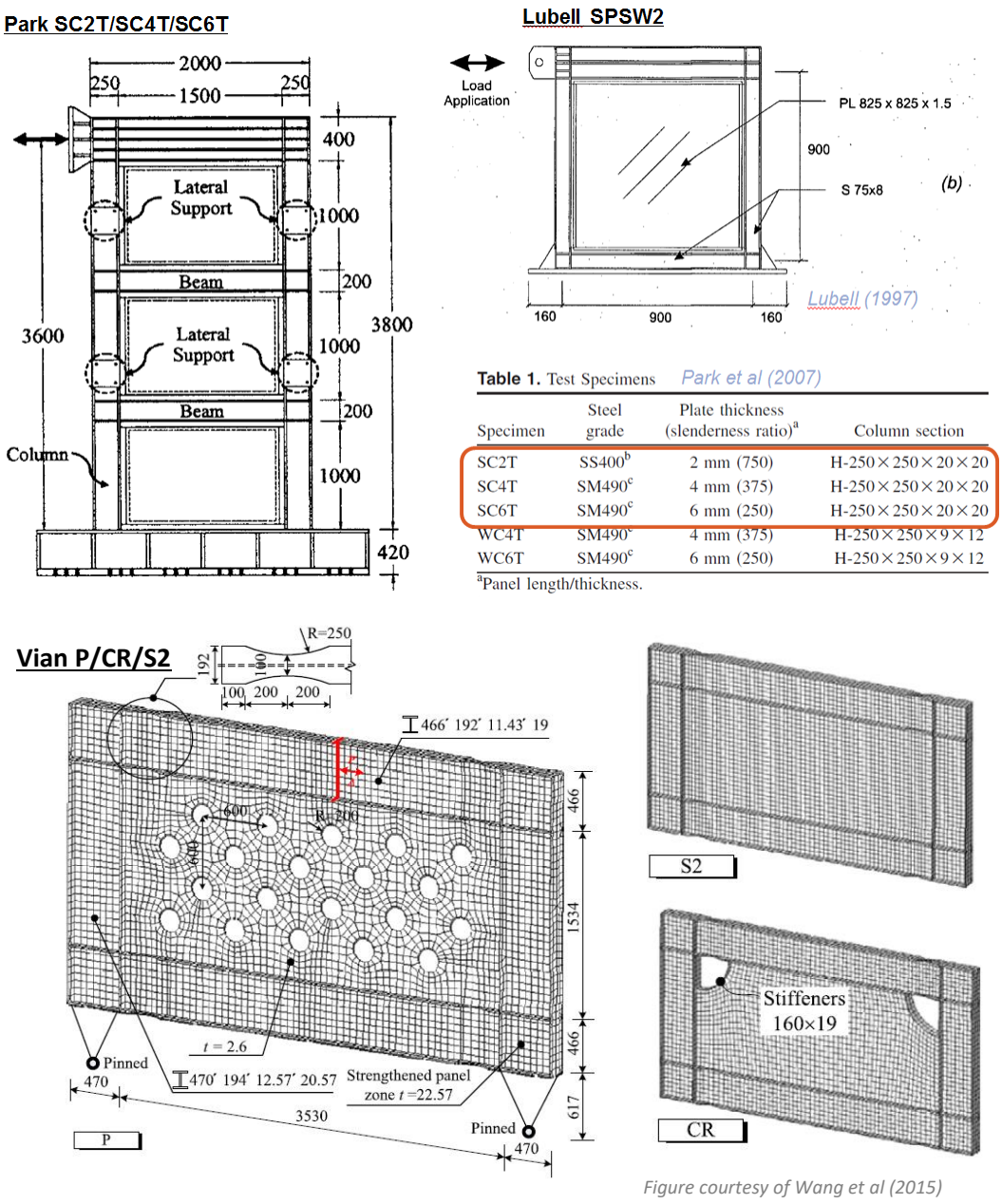

Table 1. Test Specimens *Park et al (2007)*

Specimen	Steel grade	Plate thickness (slenderness ratio)[a]	Column section
SC2T	SS400[b]	2 mm (750)	H-250×250×20×20
SC4T	SM490[c]	4 mm (375)	H-250×250×20×20
SC6T	SM490[c]	6 mm (250)	H-250×250×20×20
WC4T	SM490[c]	4 mm (375)	H-250×250×9×12
WC6T	SM490[c]	6 mm (250)	H-250×250×9×12

[a]Panel length/thickness.

Figure courtesy of Wang et al (2015)

Figure D1.2 Geometry layout of selected specimens for FE modelling verification

D1.2.2 Mesh Refinement

Mesh refinement study (*h*-refinement) was carried out to choose the optimum mesh size. Since the welded infill-to-boundary element connection is not the focus of this study, the infill plate was assumed to be attached directly (common nodes) to the horizontal and vertical boundary elements. A uniform mapped mesh was applied to the entire structure. Nonlinear static pushover analysis was performed, and some global performance criterions were chosen to assess the convergence of the mesh since points of singularity exist at the corners. Performance parameters studied include maximum total displacement, maximum Von Mises stress, roof displacement and the base shear

of the system. All errors were evaluated as the average of all load steps during the pushover analysis. Table D1.1 summarizes the error for four different meshes assuming the finest mesh (case 4) is the exact solution.

Table D1.1 Summary of mesh refinement study

Case	Num. of Nodes	Num. of Element	Total CPU Time(s)	Element Quality		Average Error [a]			
				Average	Standard Deviation	max Total Displ.	max VM Stress	Roof Displ.	Base Shear
1	2368	2327	153.3	0.9281	0.1425	-1.51%	-8.98%	0.12%	0.39%
2	6844	6784	420.7	0.9862	0.0469	-2.81%	-3.03%	-0.26%	0.08%
3	9389	9308	576.3	0.9598	0.1046	-1.54%	-0.04%	0.11%	0.23%
4	10384	10338	632.5	0.9872	0.0214	-	-	-	-

[a.] This error is the average of all load steps relative to the Case 4 solution

It can be observed that as the number of elements increases, the overall element quality increases and the max Von Mises stress solution is converging. There are some fluctuations for the other performance parameters with mesh refinement; however, the errors are all under 0.5% except the maximum total displacement, where the error is less than 2%. Therefore, it was regarded as adequate to use case 3 level of mesh density for other analysis.

D1.3 Initial Imperfection

Initial imperfections of the thin infill plates were added based on the following two considerations: 1) in real construction, the infill plates upon mounting are already in a slightly deformed shape due to fabrication process and handling 2) the analysis will encounter nonlinear buckling problem because it is difficult for the solver to initiate the buckling of perfectly flat plates and convergence difficulties will occur. Therefore, manually introducing initial imperfection is necessary from both practical and analysis point of views.

In order to study the effect of the amplitude of the initial imperfection, several different cases were compared. The initial imperfection pattern was chosen to be the lowest elastic buckling mode shape for the three infill plates. The peak buckling magnitudes used varied from 0.01% to 2% of the width of the panel. The load-displacement results under mesh refinement were consistent with the work done by Alinia and Sarraf Shirazi (2009), where they reason that since shear walls are slender, they normally buckle at an early stage and the following post-buckling behavior will not be affected significantly by the level of imposed initial imperfection.

In addition to post-buckling behavior, however, the early-stage buckling is also an important aspect of behavior to look at. Figure D1.3 shows the analysis results only up to partial yielding of the infill plate. Little difference can be observed from the force-displacement curve. The stiffness

versus displacement curve provides more information on the early-stage buckling behavior. It can be seen that if the initially applied imperfection is too large, such early-stage buckling will not be detected by the numerical simulation. 1% panel width imperfection was finally chosen to match the experimental initial stiffness while still being able to capture the early-stage buckling behavior.

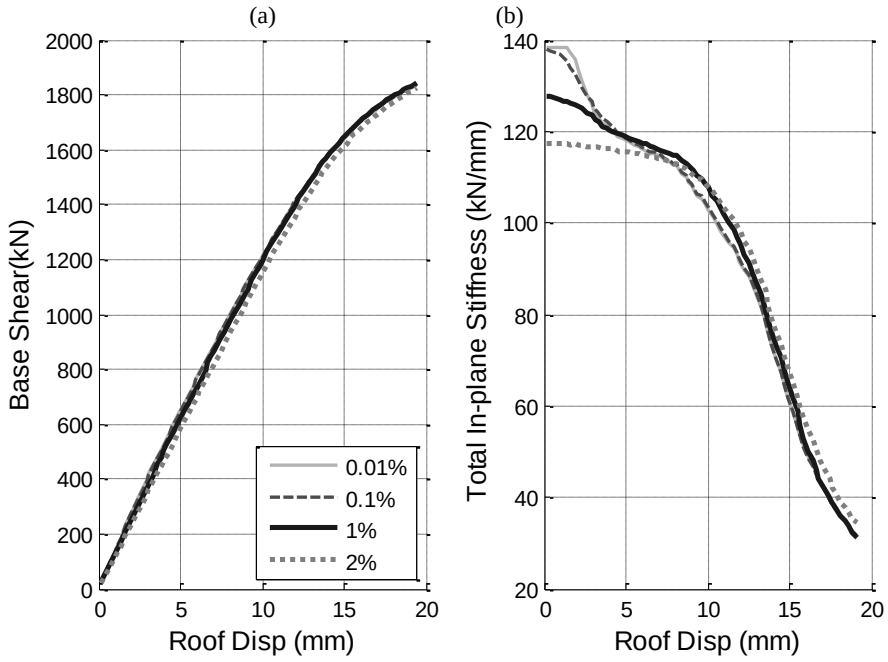

Figure D1.3 Initial imperfection study results
(a) Total base shear vs. Roof displ. (b) Total in-plane stiffness vs Roof displ.

D1.4 Material Modeling

It is known that the cyclic stress-strain responses may be different from the monotonic responses. Under cyclic loads, material response continues changing until cyclic stability is reached. Based on the nature and stability of dislocation substructure of the material at the beginning of the loading, the material will either cyclically harden (gradual saturation/stabilization of dislocations of initial low dislocation density) or cyclically soften (rearrangement of dislocations into a new configuration of initial high dislocation density)(Hertzberg et al. 2012). For commonly used structural steels, strain hardening is expected with increasing plastic strain during cyclic loading. At the same time, the Bauschinger effect, as one typical example of cyclic softening phenomena, is expected when load reverses during cyclic straining.

In addition to the simple elastic perfectly plastic model, with or without strain hardening, several power-function types of material models have been proposed in the literature to characterize the stress-strain response for monotonic or cyclically stabilized state, among which, Ramberg-Osgood and Menegotto-Pinto are commonly used for steel to describe the relation between equivalent stress and equivalent strain in J2 plasticity model. With the benefits of simplicity and less computational demand, bilinear hardening model derived from true stress-strain data have been

the most popular choice for finite element modeling of steel material. However, such simplified model may not always work well to capture the cyclic backbone curves. The power function material models often could better characterize the gradual cyclic strain hardening of the material. The following subsection compares the performances of bilinear and Ramberg-Osgood models for the same FEM model. For details of the plasticity formulation, the reader is referred to ANSYS Mechanical APDL Theory Manual(ANSYS 2013).

D1.4.1 Defining Input Uniaxial Stress-Strain Data

Bilinear Plastic with Strain Hardening

Bilinear plasticity model is one of the simplest and most commonly used material models for steel, where only the yield strength and straining hardening ratio needs to be specified. Yielding strength and strain hardening ratio are the true yield strength and hardening ratio based on the yield and the ultimate strengths of the uniaxial tension coupon test data. Since the entire coupon test data is not provided in the original paper, it was assumed that the strain at ultimate load is equal to 2/5 of the fracture strain, which results in approximately 0.15 ultimate strain, the common value used for structural steel. The energy dissipated by the bilinear model was set to be approximately equal to the coupon test result. Table D1.2 summarizes the key parameters used in the bilinear with hardening material model.

Table D1.2 Summary of data used for bilinear plasticity with hardening model

	Engineering		Actual		Engineering		Actual		Strain Hardening Modulus E_t (MPa)	Elastic Modulus, E (MPa)
PL	**ε_y**	**σ_y(MPa)**	**ε_y**	**σ_y(MPa)**	**ε_u**	**σ_u(MPa)**	**ε_{UTS}**	**σ_{UTS}(MPa)**		
2	0.001755	351	0.001753	351.62	0.1460	450.00	0.1363	515.70	1219.74	200527
4	0.00196	392	0.001958	392.77	0.1372	461.18	0.1286	524.45	1040.05	200588
6	0.001885	377	0.001883	377.71	0.1316	509.46	0.1236	576.50	1632.81	200566
9	0.001815	363	0.001813	363.66	0.1584	511.27	0.1470	592.25	1574.05	200545
12	0.002205	441	0.002203	441.97	0.1636	558.23	0.1515	649.55	1390.22	200662
16	0.00169	338	0.001689	338.57	0.1732	520.00	0.1597	610.06	1717.80	200507
20	0.001665	333	0.001664	333.55	0.1716	512.31	0.1584	600.22	1701.68	200500

Ramberg-Osgood Functions

In earthquake engineering, Ramberg-Osgood functions are often used to model the behavior of structural steel materials and components. These are basically normalized power functions. An arbitrary strain, ε_0, for which the nonzero plastic component of strain, $\varepsilon_{plastic}$ is chosen to normalize the power function (Bruneau et al. 2011). For common structural steels, if the parameters for Ramberg-Osgood model are determined by matching the yield and ultimate strength, it will lead to some extra energy dissipation capability in comparison with the monotonic energy dissipation

abilities (Figure D1.4). Table D1.3 summarizes the key parameters used in the Ramberg-Osgood material model.

Since ANSYS does not have embedded Ramberg-Osgood materials, the fitted curves were input as break points on a multi-linear kinematic hardening curve. Plastic strains were derived from the given data by deducting the elastic strain component from the total strain.

Table D1.3 Summary of data used for Ramberg-Osgood model

PL	ε_0	σ_0(MPa)	ε_B	σ_B(MPa)	m_A	m_B	n	a
2	0.001753	351.616	0.167631	532.125	0.9	0.014247	13.3804	5.41795E+33
4	0.001958	392.7683	0.158285	540.2682	0.9	0.015315	15.9944	2.18451E+40
6	0.001883	377.7106	0.152292	593.2655	0.9	0.017481	12.1807	1.06141E+30
9	0.001813	363.6588	0.180653	612.4986	0.9	0.015216	11.1602	2.31797E+27
12	0.002203	441.9724	0.186065	672.3854	0.9	0.016208	13.0072	3.15643E+31
16	0.001689	338.5712	0.195978	632.58	0.9	0.014488	9.78525	6.37802E+23
20	0.001664	333.5544	0.194332	622.1977	0.9	0.014372	9.81603	8.88078E+23

D1.4.2 Comparison

The Park SC4T specimen was used to compare the validity of bilinear and Ramberg-Osgood models. From Figure D1.5, it is clear that the bilinear kinematic hardening model failed to capture the backbone curve of the cyclic hysteresis loops. Such failure is believed to be mainly due to the choice of material model. The same simulation curve (black dotted line in Figure D1.5) was produced by the original authors (Park et al. 2007) with another FEM software and the same bilinear model. On the contrary, the multilinear kinematic hardening model with Ramberg-Osgood input points performed satisfactorily in matching hysteresis backbone curve and the distribution of stresses. This might be due to the gradual yielding of material and the extra energy dissipation capacity provided by the Ramberg-Osgood model. This allows the match for cyclic backbone curve by simple pushover analysis, of which the stress histories are very different from static cyclic analysis. Generally, the cyclic analysis responses also matched the test results reasonably well, with slight larger deviation at the last stage of cyclic deformation. This might be because of the numerical stabilization damping(ANSYS 2013), applied to overcome the severe convergence issue at large drift levels, became too high at the last set of drift reversals. The analysis results were also capable of showing the location of critical regions (e.g. column plastic hinge zone) similar to the test observations.

Since the Ramberg-Osgood model worked well for the SC4T specimen, it was used in the analyses of the other specimens, including Park SC2T, SC6T, Lubell SPSW2 and Vian P/CR/S2, to test its general applicability. Results will be shown later.

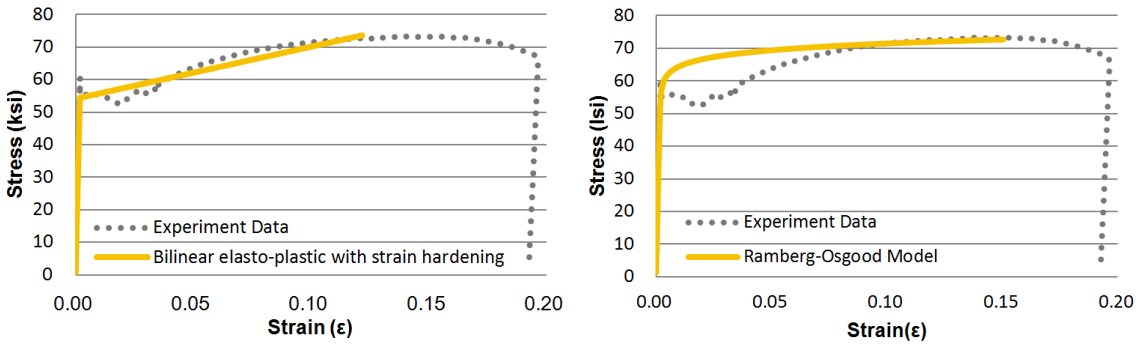

Figure D1.4 Example of data fitting by (a) Bilinear with Hardening (b) Ramberg-Osgood model

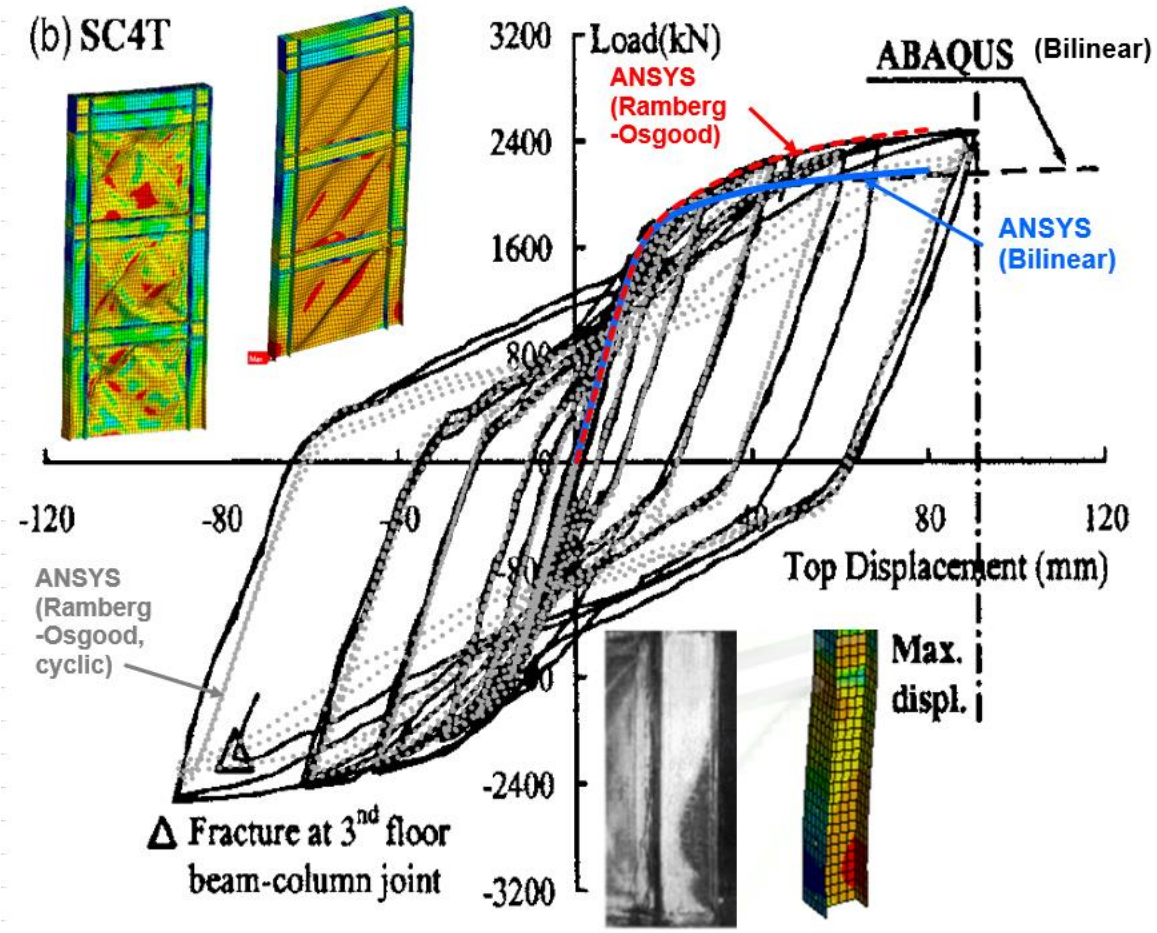

Figure D1.5 Validation of Park SC4T specimen and comparison of Ramberg-Osgood and Bilinear plasticity with strain hardening material model

D1.5 Solver Options

Since ANSYS is a widely used commercial software, there is little flexibility in modifying solution algorithms. Still, some comparisons have been made to compare the efficiency of different solvers and Newton-Raphson (N-R) options. To save some computation time, Lubell SPSW2 specimen was used for this study (Table D1.4). Since the matrix coefficient reordering algorithms are employed in the Sparse Direct Solver, Direct Solvers are found to be more efficient than Iterative Solvers in terms of solution time for the specific problem that is being analyzed. However, iterative solvers require less memory, which is beneficial for large FEM problems. Such savings of memory is mainly due to the nature of the algorithms of the Conjugate Gradient type of iterative solvers where zero entries are not stored. Considering the N-R options, little differences were observed, which is likely to be due to 1) the simple nature of the force-displacement relationship of the system, and 2) balance between longer stiffness matrix update time/ fewer iterations per load step vs. less stiffness matrix update time/more iteration per load step. For the later analysis, sparse direct solver and full N-R will be used.

Table D1.4 Comparison of different solver options

Comparison of different solver options Case	Solver Type	Newton-Raphson Option	Total CPU time(s)	Elapsed time spend computing solution(s)	Max total memory used
1	Direct[a]	Full	1730.9	878.6	198MB
2	Direct[a]	Modified	1734.1	874.5	198MB
3	Iterative[b]	Full	2724.0	1387.1	112MB
4	Iterative[b]	Modified	2733.8	1395.6	112MB

a. Sparse Direct Solver uses equation reordering (permuting rows and columns of stiffness matrix [K] and rows of force vector{F}) to minimize fill-in. Two different matrix coefficient reordering algorithms are used – Minimum Degree ordering and the METIS ordering. The choice of which one to use is automated in the solver algorithm.

b. Iterative Solver includes Jacobi Conjugate Gradient (JCG), Preconditioned Conjugate Gradient (PCG) and Incomplete Cholesky Conjugate Gradient (ICCG) solver (internally developed, unpublished work).

D1.6 Validation of Existing Test Results

Based on the previous studies on various aspects of finite element modeling of SPSW systems, the other six specimens were modeled and analyzed. It can be seen that for all specimens (Figure D1.6 to D1.11) that have been modeled, Ramberg-Osgood model was able to match the cyclic backbone curve generally well and also provided useful information on the critical regions [e.g. column yield zone (Figure D1.6 & D1.7), flexural deformation at corners (Figure D1.8), and overall out-of-plane deformation of the boundary beam (Figure D1.10)]. Cyclic analysis results matched the test results very well for specimens with thicker infill plates but did not match the test results for specimens with thinner plates at large drift ratio very closely (the results still matched well with the test result at small drift ratios). The challenge was to apply appropriate numerical damping to overcome the severe convergence issue while having as little influences as possible on the actual behavior. One remark is that for Park SC6T specimen, something might have happened during the test since the test results showed that SC6T has almost the same elastic stiffness as the SC4T specimen.

Specimen SC6T, however, is expected to be stiffer since thicker infill plate was used in this specimen.

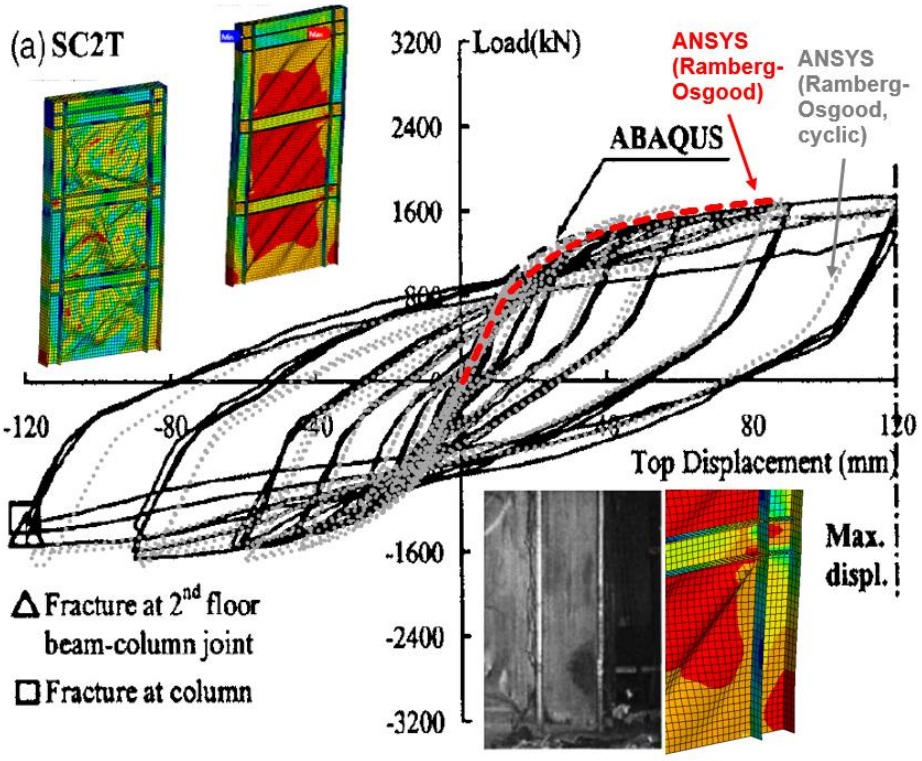

Figure D1.6 Validation of SC2T specimen results

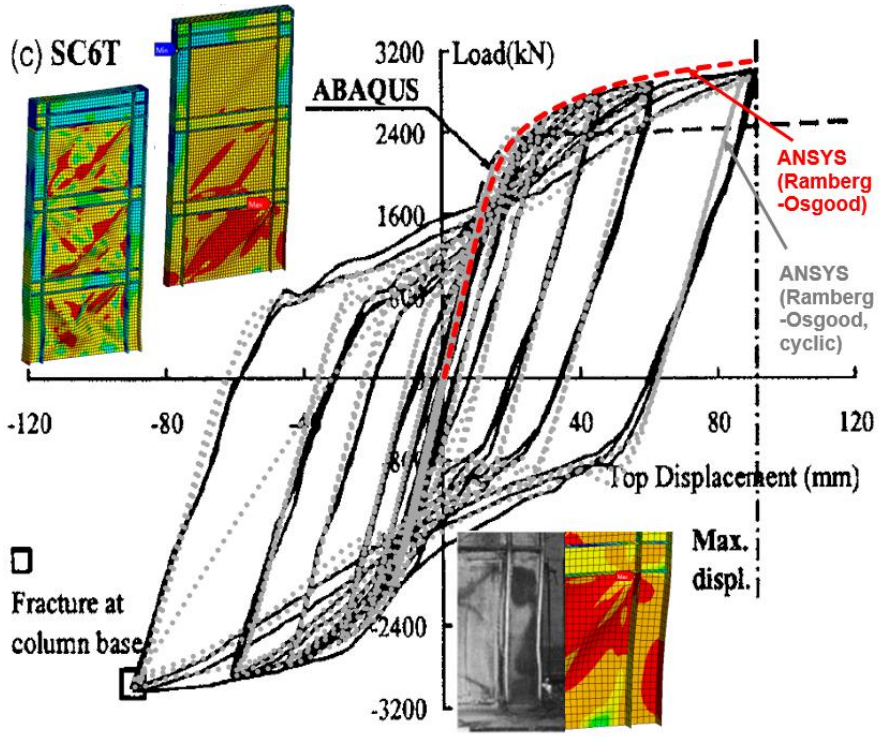

Figure D1.7 Validation of SC6T specimen results

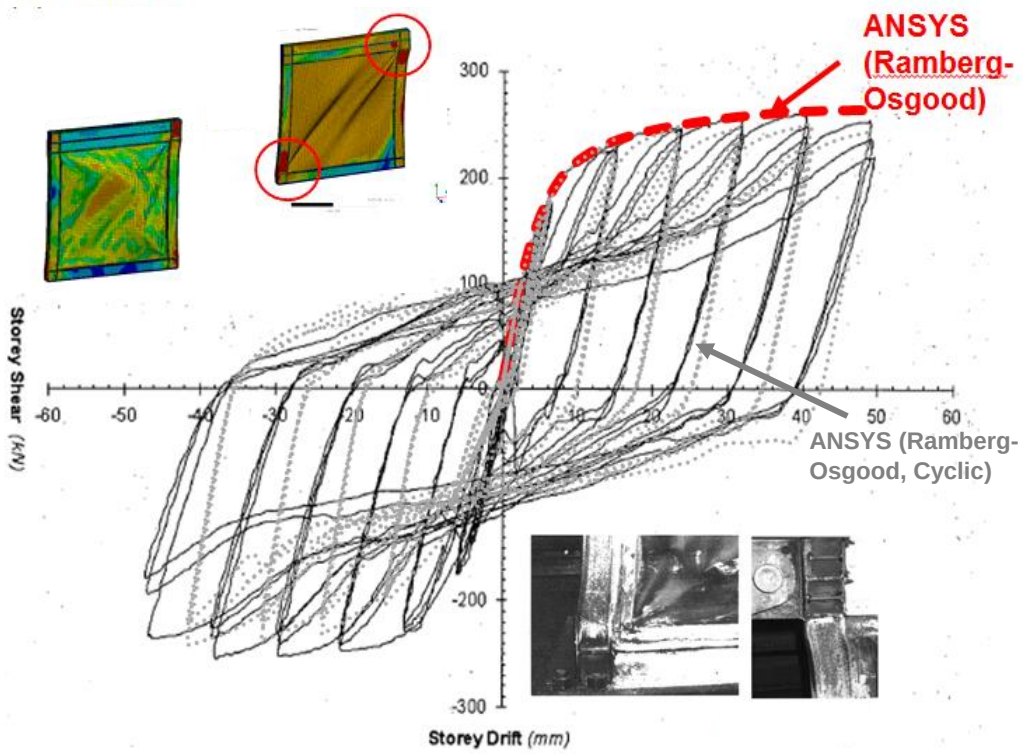

Figure D1.8 Validation of Lubell SPSW2 specimen results

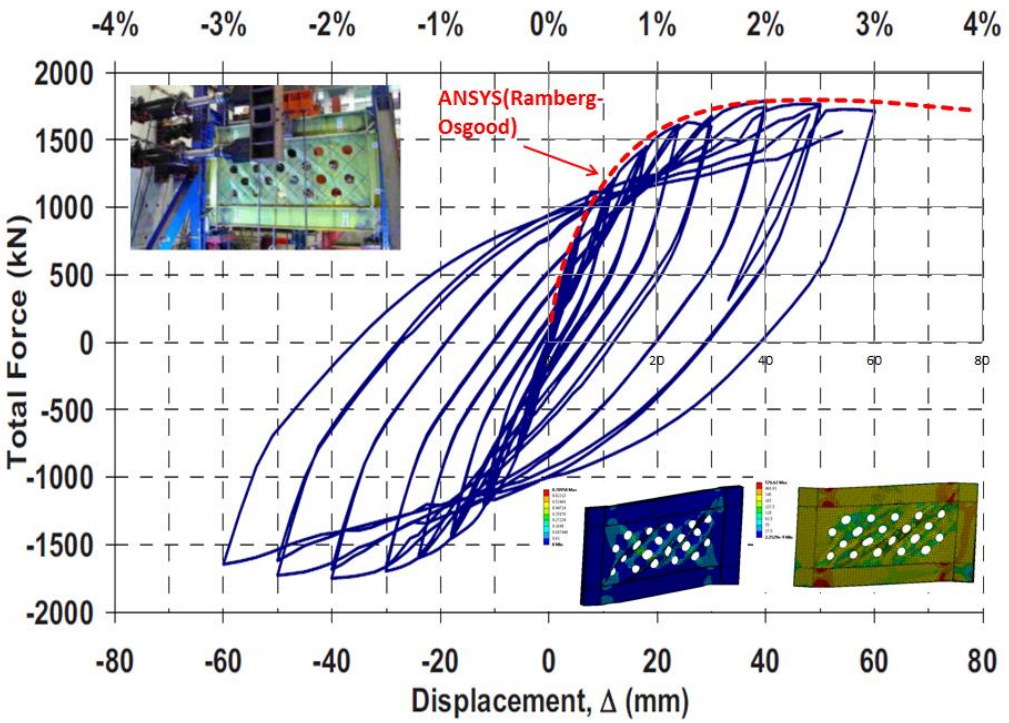

Figure D1.9 Validation of Vian specimen *P* results

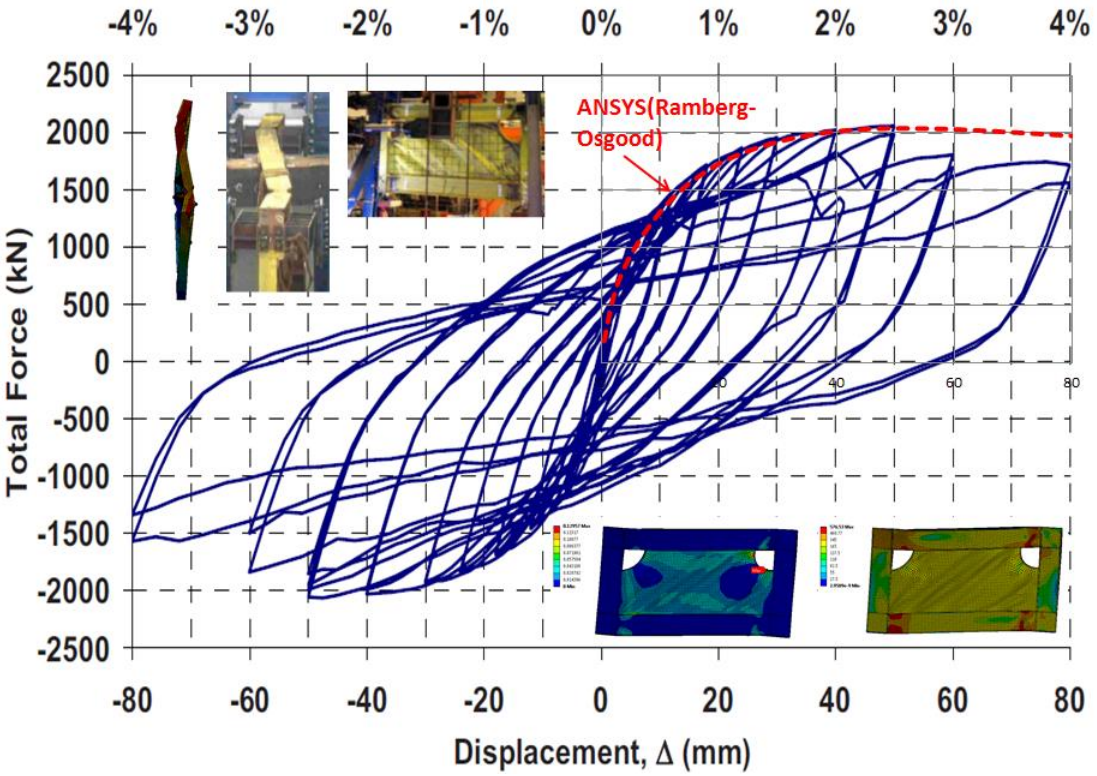

Figure D1.10 Validation of Vian specimen *CR* results

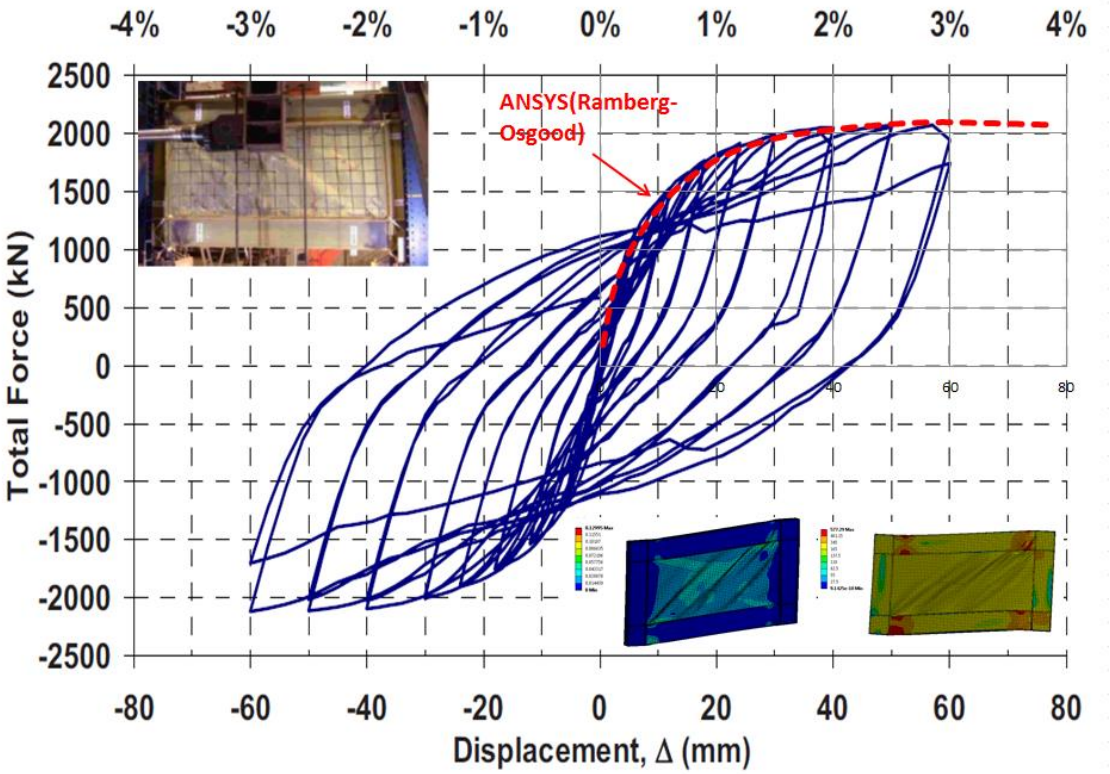

Figure D1.11 Validation of Vian specimen *S2* results

Appendix D2

D2.1 Derivation of Angle of Inclination and Shear Strength

D2.1.1 Angle of Inclination

Let *s* be the virtual width of the tension strips; the shear capacity can be computed as the summation of the tensile capacities of the tension strips within the tension field. Here, instead of the full infill width of the infill plate, an effective tension field width L_{eff} is used

$$V_{sp} = \frac{L_{eff}\cos\alpha}{s}\cdot f_{yp}t_p s\cdot\sin\alpha$$

$$V_{sp} = f_{yp}L_{eff}t_p\sin\alpha\cos\alpha \tag{D2.1-1}$$

For infinitely flexible side stiffeners,

$$L_{eff} = L_p - h_p\tan\alpha \tag{D2.1-2}$$

For side stiffeners with some rigidity

$$L_{eff} = L_p - (h_p - c)\tan\alpha \tag{D2.1-3}$$

The infinitely flexible stiffener case can be considered as a special case for the more general expression in (D2.1-3) where c=0. Let V be the shear force applied to the infill plate. The strain energy of the tension strip considering the effective tension field area is

$$W_s = \int_\Omega \frac{\sigma_s^2}{2E}d\Omega = \frac{V^2}{2Et_p}\frac{L_p h_p - (L_p - L_{eff})^2\cot\alpha}{(L_{eff}\sin\alpha\cos\alpha)^2} \tag{D2.1-4}$$

Taking L_{eff} as in Eqn. (D2.1-3), Eqn. (D2.1-4) becomes

$$W_s = \int_\Omega \frac{\sigma_s^2}{2E}d\Omega = \frac{V^2}{2Et_p}\frac{L_p h_p - (h_p - c)^2\tan\alpha}{\{[L_p - (h_p - c)\tan\alpha]\sin\alpha\cos\alpha\}^2} \tag{D2.1-5}$$

Applying the principle of least work, the angle of inclination could be obtained.

$$\frac{\partial W_s}{\partial\alpha} = 0 \tag{D2.1-6}$$

The resulting expression is a complex nonlinear polynomial as shown below and the simplified equations for calculating α is presented in the main body of the dissertation.

$$A\tan^4\alpha + B\tan^3\alpha + C\tan^2\alpha + D\tan\alpha + E = 0 \tag{D2.1-7}$$

Where

$$A = \left(1 - c/h_p\right)^3$$
$$B = -3\left(L_p/h_p\right)\left(1 - c/h_p\right)^2$$
$$C = -\left[3\left(1 - c/h_p\right)^3 - 2\left(L_p/h_p\right)^2\right]$$
$$D = \left(L_p/h_p\right)\left(5 - c/h_p\right)\left(1 - c/h_p\right)$$
$$E = -2\left(L_p/h_p\right)^2$$

D2.1.2 Shear Strength

The shear capacity of the infill plate can be obtained by considering the work conservation between work done by the external force and the internal strain energy.

$$V_{sp}(c\phi) = \mathrm{W}_{sp} = W_{pf} + W_{py} \tag{D2.1-8}$$

where ϕ is the rotation of the plastic hinge,

W_{pf} is the strain energy due to plastic hinge formation of the side stiffeners

$$W_{pf} = 4M_{pf}\phi \tag{D2.1-9}$$

And W_{py} is the strain energy by the yielding of the infill plate

$$W_{py} = f_{yp}t_p L_{eff} \sin\alpha\cos\alpha(c\phi) \tag{D2.1-10}$$

Plug in the expression of L_{eff} in Eqn.(D2.1-3),

$$W_{py} = f_{yp}t_p(L_p\cos\alpha - (h_p - c)\sin\alpha)\sin\alpha(c\phi) \tag{D2.1-11}$$

Where M_{pf} is the plastic moment capacity of the effective side stiffener.

Simplifying Eqn.(D2.1-8) after plugging in (D2.1-9) and (D2.1-11), the shear capacity of infill plate can be obtained as

$$V_{sp} = \frac{4M_{pf}}{c} + f_{yp}L_{eff}t_p \sin\alpha\cos\alpha$$
$$V_{sp} = \frac{1}{2} f_{yp}t_p[L_p - (h_p - 2c)\tan\alpha]\sin 2\alpha \tag{D2.1-12}$$

The internal plastic hinge will occur at the point of maximum bending moment (plastic capacity) where the shear in the side stiffener is zero. Assuming the angle of plastic hinge rotation is ϕ and making the work done by the plastic hinge rotation equal to that done by the tension field stresses.

$$c(f_{yp}t_p)\cdot\sin^2\alpha\cdot(\frac{c}{2}\phi)=2M_{pf}\phi$$

Solving this equation, the expression for *c* can be determined as follows,

$$c=\frac{2}{\sin\alpha}\sqrt{\frac{M_{pf}}{f_{yp}t_p}} \qquad \text{(D2.1-13)}$$

D2.2 Derivation of the Proposed Equivalent Brace Model

The derivation presented here assumes that X-brace is needed to capture system resistance in both directions. Assume the tension and compression capacity ratio is

$$\beta = \frac{\sigma_c}{\sigma_t} \sim \frac{\tau_{cr}}{f_{yp}} \tag{D2.2-1}$$

Assume the yielding strain in tension and compression is the same. The total shear strength of the shear wall can be determined by multiplying the shear wall stiffness to the yielding displacement,

$$V = K_{spsw}\Delta \tag{D2.2-2}$$

In the equivalent brace model, the shear capacity is provided by the braces in tension and in compression,

$$V = V_t + V_c \tag{D2.2-3}$$

Define δ_t as the elongation of the brace in tension, and δ_c the shortening of the compression brace, E_t is equal to the young's modulus of steel E, and $E_c=\beta E_t$, and the shear capacity provided by the brace in tension and compression can be determined by the horizontal component of the axial force in the corresponding brace,

$$V_t = \frac{EA_{EB}}{L_{EB}}\delta_t \sin\theta = \frac{EA_{EB}}{L_{EB}}\left(\Delta \sin\theta\right)\sin\theta \tag{D2.2-4}$$

$$V_c = \frac{\left(\beta E\right)A_{EB}}{L_{EB}}\delta_c \sin\theta = \frac{EA_{EB}}{L_{EB}}\beta\left(\Delta \sin\theta\right)\sin\theta \tag{D2.2-5}$$

$$L_{EB} = L \diagup \sin\theta \tag{D2.2-6}$$

Re-arrange and simplify the above, we can get

$$A_{EB} = \frac{K_{spsw}L}{(1+\beta)\,\mathrm{E}\cdot\sin^3\theta} \tag{D2.2-7}$$

If the shear buckling component of the infill panel can be neglected, the equivalent brace area can be simplified to:

$$A_{EB} = \frac{K_{spsw}L}{\mathrm{E}\cdot\sin^3\theta} \tag{D2.2-8}$$

Accordingly, the yield strain, ε_y, of the equivalent brace can be obtained by dividing the yielding elongation, δ_y, of the brace by the length of the brace, and the yielding elongation can be further related to the shear wall yielding displacement, Δ_y,

$$\varepsilon_y = \frac{\delta_y}{L/\sin\theta} = \frac{\Delta_y \sin\theta}{L/\sin\theta} \tag{D2.2-9}$$

Assume a simple elastic—perfectly plastic force-displacement relationship and define

$$\Delta_y = \frac{V_{u\_spsw}}{K_{spsw}} \tag{D2.2-10}$$

Plug Eqn.(D2.2-10) into Eqn.(D2.2-9), we can get

$$f_{EBy} = E\varepsilon_y = \frac{EV_{u\_spsw}\sin^2\theta}{K_{spsw}L} \tag{D2.2-11}$$

Appendix E1

Basic Characteristics of Selected Ground Motion Records

According to the information provided by J.Baker for the PEER tall building project by Lai et al.(2015), the following is a summary of the basic characteristics of the selected ground motion with respect to their target spectrum.

Table E1-1 Target Response Spectra Values ($S_{a,g}$) for 5% Damping Level

Hazard Level	Period (s)												
	0.010	**0.100**	**0.200**	**0.300**	**0.500**	**0.750**	**1.000**	**2.000**	**3.000**	**4.000**	**5.000**	**7.000**	**10.000**
50/30	0.175	0.306	0.396	0.383	0.313	0.238	0.186	0.089	0.052	0.036	0.027	0.019	0.010
10/50	0.491	0.849	1.077	1.078	0.963	0.804	0.665	0.391	0.257	0.186	0.149	0.107	0.053
02/50	0.763	1.307	1.640	1.667	1.530	1.337	1.144	0.727	0.503	0.371	0.309	0.220	0.110

Table E1-2 50/30 Set of Records (43 Years Return Period)

Record No.	NGA No.	Earthquake	Station	Magnitude	Distance (km)	*Vs30* (m/s)	Scale Factor
1	162	Imperial Valley-06	Calexico Fire Station	6.5	10.5	231	0.869
2	183	Imperial Valley-06	El Centro Array #8	6.5	3.9	206	0.397
3	316	Westmorland	Parachute Test Site	5.9	16.7	349	0.570
4	721	Superstition Hills-02	El Centro Imp. Co. Cent	6.5	18.2	192	0.504
5	728	Superstition Hills-02	Westmorland Fire Sta	6.5	13.0	194	0.605
6	882	Landers	North Palm Springs	7.3	26.8	345	1.151
7	1144	Gulf of Aqaba	Eilat	7.2	44.1	355	1.596
8	1794	Hector Mine	Joshua Tree	7.1	31.1	379	1.034
9	2650	Chi-Chi, Taiwan-03	TCU116	6.2	22.1	493	0.940
10	2715	Chi-Chi, Taiwan-04	CHY047	6.2	38.6	170	1.308
11	3264	Chi-Chi, Taiwan-06	CHY024	6.3	31.1	428	1.147
12	3747	Cape Mendocino	College of the Redwoods	7.0	31.5	493	0.772
13	3943	Tottori, Japan	SMN015	6.6	9.1	617	1.130
14	4031	San Simeon, CA	Templeton - 1-story Hospital	6.5	6.2	411	0.543
15	4204	Niigata, Japan	NIG014	6.6	28.4	128	0.950
16	4854	Chuetsu-oki	Nadachiku Joetsu City	6.8	35.9	571	1.376
17	4881	Chuetsu-oki	Nagaoka Kouiti Town	6.8	20.8	294	1.145
18	5990	El Mayor-Cucapah	El Centro Array #7	7.2	27.9	211	0.683
19	6891	Darfield, New Zealand	CSHS	7.0	43.6	638	1.488
20	8134	Christchurch, New Zealand	Styx Mill Transfer Station	6.2	11.3	248	0.754

Table E1-3 10/50 Set of Records (475 Years Return Period)

Record No.	NGA No.	Earthquake	Station	Magnitude	Distance (km)	*Vs30* (m/s)	Scale Factor
1	169	Imperial Valley-06	Delta	6.5	22.0	242	1.936
2	179	Imperial Valley-06	El Centro Array #4	6.5	7.1	209	1.460
3	185	Imperial Valley-06	Holtville Post Office	6.5	7.5	203	1.840
4	721	Superstition Hills-02	El Centro Imp. Co. Cent	6.5	18.2	192	1.924
5	728	Superstition Hills-02	Westmorland Fire Sta	6.5	13.0	194	2.000
6	776	Loma Prieta	Hollister - South & Pine	6.9	27.9	282	1.672
7	777	Loma Prieta	Hollister City Hall	6.9	27.6	199	1.824
8	778	Loma Prieta	Hollister Differential Array	6.9	24.8	216	1.842
9	900	Landers	Yermo Fire Station	7.3	23.6	354	2.000
10	1158	Kocaeli, Turkey	Duzce	7.5	15.4	282	1.407
11	1203	Chi-Chi, Taiwan	CHY036	7.6	16.0	233	1.691
12	1528	Chi-Chi, Taiwan	TCU101	7.6	2.1	389	1.887
13	1605	Duzce, Turkey	Duzce	7.1	6.6	282	0.993
14	3744	Cape Mendocino	Bunker Hill FAA	7.0	12.2	566	1.911
15	4847	Chuetsu-oki	Joetsu Kakizakiku Kakizaki	6.8	11.9	383	1.520
16	5827	El Mayor-Cucapah	MICHOACAN DE OCAMPO	7.2	15.9	242	1.389
17	5975	El Mayor-Cucapah	Calexico Fire Station	7.2	20.5	231	1.655
18	6888	Darfield, New Zealand	Christchurch Cathedral College	7.0	19.9	198	1.803
19	6952	Darfield, New Zealand	Papanui High School	7.0	18.7	263	1.611
20	6960	Darfield, New Zealand	Riccarton High School	7.0	13.6	293	1.956

Table E1-4 02/50 Set of Records (2475 Years Return Period)

Record #	NGA #	Earthquake	Station	Magnitude	Distance (km)	*Vs30* (m/s)	Scale Factor
1	285	Irpinia, Italy-01	Bagnoli Irpinio	6.9	8.2	650	6.000
2	737	Loma Prieta	Agnews State Hospital	6.9	24.6	240	5.469
3	776	Loma Prieta	Hollister - South & Pine	6.9	27.9	282	2.939
4	778	Loma Prieta	Hollister Differential Array	6.9	24.8	216	3.239
5	900	Landers	Yermo Fire Station	7.3	23.6	354	3.888
6	1104	Kobe, Japan	Fukushima	6.9	17.9	256	3.726
7	1121	Kobe, Japan	Yae	6.9	27.8	256	4.955
8	1148	Kocaeli, Turkey	Arcelik	7.5	13.5	523	6.000
9	1158	Kocaeli, Turkey	Duzce	7.5	15.4	282	2.473
10	1176	Kocaeli, Turkey	Yarimca	7.5	4.8	297	2.342
11	1193	Chi-Chi, Taiwan	CHY024	7.6	9.6	428	2.963
12	1503	Chi-Chi, Taiwan	TCU065	7.6	0.6	306	1.429
13	1605	Duzce, Turkey	Duzce	7.1	6.6	282	1.746
14	3750	Cape Mendocino	Loleta Fire Station	7.0	25.9	516	3.916
15	5774	Iwate	Nakashinden Town	6.9	29.4	276	4.234
16	5831	El Mayor-Cucapah	EJIDO SALTILLO	7.2	17.3	242	3.937
17	5838	El Mayor-Cucapah	El Centro - Meloland Geotechnic	7.2	29.0	186	4.617
18	6889	Darfield, New Zealand	Christchurch Hospital	7.0	18.4	194	3.586
19	6942	Darfield, New Zealand	NNBS North New Brighton School	7.0	26.8	211	4.034
20	6952	Darfield, New Zealand	Papanui High School	7.0	18.7	263	2.832

Appendix E2

Design Revisions for HPSPSW Design Cases

The evolutions of design revisions for HPSPSW C9-3 and C20-3 are provided in this section. Figure E2.1—Figure E2.3 show the peak story drift, floor acceleration, residual drift responses as well as the column demand-to-capacity ratios for each of the revised designs. Figure E2.4-Figure E2.8 show the same information for design iterations for case C20-3.

C9-3

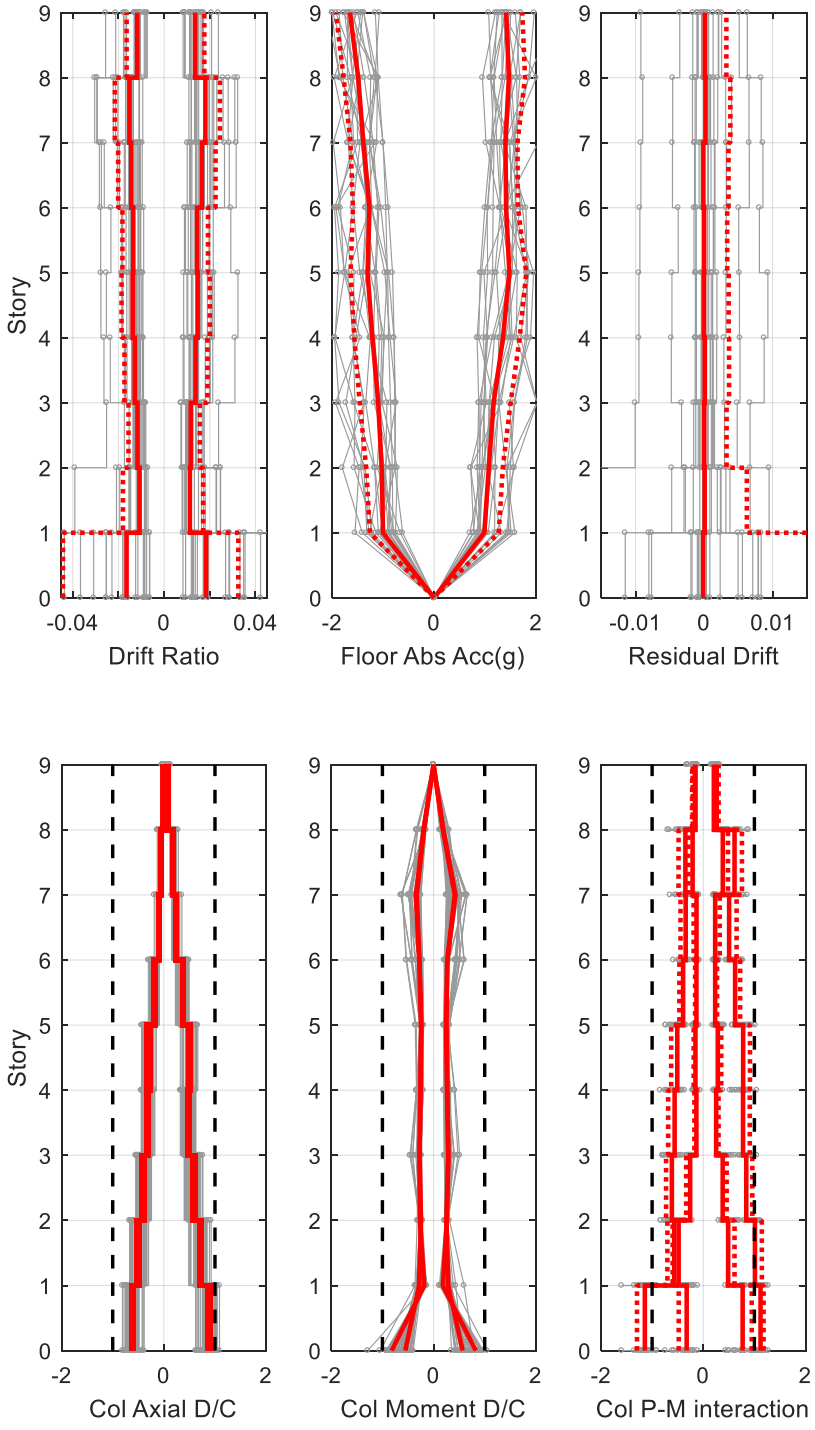

Figure E2.1 Drift, acceleration and column demand-capacity responses of design case C9-3 at 02/50 level motions

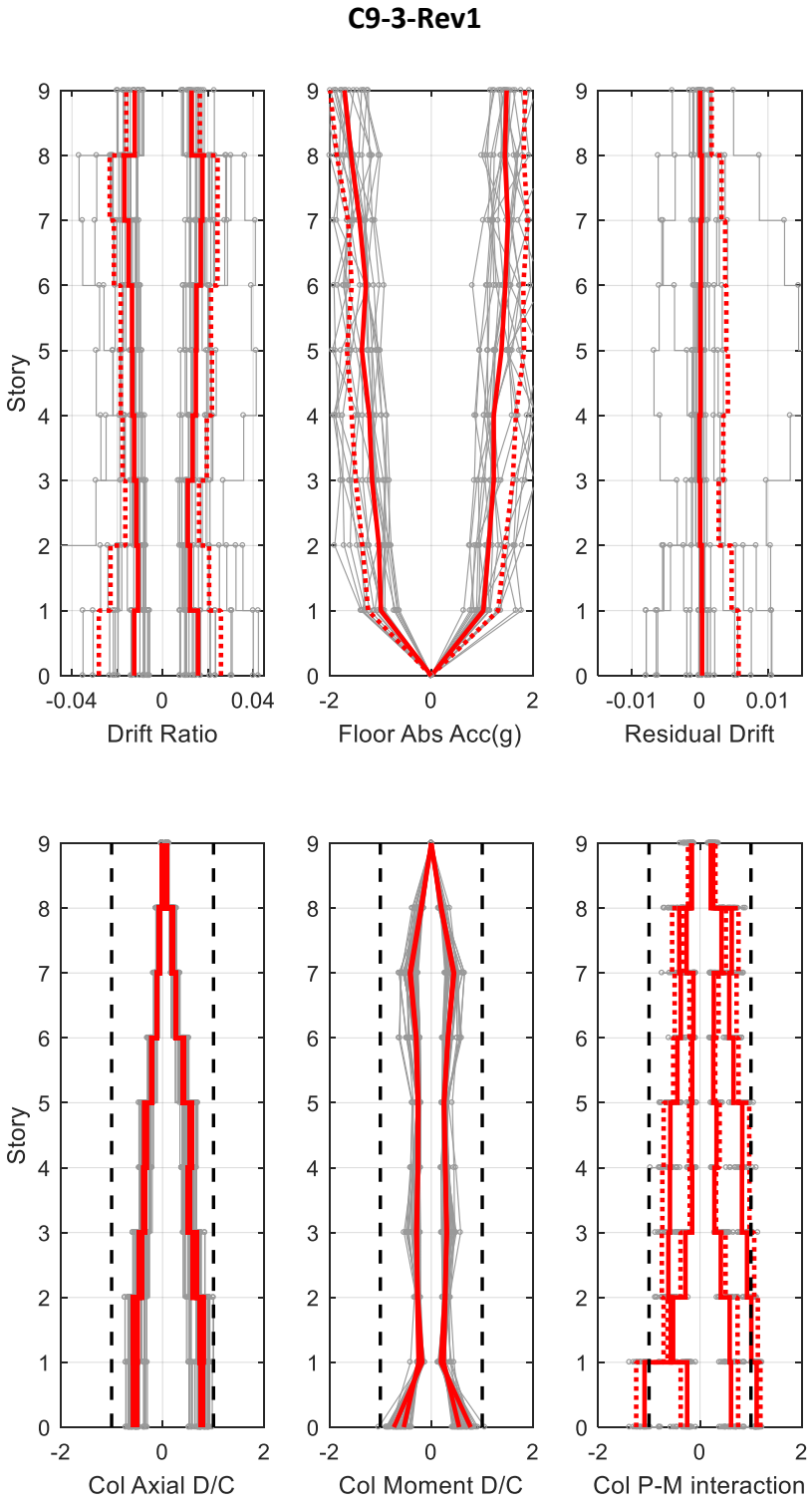

Figure E2.2 Drift, acceleration and column demand-capacity responses of design revision 1 for C9-3 at 02/50 level motions

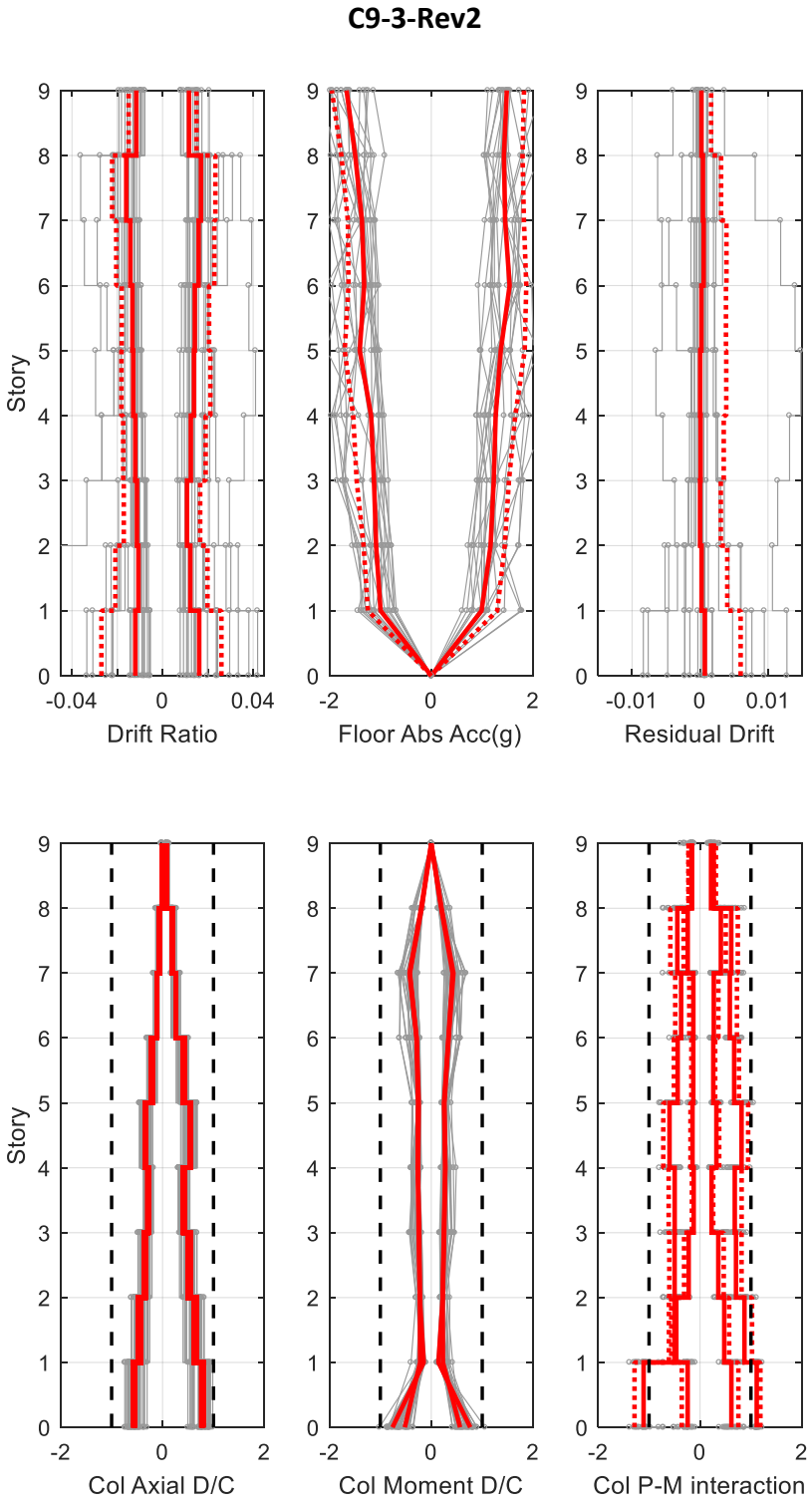

Figure E2.3 Drift, acceleration and column demand-capacity responses of design revision 2 for C9-3 at 02/50 level motions

C20-3

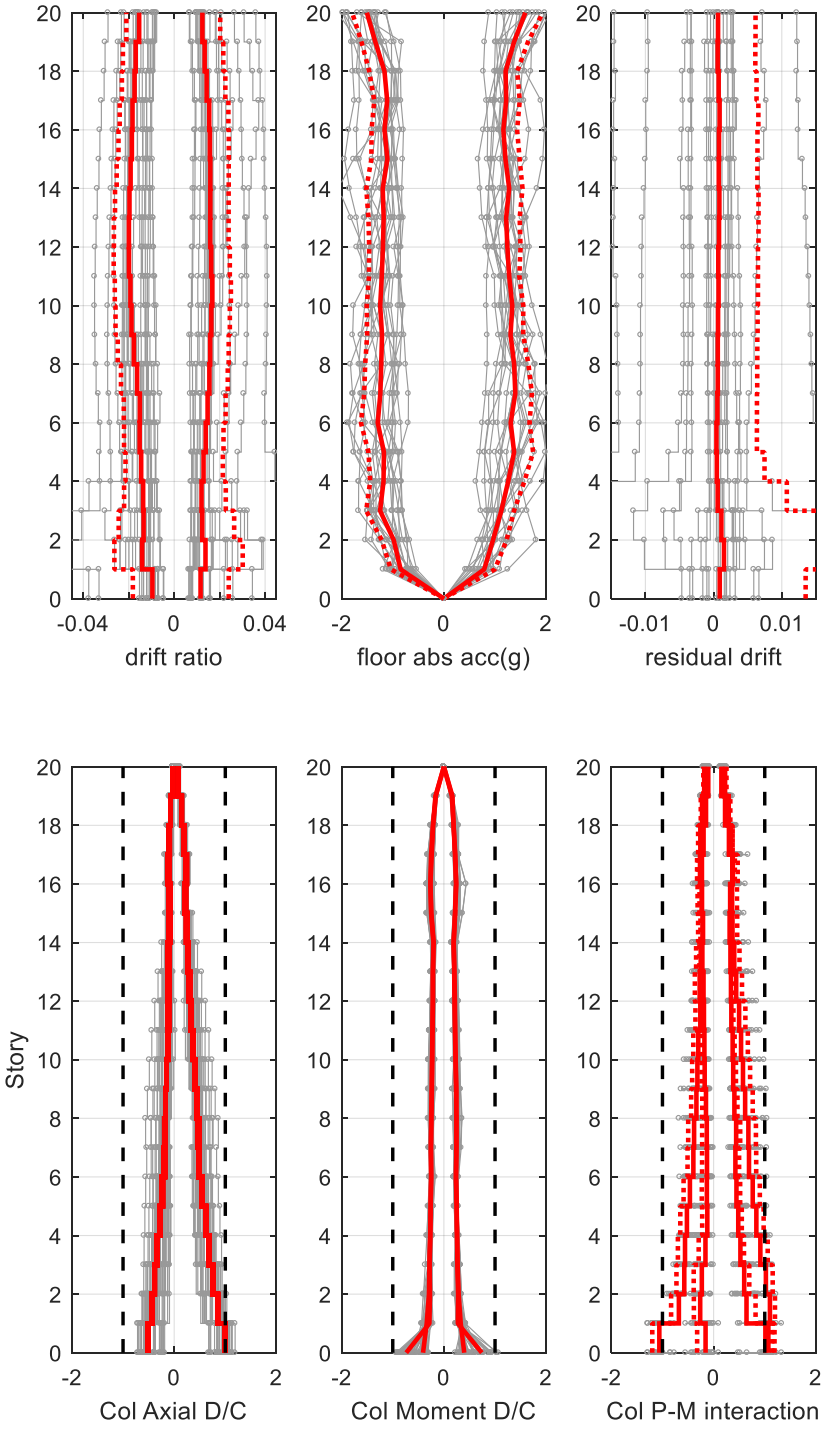

Figure E2.4 Drift, acceleration and column demand-capacity responses of design case C20-3 at 02/50 level motions

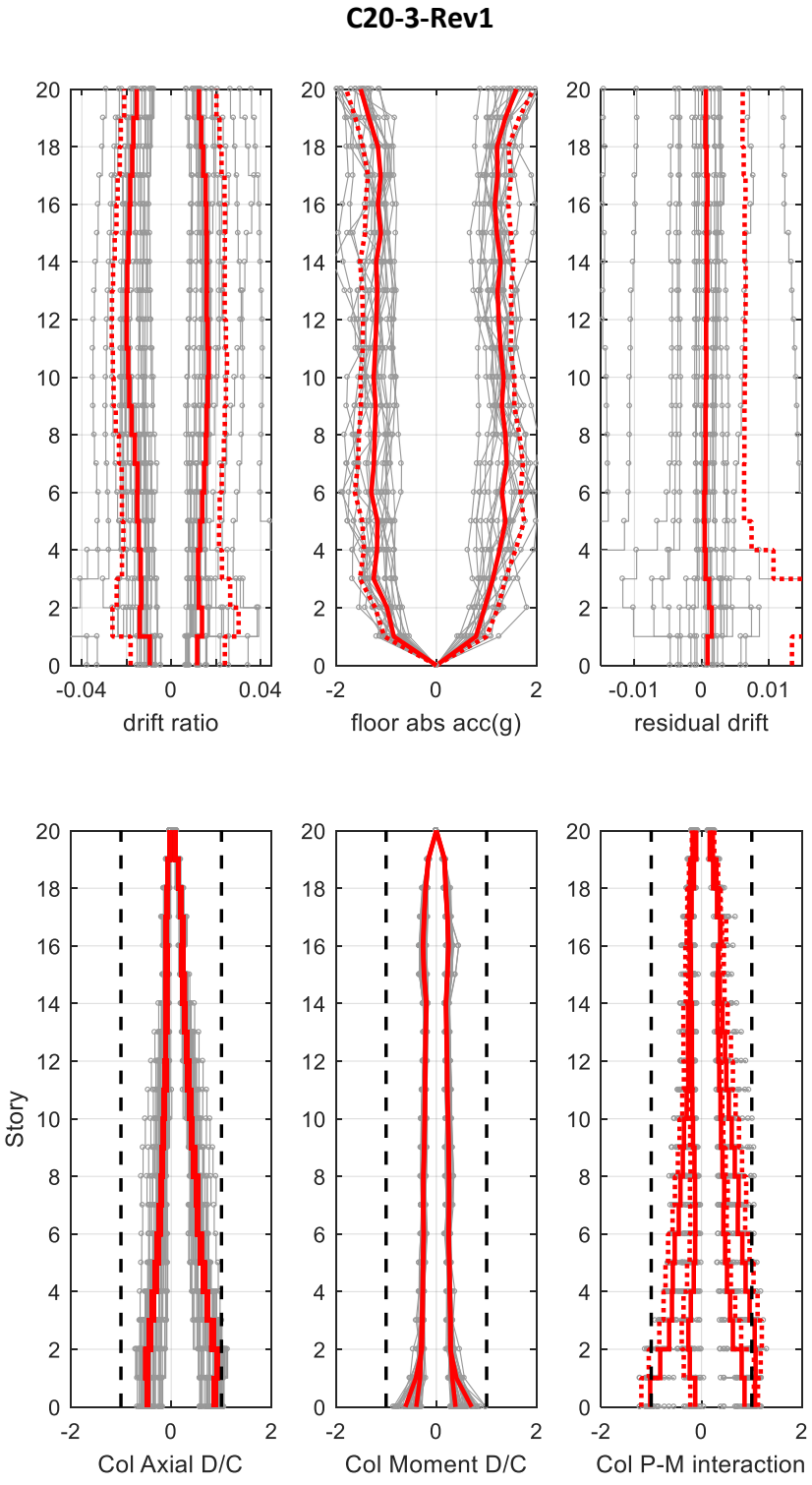

Figure E2.5 Drift, acceleration and column demand-capacity responses of design revision 1 for C20-3 at 02/50 level motions

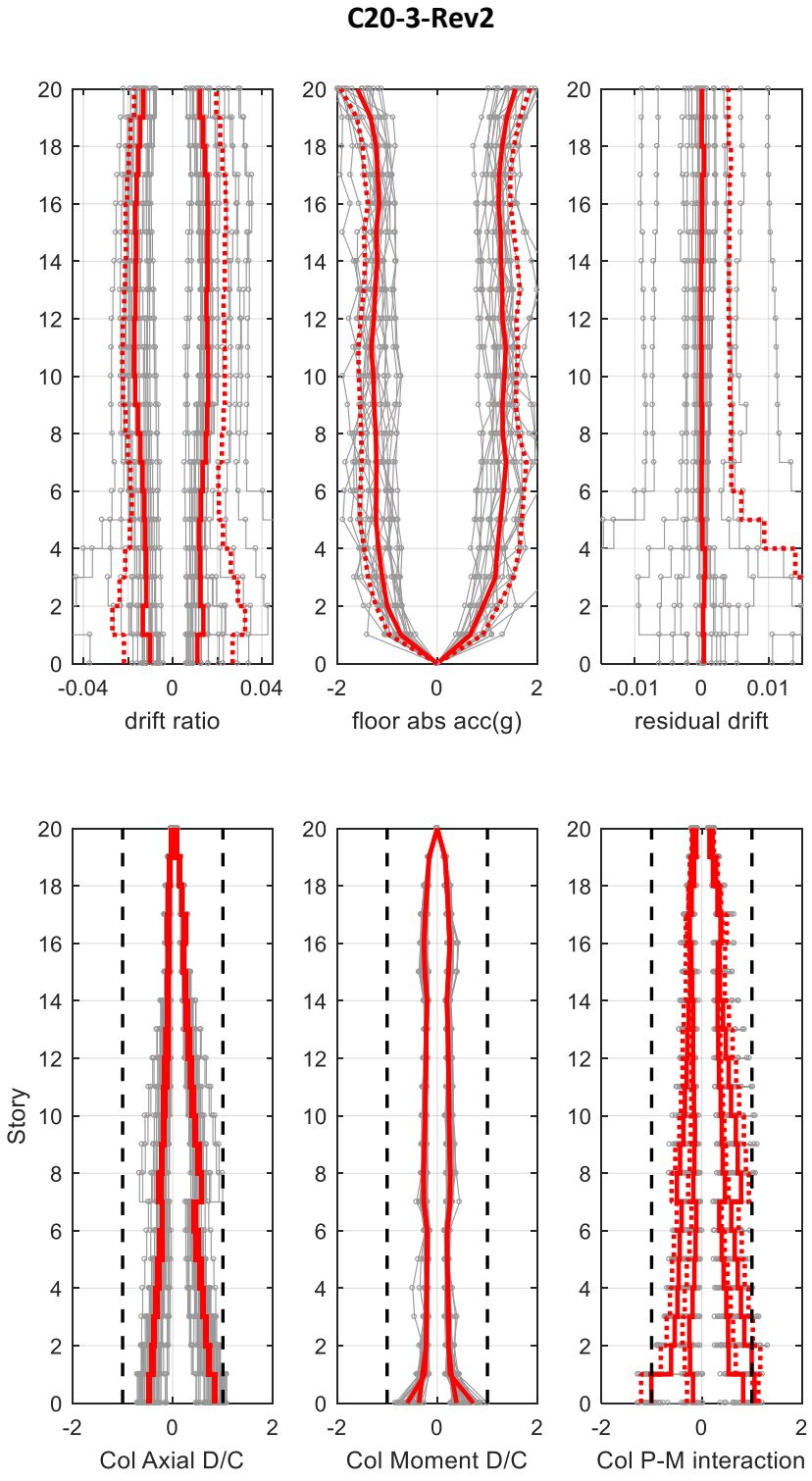

Figure E2.6 Drift, acceleration and column demand-capacity responses of design revision 2 for C20-3 at 02/50 level motions

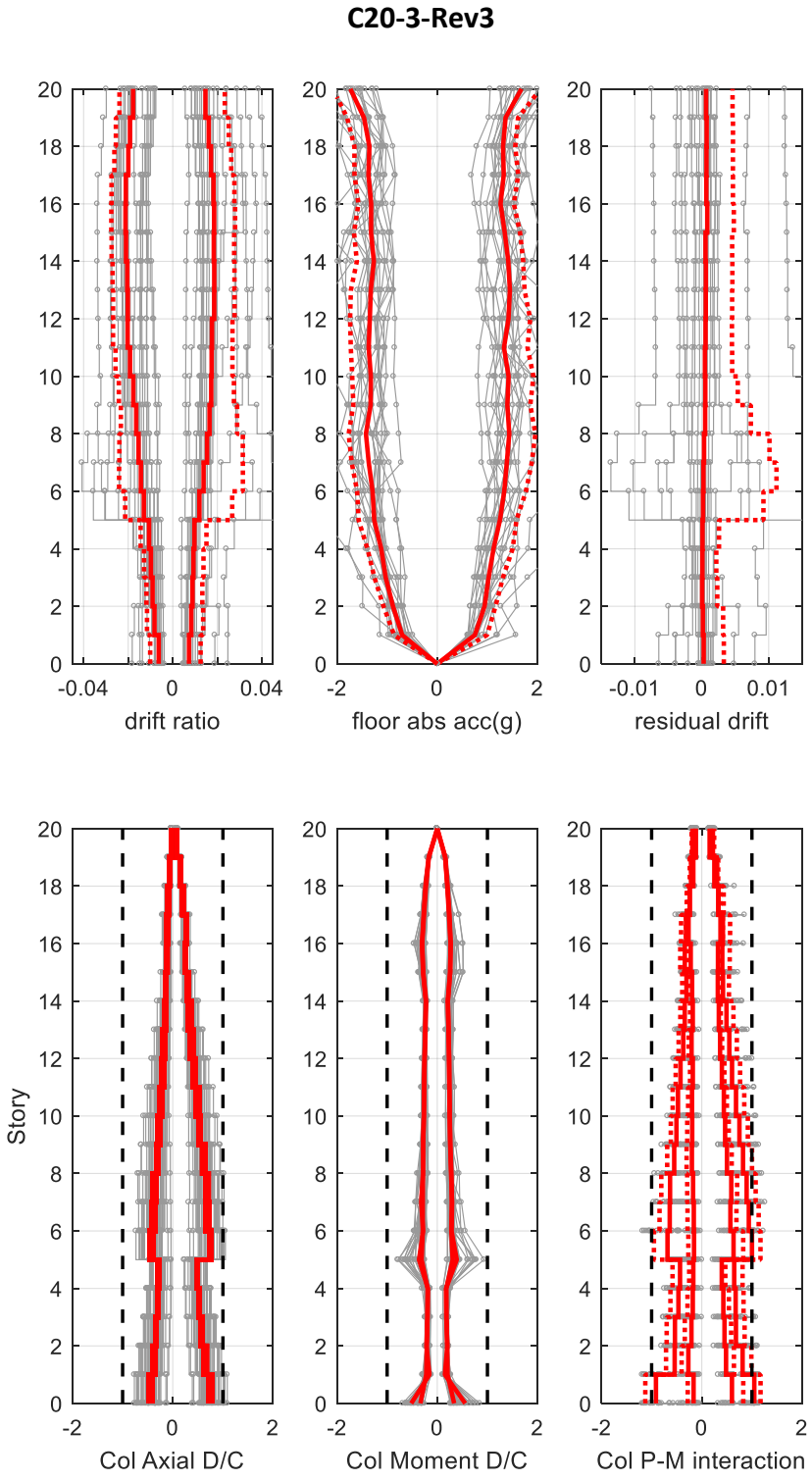

Figure E2.7 Drift, acceleration and column demand-capacity responses of design revision 3 for C20-3 at 02/50 level motions

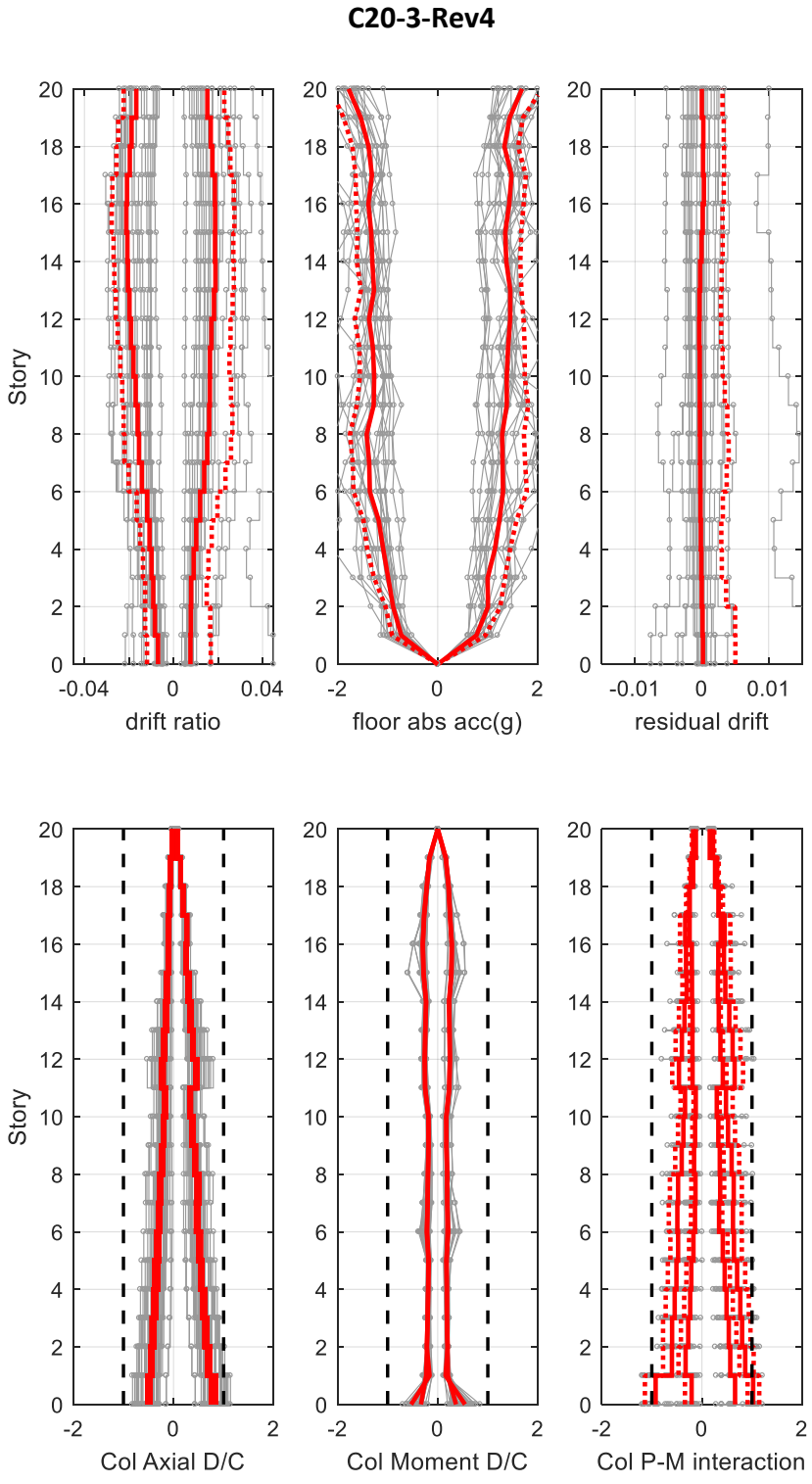

Figure E2.8 Drift, acceleration and column demand-capacity responses of design revision 4 for C20-3 at 02/50 level motions